

BACKWATER EFFECTS OF PIERS AND ABUTMENTS

by

H. K. Liu, J. N. Bradley, E. J. Plate



Prepared by the
Civil Engineering Section
Colorado State University
Fort Collins, Colorado

in cooperation with
The U. S. Department of Commerce
Bureau of Public Roads

October 1957



U18401 1421146

CER57HKL10

ACKNOWLEDGMENTS

Mr. Carl F. Izzard, Chief, Division of Hydraulic Research representing the sponsor initiated this project and has contributed much time and effort to this work. Dr. John S. McNown, Consultant to the Division of Hydraulic Research, Bureau of Public Roads, has given valuable comments and suggestions in general and has suggested in particular the comparison of flow through an open channel constriction with the free streamline problem of flow through a two-dimensional orifice. Mr. Dassel E. Hallmark of the Bureau of Public Roads participated in the collection of laboratory data, as well as in the analysis of the data. Mr. Hugh E. Berger of the Bureau of Public Roads also participated in the testing program.

Of the Colorado State University staff, the authors are indebted to Dr. M. L. Albertson, Director of the Research Foundation and Professor of Civil Engineering at Colorado State University, whose comments, discussion, and supervision of this research together with his critical review of this report are extremely appreciated, and to Dr. D. F. Peterson, Jr., formerly Head of the Civil Engineering Department for assisting in the operation of this research. The authors are also indebted to Dr. A. R. Chamberlain, Chief of the Civil Engineering Section, who has contributed much of his technical and supervisory talent to this research; to Mr. R. V. Asmus, Shop Supervisor of the Hydraulics Laboratory, under whose supervision the experimental equipment was constructed and maintained; and to the following graduate students who participated in this research: Messrs. A. H. Makerechian, Y. A. Wang, P. K. Mohanty, H. S. Nagabhushanaiah, R. C. Malhotra, and many others.

FOREWORD

Since November 1954 the Bureau of Public Roads, U. S. Department of Commerce, has sponsored a research project in cooperation with Colorado State University to study the backwater effects of bridge piers and abutments. This has been conducted in the Hydraulics Laboratory of the Civil Engineering Department, through the State University Research Foundation.

The research is intended to provide a sound method of designing bridge waterways in accordance with the general criterion that ". . . the waterway provided shall be sufficient to insure the discharge of flood waters without undue backwater head . . ." as quoted from Article 3.1.1 of the Standard Specifications for Highway Bridges, American Association of State Highway Officials.

This report presents a study of backwater effects and related problems for clear-water flowing through a local constriction. The constriction is caused by bridge abutments with or without piers in an open channel with a rigid boundary.

Both the experimental and analytical work reported herein, except Chapter VI, was under the direct supervision of H. K. Liu, Assistant Professor at Colorado State University. Chapter VI was prepared by J. N. Bradley, hydraulic engineer of the Bureau of Public Roads. E. O. Plate, former graduate student of the University, participated in the experimental work as well as the analysis of data presented in Chapter V.

TABLE OF CONTENTS

<u>Chapter</u>	<u>Page</u>
ACKNOWLEDGEMENTS	i
FORWARD	iii
LIST OF DATA TABLES IN APPENDIX B	ix
LIST OF DATA TABLES IN APPENDIX C	x
LIST OF FIGURES IN CHAPTER I	xi
LIST OF FIGURES IN CHAPTER II	xii
LIST OF FIGURES IN CHAPTER III	xiii
LIST OF FIGURES IN CHAPTER IV	xv
LIST OF FIGURES IN CHAPTER V	xvi
LIST OF FIGURES IN CHAPTER VI	xxi
ABSTRACT	xxiii
I INTRODUCTION	1
Notations and Definitions	5
Figures in Chapter I	14
II REVIEW OF LITERATURE	25
Figures in Chapter II	38
III THEORETICAL ANALYSIS	41
Continuity Equation	43
Momentum Equation	43
Energy Equation	45
Equation of Maximum Backwater	59

TABLE OF CONTENTS [Continued]

<u>Chapter</u>	<u>Page</u>
Method of Free Streamline Analysis	71
Two-dimensional Flow Around Cylinders	73
Dimensional Analysis	79
Figures in Chapter III	83
IV EQUIPMENT AND PROCEDURE	95
Equipment	95
Procedure	102
Figures in Chapter IV	107
V PRESENTATION AND ANALYSIS OF DATA	117
Part I Flow Geometry	119
Water Surface Profiles	119
Coefficient of Contraction	122
Location of the Maximum Backwater	123
Part II Energy Loss	127
Part III Maximum Backwater	131
Simple Normal Crossing	132
Abnormal Stage - Discharge Condition	146
Dual Bridges Crossing	148
Bridge Girders Partially Submerged	151
Skew Crossing	154
Eccentric Crossing	157
Piers	159
Flood Plain Models	170
Figures in Chapter V	173

TABLE OF CONTENTS [Continued]

<u>Chapter</u>	<u>Page</u>
VI ANALYSIS OF DATA FROM AN ENGINEERING APPROACH	225
Dissimilarities in Model and Prototype	225
Approach to Analysis	230
Backwater Coefficient	233
Location of Maximum Backwater	244
Difference in Level Across Embankments	246
Dual Bridges	251
Abnormal Stage-Discharge Condition	254
Bridge Girders Partially Submerged	258
Prototype Verification	261
Practical Applications	262
Figures in Chapter VI	263
VII SUMMARY AND CONCLUSIONS	285
VIII RECOMMENDATIONS FOR FUTURE RESEARCH .	297
BIBLIOGRAPHY	299
APPENDIX A - FREE STREAMLINE PROBLEM	303
APPENDIX B - TABLES	312
APPENDIX C - TABLES	341

DATA TABLES IN APPENDIX B

Table

1	Simple normal crossing
2	Abnormal stage-discharge condition
3	Dual bridges contraction
4	Bridge girders partially submerged
5	Skew crossing
6	Eccentric crossing
7	Piers with and without abutments
8	Flood plain model

DATA TABLES IN APPENDIX C

Table

1	Simple normal crossing with 45 degree wing-wall abutment
2	Flood-plain model with 45 degree wing-wall abutment
3	Simple normal crossing with 30 degree WW, 60 degree WW, 90 degree WW, 90 degree VW
4	Simple normal crossing with 1:1½ spill-through abutment
5	Flood-plain model with 1:1½ spill-through abutment
6	Piers with 45 degree wing-wall abutments
7	Piers with 1:1½ spill-through abutments
8	Eccentric crossing
9	Skew crossing with 45 degree wing-wall abutment
10	Skew crossing with 1:1½ spill-through abutment
11	Dual bridges with pile bents
12	Dual bridges contraction
13	Abnormal stage-discharge condition with 45 degree wing-wall abutment
14	Abnormal stage-discharge condition with 1:1½ spill-through abutment
15	Bridge girders partially submerged
16	Bridge girders submerged

FIGURES IN CHAPTER I

Fig. No.

- 1-1 Definition sketch for simple normal crossing with vertical-wall abutments
- 1-2 Definition sketch for simple normal crossing with wing-wall abutments
- 1-3 Definition sketch for simple normal crossing with spill-through abutments
- 1-4 Definition sketch for abnormal stage-discharge condition
- 1-5 Definition sketch for dual bridges contraction
- 1-6 Definition sketch for bridge girder partially submerged
- 1-7 Definition sketch for skew crossing
- 1-8 Definition sketch for eccentric crossing
- 1-9 Definition sketch for simple normal crossing with piers
- 1-10 Definition sketch for skew crossing with piers
- 1-11 Definition sketch for flood-plain model
- 1-12 Definition sketch of terms used in flood-plain model

FIGURES IN CHAPTER II

Fig. No.

- 2-1 Classification by Rehbock and Yarnell for flow through a contracted opening
- 2-2 Variation of backwater ratio $[h_1^*/\Delta h]_{base}$ with contraction ratio m and Manning roughness n .
- 2-3 Variation of correction factor K_c with discharge coefficient ratio c/c'

FIGURES IN CHAPTER III

Fig. No.

- 3-1 Dimensionless specific-energy diagram for two dimensional flow
- 3-2 Dimensionless discharge diagram for two-dimensional flow
- 3-3 Illustration showing difference of water surface elevation caused by channel contraction
- 3-4 Discharge diagram for various specific heads
- 3-5 Correction coefficient for Borda loss
- 3-6 Variation of theoretical backwater ratio $[h_1/h_n]$ for contraction backwater with opening ratio M and Froude number F_n
- 3-7 Measured water surface profile along the center line for $Q = 2.5$ cfs and $B = 7.9$ ft at different opening ratios M
- 3-8 Sketch showing the center line profile of contraction backwater for $Q = 2.5$ cfs and $B = 7.9$ ft at different opening ratios M
- 3-9 Variation of theoretical contraction backwater with measured resistance backwater at various depths of the contracted flow
- 3-10 Upper limiting flow conditions for the resistance backwater
- 3-11 Theoretical pressure and velocity distribution along the upstream face of the contraction
- 3-12 Theoretical pressure distribution along the upstream bank and along the centerline of the contraction
- 3-13 Irrotational flow around a cylinder
- 3-14 Irrotational flow around a cylinder in a narrow channel

Fig. No.

3-15 Two-dimensional flow around a cylinder at
 $Re = 1.86 \times 10^5$

3-16 Drag coefficient of a cylinder in a two-dimensional
flow

FIGURES IN CHAPTER IV

Fig. No.

- | | |
|------|---|
| 4-1 | General elevation of experimental flume |
| 4-2 | Patterns of bed roughness |
| 4-3 | Photo of the baffle and screen at the entrance of flume |
| 4-4 | Photo of the adjustable tailgate |
| 4-5 | Photo of the point gage and carriage |
| 4-6 | Models of wing-wall abutments |
| 4-7 | Models of spill-through abutments and vertical-board models |
| 4-8 | Pier models |
| 4-9 | Models of submerged bridge girders |
| 4-10 | Photo of Pitot tube used to take velocity profiles |
| 4-11 | Photo of wing-wall abutments in 4-ft flume |
| 4-12 | Photo of spill-through abutments in 4-ft flume |

FIGURES IN CHAPTER V

Fig. No.

- 5-1 Water surface profile along the upstream face of the embankment for vertical-board model
- 5-2 Water surface profile along the bank and the centerline for vertical-board model
- 5-3 Variation of theoretical coefficient of contraction C_c with opening ratio M [after von Mises]
- 5-4 Variation of experimental coefficient of contraction C_c with opening ratio M for vertical-board model
- 5-5 Variation of experimental coefficient of contraction C_c with opening ratio M for wing-wall abutments
- 5-6 Variation of experimental coefficient of contraction C_c with opening ratio M for spill-through abutments
- 5-7 Approximate location of maximum backwater
- 5-8 Effect of channel slope on the location of maximum backwater
- 5-9 Effect of abutment geometry on the location of maximum backwater
- 5-10 Effect of abutment geometry due to height of model on the entrance conditions of flow
- 5-11 Effect of Froude number on the location of maximum backwater [$n = 0.024$]
- 5-12 Effect of Froude number on the location of maximum backwater [$n = 0.045$]
- 5-13 Flow pattern of a simple normal crossing for spill-through abutments
- 5-14 Breakdown of energy losses for vertical-board model when $n = 0.024$
- 5-15 Breakdown of energy losses for vertical-board model when $n = 0.045$
- 5-16 Breakdown of energy losses for wing-wall abutments

Fig. No.

- 5-17 Breakdown of energy losses for spill-through abutments
- 5-18 Effect of discharge on the maximum backwater
- 5-19 Effect of bed roughness on the maximum backwater
- 5-20 Effect of channel slope on the maximum backwater
- 5-21 Variation of backwater ratio h_1^*/h_n with opening ratio M , channel slopes, width-depth ratios, and Reynolds numbers
- 5-22 Variation of experimental backwater ratio h_1^*/h_n with opening ratio M and Froude number F_n
- 5-23 Variation of theoretical backwater ratio h_1^*/h_n with opening ratio M and Froude number F_n
- 5-24 Effect of discharge on backwater ratio h_1^*/h_n
- 5-25 Effect of channel slope on backwater ratio h_1^*/h_n
- 5-26 Effect of channel roughness on backwater ratio h_1^*/h_n
- 5-27 Effect of abutment type on backwater ratio h_1^*/h_n
- 5-28 Effect of abutment geometry on backwater ratio h_1^*/h_n for wing-wall abutments
- 5-29 Effect of abutment geometry on backwater ratio h_1^*/h_n for spill-through abutments
- 5-30 Effect of abutment length on backwater ratio h_1^*/h_n for wing-wall abutments
- 5-31 Effect of abutment length on backwater ratio h_1^*/h_n for spill-through abutments
- 5-32 Variation of correction factor $\bar{\phi}$ with Froude number F_n and opening ratio M for vertical-board model
- 5-33 Variation of correction factor $\bar{\phi}$ with Froude number F_n and opening ratio M for wing-wall abutments
- 5-34 Variation of correction factor $\bar{\phi}$ with Froude number F_n and opening ratio M for spill-through abutments

Fig. No.

- 5-35 Variation of $[h_1/h_n]^3$ with F_n^2 and M as the third variable for vertical board model
- 5-36 Empirical backwater equation compared to experimental data for vertical-board model
- 5-37 Variation of $[h_1/h_n]^3$ with F_n^2 and M as the third variable for wing-wall abutments
- 5-38 Variation of $[h_1/h_n]^3$ with F_n^2 and M as the third variable for spill-through abutments
- 5-39 Variation of $[h_1/h_n]^3$ with $F_n^2 [1/M^2 - 1]$ for vertical-board model
- 5-40 Variation of $[h_1/h_n]^3$ with $F_n^2 [1/M^2 - 1]$ for 45 degree wing-wall abutments
- 5-41 Variation of $[h_1/h_n]^3$ with $F_n^2 [1/M^2 - 1]$ for 1:1½ spill-through abutments
- 5-42 Variation of $[h_1/h_n]^3$ with $F_n^2 [1/M^2 - 1]$ for various wing-wall abutments
- 5-43 Variation of $[h_1/h_n]^3$ with $F_n^2 [1/M^2 - 1]$ for various spill-through abutments
- 5-44 Variation of $[h_1/h_n]^3$ with $F_n^2 [1/M^2 - 1]$ and abutment geometry
- 5-45 Variation of $[h_1/h_n]^3$ with F_A^2 and M for vertical-board model
- 5-46 Variation of $[h_1/h_A]^3$ with F_A^2 and M for wing-wall abutments
- 5-47 Variation of $[h_1/h_n]^3$ with F_A^2 and M for spill-through abutments
- 5-48 Variation of $[h_1/h_n]^3$ with F_A^2 and M for vertical-board model in a horizontal channel
- 5-49 Backwater of dual bridges contraction for wing-wall abutments
- 5-50 Backwater of dual bridges contraction for spill-through abutments
- 5-51 Variation of $[h_1/h_n]^3 - 1$ with $F^2[1/M^2 - 1]$ and L_D of dual bridges contraction for wing-wall abutments

Fig. No.

- 5-52 Variation of $[h_1/h_n]^3 - 1$ with $F^2 [1/M^2 - 1]$ and L_D of dual bridges contraction for spill-through abutments
- 5-53 Coefficient C_{WW} and C_{ST} as a function of L_D for dual bridges contraction
- 5-54 Backwater ratio h_1/h_n for bridge girders partially submerged with wing-wall abutments
- 5-55 Backwater ratio h_1/h_n for bridge girders partially submerged with spill-through abutments
- 5-56 Variation of $M - M^*$ with z/h_1 and M for bridge girders partially submerged with wing-wall abutments
- 5-57 Contour of the water surface elevation in the vicinity of a skew crossing
- 5-58 Variation of h_u with M [base curve] for vertical-board model at $F_n = 0.332$
- 5-59 Variation of M^* with M for vertical-board model at skew crossing
- 5-60 Variation of h_n with M [base curve] for wing-wall abutments at $F_n = 0.332$
- 5-61 Variation of M^* with M for skew crossing of wing-wall abutments with faces perpendicular to roadway
- 5-62 Variation of M^* with M for skew crossing of wing-wall abutments with faces parallel to the main direction of flow
- 5-63 Variation of h_u with M [base curve] for spill-through abutments at $F_n = 0.332$
- 5-64 Variation of M^* with M for skew crossing of spill-through abutment with faces perpendicular to roadway
- 5-65 Variation of M^* with M for skew crossing of spill-through abutment with faces parallel to the main direction of flow
- 5-66 Effect of eccentric crossing on h_1 for vertical-board model

Fig. No.

- 5-67 Effect of eccentric crossing on h_1 for wing-wall abutments
- 5-68 Effect of eccentric crossing on h_1 for spill-through abutments
- 5-69 Variation of M^* with M at $e = 1$, for wing-wall and spill-through abutments
- 5-70 Effect of bed roughness in the contraction on the maximum backwater
- 5-71 Shape factor s for piers with wing-wall abutments
- 5-72 Shape factor s for piers with spill-through abutments
- 5-73 Variation of h_1^* with M^* for wing-wall abutments with piers at $F_n = 0.332$
- 5-74 Variation of h_1^* with M^* for spill-through abutments and piers at $F_n = 0.332$
- 5-75 Variation of $h_{UR} - h_n$ with M^* for skew crossing with piers and wing-wall abutments at $F_n = 0.332$, $\phi = 30$ degrees
- 5-76 Variation of M^* with M for flood-plain model with vertical-board constriction
- 5-77 Variation of M^* with M for flood-plain model with wing-wall abutments
- 5-78 Variation of M^* with M for flood-plain model with spill-through abutments

FIGURES IN CHAPTER VI

Fig. No.	
6-1	Example of flow lines produced by channel contraction
6-2	Operational differences between model and prototype
6-3	Water surface measurements at shore line - Oneida Creek, New York
6-4A	Base curve of backwater coefficient K_b for 45 degree wing-wall abutments
6-4B	Base curve of differential level ratio ϵ_b for 45 degree wing-wall abutments
6-5A	Base curve of backwater coefficient K_b for all types of wing-wall abutments
6-5B	Base curve of differential level ratio ϵ_b all types of wing-wall abutments
6-6A	Base curve of backwater coefficient K_b for 1:1½ spill-through abutments
6-6B	Base curve of differential level ratio ϵ_b for 1:1½ spill-through abutments
6-7A	Base curve of backwater coefficient K_b for all types of spill-through abutments
6-7B	Base curve of backwater coefficient ϵ_b for all types of spill-through abutments
6-8	Total backwater coefficient $K_b + \Delta K_p$ for bents with circular piles and spill-through abutments
6-9	Incremental backwater coefficient ΔK_p for piers, wing-wall, and spill-through abutments
6-10A	Total differential level ratio $\epsilon_b + \Delta \epsilon_p$ for round double-shaft piers and spill-through abutments
6-10B	Incremental differential level ratio $\Delta \epsilon_p$ for round double shaft piers and spill-through abutments

Fig. No.

- 6-11 Incremental differential level ratio $\Delta\epsilon_p$ for various piers and pile bents with wing-wall and spill-through abutments
- 6-12A Incremental backwater ratio ΔK_e for eccentric crossing and wing-wall and spill-through abutments
- 6-12B Incremental differential level ratio $\Delta\epsilon_e$ for eccentric crossing and wing-wall and spill-through abutments
- 6-13 Incremental backwater coefficient ΔK_s for skew crossing and wing-wall abutment
- 6-14 Incremental backwater coefficient ΔK_s for skew crossing and spill-through abutment
- 6-15 Incremental differential level ratio $\Delta\epsilon_s$ for wing-wall and spill-through abutments
- 6-16 Distance to point of maximum backwater with or without piers
- 6-17 Backwater multiplication factor η for dual bridges contraction for wing-wall and spill-through abutments
- 6-18A Differential-level multiplication factor η_3 of dual bridges contraction for wing-wall and spill-through abutments
- 6-18B Differential-level multiplication factor η_{3B} of dual bridges contraction for wing-wall and spill-through abutments
- 6-19 Backwater coefficient K_A for abnormal stage-discharge condition
- 6-20 Differential level ratio ϵ_A for abnormal stage-discharge condition
- 6-21 Discharge coefficient for bridge girders submerged
- 6-22 Discharge coefficient for bridge girders partially submerged

ABSTRACT

The purpose of the research reported herein is to determine the maximum height of backwater caused by a given local constriction in an otherwise prismatic channel. The experiments were conducted in a flume 73.5 ft long and 2 ft deep. For runs prior to run no. 121, the flume width was 4 ft and for the remaining experiments, the flume width was maintained at 7.9 ft. The slope of the flume could be adjusted by raising or lowering the jacks underneath the flume. The flow system was recirculatory.

Two kinds of artificial bed roughness were used in the flume. Manning's n was approximately 0.024 for the bar roughness, and 0.045 for the baffle roughness. The constriction was formed by models of either bridge abutments or piers, or a combination of both. Types of abutments used extensively in the experiments were 45 degree wing-wall, $1:1\frac{1}{2}$ spill-through, and vertical-board. Tests on piers were not extensive. The various crossing conditions tested were:

- [a] simple normal crossing
- [b] abnormal stage-discharge condition
- [c] dual-bridges contraction
- [d] bridge girders partially submerged
- [e] skew crossing
- [f] eccentric crossing
- [g] piers with and without abutments
- [h] flood-plain models

A uniform flow was established before the models were placed and the normal depth and the Froude number of this normal

flow condition were used as reference variables. Also the opening ratio, denoting the ratio of the width of the opening to the channel width has been used in the analysis.

In Chapter III, the basic principles of open channel flow through a constriction is discussed extensively. The maximum backwater is defined as the difference between the maximum depth of the backwater and the normal depth of flow. The maximum backwater caused by local constriction is classified as [a] contraction backwater and [b] resistance backwater. An equation to be used as a criterion for separating the resistance backwater from the contraction backwater has been obtained from theoretical considerations.

The application of hydrodynamics to the problem of an open channel constriction is discussed at length in this chapter. Dimensional analysis is applied to the problem in order to study the effect of many variables on the maximum backwater. It was found that both the channel slope and the channel roughness can be eliminated as variables if the normal depth and the Froude number of the normal flow are used.

Analysis of data is made both in Chapter V and Chapter VI. In Chapter V, the method of analysis is analytical with a view to understanding the effect of various primary variables on the maximum backwater. In the case of a simple normal crossing, an empirical formula for computing the maximum backwater caused by the vertical board constriction has been established. Furthermore, a set of graphs of maximum backwater has been established for other types of abutment models. A method of computing qualitatively the various energy losses of the flow in the constriction zone has been found. In analyzing

the data of other crossing conditions, a method of so-called effective opening ratio M^* has been applied with considerable success.

In Chapter VI the method of analysis is less accurate but very easy for highway engineers to use. The general principle of this method is the conservation of energy. A number of graphs based upon laboratory data have been developed for determining the maximum backwater and the differential level of water surface across the embankment.

I. INTRODUCTION

In general, bridge crossings interfere with the natural flow of a stream. Where a bridge spans an entire valley, the bridge piers offer the only obstruction of the flow, which is minor. In the usual case, however, roadway embankments are extended out onto the flood plain, for the purpose of reducing the cost of the bridge structure. In so doing, the highway crossing introduces a sudden constriction in the stream at the bridge during flood. This constriction causes a rise in stage upstream and an increase in velocity through the bridge. One of the problems of the designer is to provide the minimum waterway area, consistent with structural stability and optimum long-range cost to the highway user.

The decision of the designer must be based not only on hydraulic considerations but also on hydrologic and economic factors. From a hydrologic standpoint, it is necessary to choose a design flood for the structure and make provision for passing greater floods without severe damage to the structure proper. Economic factors include initial cost, operating costs, maintenance, possible flood damage, interruption to traffic and others. The hydrologic and economic considerations are beyond the scope of this research.

Highway engineers have long recognized that constricting the flow in a river results in a rise in stage upstream. It has been observed that extreme amounts of such backwater were frequently associated with severe scour around abutments and piers, sometimes resulting in destruction of part or all of the

bridge. On occasion the difference in water surface elevation on the flood plain from one side of the approach roadway to the other side has been noted by upstream property owners, some of whom have successfully brought suit against the responsible highway department for property damage caused by the increased stage. These occurrences have served to make highway departments more conscious of the need for predetermining how proposed bridges will affect the flow in rivers. As the subject was explored, it became evident that existing methods of computing backwater were not reliable, or were too cumbersome to be used readily by highway engineers.

In recognition of these facts the Bureau of Public Roads arranged a cooperative research project with Colorado State University in November 1954. This report covers the experimental investigation of backwater caused by various model bridges placed in a sloping flume having a rigid bed, analysis of the data, development of a working method of design and verification of that method by comparison with measurements of flood flow through actual bridges. The model tests were necessarily idealized by using only a straight channel of uniform cross section. The true effect of the constriction caused by the bridge was obtained by establishing steady uniform flow in the flume and then recording the changes in flow produced by placing the constriction while holding the discharge constant. The flume was of sufficient length to permit normal flow to be reestablished downstream.

The very real problem of scour was deliberately eliminated by use of the rigid boundary. As experience has proven, the analysis of the mechanics of flow was difficult enough without involving a moving bed. Research is now continuing with a similar

flume having a sand bed in which an attempt will be made to discover how scour within the bridge waterway affects backwater.

The research has produced a direct and relatively simple method of estimating the backwater caused by bridges with usual abutment and pier types. The method has been verified by field measurements on bridges up to about 200 ft in length. Application of the model results to waterway openings of great width relative to depth has not been proven, nor is it known how the results might apply to multiple openings.

An eminently practical result is the demonstration that the length, and hence the cost, of a bridge at a given site varies within wide limits depending on the amount of backwater considered tolerable for a given flood. The basis of an engineering economic study of the total cost of owning and operating the bridge is thus provided when floods of different recurrence intervals are considered.

Another fact, confirming results obtained by other investigators, is the proof that the total drop in water surface across the embankment was invariably greater than the actual increase in upstream stage above the stage which would exist if the bridge were not constricting the flow. It was found that the water surface at the downstream side of the bridge was below the normal elevation of the unconfined flow but would gradually approach the normal surface profile in the downstream direction as the flow expanded to the full width of the channel. This fact could be important in court cases where a litigant might construe the drop in water surface across the embankment as being equal to the amount by which the bridge had

raised the upstream stage, which is not true. The drop in water surface across embankments also has a bearing on the stability of embankments subject to overflow since the height of free fall off the downstream shoulder affects the possible erosion as the embankment begins to be overtopped. This also affects length of bridge necessary to keep the head across the embankment within reasonable limits at the roadway grade elevation for which the roadway is expected to come into operation as an emergency spillway to discharge flood waters in excess of the design flood for unhindered traffic.

The laboratory testing was performed in the Hydraulics Laboratory of the State University by the personnel of the Civil Engineering department. The variables to be studied and the outline of the testing program were determined jointly by the laboratory staff and the personnel of the Bureau of Public Roads in order to meet the urgent need of designing bridge waterways for the Interstate highway system. Analyses of the data were made independently by the laboratory staff and the staff of the Bureau of Public Roads. The approach to the analysis made by the laboratory staff is based upon the present knowledge of fluid mechanics as applied to the problem of backwater caused by channel constrictions. Formulas and graphs relative to this approach may be extended to a certain degree to the prototype problem. They will yield accurate information for the flow conditions similar to the ones under which they were developed. In the analysis developed by the staff of the Bureau of Public Roads it has been necessary, in some cases, to sacrifice accuracy for the sake of ease of application. Since each of these two approaches has its own merits, both are presented in this report.

The following are the symbols most commonly used in this report. They have been defined where they first appear within the text. For further clarification please refer to the definition sketches, Figs. 1-1 to 1-12.

NOTATIONS AND DEFINITIONS

Symbol	Unit	Definition
A_i	ft ²	Area of flow at section i
A_n	ft ²	Normal area at bridge site before the bridge is in place
A_{ni}	ft ²	Opening area at section i with water at normal depth
A_p	ft ²	Projected area of piers normal to flow, between normal water surface and stream bed
A_σ	ft ²	Area of a sub-section σ of a cross-section of the flow
B	ft	Width of channel
b	ft	Width of opening
b_c	ft	Critical opening width = $\sqrt{\frac{Q}{2.7gH_n^3}}$
b_m	ft	Bottom width for spill-through abutments [models]
b'	ft	Minimum width of jet = $b \cdot C_c$
b^*	ft	Equivalent b for the method of effective M
C_{DA}	-	D'Aubuisson's pier coefficient
C_{NA}	-	Nagler's pier coefficient
C_{RE}	-	Rehbock's pier coefficient
C_c	-	Coefficient of contraction
C_D	-	Drag coefficient for flow around cylinders

Symbol	Unit	Definition
C_d	-	Discharge coefficient for submerged bridge girders
C_K	-	Kindsvater and Carter's discharge coefficient
C_m	-	Coefficient for momentum energy loss
C_p	-	Coefficient for abnormal stage-discharge analysis
C'_p	-	Coefficient for abnormal stage-discharge analysis
C''_p	-	Coefficient for abnormal stage-discharge analysis
C_s	-	Coefficient for double submerged bridge girders analysis
C'_s	-	Coefficient for double submerged bridge girders analysis
C_{ST}	-	Coefficient for spill-through abutments
C_{WW}	-	Coefficient for wing-wall abutments
D	ft	Pier diameter
E_b	ft	Energy loss caused by contraction
E_e	ft	Excess friction loss
E_{fi-j}	ft	Friction head loss between sections i and j
E_{i-j}	ft	Total energy loss between sections i and j
E_m	ft	Energy loss due to momentum loss of jet
E_{ni-j}	ft	Normal head loss between sections i and j
E_n	ft	Normal head loss
E_r	ft	Residual loss produced by boundary resistance

Symbol	Unit	Definition
e	-	Eccentricity defined as $1 - [\text{length of short abutment}/\text{length of long abutments}]$ or $1 - [Q_L/Q_R]$ where $Q_L < Q_R$
F_i	-	Froude number at section i
F_D	lb	Total drag acting on a cylinder
F_n	-	Froude number for unobstructed flow $= \frac{V}{\sqrt{gh_n}}$
F_{i-j}	lb	Boundary friction force between sections i and j
f	-	Darcy-Weisbach friction factor
f_i	-	Denotes function
G	-	Function of M
g	ft/sec ²	Acceleration of gravity
H	ft	Specific head
H_i	ft	Specific head at section i
H_n	ft	Normal specific head
h	ft	Flow depth
h_A	ft	Depth at model entrance before model is put in for effect of abnormal stage-discharge condition
h_B	ft	Depth in a channel of width B
h_b	ft	Depth in a channel of width b
h_c	ft	Critical depth = $\sqrt[3]{Q^2/gw^2}$
h_f	ft	Friction head loss
h_i	ft	Depth at section i
h_l	ft	Depth at section l
h_4	ft	Depth at section IV
h_n	ft	Normal depth

Symbol	Unit	Definition
h_{UL}	ft	Stagnation depth upstream left
h_{UR}	ft	Stagnation depth upstream right
h_u	ft	Average stagnation depth upstream
h_{DL}	ft	Stagnation depth downstream left
h_{DR}	ft	Stagnation depth downstream right
h_D	ft	Average stagnation depth downstream
Δh_s	ft	Differential level across roadway embankment [$\Delta h_s = \Delta h$ in Chapter VI]
Δh	ft	$h_1^* + h_3^* + SoL_{1-3}$ Difference in water surface elevation between section I and section III
h_1^*	ft	Maximum backwater for normal crossing [above normal depth]
h_d^*	ft	Maximum backwater for dual crossing cases [above normal depth]
h_3^*	ft	Vertical distance from water surface on downstream side of embankment
Δh_1^*	ft	Additional backwater caused by piers at section I
h_s^*	ft	Backwater at section I produced by partial submergence of bridge superstructure
J	A_p / A_{n2}	Ratio of area obstructed by piers to gross water area based on normal water surface at section II
K^*	-	$k_b + \Delta k_p + \Delta k_e + \Delta k_s$ Total backwater coefficient
K_b	-	Backwater coefficient [base curve]
ΔK_e	-	Incremental backwater coefficient for eccentricity

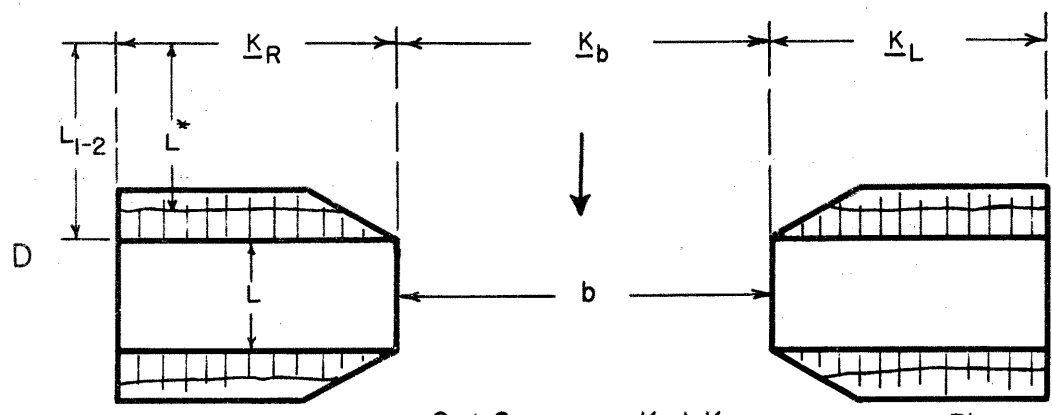
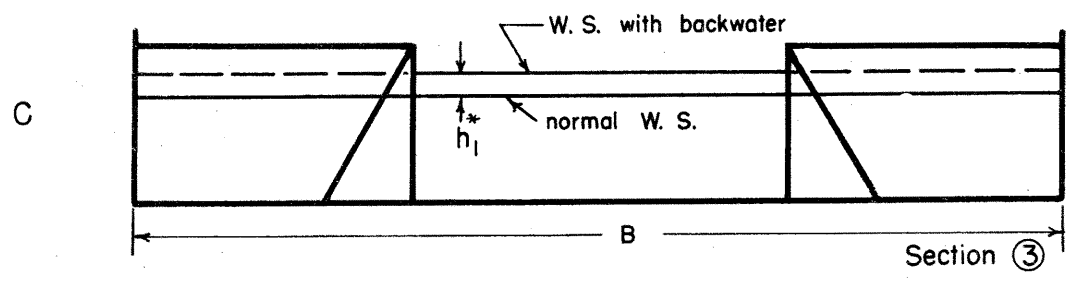
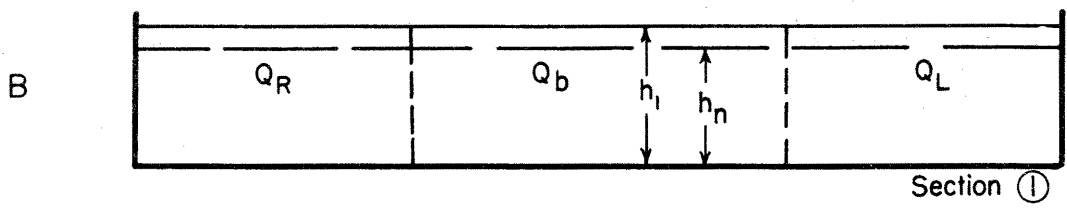
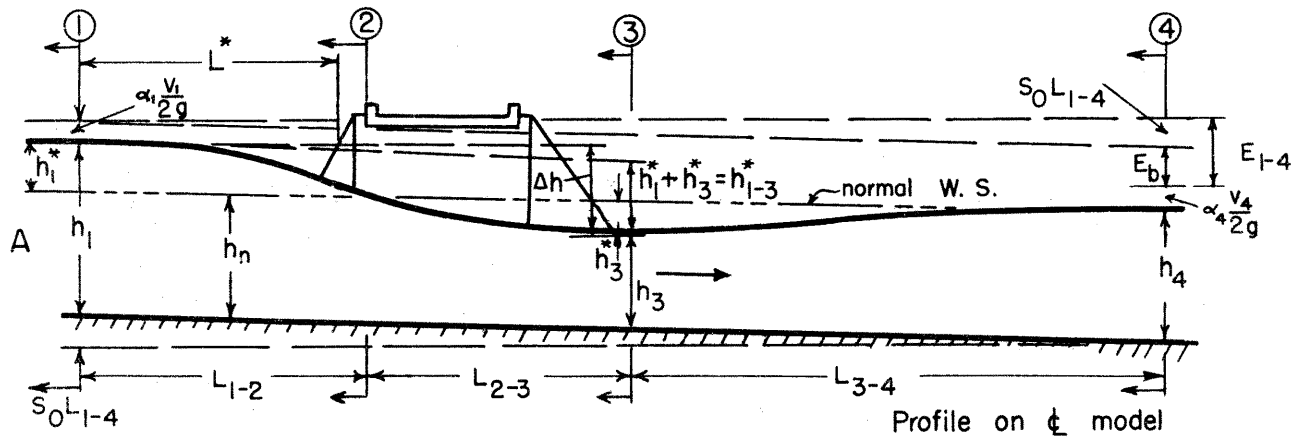
Symbol	Unit	Definition
ΔK_p	-	Incremental backwater coefficient for piers
ΔK_s	-	Incremental backwater coefficient for skew crossing
K_A	-	Backwater coefficient for abnormal stage-discharge condition [base curve]
K_d	-	Backwater coefficient for dual bridges crossing [base curve]
$\frac{K}{\sigma}$	ft ³ /sec	Conveyance of a sub-section of a cross-section of the flow
$\frac{K}{1}$	ft ³ /sec	Total conveyance at section I
$\frac{K}{R}$, $\frac{K}{ctr}$, and $\frac{K}{L}$	ft ³ /sec	Conveyance of that portion of the natural flood plain obstructed by the roadway embankment [subscript refers to right, center or left side, facing downstream]
k	ft	Channel roughness elevation
L	ft	Length of throat
L_D	ft	Distance between dual bridges
L_{i-j}	ft	Distance between sections i and j
L^*	ft	Distance between section I and section II [Chapter V] Distance from water surface on up-stream side of roadway embankment to point of maximum backwater [Chapter VI]
ℓ	ft	Model height
M	-	Opening ratio $bh_n/Bh_n = b/B$ or $Q_{ctr}/Q = Q_{ctr}/Q_R + Q_{ctr} + Q_L$
M_c	-	Critical opening ratio
M^*	-	Effective M value for method of effective M

Symbol	Unit	Definition
ΔM	-	$[M - M^*]$
M'	-	M based on jet width = $C_c b/B$
m	-	Contraction ratio $[1 - M]$
N	-	Number of piers
n	ft ^{1/6}	Manning's roughness coefficient
\bar{P}	lb	Total boundary pressure at section II
p_i	lb/ft ²	Local pressure at section i
Δp	lb/ft ²	Pressure difference
Q	cfs	Total discharge
$Q_B = Q$	cfs	Total discharge over channel width B
Q_b, Q_{ctr}	cfs	Discharge over channel width b
Q_R, Q_L	cfs	Partial discharge of that portion of the flood plain obstructed by the roadway embankments [subscript refers to right or left side, facing downstream]
Q_σ	cfs	Discharge of a sub-section of a cross-section of the flow
q	cfs/ft	Unit discharge
q_{max}	cfs/ft	Maximum unit discharge = Q/b_c
R	ft	Hydraulic radius
R_b	ft	Hydraulic radius of bed
R_e	-	Reynolds number Vh/ν
R_i	ft	Hydraulic radius of a sub-section of flood plain or main channel
R_σ	ft	Hydraulic radius of a sub-section of cross-section of the flow
S	-	Energy gradient
S_f	-	Friction slope
S_o	-	Flume slope

Symbol	Unit	Definition
$S_{OL_{1-4}}$	ft	Fall in channel between sections I and IV
ST 1: λ	-	Abbreviation of spill-through model with side slope 1: λ
ST	-	Standard spill-through model 1:1 $\frac{1}{2}$
s	-	Pier correction factor for method of effective M
T	-	Temperature
t'	-	Ratio of abnormal to normal depth of flow, previous to constriction in place
u	ft/sec	Local velocity along x direction
v	ft/sec	Local velocity along y direction
VW	-	Abbreviation for vertical-wall model
VB	-	Abbreviation for vertical-board model
V	ft/sec	Normal velocity = $Q/h_n B$
V_i	ft/sec	Average velocity at section i
V_{ni}	ft/sec	Hypothetical velocity Q/A_{ni} at section i
V_j	ft/sec	Average jet velocity
WW	-	Abbreviation for standard wing-wall abutment [model]45 $^\circ$
WW ϕ	-	Abbreviation for wing-wall model with angle of throat inlet ϕ°
w	ft	Local channel width
x	ft	Variable distance from the upstream face of the constriction
y	ft	Variable
z	ft	Distance from channel bed to bottom of bridge deck
Δz_{i-j}	ft	Difference in bed elevation between sections i and j

Symbol	Unit	Definition
z_o	ft	Distance of center of gravity of normal area from the water surface
β_i	-	Correction factor for non-hydrostatic pressure distribution at section i
β'	-	Correction factor for velocity head in Nagler's formula
γ	lb/ft ³	Specific weight of fluid
δ_o	-	Rehbock's pier shape factor
$\Delta\epsilon_e = \Delta\left[\frac{h_1^*}{h_1^* + h_3^*}\right]_e$		Incremental differential level ratio for eccentricity
$\Delta\epsilon_p$	-	Incremental differential level ratio for piers
$\Delta\epsilon_s$	-	Incremental differential level ratio for skew
ϵ_A	-	Differential level ratio abnormal flow condition [base curve]
$\epsilon_b = \frac{h_1^*}{h_1^* + h_3^*}$		Differential level ratio normal flow condition [base curve]
ϵ^*	-	$\epsilon_b + \Delta\epsilon_e + \Delta\epsilon_p + \Delta\epsilon_s$ Total differential level ratio
η	-	Backwater multiplication factor for dual bridges crossing
θ'	-	Correction coefficient in Nagler's formula = 0.3
$\alpha_{ei} = \frac{\sum qv^2}{\sum QV_i^2}$		Energy correction factor for non-uniform distribution of velocity at section i
$\alpha_{mi} = \frac{\sum qv}{QV_i}$		Momentum correction factor for non-uniform distribution of velocity at section i
μ	lb sec/ft ²	Dynamic viscosity
ν	ft ² /sec	Kinematic viscosity

Symbol	Unit	Definition
ρ	slugs/ft ³	Unit mass density of fluid
σ	-	A subscript denoting a sub-section of a cross-section of flow
τ	lb/ft ²	Average boundary shear stress
τ_o	lb/ft ²	Normal boundary shear stress
ϕ	-	Angle of skew
Φ	1/ Ψ	Correlation coefficient between constriction and resistance back-water
Ψ	-	Correlation coefficient between constriction and resistance back-water
$W = \phi + i\Psi$	-	Complex potential function
$z = x + iy$	-	Complex number



$$M = 1 - \left(\frac{Q_R + Q_L}{Q} \right) \text{ or } 1 - \left(\frac{K_R + K_L}{K_I} \right)$$

Fig. No. I-2 Definition sketch for simple normal crossing with wing-wall abutments.

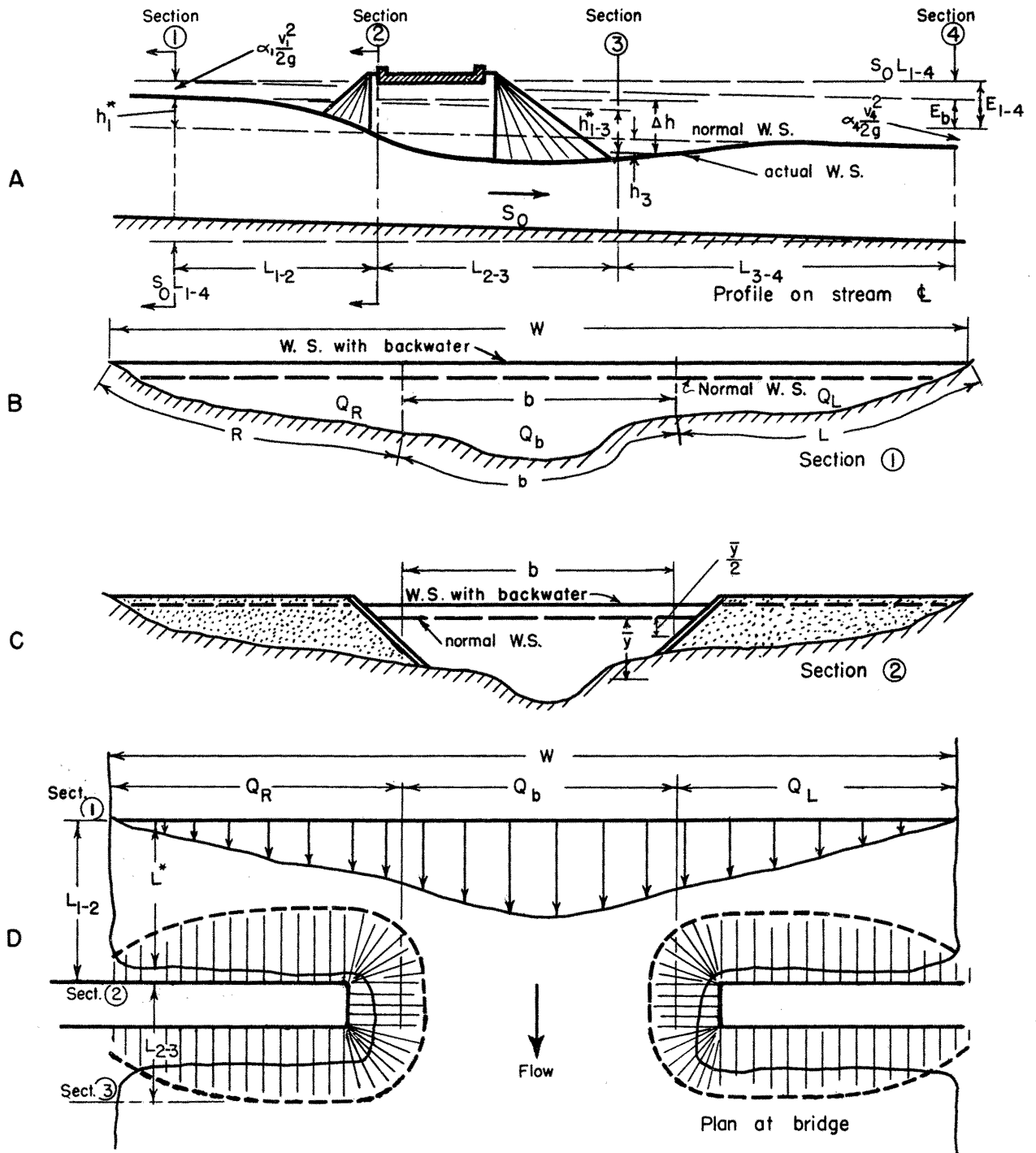


Fig. No. 1-3 Definition sketch for simple normal crossing with spill-through abutments.

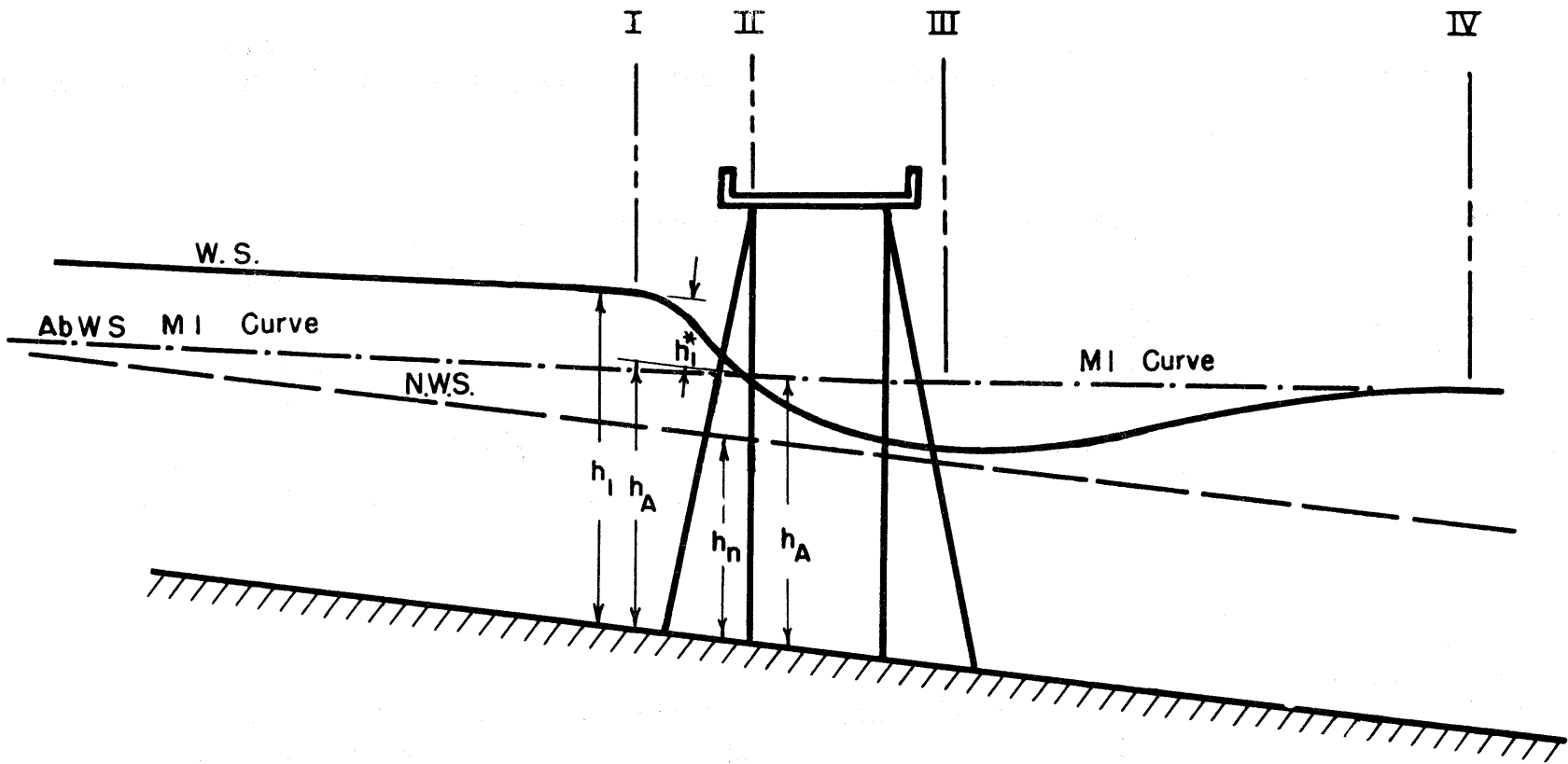


Fig. No. I-4 Definition sketch for abnormal stage-discharge condition.

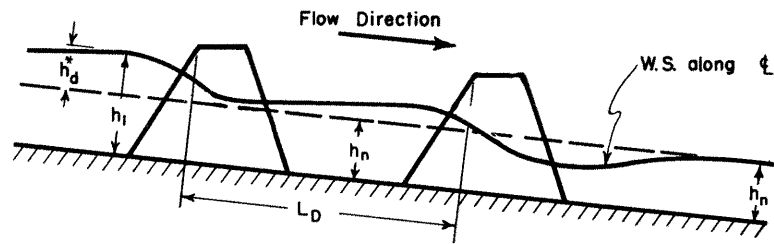
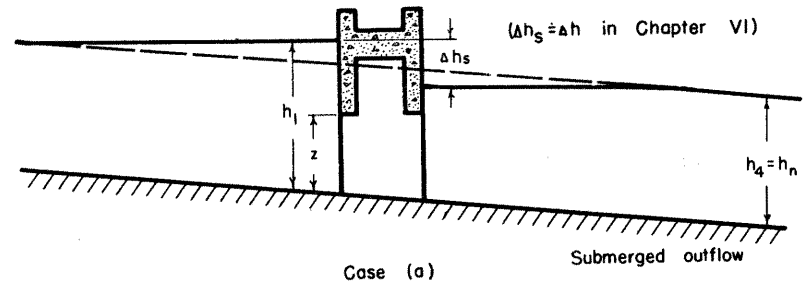
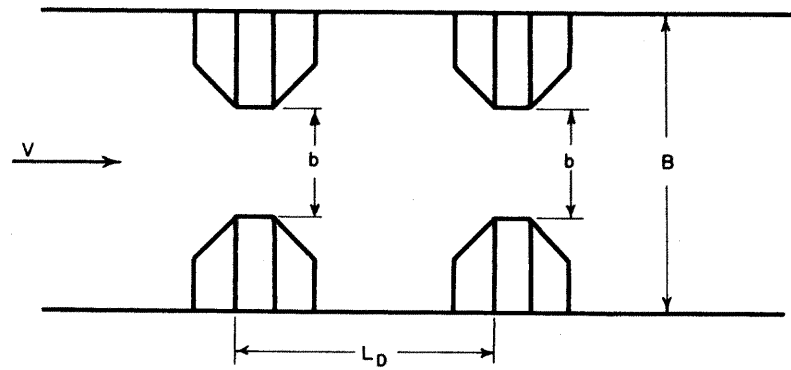


Fig. No. I-5 Definition sketch for dual bridges contraction.



Case (a)

Submerged outflow



Case (b)

Free outflow

Fig. No. I-6 Definition sketch for bridge girder partially submerged.

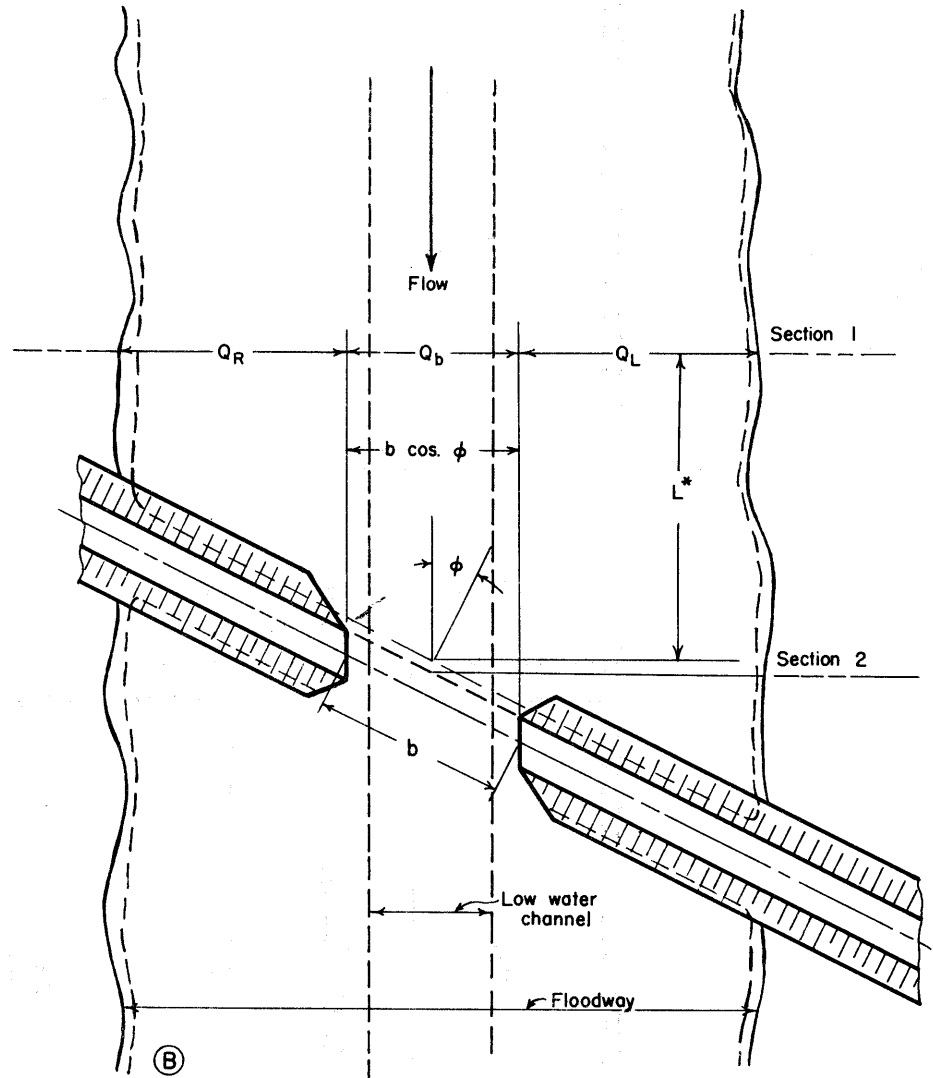
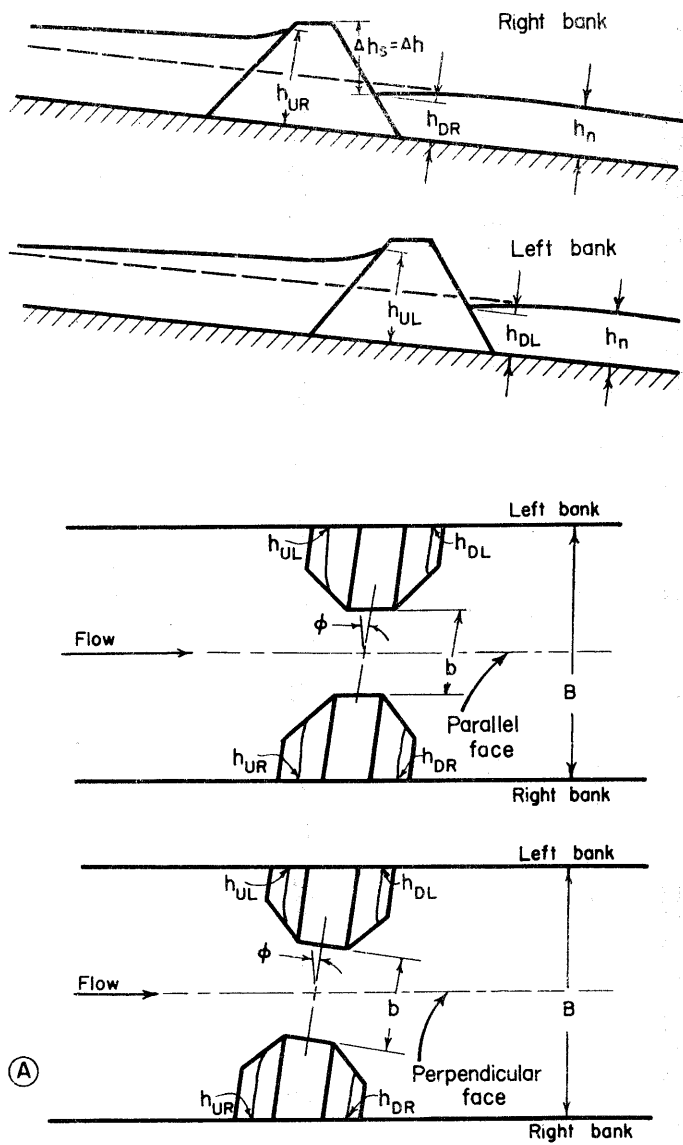
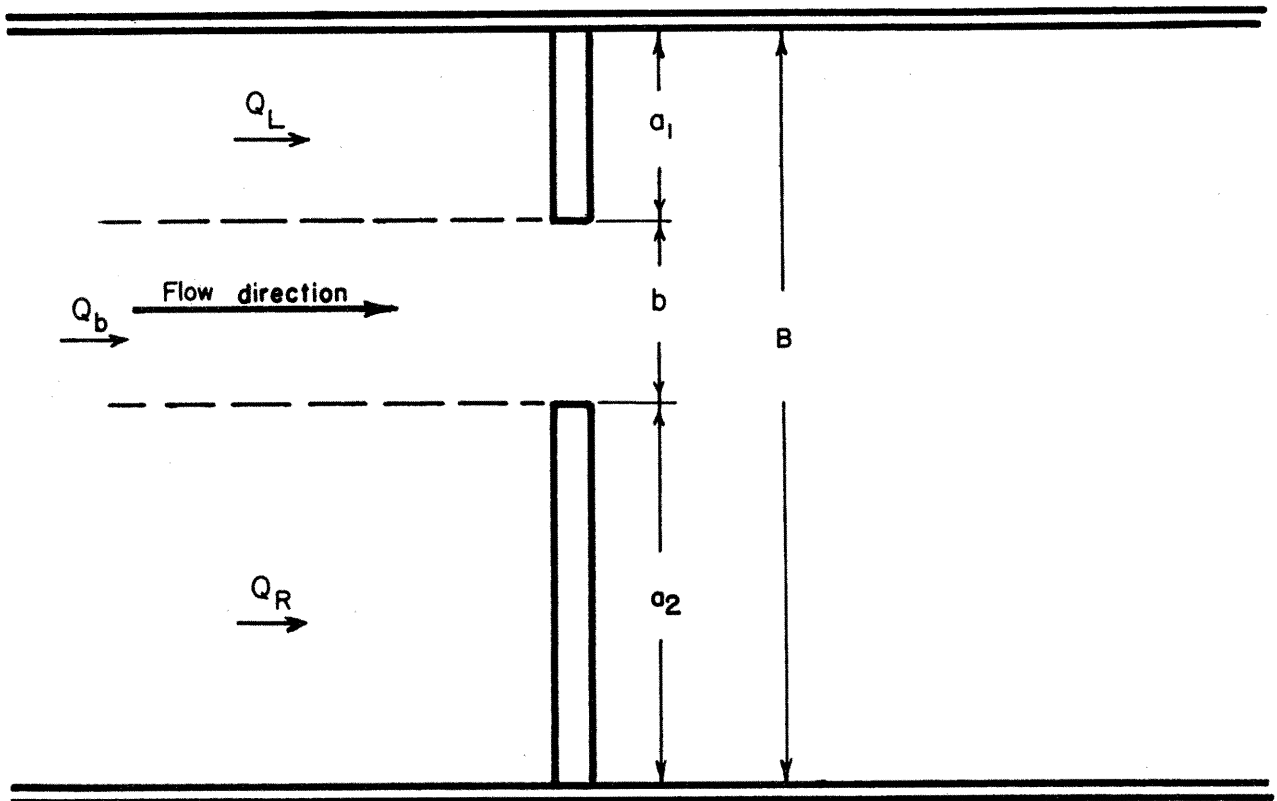


Fig. No. 1-7 Definition sketch for skew crossing



eccentricity $e = 1 - \frac{a_1}{a_2}$ (Chapter V)

or $e = 1 - \frac{Q_L}{Q_R}$, $Q_L < Q_R$ (Chapter VI)

Fig. No. I-8 Definition sketch for eccentric crossing.

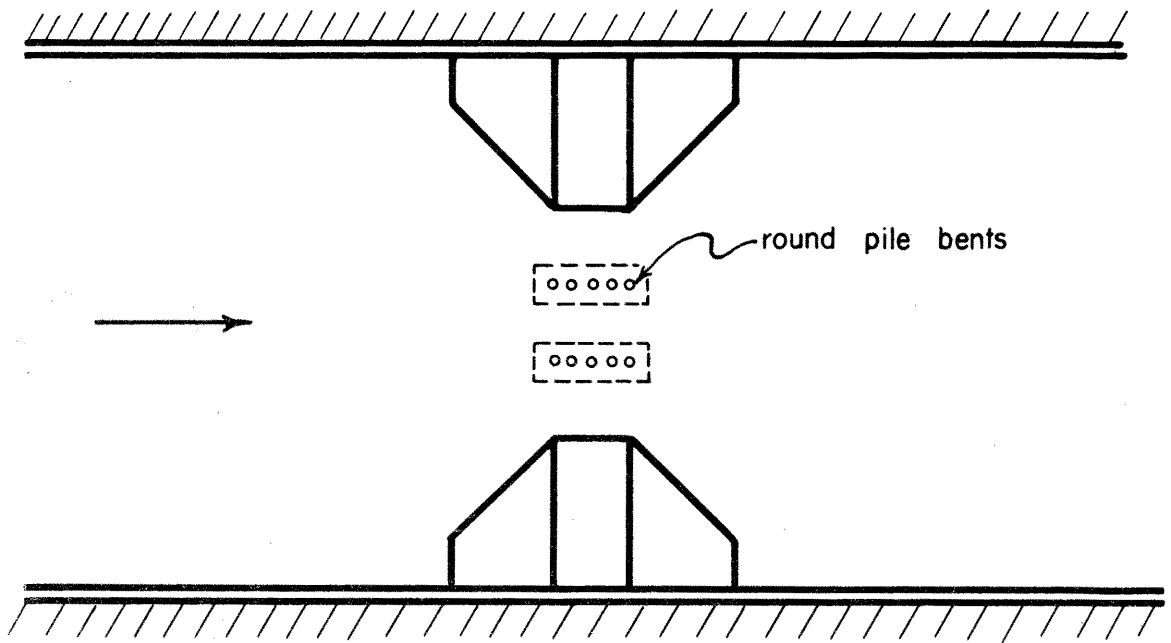


Fig.No.1-9 Definition sketch for simple normal crossing with pile bents

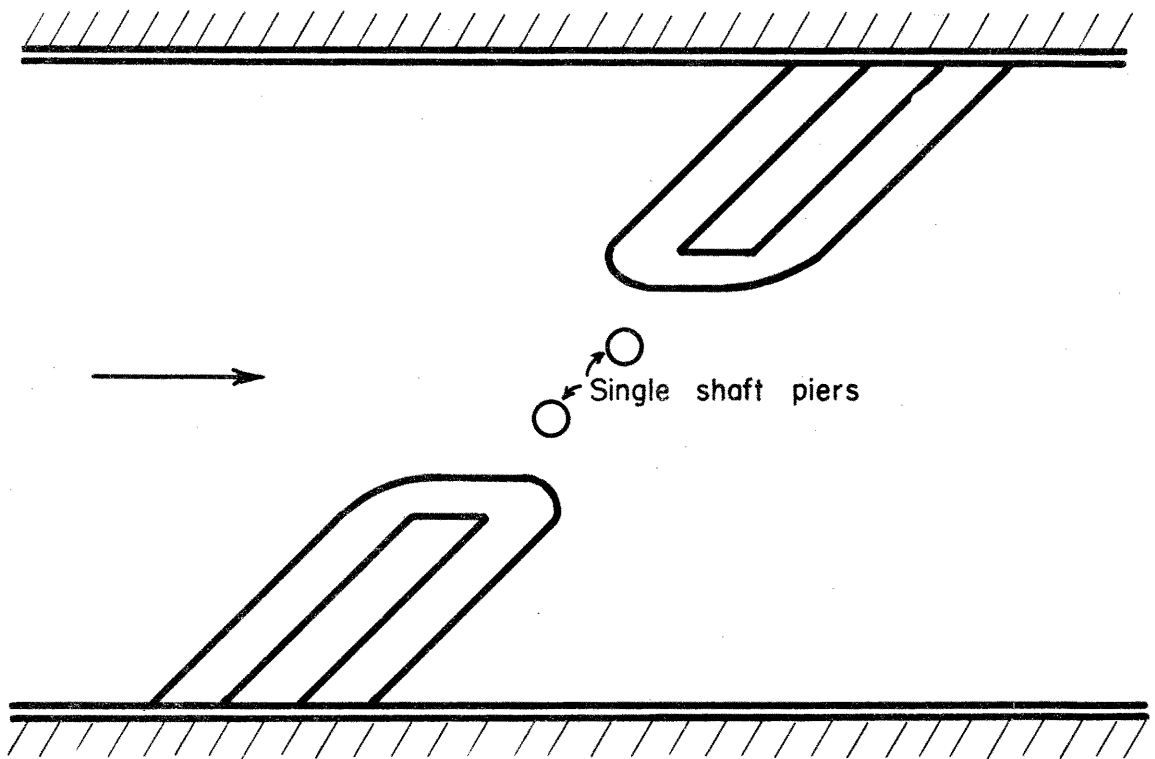
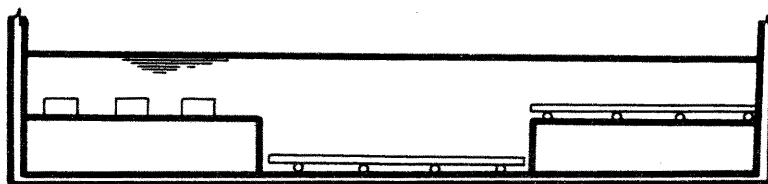
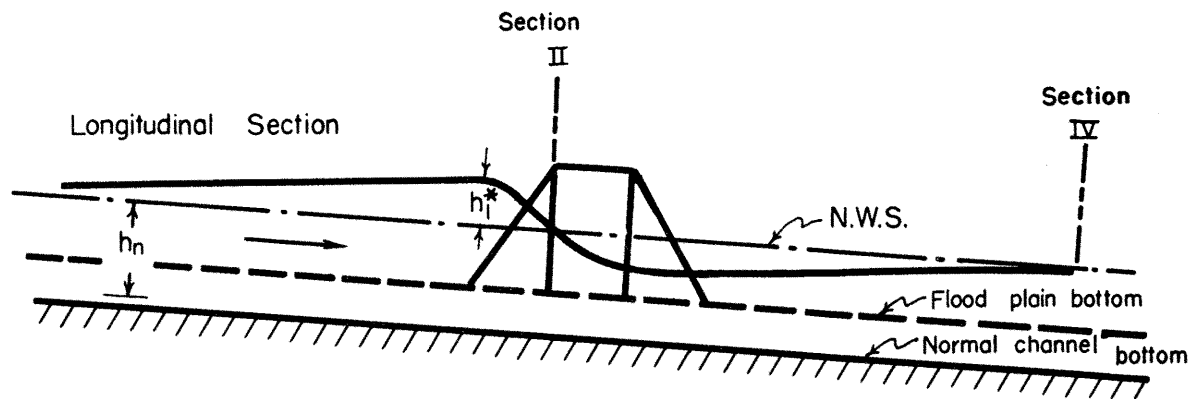
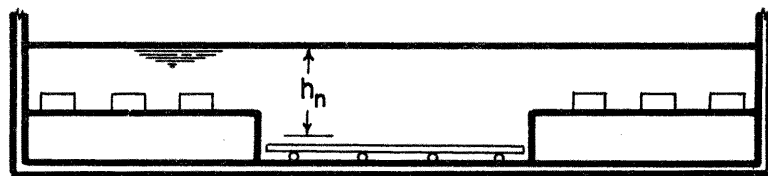


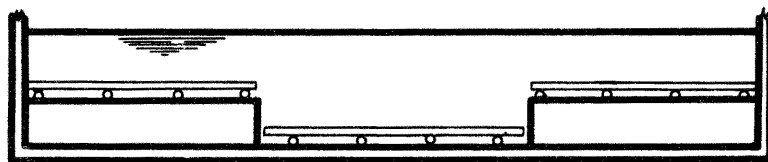
Fig.No.1-10 Definition sketch for skew crossing with piers



Roughness arrangement 1

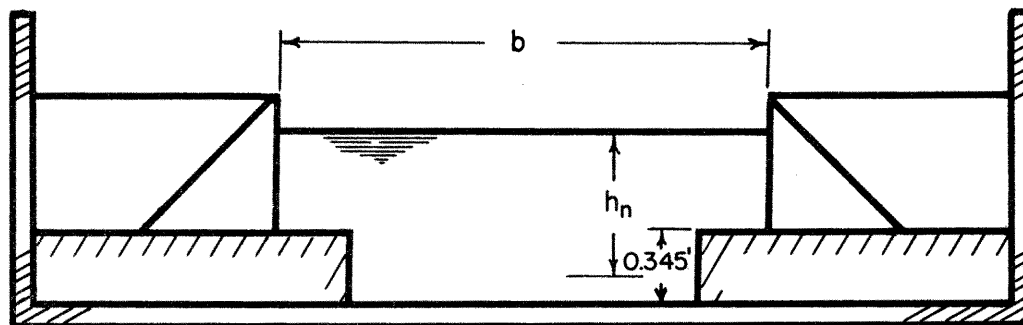


Roughness arrangement 2



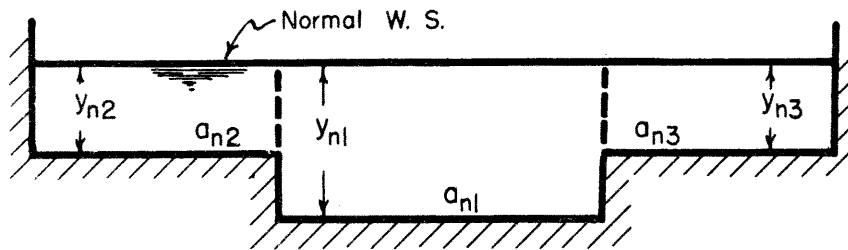
Roughness arrangement 3

Cross section of unobstructed channel



Cross section of contracted section

Fig. No. I-II Definition sketch for flood-plain model



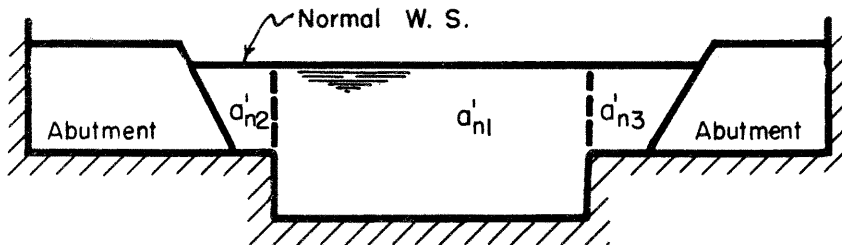
For uncontracted section:

y_{n1}, y_{n2}, y_{n3} depth from normal water surface to bottom in subdivision 1, 2, & 3

a_{n1}, a_{n2}, a_{n3} area under normal water surface in subdivision 1, 2, & 3.

$$h_n = 2 \frac{\frac{1}{2} y_{n2} a_{n2} + \frac{1}{2} y_{n1} a_{n1} + \frac{1}{2} y_{n3} a_{n3}}{a_{n1} + a_{n2} + a_{n3}} = 2 \frac{\sum_{\sigma=1}^3 \frac{1}{2} a_{n\sigma} y_{n\sigma}}{\sum_{\sigma=1}^3 a_{n\sigma}}$$

$$V_n = \frac{Q}{\sum_{\sigma=1}^3 a_{n\sigma}}$$



For contracted section:

$a'_{n1}, a'_{n2}, a'_{n3}$ area under normal water surface for subdivision 1', 2', & 3'.

$$M = \frac{\sum_{\sigma=1}^{3'} a'_{n\sigma}}{\sum_{\sigma=1}^3 a_{n\sigma}} \quad F_n = \frac{V_n}{\sqrt{g h_n}}$$

Fig. No. I-12 Definition sketch of terms used in flood-plain model.

II. REVIEW OF LITERATURE

Late in the eighteenth century, hydraulic engineers began to study the subject of flow through contracted sections. Some of the investigators, such as Boussinesq [2] and Jaeger [13], used mathematical analysis while others, such as Rehbock, [24] Nagler [23], Lane [19], and Yarnell [36, 37], employed the empirical approach. In recent years the use of dimensional analysis in hydraulic research has modified data evaluation as well as experimental procedure. However, experimentation on open channel constrictions using this new approach has been limited. The most recent laboratory investigations using the approach of dimensional analysis include those by Kindsvater and Carter [16] and by Tracy and Carter [32].

Yarnell [36, 37] made a very extensive literature review on the study of backwater caused by pier contraction in 1934. He also made a very complete bibliography up to that time. Continuing Yarnell's work, Garrett [4] compiled a bibliography up to 1956.

As pointed out by Rehbock [24] a general theoretical method to determine the backwater due to piers cannot be found readily because of mathematical difficulty, since the energy loss so produced is largely through the action of resistance which is so complex that no exact mathematical interpretation is feasible. In this chapter only those publications which are most useful to the current research are reviewed.

According to the D'Aubuisson theory [36], the velocity in the contraction zone is

$$V_2 = C_{DA} \sqrt{2g[H_1 - h_2]} = C_{DA} \sqrt{2g[V_1^2/2g + h_1 - h_2]}$$

or

$$h_1 - h_2 = \frac{Q^2}{2g} \left[\frac{1}{C_{DA}^2 b^2 h_2^2} - \frac{1}{B^2 h_1^2} \right] \quad [2-1]$$

where C_{DA} is D'Aubisson's pier coefficient,

H_1 is the specific head at Section I in ft,

h_1 is the depth at Section I in ft,

h_2 is the depth at Section II in ft,

V_1 is the velocity at Section I in ft,

g is the acceleration of gravity in ft/sec²,

Q is the total discharge in cfs,

b is the width of constriction in ft,

B is the width of channel in ft,

h_4 is the depth at Section IV in ft,

h_n is the normal depth.

The true maximum backwater should be defined $h_1^* = h_1 - h_n$
 $= h_1 - h_4$ instead of $h_1 - h_2$. For practical purposes, however,
 h_n can be substituted for h_2 , which results in

$$C_{DA} = \frac{Q}{\sqrt{2gb^2h_n^2[h_1^* + V_1^2/2g]}}$$

or

$$h_1^* = \frac{1}{C_{DA}^2 M^2} \frac{V_n^2}{2g} - \frac{V_1^2}{2g} \quad [2-2]$$

where M is the opening-channel width ratio or opening ratio,
 V_n is the normal velocity in ft/sec,
 h_1^* is the maximum backwater in ft.

Nagler's [23] formula is

$$Q = C_{NA} b \sqrt{2g} \left[h_n - \theta' \frac{V_n^2}{2g} \right] \sqrt{h_1 - h_n + \beta' V_1^2 / 2g} \quad [2-3]$$

where β' is a function of contraction ratio

$$C_{NA} \text{ is the Nagler's pier coefficient,}$$

$$\theta' \text{ is a correction factor} = \frac{h_n - h_2}{V_n^2 / 2g}$$

Nagler assumed that $\theta' = 0.3$.

E. W. Lane [19] also conducted a study on the problem of open channel flow through constrictions. He introduced sharp-edged vertical models in his experiments which was a sound first step toward the final solution of obtaining formulas for backwater due to constrictions.

Lane is the first investigator who studied the flow contraction caused by the contraction of the channel itself. Most of the investigators dealt with contractions created by placing piers in the flow until Kindsvater, Carter and Tracy [16 and 17] made their investigation. His analysis was mainly based upon formulas by D'Aubuisson and Weisbach. He correlated the discharges and difference of surface elevation upstream and downstream from the constriction by introducing empirical discharge coefficients. There was no definite unique correlation given. He did indicate that there may exist a correlation between the backwater ratio and the coefficient of discharge.

Rehbock [24] conducted extensive research to determine the backwater height caused by piers. The models of the piers

had a thickness varying from 0.147 in. to 4.72 in. with most of them being 1.18 in. The length of most piers was about 7.87 in. The flume width was 15.75 in. The discharge was not mentioned in the report. Rehbock divided the channel flow passing through a constriction into three classes:

Class I when

$$m \leq \frac{1}{0.97 + 21 \frac{F_n^2}{2}} - 0.13 \quad [2-4]$$

Class II when

$$\frac{1}{0.97 + 21 \frac{F_n^2}{2}} - 0.13 < m < 0.05 + [0.9 - 2.5 \frac{F_n^2}{2}]^2 \quad [2-5]$$

Class III when

$$m > 0.05 + [0.9 - 2.5 \frac{F_n^2}{2}]^2 \quad [2-6]$$

where F_n is the Froude number of the unobstructed flow
 m is the total width of the piers divided by the channel width. Such a classification is shown in Fig. 2-1 .

Rehbock reasoned that since the law of resistance loss due to the presence of a constriction is still mathematically unknown, an exact theoretical solution to the problem of computing backwater cannot be obtained. Therefore, model studies to develop empirical formulas must be used. In his study, the following independent variables were used: discharge Q , width of channel B , depth of unobstructed flow h_n , number of piers N , thickness of the piers D , form of the piers and roughness of the piers. Rehbock assumed that the maximum backwater

h_1^* is proportional to the velocity head of the unobstructed flow

$$h_1^* = C_{RE} \frac{V_n^2}{2g}, \quad [2-7]$$

where C_{RE} is Rehbock's pier coefficient.

He found that the roughness of the piers is not an important factor and also that the roughness and the slope of the channel have no direct effect on the maximum backwater since they are already taken into account in the determination of the normal depth h_n for the unobstructed channel. He proposed the following formula to compute C_{RE} for class I flow

$$C_{RE} = [\delta_o - m[\delta_o - 1]] [0.4m + m^2 + 9m^4] [1 + F_n^2] \quad [2-7a]$$

therefore

$$h_1^* = [\delta_o - m[\delta_o - 1]] [0.4m + m^2 + 9m^4] [1 + F_n^2] \frac{V_n^2}{2g} \quad [2-8]$$

where

$$m = \frac{\Sigma ND h_n}{B h_n} = \frac{\Sigma ND}{B} = \text{contraction ratio} \quad [2-9]$$

δ_o is called pier shape factor and depends upon the pier geometry. Eq 2-8 indicates that the backwater ratio $\frac{h_1^*}{h_n}$ is proportional to $[1 + F_n^2] \frac{V_n^2}{2g}$, a function of the Froude number. For a given contraction ratio pier form effects the backwater in two ways:

- a. It can affect the point of separation which in turn effects energy dissipation, and
- b. It can change the effective opening area and therefore, affects the maximum backwater.

Such effects owing to the pier form depend, furthermore, on the contraction ratio. The empirical term $[\delta_o - m[\delta_o - 1]]$ is thus explained. The contraction ratio has a major effect upon the backwater indicated by the factor $[0.4m + m^2 + 9m^4]$.

Rehbock found that the pier form has a very important effect upon the backwater as indicated by the factor $\delta_o - m[\delta_o - 1]$. For instance, with a semi-circular nose the backwater reduces to about 37% of that of a rectangular pier. With a given nose the smallest backwater height was observed when the total length of pier amounts to from three to five times its width. In summary, Rehbock found that the maximum backwater caused by pier obstruction depends on the contraction ratio m , the Froude number of the unobstructed flow and the pier geometry.

D. L. Yarnell [36, 37] conducted about 2600 experiments to verify different backwater formulas existing at the time, such as those of D'Aubuisson, Weisbach, Nagler and Rehbock. He also made an intensive literature review [36]. His channel was 10' x 10' x 312'. Discharge varied from 10 to 160 cfs. He determined experimentally the coefficients used in different formulas for various kinds of pier shape, dimension, and orientation. The size of pier was 14 in. in width and several feet in length. His classification of flow was according to whether the flow condition in the constricted section was at critical stage. Comparison of such classification with Rehbock's is shown in Fig. 2-1. Yarnell concluded that:

- a. Weisbach's formula is theoretically unsound,
- b. As long as the velocities are slow enough to keep within Rehbock's Class I flow, anyone of the three formulas will give results close enough for practical purposes, if the proper coefficient is used.

This coefficient varies with channel contraction as well as the pier shape,

- c. The height of the backwater due to bridge piers varies directly as the depth of unobstructed channel,
- d. For the lower velocities, the more efficient shapes are lens-shaped nose and tail or a similar shape,
- e. The optimum ratio of pier length to width probably varies with the velocity and is generally between 4 and 7,
- f. Placing the piers at an angle with the current has an insignificant effect on the amount of backwater if the angle is less than 10° ,
- g. Placing the piers at an angle of 20° or more with the current materially increases the amount of backwater, the increase depending upon the quantity of flow, the depth, and the channel contractions.

A summary of Yarnell's work is given by Woodward and Posey [35].

Kindsvater and Carter [16] and with Tracy [17], on the basis of laboratory investigation, proposed a method of estimating the discharge through a contracted section, which is caused by the installation of abutments [see Fig. 1 - 1]. A combination of an energy equation and continuity equation results in the discharge equation

$$Q = C_K b h_3 \sqrt{2g [\Delta h + \alpha_1 V_1^2 / 2g - E_{f1-3}]} \quad [2-10]$$

where Q = discharge in cfs;

C_K = Kindsvater's discharge coefficient;

b = Width of the contracted opening;

h_3 = flow depth at section III;

g = gravitational acceleration;

Δh = difference in elevation of the water surface between sections I and III

$\alpha \frac{V_1^2}{2g}$ = weighted average velocity head in feet at section I, where V_1 is the average velocity at section I, and α_1 is a coefficient which takes into account the variation in velocity in section I.

E_{f1-0} = The head loss in feet due to friction between sections I and III.

By the aid of dimensional analysis, the discharge coefficient is found to be a function of the following variables

$$C_K = C_K [F, m, \frac{h_3}{b}, \frac{L}{b}, e, \phi, \text{abutment type}] \quad [2-11]$$

where

$$F = \frac{Q}{bh_3 \sqrt{gh_3}}$$

which is a Froude number

$m = 1 - b/B$, which is called contraction ratio [2-12]

L = length equivalent to the contracted opening in the flow direction

e = eccentricity of the opening, see Fig. 1-8.

ϕ = skew angle of the abutment with respect to the flow, see Fig. 1-7.

In case of an irregular, natural channel, the contraction ratio m can be evaluated from

$$m = 1 - \frac{K_b}{K_B} \quad [2-13]$$

in which K_b is the conveyance of that part of the approach channel which occupies an area of width b , and K_B is the conveyance of the total section. Conveyance is defined in terms of the Manning formula as

$$K = \frac{1.49}{n} AR^{2/3} \quad [2-14]$$

in which A is the area, R is the hydraulic radius, and n is the Manning's roughness factor.

By ignoring the ratio h_3/b , in Eq 2-11, which was shown by experiment to be insignificant, Kindsvater and Carter defined a standard condition such that $F = 0.5$, $e = 1$, $\phi = 0^\circ$ with the abutment type vertical-faced with square-edges. From the experimental data for the standard condition, a family of base curves showing the relationship between C_K , m , and L/b was constructed [not shown in the current report]. If the discharge coefficient for the standard condition is designated as C'_K , the value of C'_K should be adjusted for the effects of F , e , ϕ and abutment type. Such an adjustment value of discharge coefficient can be substituted into Eq 2-10 for computing the discharge. A set of figures for the adjustment of C'_K was given by Kindsvater and Carter in their report [14].

To apply this method for computing discharge, the stages of the flow in the vicinity of the constriction must be obtained

from the field measurement in addition to such information as contraction ratio and abutment geometry. This process of computing the discharge is just the opposite to the one of computing the maximum backwater. In the later case, the stages of the flow in the vicinity of the constriction is unknown, but the discharge, which is a design discharge for a certain flood frequency, is always given. In Eq 2-10, if Q and b are known and if C_K can be estimated, the remainder of the terms which represent the flow stages can be expressed as a function of the discharge and the discharge coefficient. This is to say that a laboratory investigation intended for determining the discharge characteristics for an open-channel constriction can be adopted to determine the maximum backwater as well and vice versa.

By extending the previous investigation [16 and 17] on discharge coefficients for open-channel constriction, and using the data and certain computation procedures in that investigation, Tracy and Carter [32] proposed the following method for computing the maximum backwater:

The maximum backwater h_1^* measured upstream at a distance b can be divided by Δh which is the difference in water surface elevation between section I and section III for the constricted channel, see Fig. 1-1. The ratio $h_1^*/\Delta h$, according to Tracy and Carter, has been shown by laboratory data to be a function primarily of the percentage of channel contraction. The influences of bed roughness and constriction geometry are secondary. Variables characteristic of the flow, such as the Froude number, the depth and constriction length are largely unimportant in their effect on this ratio. Fig. 2-2 shows the

variation of $[h_1^*/\Delta h]_{\text{base}}$ with the contraction ratio m and the Manning's roughness factor n , where $[h_1^*/\Delta h]_{\text{base}}$ is the ratio $h_1^*/\Delta h$ for a channel having a vertical-faced constriction with square-edged abutments. [Note by the current authors: The word "base" corresponds to "standard" defined previously [16 and 17] except that for the cases of eccentricity and skew in which the ratio $h_1^*/\Delta h$ was not defined by Tracy and Carter.]

Letting

$$K_c = \frac{h_1^*/\Delta h}{[h_1^*/\Delta h]_{\text{base}}},$$

where $h_1^*/\Delta h$ is for any type of abutments, it was found that K_c varies with the contraction ratio and the ratio of existing discharge coefficient C_K to the discharge coefficient C'_K for the base condition, see Fig. 2-2. The discharge coefficient C_K is Kindsvater's discharge coefficient which was mentioned previously.

Tracy and Carter claimed that the quantity Δh can be computed from

$$\Delta h = \frac{Q^2}{2gb^2h_3^2C_K^2} - \alpha_1 \frac{V_1^2}{2g} E_{f1-3} \quad [2-15]$$

In application, $h_1^*/\Delta h$ is selected from Fig. 2-2. The ratio $h_1^*/\Delta h$ is then adjusted for a constriction-geometry effect by the factor K_c obtained from Fig. 2-3. The adjusted ratio $h_1^*/\Delta h$ may be multiplied by Δh to yield the value of h_1^* .

The data used by Tracy and Carter were obtained in a channel having a level bottom. The difficulty of using the data

from a level channel is the lack of standards representing the unobstructed flow conditions, because in a certain channel the velocity, the depth, and the energy gradient of the unobstructed flow vary from section to section for a given discharge (which means that the flow is non-uniform). Such standards are in general very essential for both theoretical and laboratory investigation.

This method cannot be used directly to estimate the maximum backwater h_1^* , because the ratio $h_1^*/\Delta h$ contains Δh which is an independent variable itself. This method constitutes a process of trial and error which is not convenient to use in computing the backwater.

Izzard [12] in discussing the work of Tracy and Carter pointed out:

"the following distinction between the objectives of the hydrologic engineer and those of the highway designer is important: The former is expected to achieve a fairly high standard of accuracy in his estimate of the flood discharge as computed from backwater, and that estimate is the end result. The highway engineer, however, reverses the computation and wants to know approximately how much backwater can be expected for floods of various frequencies whose peak discharge can probably be estimated no more accurately than $\pm 20\%$ [unless a gaging station having a long record happens to exist nearby]. Obviously, then, the highway engineer does not have to work to the close tolerances expected of the engineer who is gaging streams."

Izzard [11] proposed the following formula for computing backwater:

$$h_1 - h_n = h_1^* = K_b \frac{V_n^2}{2g} \quad [2-16]$$

where $V_{n2} = \frac{Q}{bh_n}$ is a hypothetical velocity and K_b is called the backwater coefficient which must be obtained from experiments.

More discussion of this approach will be given in Chapter VI of the current report.

By using Carter and Tracy's data, Izzard [12] developed a simple graph correlating the maximum backwater contraction ratio and Froude number. As pointed out by Izzard, his graphical correlation is encouraging, but not conclusive owing to limited data. The effect of other variables such as channel slope, channel roughness, skew crossing, eccentricity and piers is still unknown.

From review of previous research, it is evident that further study of backwater caused by bridge constriction is needed for planning and designing bridges across rivers.

BRIDGE PIERS AS CHANNEL OBSTRUCTIONS

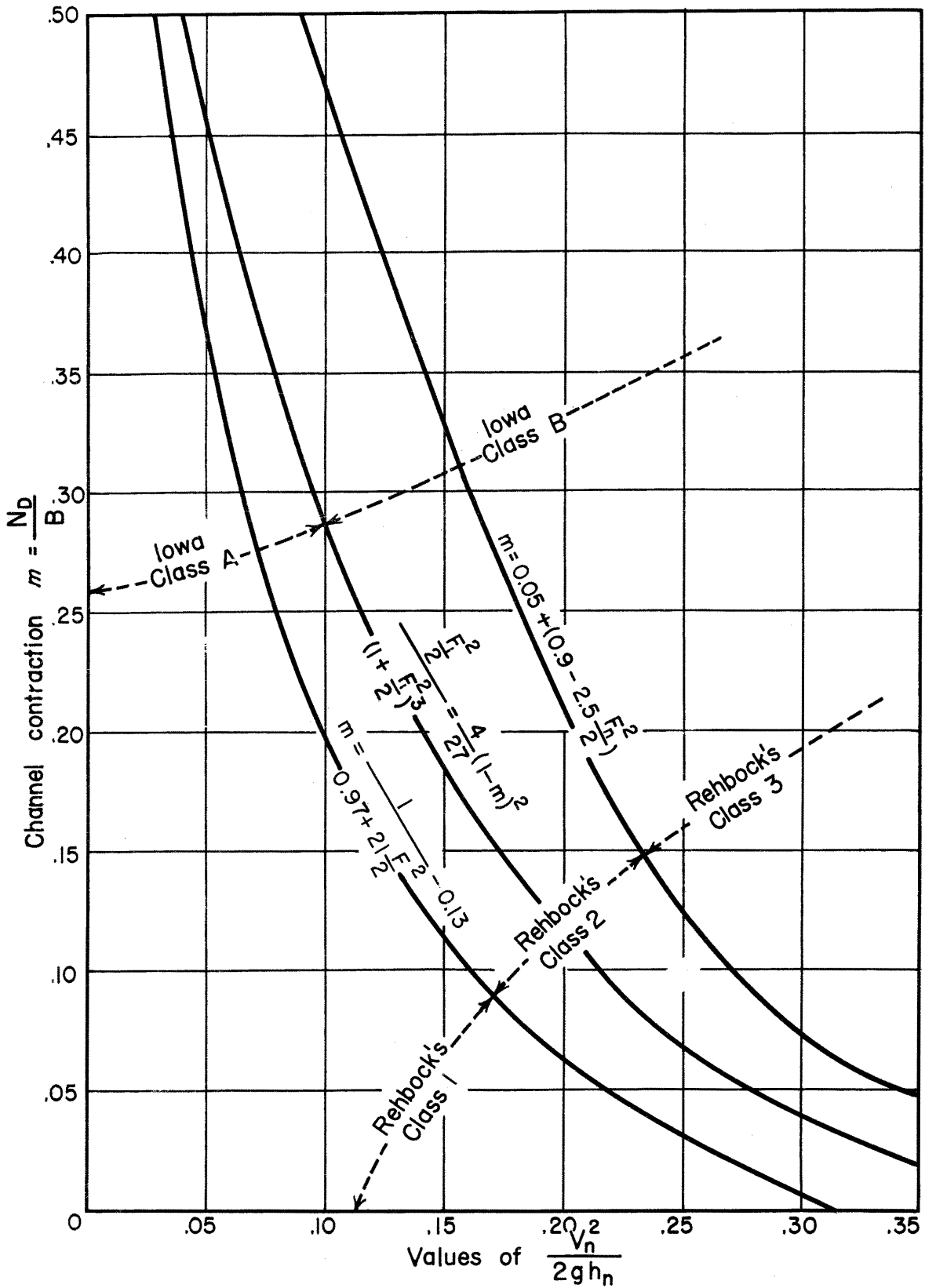


Fig. No. 2-1 Classification by Rehbock and Yarnell for flow through a contracted opening.

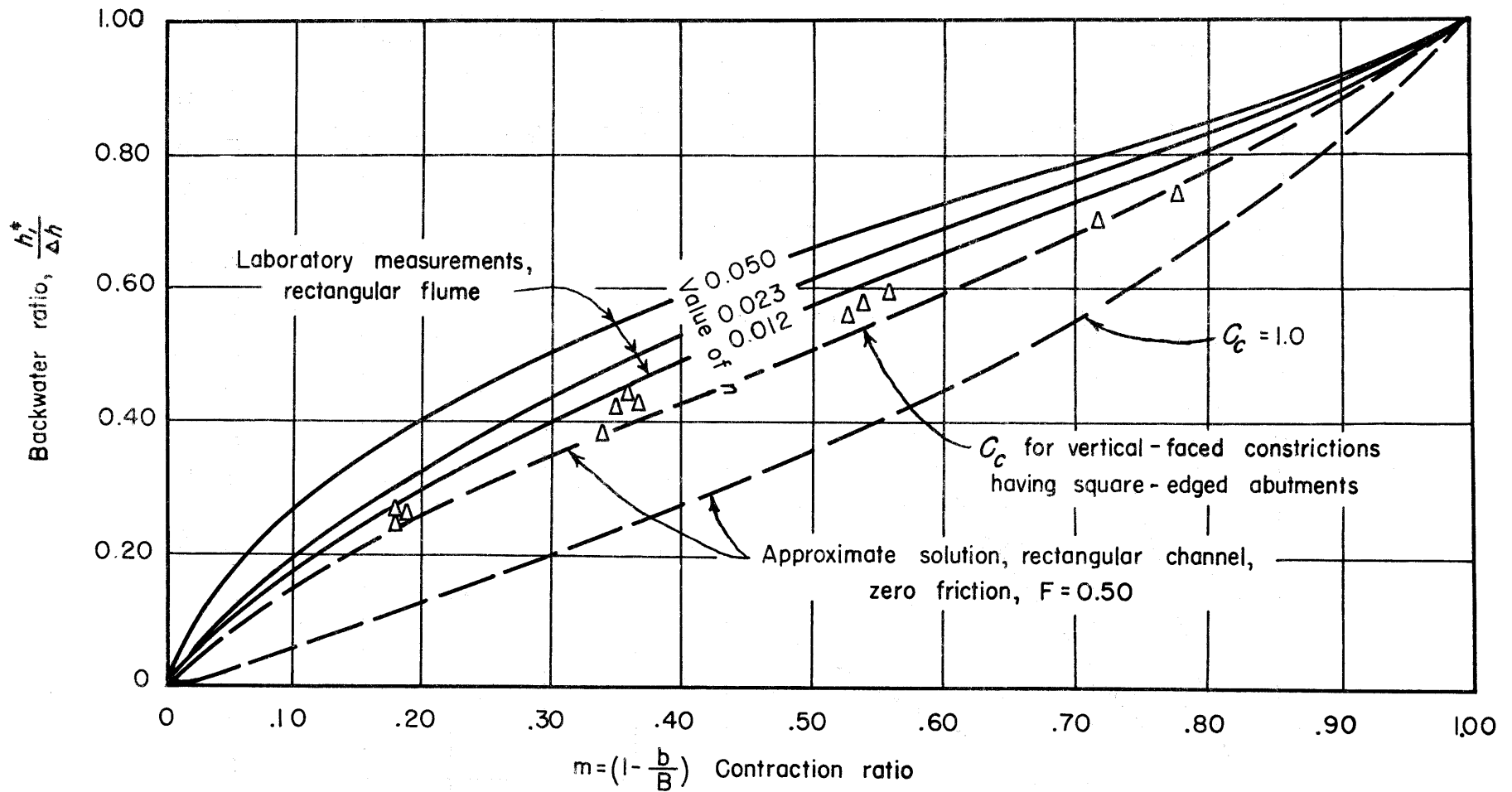


Fig. No.2-2 Variation of backwater ratio $[\frac{h_1^*}{\Delta h}]_{base}$ with contraction ratio m and Manning roughness n .

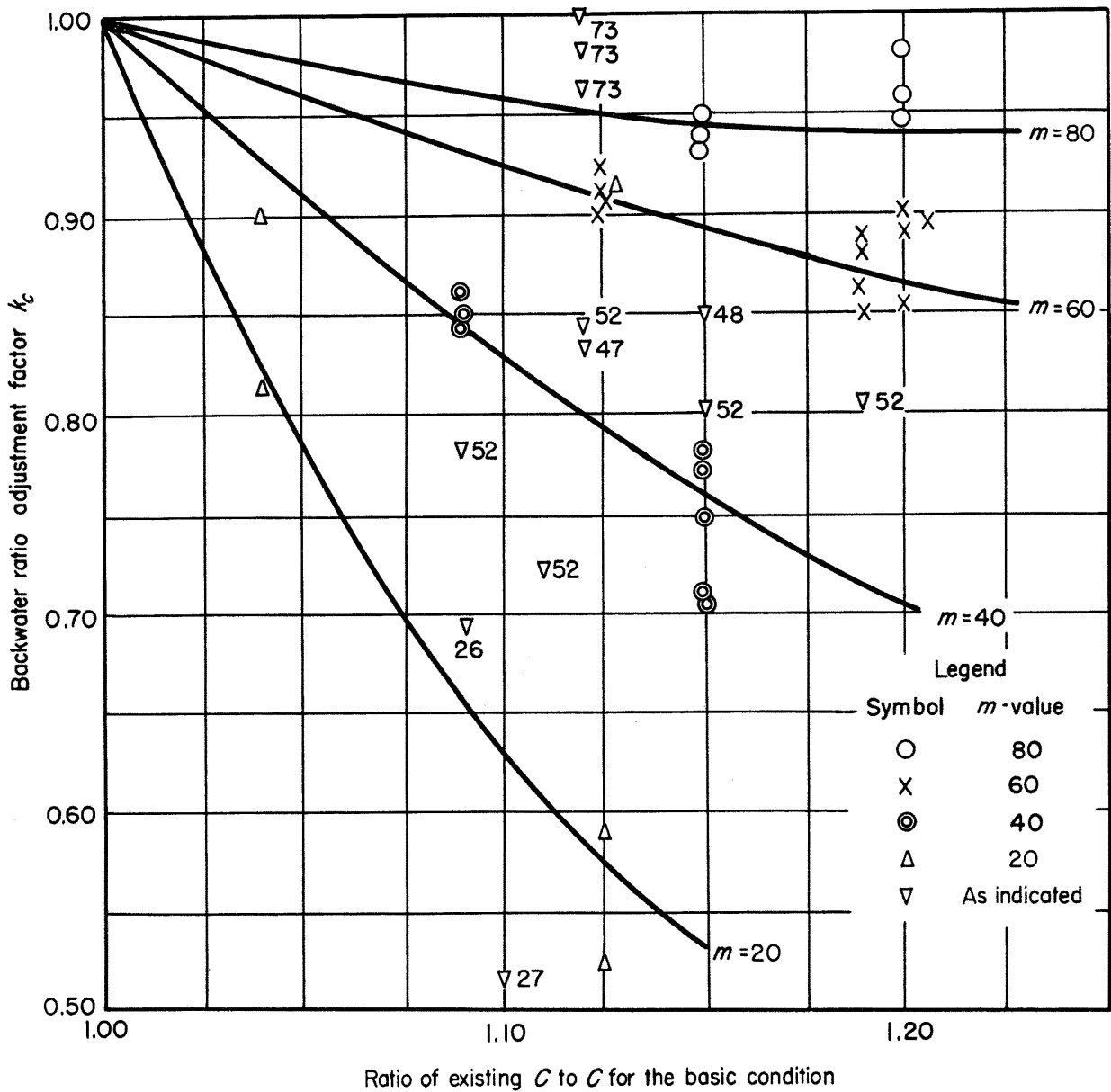


Fig. No. 2-3 Variation of correction factor k_c with discharge coefficient ratio c/c'

III. THEORETICAL ANALYSIS

An open channel will flow at a normal depth if the discharge is constant, and the channel, within a sufficiently long reach, has a uniform cross-section, a uniform surface roughness, and a uniform grade. If a constriction is installed into such a channel, the flow pattern will become that as shown in Fig. 1-1. Along the centerline profile, the flow can be divided into several reaches. At section O, the flow depth is essentially unaffected by the contraction. From section O to section I, the flow depth increases to a maximum. Downstream from section I the flow depth begins to decrease through section II where the minimum bridge opening begins, until it reaches a minimum flow area at section III. From section III, the flow depth begins to increase until it reaches the normal depth at section IV.

As shown in Fig. 1-1b, the approaching flow separating from the sidewalls of the channel begins to converge toward the contracted opening. A separation zone designated as zone Ia is formed by the boundary and the converging stream. At the upstream edge of the model the converging streamline separates again -- this time from the walls of the bridge opening. A strong eddy is formed owing to separation. This eddy zone, designated as zone IIIa extends to the sidewall downstream from the model. The streamlines that separate from the abutment form a jet. The jet continues to converge until it reaches section III, where the width and the depth of the jet assume a minimum, [the vena-contracta]. Downstream from section III the jet begins to diverge until it reaches the side boundaries approximately at section IV. In this reach between sections III and IV

the jet boundaries cannot be traced distinctly owing to the lateral mixing of the jet with the surrounding water.

Along the boundary, the flow depth begins to increase from section 0 until it reaches a maximum at the stagnation point which exists at the intersection of the upstream face of the abutment and the channel wall. Along the upstream face of the abutment, the flow depth decreases gradually from the stagnation depth to a point near the edge of the abutment -- beyond which the depth decreases rapidly. The minimum flow depth is usually at the center of the eddy which is in the separation zone IIIa. The eddy is small compared to the size of zone IIIa. It can be stated that within the separation zone IIIa, the depth is essentially the same as that at section III. From section III, the flow depth along the boundary increases until it reaches the normal depth at section IV.

From this brief discussion, it is clear that an analysis of the problem of open channel flow through a local contraction is very complex. An engineer who must estimate the height of the maximum backwater, which is the maximum elevation above the normal water surface, not only needs to know how to apply an empirical formula for backwater, but he also needs to understand the fundamental nature of the problem in order to apply the formula intelligently. It is the purpose of this research to provide such information by means of model study.

Theoretical considerations, based on the continuity equation, the momentum equation, and the energy equation, are employed in order to derive an equation for the maximum backwater. Dimensional analysis is used in order to evaluate the parameters whose influence on the maximum backwater is most important. The theory of free streamlines is used to determine the location of the maximum backwater.

Continuity Equation

According to the principle of conservation of mass, the continuity equation from section 0 to section IV [Fig. 1-1] can be written as

$$\begin{aligned} Q &= V_n B h_n \\ &= V_o B h_o && [h_o = h_n, V_o = V_n] \\ &= V_1 B h_1 \\ &= V_2 b h_2 \\ &= V_3 C_c b h_3 && [\text{Assuming the vena contracta} \\ &&& \text{is at section III}] \\ &= V_4 B h_4 && [h_4 = h_n, V_4 = V_n] \quad [3-1] \end{aligned}$$

where:

- Q is the total discharge
- V_n is the normal velocity
- h_n is the normal depth
- B is the width of the channel
- b is the width of the opening
- V_i is the velocity at section i
- h_i is the depth of flow at section i = I, II, III or IV
- C_c is the coefficient of contraction.

Momentum Equation

According to the principle of conservation of force and momentum-flux, and by assuming that the pressure distribution in both sections 0 and I is hydrostatic, the momentum equation between these two sections is:

$$\frac{B}{2} \gamma [h_0^2 - h_1^2] - \bar{F}_{0-1} = \rho Q [\alpha_{m1} V_1 - \alpha_{m0} V_0] \quad [3-2]$$

where:

- α_{m0} is the momentum correction factor for non-uniform distribution of velocity at section 0
- α_{m1} is the momentum correction factor for non-uniform distribution of velocity at section I
- ρ is the density of the fluid
- \bar{F}_{0-1} is the boundary resistance between section 0 and section I
- γ is the unit weight of the fluid

Since the distance between section 0 and section I usually is great, the term \bar{F}_{0-1} is important. There is no accurate method of evaluating \bar{F}_{0-1} at the present time. Hence Eq 3-2 does not have any practical application although it is theoretically sound. The momentum equation between sections I and II is:

$$\frac{1}{2} \gamma [B h_1^2 - \beta_2 b h_2^2] - \bar{F}_{1-2} - \bar{P}_2 = \rho Q [\alpha_{m2} V_2 - \alpha_{m1} V_1] \quad [3-3]$$

where:

- \bar{F}_{1-2} is the boundary resistance between section I and section II
- β_2 is a correction factor for non-hydrostatic pressure distribution at section II
- α_{m2} is the momentum correction factor for non-uniform distribution of velocity at section II

\bar{P}_2 is the total pressure exerted on the body of water at section II by the abutment.

If the distance between sections I and II is small, the boundary resistance force \bar{F}_{1-2} can be neglected. Because the flow depth along the upstream face of the model is not known, the total pressure \bar{P}_2 cannot be evaluated accurately.

The evaluation of the momentum equation between sections II and III is even less certain owing to the unknown boundary force.

The momentum equation between sections III and IV can be written as

$$\frac{B}{2} \gamma [h_3^2 - h_n^2] - \bar{F}_{3-4} = \rho Q [\alpha_{m4} V_n - \alpha_{m3} V_3] \quad [3-4]$$

where:

\bar{F}_{3-4} is the total boundary resistance between sections III and IV,

α_{m3} , α_{m4} is the momentum correction factor for non-uniform velocity distribution at sections III and IV respectively.

It is assumed that h_3 is a constant over the entire cross-section and the pressure distribution in both sections is hydrostatic. The use of this equation will be discussed later.

Energy Equation

The cause of the backwater due to a contraction can be studied by classifying the maximum backwater into two kinds:

[a] Contraction backwater - the flow depth at the minimum contracted opening is critical. In this case

the maximum backwater is mainly governed by the energy requirement of such a critical flow,

- [b] Resistance backwater - the flow depth at the minimum contracted opening is greater than the critical depth. In this case the maximum backwater is mainly governed by the energy loss caused by flow expansion and by the increase of boundary shear.

Contraction backwater:- The cause of the contraction backwater can be explained by means of the specific energy diagram, see Fig. 3-1, and the discharge diagram, see Fig. 3-2. The flow is assumed to have no boundary resistance in a level channel or in case of sloping channel the specific energy at all sections is the same.

For a flow in a channel of a mild slope, the specific energy of the flow can be written as

$$H = h + \frac{V^2}{2g} \quad [3-5]$$

where:

H = specific energy of the flow

V = velocity of the flow

h = depth of the flow.

The velocity distribution is assumed uniform and the pressure distribution is hydrostatic. Equation 3-5 can be written in terms of H , h , Q , and B through the use of the continuity equation

$$H = h + \frac{Q^2}{B^2 h^2 2g} \quad [3-6]$$

Let

$$h_{cB} = \sqrt[3]{\frac{Q^2}{gB^2}} \quad [3-7]$$

and substitute Eq 3-7 into Eq 3-6

$$H = h + \frac{[h_{cB}]^3}{2h^2} \quad [3-8]$$

By differentiating Eq 3-8 with respect to h , putting $\left[\frac{dH}{dh}\right] = 0$ and letting this particular value of h to be designated as h_c , it is found that

$$h = h_c = h_{cB} \quad [3-9]$$

Substituting Eq 3-9 into Eq 3-8 yields

$$H = H_{\min.} = \frac{2}{3}h_c \quad [3-10]$$

The quantity h_c is called the critical depth, it is defined as the flow depth at which the specific energy head is minimum for the given discharge. From Eqs 3-7 and 3-10 the critical depth and the minimum specific energy can be calculated for a given magnitude of Q and B . Dividing Eq 3-8 by h_{cB} yields

$$\frac{H}{h_{cB}} = \frac{h}{h_{cB}} + \frac{h_{cB}^2}{2h^2} \quad [3-11]$$

Eq 3-11 is shown in Fig. 3-1. Fig. 3-1 indicates also that for a given h_{cB} , on the basis of Eq 3-7, there is a minimum specific energy $H = 1.5 h_c$ below which the flow is not possible.

Fig. 3-1 is called the specific energy diagram. The flow is classified as rapid when $h < h_{cB}$ or tranquil when $h > h_{cB}$.

Eq 3-6 may be rewritten for discharge per unit width

$$H = h + \frac{Q^2}{2gw^2h^2} = h + \frac{q^2}{2gh^2} \quad [3-12]$$

where:

- h is the local flow depth,
- w is the local channel width, and Eq 3-12 indicates that for a constant, H , and Q , the local flow depth varies also with the channel width w , or the unit discharge q .

Let the flow be narrowed from a width B to a width b while the specific energy H remains constant. The critical depth according to the given constant H is $h_c = \frac{2}{3}H$. The depth relationship between the two sections is then expressed by the discharge diagram Fig. 3-2. Figs. 3-2 and 3-3 indicate, if the approaching flow is tranquil, the flow depth decreases as the unit discharge q increases [width of the channel decreases] until q reaches a maximum beyond which the flow is not possible under the given specific head. This means that for a given specific head, there exists a minimum channel width which gives the maximum unit discharge, beyond which the flow is not possible. If the approach flow is a rapid flow, the flow depth increases as the unit discharge increases up to a maximum limit beyond which the flow is not possible under given H .

Fig. 3-2 is developed on the basis that the specific head in the converging channel is the same at all sections. Because the energy loss of a converging flow is small, the condition stated

above is true as a first approximation for flow that converges gradually. Let h_B be the depth in the approach channel, and assume $h_B > \frac{2}{3}H = h_c$, i.e., the approaching flow is tranquil. Let

$$h_{cw} = \sqrt[3]{\frac{Q^2}{w^2g}} \quad [3-13]$$

The magnitude of h_{cw} can be computed for a given Q and w . If h_{cw} computed from Eq 3-13 is less than $\frac{2}{3}H$, the flow having a width w is tranquil, i.e. $h > h_c$. If $h_{cw} = \frac{2}{3}H = h_c$, the flow having a width w is critical, i.e., $h = h_c$. If h_{cw} computed from Eq 3-13 is greater than $\frac{2}{3}H$, the flow having a width w is impossible under the given head H .

For flow through a contracted channel of width b ,

let

$$h_{cb} = \sqrt[3]{\frac{qb^2}{g}} \quad [3-14]$$

where:

$$q_b = \frac{Q}{b}$$

The following statements may be made:

- a. If $h_{cb} < h_c = \frac{2}{3}H$, the flow in the contracted channel is tranquil, that is $h_b > h_c$, h_b denotes the flow depth in the channel of width b .
- b. If $h_{cb} = h_c = \frac{2}{3}H$, the flow in the contraction is critical, that is $h_b = h_c$.

- c. If $h_{cb} > h_c = \frac{2}{3}H$, the flow is impossible under the given conditions. That is to say that for a given H and Q , there exists a minimum opening width b_c and a corresponding maximum unit discharge $q_{\max} = \frac{Q}{b_c}$. If the width is decreased the flow is impossible under given conditions. The magnitude of b_c can be found as follows:

$$\frac{2}{3}H = h_c = h_{cb} = \sqrt[3]{\frac{Q^2}{b_c^2 g}}, \quad [3-15]$$

$$b_c = \sqrt{\left[\frac{27}{8}\right] \frac{Q^2}{gH^3}} \quad [3-16]$$

When the constriction is so small that it calls for q larger than q_{\max} at a given H , part of the Q has to be stored temporarily upstream from the constriction until H is increased sufficiently to force the total discharge through the constriction.

Eq 3-15 and Fig. 3-4 demonstrate the necessity of increasing the specific head in order to increase q_{\max} through the constriction.

As shown in Fig. 3-1, for tranquil flow $h > h_c$ the specific head increases as the depth of the flow increases. The increase of depth is accomplished as soon as the constriction is installed because of the work done on the flow. In case of an ideal fluid, the specific head thus increased would be the same throughout the flow, and would remain the same because of no loss of energy.

In case of a real fluid, the increase of depth, and therefore the increase of the specific head as a result of work done

on the flow by installing the constriction, is accompanied by a reduction of velocity. Therefore, the energy loss owing to the boundary resistance is reduced. In other words, the friction slope between the sections 0 and I is less than that of a normal flow. Thus, the specific head at section I is maintained to be such that the total discharge can pass through the contracted opening.

The difference between the maximum depth required by the critical flow at the constriction and the normal depth of the uncontracted flow is called the contraction backwater. The contraction backwater is independent of the flow condition below the contraction since the flow is critical at the contraction.

The foregoing discussion is based upon the assumption that the specific head H of a flow of varying width is a constant. Because the energy loss of a converging flow is comparatively small, the foregoing principle can be applied to a converging, open channel flow; i.e., the specific head is constant in the converging zone. Let $h_B = h_n$ for the uncontracted channel, the contraction backwater is defined as $h'_B - h_B$, where h'_B is taken from Fig. 3-1 according to $H' = \frac{3}{2} \sqrt[3]{Q^2/b^2g}$. Because h'_B depends only upon Q/b , it is independent of the flow conditions downstream from the contracted opening. This corresponds also to the properties of critical flow which occurs in the contracted section.

Resistance backwater:- For the convenience of illustration, it was assumed in the previous section that the backwater is caused by excessive contraction only. This implies that there would be no backwater above normal unless the opening is so small that a given discharge cannot be forced through it for a

given specific head. For this condition the depth of flow would pass through critical depth where the contraction is minimum. This approximation is not sufficient, however, for analyzing actual flow conditions because the energy dissipation downstream requires additional backwater upstream from the contraction to overcome this loss.

Referring to Fig. 1-1, the equation expressing the conservation of energy between section I and section IV in a channel having a mild slope can be written as

$$\Delta z_{1-4} + h_1 + \alpha_{e1} \frac{V_1^2}{2g} = h_n + \alpha_{e4} \frac{V_n^2}{2g} + E_{1-4} \quad [3-17]$$

where:

Δz_{1-4} is the difference in bottom elevation between the two sections.

The total head loss E_{1-4} between sections I and IV is caused by dissipation of energy. Results obtained from model tests can be applied to prototype condition only if the similarity of model and prototype extends also to the similarity of the different processes of energy dissipation. Therefore, the knowledge of the head losses encountered in flow through a contracted section is needed. The tools for separating the losses are the energy equations and the momentum equation.

The different losses of energy can best be explained by discussing them from section to section. Between sections 0 and I, the boundary resistance loss is less than the normal loss owing to the reduction in velocity in the backwater reach. The stored energy is consumed entirely between sections I and IV and principally between sections II and IV.

It is generally known that there is very little excess energy loss due to the convergence of flow. This fact is confirmed later in this study by experiments. It was found through this study that the specific energy at section I is approximately equal to that at section II. The energy loss between sections I and II is caused mainly by the boundary resistance. This energy loss is approximately equal to the difference in bottom elevation of the two sections. An additional small amount of energy loss may be caused by separation that occurs along the wall a short distance upstream from the stagnation point.

The following assumptions are made for flow between section I and section II:

- a. Pressure distribution is hydrostatic at both section I and section II,
- b. Velocity is uniform and parallel to the bottom at both sections,
- c. Energy loss is equal to the normal boundary resistance slope S_o multiplied by the distance between the two sections.

With these assumptions the following energy equation can be written between sections I and II:

$$h_1 + \frac{Q^2}{2gB^2h_1^3} = h_2 + \frac{Q^2}{2gb^2h_2^3} \quad [3-18]$$

Between sections II and III, the energy loss caused by the boundary resistance increases because of the appreciable increase of velocity. Such an increase of velocity depends not only upon the channel contraction but also upon the further contraction of the jet. The smaller the coefficient of contraction,

the greater is the boundary-resistance loss. This resistance loss occurs within a small reach between sections II and III.

In addition to the boundary-resistance loss within this reach, there is also an energy loss caused by the internal shear which accompanies separation. The separation occurs near the upstream edge of the abutment. If the upstream edge is sharply defined, separation can always be found at this point, which is in section II. In case the abutment has no sharp edge, the location of the point of separation is not clearly defined, and can only be calculated approximately by using the boundary layer theory or measured in the laboratory. In general, it is influenced by the geometric characteristics of the abutment and the Reynolds number of the flow.

At the region where the streamlines leave the boundary, the velocity gradient is usually very great. Considerable energy is dissipated directly into heat through viscous action. The work done by the shear per unit volume of the fluid per unit time is equal to $\tau du/dy$, in which τ is the unit shear stress, and du/dy is the mean velocity gradient [in a horizontal plane] transverse to the flow. For viscous flow this rate is equal to $\mu [d\bar{u}/dy]^2$, in which μ is the coefficient of dynamic viscosity. The zone of the high velocity gradient and intense shear is called the vortex-layer. For an ideal fluid this is called a vortex sheet because the thickness of this zone is theoretically nil -- hence, the velocity distribution is discontinuous across the sheet. Since these viscous vortex layers are highly unstable, the rolling-up process to form an eddying pattern begins almost immediately downstream from the point of separation. Part of the energy from the main stream is dissipated directly into heat by viscous action,

and part of it is converted first into eddies and turbulence and then into heat. As soon as the eddies start forming, lateral mixing of these eddies follows immediately, consequently additional loss of energy results. The total energy loss caused by separation varies with such factors as the opening ratio, the discharge, and the model geometry.

The reach between sections III and IV is usually called the "jet-expansion zone". Within this zone the energy loss is greater than that for normal flow. It can be classified into:

- a. Energy loss caused by lateral mixing of eddies or lateral exchange of momentum,
- b. Energy loss caused by the boundary resistance.

Energy loss caused by lateral mixing:- The energy loss caused by lateral mixing of eddies can be expressed by the formula

$$E_m = C_m \frac{(V_3 - V_4)^2}{2g} \quad [3-19]$$

where:

E_m is the loss of energy head caused by lateral mixing,

$(V_3 - V_4)^2 / 2g$ is a theoretical expression, known as the Borda loss, for computing the energy loss caused by sudden expansion of flow in a pipe,

C_m is a coefficient.

Archer [1] found that for gradual expansion of pipe flow the measured head loss is slightly different from $(V_3 - V_4)^2 / 2g$. A correction factor such as shown in Fig. 3-5 was obtained by Archer. For lack of accurate information, Archer's correction factor will be used as C_m to compute E_m .

Energy loss caused by boundary resistance:- The energy loss due to boundary resistance can be assumed proportional to the boundary shear. The boundary shear between sections III and IV can be evaluated from laboratory data by using the following equation:

$$\bar{F}_{3-4} = \frac{B}{2} \gamma [h_3^2 - h_4^2] + \rho Q [\alpha_{m3} V_3 - \alpha_{m4} V_4] \quad [3-4]$$

in which:

α_{m3} , α_{m4} can be assumed to be unity,

h_3 , h_4 , and Q are measured directly,

V_4 can be computed, and

V_3 can be computed after the vena contracta is measured.

$$\text{Assuming } S_o = C_f \tau_o = C_f \gamma h_n S_o \quad , \quad [3-20]$$

$$S_f = C_f \tau = C_f \frac{\bar{F}_{3-4}}{BL_{3-4}} \quad [3-21]$$

where:

S_o is the normal energy loss per unit length in the flow direction,

S_f is the average energy loss per unit length between sections III and IV,

C_f is a proportion factor,

τ_o is the normal boundary shear,

τ is the average boundary shear = \bar{F}_{3-4}/BL_{3-4} .

From Eq 3-21, $C_f = 1/\gamma h_n$, therefore,

$$S_f = \frac{1}{\gamma h_n} \frac{\bar{F}_{3-4}}{BL_{3-4}} \quad [3-22]$$

The total energy loss due to boundary resistance between sections III and IV is

$$E_{f^{3-4}} = S_f L_{3-4} = \frac{\bar{F}_{3-4}}{\gamma B h_n} \cdot \quad [3-23]$$

Now $E_{n^{3-4}}$ = total normal energy loss between sections III and IV

$$= S_o L_{3-4} \quad [3-24]$$

therefore,

$$\begin{aligned} E_{e^{3-4}} &= \text{total excess resistance loss between sections} \\ &\quad \text{III and IV} \\ &= [S_f - S_o] L_{3-4} = \frac{\bar{F}_{3-4}}{\gamma B h_n} - S_o L_{3-4} \cdot \quad [3-25] \end{aligned}$$

In summary, the energy loss between sections 0 and IV can be stated as follows:

- a. Between sections 0 and I, the energy loss is less than the normal energy loss,
- b. Between sections I and II, the energy loss is approximately equal to the normal energy loss.
- c. Between sections II and III, the energy loss is greater than the normal energy loss owing to greater boundary resistance and also to energy loss accompanying separation and lateral mixing.
- d. Between sections III and IV, the energy loss is usually much greater than the normal energy loss owing to greater boundary resistance and also to lateral mixing.

Therefore,

$$\begin{aligned} E_{3-4} &= E_{f3-4} + E_m \\ &= E_{n3-4} + E_{e3-4} + E_m \end{aligned} \quad [3-26]$$

in which E_{n3-4} , E_{e3-4} , E_m can be computed according to Eqs 3-24, 3-25 and 3-19 respectively.

A reduction of energy loss means a reduction in the energy gradient. Likewise, an increase of energy loss means an increase in the energy gradient. A sketch of the energy gradient for flow through a contraction is shown in Fig. 1-1. Downstream of section IV, where the flow resumes its normal flow condition, the normal energy gradient, which is governed by the normal flow conditions, remains parallel to the channel slope. The excess energy loss between sections II and IV has to be supplied from upstream. A steeper energy gradient can be drawn between section IV and section II. The vertical distance between the energy gradient line and the channel bottom at section II is the specific head H_2 required at that section in order to maintain the flow. Since the specific head H_1 at section I is approximately equal to that of section II, [i.e., $H_1 = H_2$], the quantity H_2 may be considered the required specific head at section I. Such an increase of specific head $H_2 - H_4$ is a result of the backwater between sections 0 and I. Notice that

$$H_4 = h_4 + \frac{V_4^2}{2g} = h_n + \frac{V_n^2}{2g} = H_n = h_o + \frac{V_o^2}{2g} = H_o \quad [3-27]$$

Therefore,

$$H_2 - H_4 = H_2 - H_n = H_2 - H_0 \quad [3-28]$$

and

$$H_0 - H_4 = 0 \quad [3-29]$$

where:

H_n is the specific head of the normal flow,
 H_0 , H_4 are the specific heads at sections 0 and
 IV respectively.

Eq 3-28 means that the total energy gain in the backwater reach between sections 0 and I is completely dissipated between sections II and IV.

It is reasonable to expect that for a given Q , h_n , and B , the smaller the opening b , the longer the distance L_{2-4} -- which means the further section IV is downstream. Furthermore, for a given Q , h_n , and B , the smaller the opening b , the greater the energy gradient and the greater the specific head H_2 . As long as H_2 is greater than $\frac{3}{2}h_{cb} = \frac{3}{2}\sqrt[3]{Q^2/b^2g}$, the backwater is classified as resistance backwater. The limiting case is when $H_2 = \frac{3}{2}\sqrt[3]{Q^2/b_c^2g}$ and the corresponding opening width b_c is the critical width of the opening. A further reduction of b , i.e., $b < b_c$, causes backwater classified as contraction backwater. In this case the contraction backwater is independent of the downstream flow condition.

Equation of Maximum Backwater

The principles of specific energy, discharge diagram for contraction backwater, the mechanics of the flow through

an open channel contraction and expansion, and the factors affecting energy loss for resistance backwater have been discussed extensively. Because there is no available mathematical formula at the present time to predict the amount of energy loss, it is necessary to use experiments in pursuit of a satisfactory method of estimating the maximum backwater.

In the light of these facts, it is hoped that the problem might be analyzed in the following manner:

- a. By making certain assumptions about factors such as the velocity distribution, pressure distribution and separation, the change of water surface configuration can be approximately expressed by the use of the specific energy and discharge diagrams.
- b. By using experimental data, some coefficient to correct for these assumptions can be introduced into the expression.

The purpose of the following analysis is to correlate the maximum backwater height with the discharge and the degree of the contraction, under the condition that the flow is critical at the minimum cross-section of the contraction. The application of this approach to the case when the flow is less than critical in the contraction will also be discussed in the latter part of the current report.

In addition, the following conditions are observed:

- a. Non-uniform distribution of velocity at both sections I and II.
- b. Non-hydrostatic pressure distribution at section II.
- c. Hydrostatic pressure distribution at section I.
- d. Contracted opening at section II is smaller than

- b due to separation at the edge of the abutment.
- e. The water surface at section II is level across the constriction.
- f. The contracted width is the same in any plane parallel to the bottom of the channel.

The specific head at any section of the flow which may have non-uniform velocity distribution, and non-hydrostatic pressure distribution is:

$$H = \alpha_e \frac{V^2}{2g} + \beta h \quad [3-30]$$

where α_e , β are coefficients to correct for non-uniform velocity and for non-hydrostatic pressure respectively. Eq 3-30 can be written also as

$$H = \frac{\alpha_e Q^2}{2gw^2h^2} + \beta h \quad [3-31]$$

or

$$H = \alpha_e h \frac{F^2}{2} + \beta h \quad ; \quad [3-32]$$

where

$$F^2 = \frac{Q^2}{gh^3w^2} \quad , \quad [3-33]$$

F is known as the Froude number .

Letting

$$h_{cw} = \sqrt[3]{\frac{\alpha_e Q^2}{\beta gw^2}} \quad [3-34]$$

Eq 3-31 becomes

$$H = \frac{\beta h_{cw}^3}{2h^2} + \beta h \quad . \quad [3-35]$$

Under critical flow conditions

$$\frac{dH}{dh} = 0$$

$$h = h_c = h_{cw} \quad . \quad [3-36]$$

Substituting Eq 3-36 into Eq 3-35 yields

$$H = \frac{3}{2} \beta h_c$$

or

$$h_c = \frac{2}{3} \frac{1}{\beta} H \quad [3-37]$$

i.e., at critical flow

$$\frac{2}{3} \frac{1}{\beta} H = h_c = h_{cw} = \sqrt[3]{\frac{\alpha e Q^2}{\beta g w^2}} \quad . \quad [3-38]$$

The continuity equation is [Fig. 1-1]

$$Q = Bq_1 = wq = bq_2$$

where:

q_1 is the unit discharge at section I

q_2 is the unit discharge at section II

or

$$q_1 = \frac{b}{B} q_2 = M q_2 \quad [3-39]$$

where

$$M = b/B \quad [3-40]$$

The quantity M is called the opening ratio in this report. It is a ratio of the width of the contracted opening to the width of the approach channel. Notice that

$$M = 1 - m \quad [3-41]$$

where m is previously defined as the contraction ratio. Unless mentioned otherwise, the term opening ratio is used throughout the current report. The relation between the unit discharge q and the Froude number F can be written as:

$$q^2 = \frac{1}{\alpha_e} g h^3 F^2 \quad [3-42]$$

For section I:

$$q_1^2 = \frac{1}{\alpha_{e1}} g h_1^3 F_1^2 \quad [3-43]$$

where the subscript 1 denotes section I.

From Eq 3-34

$$q_2^2 = \frac{\beta_2}{\alpha_{e2}} g h_{c2}^3 \quad [3-44]$$

where the subscript 2 denotes section II,

α_{e2} is the energy correction factor for non-uniform flow at section II,

β_2 is the correction factor for non-hydrostatic distribution of pressure at section II, and

h_{c2} is the critical depth of flow at section II.

Substituting

$$h_{c2} = \frac{2}{3} \frac{1}{\beta_2} H_2$$

from Eq 3-38 into Eq 3-44 and making the use of

$$H_1 = H_2$$

yields

$$q_2^2 = \frac{\beta_2}{\alpha_{e2}} g \left[\frac{2}{3\beta_2} H_1 \right]^3 \quad . \quad [3-45]$$

From Eq 3-32

$$H_1 = \alpha_{e1} h_1 \frac{F_1^2}{2} + \beta_1 h_1 \quad . \quad [3-46]$$

Combining Eqs 3-46 and 3-45, yields

$$q_2^2 = \frac{8}{27} \frac{1}{\alpha_{e2}\beta_2^2} g h_1^3 \left[\frac{\alpha_{e1} F_1^2}{2} + \beta_1 \right]^3 \quad . \quad [3-47]$$

Combining Eqs 3-39, 3-43 and 3-47 then gives

$$F_1^2 = \frac{8}{27} \frac{\alpha_{e1}}{\alpha_{e2}\beta_2^2} M^2 \left[\frac{\alpha_{e1} F_1^2}{2} + \beta_1 \right]^3 \quad . \quad [3-48]$$

Based upon the assumption that hydrostatic distribution of pressure prevails throughout section I,

$$\beta_1 = 1$$

Therefore,

$$F_1^2 = \frac{8}{27} \frac{\alpha_{e1}}{\alpha_{e2}\beta_2} M^2 \left[\frac{\alpha_{e1}F_1^2}{2} + 1 \right]^3 \quad [3-49]$$

In which the coefficient α_{e1} , α_{e2} , β_2 are expected to be a function of the opening ratio, Froude number of the uncontracted flow, and the geometry of the abutments which form the contraction. In case the velocity distribution is uniform, the pressure distribution is hydrostatic in any section,

$$\alpha_{e1} = \alpha_{e2} = 1, \quad \beta_2 = 1$$

Therefore, Eq 3-49 can be written as

$$F_1^2 = \frac{8}{27} M^2 \left[\frac{F_1^2}{2} + 1 \right]^3 \quad [3-50]$$

Since Eq 3-50 is a cubic equation, there are three roots of F_1^2 for a given value of M . The first root gives F_1^2 greater than 1, which is for the case that the upstream flow is rapid; the second root gives F_1^2 smaller than 1, which means the upstream flow is tranquil flow; and the third root gives F_1^2 as being negative, which has no physical meaning. Since the upstream flow condition is usually tranquil in natural streams, the second root is chosen, namely

$$F_1^2 = 2 \left[\frac{3}{M} \sin\left(\frac{\theta}{3} - 30^\circ\right) - 1 \right] \quad [3-51]$$

where $\cos \theta = -M$.

Eq 3-51 has been derived by Yarnell [Fig. 2-1] for classifying flow through a contraction. If the Froude number F_1 of the flow is less than that given by Eq 3-51 for a certain M , the flow is tranquil in the contracted section [known as Iowa Class A flow]; if the Froude number F_1 of the flow is greater than that given by Eq 3-51 for a certain M , the flow in the contracted section is critical [known as Iowa Class B flow].

In the current report the backwater for Class A is called the resistance backwater and that for Class B is contraction backwater. Eqs 3-50 and 3-51 or more generally Eq 3-48 or 3-49, define the upper limiting condition for the resistance backwater and also the lower limiting condition for the contracted backwater.

The Froude number F_1 of the upstream portion of the flow can be written in terms of F_n , the Froude number of the normal uncontracted flow, and h_1/h_n , the ratio of the total maximum depth with backwater to the depth of the uncontracted flow:

$$F_1^2 = \frac{\alpha_{e1} V_1^2}{g h_1} = \frac{\alpha_{e1} F_n^2}{[h_1/h_n]^3} \quad [3-52]$$

Substituting Eq 3-52 into Eq 3-51 and assuming

$$\alpha_{e1} = 1$$

for uniform distribution of velocity, yields

$$\left[\frac{h_1}{h_n} \right]^3 = \frac{F_n^2}{2 \frac{3}{M} \sin\left[\frac{\theta}{3} - 30^\circ\right] - 1} = \left[1 + \frac{h_1^*}{h_n} \right]^3 \quad [3-53]$$

Eq 3-53 shows that the total maximum depth of the backwater h_1 can be computed, for the case of critical flow at the contracted section, if the Froude number of the uncontracted flow, and the degree of contraction are known. Fig. 3-6 is a plot of Eq 3-53. This shows that for a given value of F_n , there is an upper limiting value of M beyond which there is no contraction backwater. Furthermore, the larger F_n is the larger M should be. Finally, for $F_n = 1$, any amount of contraction will cause contraction backwater and for $F_n = 0.1$, M can be as low as 0.185.

Eq 3-53 is derived as a mathematical solution for the lower limiting case of the contraction backwater and the upper limiting case of the resistance backwater. In order to see the justification of the assumption that Eq 3-53 can be modified by introducing empirical coefficients so that it is also applicable to the general case of resistance backwater, the following facts have been observed:

- a. For a given opening ratio M the maximum depth of the backwater increases as the discharge increases regardless of whether the flow is critical or tranquil at the contracted section.
- b. For a given discharge, the maximum depth of the backwater increases as M decreases regardless of whether the flow condition in the constriction is critical or not.
- c. In both cases, the backwater caused by the constriction is dependent upon the same variables such as F_n and M .

Fig. 3-7 is a series of record of the water surface profiles along the center line of a steady flow through a contracted opening. The change of surface profile was caused by the change of the opening ratio. For this particular case, Q was 2.5 cfs, B was 7.9 ft and M changed from 0.25 to 0.75.

The water surface profiles for critical flow at the contraction can be sketched as shown in Fig. 3-8 after the critical depth $h_c = h_{cb}$, and the maximum depth of the backwater h_B are computed. For given Q and M , the quantity h_{cb} can be computed according to Eq 3-14 and the quantity h_B can be computed from Eq 3-51. The trend of Fig. 3-8 is similar to Fig. 3-7.

Fig. 3-9 indicates h_B vs h_{cb} as computed for the case of critical flow at the contraction and indicates also h_1 vs h_2 taken from Fig. 3-7 for the case of tranquil flow at the contraction. The two curves have a similar trend.

On the basis of the above analysis, Eqs 3-49, 3-50, 3-51, 3-52 and 3-53, which are for the upper limiting conditions of the resistance backwater, can be modified by empirical coefficients so that they can be used for the case of resistance backwater. Such introduction of empirical coefficients will be made after the simplification of Eq 3-53 shown in the following.

In Eq 3-53 the effect of M on h_1/h_n is not expressed explicitly. The following approximation can be introduced in order to express the effect of M more conveniently.

From Eq 3-49

$$F_1^2 = \frac{8}{27} \frac{\alpha e_1^4}{\alpha e_2 \beta_2^2} M^2 \left[\frac{F_1^2}{2} + \Delta \right]^3 \quad [3-54]$$

where

$$\Delta = \frac{1}{\alpha_{e1}} \leq 1$$

because

$$\alpha_{e1} \geq 1 \quad .$$

Let

$$\frac{F_1^2}{2} = X \quad [3-55]$$

Eq 3-54 becomes

$$2X = \frac{8}{27} \Psi M^2 [X + \Delta]^3$$

where,

$$\Psi = \frac{\alpha_{e1}^4}{\alpha_{e2}\beta_2^2}$$

or,

$$2X = \Psi \frac{8}{27} M^2 [X^3 + 3\Delta X^2 + 3\Delta^2 X + \Delta^3] \quad . \quad [3-56]$$

Because F_1 is usually much less than unity, and Δ is also less than unity the terms X^3 , $3\Delta X^2$ can be neglected.

Solving for X yields

$$X = \frac{\Psi \frac{4}{27} M^2 \Delta^2}{1 - \Psi \frac{4}{9} M^2 \Delta^2} \quad .$$

Because

$$\begin{aligned}
X &= \frac{F_1^2}{2} = \frac{V_1^2}{2gh_1} = \frac{Q^2}{2gB^2h_n^3} \frac{h_n^3}{h_1^3} \\
&= \frac{1}{2} \frac{F_n^2}{[h_1/h_n]^3} \quad [3-57]
\end{aligned}$$

therefore,

$$\left[\frac{h_1}{h_n}\right]^3 = \frac{3}{2} F_n^2 \left[\frac{9}{4\psi M^2 a^3} - \frac{1}{\Delta} \right] \quad [3-58]$$

In case the velocity is uniform, the pressure distribution is hydrostatic, $\psi = 1$, $\Delta = 1$, and

$$\left[\frac{h_1}{h_n}\right]^3 = \frac{3}{2} F_n^2 \left[\frac{9}{4M^2} - 1 \right] \quad [3-59]$$

Eq 3-59 is an approximation of Eq 3-53, Fig. 3-10 shows the comparison of Eq 3-59 with Eq 3-53. They agree very well except when M approaches unity. In this case the required F_1 approaches F_n , and the error introduced by neglecting terms of higher order becomes appreciable.

The terms ψ , and Δ were originally introduced into Eq 3-58 for correcting the non-uniform velocity distribution and non-hydrostatic pressure distribution. If ψ is defined as an empirical coefficient which correlates the resistance backwater to the contraction backwater, and if $\Delta = 1$ and $\phi = 1/\psi$, then Eq 3-59 can be written as

$$\left[\frac{h_1}{h_n}\right]^3 = \frac{3}{2} F_n^2 \left[\frac{9\phi}{4M^2} - 1 \right] \quad [3-60]$$

which is a general equation for the resistance backwater. More discussion of Eq 3-60 will be presented in Chapter V.

Method of Free Streamline Analysis

The pattern of open channel flow through a contracted opening is often assumed to be similar to the flow of an ideal fluid through an orifice. Although there is much to be gained by using this approach, it is equally important to realize the differences between these two flow problems. For instance comparing [a] an open channel flow through a contraction with [b] the free streamline problem for flow out of a two-dimensional orifice, one finds no free surface, no energy loss, and no separation zone for case [b]. In this case the velocity distribution is symmetrical with respect to the vertical plane passing through the centerline of the orifice, and is identical in all the horizontal planes. The pressure is constant along the boundary of the free streamline.

Applying the transformation theorem of Schwarz-Christoffel, Von Mises was able to obtain the complex potential function of flow out of a two-dimensional orifice. He also obtained a formula to describe the width of the contracted jet. Under the supervision of J. S. McNown this problem has been solved in a manner as adopted by standard textbooks of hydrodynamics [see Appendix]. The results are summarized as follows: [See Fig. 3-11] ^{p.90}

$$\text{Continuity: } BV_o = C_c bV_j \quad [3-61]$$

where:

- B is the width of the channel,
- b is the width of the two-dimensional orifice,
- C_c is the coefficient of contraction,
- V_o is the velocity of approaching flow, and
- V_j is the velocity of the free jet along the boundary where the pressure is zero.

Geometry;

$$\frac{1}{C_c} = 1 + \frac{1}{\pi} \left(\frac{V_j}{V_o} - \frac{V_o}{V_j} \right) \cot^{-1} \left[\frac{1}{2} \left(\frac{V_j}{V_o} - \frac{V_o}{V_j} \right) \right] \quad [3-62]$$

Velocity along BC :

$$1 - \frac{y}{B/2} = \frac{2V_o}{\pi} \left[-2 \tan^{-1} \left(\frac{v}{V_j} \right) + \frac{V_j}{V_o} \tan^{-1} \left(\frac{v}{V_o} \right) + \frac{V_o}{V_j} \tan \left(\frac{V_o v}{V_j^2} \right) \right] [3-63]$$

where v is the local velocity

y is the horizontal distance from the center of the orifice.

Velocity along the upstream bank BA , where $u < V_o$ and hence

$$\frac{x}{B} = \frac{R}{\pi} \left[\ln \frac{1 + \frac{u}{V_o} R}{1 - \frac{u}{V_o} R} - \frac{1}{2R} \ln \frac{1 + \frac{u}{V_o}}{1 - \frac{u}{V_o}} + \frac{R}{2} \ln \frac{1 + \frac{u}{V_o} R^2}{1 - \frac{u}{V_o} R^2} \right] \quad [3-64]$$

where

$$R = \frac{V_o}{V_j} = \frac{C_{cb}}{B}$$

The pressure distribution along BA is

$$\frac{1}{2} \frac{\Delta p}{\rho V_o^2} = 1 - \left(\frac{u}{V_o} \right)^2 \quad [3-65]$$

where Δp is the pressure increment greater than that of the approaching flow. Velocity along the center line AC , where $u > V_o$

$$\frac{x}{b} = \frac{C_c}{\pi} \left[\ln \frac{1 + \frac{u}{V_o} R}{1 - \frac{u}{V_o} R} - \frac{1}{2R} \ln \frac{1 + \frac{u}{V_o}}{1 - \frac{u}{V_o}} + \frac{R}{2} \ln \frac{1 + \frac{u}{V_o} R^2}{1 - \frac{u}{V_o} R^2} \right] \quad [3-66]$$

and the pressure distribution along the centerline is

$$\frac{p_0 - p}{\frac{1}{2} \rho V_0^2} = \left[\frac{u}{V_0} \right]^2 - 1 \quad [3-67]$$

or writing the equation in terms of V_j and p_j where $p_j = 0$,

$$\frac{p}{\frac{1}{2} \rho V_j^2} = 1 - \left[\frac{u}{V_j} \right]^2 \quad [3-68]$$

Eq 3-63, 3-65, and 3-68 can be used to indicate approximately the water surface along the upstream face of the embankment, along the bank, and along the centerline of the stream respectively. The application is only an approximation to open channel flow through a contraction because of the assumptions used in the derivation. Theoretical curves of pressure distribution are plotted in Fig. 3-11, 3-12 according to $b/B = 0.25$, 0.5 , and 0.75 . The correlation between the depth of flow in the case of flow having a free surface and the pressure head for two-dimensional flow depends not only on the pressure distribution but also on the continuity equation. In Fig. 3-11, 3-12 both of these correction factors have been neglected.

Two-Dimensional Flow Around Cylinders

The problem of a flow around a cylindrical body has been studied extensively in recent decades. Most of the analytical study is for two-dimensional flow with no free surface. Although such study cannot be applied directly to open channel flow, a review of such study will aid to the understanding of open channel flow around piers. Such analytical study will be summarized as follows:

Flow around a cylinder can be studied from two different approaches:

- a. The fluid is assumed to be inviscid or ideal, and the flow is a potential flow. The discussion of this ideal case can yield a general description of the flow pattern.
- b. The flow pattern obtained from [a] is, at least in the vicinity of the pier, modified owing to the presence of boundary resistance.

Irrotational flow around a cylinder:- For an ideal fluid flow, there will be no resultant force upon the cylinder. In the case of a single cylinder surrounded by an infinite amount of fluid having an approaching velocity V_0 , the pressure distribution around the cylinder is as shown in Fig. 3-13. There will be two stagnation points -- one at point a and the other at point d. The pressure at points b and c will be a minimum because the maximum velocity occurs at these points. The velocity and pressure at any point can be computed because the flow condition can be described fully by a complex potential function.

The complex potential of an unlimited fluid around a cylinder can be written as [30]

$$W = V_0 \left[z + \frac{D^2}{z} \right] = \phi + i\psi \quad [3-69]$$

where:

- W is the complex potential,
- ϕ is the potential function,
- ψ is the stream function,
- z is a complex variable $z = x + iy$ in which x, y are real numbers, and $i = \sqrt{-1}$,

D is the diameter of the cylinder, and
 V_o is the approach velocity.

The complex velocity is accordingly

$$\frac{dW}{dz} = + V_o - \frac{D^2 V_o}{z^2} \quad [3-70]$$

and the magnitude of the velocity is $\left| \frac{dW}{dz} \right|$.

At point a ,

$$z = -D , \quad v_a = \left| \frac{dW}{dz} \right| = 0 .$$

At point b ,

$$z = iD , \quad v_b = 2V_o .$$

In other words, at point a the velocity is zero, and at point b the velocity is twice the approach velocity V_o . Through the use of Bernoulli's equation the pressure at points a and b can be obtained.

$$p_o + \frac{V_o^2}{2g} = p_a + \frac{v_a^2}{2g} , \quad [3-71]$$

$$v_a = 0 ,$$

$$p_o + \frac{V_o^2}{2g} = p_b + \frac{v_b^2}{2g} . \quad [3-72]$$

From Eq 3-71 and Eq 3-72

$$p_a = p_o + \frac{V_o^2}{2g} \quad [3-73]$$

$$p_b = p_o + \frac{V_o^2}{2g} - \frac{[2V_o]^2}{2g} . \quad [3-74]$$

The difference between p_b and p_a is $4V_o^2/2g$.

The pressure and velocity distributions around a single cylinder, with boundaries at infinity, are different from those around a row of cylinders in a single line transverse to the flow. See Fig. 3-14. If the cylinders are equally spaced, the streamlines passing through the mid-point between two cylinders will remain unchanged because of the symmetry of the flow, and can be considered as a rigid wall boundary. This is also the case where a single cylinder is placed in the middle of a straight channel.

It can be shown mathematically that [30]

$$W = V_0 z + V_0 c' \text{Coth} \frac{\pi z}{B} \quad [3-75]$$

is the complex potential of a flow passing through a row of cylinders spaced at a distance B ,

where:

c' is a constant depending upon the size of the piers and the spacing of the piers.

The major and minor semidiameters of the cylinders can be shown to be respectively $x_0 = 0.254B$, $y_0 = 0.25B$ which are approximately the same. The complex velocity is given by

$$\frac{dW}{dz} = V_0 - V_0 c' \frac{\pi}{B} \text{Csch} \frac{\pi z}{B} \quad [3-76]$$

When $x = 0.254B$, and $y = 0$, it can be shown that

$$\frac{dW}{dz} = 0$$

which means $x = 0.254B$, and $y = 0$ is a stagnation point.
 When $x = 0$, $y = 0.25B$,

$$\left| \frac{dW}{dz} \right| = V_o \left[\frac{2 + \pi}{2} \right] .$$

The maximum difference in pressure between a and b is,
 therefore ,

$$\frac{V_o^2}{2g} \left[\frac{2 + \pi}{2} \right] = 6.61 \frac{V_o^2}{2g}$$

which is about 65 percent greater than the pressure difference
 for unlimited flow around a single cylinder .

Real flow around a cylinder:- The measured pressure
 distribution at $Re = 1.86 \times 10^5$ in Fig. 3-15 is different from
 the theoretical curve in Fig. 3-13. The difference is caused
 by separation. It should be noted, however, that the measured
 stagnation pressure at point a is the same as the theoretical
 value because it is measured upstream from the point of separa-
 tion. The measured pressure at point b is greater than the
 corresponding theoretical pressure, and the measured pressure
 at d is smaller than the theoretical pressure at point d .
 Since the measured pressure distribution is also symmetrical
 with respect to the axis parallel to the flow, there is no lateral
 force acting on the cylinder . However, the unbalanced pressure
 distribution between the front and the back of the circular cylin-
 der results in a drag force called form drag acting along the
 direction of the flow. In addition to the form drag acting on
 the cylinder, there is also a force of boundary drag owing to the
 viscous effect. The total longitudinal force including both the

form drag and the boundary drag is normally called the total drag F_D . The coefficient of drag C_D is defined as

$$C_D = \frac{F_D}{\frac{1}{2} \rho V_o^2} \quad [3-77]$$

The drag coefficient C_D is mainly a function of Reynolds number defined as

$$Re = \frac{V_o D}{\nu} \quad [3-78]$$

where D is the diameter of the circular cylinder. For an ideal fluid, C_D is zero.

Fig. 3-16 indicates the drag coefficient C_D varies with the Reynolds number $V_o D / \nu$. The following is taken mainly from Goldstein's discussion [8].

Fig. 3-16 shows the relative contributions to the total drag of a circular cylinder made by skin-friction and by normal drag for the value of Re less than about 2×10^4 . Except at $Re = 10$ and 20 the form drag was predicted from measurements of normal pressure [form drag] and the boundary shear drag. The boundary drag and form drag at $Re = 10$ and 20 were determined by Thom [8] from a numerical solution of the equations for the flow of a viscous fluid around a cylinder. The figure shows that at $Re = 10$ the contribution of the boundary drag amounts to about 43% of the total drag. The contribution then decreases with increasing Re , and becomes quite small at $Re = 10^4$. A broken line in the diagram shows that the boundary drag over the range $30 < Re < 10^4$ is closely given by the relation $C_D = 4 Re^{-1/2}$. This relation is due to Thom [8], who calculated

the skin-friction up to 60 degrees from the forward stagnation point [point a Fig. 3-15] by using his approximate solution in closed form of the boundary layer equations, and took values between 60 degrees and 90 degrees from experiment. The relation has been verified up to $Re = 4 \times 10^4$ by Schiller and Linke [8] with the accuracy obtained by experiment.

The discussion of flow around cylinders is so far limited to two-dimensional flow. It has been shown that the flow pattern away from the vicinity of the cylindrical boundary can be treated as irrotational flow, and the flow near the cylindrical boundary can be studied by the use of the boundary layer approach. However, for gravitational flow around cylinders [i.e., flow with a free surface] none of the previous theories has a direct application. The problem is mathematically very complex. The mechanics of the flow is also complex, because both the Reynolds number and the Froude number have influence on the drag coefficient. Further laboratory measurements of the distribution of pressure, shear, and velocity are needed for gravitational flow around cylinders and piers.

Dimensional Analysis

In the science of experimental research the method of dimensional analysis is a very necessary tool for correlating experimental data. According to the procedure, a dependent variable is listed as a function of variables which will affect its value. Such a group of independent variables together with the one dependent variable can be grouped into a number of dimensionless terms by using the π -theorem [33]. The dependent variable appears only in one of the dimensionless terms.

The maximum backwater h_1^* can be listed as a function of the following variables: total discharge Q , width of the channel B , width of the contracted opening b , slope of the channel S_0 , roughness of the channel k , gravitational acceleration g , density of the fluid ρ , viscosity of the fluid μ , abutment-geometry factor, pier-geometry factor, channel geometry, characteristics of turbulence in the approaching channel, velocity distribution of the approaching flow, roughness of the model, and orientation of the constriction with respect to the approaching flow [such as skew crossing and eccentric crossing]. Because there are many independent variables affecting the maximum backwater, the analysis of this problem becomes very complex. In order to reduce the problem to its simplest form, it is necessary to restrict the dimensional analysis to the case of simple normal crossing, i.e., the roadway is perpendicular to the flow, and the contraction is symmetrical with respect to the flow centerline. It is assumed that all the other cases can be related empirically to the normal crossing.

If the considerations are confined to constant abutment and channel geometry, then h_1^* can be expressed as a function of the remaining independent variables, or

$$h_1^* = f_1[Q, B, b, S_0, k, g, \rho, \mu] \quad . \quad [3-79]$$

Because the channel roughness cannot always be represented by a single length dimension, Eq 3-79 cannot be considered as being very useful. Therefore, variables h_n and V_n are used instead of k , S_0 , and Q through the following operation.

The normal depth for the uncontracted channel can be listed as a function of variables shown in the following equation.

$$h_n = f_2[Q, S_o, k, B, \rho, \mu] \quad . \quad [3-80]$$

This equation can be expressed implicitly without losing any generality by writing

$$f_3[h_n, Q, S_o, k, B, \rho, \mu] = 0 \quad . \quad [3-81]$$

If the flow is uniform, that is, a normal depth prevails throughout the channel, the channel slope is equivalent to the energy gradient. Since

$$S_e = S_o = \frac{h_f}{L} = f \frac{1}{4R} \frac{V_n^2}{2g}$$

where

$$f = \text{function} \left[\frac{V_n R}{\nu}, \frac{k}{R} \right]$$

and is called the Darcy-Weisbach resistance coefficient and R is the hydraulic radius. For a very wide rectangular channel, $R = h_n$, therefore, the energy gradient can be expressed by the following function:

$$S_e = S_o = \text{function} \left[\frac{V_n h_n}{\nu} \frac{k}{h_n}, \frac{V_n^2}{2gh_n} \right] \quad . \quad [3-82]$$

The equation of continuity is

$$Q = V_n B h_n \quad . \quad [3-83]$$

By treating Eq 3-81, 3-82 and 3-83 as three simultaneous equations having three unknowns, Q , k and S_o , the solution for Q , k , and S_o can be written as

$$\begin{aligned} Q &= \text{function } [V_n, h_n, B] \\ k &= \text{function } [V_n, h_n, B, \rho, \mu] \\ S_e &= \text{function } [V_n, h_n, \rho, \mu, B, g] \quad . \quad [3-84] \end{aligned}$$

Substituting Eq 3-84 into Eq 3-79

$$h_1^* = f_4[V_n, h_n, B, b, \rho, g, \mu] \quad . \quad [3-85]$$

The effects of channel roughness and slope are only reflected in the normal depth and the normal mean velocity of the flow.

If V_n , h_n , and ρ are chosen as repeating variables, and the π -theorem is applied, Eq 3-85 reduces to the following dimensionless equation, if model type is included:

$$\frac{h_1^*}{h_n} = f_5\left[\frac{V_n}{\sqrt{gh_n}}, \frac{V_n h_n}{\nu}, \frac{B}{h_n}, \frac{b}{B}, \text{model type}\right] \quad . \quad [3-86]$$

In case of 1:1½ spill-through abutment, the average opening width below normal water surface $b + 1\frac{1}{2}h_n$ will be used to replace b .

Equation 3-86 is the final equation obtained from dimensional analysis. It is used for planning the experimental work and for analyzing the data.

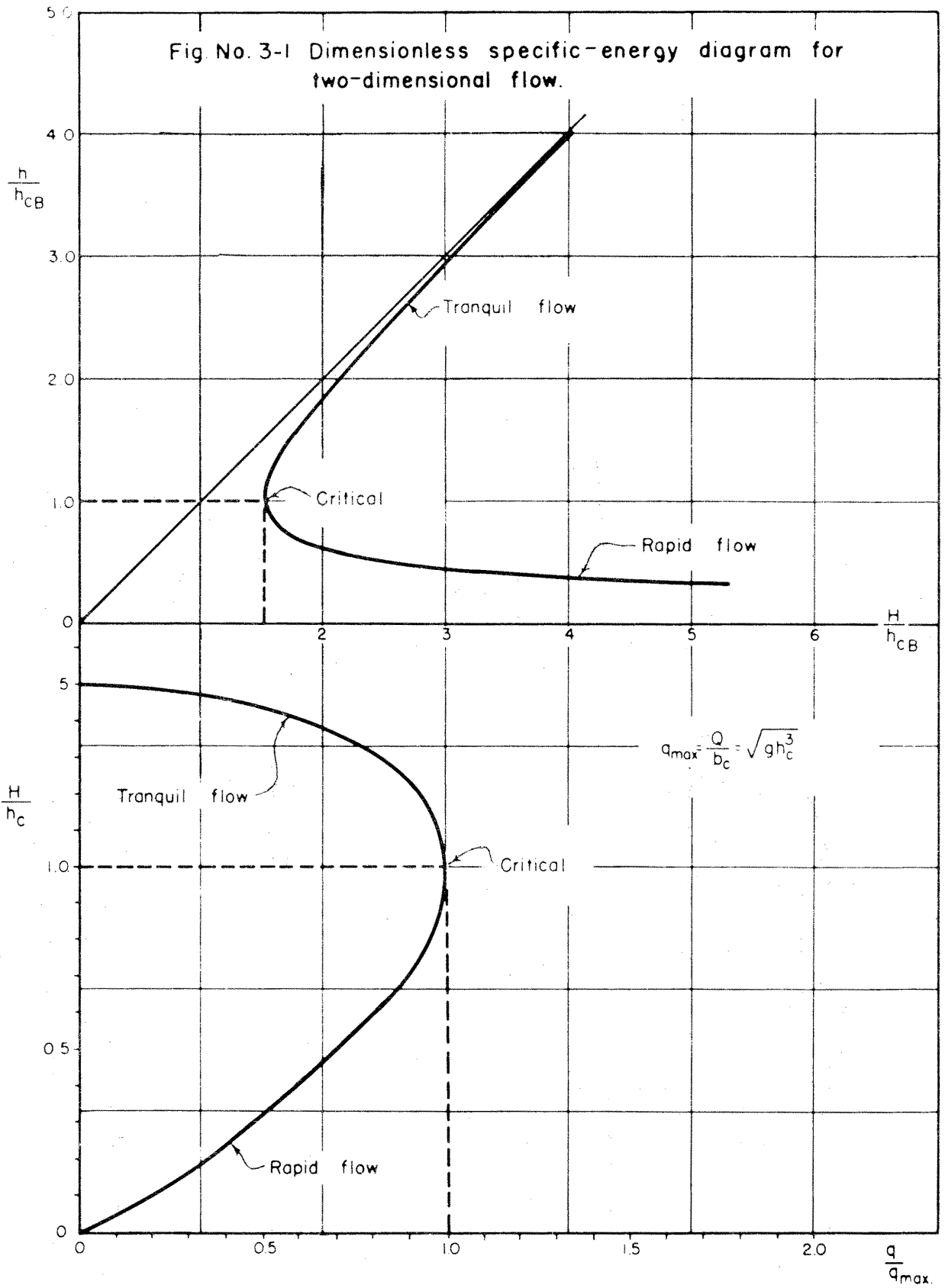


Fig. No. 3-2 Dimensionless discharge diagram for two-dimensional flow.

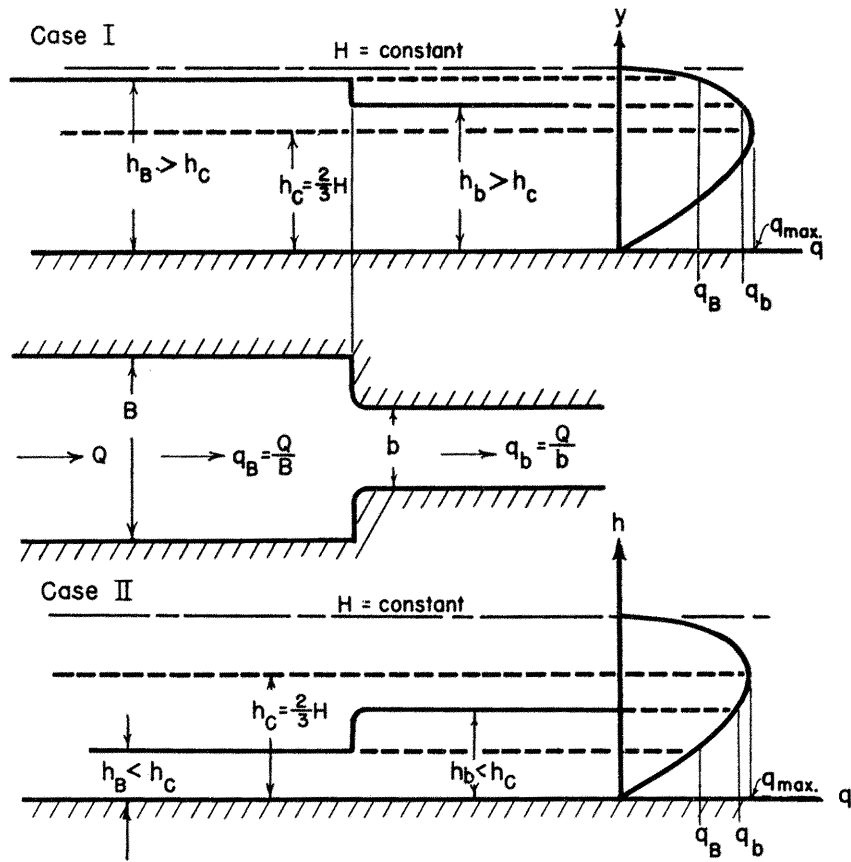


Fig. No. 3-3 Illustration showing difference of water surface elevation caused by channel contraction.

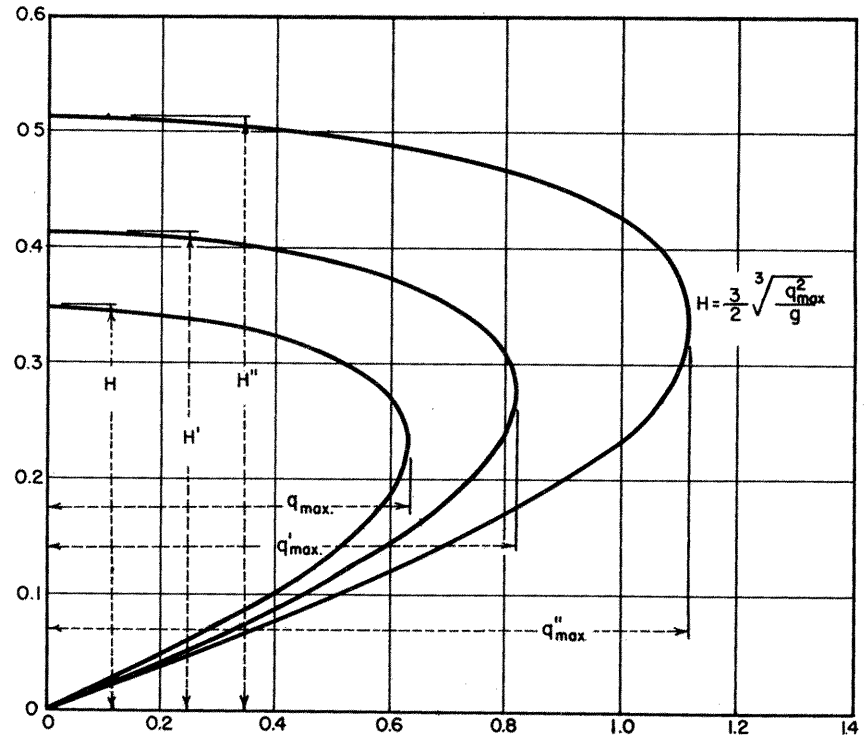


Fig. No. 3-4 Discharge diagram for various specific heads

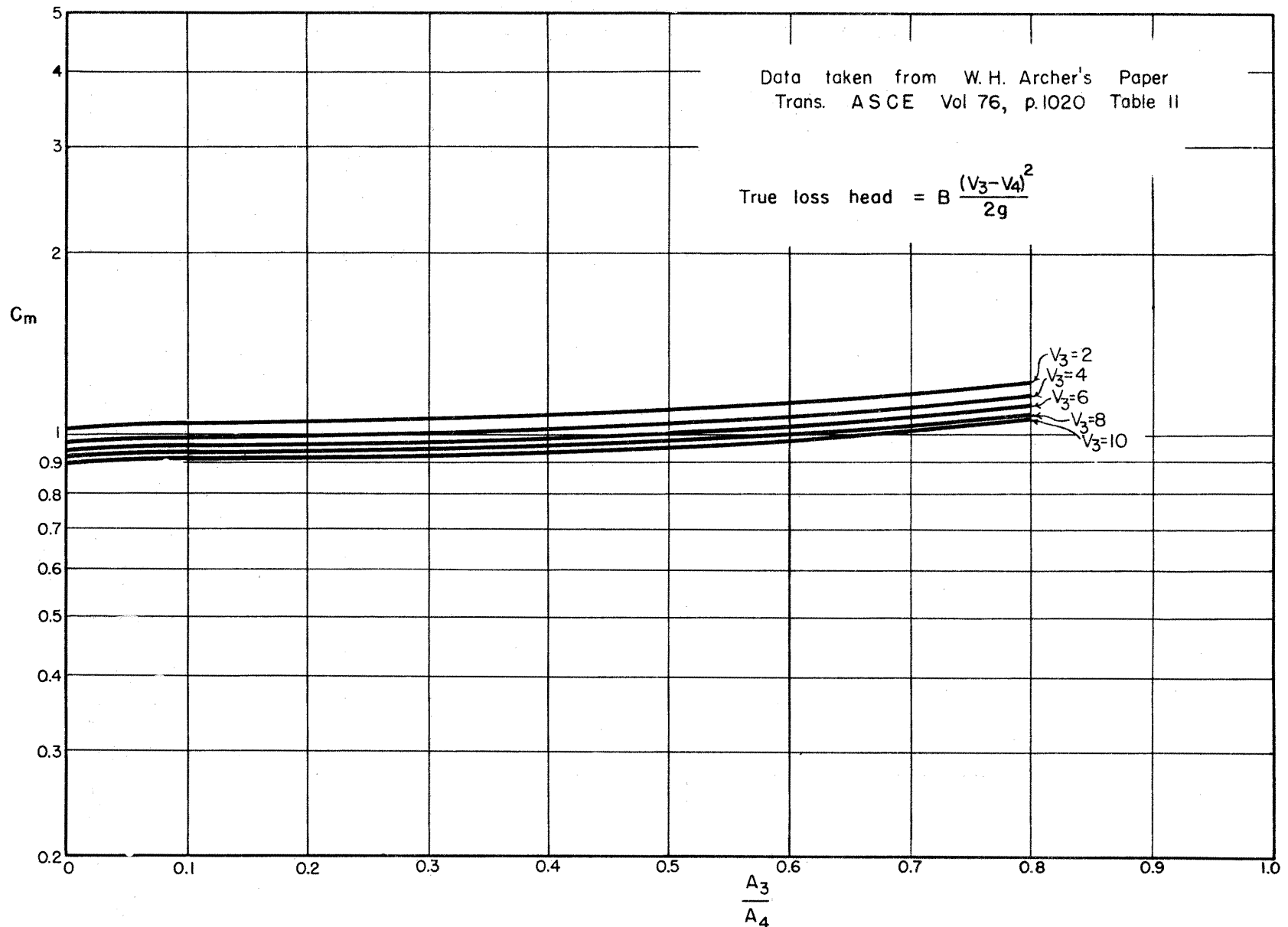


Fig.No.3-5 Correction coefficient for Borda loss

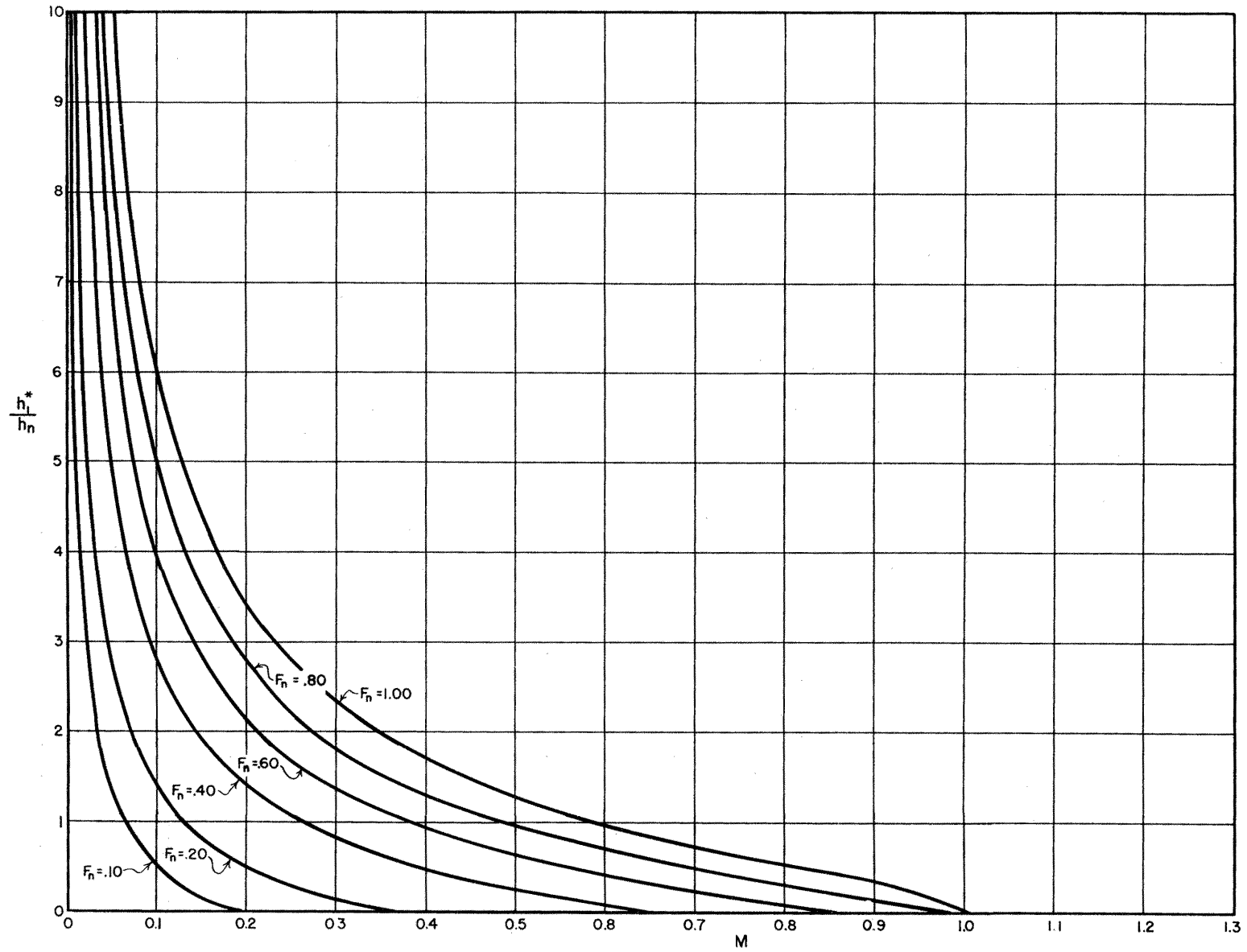


Fig. No. 3-6 Variation of theoretical backwater ratio (h_1^*/h_n) for contraction backwater with opening ratio M and Froude number F_n

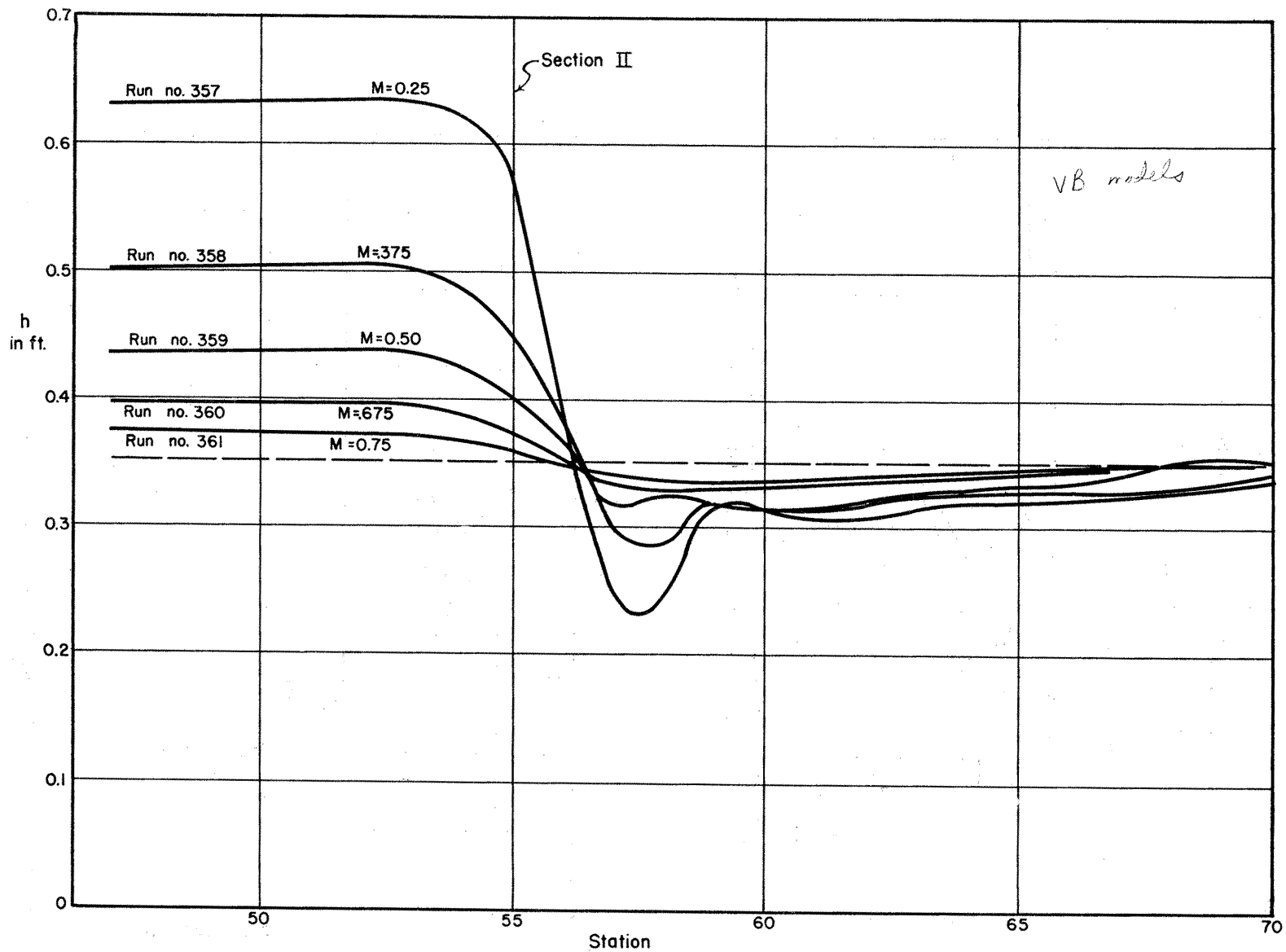


Fig. No. 3-7 Measured water surface profile along the center line for $Q=2.5\text{cfs}$ and $B=7.9\text{ft.}$ at different opening ratios M

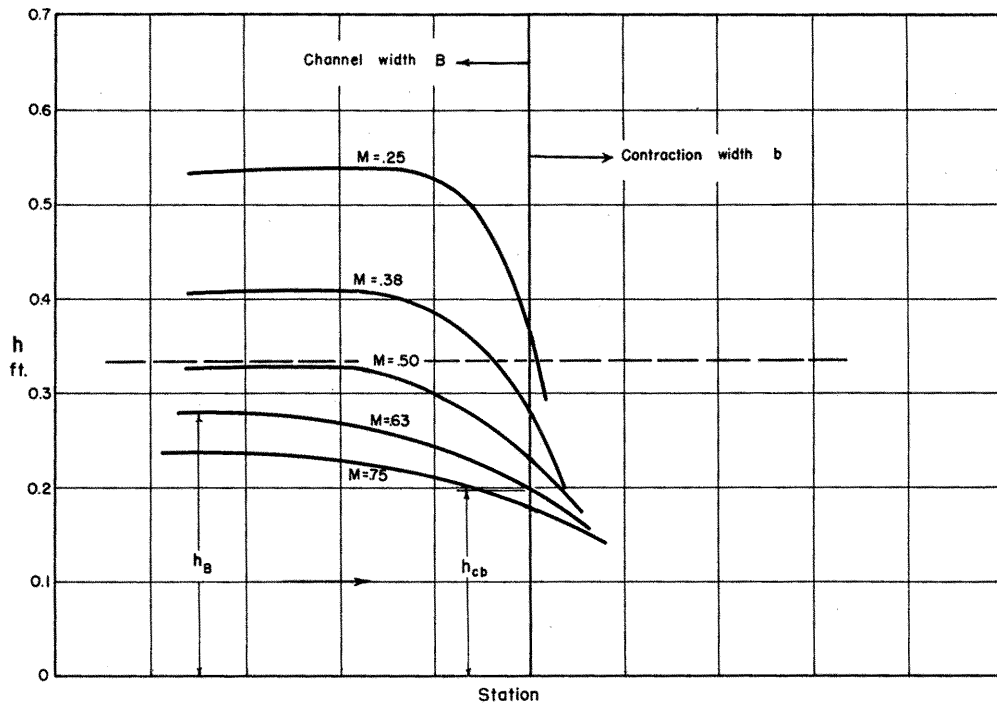


Fig. No. 3-8 Sketch showing the center line profile of contraction backwater for $Q=2.5\text{cfs}$ and $B=7.9\text{ft.}$ at different opening ratios M .

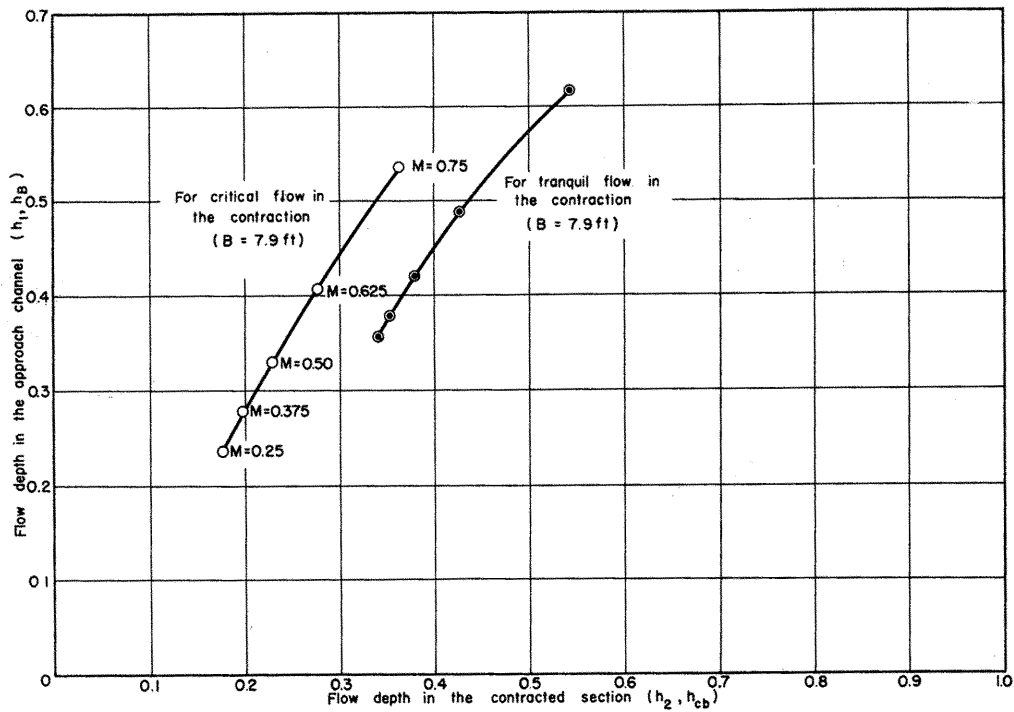


Fig. No. 3-9 Variation of theoretical contraction backwater with measured resistance backwater at various depths of the contracted flow

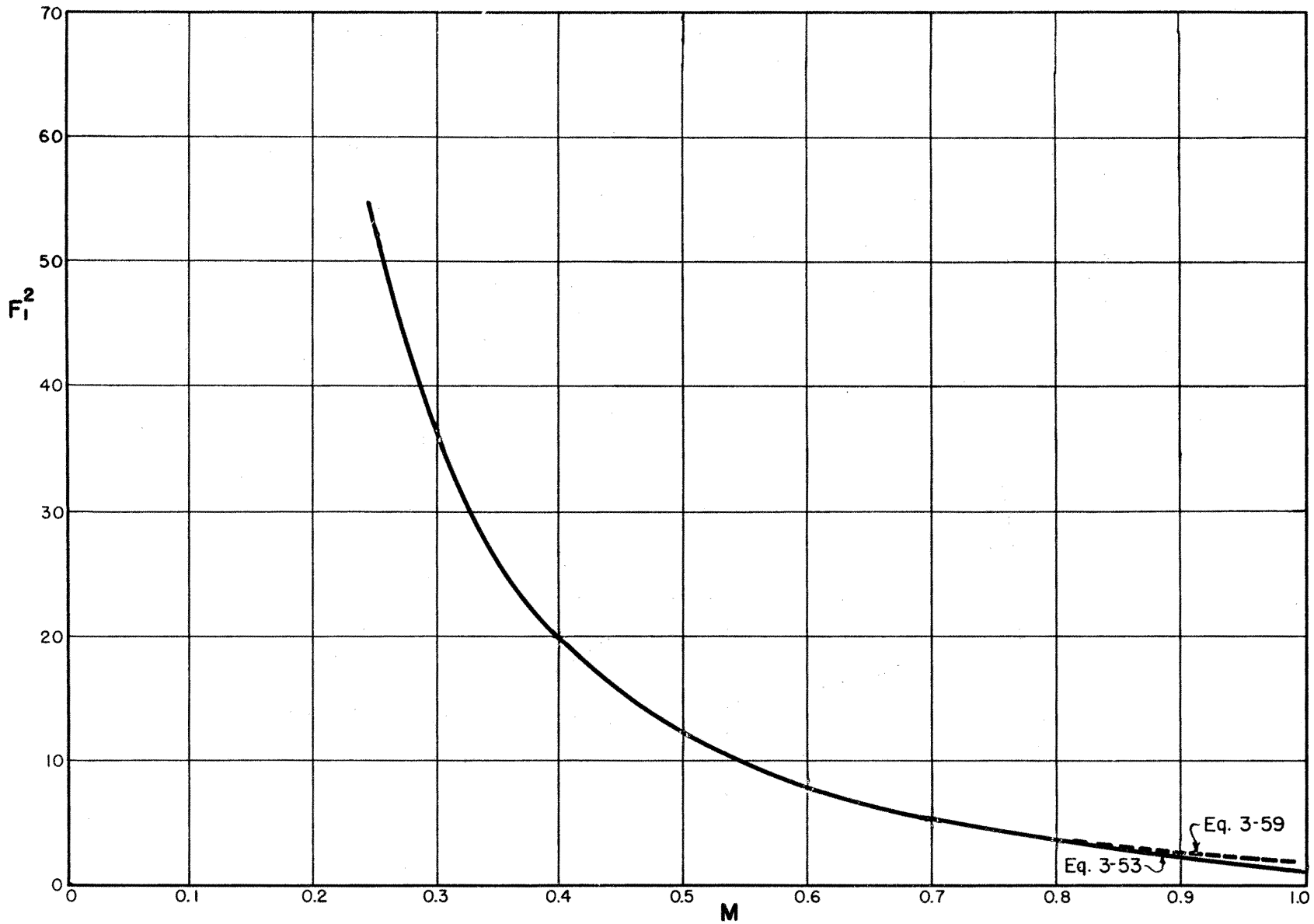


Fig. No. 3-10 Upper limiting flow conditions for the resistance backwater.

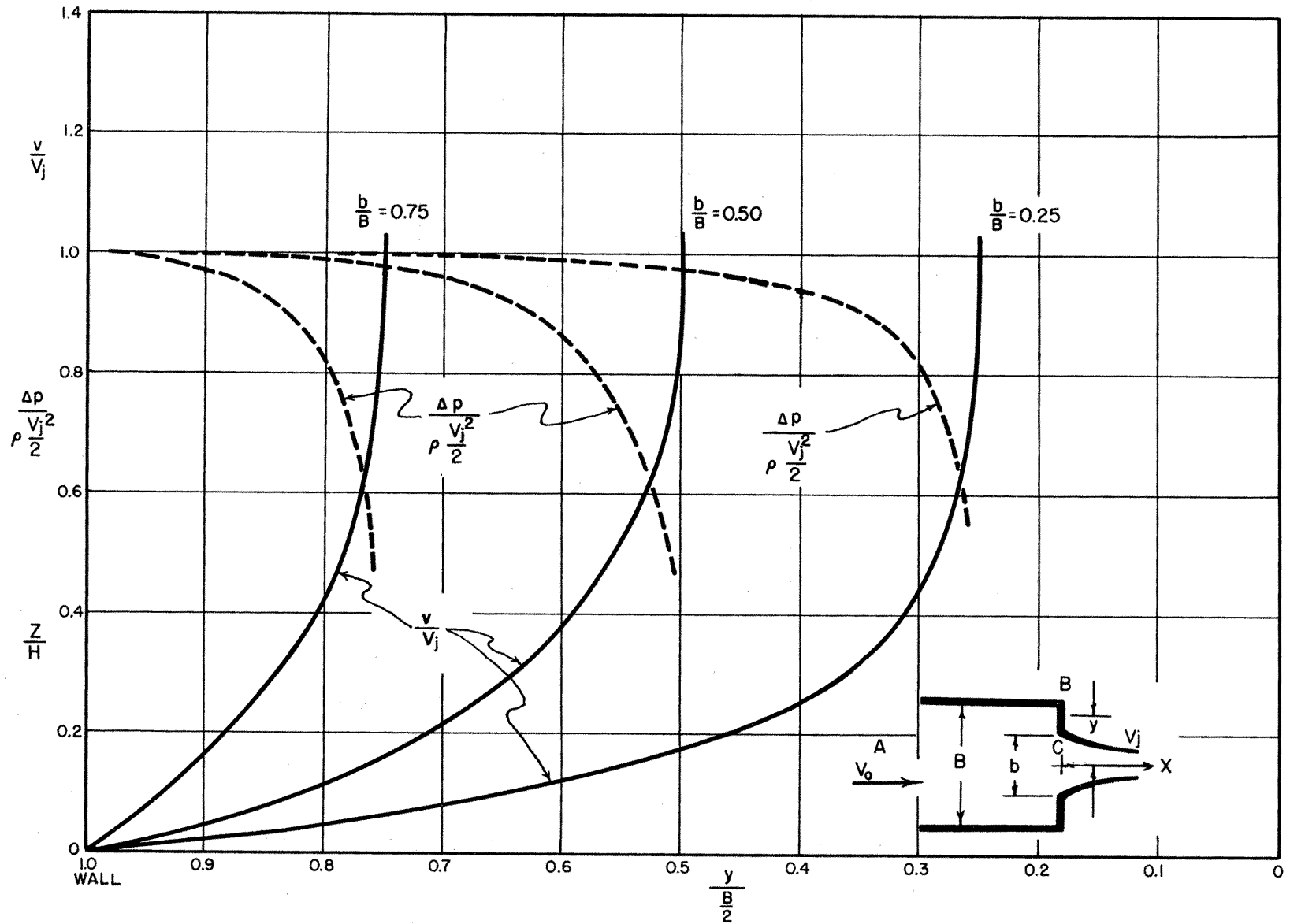


Fig. No. 3-II Theoretical pressure and velocity distribution along the upstream face of the contraction

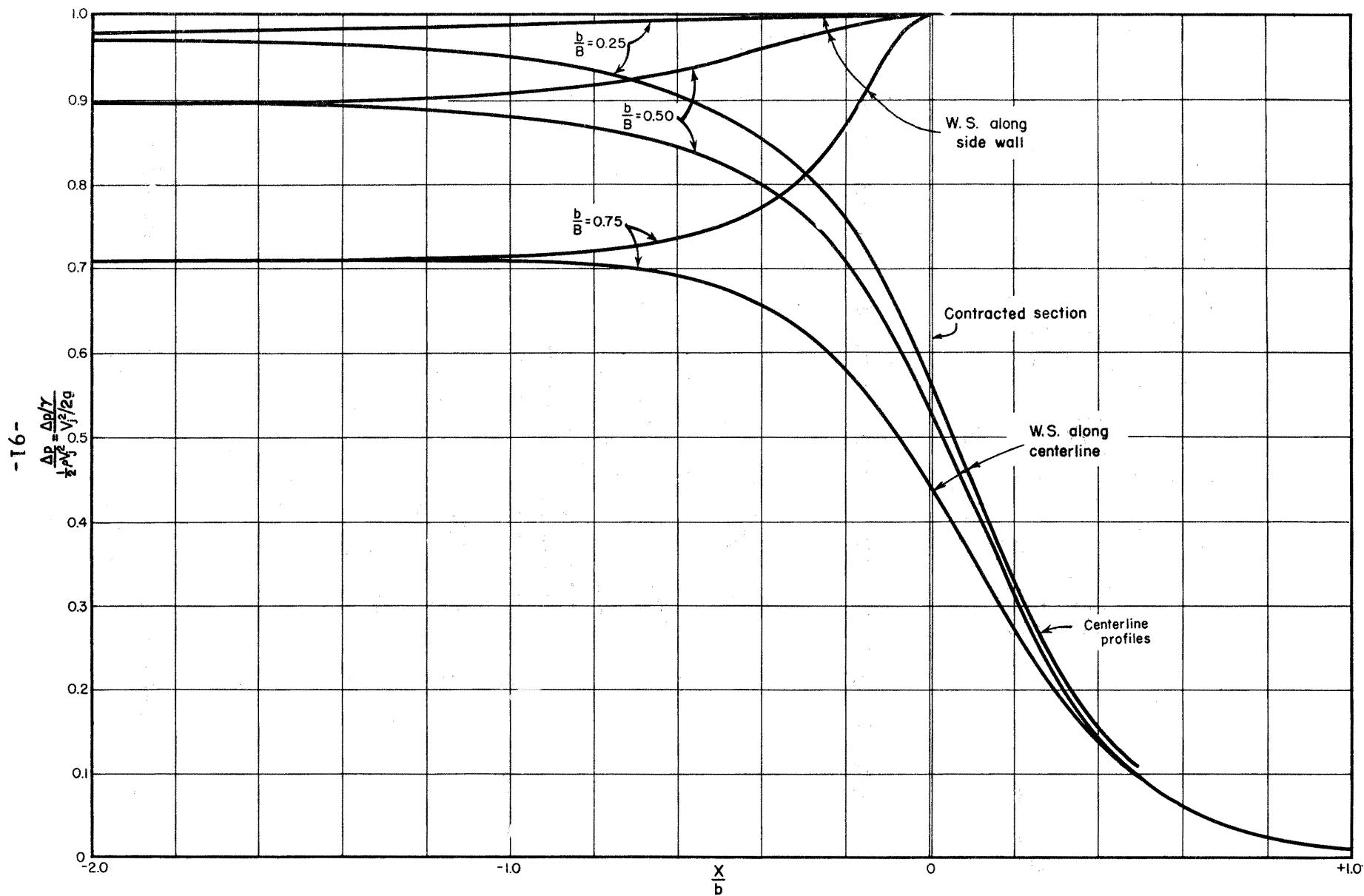


Fig. No. 3-12 Theoretical pressure distribution along the upstream bank and along the centerline of the contraction

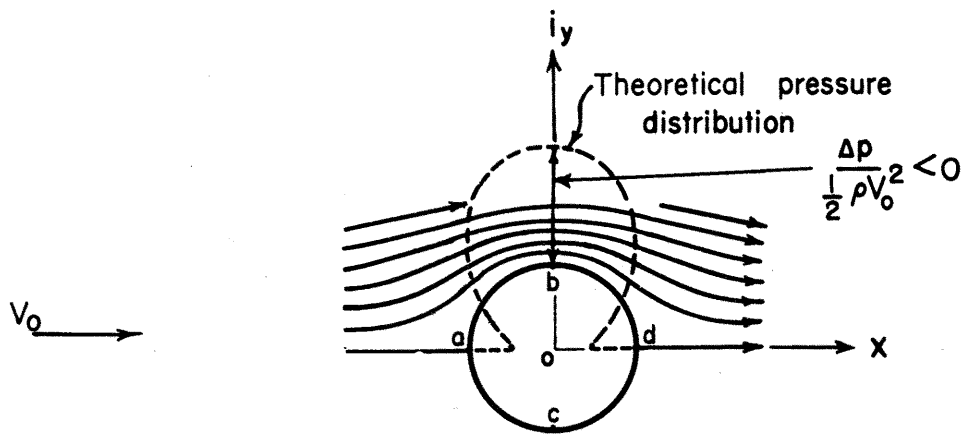


Fig. No. 3-13 Irrotational flow around a cylinder

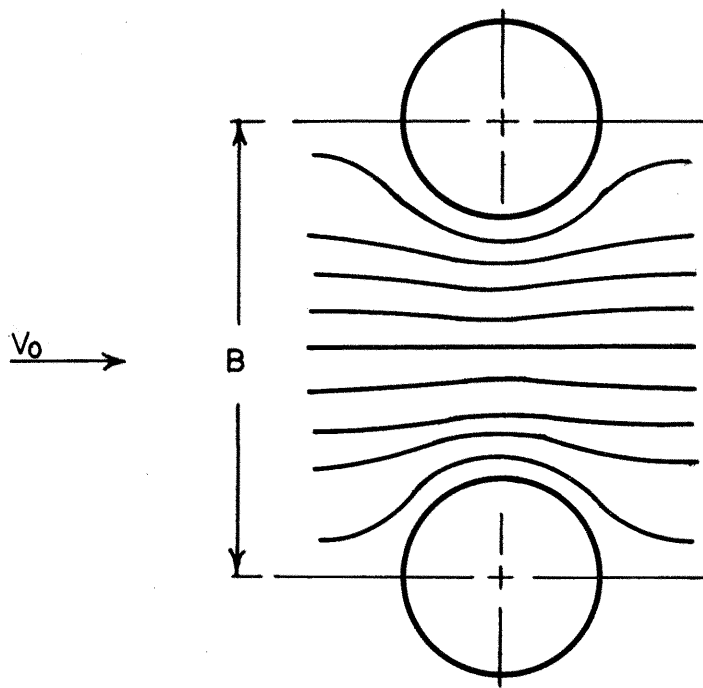


Fig. No. 3-14 Irrotational flow around a cylinder in a narrow channel.

$$R = 1.86 \times 10^5$$

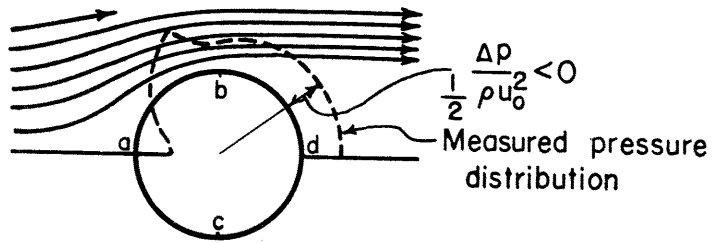


Fig. No. 3-15 Two-dimensional flow around a cylinder at $Re = 1.86 \times 10^5$

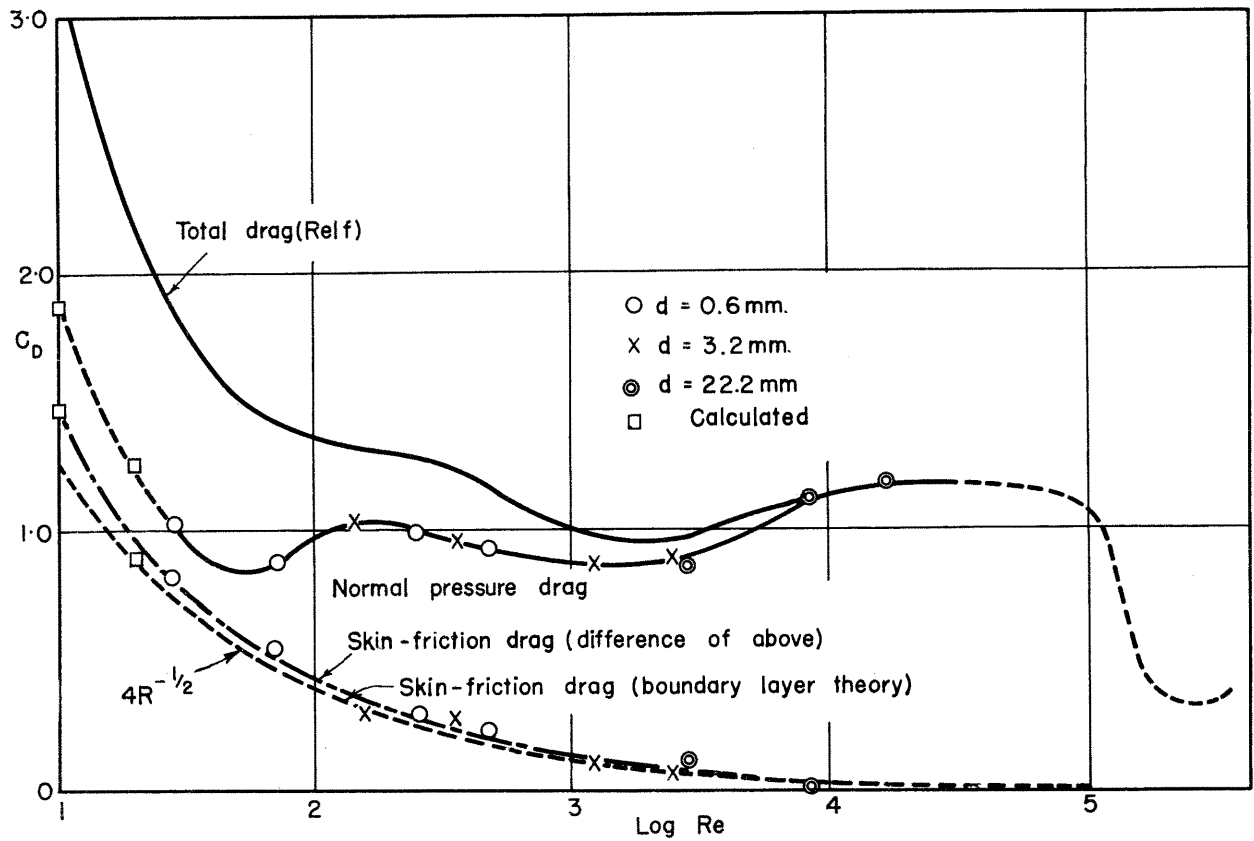


Fig. No. 3-16 Drag coefficient of a cylinder in a two-dimensional flow

IV. EQUIPMENT AND PROCEDURE

Equipment

The equipment used in the testing may be divided into: [1] the flume, [2] the supply system, [3] the measuring devices, and [4] the models.

Flume

The flume, see Fig. 4-1, is of adjustable slope type, 73.5 ft long and 2 ft deep. For run Nos. 1-66, its width was 4 ft, for all runs thereafter it was widened to 7.9 ft. The floor and the walls are of $\frac{1}{2}$ -in. painted plywood, braced by 2-in. by 4-in. ribs every 18 in. The bottom of the flume rests on a pair of 6-in. I-beams, 4 ft apart. These are supported by pairs of screw-jacks at 8 ft to 10 ft intervals along the length of the flume. A rail is mounted on the top of each flume wall by means of adjustable screws at 1-ft intervals. These serve as guide rails for the instrument carriage.

Tests were conducted on two different kinds of roughness. The first kind, see Fig. 4-2a, consisted of a mesh of $\frac{1}{4}$ -in. reinforcing bar spaced at 6 in. longitudinally and 12 in. transversely. The longitudinal bar rested directly on the flume floor so that the transverse bar was held $\frac{1}{4}$ in. above the floor. For creating the second kind of roughness, see Fig. 4-2b, the mesh was turned upside down so that the transverse bars rested on the floor. Sheet metal angles 6 in. long and 1 in. high were put under the transverse bar, with a transverse distance of 6 in. between, in such a fashion that a staggered roughness pattern was obtained

as shown in the sketch. The Manning n was approximately 0.024 for the bar roughness and approximately 0.045 for the baffle roughness.

Supply System

From runs Nos. 1 to 120 the water was recirculated entirely within a pipeline. It was drawn by a centrifugal pump of 9 cfs capacity in a 14 in. supply pipe to be delivered at the flume entrance. A valve in the supply pipe served to control the discharge. To introduce uniform distribution of discharge at the entrance a diffuser section was attached to a transverse float bar, two honey comb lattice works, and three hardware cloth screens -- placed in series in that order to insure uniform velocity distribution and reduce excessive turbulence. See Fig. 4-3. After the flume was widened to 7.9 ft, the diffuser section and the float bar were abandoned in favor of a rectangular weir. The depth in the tailbox was kept constant to insure a minimum in head variation on the pump.

It was decided to draw water directly from the large Hydraulics Laboratory sump after run No. 121. The water was pumped through a 14-in. pipe line and dropped into the entrance section. Lattice works and a float bar were needed to smooth the water surface and reduce excessive turbulence. The water was conveyed back to the sump.

After run No. 760 the tests were made in another flume [73.5 ft in length]. Here the 14-in. pipe was connected to a manifold type diffuser at the flume entrance. This permitted the use of one lattice screen and one float bar only.

An adjustable tailgate having two sets of vertical slats was attached to the downstream end of the flume for the purpose of counteracting the drawdown effect of the drop-off at the end of the flume. See Fig. 4-4. This maintained a water surface slope very nearly parallel to the flume floor at the downstream end of the flume.

Measuring Devices

For measuring water surface profiles, piezometers were connected to openings in the side wall about 1 in. above the flume floor at 4-ft intervals along the length of the flume. A carriage-mounted point-gage was used to measure the surface elevation at any point within the flume. See Fig. 4-5. The point gages were equipped with a vernier to measure to the nearest 0.001-ft, and were correlated with the flume bottom by means of metal reference plates screwed on the floor. The carriage traveled along the flume on the rails mounted on the side walls and the point gage could be moved across the flume on two rails mounted on the carriage. A steel tape fixed on the flume wall and another one arranged on the carriage provided readings for longitudinal and transverse locations of the point gage.

One stationary point gage was used near the downstream end of the flume during the runs Nos. 67-121 to determine normal depth. It was believed that its position was far enough downstream from the model for re-establishment of normal depth, and yet far enough upstream from the end of the flume to be unaffected by drawdown. After run No. 200 a more accurate method of determining the normal depth was adopted [see procedure: establishing normal depth].

The discharge was measured by a 10-in. orifice which was located in the supply line. A differential manometer registered the pressure difference across the orifice plate, and the discharge could be read from a calibration chart.

Velocity profiles were taken occasionally by using a Pitot tube mounted to the carriage. The Pitot tube was calibrated and the coefficient was found to be close to unity. A coefficient of unity was therefore assumed throughout the testing.

An engineers level and a rod were used for setting the flume slope, adjusting the rails, and determining the relative elevations of all measurement devices. Confetti of either aluminum powder or potassium permanganate was used for studying the rollers and eddies as well as the flow pattern. The water used in the tests was city water, its temperature was measured with a thermometer and recorded.

Models

The types of bridge-crossing models studied in this report are:

1. Simple normal crossing,
2. Abnormal stage-discharge condition,
3. Dual bridges crossing,
4. Bridge girder partially submerged,
5. Skew crossing,
6. Eccentric crossing,
7. Piers with and without abutments
8. Flood-plain crossing.

The classification of these types is according to the geometric flow condition in the contracted section. Greater detail on these crossings is presented following the discussion of the abutment models and the pier models

Abutment models:- Three types of abutments were tested; the wing-wall model, the spill-through model, and the vertical-board model. Wing-wall models and spill-through models were made from 16 and 20 gage galvanized sheet metal. The opening between the two abutments could be varied by clamping a 6-in. extension on the back end of each abutment, see Fig. 4-6 and Fig. 4-7. The vertical board models were made from $\frac{1}{2}$ -in. plywood; a strip of galvanized sheet metal was fixed to the throat side of the model to insure conditions of sharp edge entrance, see Fig. 4-7.

Pier models:- Six different kinds of pier models were tested, either separately or in combination with different abutments. These are: circular single-shaft piers, circular double-shaft piers, circular double-shaft piers, round-ended narrow piers, square pile bents, round pile bents, and H-beam pile bents. The single and double-shaft circular piers were made either of $\frac{5}{8}$ -in. steel rod or of pipe, a footing was soldered across the bottom when necessary. For sizes see Fig. 4-8.

For round ended narrow piers two pipes were attached by a $\frac{1}{8}$ -in. by $1\frac{1}{2}$ -in. plate, and the space between the pipes was filled with concrete. Another kind of round-ended narrow pier was made by welding a sheet metal rib between the two pipes and filling plywood flush outside of the pipes. The pile bents were made from steel rod welded on a $1\frac{1}{2}$ " x $\frac{1}{8}$ " steel plate. The top consisted of a piece of 2-in. by 4-in. wood.

For the H-beam bents aluminum channels were soldered together to form the H beam, the beams were then soldered on an aluminum strip, the top was a piece of wood of 2-in. by 4-in., see Fig. 4-7.

Simple normal crossing is the case where the bridge crossing is normal to the main flow direction and symmetrical with respect to the center line of the flume. Only abutment models are used in this type of crossing. A normal flow condition prevailed in the flume before the abutment models were installed. See Fig. 1-1 and 1-2.

Abnormal state-discharge condition is similar to the simple normal crossing except that the flow was at an abnormal stage-discharge condition before the abutment models were installed, see Fig. 1-4. The abnormal stage-discharge condition is the only case in this report where the flow was not set at normal flow before the abutments were installed.

Dual bridges crossing is the case where there are two bridge crossings parallel to each other. The crossings are normal and symmetrical with respect to the main flow, see Fig. 1-5.

Bridge girder partially submerged is the case which changes the simple normal crossing by adding a model of bridge girder supported by the two abutments. The lower part of the girder is submerged in the flow. The models of the bridge girder were so constructed that the degree of submergence could be changed. Two types of bridge girder models were used in connection with the 45 degree wing-wall abutments and 1:1½ spill-through abutments. The first one was made of ½-in. plywood with four girders ½-in. thick. The model was 1 ft wide which is the same as the top width of the abutment models. Each end of the girder could be adjusted so that it contacted tightly either the spill-through abutment or the wing-wall abutment. The second one consisted of a plywood deck, 1 ft wide to which a sheet-metal angle was attached on the upstream side. The ends of the angle could be adjusted for both

types of abutments. See Fig. 1-6 for the general arrangement and Fig. 4-9 for the bridge girder models.

Skew crossing is the case where the center line of the roadway does not intersect the center line of the flow at a right angle. The intersection angle is ϕ , see Fig. 1-7. In the case in which the front face of the abutments is perpendicular to the roadway, the geometry of the abutment models remained the same as shown in Figs. 4-6 and 4-7. In the case where the front face of the abutments is parallel to the direction of the flume, the geometry of the abutment was changed accordingly. The top width of the roadway is $\text{Cos } \phi$.

Eccentric crossing is the case in which the center line of the contracted opening, although being parallel to the center line of the flume, does not coincide with the center line of the flume.

Piers with and without abutments is the case in which the effect of piers on the maximum backwater has been studied. The arrangement of the models is symmetrical with respect to the center line of the flume, see Figs. 1-9 and 1-10.

Flood plain crossing is the case in which the cross-section of the channel is not a simple rectangle. The cross-section is a composite section as shown in Fig. 1-12. The flood plain of each side was 3 ft wide. The center channel is 2 ft wide, and is recessed 0.345 ft below the flood plain. A variety of roughness patterns can be arranged as shown in Fig. 1-12.

Procedure

The testing procedure was as follows. First, the channel slope was set as desired and the rails adjusted accordingly. Second, normal depth was established and recorded, corresponding to the desired discharge. Finally, the models were placed, and the data taken and recorded.

Setting of Slope

With the flow in the flume the jacks under the flume were adjusted according to predetermined readings with an engineer's level and rod. The rod readings always were taken on the flume bottom directly above the jacks. The bottom actually is slightly wavy due to warping of the plywood, but the method of setting the slope gave a very satisfactory average value of slope.

Setting of Rails

The rails were adjusted parallel to the flume bottom after the flume slope had been set. Each screw supporting a rail was adjusted separately if found necessary. Both slope and rails were adjusted again whenever the discharge was changed or if there was reason to do so [for example, if the normal depth were not correct]. Because both the slope and the rails were adjusted under normal flow conditions, small deflections were possible once the model was installed and a heavier load of water resulted upstream from the model. The error of measurements introduced thereby was considered small enough to justify no further adjustment.

Establishing Normal Depth

For the first 154 runs the water surface slope was determined by means of piezometer readings. The tailgate was changed until water surface was parallel to the flume slope, according to the piezometer readings. Later it was found that the piezometer readings were not in agreement with direct water surface readings made by the point gage. This was due to the difficulty of removing all the air trapped in the piezometer tubing, and to the difficulty of reading the piezometers accurately on account of the capillary rise in the tubes. It was possible to avoid all these difficulties by use of the point gage, which had the additional advantage of giving a constant reading for uniform depth eliminating the computations formerly necessary with the piezometers. The accuracy of setting normal depth by this method was found to be quite satisfactory. The normal depth could always be re-established within a fraction of one thousandth of a foot for the same discharge, slope, and roughness.

When the effect of downstream ponding was investigated, the normal depth was established first. Then the tailgate was adjusted so that the depth at the position where the model entrance would be located was equal to the normal depth plus the desired increased depth. Actually, this position was one point on a back-water curve, and the definition of the depth is rather arbitrary, see Fig. 1-4.

Placing of Models

Once normal depth had been established, the models were placed. Beginning with run 200 all cracks between model section and between model and flume were sealed with plasticine. Furthermore, the roughness elements, which had been taken out previously

for placement of the models, were returned. Care was taken, thereby, to re-establish a consistent roughness pattern in the throat section. The importance of a systematic roughness pattern was particularly apparent during runs with piers, where the increment in backwater due to the piers was very small. A difference caused by re-arrangement of roughness, or by leaving out the roughness between the piers, could cause a change in backwater which sometimes was equal to or larger than the backwater increment caused by piers.

Data Taken

The data of primary interest were: the water surface readings at particular points, i.e. the position of maximum backwater, the section of re-established normal depth, the stagnation points in the upstream and downstream corners of model with flume side wall, and the width of the contracted jet [the vena contracta]. The methods of taking these data were:

- a. The point of maximum backwater was found by taking a water surface profile along the center line by means of the point gage. In the case of skewed crossings the position of the maximum backwater shifts to the side wall. Maximum backwater height and its position were always recorded.
- b. The section of re-established normal depth was determined by using the water surface profile along the centerline of the flume. It is the section downstream from the model where the normal depth was re-established. The continuous reading of the normal depth from this section furnished a control to determine whether the experimental conditions had remained undisturbed. If the

continuous reading downstream was different from the normal depth reading as obtained without the models, then the discharge was checked and eventually flume and rail slopes also were checked. Due to small undulations caused by the expanding jet through the constrictions, the position of the beginning of re-established normal depth could not be defined clearly. Therefore, an attempt was made to define more accurately a length parameter for the particular case of flow under consideration. There was always a reverse current along the side wall in the wake of the model where the water was flowing upstream. Some distance downstream the velocity along the side wall reversed its direction and the water flowed downstream again. The average of the position of the stagnation points between both currents on both walls was determined as the desired length parameter. It was determined by dropping potassium permanganate into the water at different positions along the walls, and thus finding the stagnation point.

- c. The water surfaces around the models were measured frequently, but in most cases, only the depth at the stagnation points was recorded. In order to average the errors due to small fluctuations, the readings were taken three times during each run. In the case of two bridges, the water surface between the two models was of a surging nature. Therefore, the stagnation depths at the downstream side of the upstream model, and the stagnation depths at the upstream side of the downstream model were determined by taking

the mean of each average of three readings of the maximum depth and of three readings of minimum depth.

- d. A measurement of the width of the vena contracta yielded results which showed considerable scatter. It was found that the position of the minimum depth along the center line was approximately equal to the position of the vena contracta. This point therefore was defined as the position of the vena contracta. The width was then measured by defining it as the width of the jet between the turbulent mixing zones on each side. This zone was made clear by inserting dye close to the upstream side of the model.

Figure 4-10 shows a typical arrangement of taking measurements. In this particular case, the velocity distribution in the contracted section was measured. Figure 4-11 shows typical flow in the vicinity of a wing-wall abutment. Figure 4-12 shows typical flow in the vicinity of a spill-through abutment.

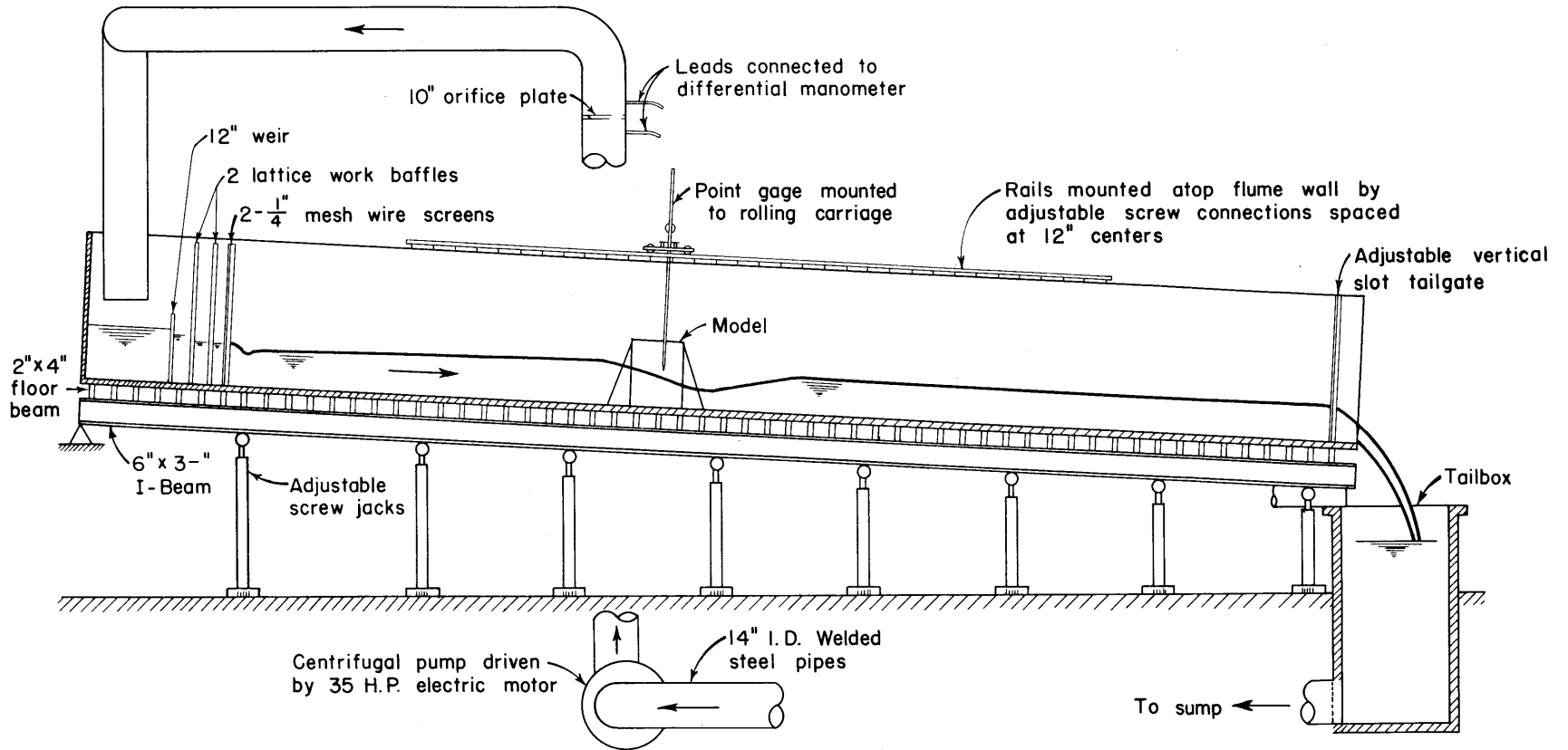


Fig. No. 4-1 General elevation of experimental flume

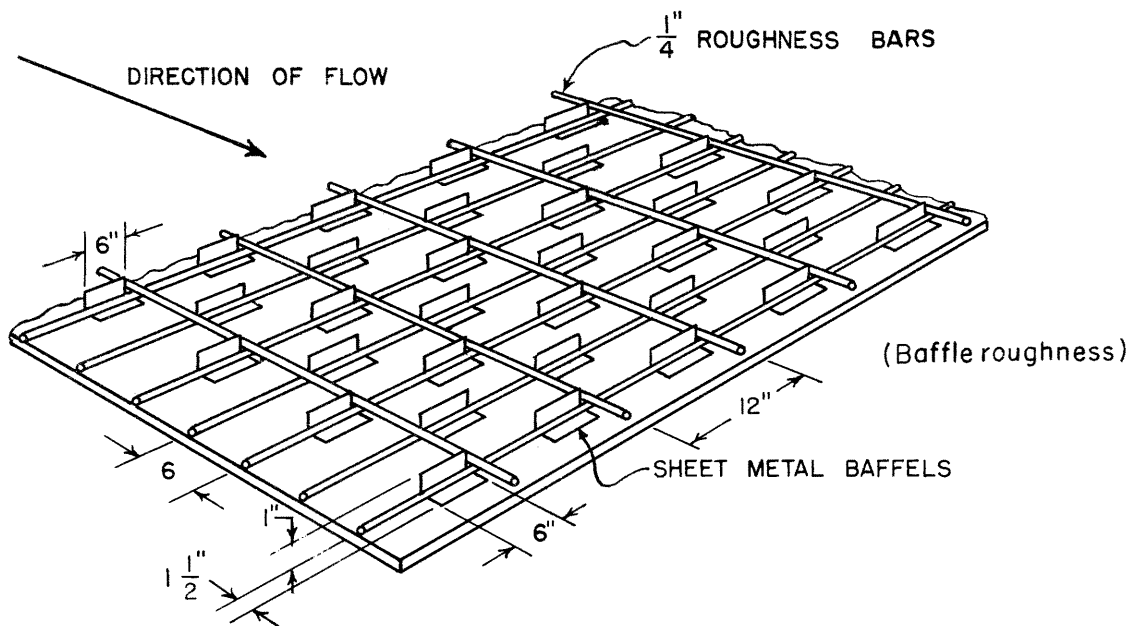
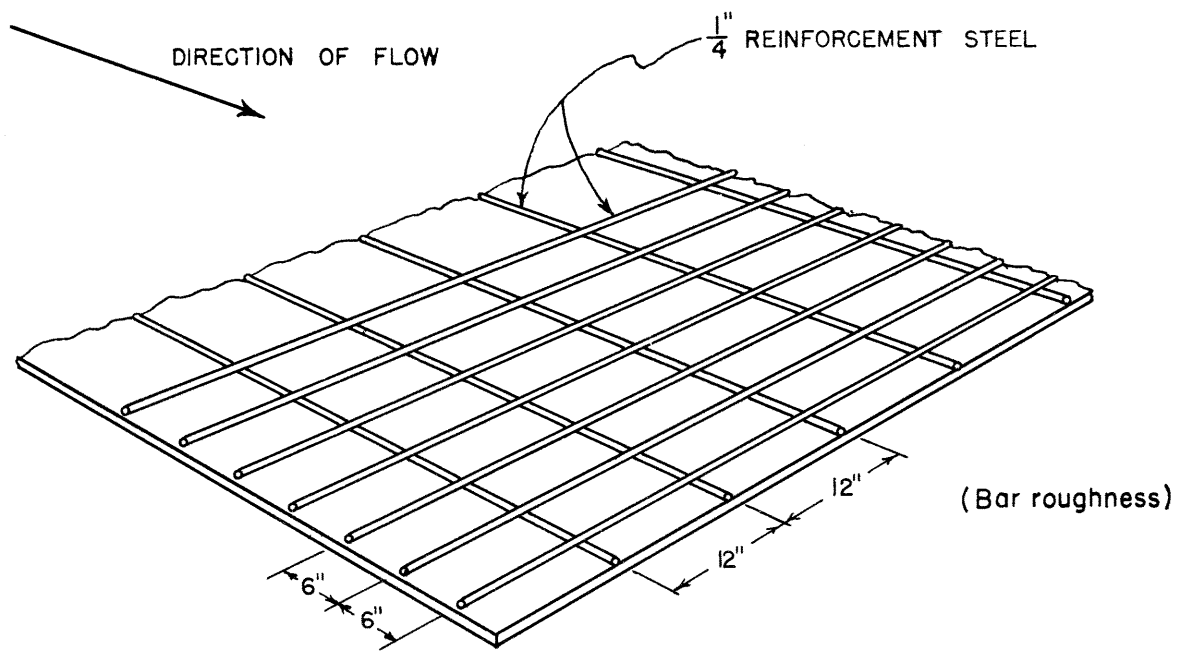


Fig.No.4-2 Patterns of bed roughness

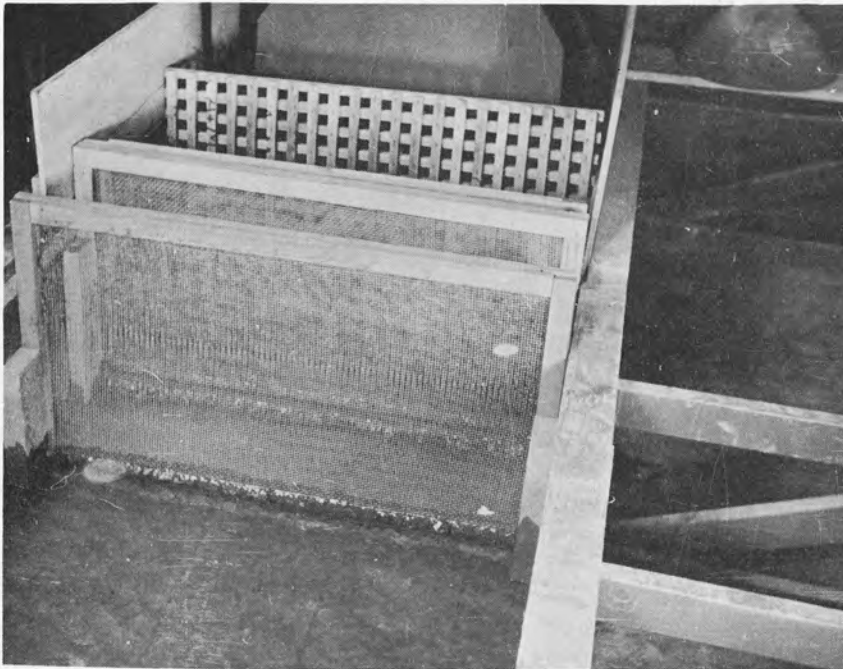


Fig. No. 4-3 Photo of the baffle and screen at the entrance of the flume

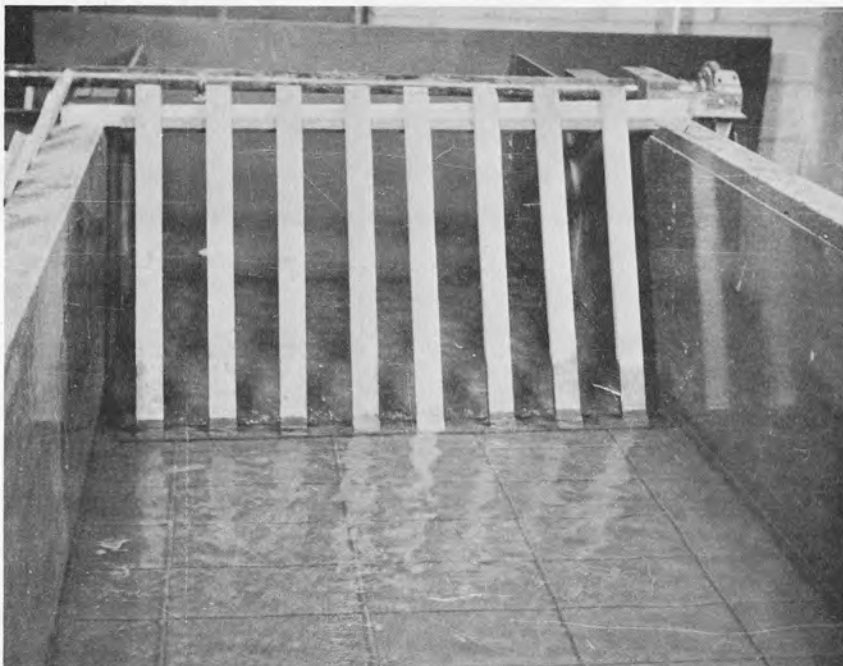


Fig. No. 4-4 Photo of the adjustable tailgate

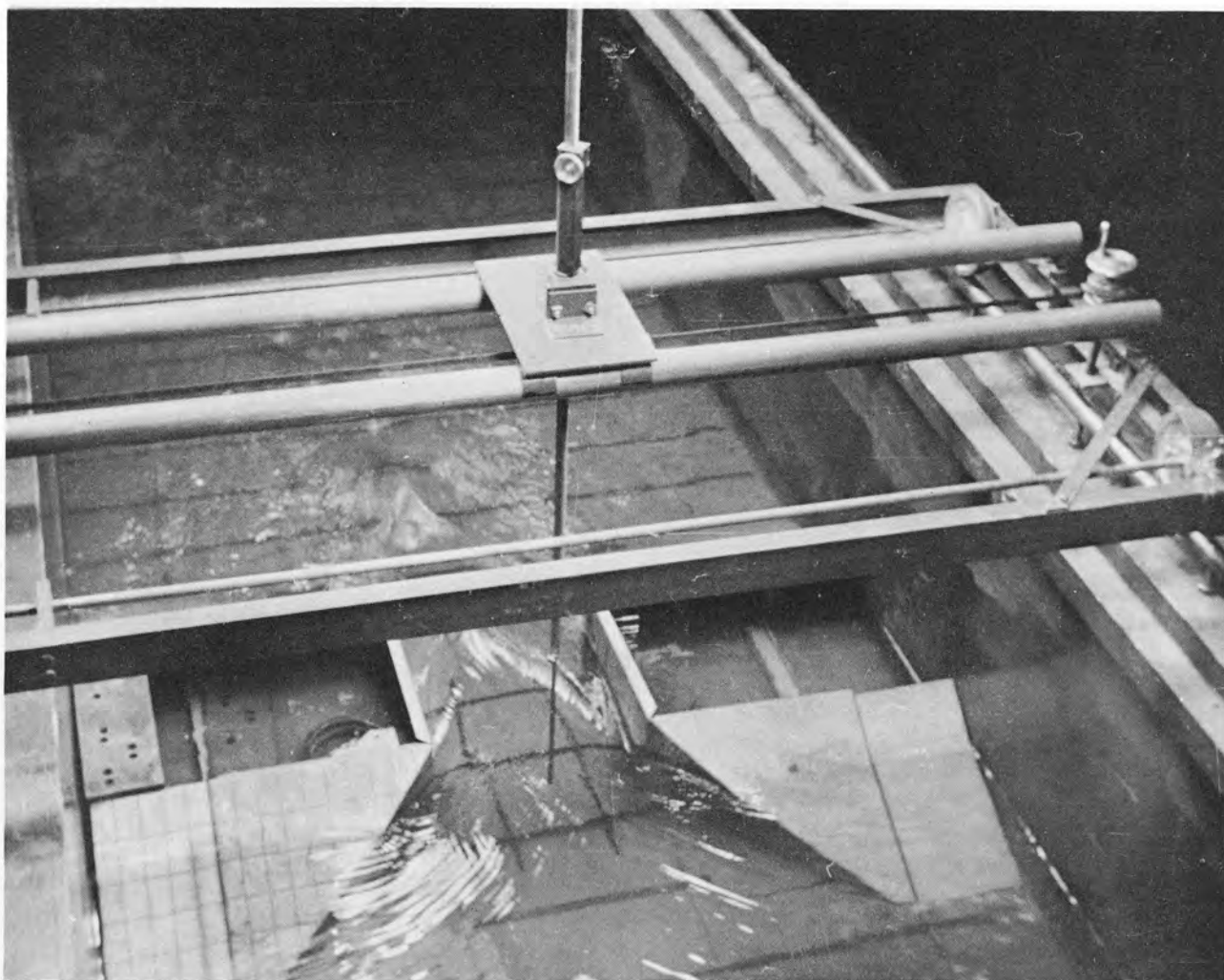
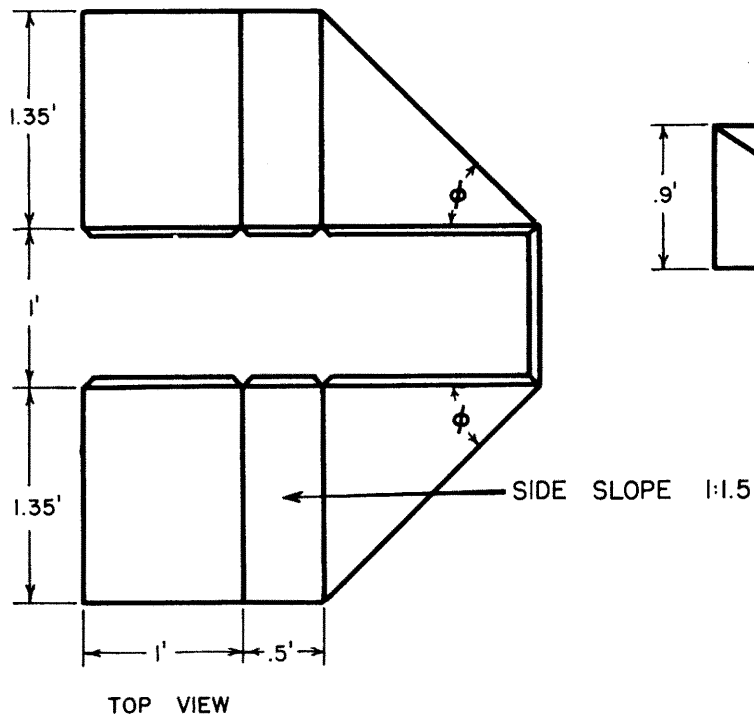
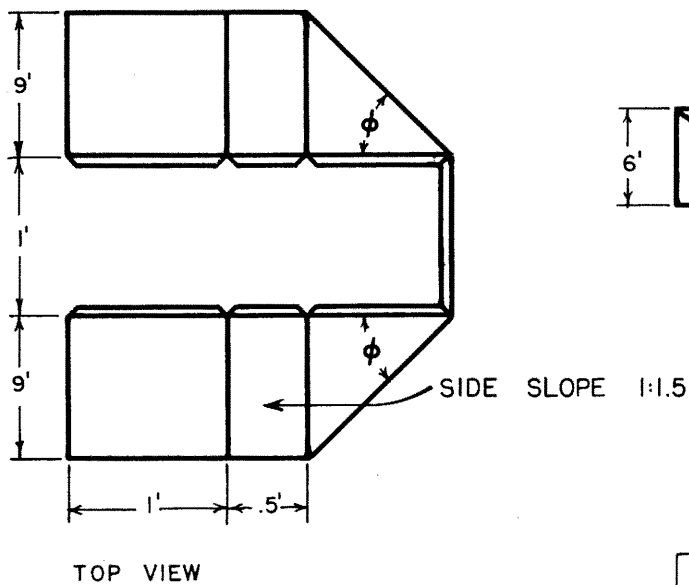


Fig No. 4-5 Photo of the point gage and carriage

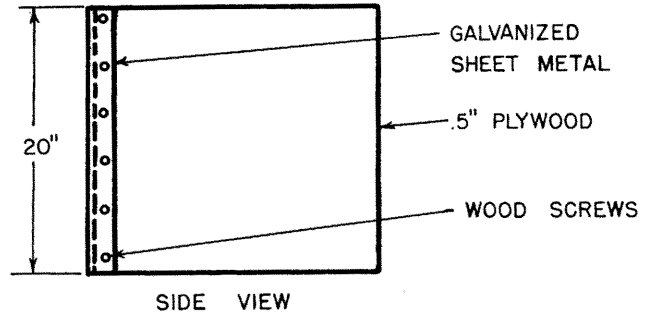
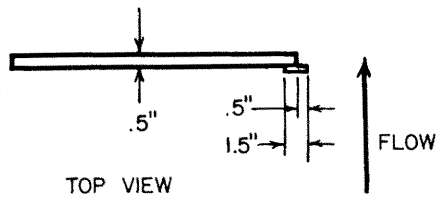


MODELS USED	$\phi = 45^\circ$	WW 45
	$\phi = 60^\circ$	WW 60
	$\phi = 90^\circ$	WW 90

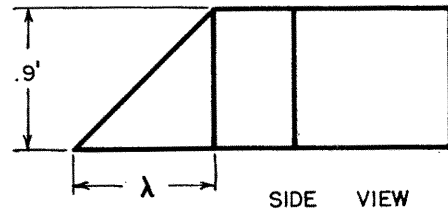
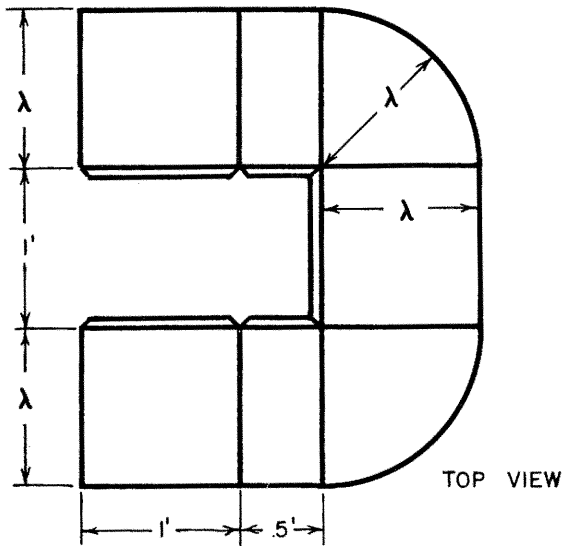


USED WERE	$\phi = 30^\circ$	WW 30
	$\phi = 45^\circ$	WW 45

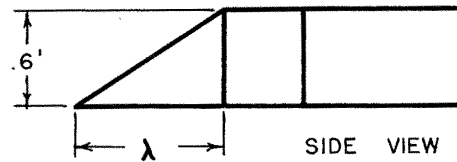
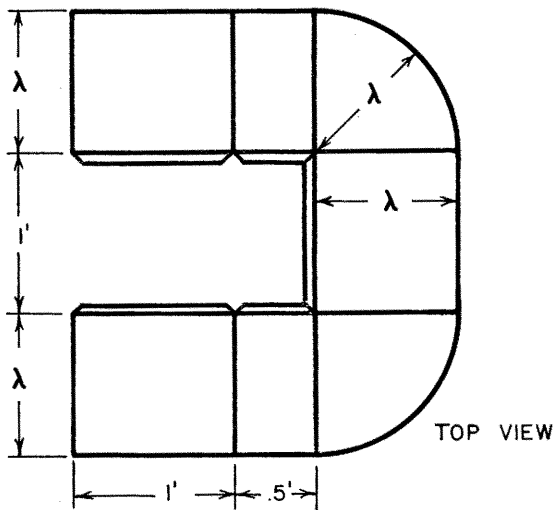
Fig. No. 4-6 Models of wing-wall abutments



VERTICAL BOARD TYPE



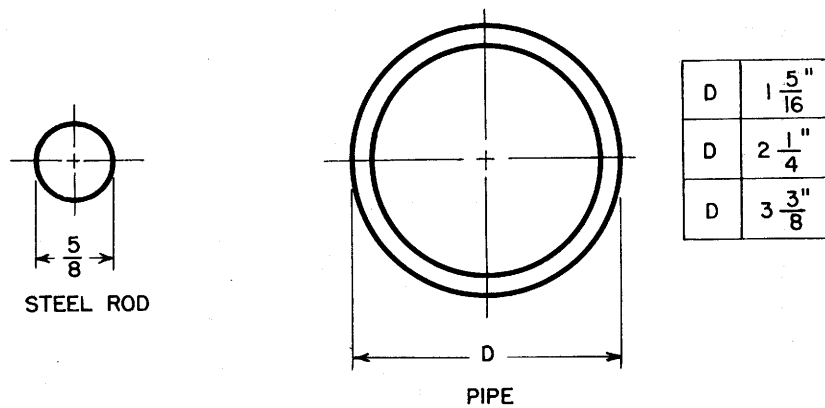
$\lambda = 0$	ST 1:0 VW
$\lambda = 0.9$	ST 1:1
$\lambda = 1.35$	ST 1:1.5



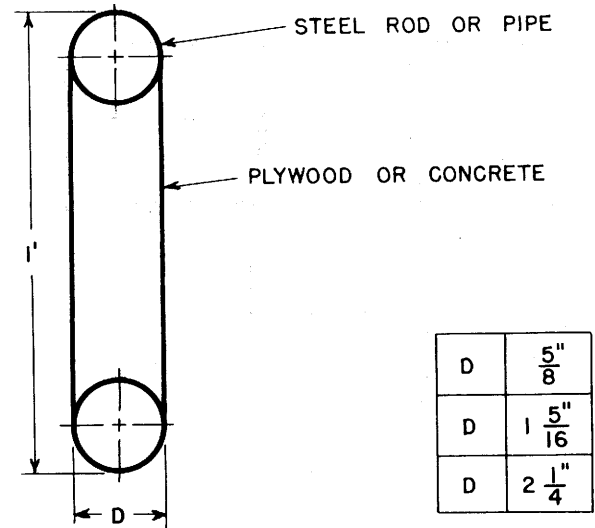
$\lambda = 0.9$	ST 1:1.5
$\lambda = 1.2$	ST 1:2

SPILL - THROUGH TYPE

Fig. No. 4-7 Models of spill-through abutments and vertical-board model.

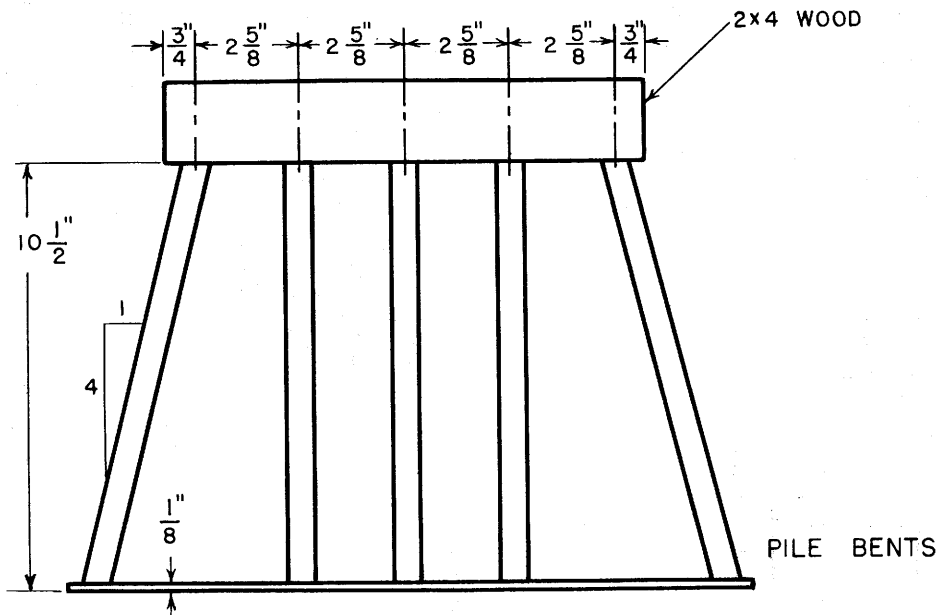


ROUND PIERS: SINGLE & DOUBLE SHAFT



ROUND ENDED NARROW PIERS

-113-



PILE BENTS

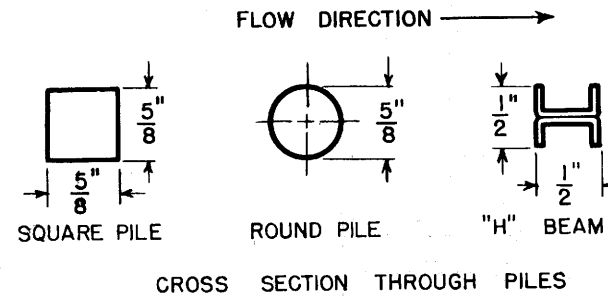


Fig. No. 4-8 Pier models

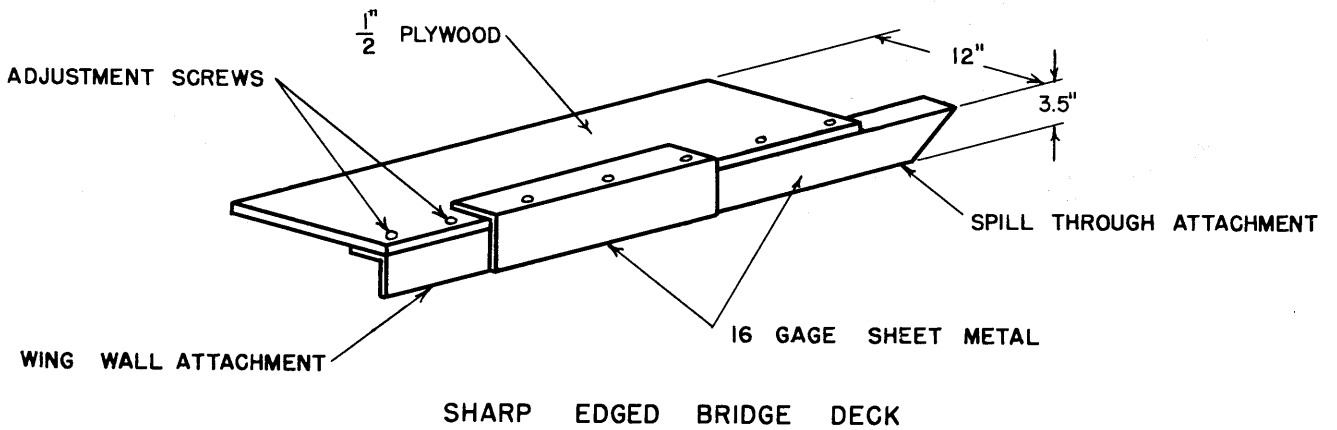
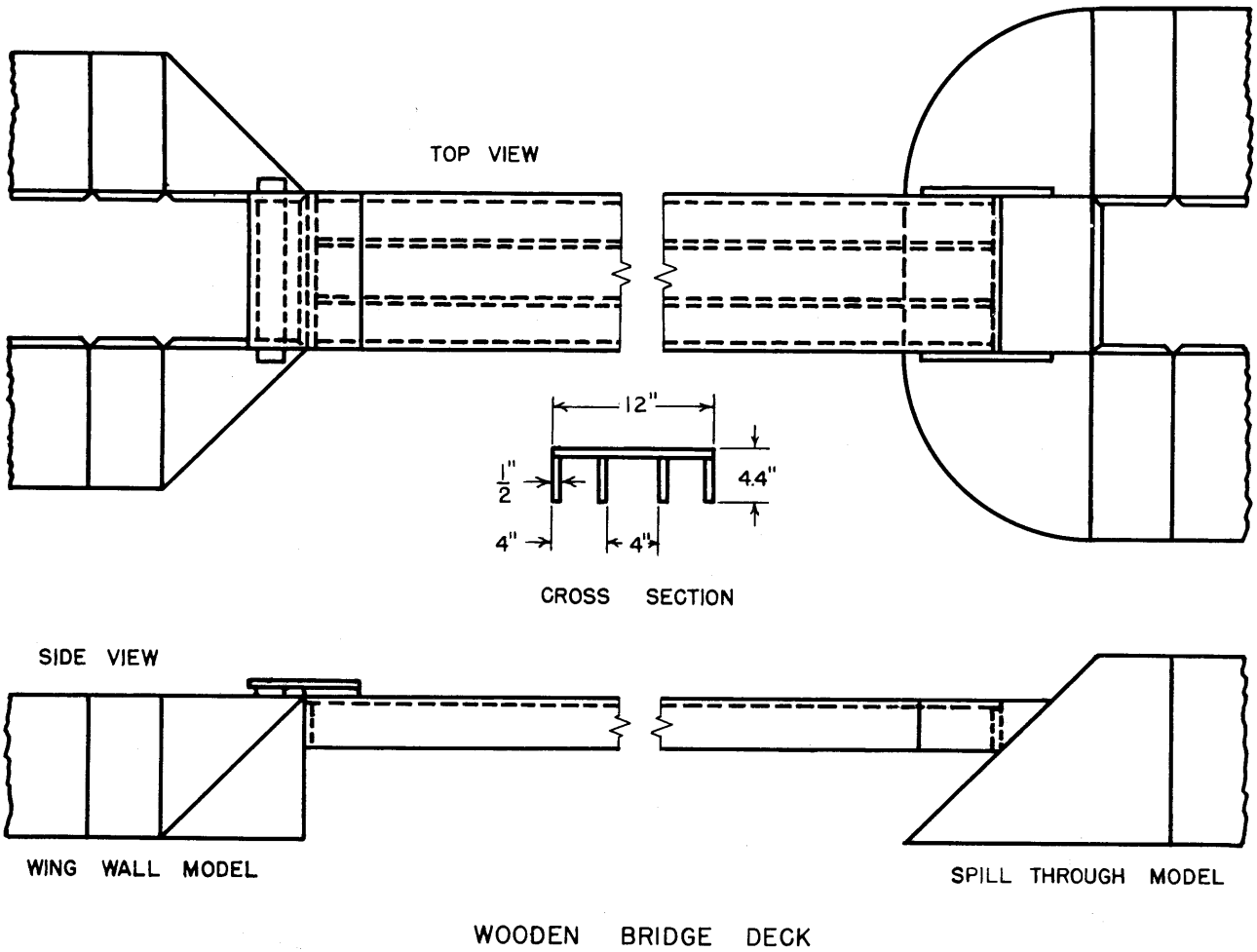


Fig. No. 4-9 Models of submerged bridge girders

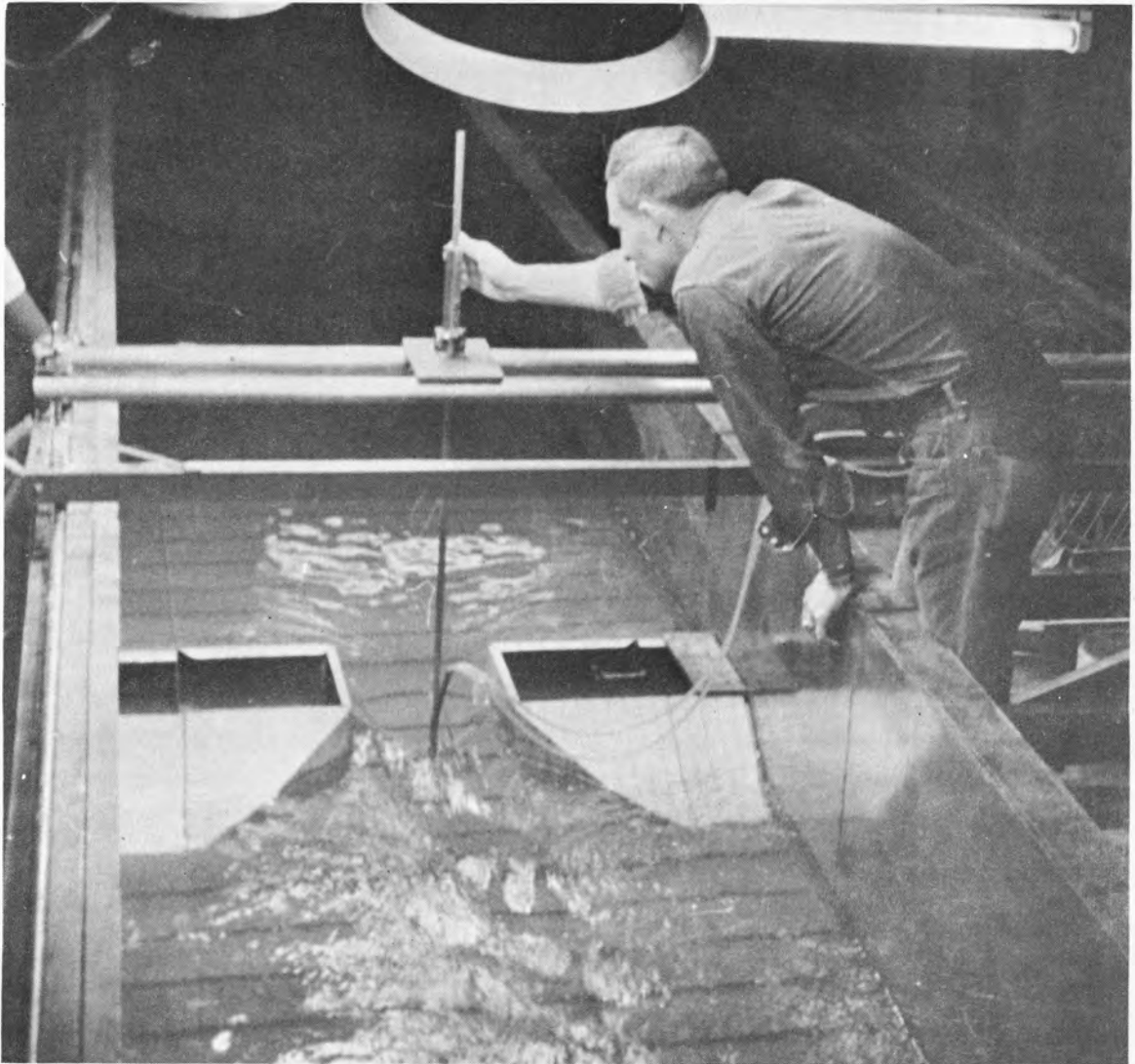


Fig. No. 4-10 Photo of Pitot tube used to
take velocity profiles



Fig. No. 4-11 Photo of wing-wall abutments
in 4-ft. flume

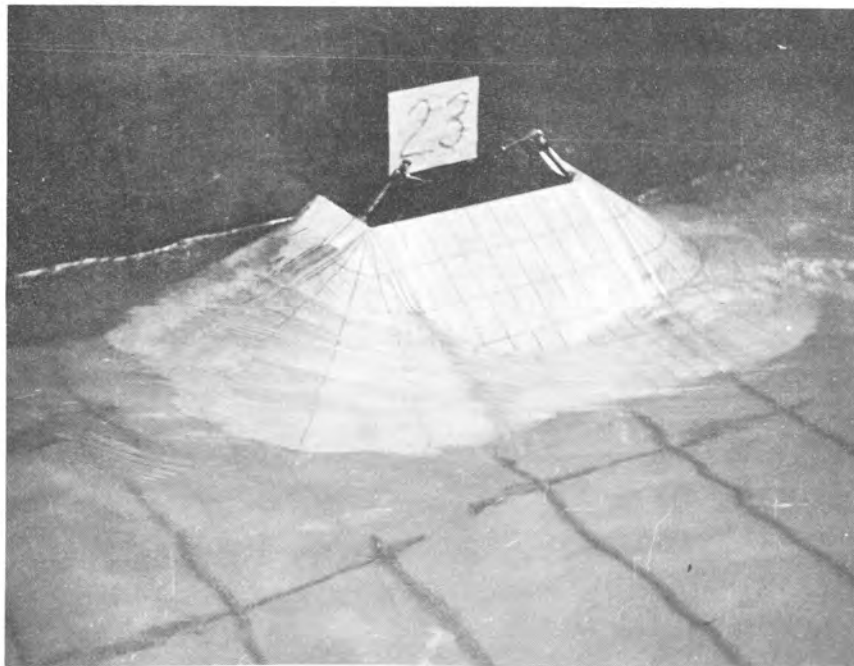


Fig. No. 4-12 Photo of spill-through abutments
in 4-ft. flume

V. PRESENTATION AND ANALYSIS OF DATA

The ultimate objective of this research is to find a practical method of estimating maximum backwater caused by a bridge contracting a stream channel. Therefore, the qualitative study of a large number of variables has been given preference over an extensive investigation of the mechanics of backwater formation. The basic principles, such as stated in Chapter III, were studied experimentally whenever possible.

Experimental data obtained from this research were numbered chronologically from 1 to 121 for earlier data obtained in a flume of 4-ft width and from 200 to 1392 for later data obtained in a flume of 7.9-ft width.

Data pertaining to the flume of 4-ft width were limited to 45 degree wing-wall abutments, and $1:1\frac{1}{2}$ spill-through abutments, [hereafter referred to as WW abutments and ST abutments respectively.] The opening was centered and perpendicular to the approaching flow. Owing to the fact that during these earlier runs the experimental procedure was not well established and the normal water surfaces were not determined exactly, the information concerning the Froude number of the uncontracted flow, and the maximum backwater are not accurate. In general, data of this group will be used only to check the conclusions based upon the data from the flume of 7.9-ft width. Some runs of this group have not been analyzed for one of the following reasons, such as: inaccuracy in determining the slope of the flume, inaccuracy in measuring the discharge, and inaccuracy in determining the elevation of the normal water surface.

Some of the data pertaining to the flume of 7.9-ft width have not been analyzed for one of the following reasons such as. fluctuation of discharge; inconsistency of bed roughness in the contracted section; abutments over-topped, and inaccuracy in establishing the normal flow condition in the uncontracted channel.

Experimental data obtained from this research are listed in Appendix B according to the conditions of contraction.

In this chapter the presentation and analysis of data will be divided into three parts:

1. Flow Geometry,
2. Energy Loss, and
3. Maximum Backwater.

The analysis of maximum backwater will be concerned about the maximum backwater along the center line of the flume, except in the cases where the maximum backwater along the center line of the flume does not exist. For such exceptional cases the analysis will be for the backwater at one of the two upstream stagnation points.

The data of the differential elevation of the water surfaces across the roadway embankment can be found from the tables in the Appendix. According to dimensional analysis the data of such differential elevation can be considered as a dependent variable similar to the maximum backwater. The data of such differential elevation are not analyzed in this chapter.

Part I. FLOW GEOMETRY

The term "flow geometry" is used here to include:

1. The water surface profile along the boundary, and along the center line;
2. The coefficient of contraction of the jet, and
3. The location of the maximum backwater.

The flow geometry of open channel flow through a contraction has been studied through the use of free streamline theory. According to this theory the velocity distribution and the pressure distribution of the flow are uniquely determined by the boundary geometry. The pressure along the jet boundary is constant, consequently the velocity along the jet boundary is also constant. The mathematics involved in the free streamline theory is rather complicated but it is included in the Appendix for reference. The application of this theory to an open channel contraction was suggested by J. S. McNown, consultant to this research. The difficulty of applying free streamline theory to the case of open channel flow through a contraction lies chiefly in the fact that the former is valid for two-dimensional flow while the latter has a free surface and is of a three-dimensional nature. The theory is based upon the assumption that along the entire free streamline the pressure is constant and consequently, the velocity is also constant. Such an assumption is not entirely valid for the jet from an open channel contraction.

Water Surface Profiles

Information concerning flood stage along the highway embankment and the river bank is needed in order to safeguard

the embankment and the farm land adjacent to the bank. For rectangular channel in the laboratory, this information can be obtained approximately by use of free streamline theory. For given boundary conditions, the velocity distribution along the boundary and along the centerline of the flow can be calculated, and the pressure distribution can be computed according to Bernoulli's theorem. In order to convert this pressure head into the flow depth, the continuity equation must be taken into consideration. The effect of non-hydrostatic pressure should be considered wherever surface curvature is pronounced and accelerations due to gravity are large. Fig. 3-11 indicates the theoretical distribution of relative pressure head and relative velocity along the embankments, in which the relative pressure head $\Delta p / \frac{1}{2} \rho V_j^2$ is the difference between the local pressure along the contracting boundary and that along the free streamline, divided by the dynamic pressure $\rho \frac{V_j^2}{2}$ of the free jet. The relative velocity v / V_j , is the ratio of the local velocity v to the jet velocity V_j . At the stagnation point, $v = 0$, therefore $\Delta p / \frac{1}{2} \rho V_j^2 = 1$; at the edge of the plate where the jet separates from the boundary, $v = V_j$, hence $\Delta p / \frac{1}{2} \rho V_j^2 = 0$. No correction was made regarding the continuity equation and non-hydrostatic pressure distribution. A theoretical water surface profile can be determined by assuming there exists a similarity between a two-dimensional flow through a slot, with an approach velocity V_0 , and open channel flow through a contraction with an approach velocity V_1 at section I. Data taken along the upstream face of a VB model are shown in Fig. 5-1. In this case the local depth of flow divided by the depth at the stagnation point was plotted against $\frac{y}{B/2}$. Verification was made only for

$b/B = 0.25$, because the length of the roadway in this case was adequately long so that the variation of water surface could be measured more satisfactorily.

Theoretical curves for $\Delta p / \frac{1}{2} \rho V_j^2$ along the upstream bank and along the center line are plotted in Fig. 3-12 for different opening-ratios; in which Δp is the difference between the local pressure and that along the free streamline. These curves resemble the experimental water surface profiles along the bank and along the center line at different opening ratios. Data taken along the upstream bank and along the center line are shown in Fig. 5-2. In order to minimize the effect of curvilinear flow on the pressure distribution along the center line, an opening ratio $b/B = 0.75$ has been chosen for comparison. The comparison was made by defining $V_j^2 / 2g = \Delta h \times 0.709$ for $b/B = 0.75$ in which 0.709 is $\frac{\Delta p / \gamma}{V_j^2 / 2g}$ for the approaching flow and $\Delta h = \Delta p / \gamma$ was measured above h_3 . The comparison is fairly satisfactory despite the assumptions used in the theory. Data deviate appreciably from the theoretical curve when $x/b > 0.1$. This might be owing to the fact that along the lateral boundary of the jet the pressure is not constant as assumed.

Although the comparison between the theory and the measurement in some cases is quite satisfactory, it should be remembered that the comparison regarding pressure distribution along the bank and the embankment can deviate considerably from theory to measurement because of:

- a. Non-uniform distribution of velocity of the approach flow, and
- b. Separation loss in the vicinity of the stagnation point.

Coefficient of Contraction

An analytical study of open channel flow through a local contraction requires the use of three basic principles as expressed by:

- a. Continuity equation,
- b. Momentum equation. and
- c. Energy equation.

In using any of these three equations, it is necessary to know the maximum jet velocity, which occurs in the section of minimum opening. If the coefficient of jet contraction is known, the maximum jet velocity can be computed through the use of the continuity equation. According to the free streamline theory, the coefficient of contraction has a minimum value of $\frac{\pi}{\pi + 2} = 0.611$ at a distance far downstream from the opening. The values of C_c measured for different values of b/B are shown in Figs. 5-4, 5-5 and 5-6 for vertical board model, 45 degree wing-wall abutments and $1:1\frac{1}{2}$ spill through abutments respectively [hereafter referred to as VB model WW and ST abutments]. No conclusion can be drawn from these figures because of scatter data.

Because open channel flow through a contraction is three dimensional in nature, it is difficult to measure the contraction coefficient of the jet. First, the boundary of the jet is not clearly defined due to the mixing action between the oncoming jet and the surrounding fluid. Second, in addition to lateral contraction which is caused directly by the geometry of constriction, there is also a vertical contraction caused by gravity. The minimum width does not necessarily correspond to the minimum depth of the jet. Furthermore, the coefficient of contraction may depend upon the distribution of the approaching velocity, the roughness of the bank

and the bed in the vicinity of the contraction and the width-depth ratio of the uncontracted flow.

The minimum jet width was observed by introducing dye at the point of separation along the abutment. It was measured by a point gage. Because information on the coefficient of contraction is very essential in studying the maximum backwater, it is suggested that research be continued on the coefficient of contraction.

Location of Maximum Backwater

The distance of the maximum drawdown is the distance between section I, where the maximum backwater occurs, and section II where the minimum opening begins.

The approaching velocity of two-dimensional flow through a slot is V_o and is theoretically at infinity upstream from the slot. The maximum pressure head p_o/γ is also at infinity upstream. For a flow in a channel having a uniform slope, the natural velocity of approach is at a distance upstream from the contraction and is equal to the normal velocity V_n of the uncontracted flow. The maximum potential caused by the contraction can be assumed to be where the velocity is equal to the normal velocity. In order to illustrate how the location of maximum backwater depends upon other variables; the following comparison between the two-dimensional flow and the open channel flow is made:

Because the slope of the water surface between sections 0 and I is extremely small, the maximum depth h_1 can be considered as the maximum potential head of the backwater. Assuming that the maximum pressure potential of the two-dimensional

constricted flow corresponds to the maximum potential head of the contracted open-channel flow, the approximate location of the maximum pressure potential obtained from the free streamline theory can be used as a guide to determine the location of the maximum backwater h_1^* . Although the location of the maximum pressure potential of the two-dimensional flow is theoretically at infinity, it can be considered approximately to be at a place, where the velocity is 1 per cent greater than the approaching velocity, i.e., $v = 1.01 V_0$. Based upon such a standard, the nominal distance L^* between the section of maximum pressure potential and the slot can be computed by use of Eq. 3-66. As shown in Fig. 5-7, the distance L^* divided by the slot width b , varies with the opening ratio. Fig. 5-7 indicates that $L^* = b$ at $b/B = 0.70$; $L^* > b$ for $b/B < 0.7$; and $L^* < b$ for $b/B > 0.7$.

The location of maximum backwater was scaled from the recorded water surface profiles and has been tabulated in Tables of Appendix B. Because the water surface slope in the vicinity of maximum backwater is rather small, it is difficult to determine exactly the location of maximum backwater. Plots of this distance to maximum backwater have been made for various flow conditions and abutment types shown in Figs. 5-8, 5-9, 5-11 and 5-12.

As shown in Fig. 5-8, the effect of channel slope is that the greater the slope, the smaller is L^*/b . This is true because the maximum backwater is referred to the channel bottom, not to a horizontal datum.

According to Fig. 5-9, the location of maximum backwater is also affected by abutment geometry which is caused by changing the model height. This is due to the fact that the entrance

condition of flow is affected by abutment geometry. If the model were prismatic [such as the vertical-wall model] or cylindrical, the change of model height would not affect the abutment geometry. The effect of abutment geometry due to varying abutment height can be understood from the following illustration:

Fig. 5-10 shows the plan view of both WW abutments and ST abutments. Each type of abutment has two different heights. The shaded area indicates the portion of the abutments submerged under the same depth [$\frac{1}{2}$ ft] of flow. For WW abutments although the horizontal projected area of submergence for the higher model [0.9 ft high] is larger than that for the lower model [0.6 ft high], and is located further upstream than that for the lower model, the flow in the vicinity of the abutments is guided along the same direction for both cases. Hence, the height of the abutment may not affect appreciably the location of the maximum backwater. For ST abutments, not only the projected areas of submergence are not the same for abutments of different height, but also the flow in the vicinity of the abutments is guided along different curvature for abutments of different height. This explains the effect of height of ST abutments on the distance L^* as shown in Fig. 5-9.

Fig. 5-11 indicates that for the VB model, $n = 0.024$, an increase in F_n decreases the ratio L^*/b . On the other hand, Fig. 5-12 indicates for the same abutments and slope but $n = 0.042$, and increase in F_n increases the ratio L^*/b . The variation of L^*/b with F_n in these two figures is not consistent which might be caused by the effect of the channel roughness. At the present, because of limited data, no conclusion can be drawn regarding the effect of F_n on L^* .

From these graphs it can be concluded, however, that the distance of the maximum backwater measured from the abutment entrance never exceeds the theoretical value shown in Fig. 5-7 which is also shown in these graphs. To assume then for a design problem that the location of the maximum backwater exists at a distance as shown in Fig. 5-7, provides a reasonable upper limit.

Fig. 5-13 shows the contours of the water surface elevation above an arbitrary datum in the vicinity of a contracted opening. In general the flow pattern changes with opening ratio, Froude number, and abutment geometry.

Part 2. ENERGY LOSS

The theoretical considerations of energy loss have been presented in Chapter III. They are briefly reviewed here as a guide for discussing the experimental results. Fig. 1-1 is needed for reference.

From section 0 to section I, the flow is entirely within the backwater reach, because the depth is greater than the normal depth, hence the average velocity is less than the normal; therefore, the energy loss is less than that accompanying the normal flow. Notice that there is a steady gain of potential energy compared to that of normal flow within this reach.

From section I to section II the flow converges from a width B to a width b . There is a small amount of energy loss due to separation in zone Ia. The average specific head of section II is assumed to be the same as that of section I, as indicated by Eq 3-18.

$$h_1 + \frac{Q^2}{2gB^2h_1^3} = h_2 + \frac{Q^2}{2gb^2h_2^3} \quad [3-18]$$

Table 5-1 gives the value of $h_1 + \frac{Q^2}{2gB^2h_1^3}$ and $h_2 + \frac{Q^2}{2gb^2h_2^3}$ obtained by using different model data. The difference is not appreciable.

At section II the abutments may cause separation to the flow. Consequently, there is a certain amount of energy loss due to separation, the amount of such loss may or may not be important depending upon the type of abutments, the opening ratio, and the other flow conditions.

TABLE 5-1

Comparison of Specific Head Between Section I and Section II

Run No.	Model Type	Q cfs	b ft	h_1 ft	$\frac{Q^2}{2gB^2h_1^3}$ ft	$H_1 = h_1 + \frac{Q^2}{2gB^2h_1^3}$ ft	h_2 ft	$\frac{Q^2}{2gb^2h_2^3}$ ft	$H_2 = h_2 + \frac{Q^2}{2gb^2h_2^3}$ ft	$\frac{H_1 - H_2}{H_1}$ per cent
301	VB	5.0	5.99	.519	.023	.542	.495	.044	.539	0.55
361	VB	2.5	6.00	.355	.012	.367	.341	.023	.364	0.83
450	VB	2.5	6.00	.532	.005	.537	.524	.010	.534	0.75
459	VB	5.0	6.00	.733	.012	.745	.724	.021	.745	0.00
455	WW	2.5	4.46	.539	.005	.544	.531	.017	.548	0.74
469	WW	5.0	2.44	.888	.008	.896	.792	.104	.896	0.00
498	WW	5.0	4.48	.549	.021	.570	.498	.078	.576	1.05

From section II to III as the flow continues to converge, additional energy loss is due to lateral mixing between the jet and the surrounding water. No information is available about the amount of energy loss within this reach.

Between sections III and IV the energy loss can be divided into three categories:

- a. Energy loss caused by the normal boundary resistance

$$E_{n3-4} = S_0 L_{3-4} \quad . \quad [3-24]$$

- b. Energy loss caused by the excess boundary resistance

$$E_{e3-4} = \frac{\bar{F}_{3-4}}{\gamma B h_n} - S_0 L_{3-4} \quad . \quad [3-25]$$

- c. Energy loss caused by lateral exchange of momentum

$$E_{m3-4} = C_m \frac{[V_3 - V_4]^2}{2g} \quad . \quad [3-19]$$

Under the assumption that the energy loss between section I and section III is equal to the normal energy loss, the distribution of energy loss between section I and IV has been computed according to Eqs 3-19, 3-24 and 3-25, as shown in Figs. 5-14 to 5-17. The distribution curves for VB, WW and ST models are similar. Although the figures are somewhat qualitative, they are quite informative. In general, the following conclusions can be stated qualitatively:

- a. The excess energy loss reaches a maximum of about 20% of the total energy loss when the opening ratio is about 0.5. Either increasing or decreasing the opening ratio M will reduce the energy loss due to excess boundary resistance.
- b. Normal energy loss increases as the opening ratio M increases. At $M = 0.5$, for VB model, it is about 20% of the total energy loss. For WW and ST models, it is about 25% of the total loss.
- c. Energy loss due to mixing decreases as the opening ratio increases. At $M = 0.5$ for all models, it is about 50% of the total energy loss.
- d. The effect of increasing channel bottom roughness is to reduce the percentage of loss owing to lateral mixing, and excess boundary resistance, and to increase the percentage of loss owing to normal boundary resistance.

Part 3. MAXIMUM BACKWATER

The main objective of this research was to determine the maximum backwater depth caused by bridge contractions. In order to understand the problem, a laboratory investigation as described is needed. It has been realized that the laboratory results cannot be applied to the complex prototype problems without modifications based upon engineering judgment. Nevertheless, a thorough understanding of the basic principles involved in the problem is very helpful to those responsible for design.

The logical approach for studying the backwater problem is to consider first the most simplified case. Results obtained from the most simplified case can be used then as a basis for the study of the more complex cases. In accordance with this approach, the discussion of the effect of different crossing conditions on the maximum backwater is presented as follows:

1. Simple normal crossing,
2. Abnormal stage-discharge condition,
3. Dual bridges crossing,
4. Bridge girders partially submerged,
5. Skew crossing,
6. Eccentric crossing,
7. Piers with and without abutments, and
8. Flood plain models

Definition sketches shown from Figs. 1-1 to 1-12 are recommended for reference.

Among the different crossing conditions, the data of simple normal crossings are sufficient for extensive analysis. The data of abnormal stage-discharge condition can be considered

sufficient only for the case that the abnormal condition in a tilted channel is caused by M1-type backwater. The data of other crossing conditions, such as dual bridge crossings and bridge girder partially submerged are not sufficient to permit complete analyses. Different methods of analysis will be discussed for these crossing conditions.

Simple Normal Crossing

The analyses of data pertaining to the simple normal crossings are divided into three parts:

- a. Discussion of variables;
- b. Equation of maximum backwater; and
- c. Empirical curves.

The significance of each independent variable of simple normal crossings will be discussed in order to find the most important ones. The equations of maximum backwater refer to the theoretical equations which have been presented in Chapter III, and will be modified by coefficients based upon experimental data. Empirical curves will be developed by plotting data according to the variables obtained from dimensional analysis and theoretical consideration.

The simplest laboratory condition for this case is obtained by using sharp-edged vertical board models [VB models] in a rectangular flume, see Fig. 4-7. Although the vertical board type of model does not find direct application in highway design practice, it does provide the most convenient means of investigating the relative influences of the basic variables on the maximum backwater.

In this case these variables include the discharge Q , the slope S_o , the roughness k , the width of bridge opening b , and the channel width B . The changes produced by any of these variables can best be demonstrated by a plot of h_1^* vs b , in which the variables have been made dimensionless by dividing by B . The variable under consideration such as Q , k , or S_o is the third variable as shown in Fig. 5-18, Fig. 5-19 or Fig. 5-20 respectively. Since only one channel width was used, these plots do not show the effect of channel width. The plots show that discharge, roughness and slope influence the maximum backwater considerably.

It was shown in Chapter III that the channel roughness and the slope can be eliminated if the normal depth and the normal mean velocity are used. This resulted in the equation

$$\frac{h_1^*}{h_n} = \text{function} \left[\frac{b}{B}, \frac{V_n}{\sqrt{gh_n}}, \frac{V_n h_n}{\nu}, \frac{B}{h_n}, \text{model type} \right] \quad [3-86]$$

If only the VB model is considered, the variable of model type can be eliminated, and Eq 3-86 can be reduced to the following expression

$$\frac{h_1^*}{h_n} = \text{function} \left[\frac{b}{B}, \frac{V_n}{\sqrt{gh_n}}, \frac{V_n h_n}{\nu}, \frac{B}{h_n} \right] \quad [5-1]$$

which contains four dimensionless parameters.

Flume experiments were made by maintaining the Froude number $V_n/\sqrt{gh_n}$ of the uncontracted flow constant, hereafter referred to simply as Froude number F_n . The influence of the opening ratio b/B , and the Reynolds number $V_n h_n/\nu$ on the backwater ratio h_1^*/h_n can be seen from Fig. 5-21. The

theoretical curve based upon Eq 3-53 at $F_n = 0.184$, is also shown for comparison. The parameter b/B has a predominant effect on h_1^*/h_n . The Reynolds number which has only two values, 5.87×10^3 and 1.25×10^4 , seems to have little or no effect on the backwater ratio h_1^*/h_n . Although there is some slight discrepancy between the two sets of data for smaller b/B -values, it cannot be attributed to the effect of $V_n h_n / \nu$, because the smaller the value of b/B , the greater is the curvature of the contracted water surface, and the smaller is the viscous effect. Therefore, the slight scatter may be attributed to experimental error.

In Fig. 5-21, the Froude number was maintained constant by changing the channel slope, from $S_o = 0.0012$ to 0.002 . From this figure, it can be seen that the channel slope does not have any influence on h_1^*/h_n , provided Froude number is used as a variable. The reason, explained in Chapter III, is that the effect of channel slope on the backwater ratio is reflected through the normal flow depth except in the case of horizontal slope $S_o = 0$. The normal depth in a horizontal channel is infinite. Such a case should be considered as an abnormal stage-discharge condition which will be discussed in the next section.

The data for Fig. 5-21 were taken in the same flume, and the width-depth ratio varied from 11 to 16.5 because of the change in depth. Despite the variation in the width-depth ratio B/h_n , however, there is no indication that it affects the backwater ratio h_1^*/h_n .

Thus Fig. 5-21 has demonstrated that the effect of three variables namely, $V_n h_n / \nu$, S_o , and B/h_n on the backwater ratio h_1^*/h_n is not appreciable. The conclusion thus obtained

is probably positive for the parameter $V_n h_n / \nu$ and S_o , but is still uncertain for the parameter B/h_n because it was not varied over a wide range. The effect of Reynolds number on the backwater ratio is commonly known to be small because, both in the flume and in the natural rivers, the Reynolds numbers are large. The conclusion regarding the effect of channel slope on the backwater ratio can be accepted because the variation of tested slope is appreciable despite the fact it was not within the slope range of natural rivers. The conclusion regarding the effect of width-depth ratio is not certain because of the limited range of data. The width-depth ratio in natural streams is usually far greater than that in the laboratory. Therefore, it is recommended that further research in a much wider flume should be done to check the results of the current investigation.

A contraction in an open channel usually creates pronounced surface curvature of the flow. Therefore, the flow pattern in the vicinity of the contraction is influenced significantly by the fluid weight or the Froude number. The data in Fig. 5-21 have demonstrated that Reynolds number, slope, and width-depth ratio [at least tentatively] are not important factors for the problem of backwater. Therefore Eq 5-1 can be reduced to the following expression

$$\frac{h_1^*}{h_n} = \text{function} \left[\frac{b}{B}, \frac{V_n}{\sqrt{gh_n}} \right] \quad [5-2]$$

The effect of the opening ratio $b/B = M$ and the Froude number $F_n = V_n / \sqrt{gh_n}$ on the backwater ratio h_1^*/h_n are shown in Fig. 5-22. The backwater ratio increases with increasing Froude number. Furthermore, for each constant value of

the Froude number, the backwater ratio decreases with increasing opening ratio, as shown in Fig. 5-21 for a single value of F_n .

In order to examine the trend of the variation of h_1^*/h_n with M for different values of the Froude number, the theoretical equation of maximum backwater, Eq 3-53 was plotted as shown in Fig. 5-23. From Fig. 5-23, it can be seen that as M approaches zero, h_1^*/h_n approaches infinity asymptotically for all Froude numbers. Furthermore, all the curves have a point of inflection at intermediate values of M and then h_1^*/h_n decreases suddenly at the larger M -values, because as $M \rightarrow 1.0$, $h_1^* \rightarrow 0$. The group of curves converge as M decreases, and diverge as M increases. Such a trend can be observed also from Fig. 5-22.

A direct comparison between the theoretical equation [Eq 3-53] at $F_n = 0.184$, and the experimental data at the same Froude number can be seen from Fig. 5-21. The data follow the general trend of the theoretical curve. However, there is considerable discrepancy between the data and the theoretical curve. Such discrepancy is owing to the assumptions used in the derivation of the theoretical curve. In order to make use of the theoretical analysis, it is necessary to introduce an empirical coefficient ϕ into Eqs 3-51 and 3-53 as expressed by Eq 3-60 to fit experimental data.

Fig. 5-23 indicates that for a certain Froude number there is a limiting value of M at which h_1^*/h_n goes to zero. The limiting value of M can be obtained through Eq 3-53 by putting $h_1 = h_n$, i.e. $h_1^* = 0$.

The resemblance between Fig. 5-22 and Fig. 5-23 is a further demonstration that analysis of maximum backwater based upon the assumption of critical flow at the contraction is logical and useful.

The variation of Froude number in Fig. 5-22 was obtained by varying the discharge, the channel slope and the channel roughness. If the position of the curves for different values of the Froude number is consistent, it is an experimental proof that the influence of discharge, channel slope, and channel roughness is reflected completely in the Froude number. Figs. 5-24, 5-25 and 5-26 show the variation of h_1^*/h_n with F_n and M based upon the data taken for various discharges, channel slopes, and channel roughnesses. It may be seen that h_1^*/h_n varies consistently with F_n for a constant value of M . Note that in Fig. 5-24 three discharges are indicated by three different symbols; in Fig. 5-25 two slopes are indicated by two different symbols; and in Fig. 5-26 two kinds of roughness are indicated by two different symbols. The consistent variation in these plots verifies Eq 5-2 and the assumption that the influence of discharge, slope, and roughness are included in the Froude number.

Because other types of abutments are more practical than the vertical board, the effect of abutment geometry on the backwater must be studied. Fig. 5-27 shows that the type of abutment influences considerably the backwater ratio. This may be interpreted as indicating that the flow pattern is affected by the entrance condition which depends considerably upon the abutment geometry. The curve for VB abutments is the upper curve in Fig. 5-27; the curve for WW abutments is the lowest; and the curve for ST abutments lies between the two. The position for the curve of the ST abutments depends upon how the opening ratio is defined. The curve shown in Fig. 5-27 is for M defined as the ratio of the average width of the contraction at normal flow depth to the width of the approach channel. Should M be defined as the top-width

divided by the channel width, the curve would be shifted toward the right; and if M is defined as the bottom width divided by the channel width, the curve will be shifted toward the left. For the case of a large ratio of contracted-opening to depth b/h_n , the different definitions of opening ratio M for ST abutments does not affect the value of M appreciably.

Fig. 5-27 shows that for a given normal flow condition, the effect of model geometry on backwater becomes less significant as the opening ratio M decreases. As M becomes small, all three curves tend to approach the same curve, that is, the curve for the VB model. It can be concluded that if other conditions remain constant, the flow pattern at small values of the opening ratio is governed primarily by the opening ratio and is not affected appreciably by the geometry of the abutments.

That the entrance condition of the flow can be changed also by using different heights of abutments has been explained previously, see Fig. 5-10. For WW abutments, the change of entrance condition due to change of abutment height is not significant enough to affect h_1^*/h_n as can be seen from Fig. 5-28. For ST abutments the rather marked effect of abutment height can be seen clearly from Fig. 5-29.

Within the test range, the model length does not have any significant effect on the backwater ratio h_1^*/h_n as shown in Figs. 5-30 and 5-31 for WW and ST abutments respectively.

Equation of maximum backwater:- A study of the measured data from laboratory experiments confirms the result obtained from dimensional analysis

$$\frac{h_1^*}{h_n} = \text{function} \left[\frac{b}{B}, \frac{V_n}{\sqrt{gh_n}}, \text{model} \right] \quad [5-3]$$

Any suitable empirical or theoretical equation for the maximum backwater, therefore, must include the parameters given in Eq 5-3. For an analysis of this type of problem, three basic equations should be considered:

1. The continuity equation
2. The momentum equation, and
3. The Bernoulli equation.

In applying the continuity equation, it is necessary to make assumptions regarding the distribution of velocity and the coefficients of contraction. When using the momentum equation, it is necessary to evaluate the forces exerted by the boundary to the flow in addition to the velocity distribution and the pressure distribution. In applying the Bernoulli equation, it is necessary to evaluate along each streamline the energy loss, velocity distribution, and pressure distribution. All indicate that there are unknown quantities which must be evaluated through experiment.

Eq 3-60 was obtained in Chapter III:

$$\left[\frac{h_1}{h_n}\right]^3 = \frac{3}{2}F_n^2 \left[\frac{9\phi}{4M^2} - 1 \right] \quad [3-60]$$

This equation was based upon the continuity equation and the Bernoulli equation. As pointed out in Chapter III, the coefficient ϕ has three meanings.

- a. It corrects for non-uniform velocity distribution in sections I and II, and non-hydrostatic pressure distribution in section II.
- b. It corrects for the deviation of the actual flow conditions from the conditions of critical depth at the entrance of the contraction.

- c. It corrects for the approximation obtained by neglecting terms of higher order in Eq 3-54.

Because the correction stated under c becomes significant only for values of M larger than 0.8, which is beyond the range of laboratory data, it need not be considered.

According to the correction stated under a, the velocity distributions in sections I and II depend on the opening ratio, the abutment geometry and the Froude number. Hence ϕ is a function of M , F_n and abutment type.

Regarding the correction stated under b, it is noted that the assumption of critical depth at the contraction becomes more realistic, the smaller the value of M and the larger the Froude number F_n . The term $\bar{\phi}$ becomes unity in case the assumption of critical depth at the contraction is fulfilled, therefore for small values of M and large values of F_n the coefficient $\bar{\phi}$ approaches values close to unity. However, correction for non-uniform velocity distribution and non-hydrostatic pressure distribution prevents $\bar{\phi}$ from reaching unity.

By inserting into Eq 3-60 the values of h_1^*/h_n , F_n and M obtained through measurement, $\bar{\phi}$ values can be computed. Fig. 5-32 shows the variation of the $\bar{\phi}$ -values with F_n with M as a third variable for the VB model. These curves indicate the trend that for constant Froude number, the larger the M , the larger the value of $\bar{\phi}$; and for a constant value of M , the smaller the Froude number, the larger the value of $\bar{\phi}$. The $\bar{\phi}$ -value approaches unity for all values of M when F_n approaches unity, and $\bar{\phi}$ approaches infinity for all values of M as F_n approaches zero.

Fig. 5-33 and 5-34 are $\bar{\phi}$ -values as a function of M with F_n as a third variable for WW abutments and ST abutments respectively. These two figures are very similar, which means that the geometric effect of the WW abutments and ST abutments on the $\bar{\phi}$ -value is approximately the same.

Notice that all experimental $\bar{\phi}$ -values shown in Figs. 5-32, 33 and 34 are greater than unity, which means that within the experimental range the flow in the contracted section is not at critical stage, the distribution of velocity is not uniform, and the distribution of pressure is not hydrostatic. Furthermore for the same value of F_n and M , the $\bar{\phi}$ -value from Fig. 3-32 is larger than the $\bar{\phi}$ -value from either Fig. 3-33 or 3-34. Assuming that the correction for the flow in the contracted section, not being at critical stage, is the same for all abutment-types when F_n and M are the same, the larger $\bar{\phi}$ -value for the VB model means that the distribution of velocity deviates more from being uniform, and the distribution of pressure deviates more from being hydrostatic in this case.

It is clear from Figs. 5-32, 5-33 and 5-34 that the $\bar{\phi}$ -value is a function of F_n , M , and model type. For each model an empirical equation of $\bar{\phi}$ expressed as a function of F_n and M can be obtained. Such an equation for either ST or WW abutments, if obtained, does not have appreciable practical use. The equation of the $\bar{\phi}$ -value for the VB model alone will illustrate the function of F_n and M . The method of obtaining such an equation is now explained.

In Chapter III the following equation was given:

$$\left[\frac{h_1}{h_n}\right]^3 = \frac{F_n^2}{F_1^2} \quad [3-53]$$

where

$$F_1^2 = \frac{2}{\frac{3}{M} \sin\left[\frac{\phi}{3} - 30^\circ\right] - 1} \quad [3-51]$$

This equation is for the upper limit of resistance backwater having uniform velocity distribution and hydrostatic pressure distribution in the contraction. Eqs 3-53 and 3-51 show that $[h_1/h_n]^3$ varies directly with F_n^2 , and apparently in a complex way with some function of M . The boundary conditions are:

$$\text{when } F_n = 0, \quad \frac{h_1}{h_n} = 0$$

$$\text{when } M = 1, \quad F_1 = 1, \quad F_n = 1, \quad \text{and} \quad \frac{h_1}{h_n} = 1 \quad [5-4]$$

Assume that $[h_1/h_n]^3$ for the VB model varies practically with F_n^2 and let the function of M of Eq 3-51 change to fit the laboratory data. An equation relating $[h_1/h_n]^3$, F_n^2 and M can be obtained for the VB model from experiments. For the VB model the variation of $[h_1/h_n]^3$ with F_n^2 and M is shown in Fig. 5-35. A series of straight lines can be drawn through the data. The general equation for the straight line is

$$\left[\frac{h_1}{h_n}\right]^3 = GF_n^2 + 1 \quad [5-5]$$

where G is the slope of the straight line and is a function of M . Notice that Fig. 5-35 satisfies the boundary value of Eq 5-4. The best fitting empirical equation for G to satisfy Eqs 5-4 and 5-5 is

$$G[M] = 4.483 \left[\frac{1}{M^2} - \frac{2}{3}(2.5 - M) \right] \quad . \quad [5-6]$$

Substituting $G(M)$ into Eq 5-5 and rearranging terms

$$\left[\frac{h_1}{h_n} \right]^3 - 1 = 4.483 F_n^2 \left[\frac{1}{M^2} - \frac{2}{3}(2.5 - M) \right] \quad . \quad [5-7]$$

By combining Eq 5-7 and 3-60 the equation for $\bar{\phi}$ can be obtained as

$$\bar{\phi} = 1.33 \left[1 - \frac{2}{3} M^2 \left(2 - M - \frac{1}{3 F_n^2} \right) \right] \quad . \quad [5-8]$$

Eq 5-7 is an empirical equation for determining the maximum backwater for the VB model. Substitute

$$h_1 = h_n + h_1^* \quad . \quad [5-9]$$

Eq 5-7 results in

$$\left[\frac{h_1^*}{h_n} \right]^3 = 4.483 F_n^2 \left[\frac{1}{M^2} - \frac{2}{3}(2.5 - M) \right] + 1 \quad . \quad [5-10]$$

The variation of $[h_1^*/h_n]^3$ with $F_n^2 [1/M^2 - \frac{2}{3}(2.5 - M)]$ for VB data is shown in Fig. 3-36. Eq 5-7 is also shown for comparison. It shows that Eq 5-7 fits the data very well. Therefore it can be used to compute the backwater caused by the VB contraction.

Similar to Fig. 5-35, are Figs. 5-37 and 5-38 showing the variation of $[h_1/h_n]^3$ with F_n^2 and M for WW and ST abutments respectively. In these two figures, data for a given M -value do not follow a straight line. This implies that $[h_1/h_n]^3$

does not vary linearly with F_n^2 . This is because the entrance condition of the flow varies with F_n . No attempt has been made to find empirical equations to fit the data because of the limited usefulness of these equations.

Empirical curves:- Based upon Eq 5-7, significant parameters can be developed for presenting data by simple empirical curves. Eq 5-7 can be changed into the following form and still satisfy the boundary conditions as indicated by Eq 5-5.

$$\left[\frac{h_1}{h_n}\right]^3 - 1 = F_n^2 \left[\frac{1}{M^2} - 1\right] G' \quad [5-11]$$

where G' is a new function of M . Comparing Eq 5-11 with Eq 5-7 yields,

$$G' = 2.98 \left[1.5 - \frac{M^2}{M+1} \right] \quad [5-12]$$

A plot of $[h_1/h_n]^3$ with $F_n^2 [1/M^2 - 1]$ has been prepared for the VB model in Fig. 5-39 which indicates that when $F_n^2 [1/M^2 - 1] \rightarrow 0$, $[h_1/h_n]^3 \rightarrow 1$.

The value of $F_n^2 [1/M^2 - 1]$ approaches zero either by letting F_n^2 approach zero or by letting M approach unity. When the value of F_n approaches zero either the normal velocity in the uncontracted channel must approach zero, or the normal depth in the uncontracted channel must approach infinity. In either case the maximum backwater h_1^* caused by channel contraction is insignificant. On the other hand, as the opening ratio M approaches unity the maximum backwater depth h_1 approaches h_n . Data for different Froude numbers fall very well on a single curve. At any point the tangent of the curve

varies with $F_n^2 [1/M^2 - 1]$. The advantage of using Fig. 5-39 instead of Fig. 5-35 is two-fold:

- a. According to Fig. 5-35, interpolation is needed for an M -value other than those indicated by the curves. No interpolation is needed if Fig. 5-39 is used because there is only one curve.
- b. According to Fig. 5-35 extrapolation is needed for $F_n > 0.416$, such extrapolation is not necessary if Fig. 5-39 is used as long as $F_n^2 [1/M^2 - 1] < 2.6$.

The same plot has been prepared for other abutment types as shown in Figs. 5-40 to 5-43, namely for WW 45 degree, WW 90 degree, WW 60 degree and WW 30 degree abutments, and ST 1:1½, ST 1:1, and ST 1:2 abutments. These curves can be constructed with a relatively small number of data. Fig. 5-40 and Fig. 5-41, which are for WW and ST models respectively, indicate that Froude number may enter as a possible third variable. This may be explained by the fact that the entrance condition for a model other than VB changes with Froude number. The advantage of using VB model to simplify the problem is then clearly demonstrated. It can be found from Figs. 5-40, 5-41 that the scatter of data for $[h_1/h_n]^3$ is mostly within 8 per cent, which means 2 per cent for h_1/h_n . Considering the wide range of data, the correlation is exceedingly good.

The curves for different models as shown in Fig. 5-39 to Fig. 5-43 are replotted for comparison in Fig. 5-44 where it may be seen that the VB model gives the largest maximum backwater and the WW60 degree model gives the least maximum backwater if other variables are held constant.

The data for simple normal crossings are listed as Table I in the Appendix B.

Abnormal Stage-Discharge Condition

Abnormal stage-discharge condition at the proposed bridge crossing can be caused by a dam downstream or flood flow in another river whose confluence with the river under consideration is a short distance downstream. In the laboratory, this backwater which is known as an M1 curve can be obtained by raising the tailgate to cause ponding in the downstream section of the flume. The changing of depth due to the effect of an M1 curve varies from maximum at the tailgate to zero at some distance far upstream from the tailgate.

The depth measured at section II is chosen as the reference depth h_A , see Fig. 1-4. After the model was in place, the maximum backwater was measured. The difference between h_1 and h_A is defined as the maximum backwater caused by the contraction.

Experiments for this abnormal condition have been made for VB, ST and WW abutments. Data for this condition are tabulated in Table 2 in Appendix B. For ST and WW abutments, two values of Froude number were used, $F_n = 0.289$ and $F_n = 0.332$. For the VB model $F_n = 0.289$ was used. The range of $[(h_A - h_n)/h_n]$ varies from zero to forty per cent.

In analyzing the simple normal crossing case, graphs showing the variation of $[h_1/h_n]^3$ with F_n^2 and M was found to be satisfactory, see Figs. 5-35, 5-37 and 5-38. The same type of plot may be used for the present case provided the proper depth and Froude number are defined to take into consideration the abnormal stage-discharge effect.

In the case of a simple normal crossing, the reference depth is the normal depth. In case of flow having abnormal stage-discharge, however, the desired reference depth is the depth at the section where the maximum backwater is expected to occur after the contraction is installed. Since the location of the maximum backwater is not generally known, the reference depth has been defined as the depth measured at section II before the contraction is in place. Thus

$$h_A = h_n [1 + \text{ratio of increase at section II}] \quad [5-13]$$

where h_A is the reference depth for the abnormal stage-discharge condition. The reference depth measured at section II is greater than the depth if measured at section I; hence $h_1/h_A < 1$ for $M = 1$. The reference Froude number can be defined as:

$$F_A = \frac{Q}{h_A B \sqrt{gh_A}} \quad [5-14]$$

Plots showing the variation of $[h_1/h_A]^3$ with F_A^2 and M are given in Figs. 5-45, 5-46 and 5-47. In all cases a series of curves can be drawn, these curves do not pass through the point $[h_1/h_A]^3 = 1$ for $F_A = 0$ as compared to the curves for the case of the simple normal crossing. The reason is that h_A and h_1 were not measured at the same section.

For the case that the flow has a horizontal bed, the reference depth h_A can also be taken as the depth measured at section II. However, in this case $h_1/h_A > 1$ for $M = 1$, because the backwater curve is the H2-type instead of M1. Based upon this reference depth, F_A and $[h_1/h_A]$ were computed. Fig. 5-48

shows the variation of $[h_1/h_A]^3$ with F_A^2 and M . The curves do not coincide with those in Fig. 5-35 which is for data from a sloping channel. This discussion leads to the conclusion that data taken in a horizontal channel do not represent flow conditions in sloping channels. Fig. 5-48 does not coincide with Fig. 5-45 which is for an abnormal stage-discharge condition of M1 type of backwater curve.

Data of abnormal stage-discharge conditions are in Table 2 of Appendix B.

Dual Bridges Crossing

Whenever there is heavy traffic crossing a river or a stream, there is usually more than one bridge crossing. Dual bridges may be built for many purposes, such as for highways and for railroads. According to modern development of divided highway construction, two bridges of identical design, placed parallel and only a short distance apart, are becoming more common. It is to be expected that the backwater produced by dual bridges contraction [hereafter called dual contractions] would be higher than that for a single bridge. As the combinations of dual contractions encountered in the field would be innumerable, it was necessary to restrict the model tests to the simplest arrangement, namely: identical parallel bridge crossings normal to the flow, see Fig. 1-5. The abutments were restricted to the WW model and the ST model. The distance between the two bridges was limited to the range permissible in the flume. The maximum backwater h_d^* upstream from the first contraction depends not only upon the variables discussed in the case of a simple normal crossing but also on L_D , the distance between the two bridges.

The effect of L_D on the maximum backwater is reasoned as follows: If $L_D = 0$, the two contractions are represented by one only and the backwater can be determined by the method discussed for the simple normal crossing. If $L_D > 0$, the jet coming from the first contraction enters into a zone of backwater caused by the second contraction downstream. Owing to the effect of higher tailwater depth, there will be a different force-momentum flux, and different energy dissipation for the oncoming jet. Consequently, the maximum backwater h_d^* will be higher than h_1^* which is for a single contraction. If the distance between the two contractions is fairly great, the backwater effect of the second contraction will not affect materially the oncoming jet from the first contraction. Consequently, the maximum backwater will not be affected appreciably. Other conditions remaining the same, there will be a value of $L_D = L_{DC}$ which gives the highest maximum backwater. In this study it is expected to determine the effect of L_D , and to determine the magnitude of L_{DC} . Needless to say, in the design of a dual crossing, the L_{DC} -value should always be avoided.

The magnitude of L_{DC} depends upon such variables as the Froude number, the opening ratio, and the model type. With the limited amount of data, it is not possible to evaluate the effects of all these variables. In this study the opening ratio was varied approximately from 0.35 to 0.75. The length L_D was varied from 0 to 10 ft, which is about 20 times the normal flow depth. The effect of Froude number cannot be studied because of limited data.

Let h_d^* and h_1^* denote the maximum backwater for dual contractions and for a simple normal crossing respectively.

Plots are given, see Figs. 5-49 and 5-50, showing variation of $[h_d^* - h_1^*]$ with L_D and M with a constant Froude number for two WW models and two ST models. The difference $[h_d^* - h_1^*]$ is the increase of maximum backwater due to the existence of the second contraction downstream. The two plots are different from each other, which means that there is an effect due to abutment geometry. Figs. 5-49 and 5-50 indicate that for a given Froude number, abutment type, and spacing of the two bridges, the smaller the M , the larger the $[h_d^* - h_1^*]$. Along any one curve of $M = \text{constant}$, $[h_d^* - h_1^*]$ varies with L_D . Furthermore h_d^* is independent of L_D , therefore h_1^* is the highest, if $[h_d^* - h_1^*]$ is a maximum.

The L_D -value which corresponds to maximum $[h_d^* - h_1^*]$ is designated as L_{DC} according to the definition. Figs. 5-49 and 5-50 seem to indicate that L_{DC} increases with decrease of M because the tailwater depth below the first contraction increases as M decreases, and L_{DC} is expected to increase with the tailwater depth. The range of L_D is not sufficient to determine the L_{DC} value which will give highest backwater.

In analyzing the case of simple normal crossings it was found that by plotting $[h_1/h_n]^3$ with $F_n^2[1/M^2 - 1]$, data of the same abutment type fell along a single curve, see Fig. 5-39 to Fig. 5-43. Another type of plot using $[h_1/h_n]^3 - 1$ and $F_n^2[1/M^2 - 1]$ was made but not reported; it showed that data fell on a straight line, the slope of the line is not 1.0, but varies slightly with abutment geometry. Following such an analysis, data for dual bridges crossing were plotted as $[h_1/h_n]^3 - 1$ against $F_n^2[1/M^2 - 1]$ as shown in Figs. 5-51 and 5-52 for WW and ST abutments respectively. From these two figures, straight, parallel

lines can be obtained for different values of L_D . The third variable L_D is not expressed dimensionlessly because of insufficient data. From dimensional analysis the third variable can be expressed either as L_D/h_n or L_D/B . Only one value of Froude number was used for ST abutments. Three values of Froude number were used for WW abutments -- in which case F_n does not enter as a third variable as can be seen from Fig. 5-51. Empirical equations can be obtained from these two figures. For WW abutments

$$\left[\left(\frac{h_1}{h_n}\right)^3 - 1\right]^{1.305} = C_{WW} F_n^2 \left[\frac{1}{M^2} - 1\right] \quad [5-15]$$

For ST abutments

$$\left[\left(\frac{h_1}{h_n}\right)^3 - 1\right]^{1.25} = C_{ST} F_n^2 \left[\frac{1}{M^2} - 1\right] \quad [5-16]$$

Both C_{WW} and C_{ST} are shown in Fig. 5-53 as a function of L_D . According to the data, the greater the L_D , the greater the coefficient C_{WW} and C_{ST} -- therefore, the higher the backwater. For each type of abutment there must be a value of L_D which creates the highest maximum backwater, it is concluded that the experimental range of L_D is not large enough to give the maximum value of C_{WW} and C_{ST} , corresponding to the highest value of $[h_1/h_n]$. Data for dual contractions are listed as Table 3 in Appendix B.

Bridge Girders Partially Submerged

If the contracted opening is not adequate for a given flood, the backwater will be forced so high that it may overtop

the bridge superstructure or it may partly submerge the upstream girder of the bridge. In the latter case, the contraction due to the bridge crossing acts as an orifice, see Fig. 1-6. The problem of studying backwater then becomes a problem of studying the discharge coefficient of such an orifice.

Laboratory models have been made to study this problem. The bridge girder was substituted by a wooden box of 1-ft width, see Figs. 1-6 and 4-9. The distance z between the bottom of the box and the flume bottom could be varied easily. The length of the box matched with the contracted opening length so that there was no problem of sealing the joints. Both WW and ST abutments were tested. Most tests were made by using $F_n = 0.332$ for the ST abutments, and $F_n = 0.297$ for the WW abutments. The method of studying the maximum backwater by use of the discharge coefficient, with the bridge girder partially submerged, is presented in Chapter VI. By the use of dimensional analysis the ratio of the maximum backwater depth to the normal depth can be expressed by the following variables:

$$\frac{h_1}{h_n} = f \left[M, F_n, \frac{z}{h_n}, \text{abutment type}, \frac{B}{h_n} \right] \quad [5-17]$$

Figs. 5-54 and 5-55 show the variation of h_1/h_n with z/h_n and M for WW and ST abutments respectively. In each of these two figures the abutment type, the Froude number, and the width-depth ratio were held constant. Because of limited data, the series of dimensionless curves cannot be completed. In general it can be expected that along the curve of a constant M , the smaller the value of z/h_n , the greater the magnitude of h_1/h_n . Furthermore, it is expected there is an upper limit of z/h_n

beyond which h_1/h_n remains unchanged. The z -value in this case should be greater than h_2 -- the depth at section II when the bridge girder is not submerged.

In the foregoing analysis the parameters used for analyzing data of dual contractions, and partially submerged bridge girders are derived from the case of simple normal crossing. A new method utilizing the effective opening ratio M^* has been found successful in correlating data of partially submerged bridge girders. This method was found satisfactory also for correlating data of other conditions reported hereafter.

Using experimental data, the backwater depth for the simple normal crossing with certain abutments and under certain flow conditions can be plotted against opening ratio M as a base curve. The measured depth h_1 or h_1^* for a contraction condition other than a simple normal crossing, but with the same abutments and flow conditions, is superposed on the base curve for the simple normal crossing. The opening ratio thus found is called effective opening ratio M^* . In application if the M^* -value is known for a certain contraction, the backwater depth for this contraction can be obtained from the known information of a simple normal crossing.

The method of effective opening ratio can be applied to the case of bridge girders partially submerged as follows: The effective opening ratio M^* under certain flow conditions for WW abutments can be found, and the difference between actual opening ratio and the effective opening ratio $M-M^*$ is plotted against z/h_1 with M as the third variable, see Figs. 5-56. Because h_1 and possibly M^* are functions of Froude number, the Froude number does not appear in Fig. 5-56 as third variable.

In order to use Fig. 5-56, a simple trial and error procedure is needed. By assuming the value of h_1 , the value of M^* can be found from Fig. 5-56. The values of h_1 and M^* should fall also on the base curve of h_1 vs M under the same flow condition with the same abutments. Data for bridge girder partially submerged are included in Table 4 of Appendix B.

Skew Crossing

The skew crossing was obtained by placing the abutments on a skew angle ϕ with respect to the longitudinal direction of the flume, see definition sketch Fig. 1-7. The abutments were installed after the normal flow was established. Measurements indicate that the flow pattern in the vicinity of the contracted section differs considerably from the case of the simple normal crossing -- refer to Fig. 5-13. With the skew crossing, the flow pattern is no longer symmetrical with the center line of the channel, see Fig. 5-57, the water surface contour. The section I, where the maximum backwater h_1 is usually measured, cannot be defined in this case. Data show that the maximum depth may occur at the upstream left or right stagnation points and depends upon the opening ratio and skew angle. Flow depth h_{UL} , h_{UR} , h_{DL} , and h_{DR} were measured at the points P_{UL} , P_{UR} , P_{DL} and P_{DR} respectively, see Fig. 1-7.

There are two ways to orient the face of the model abutment, see Fig. 1-7:

- a. Parallel to the center line of the approaching channel, and
- b. Perpendicular to the center line of the roadway.

It is difficult to conclude which arrangement gives the least

backwater. Case a is suitable for the upstream abutment while case b is suitable for the downstream abutment.

Data for skew crossings were taken for VB, WW and ST abutments, see Table 5 in Appendix B. Skew angles varied at 15 degrees, 30 degrees and 45 degrees. It was found in the tests that a skew angle equal to or less than 15 degrees does not affect appreciably the depth at the stagnation point. Therefore, testing of the 15-degree skew angle was not completed. Froude numbers used were 0.289 and 0.332. For skew crossings the opening ratio M is defined as $M = [b \cos \phi]/B$, where ϕ is the skew angle. In order to obtain a wider range of M -values for ST and WW abutments, it was necessary to alter the abutment for wider openings. This might introduce some uncertainty into the data because the abutment shape is no longer standard.

The method of effective opening ratio M^* was applied to this case. In order to obtain the effective opening ratio, it is necessary to plot a base curve. The base is obtained by plotting the average of h_{UR} and h_{UL} as h_u [for the simple normal crossing] against M for a given model at a given Froude number. The effective opening ratio M^* can be found by superposing on the base curve the reading h_{UR} or h_{UL} of the skew crossing. The corresponding opening ratio is called the effective opening ratio M^* of a skew crossing according to h_{UR} or h_{UL} respectively for a given abutment at a given Froude number. Data of the VB model analyzed by this method is presented in the following to illustrate the procedure.

Fig. 5-58 shows the base curve h_u vs M of the simple normal crossing for the VB model at $F_n = 0.332$. If the value of h_{UR} of the skew crossing at opening ratio M is superposed on the base curve, the effective opening ratio can be obtained.

Fig. 5-59 shows a plot of M vs M^* for VB model at $F_n = 0.332$. Notice that M^* is also a function of skew angle. A straight line $M = M^*$ is drawn for reference. The fact that all data fall above the line means that the effective opening ratio of skew crossings is greater than the actual opening ratio. It is equivalent to saying that for the same opening ratio, the backwater h_{UR} of a skew crossing is less than h_u , the average of water h_{UR} and h_{UL} of a simple normal crossing. The reason for this is that for the same opening ratio of a given channel, the opening width b of a skew crossing is actually greater than that of a simple normal crossing. In general M^* depends upon M , ϕ , F_n and abutment geometry.

Fig. 5-60 is the base curve for the WW abutment at $F_n = 0.332$. Fig. 5-61 is a plot of M vs M^* for the WW abutment with the abutment face perpendicular to the roadway. Fig. 5-62 is a plot of M vs M^* for the WW abutment with the abutment face parallel to the center line of the channel.

From Figs. 5-61 and 5-62, it can be seen that some of the data fall below the line $M = M^*$ -- which means that in this case M^* is smaller than M , i.e., the backwater h_{UR} of a skew crossing is greater than h_u of a simple normal crossing if the opening ratio remains the same. However, such an effect is not important because it happens when ϕ is small or when M is large as shown in these two figures.

Fig. 5-63 is the base curve for the ST abutment at $F_n = 0.332$; Fig. 5-64 is a plot of M vs M^* for the ST abutment with the abutment face perpendicular to the roadway. It shows that M vs M^* is independent of skew angle. Fig. 5-65 is a plot of M vs M^* for the ST abutment with the abutment face

parallel to the center line of the flume. It shows that M^* is generally greater than M , which means h_{UR} is smaller than h_u for the same opening ratio.

Eccentric Crossing

Bridge abutments are almost invariably placed back from the normal low water channel. During floods, however, the river occupies the entire flood plain. The flood plain, however, is not always symmetrical with respect to the normal channel. Consequently, the bridge span becomes eccentric with respect to the axis of the flood plain. The degree of eccentricity e was defined in this chapter as the difference between unity and the ratio of the lengths of the short roadway to the long roadway, see Fig. 1-8. When $e = 1$, it corresponds to a bridge for which only one roadway extends into the river, and when $e = 0$ it corresponds to the case of a normal crossing.

For the VB model degrees of eccentricity varying from zero to unity have been tested. When the eccentricity is unity, the roadway embankment is from one side of the channel only. This case could be treated as a hypothetical case of simple normal crossing by considering the opposite bank of the channel as the center line of the flow and the hypothetical channel has twice the channel width, if the boundary layer developed along the bank is assumed negligible. For practical application, this assumption implies that the bank adjacent to the opening must be straight and hydraulically smooth. Figs. 5-66, 5-67 and 5-68 show the comparison of the magnitude of h_1 between the simple normal crossing and the eccentric crossing of $e = 1$, for VB, WW and ST abutments respectively. Except for ST abutment, the difference in h_1 is negligible.

In the case of eccentric crossing, the maximum backwater h_1^* cannot be determined very simply because of the unsymmetrical flow pattern. For approximation it may be considered still to be on the center line of the opening.

For ST abutments the effect of eccentricity on h_1 becomes more significant as shown in Fig. 5-68. By comparing these three Figures, it can be concluded that among the three types of abutments tested, the backwater depth h_1 caused by eccentricity of ST abutments changes most appreciably, and that caused by eccentricity of the VB contraction does not change appreciably. This indicates that the flow pattern pertaining to the ST abutments is easily affected by eccentricity while the flow pattern pertaining to the VB contraction is least affected by eccentricity.

The effect of eccentricity on the stagnation depth has been studied by use of the method of effective opening ratio. The value of M^* for measured h_{UL} was found from a base plot of h_U with M for simple normal crossing of the same abutment type at the same Froude number. The value of M^* varies linearly with M as shown in Fig. 5-69. Notice that for all cases, M^* is less than M , which means the magnitude of h_{UL} of eccentric crossing is generally larger than that of the simple normal crossing for the same abutments at the same Froude number.

Fig. 5-69 yields a very convenient correlation between normal crossings and eccentric crossings. In order to estimate the effect of eccentricity, the value of M has to be multiplied by a factor of proportionality which is the slope of the straight line. Such a factor depends on the model type, the Froude number, and the degree of eccentricity. More experimental data on the effect of eccentricity on the maximum backwater are needed in order to complete this graph.

The data for eccentric crossings are in Table 6 of Appendix B.

Piers

Most bridges have piers built in the stream channel to support the superstructure. The channel contraction is caused either by piers alone, if the abutments lie outside the channel, or by a combination of piers and abutments.

A study of the effect of piers on the backwater is therefore desirable. The shapes and sizes of piers encountered in practice vary considerably. Only certain common types could be considered in this research. These are:

- a. single shaft circular pier,
- b. double shaft circular pier,
- c. round-ended narrow pier,
- d. round pile bent,
- e. square pile bent, and
- f. H-pile bent.

Detailed descriptions of these piers are shown in Fig. 4-8. Froude numbers of 0.289, 0.298, and 0.332 were used in the testing.

Extensive studies on the backwater caused by piers alone have been made previously by Rehbock [24], Yarnell [36], and Nagler [23]. It is therefore possible to analyze the present data by these methods derived by previous investigators.

If the combined effects of piers and abutments are to be investigated, the problem is considerably more involved: Considerable error may result if the additional backwater caused by piers is assumed to be equal to the difference between the

total backwater and the backwater caused by the abutments. It was pointed out that in the case of a normal crossing without piers, the influence of abutment geometry changes with the flow depth. If this is also true for piers in place, then it is not possible to evaluate separately the additional effect of abutment geometry and the influence of piers on the backwater. This consideration makes clear that it is not possible to apply methods for piers alone to the case of the combination of piers and abutments. A further complication arises from the considerations given in Chapter III for the case of flow around a circular shaft: The head-loss caused by a pier varies not only with the size of the pier but also with the approaching flow conditions. One finds, therefore, that the pier size D , as well as the number of piers N , will enter as separate variables -- i.e., if the additional headloss is expressed by a function of sND/B , where s is a function ϕ of pier shape and size.

From the foregoing considerations, it is concluded that an accurate method of computing maximum backwater for the case of piers with abutments cannot be found without an extensive study. However, owing to the fact that piers cause a relatively small amount of backwater, an approximate but safe method may still be obtained.

It was found that the artificial bed roughness in the throat section is of considerable influence on the backwater. In some cases the influence of the artificial bed roughness in the contracted opening may even be larger than that of piers. A series of tests had been conducted to demonstrate this effect for the case of $b/B = 0.563$ with pile bents, the differences between tests of maximum backwater with and without roughness in the contraction can be seen

from Fig. 5-76. For example, h_1^* was 0.041 ft for the case of WW abutments with bar roughness [$n = 0.024$] in the contraction, and h_1^* was 0.039 for the case of WW abutments, without bar roughness in the contraction. After one pile bent was added, h_1^* became 0.040 for the case without bar roughness, which was still less than h_1^* for the case of no piles but with bar roughness. The effect of bed roughness in the contraction on the maximum backwater becomes more important as the number of piers increases. Notice that in Fig. 5-70, the difference between the two h_1^* -values increases as the number of piers increases. This fact can be used to explain some of the data scatter reported in Table 7 of Appendix B.

Piers only:- It was found that the backwater caused by a few piers is very small and the error of measurement may often be almost equal to the backwater.

The methods available for computing the backwater caused by piers are those of Rehbock [24], d'Aubuisson [36], Nagler [23], and Weisbach [36].

Rehbock [24] assumed the backwater proportional to the velocity head of the unobstructed flow, or

$$h_1^* = C_{RE} \frac{V_n^2}{2g} \quad [2-7]$$

where

$$C_{RE} = [\delta_o - m(\delta_o - 1)] [0.4m + m^2 + 9(m)^4] [1 + F_n^2] \quad [2-7a]$$

where δ_o is a form index of the pier,

m is the contraction ratio = $\frac{ND}{B}$, see Eq 2-9.

For round-ended narrow piers and single round shaft piers the values of the coefficient δ_o computed for present data compare reasonably well with the ones given by Rehbock. Rehbock did not furnish coefficients for other types of piers used in this research. These coefficients for all piers tested have been computed from the data, see Table 5-2. A comparison of computed backwater heights according to Rehbocks coefficient with measured backwater heights is given in Table 5-3. For $Q = 5$ cfs, the backwater computed from Rehbock's formula is smaller than the measured backwater. For $Q = 3$ cfs, the computed backwater is comparable to the measured backwater.

D'Aubuisson assumed the backwater height to be equal to the difference between the velocity head at the pier side, and the velocity head at the section of maximum backwater. For the former he used the velocity head of the normal section multiplied by a factor of proportionality $1/C_{DA}^2$ which depends on the pier type. Thus he obtained the following equation:

$$h_1^* = \left[\frac{1}{C_{DA}^2} \frac{V_n^2}{2g} \right] - \frac{V_1^2}{2g} \quad [2-2]$$

The coefficients C_{DA} from current data compare reasonably well with the ones given by Yarnell [36] for round ended narrow piers and double shaft piers, Yarnell did not give coefficients for other pier types. Coefficients for all piers tested have been computed from present data, see Table 5-2. The backwater heights computed from D'Aubuisson's equation compared unusually well with the measured ones as shown in Table 5-3.

By using the coefficient for round-ended narrow piers $C_{NA} = 0.934$ and for double circular shaft $C_{NA} = 0.892$ as

given by Yarnell, the backwater was computed according to Nagler's backwater formula:

$$Q = C_{NA} b \sqrt{2g} \left[h_n - \theta' \frac{V_n^2}{2g} \right] \sqrt{[h_1 - h_n] + \beta' \frac{V_1^2}{2g}} \quad [2-3]$$

or

$$h_1^* = h_1 - h_n = \frac{Q^2}{C_{NA}^2 b^2 2g \left[h_n - \theta' \frac{V_n^2}{2g} \right]^2} - \beta' \frac{V_1^2}{2g}$$

where θ' is 0.3 according to Yarnell, and β' is obtained from Fig. 2 of Yarnell's report [36]. Table 5-3 shows that Nagler's method does not compare well with the present data. Therefore, Nagler's method was not used. The method of Weisbach has been found unsound by Yarnell [36], therefore, it is not included in this report.

The data for piers only are in Table 7 of Appendix B.

TABLE 5-2

Comparison of Pier Coefficients

Pier Type	Rehbock's form index δ_o			D'Aubisson Coef. K_{DA}		Nagler's Coef. K_{NA}	
	Authors	Yarnell	Rehbock	Authors	Yarnell	Authors	Yarnell
Round Narrow	3.21	3.35	$1.27 + \frac{1}{2} \frac{L}{D}$	1.052	1.079	0.910	0.934
Single Shaft	3.46	-	2.51	1.043	-	-	-
Double Shaft	5.23	6.13	-	0.996	0.991	0.949	0.892
Round Pile	10.51	-	-	0.918	-	0.878	-
Square Pile	10.61	5.03	-	0.928	1.003	0.900	0.885

Note: L = length of piers

D = thickness of piers

Round Ended Narrow Piers - In the experiments by the authors L/D varied from 5 to 20 times. The coefficient is the average value. Yarnell used L/D equal to 4 only.

Square Pile Bents - The models used by Yarnell included bracings whereas the models in the author's experiments had no bracings.

TABLE 5-3

Comparison of Maximum Backwater Computed from Various Formulas

Run No.	Type of Model	N [Number of Piers]	Discharge	M [$=\frac{B-ND}{B}$]	h_n	h_1^* [= Backwater height]			
						Measured Backwater Height	From Rehbock's Method	From d'Aubuisson Method	From Nagler's Method
594	Round	4	5 cfs	.899	0.416	0.007	0.0037	0.0083	0.012
595	Narrow	2	"	.949	"	0.003	0.0017	0.0042	0.007
1120	"	12	"	.921	0.484	0.004	0.0034	0.0033	0.0063
1121	"	16	"	.895	"	0.006	0.005	0.0045	0.0057
1122	"	8	"	.895	"	0.006	0.0034	0.0046	0.0058
1123	"	6	"	.921	"	0.004	0.0024	0.0027	0.0064
1124	"	4	"	.947	"	0.003	0.0016	0.0012	0.0064
1125	"	2	"	.974	"	0.001	0.00074	0.000	0.0055
1133	"	16	3 cfs	.895	0.360	0.004	0.0032	0.0029	0.0040
1134	"	12	"	.921	"	0.002	0.0024	0.0018	0.0044
1135	"	8	"	.947	"	0.001	0.0015	0.0005	0.0014
1136	"	8	"	.895	"	0.002	0.0022	0.0026	0.0035
1137	"	6	"	.921	"	0.001	0.0016	0.0016	0.0022
596	single	4	5 cfs	.848	0.416	0.013	0.0081	-	-
597	shaft	2	"	.924	"	0.007	0.0035	-	-
608	"	2	"	.924	0.484	0.002	0.0025	-	-
609	"	4	"	.848	"	0.008	0.0057	-	-
610	"	2	"	.949	"	0.003	0.0016	-	-
611	"	4	"	.899	"	0.006	0.0035	-	-
1110	"	2	"	.974	"	0.006	0.00075	-	-
1111	"	4	"	.947	"	0.003	0.00152	-	-

TABLE 5-3 -- Continued

Run No.	Type of Model	N [Number of Piers]	Discharge	M [$=\frac{B-ND_1}{B}$]	h_n	h_1^* [= Backwater height]			
						Measured Backwater Height	From Rehbock's Method	From d-Aubuisson Method	From Nagler's Method
1112	single shaft	6	5 cfs	.921	0.484	0.006	0.00248	-	-
1113	"	8	"	.895	"	0.008	0.00346	-	-
1126	"	8	"	.947	"	0.002	0.0015	-	-
1127	"	12	"	.921	"	0.003	0.0025	-	-
1128	"	16	"	.895	"	0.003	0.0035	-	-
1145	"	16	3 cfs	.895	0.360	0.003	0.0022	-	-
1147	"	12	"	.921	"	0.001	0.0016	-	-
1151	"	8	"	.895	"	0.002	0.0022	-	-
1152	"	6	"	.921	"	0.001	0.0016	-	-
1154	"	4	"	.947	"	0.001	0.0010	-	-
623	double shaft	2	5 cfs	.926	0.484	0.006	-	0.0063	0.0097
624	"	2	"	.949	"	0.004	-	0.0045	0.0094
1114	"	8	"	.895	"	0.011	-	0.0081	0.0098
1115	"	6	"	.921	"	0.005	-	0.0039	0.0098
1116	"	4	"	.947	"	0.008	-	0.0039	0.0098
1129	"	16	"	.895	"	0.007	-	0.0077	0.0128
1130	"	12	"	.921	"	0.006	-	0.0055	0.0097
1131	"	8	"	.947	"	0.004	-	0.0039	0.0094
1132	"	4	"	.974	"	0.001	-	0.0020	0.0085
1146	"	16	3 cfs	.895	0.360	0.006	-	0.0043	0.0061
1148	"	12	"	.921	"	0.003	-	0.00396	0.0061
1149	"	8	"	.947	"	0.001	-	0.00363	0.0058
1150	"	8	"	.895	"	0.004	-	0.00428	0.0059
1153	"	6	"	.921	"	0.002	-	0.00394	0.0062
1155	"	4	"	.947	"	0.002	-	0.00363	0.0059

TABLE 5-4
Shape Factor for Piers with Abutments

Abutment Type	D/h _n Diameter of the Piers Normal Depth	s = Pier Shape Factor				
		Single Shaft	Double Shaft	Round Nar- row	Round Pile	Square Pile Bents
Wing-wall	0.10	-	-	-	0.944	1.08
	0.15	0.412	0.722	0.458	1.30	1.80
	0.20	0.404	0.722	0.500		
	0.25	0.405	0.720	0.516		
	0.30	0.414	0.732	0.536		
	0.35	0.428	0.746	0.560		
	0.40	0.450	0.770	0.590		
	0.45	0.478	0.798	0.624		
	0.50	0.510	0.828	0.668		
	0.55	0.554	0.864	0.712		
	0.60	0.598	0.904	0.760		
Spill-through	0.10	0.180	0.390	0.340	0.77	1.02
	0.15	0.274	0.470	0.420		
	0.20	0.344	0.540	0.480		
	0.25	0.400	0.588	0.538		
	0.30	0.456	0.636	0.578		
	0.35	0.498	0.674	0.616		
	0.40	0.530	0.700	0.648		
	0.45	0.558	0.724	0.670		
	0.50	0.580	0.744	0.688		
	0.55	0.600	0.760	0.708		
	0.60	0.616	0.776	0.720		

Piers and abutments:- The head loss caused by piers in addition to the abutments will be a function of the properties of the piers and abutments and the properties of the flow. The pier properties are the size D , the shape, and the number of piers N . Since the size and number of piers are predetermined, the only factor that can be adjusted to fit experimental results is the shape factor.

By use of the pier shape factor the method of effective opening ratio can be applied to this case as follows:

The effect of the piers is to increase the backwater as compared to that of the simple normal crossing. One might therefore assume that the effect of piers is expressed through a decrease of M of the normal crossing case, designated by M^* . The difference $M - M^*$ is a function of the properties of the piers and abutments and of the properties of flow. It was assumed that

$$M - M^* = s \frac{ND}{B} \quad , \quad [5-18]$$

where s is a function of pier shape, pier diameter, abutment geometry, and unobstructed flow conditions. In order to determine s from the data, Eq 5-18 can be written as

$$s = [M - M^*] \frac{B}{ND} \quad . \quad [5-19]$$

For each run, M^* was determined from a base plot of h_1^* vs M of simple normal crossing without piers by superposing the h_1^* -value of the same crossing conditions with piers. The coefficient s was plotted against D/h_n as shown in Figs. 5-71 and 5-72. Although the data scatter somewhat, an average curve

correlating s with D/h_n can be drawn for each combination of abutment type and pier type. These two figures indicate the effect of abutment type changes on the trend of s vs D/h_n . The s -value for pile bents differs considerably from the one for piers. Based upon these two figures, the average value of s for all the pier types and abutment types tested are summarized in Table 5-4.

In order to use the method of effective opening ratio to estimate the maximum backwater, it is necessary to compute the effective opening ratio M^* , by using the formula

$$M^* = M - s \frac{ND}{B} \quad [5-20]$$

where s is taken from Figs. 5-71 or 5-72 or Table 5-4, according to the abutment type. After M^* has been obtained, the backwater h_1^* can be computed by using the method described for the case of a simple normal crossing. Fig. 5-73 is for WW abutments at $F_n=0.332$. Type of piers is the third variable in these figures. The curve is the computed h_1^* based upon M^* . This curve is in fact also the base curve of h_1^* vs M for the same flow condition without piers, where M is defined as b/B . The measured backwater h_1^* are shown as data. The agreement is satisfactory. Fig. 5-74 is another sample but for ST abutments.

The method of effective M can be extended to dual bridges crossing with piers. From analysis it was found that the coefficient s which is derived from the simple normal crossing with piers can also be used for these cases.

In the case of a skew crossing, the effective M , i.e., M^* was calculated according to Eq 5-20, in which s is the same as that for a simplified normal crossing with piers, and $M = [b \cos \phi] / B$. The measured backwater $[h_{UR} - h_n]$ is plotted against M^* as compared to the curve of skew without piers shown in Fig. 5-75. The agreement between $[h_{UR} - h_n]$ measured and $[h_{UR} - h_n]$ predicted is very good.

This finding permits the conclusion that the coefficient s derived from data of the simple normal crossing with piers is dependent upon the abutment type, the pier type, and the ratio of D/h_n ; and is independent of such variables as Froude number and opening condition.

Data of maximum backwater caused by piers and abutments are in Table 7 of Appendix B.

Flood Plain Models

In order to simplify the problem, most of the model tests in this research were performed in a rectangular channel having uniform roughness. Natural waterways, however, seldom have rectangular channels. Rivers confined within the main channel during low flow may extend to the wide flood plain during flood. The roughness of the main channel may be considerably different from that of the flood plain. Trees and vegetation on the flood plain tend to produce a roughness which is greater than that of the main channel.

Some experiments have been conducted to explore the possibility of applying results obtained in rectangular channels to the cases consisting of a main river channel and a flood plain. These tests are referred here as the ones for flood plain model.

The experiments on composite area were performed on a flood plain of 7.9 ft width, having a main rectangular channel which is 1.97 ft wide in the center and is 0.354 ft below the flood plain, see Fig. 1-11. The roughness arrangement was a combination of bar and baffle roughness, as VB model WW and ST abutments were used in the study.

Because the channel cross-section is not rectangular, the method developed for normal crossing has to be modified before it can be applied to the case of a flood plain model. This requires new definitions for Froude number, opening ratio, and normal depth. These definitions should satisfy two conditions:

- a. If applied to rectangular channels, the terms should reduce to the ones previously employed for analysis of the simple normal crossing.
- b. The definition of the terms should be based on data which are accessible to the designing engineer, such as rating curves and topographic maps.

Although the data on the flood plain model are not sufficient to draw definite conclusions, a reasonable correlation seems possible by using the method of effective opening ratio M^* , if the following definitions are employed, see Fig. 1-12.

- a. The normal depth is defined as twice the distance from the normal water surface to the center of gravity of the cross-sectional area below the normal water surface.
- b. The mean velocity is defined as the total discharge divided by the cross-sectional area below the normal water surface.

- c. The opening ratio M is defined as the ratio of the contraction area below the normal water surface to the uncontracted cross-sectional area of the flow below the normal water surface.
- d. The Froude number was based on the depth defined above and the mean velocity.

The plots of M vs M^* are given in Figs. 5-76 to 5-78. The data do not suffice to draw final conclusions. However, the following may be stated tentatively:

- a. For the VB model, the conservative design is to use $M = M^*$. The line $M = M^*$ fits the data of $F_n = 0.337$ rather well. However, the data of smaller Froude number deviate considerably. This deviation is on the safe side. That is, a larger backwater will be obtained if $M = M^*$ is used.
- b. For the WW model, a straight line relation exists between M and M^* around which there exists some scatter. This straight line deviates from $M = M^*$ which means that M should be defined so that for large openings the value of M decreases whereas for small openings it increases.
- c. The same trend as that for the WW model can be observed for the ST model. However, owing to the pronounced effect of the baffle roughness, the data deviate in a consistent manner from the straight line.

In conclusion it may be stated that further investigation and more data are needed in order to correlate the data for the flood plain model to those for the normal crossing.

Data of flood plain model are listed as Table 8 in Appendix B.

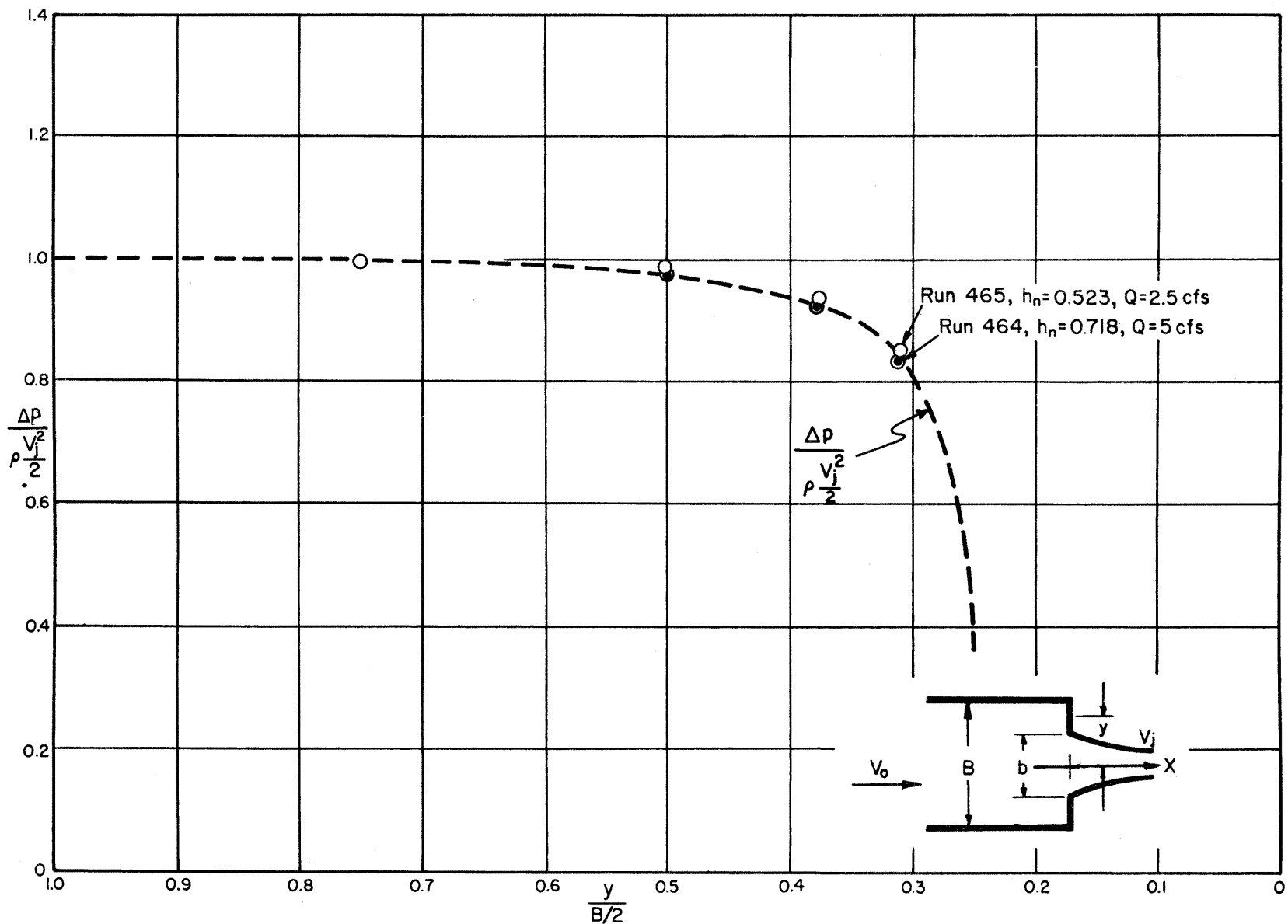


Fig. No. 5-1 Water surface profile along the upstream face of the embankment for vertical-board model.

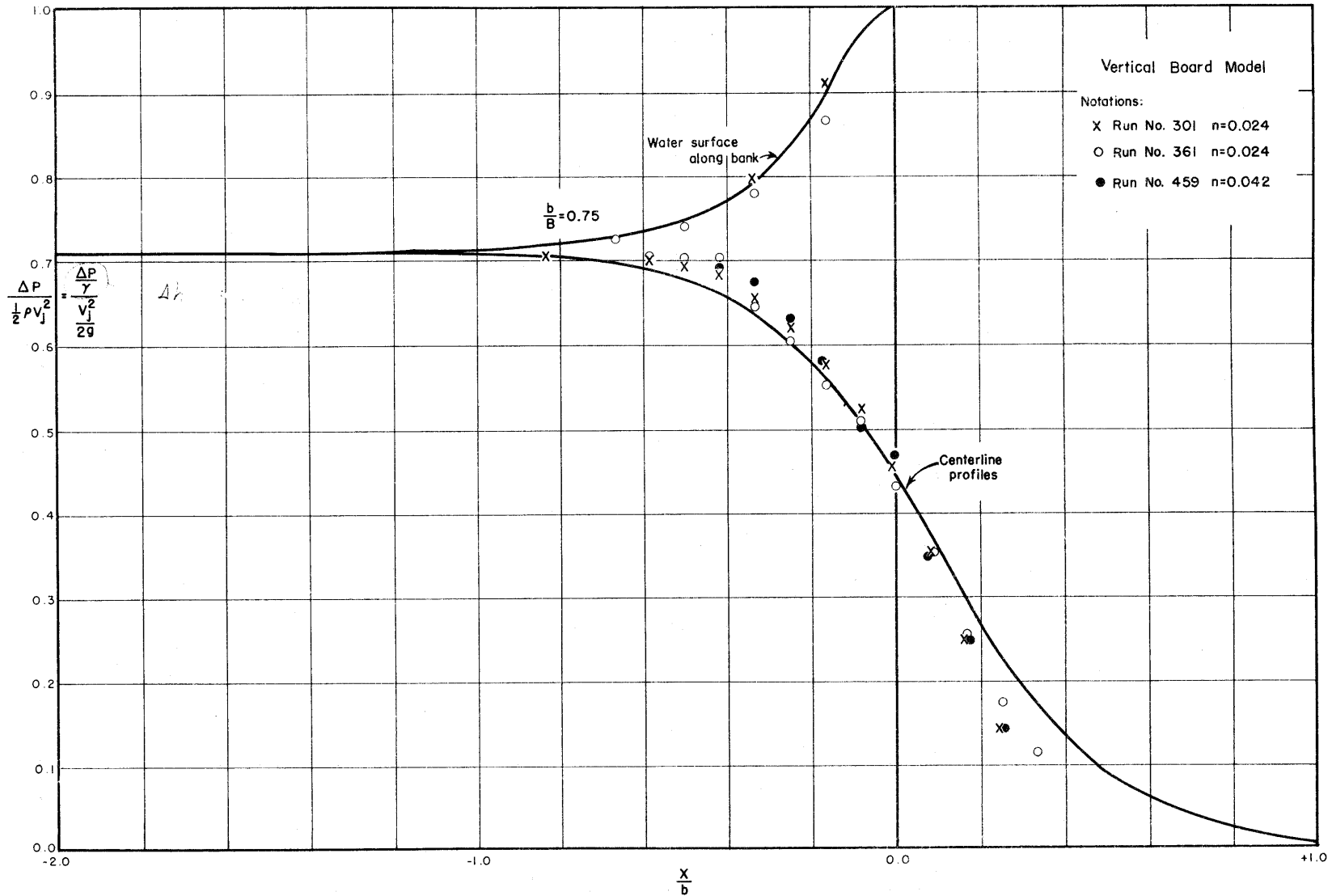


Fig. No. 5-2 Water surface profile along the centerline for vertical board model

Fig. 122

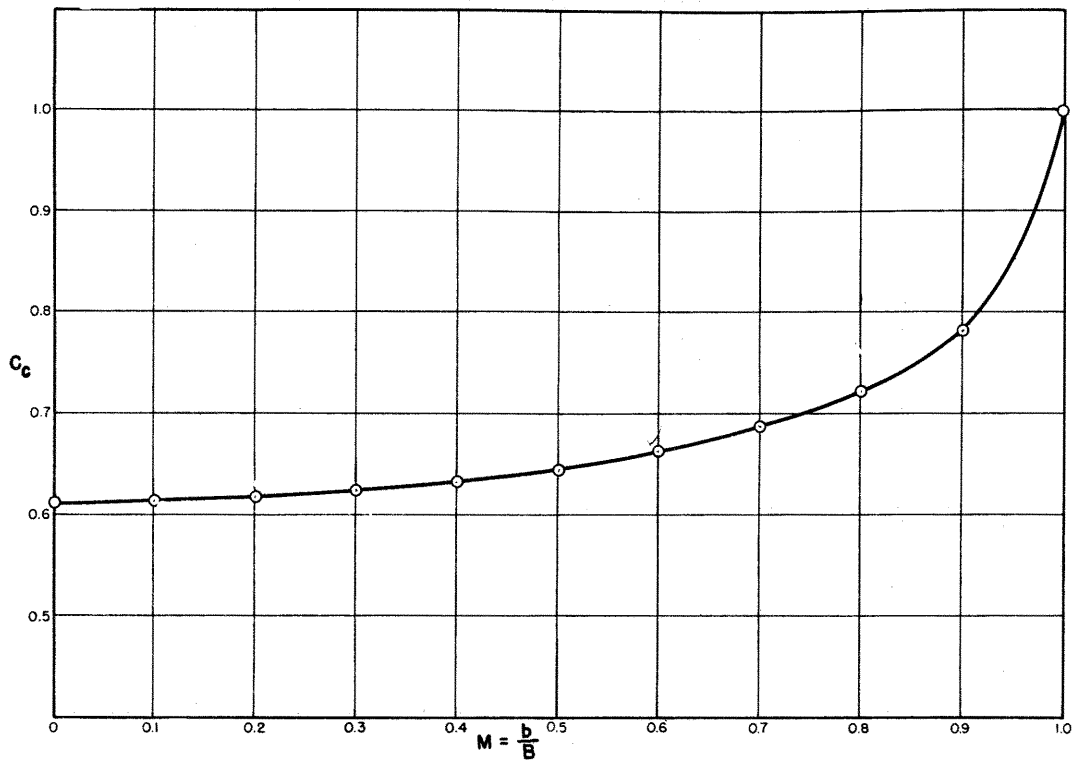


Fig. No. 5-3 Variation of theoretical coefficient of contraction C_c with opening ratio M [after von Mises]

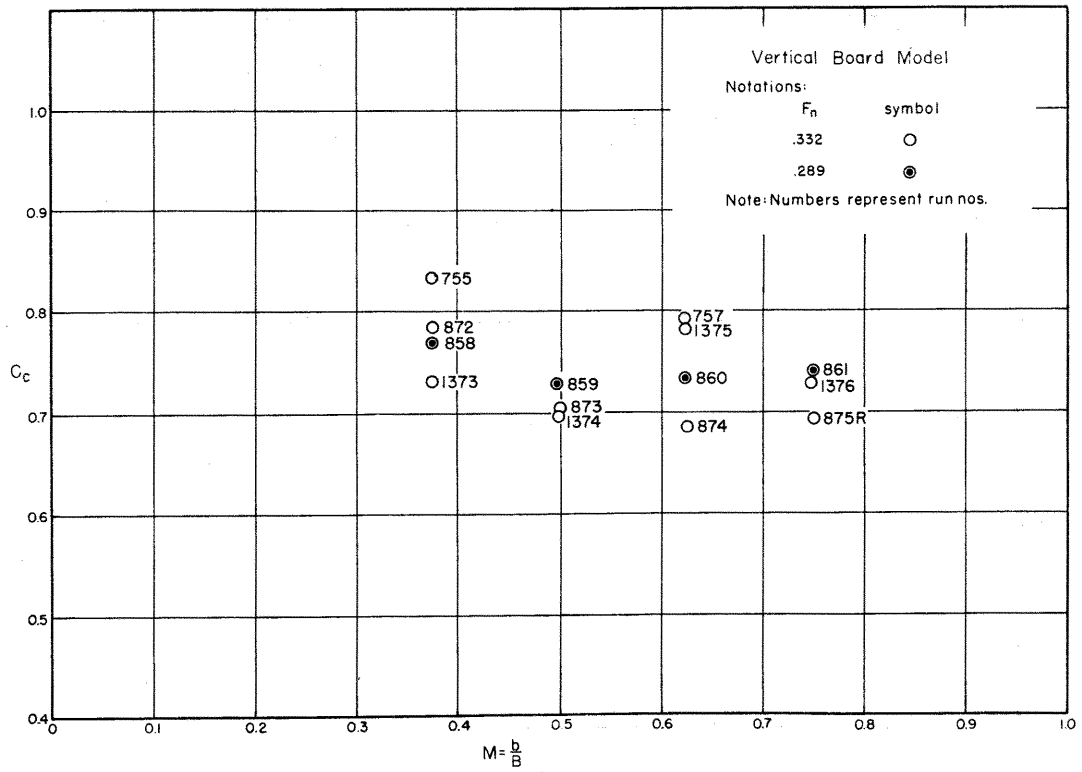


Fig. No. 5-4 Variation of experimental coefficient of contraction C_c with opening ratio M for vertical-board model.

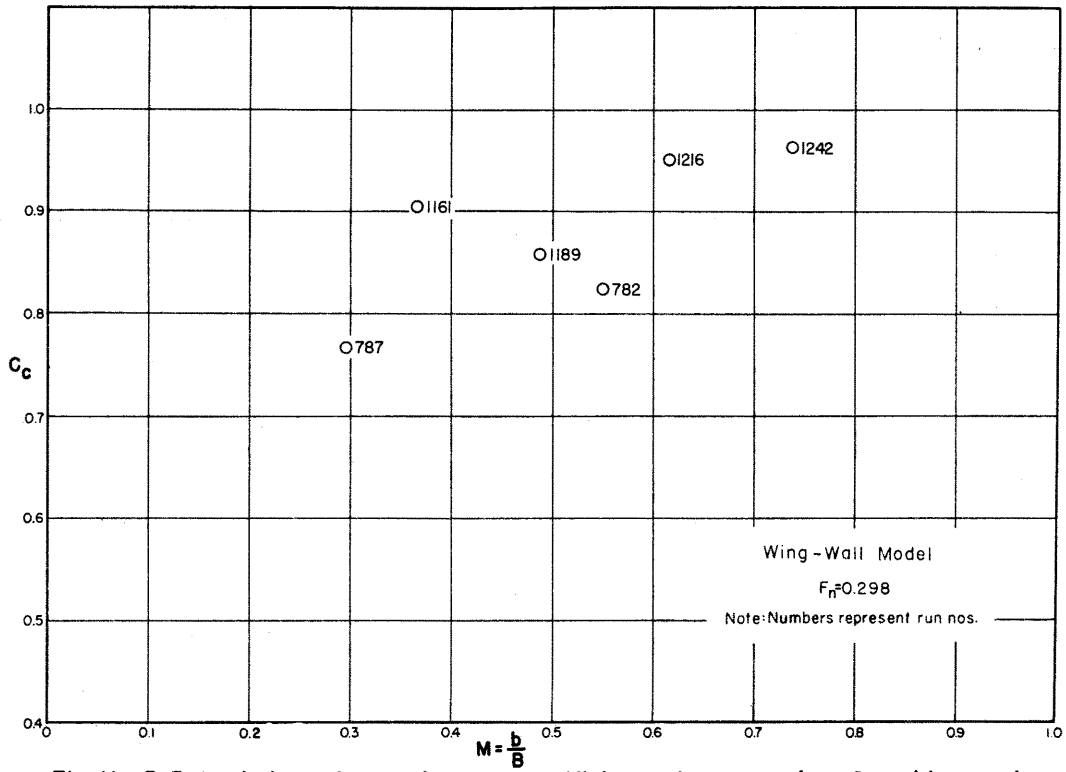


Fig. No. 5-5 Variation of experimental coefficient of contraction C_c with opening ratio M for wing-wall abutments.

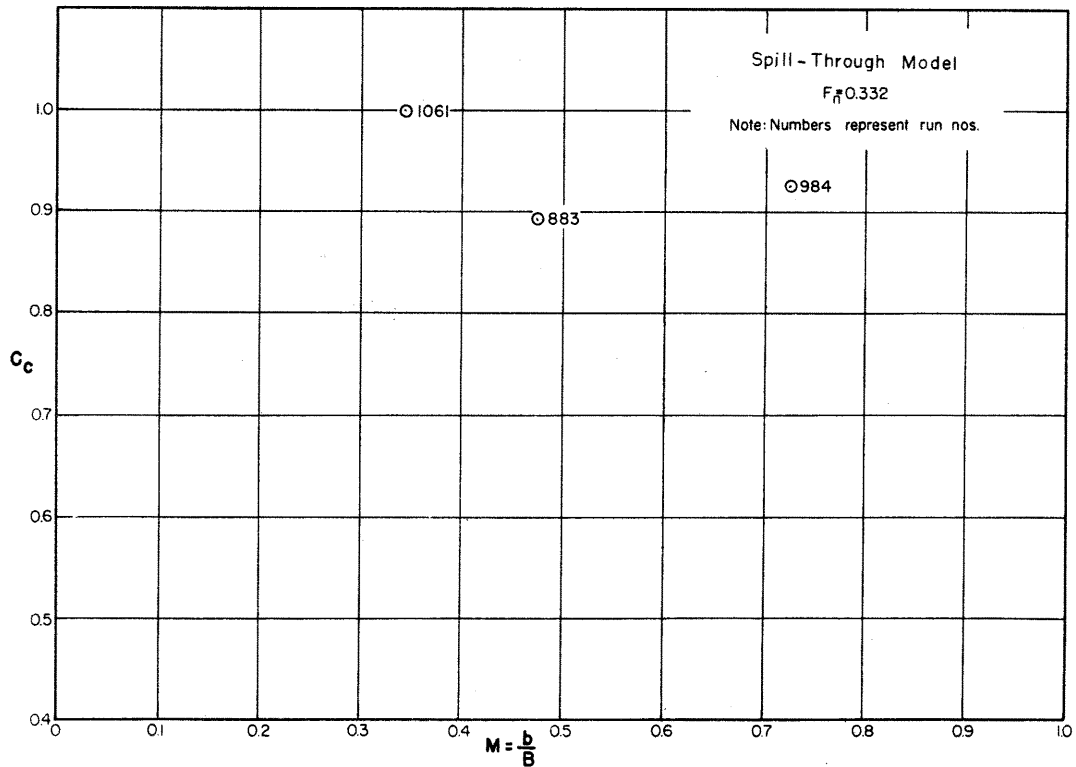


Fig. No. 5-6 Variation of experimental coefficient of contraction C_c with opening ratio M for spill-through abutments.

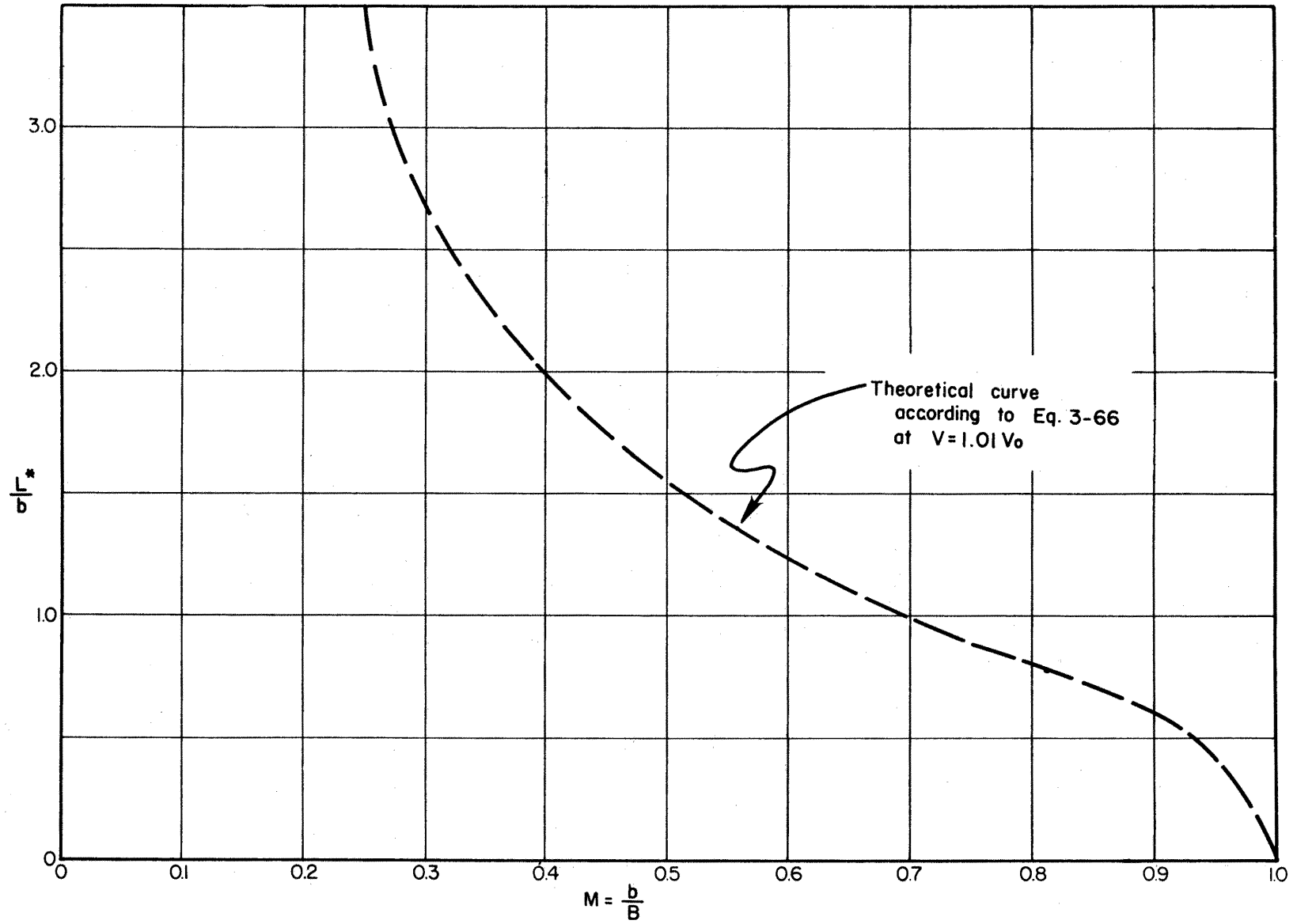


Fig. No. 5-7 Approximate location of maximum backwater

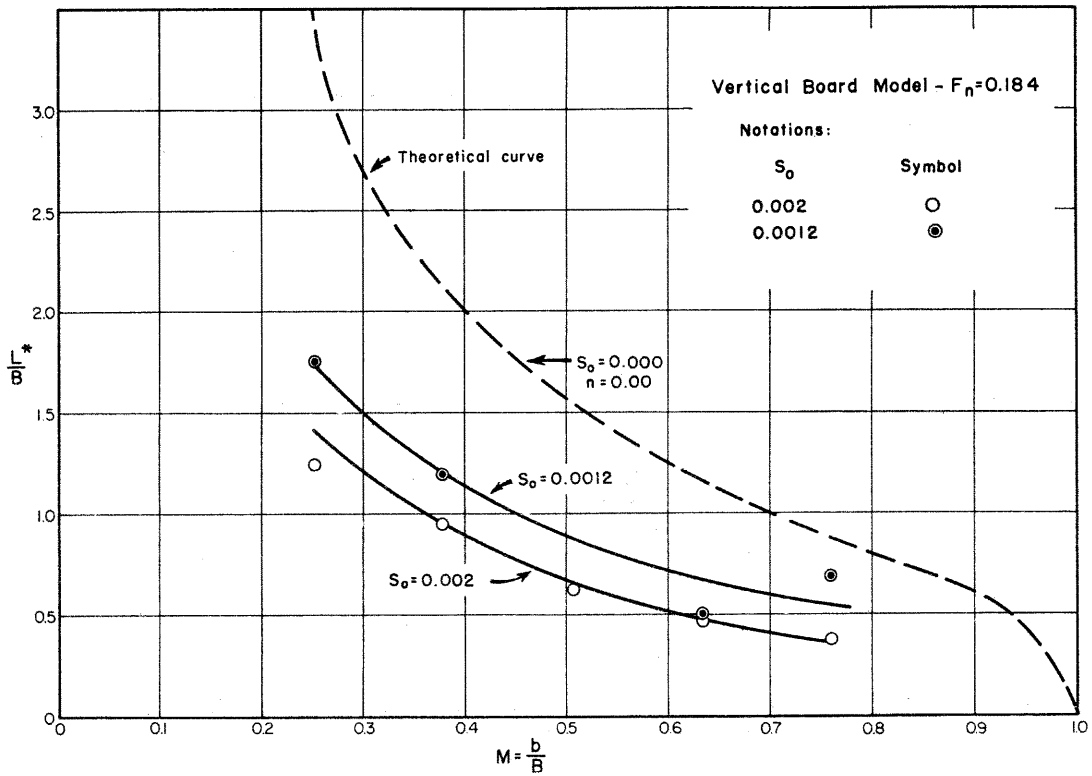


Fig.No.5-8 Effect of channel slope on the location of maximum backwater.

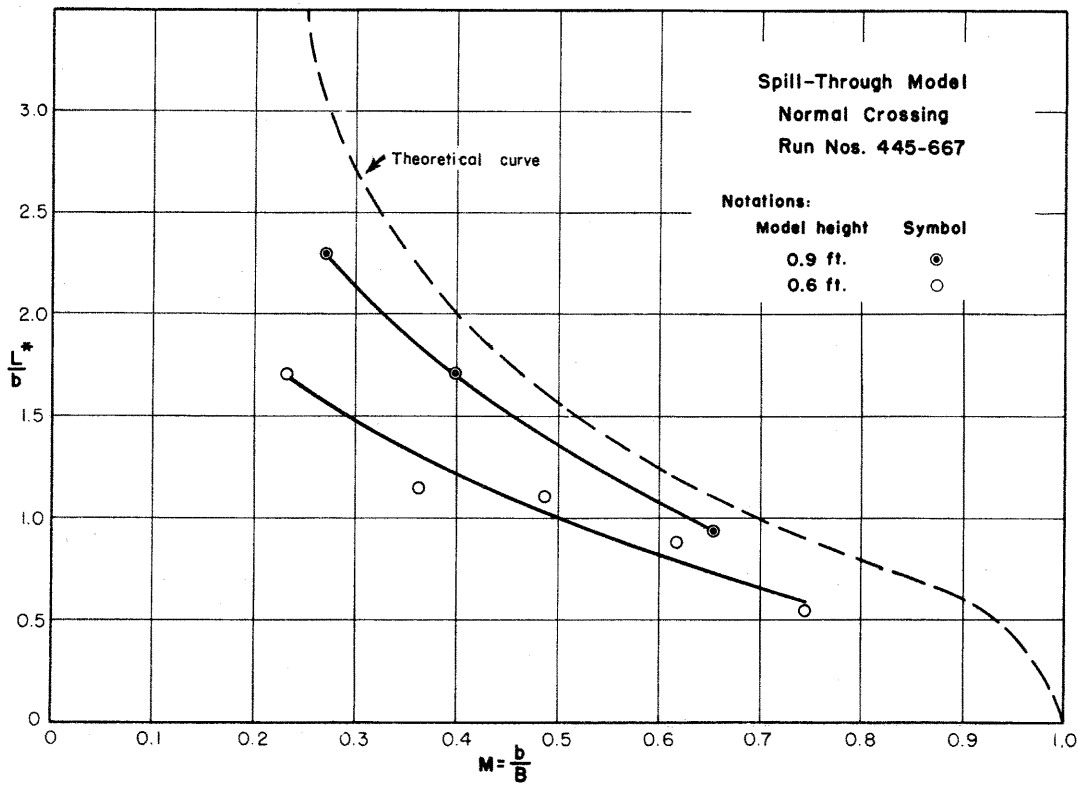


Fig.No.5-9 Effect of abutment geometry on the location of maximum backwater.

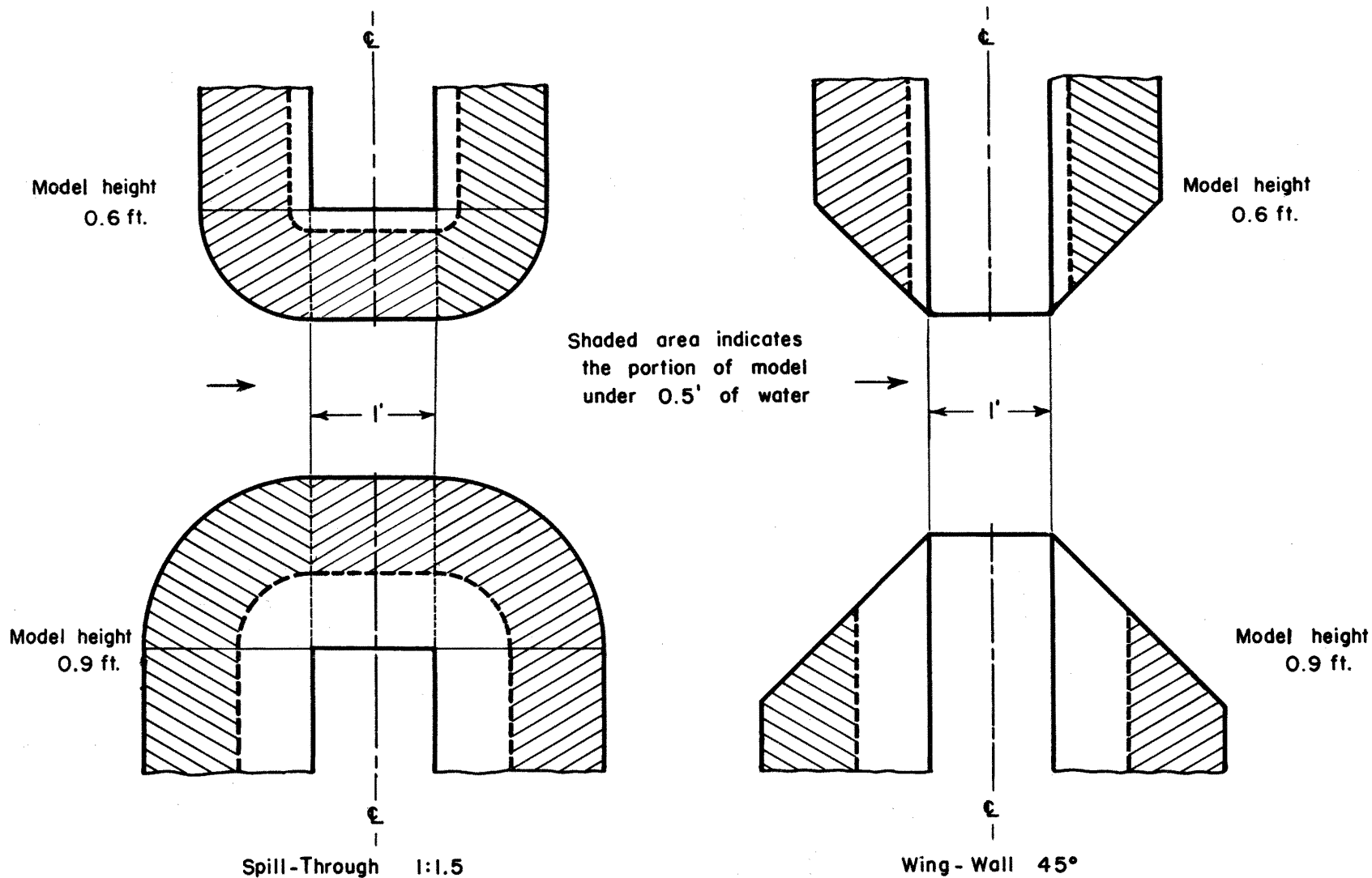


Fig.No.5-10 Effect of abutment geometry due to height of model on the entrance conditions of flow.

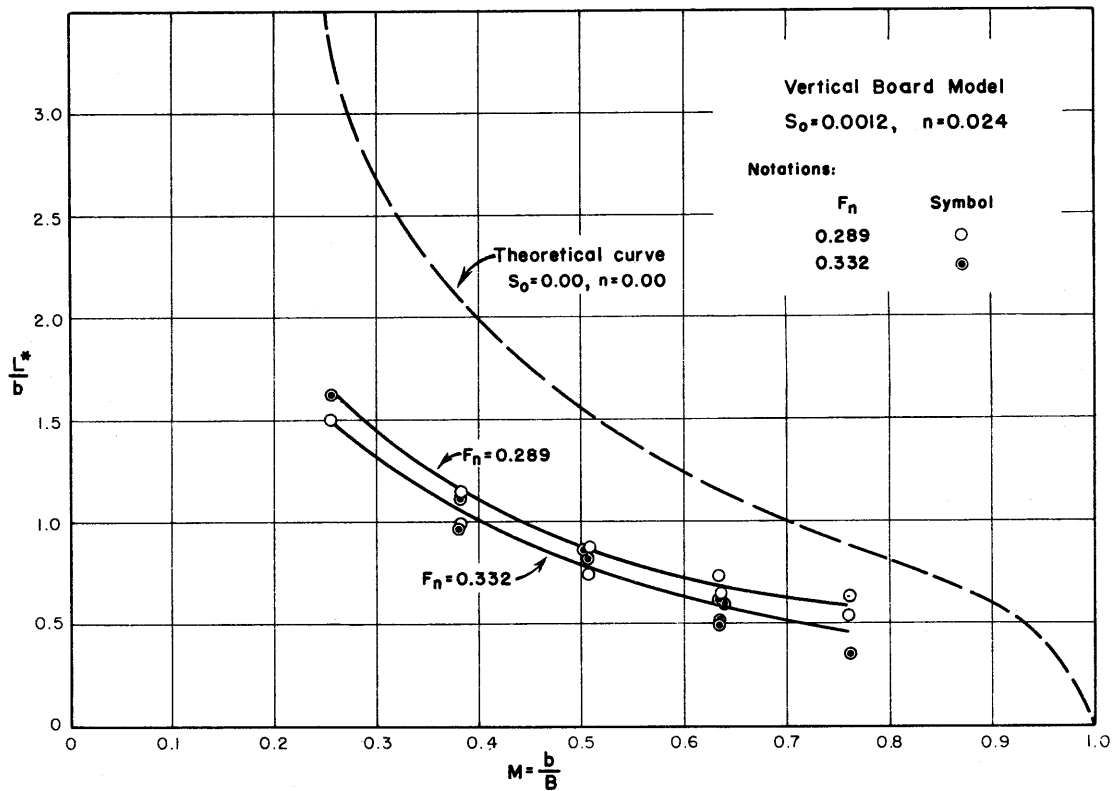


Fig.No.5-11 Effect of Froud number on the location of maximum backwater [$n=0.024$]

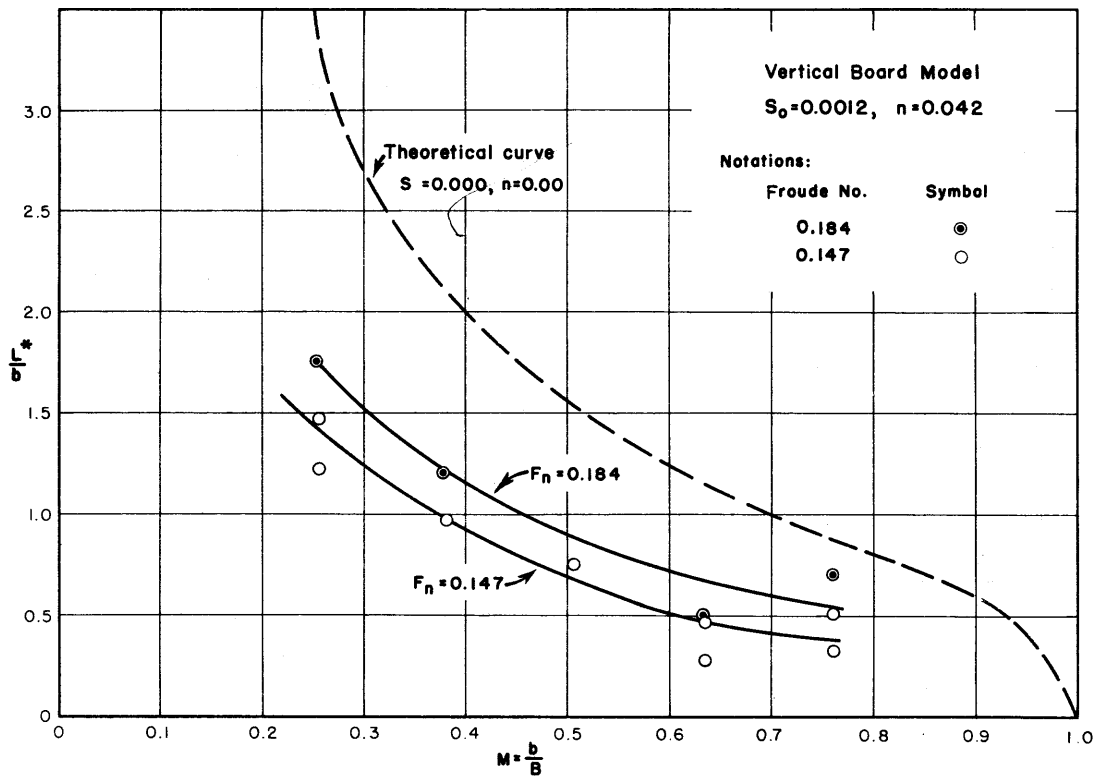


Fig.No. 5-12 Effect of Froud number on the location of maximum backwater [$n=0.042$]

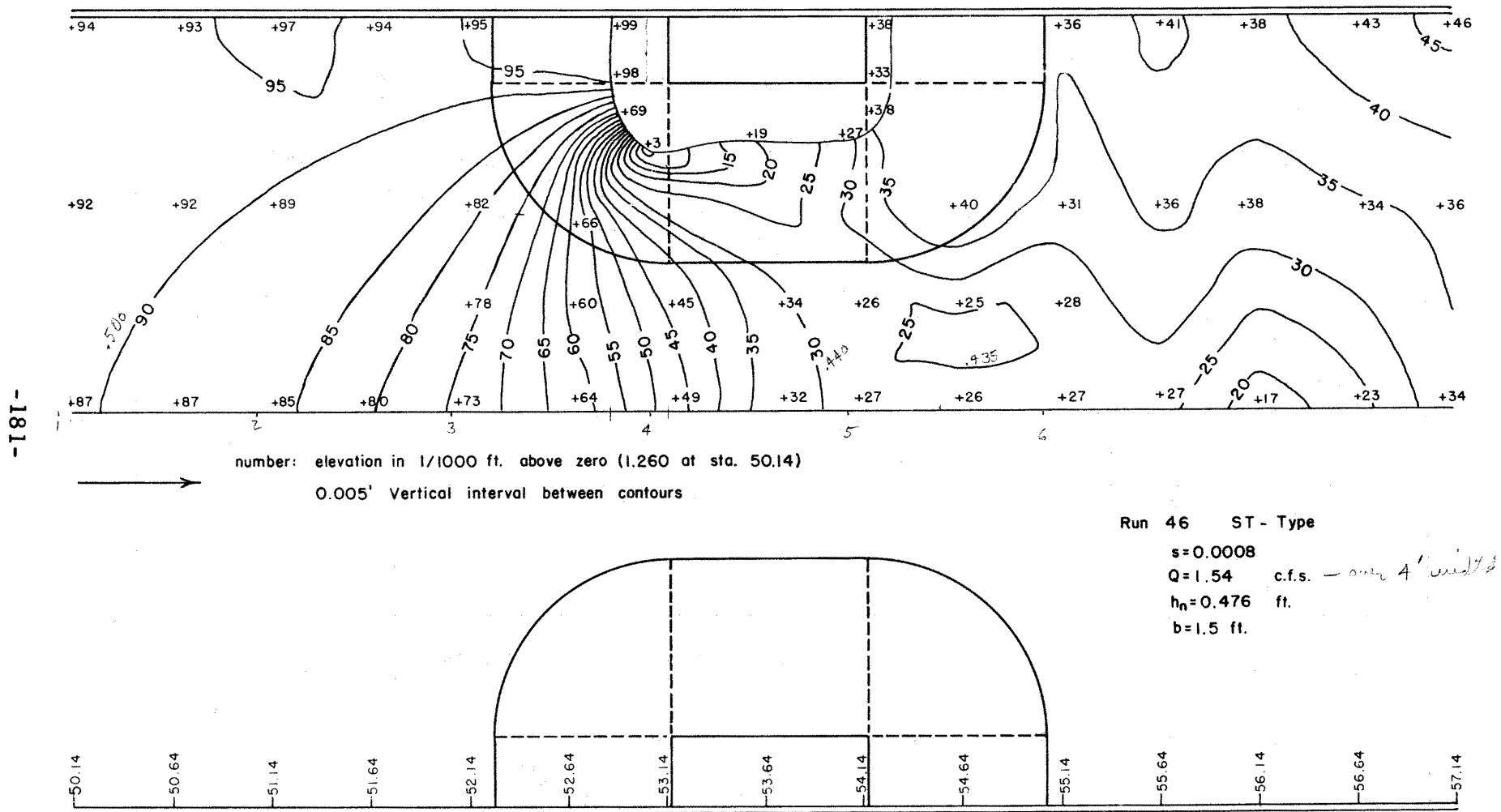


Fig. No. 5-13 Flow pattern of a simple normal crossing for spill-through abutments

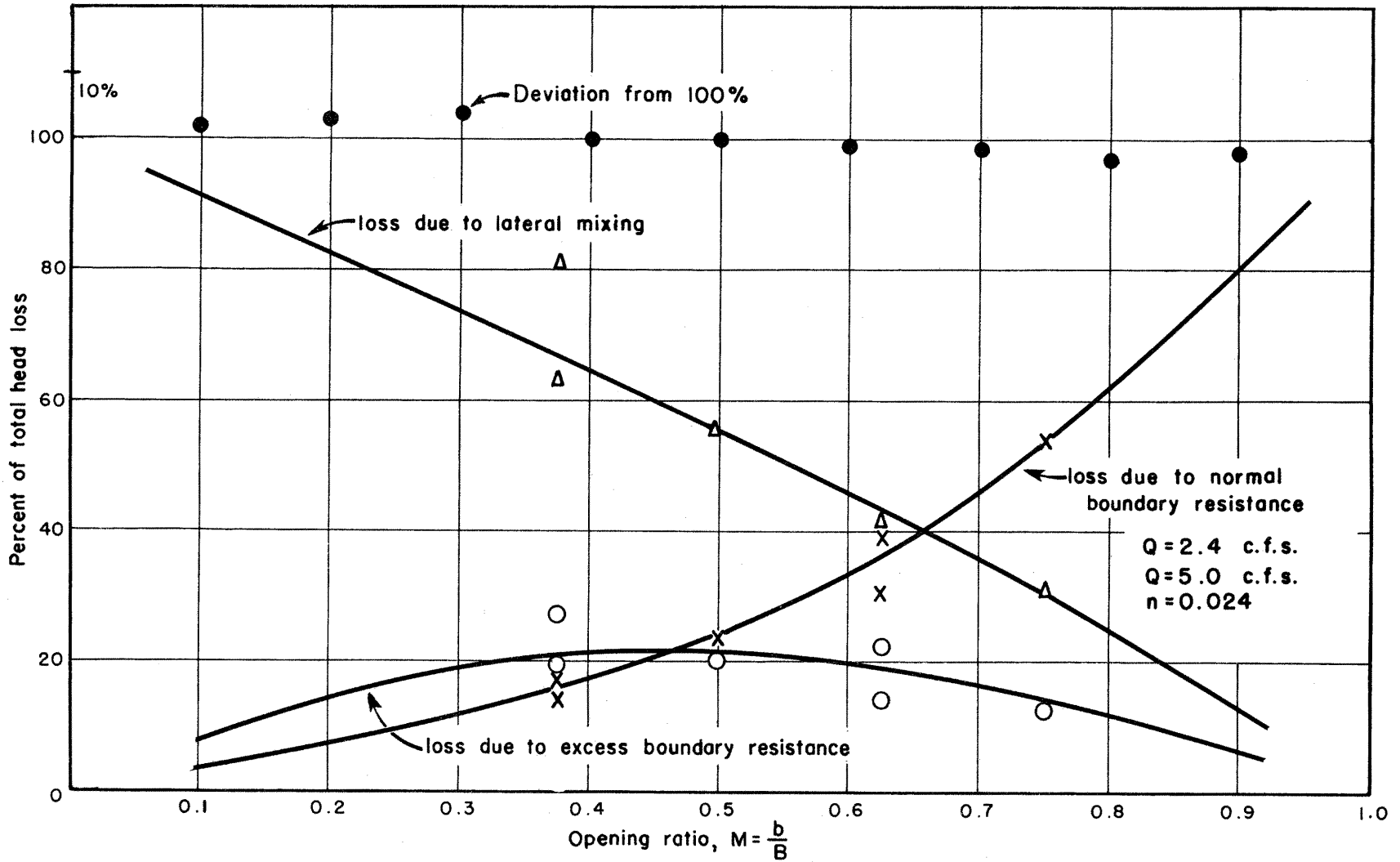


Fig. No. 5-14 Breakdown of energy losses for vertical-board model when $n=0.024$.

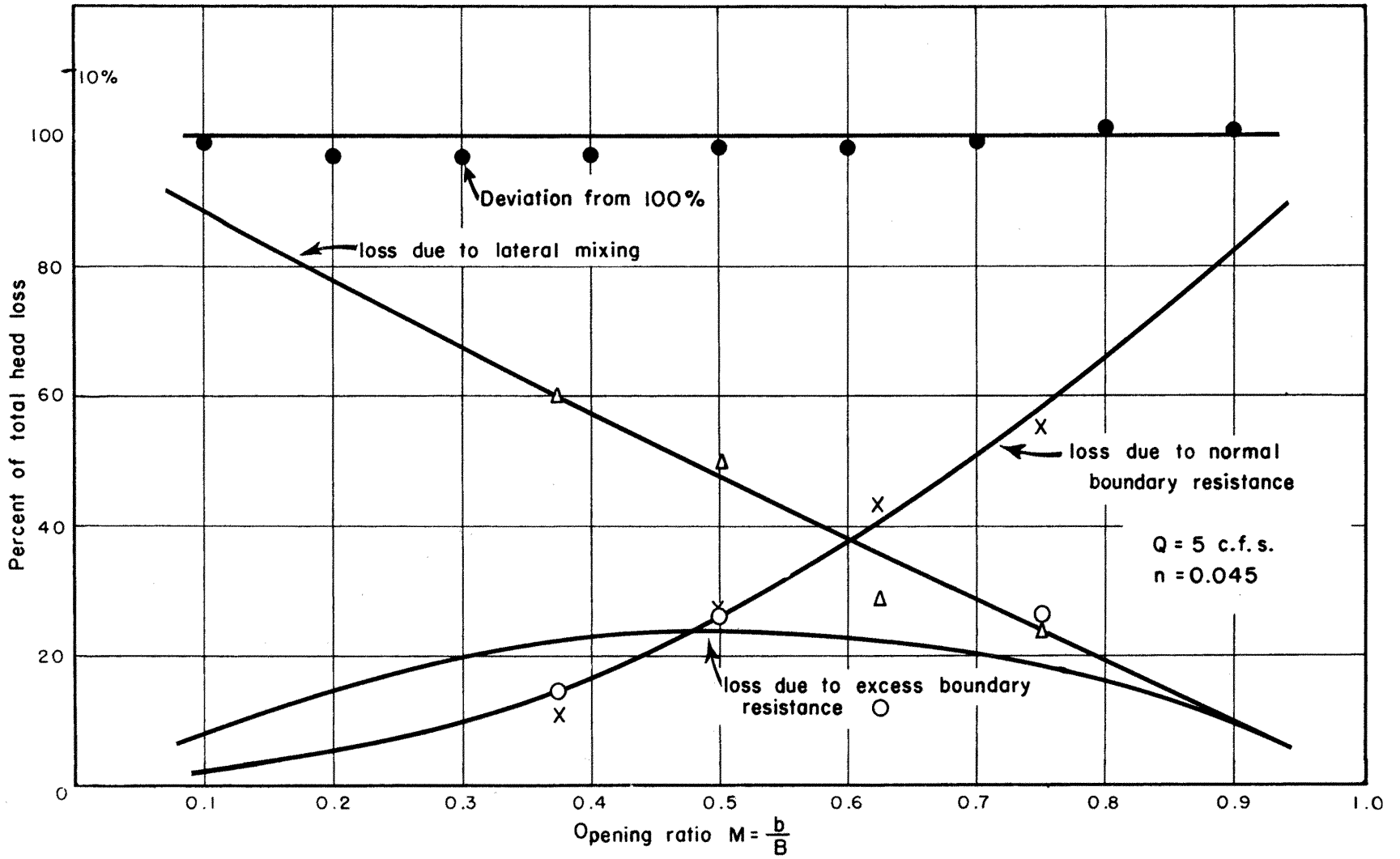


Fig. No. 5-15 Breakdown of energy losses for vertical-board model when $n=0.045$.

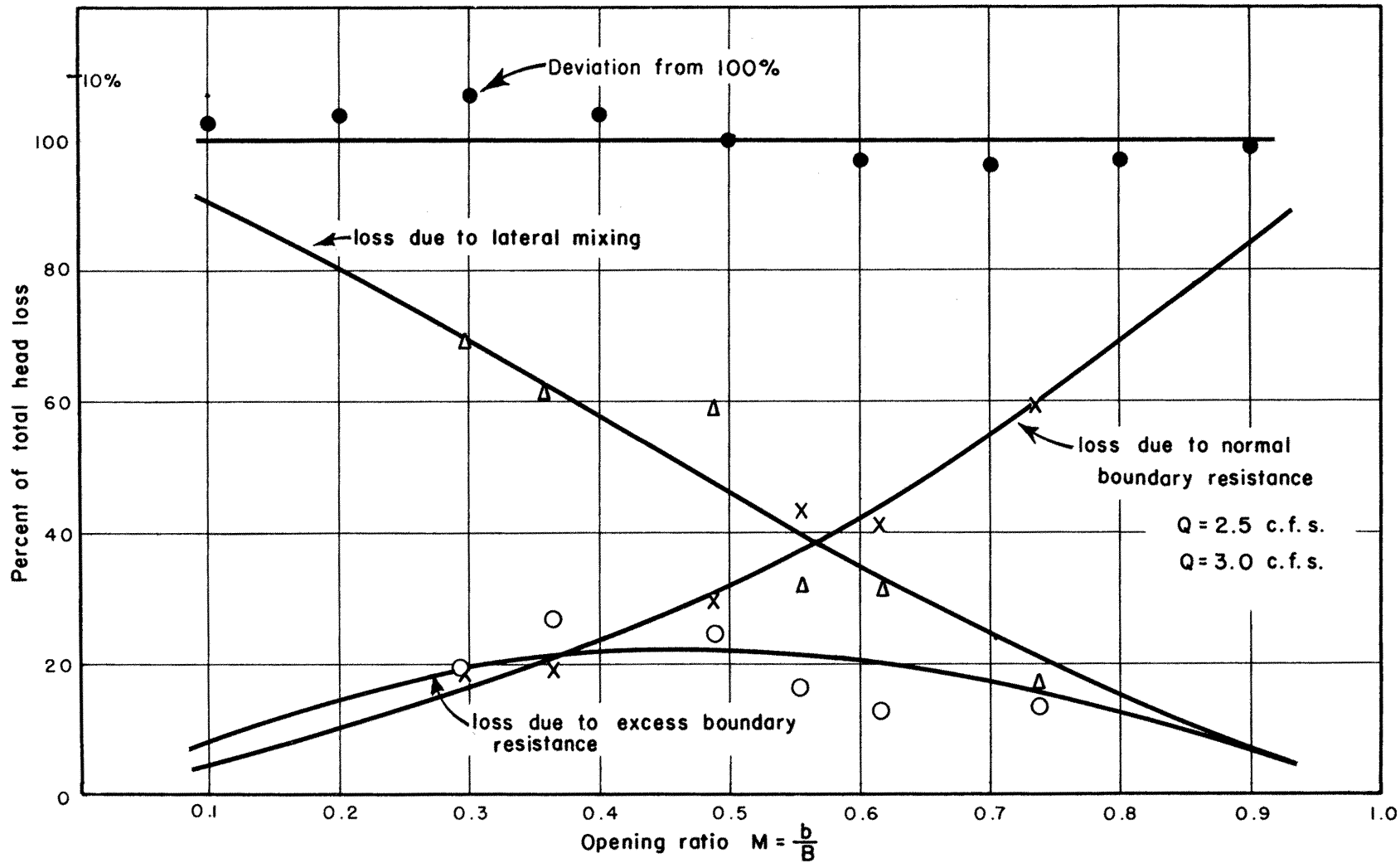


Fig.No. 5-16 Breakdown of energy losses for wing-wall abutments.

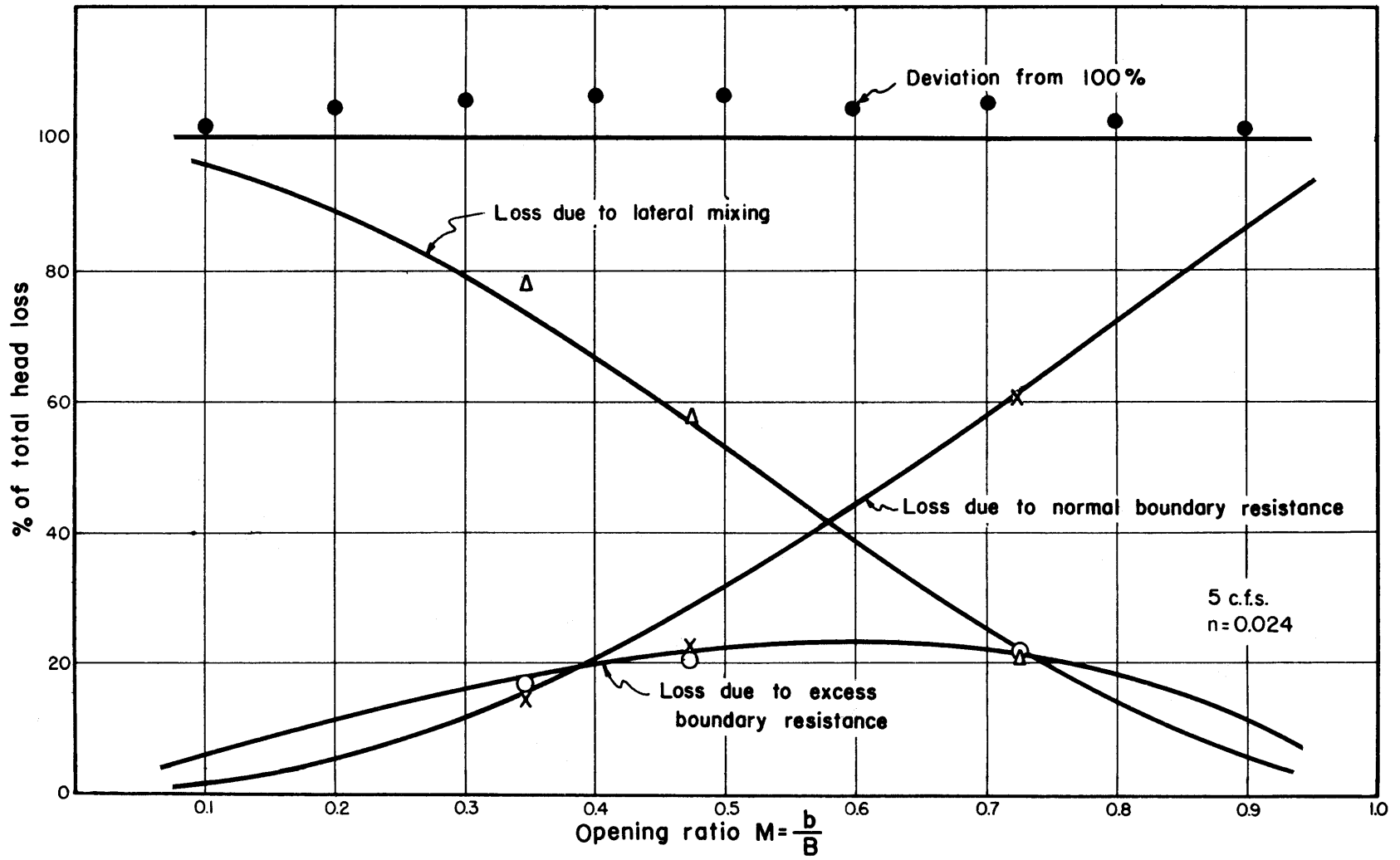


Fig. No. 5-17 Breakdown of energy for spill-through abutments.

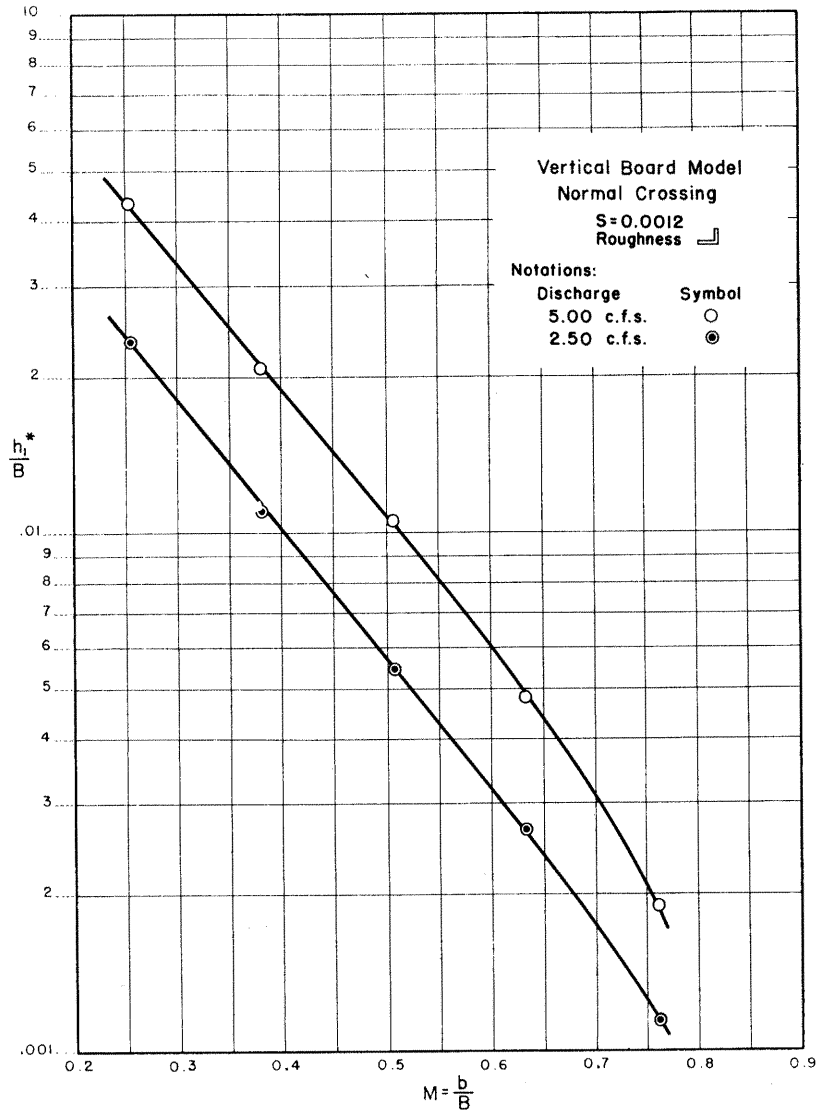


Fig.No.5-18 Effect of discharge on the maximum backwater.

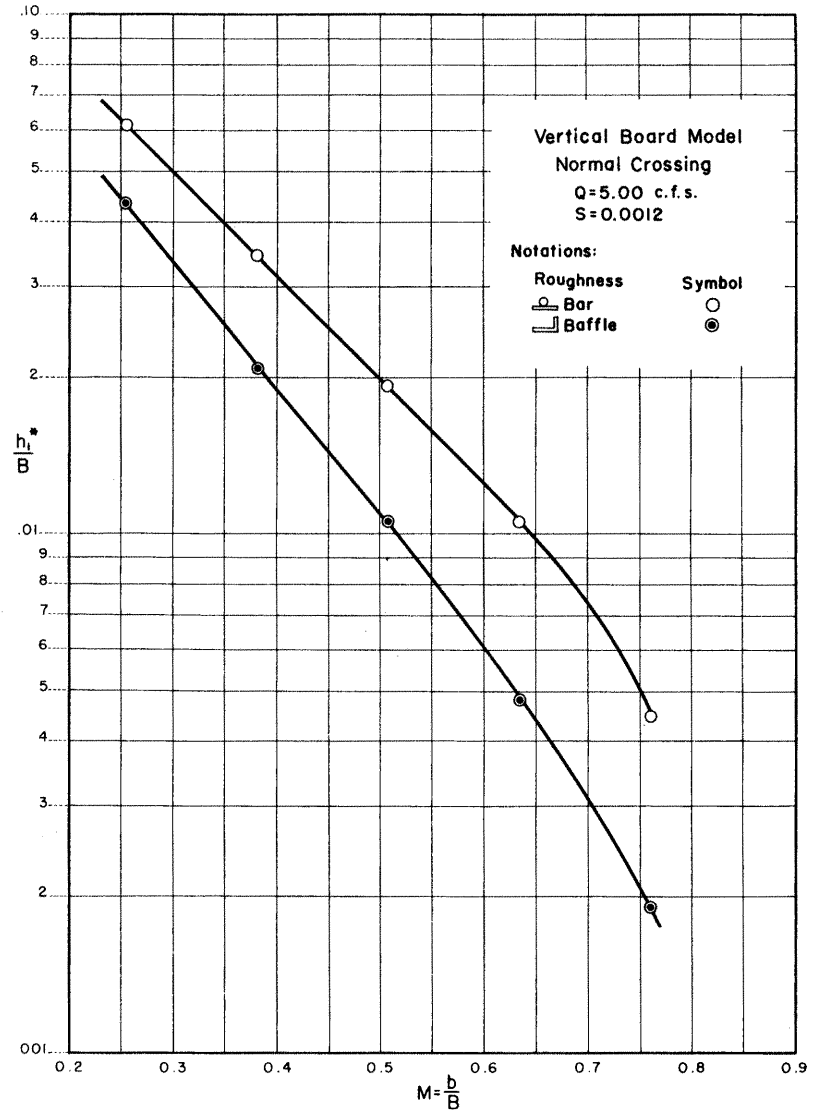


Fig.No.5-19 Effect of bed roughness on the maximum backwater.

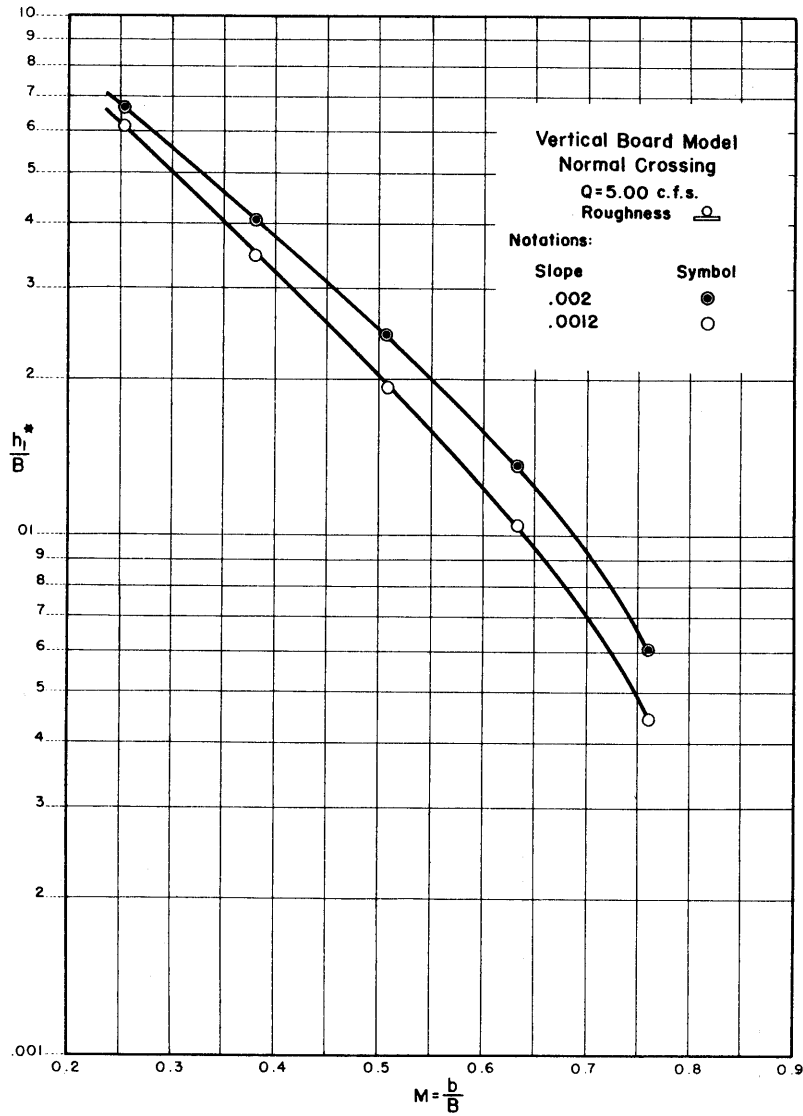


Fig.No.5-20 Effect of channel slope on the maximum backwater.

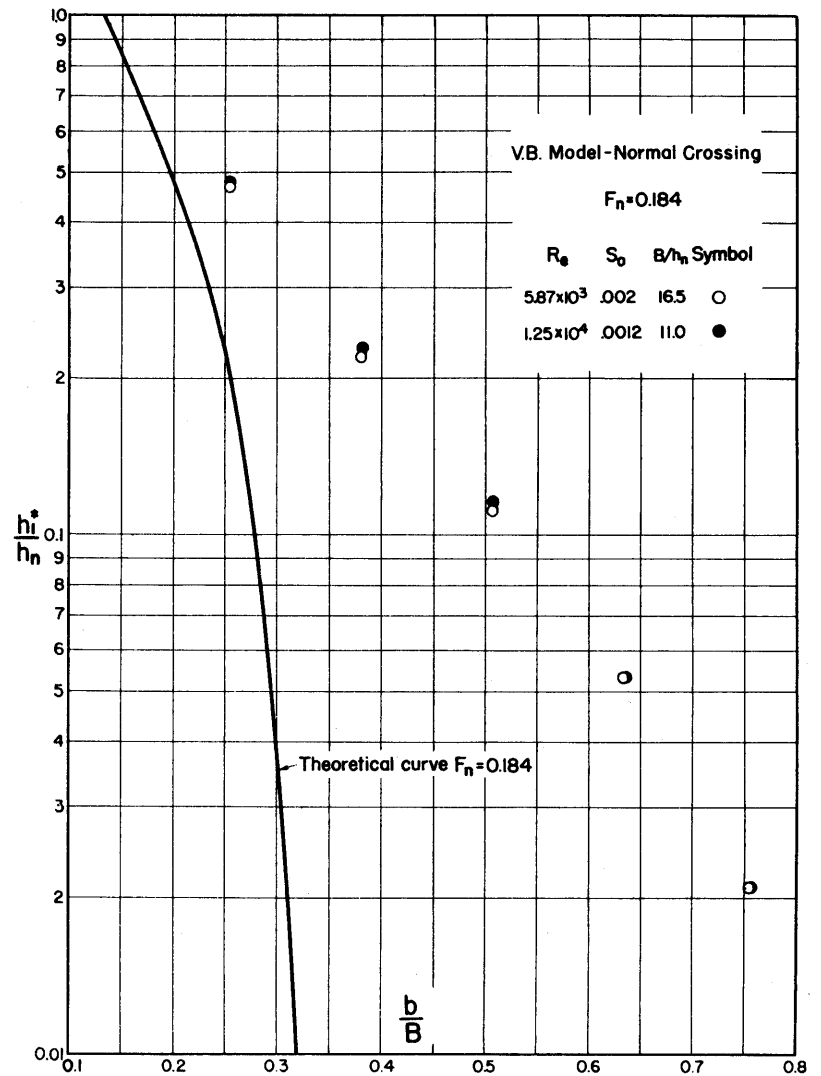


Fig.No.5-21 Variation of backwater ratio $\frac{h_1}{h_2^*}$ with opening ratio M, channel slopes, width-depth ratios, and Reynolds numbers.

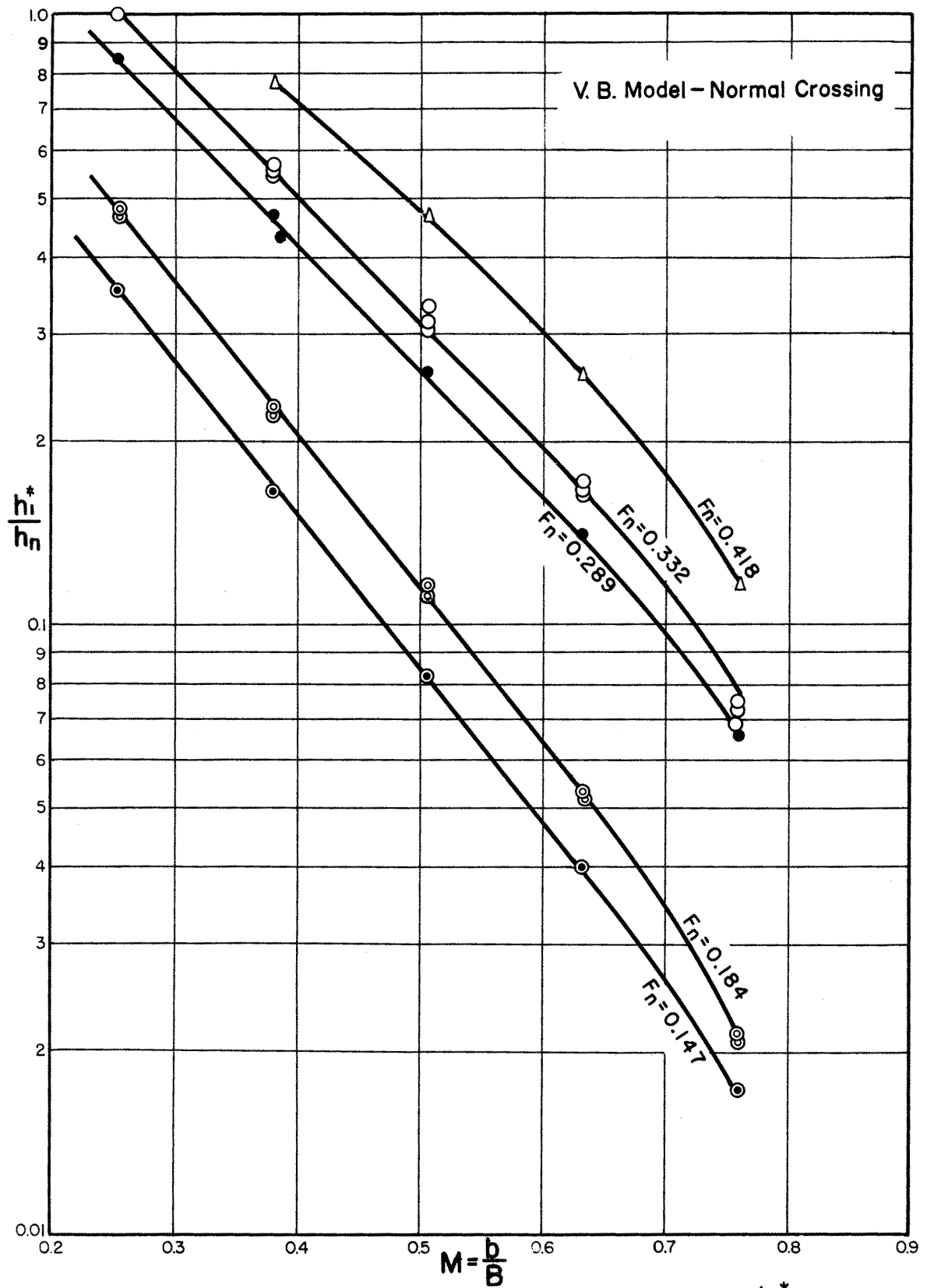


Fig. No. 5-22 Variation of experimental backwater ratio $\frac{h_1}{h_n^*}$ with opening ratio M and Froude number Fn .

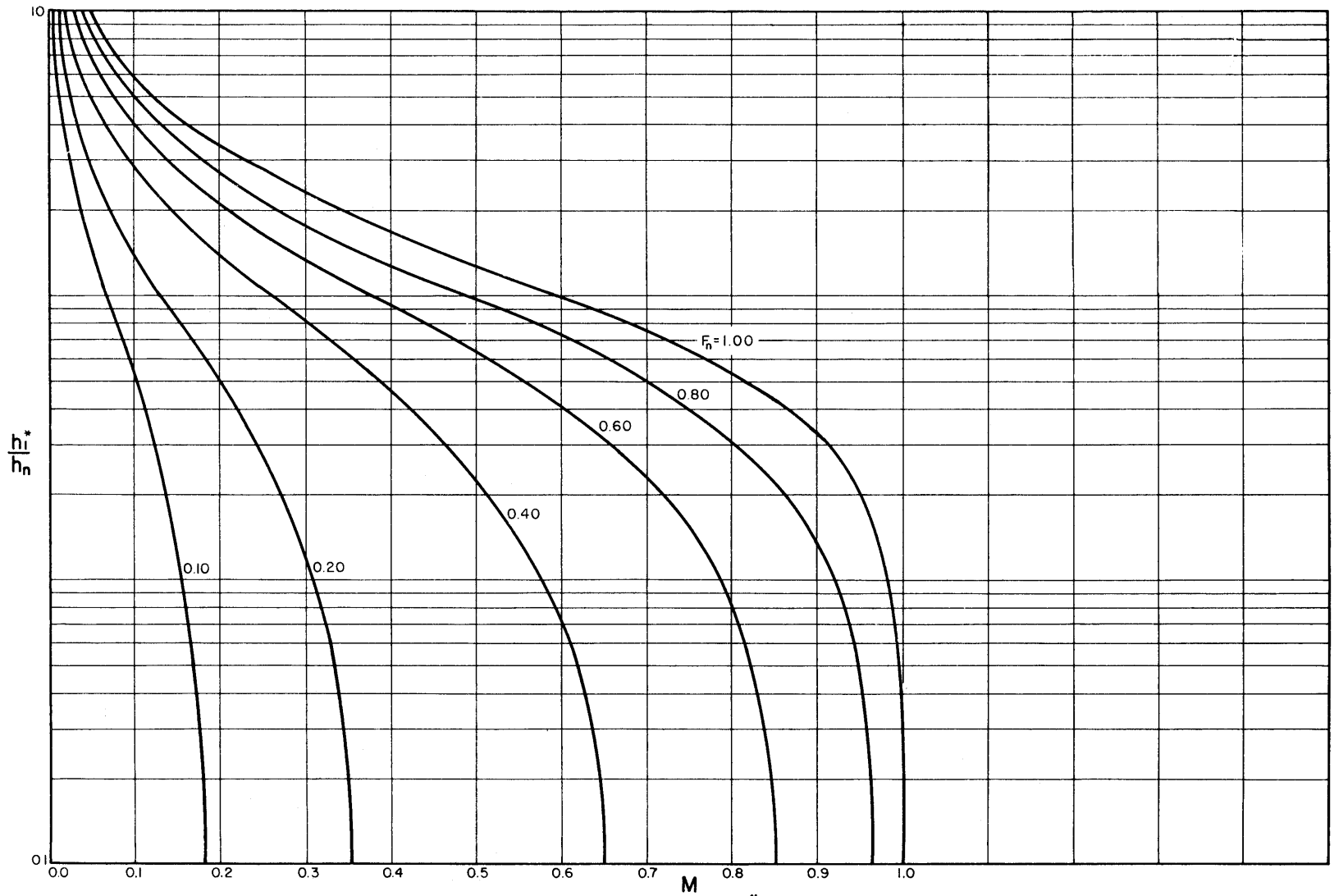


Fig.No.5-23 Variation of theoretical backwater ratio $\frac{h_1^*}{h_n}$ with opening ratio M and Froude number F_n .

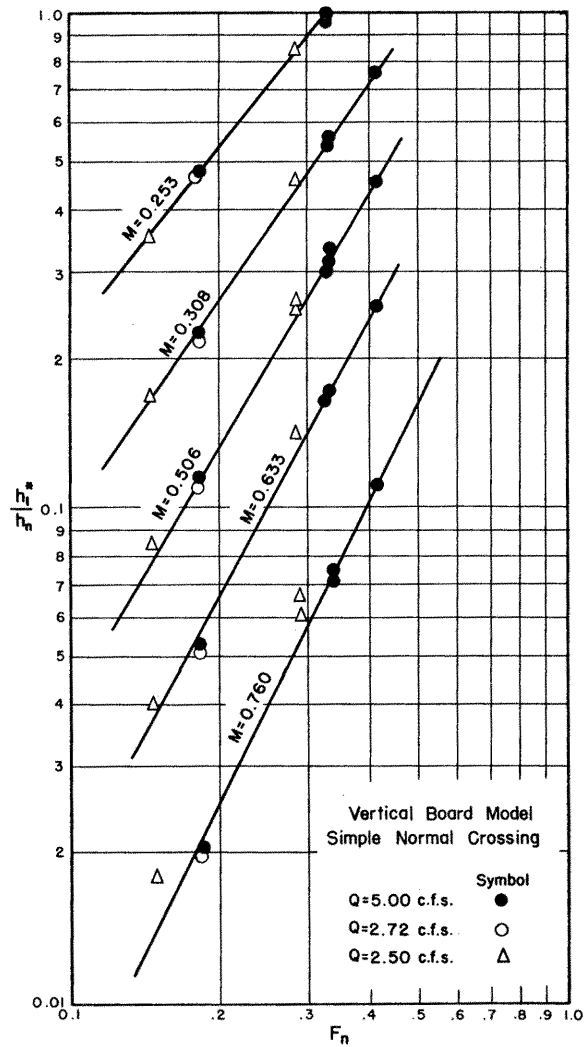


Fig. No. 5-24 Effect of discharge on backwater ratio $\frac{h_1^*}{h_n}$

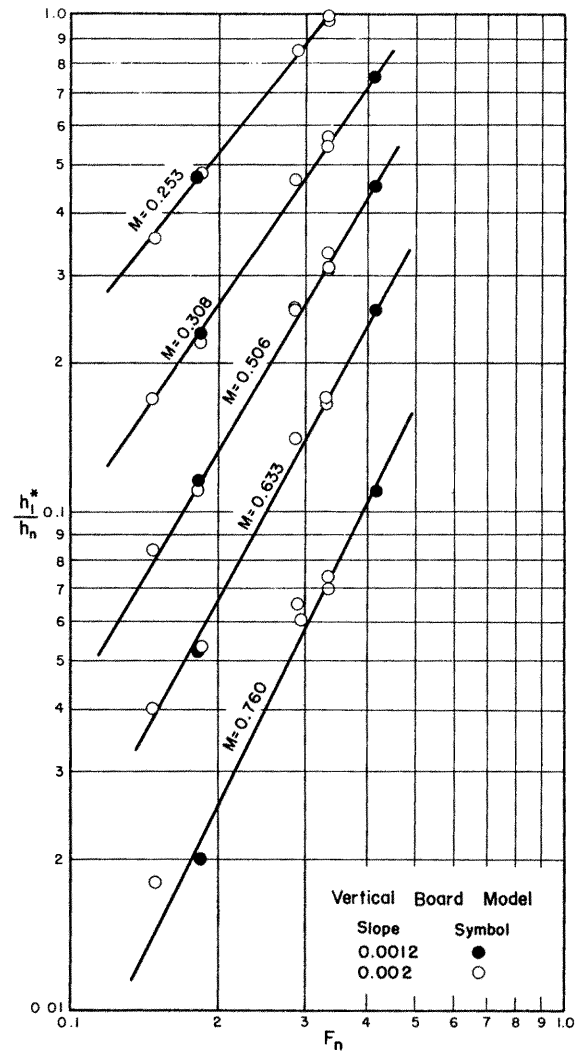


Fig. No. 5-25 Effect of channel slope on backwater ratio $\frac{h_1^*}{h_n}$

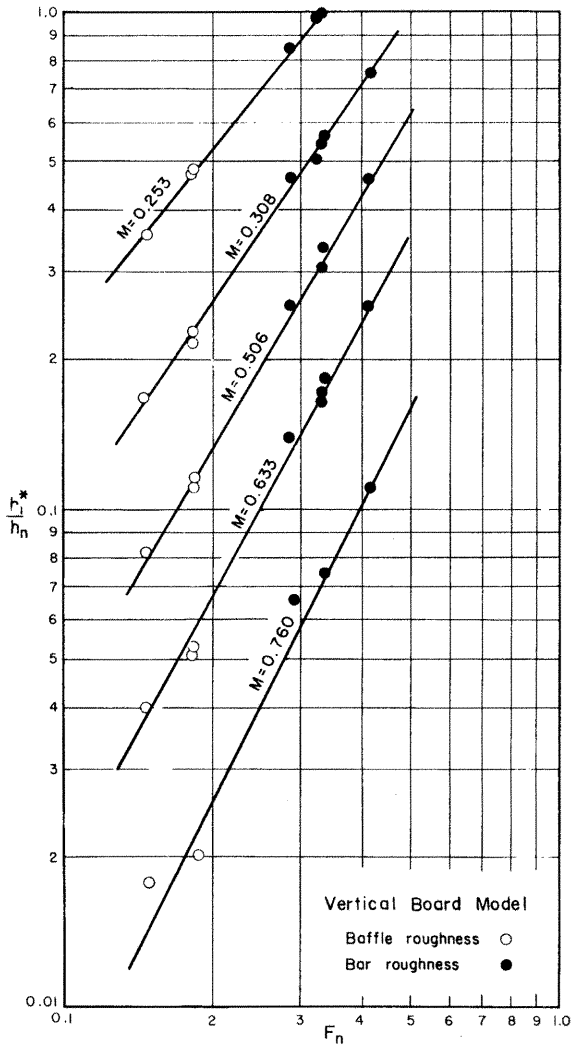


Fig. No 5-26 Effect of channel roughness on backwater ratio $\frac{h_1^*}{h_n}$

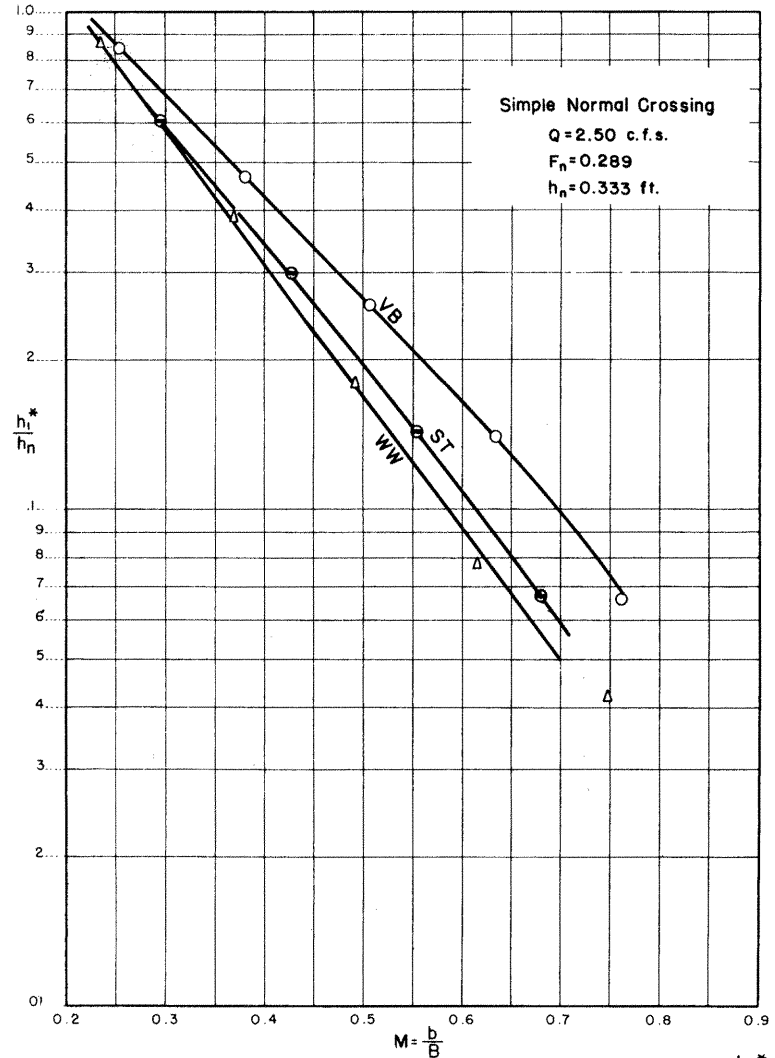


Fig. No. 5-27 Effect of abutment type on backwater ratio $\frac{h_1^*}{h_n}$

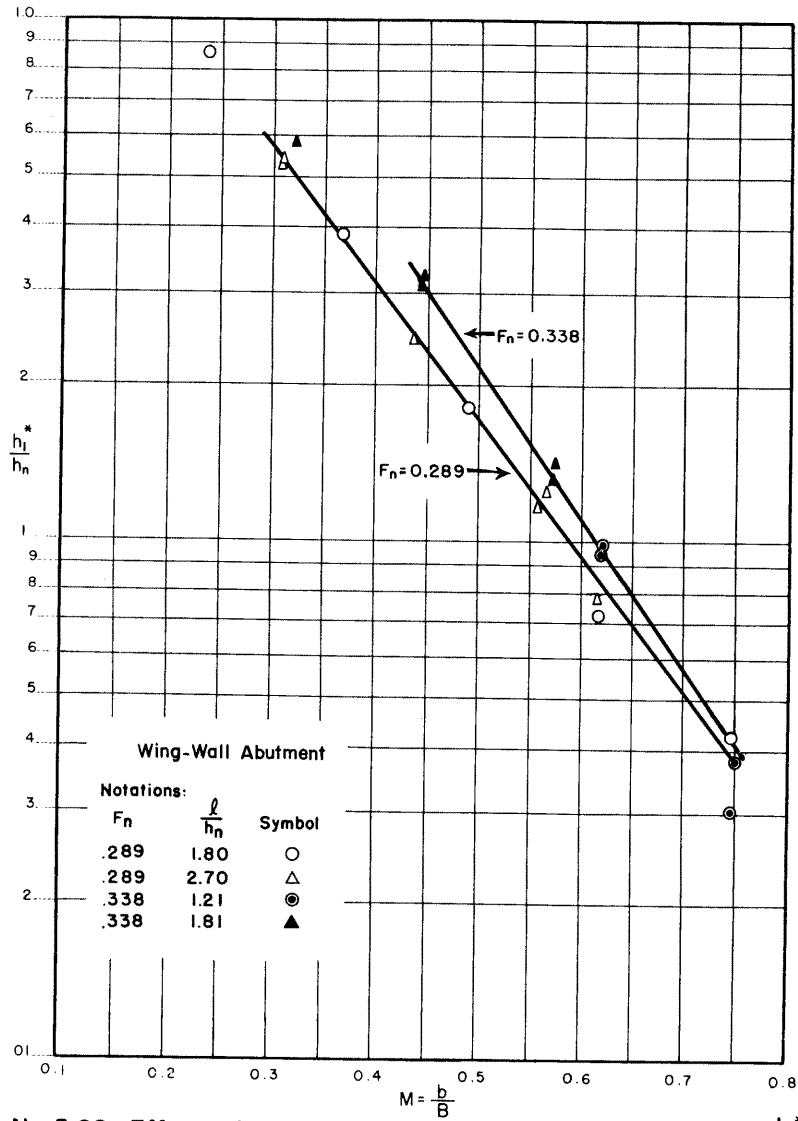


Fig. No. 5-28 Effect of abutment geometry on backwater ratio $\frac{h_1^*}{h_n}$ for wing-wall abutments.

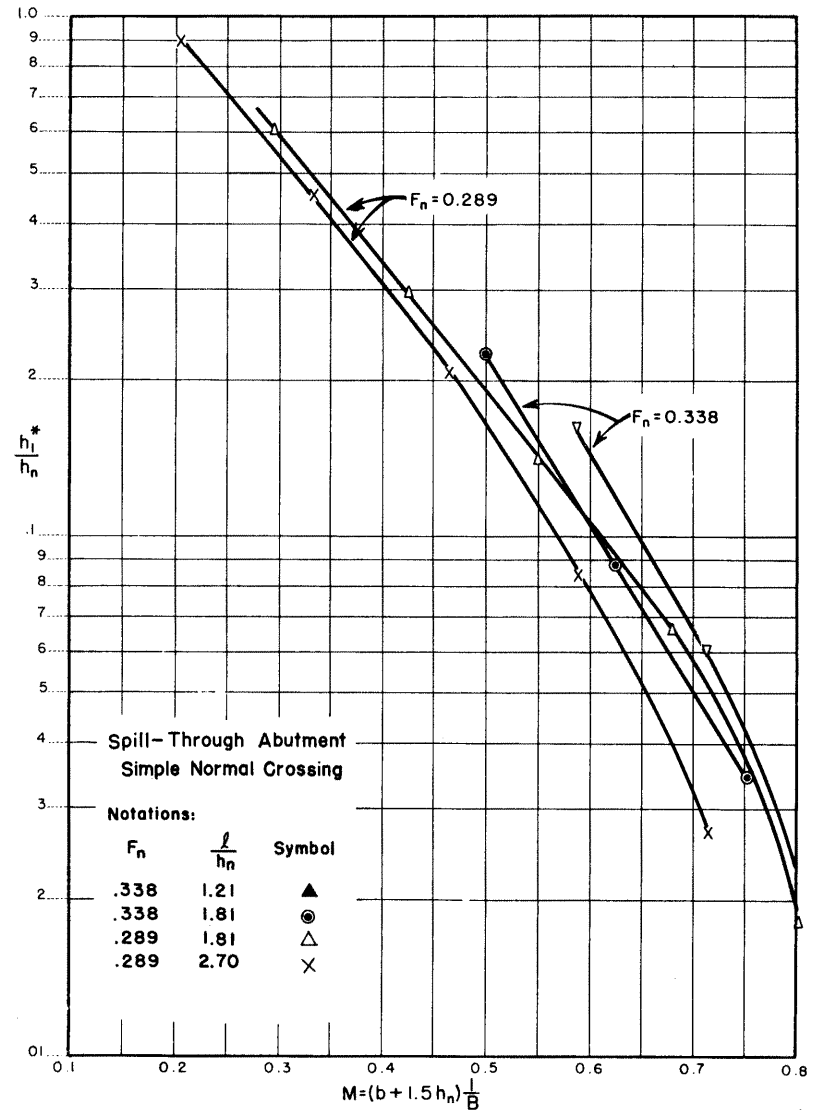


Fig. No. 5-29 Effect of abutment geometry on backwater ratio $\frac{h_1^*}{h_n}$ for spill-through abutments.

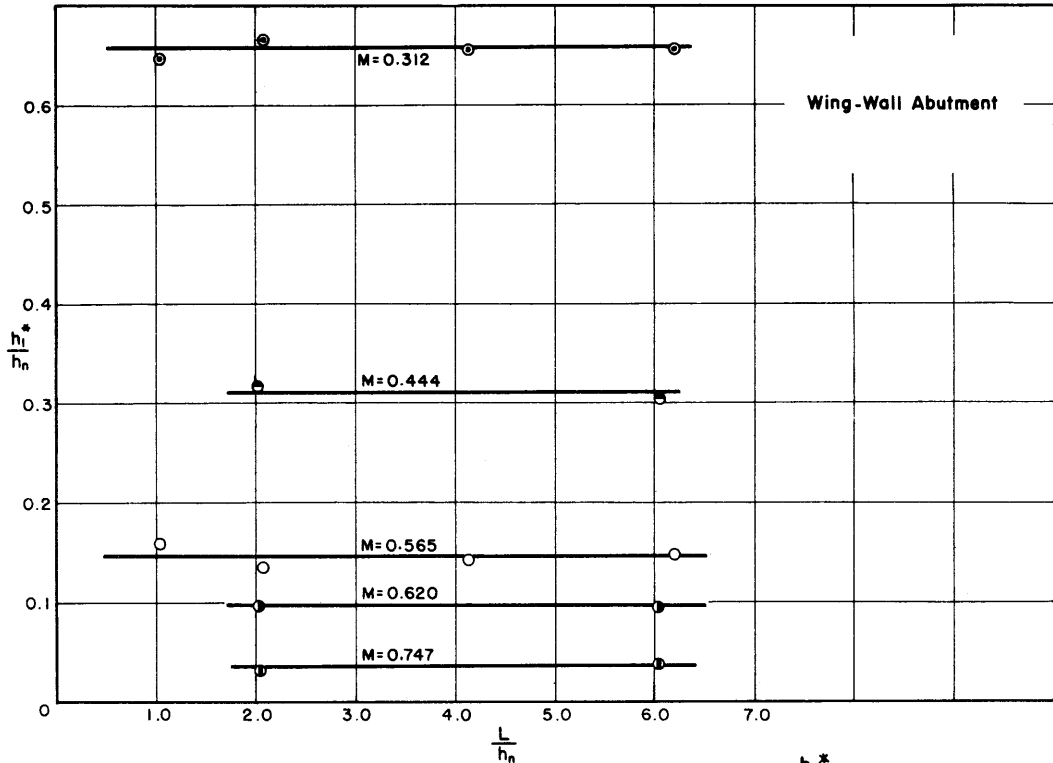


Fig. No. 5-30 Effect of abutment length on backwater ratio $\frac{h_1^*}{h_n}$ for wing-wall abutments.

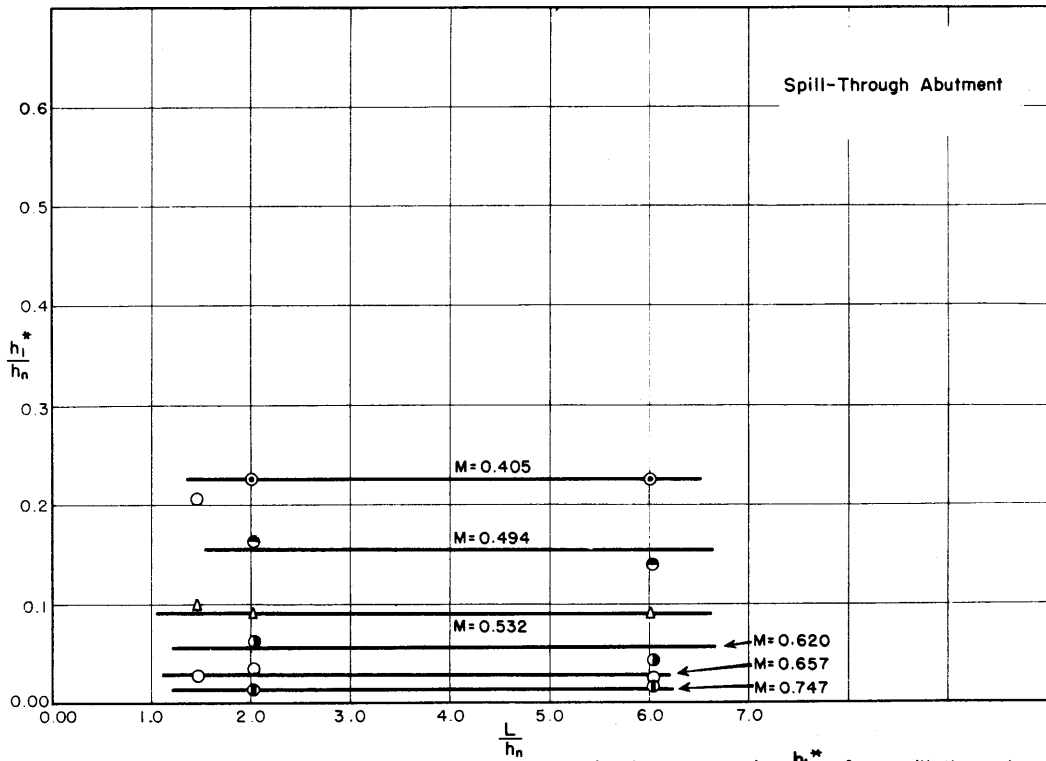


Fig. No. 5-31 Effect of abutment length on backwater ratio $\frac{h_1^*}{h_n}$ for spill-through abutments.

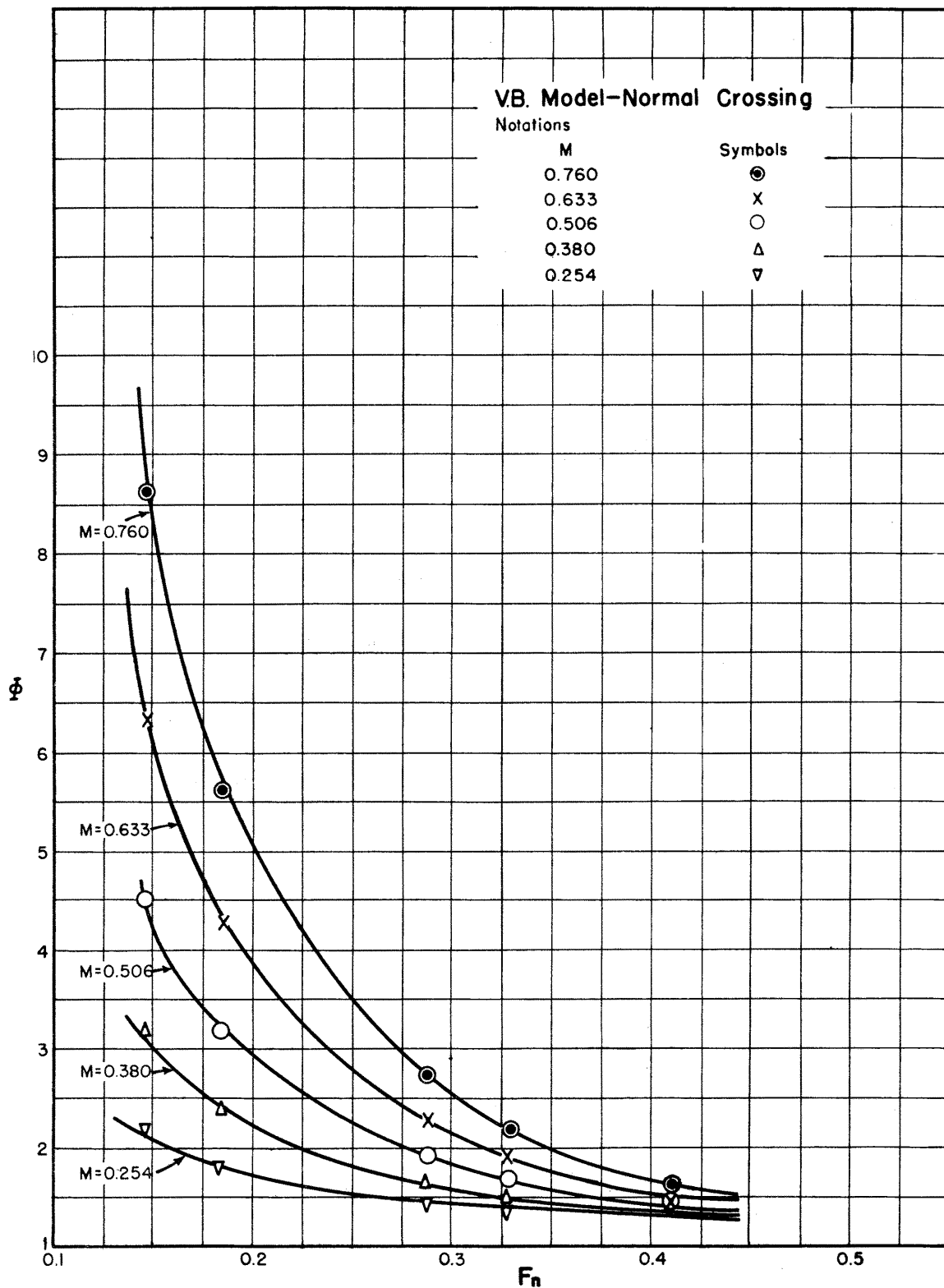


Fig.No.5-32 Variation of correction factor Φ with Froude number F_n and opening ratio M for vertical-board model.

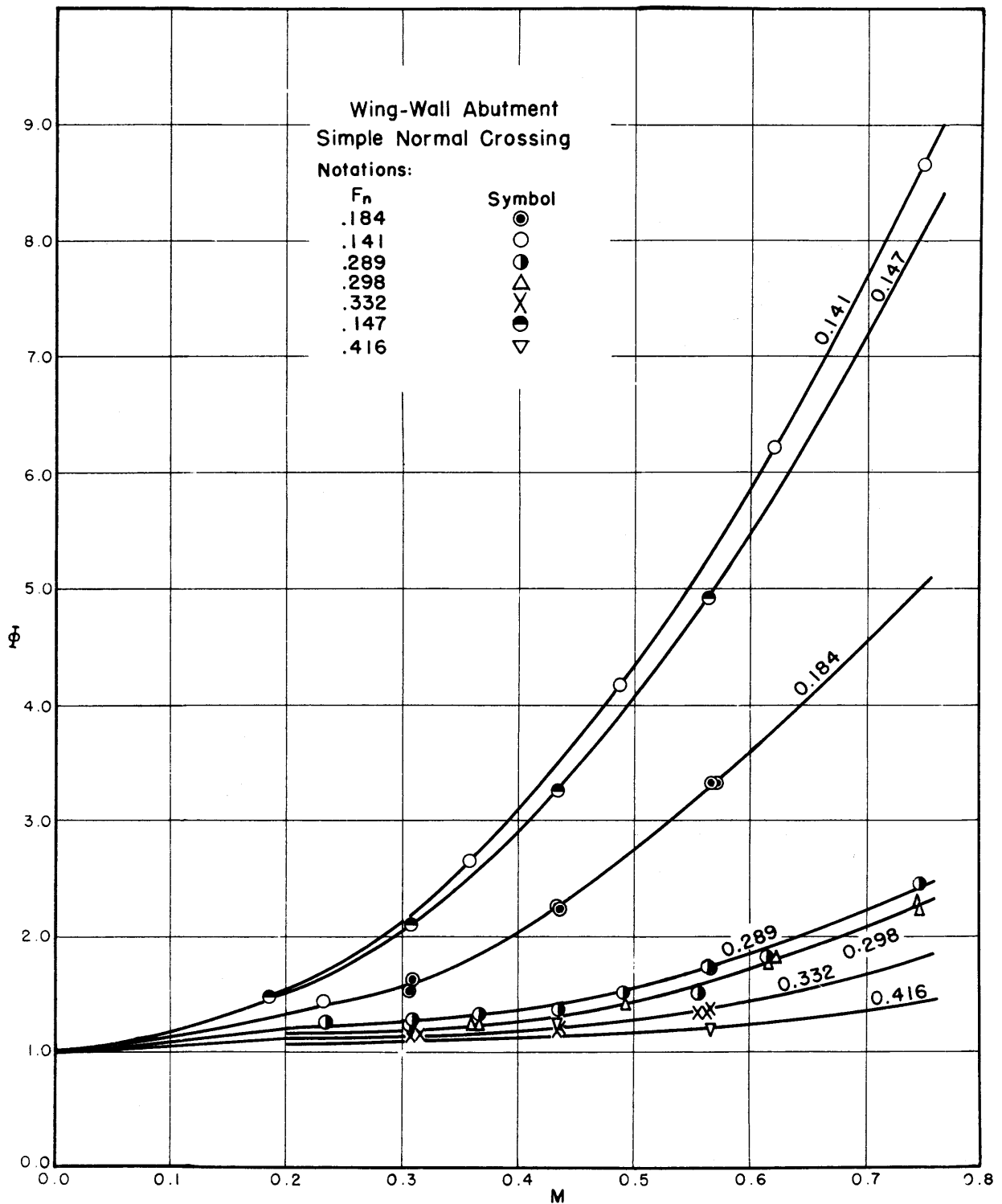


Fig. No. 5-33 Variation of correction factor Φ with Froude number F_n and opening ratio M for wing-wall abutments.

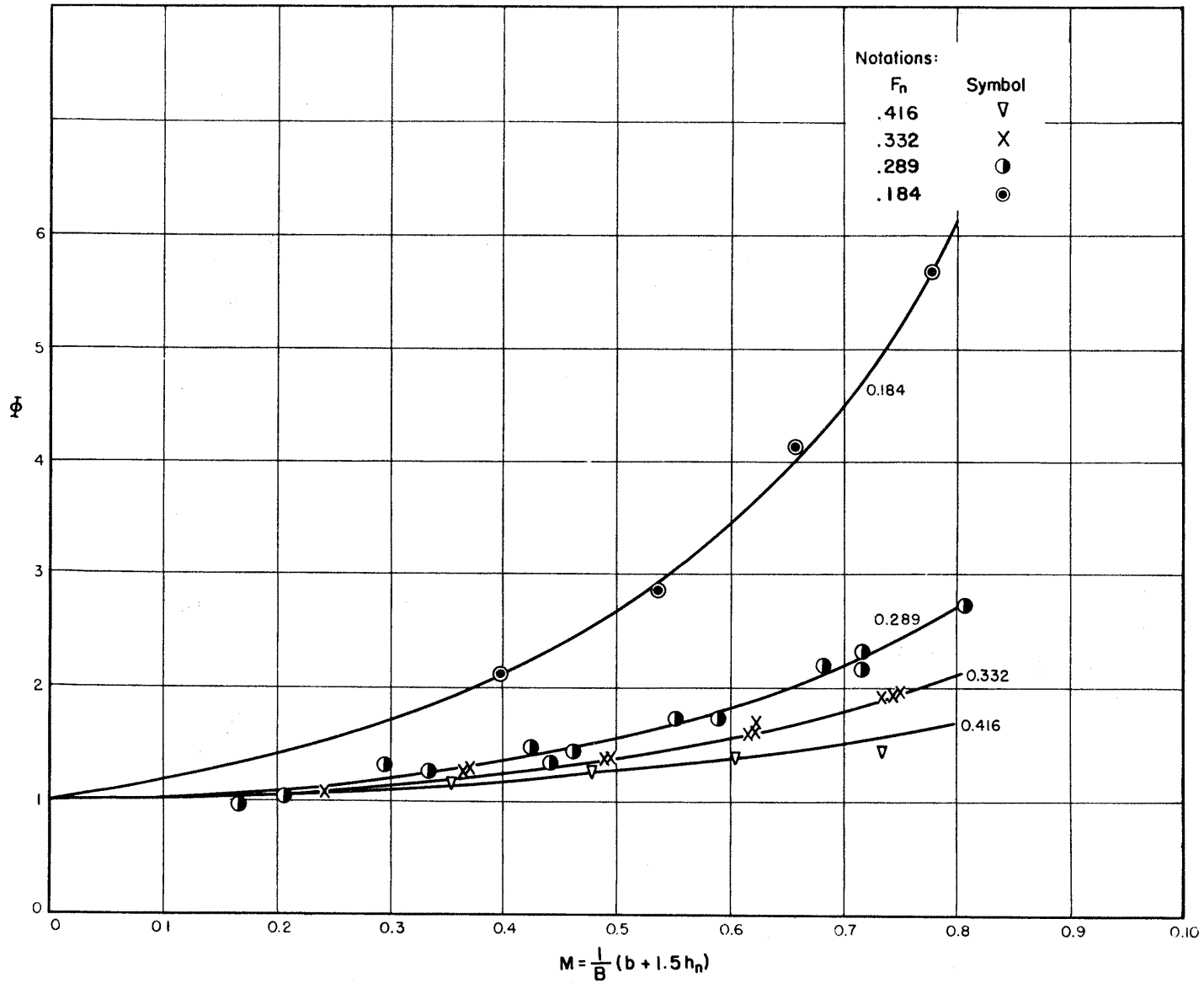


Fig. No.5-34 Variation of correction factor Φ with Froude number F and opening ratio M for spill-through abutments.

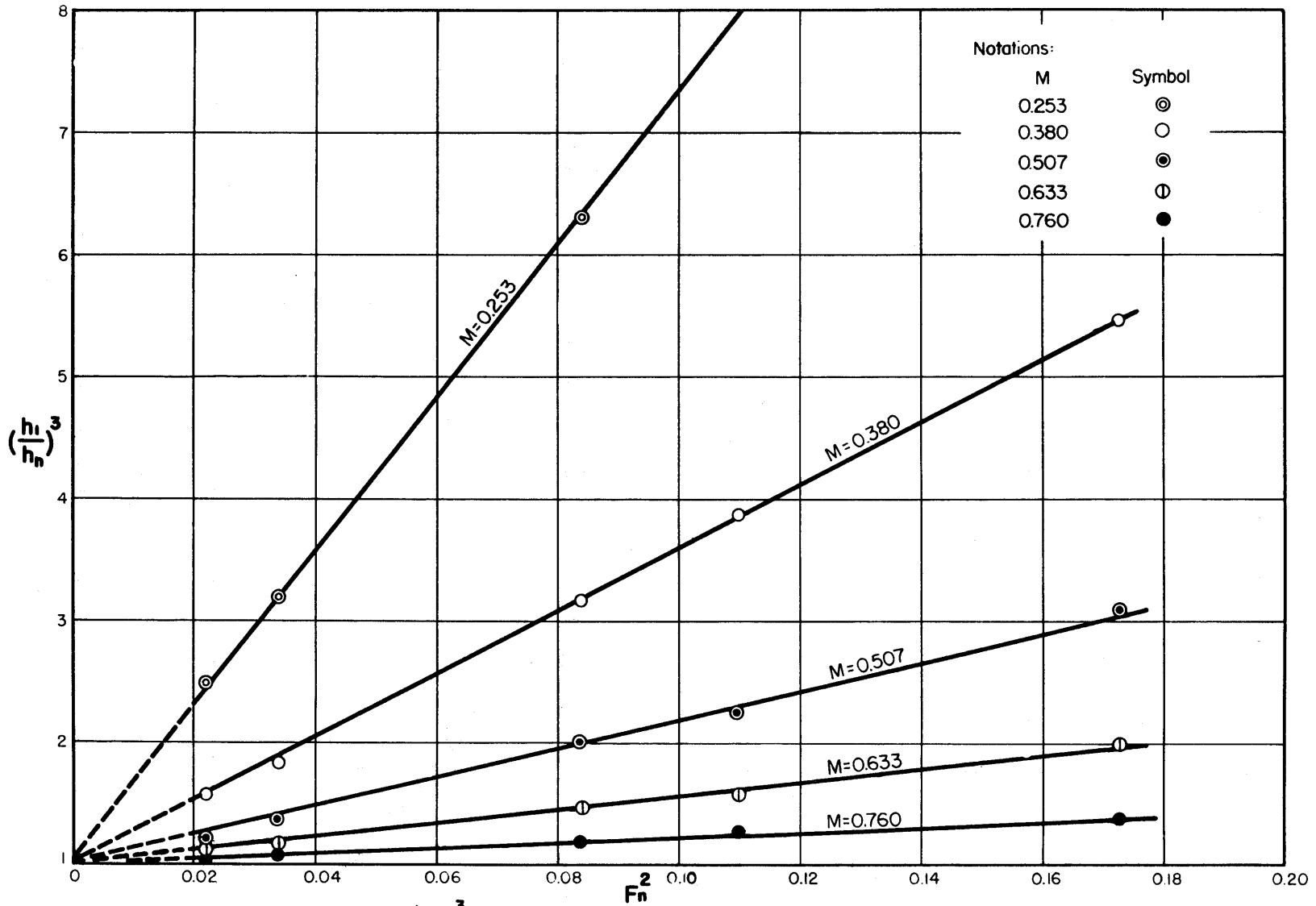


Fig.No.5-35 Variation of $(\frac{h_1}{h_n})^3$ with F_n^2 and M as the third variable for vertical board model.

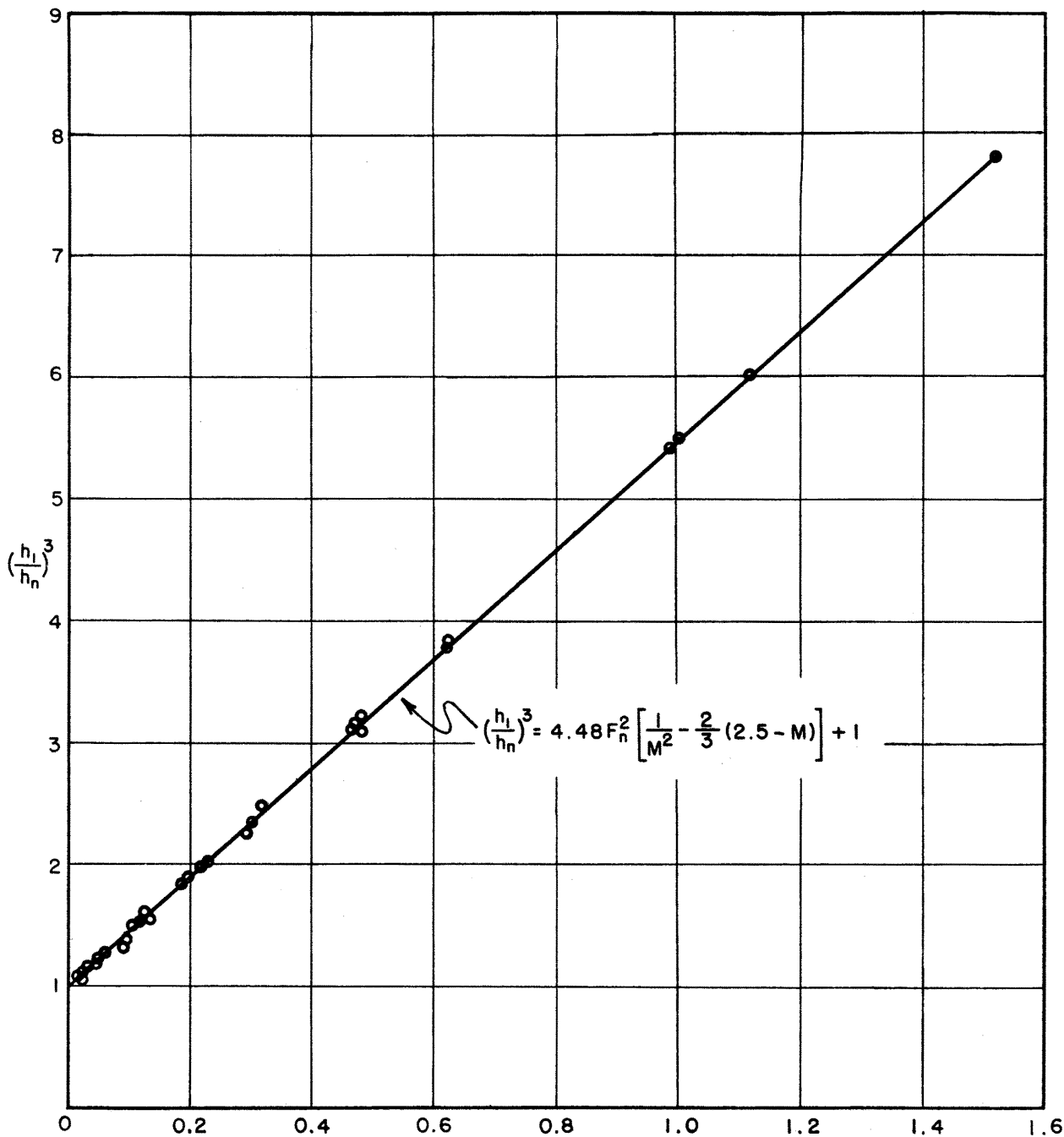


Fig. No. 5-36 Empirical backwater equation compared to experimental data for vertical board model

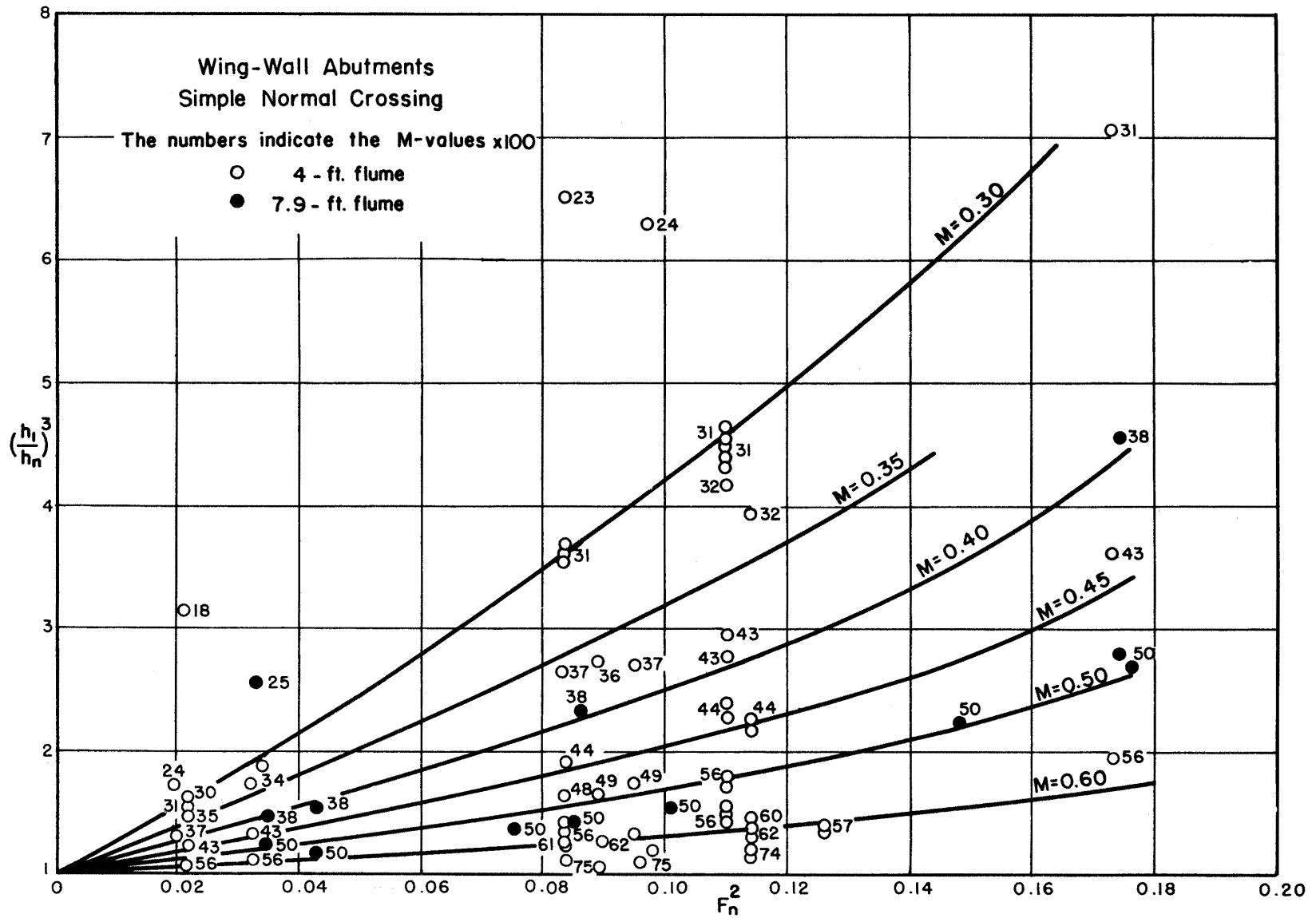


Fig. No. 5-37 Variation of $\left[\frac{h_1}{h_n}\right]^3$ with F_n^2 and M as the third variable for wing-wall abutments.

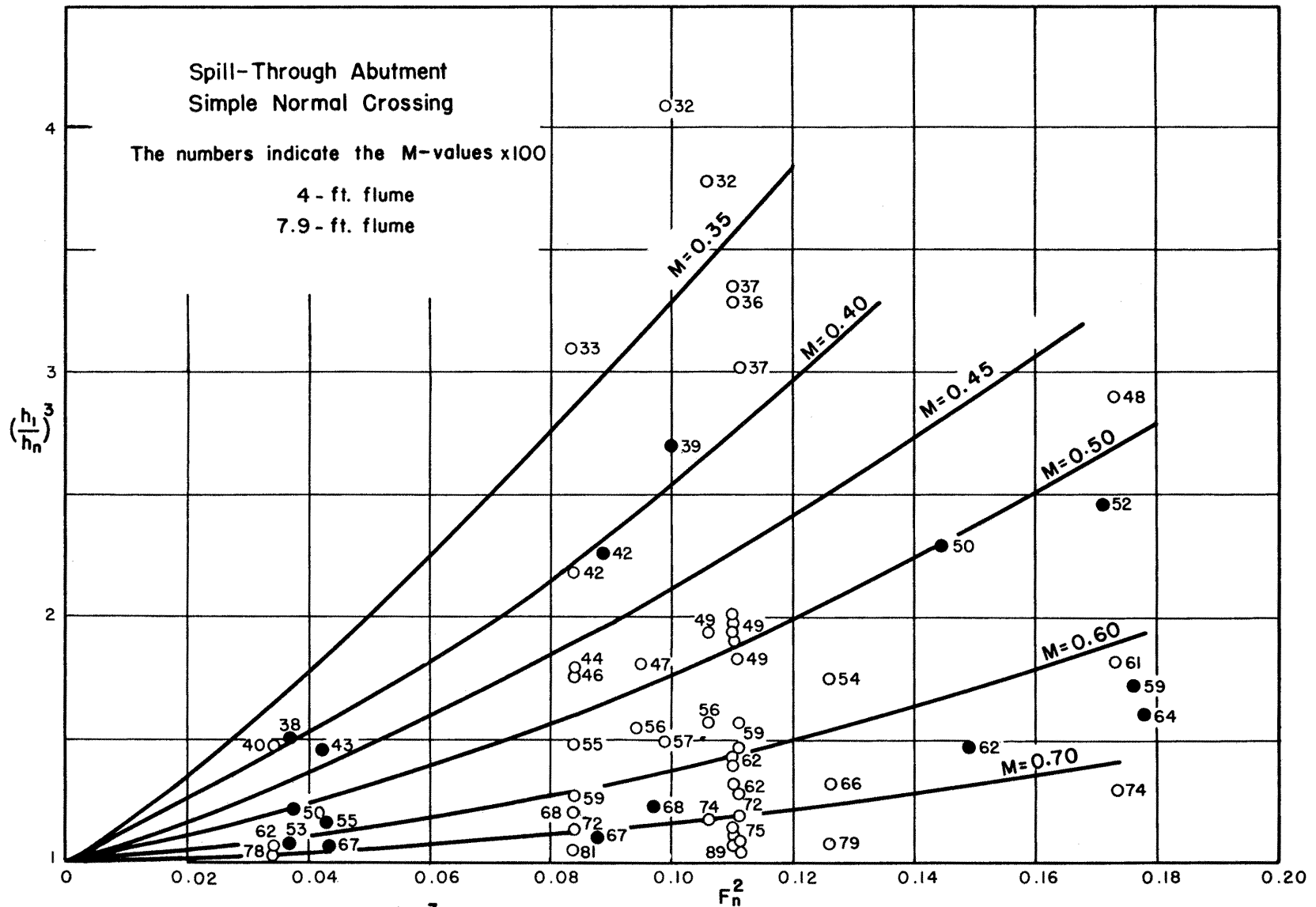
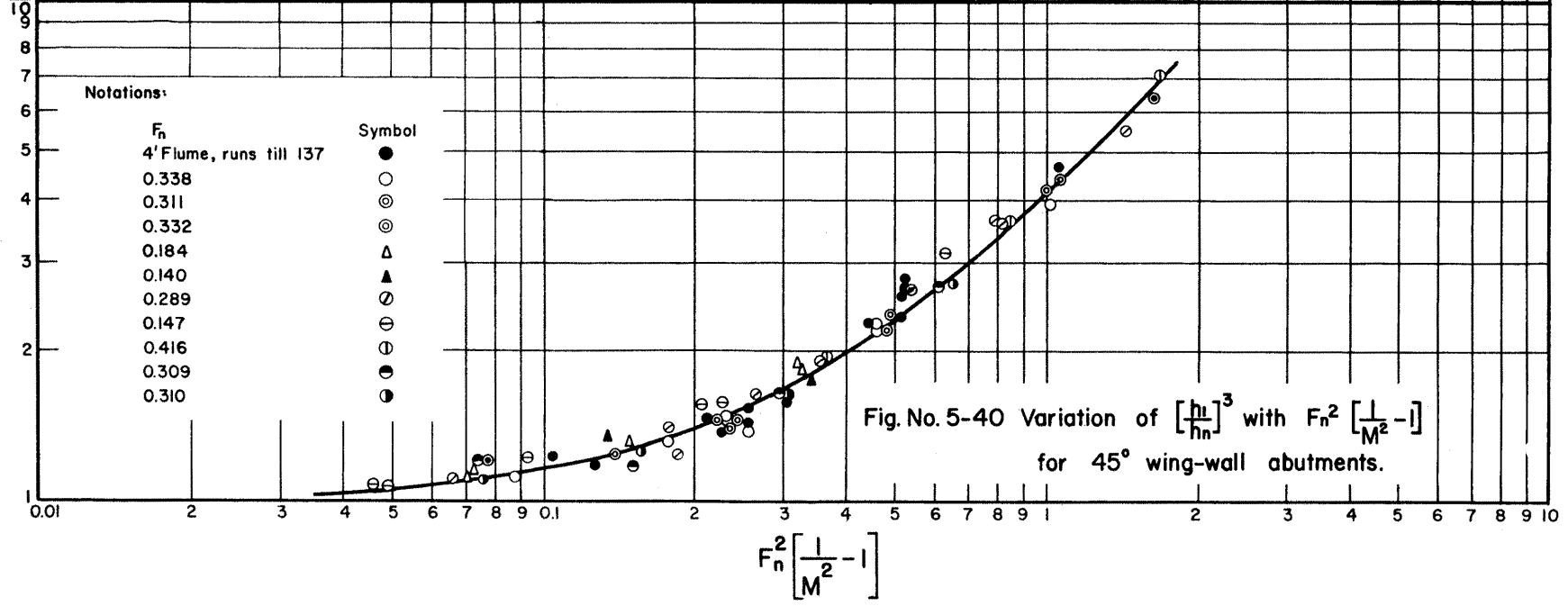
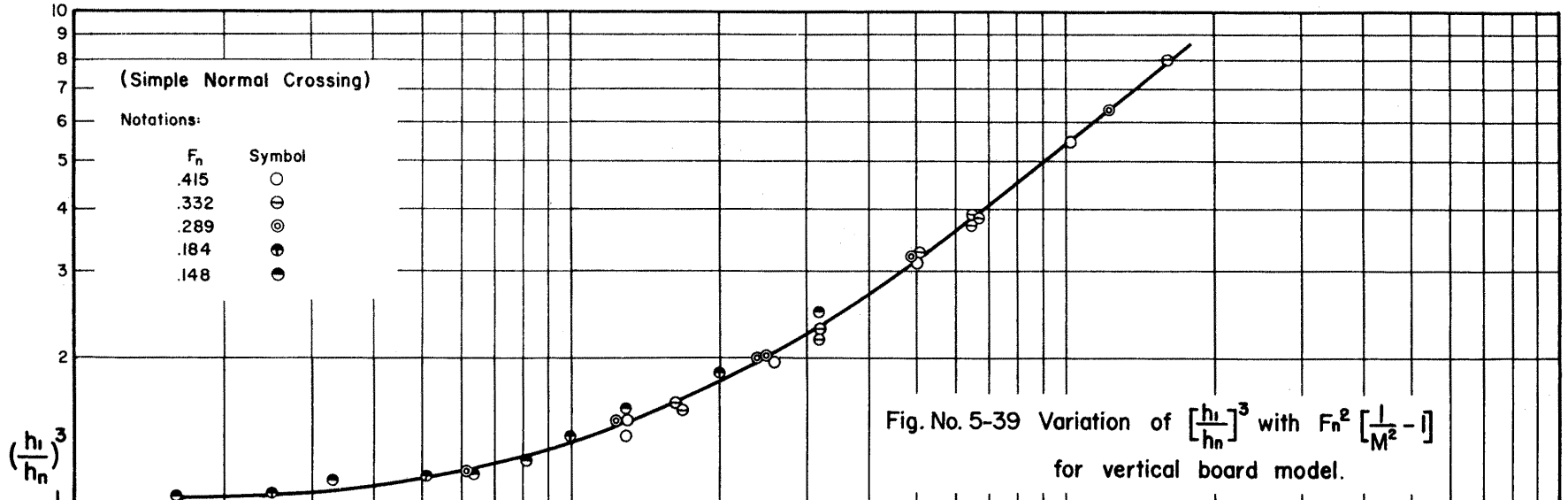


Fig. No. 5-38 Variation of $\left[\frac{h_1}{h_n}\right]^3$ with F_n^2 and M as the third variable for spill-through abutment.



$$F_n^2 \left[\frac{1}{M^2} - 1 \right]$$

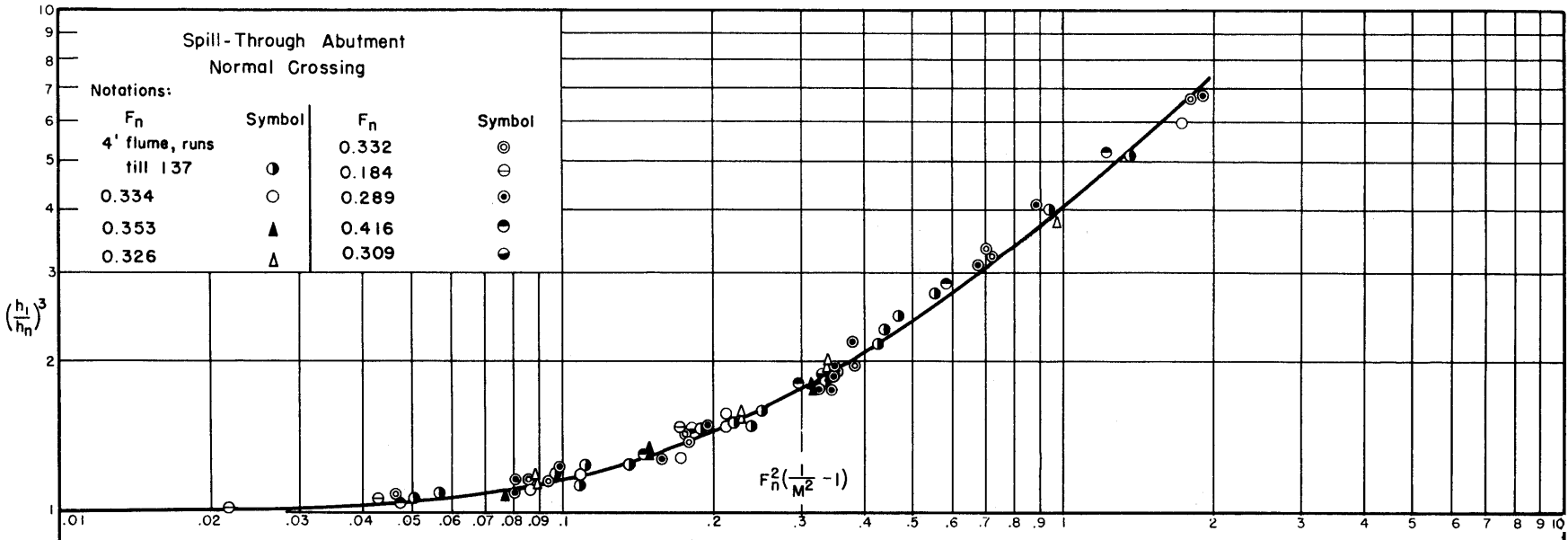


Fig. No. 5-41 Variation of $\left[\frac{h_1}{h_n} \right]^3$ with $F_n^2 \left[\frac{1}{M^2} - 1 \right]$ for $1: \frac{1}{2}$ spill-through abutments

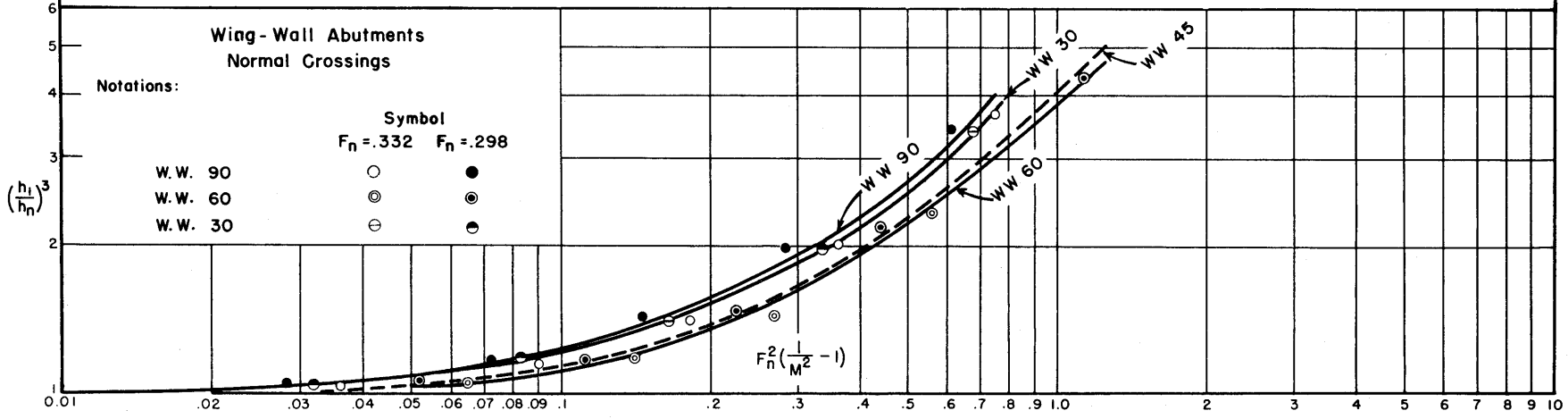


Fig. No. 5-42 Variation of $\left[\frac{h_1}{h_n} \right]^3$ with $F_n^2 \left[\frac{1}{M^2} - 1 \right]$ for various wing-wall abutments

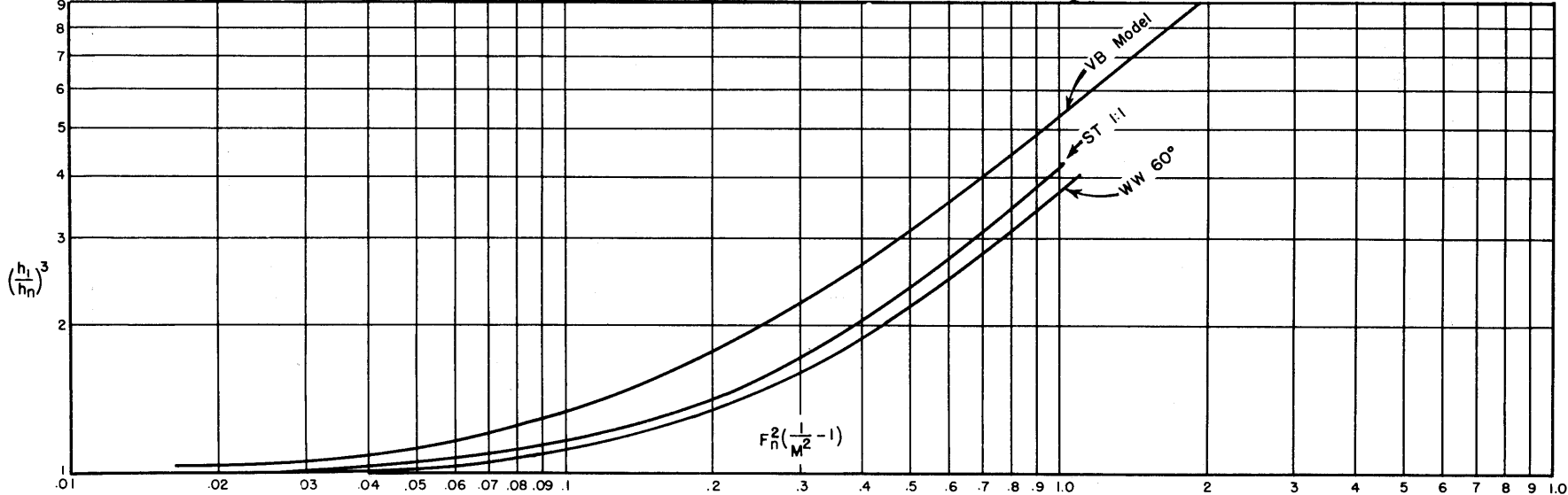
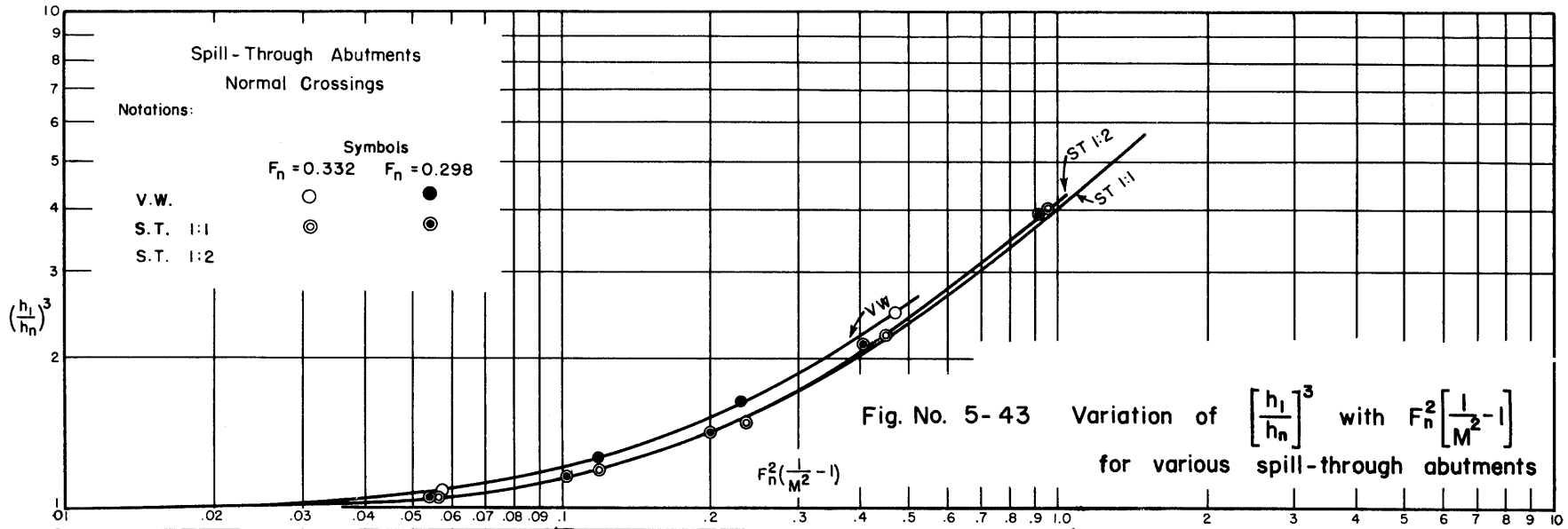


Fig. No. 5-44 Variation of $\left[\frac{h_1}{h_n}\right]^3$ with $F_n^2 \left[\frac{1}{M^2} - 1\right]$ and abutment geometry

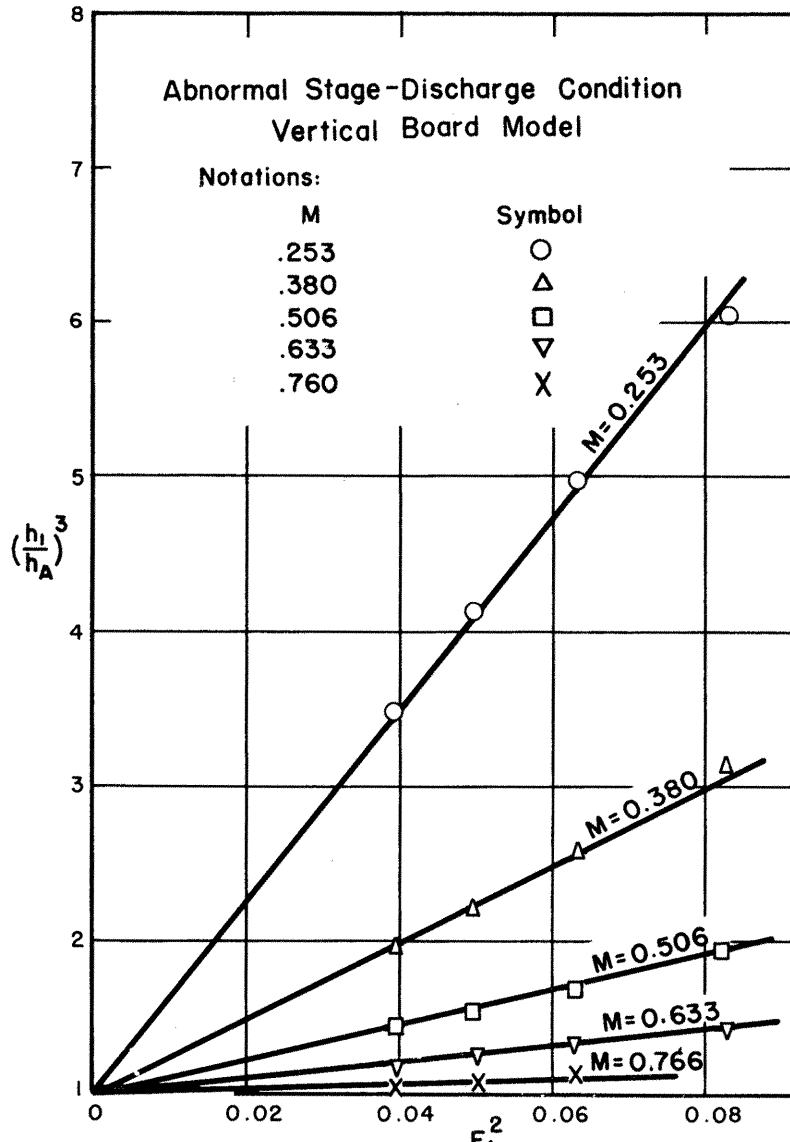


Fig. No. 5-45 Variation of $\left[\frac{h_1}{h_A}\right]^3$ with F_A^2 and M as the third variable for vertical board model.

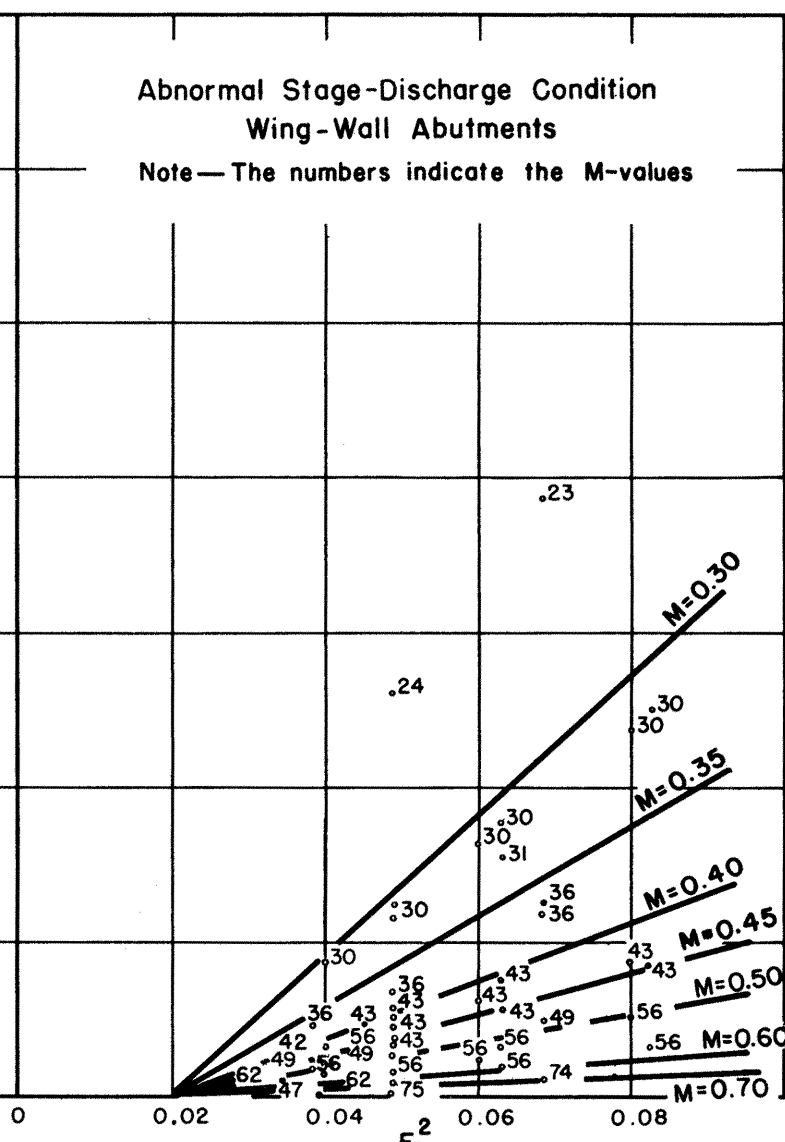


Fig. No. 5-46 Variation of $\left[\frac{h_1}{h_A}\right]^3$ with F_A^2 and M as the third variable for wing-wall abutment.

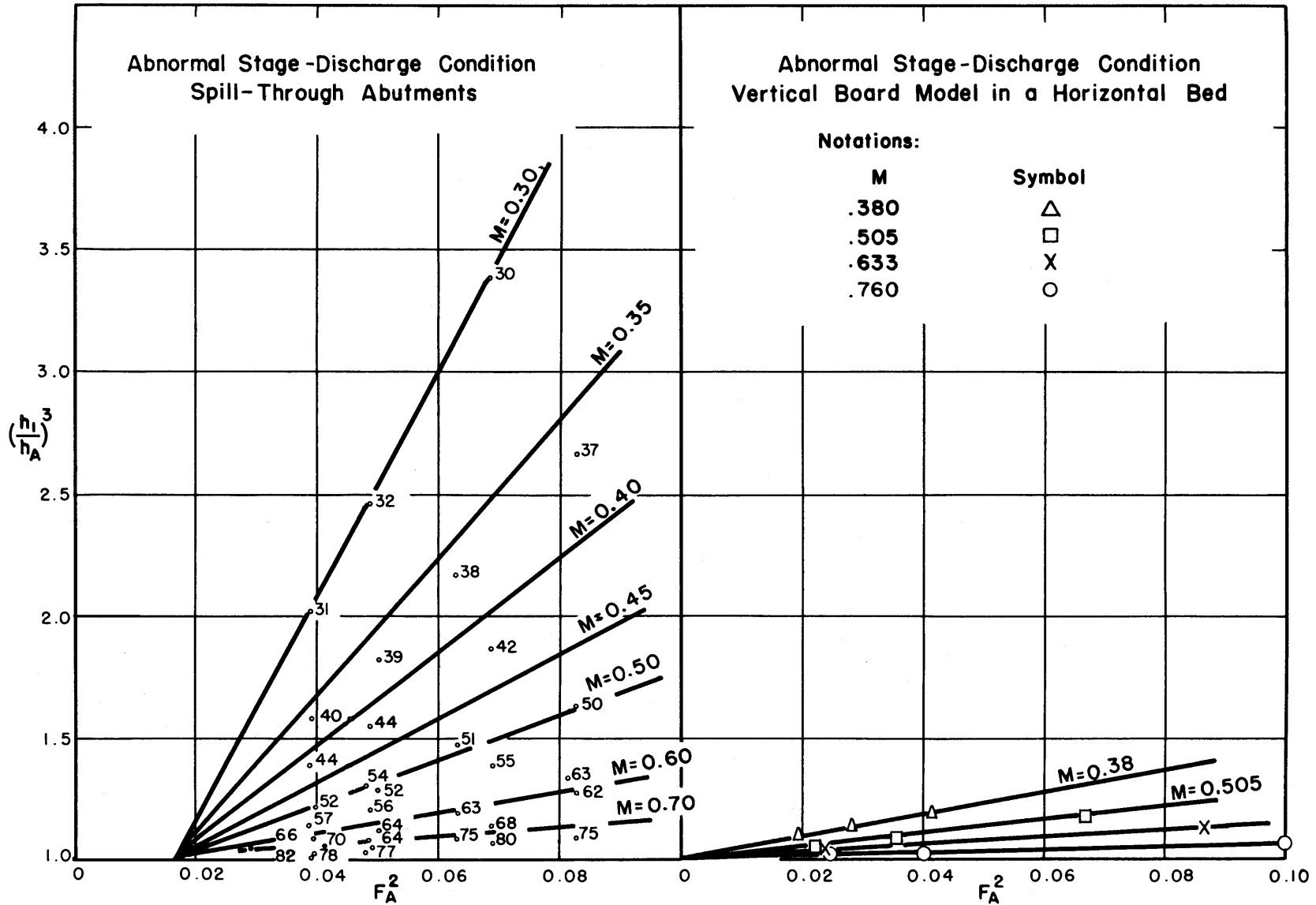


Fig. No. 5-47 Variation of $\left[\frac{h_1}{h_n}\right]^3$ with F_A^2 and M for spill-through abutments

Fig. No. 5-48 Variation of $\left[\frac{h_1}{h_n}\right]^3$ with F_A^2 and M for vertical-board model in a horizontal channel

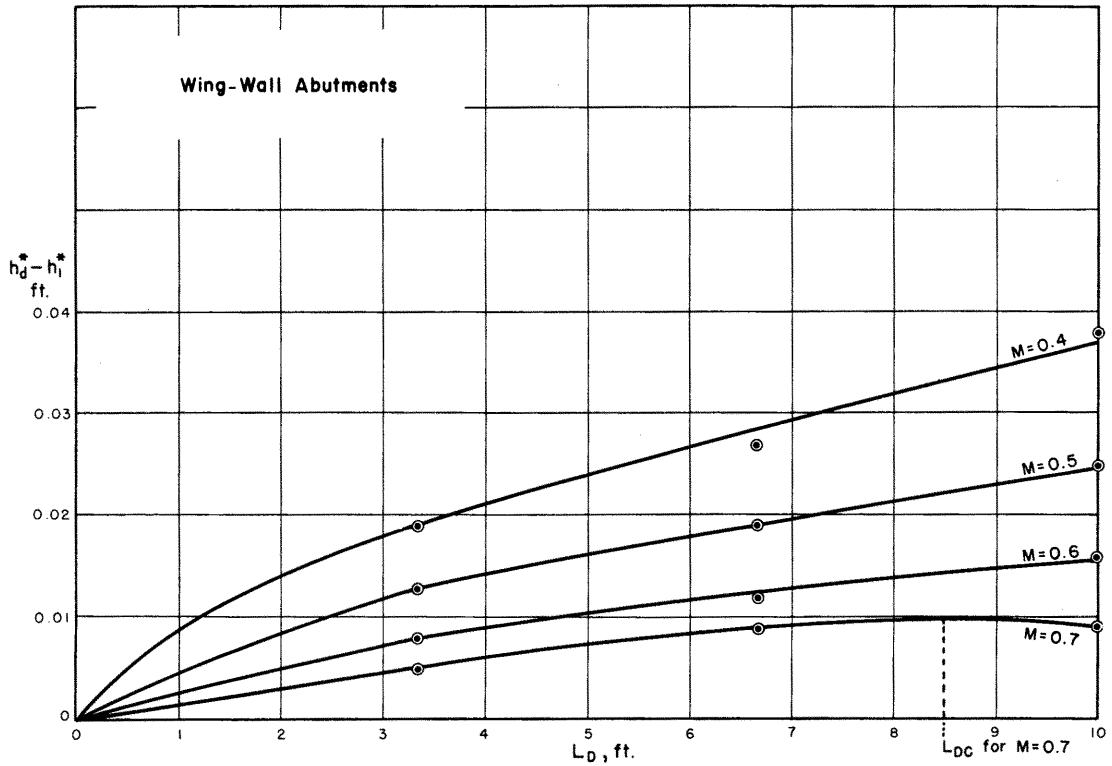


Fig. No. 5-49 Backwater of dual bridges contraction for wing-wall abutments

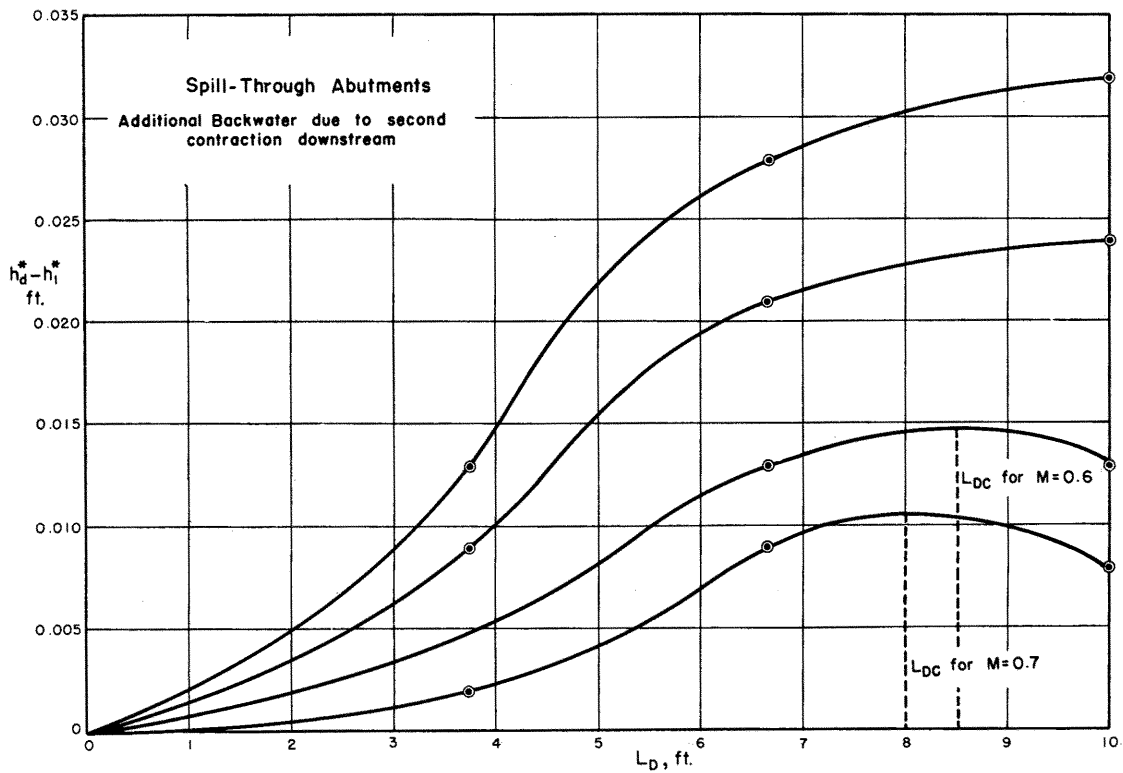


Fig. No. 5-50 Backwater of dual bridges contraction for spill-through abutments

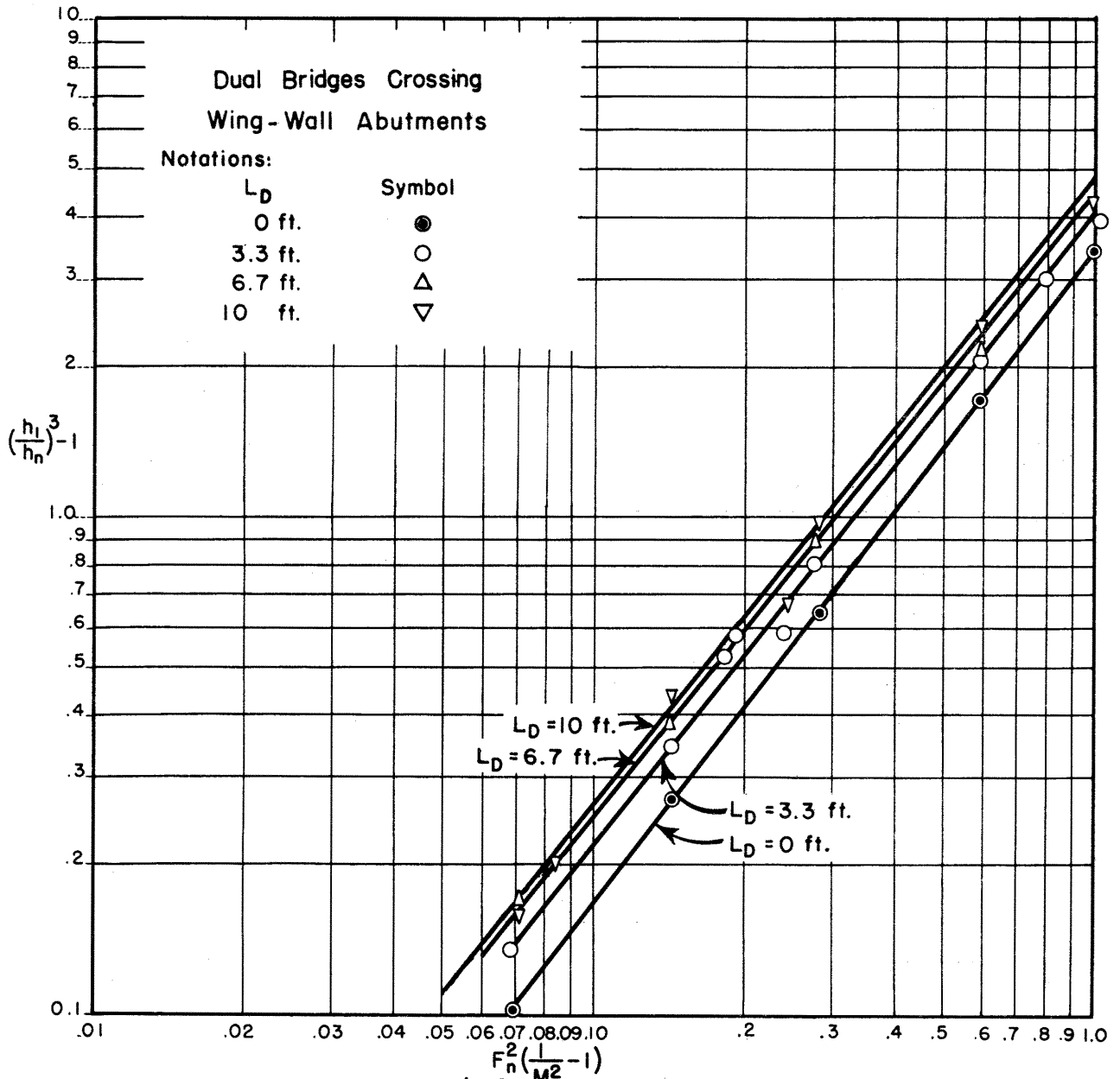


Fig. No. 5-51 Variation of $\left[\frac{h_1}{h_n} \right]^3 - 1$ with $F_n^2 \left[\frac{1}{M^2} - 1 \right]$ and L_D of dual bridges contraction -- for wing-wall abutments

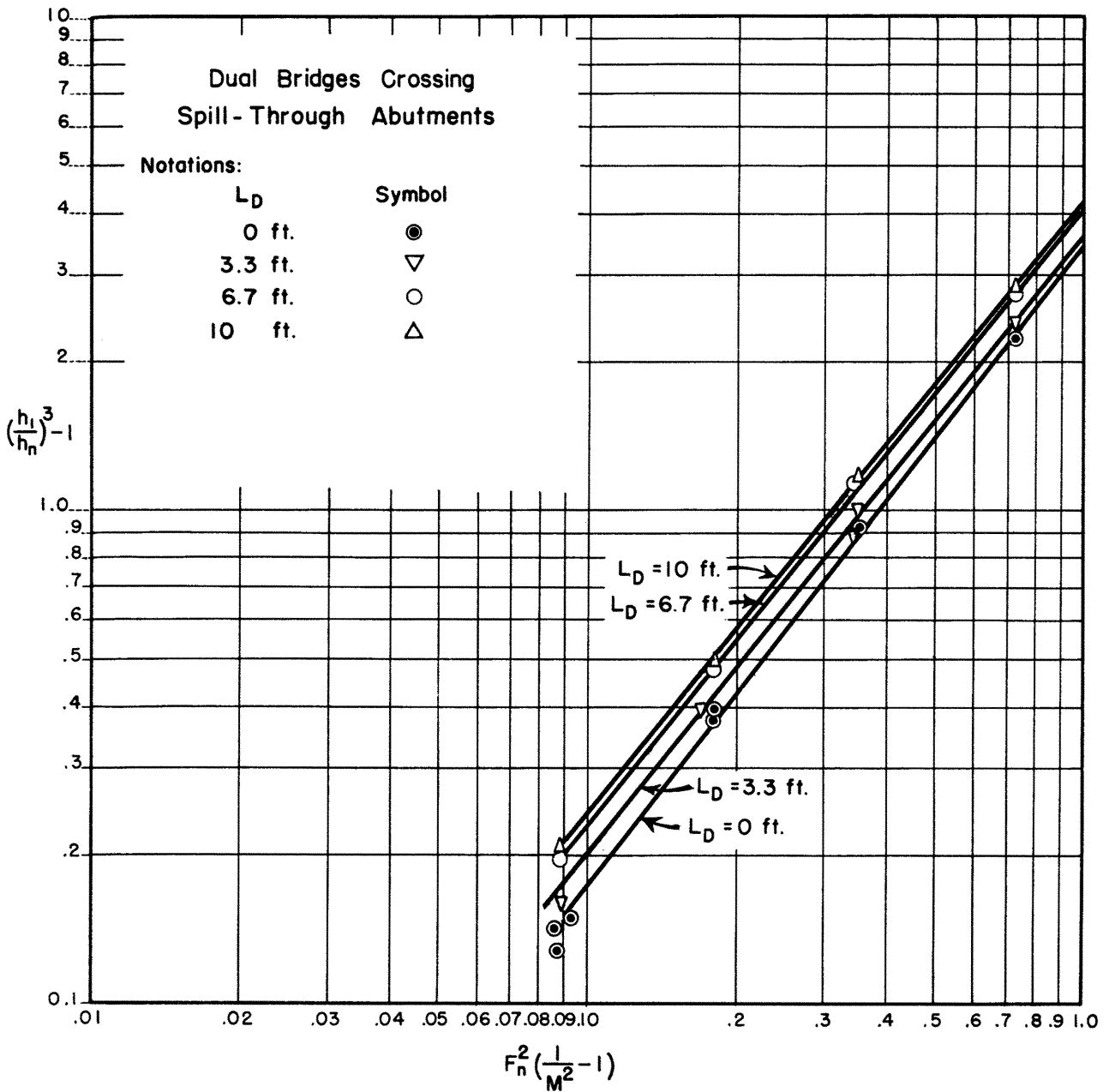
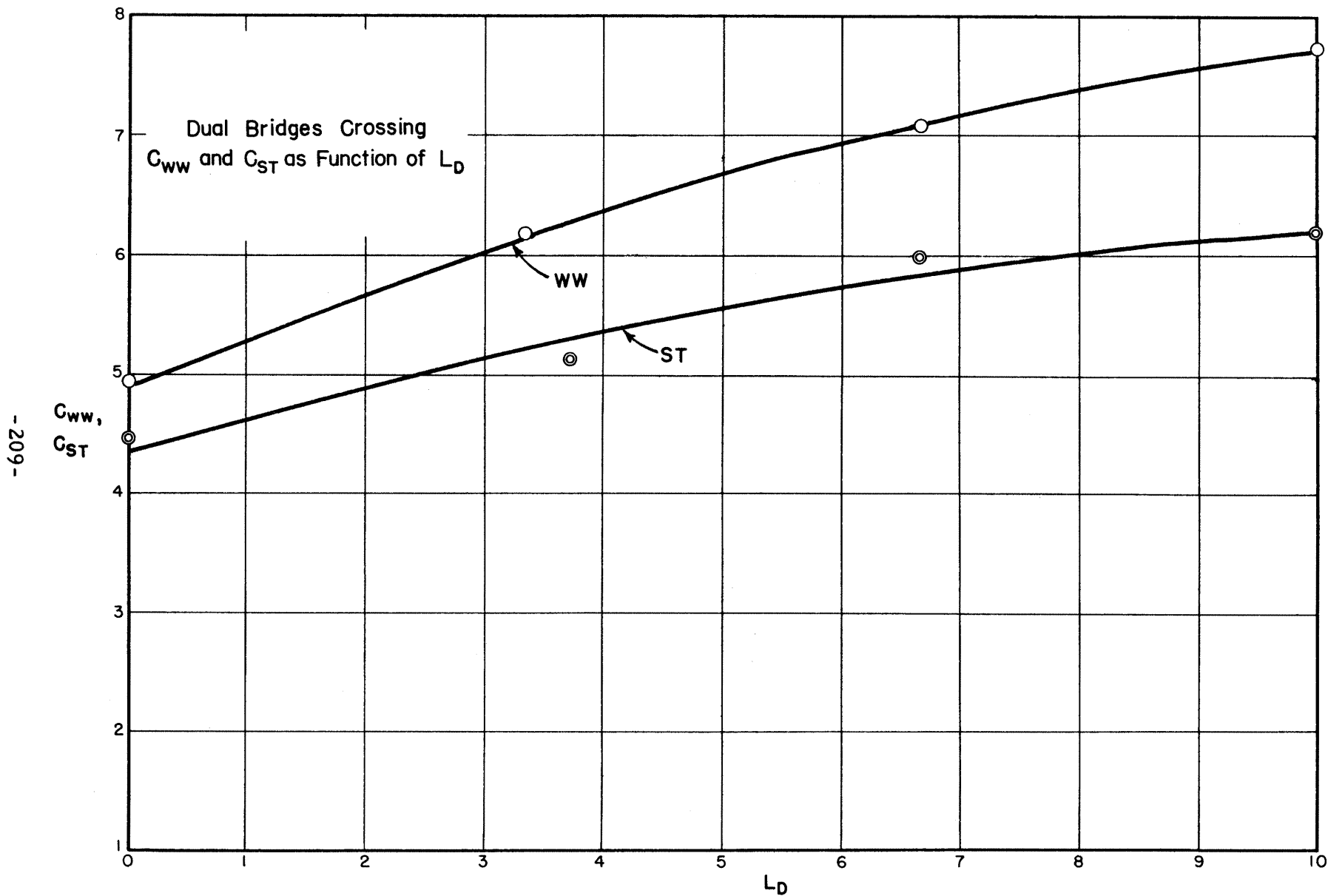


Fig. No. 5-52 Variation of $\left[\frac{h_1}{h_n} \right]^3 - 1$ with $F_n^2 \left[\frac{1}{M^2} - 1 \right]$ and L_D of dual bridges contraction for spill-through abutments



-209-

Fig. No. 5-53 Coefficient C_{ww} and C_{ST} as a function of L_D for dual bridges contraction

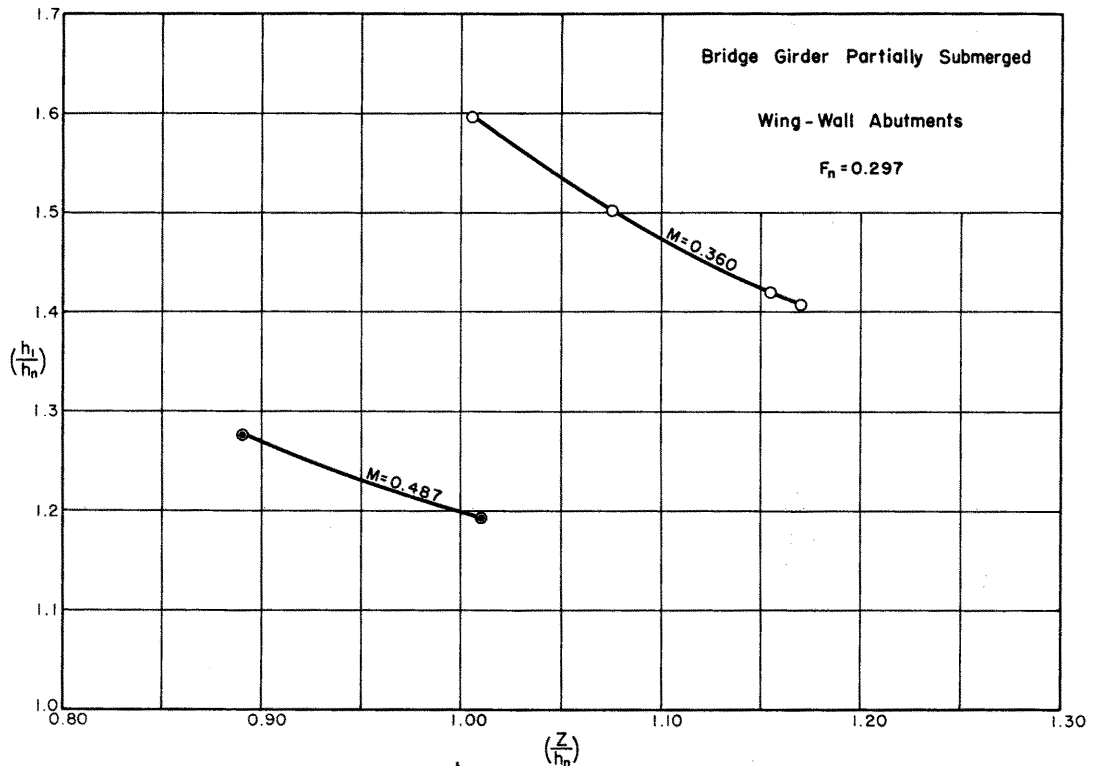


Fig. No. 5-54 Backwater ratio $\frac{h_1}{h_n}$ for bridge girder partially submerged with wing-wall abutments

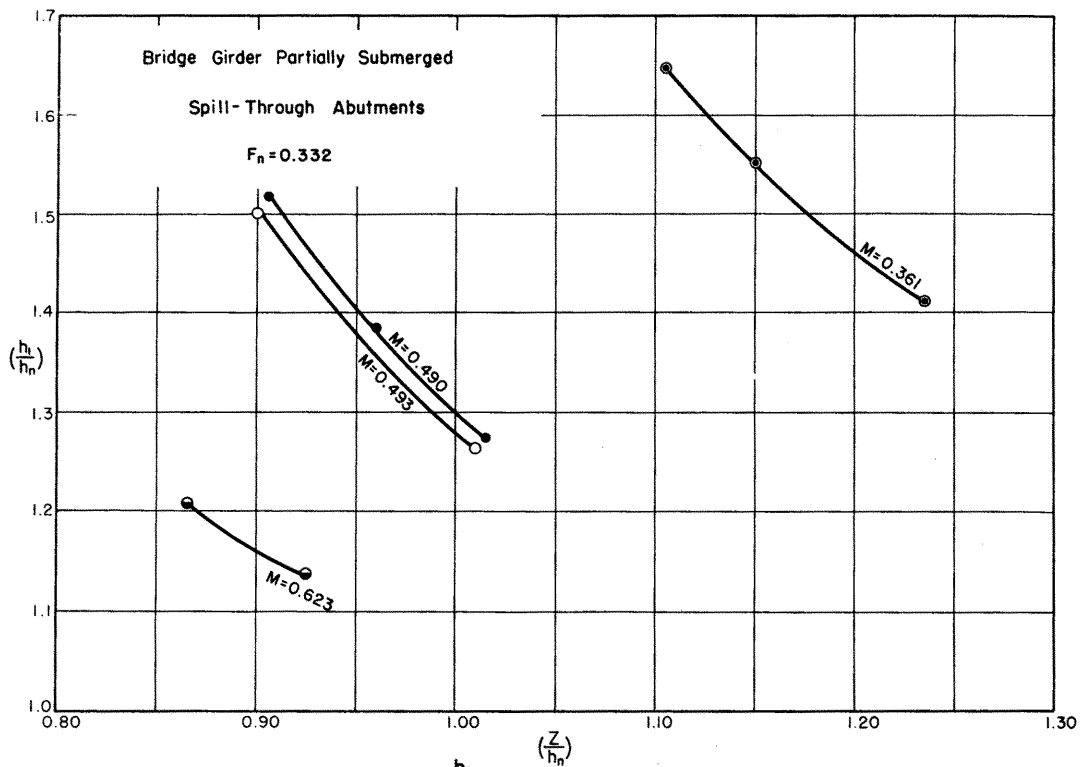
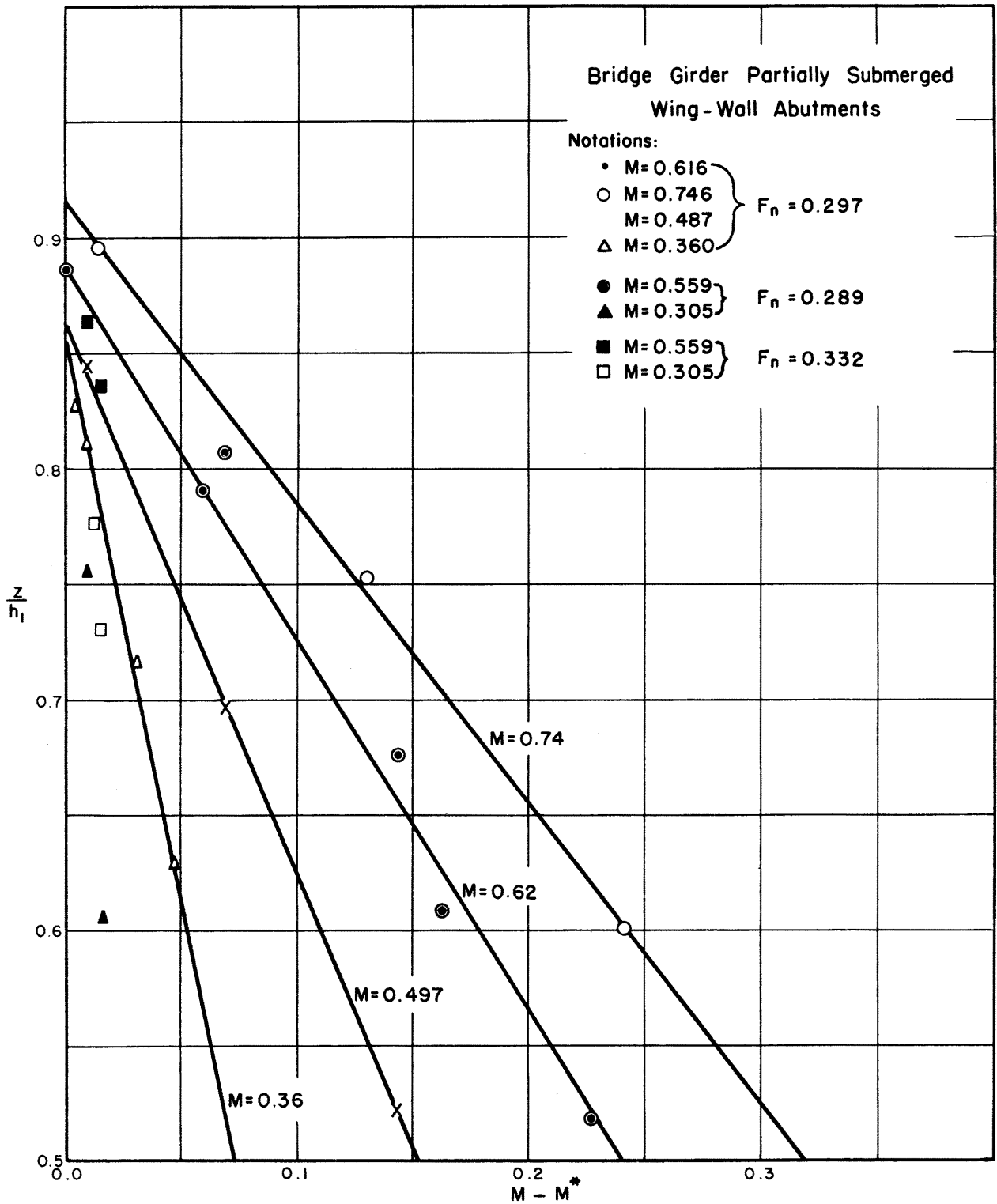


Fig. No. 5-55 Backwater ratio $\frac{h_1}{h_n}$ for bridge girder partially submerged with spill - through abutments



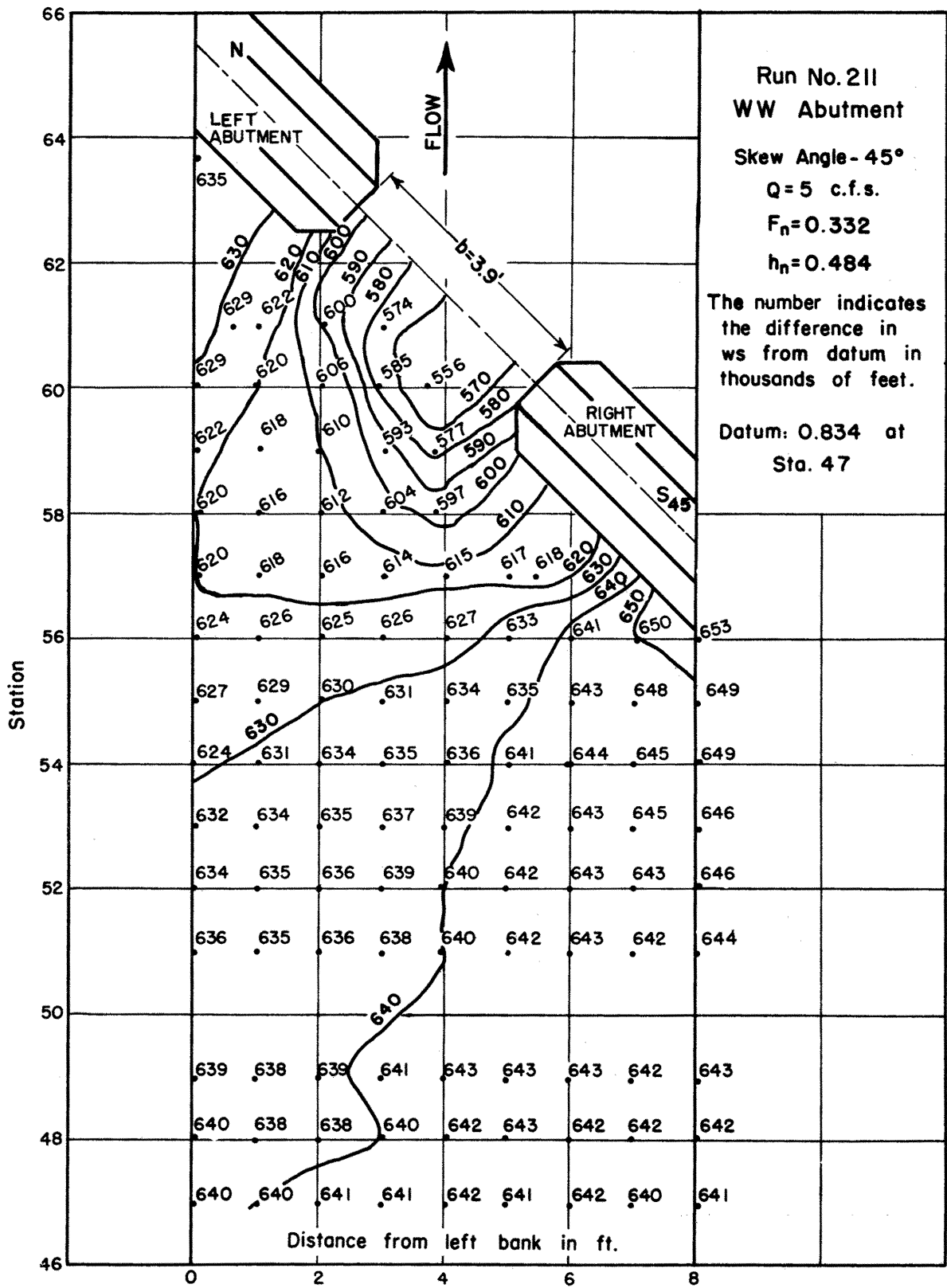


Fig. No. 5-57 Contour of the water surface elevation in the vicinity of a skew crossing

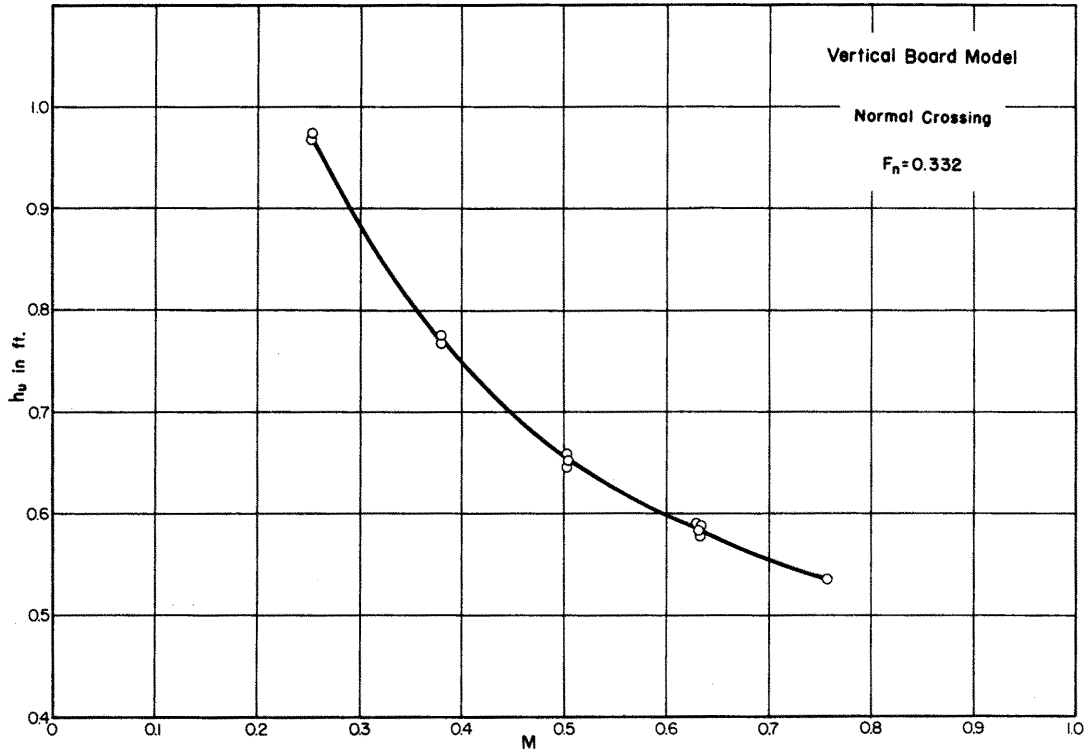


Fig. No. 5-58 Variation of h_u with M [base curve] for vertical board model at $F_n = 0.332$

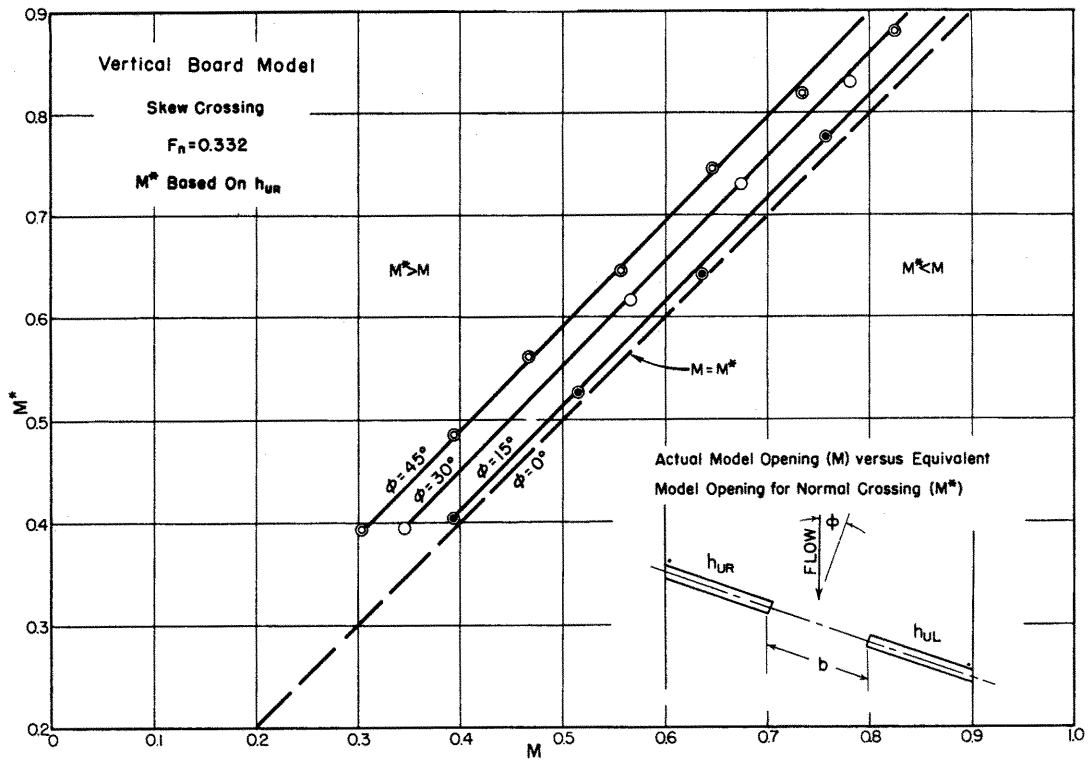


Fig. No. 5-59 Variation of M^* with M for vertical board model, skew crossing

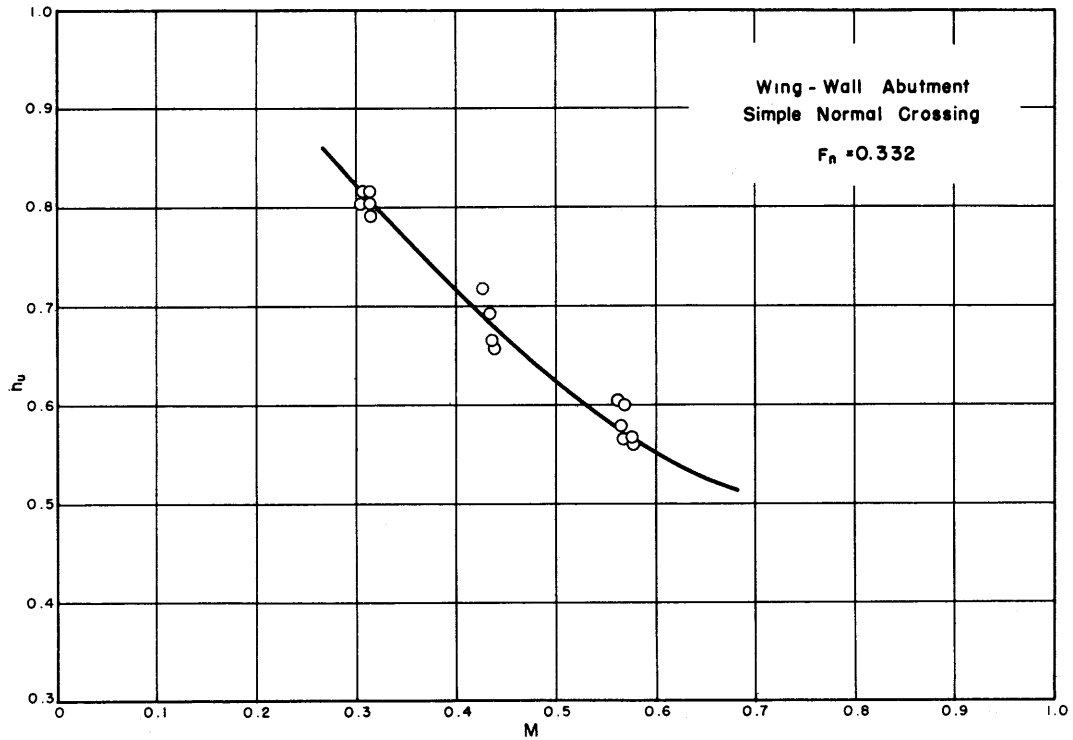


Fig. No. 5-60 Variation of h_u with M [base curve] for wing-wall abutments at $F_n = 0.332$

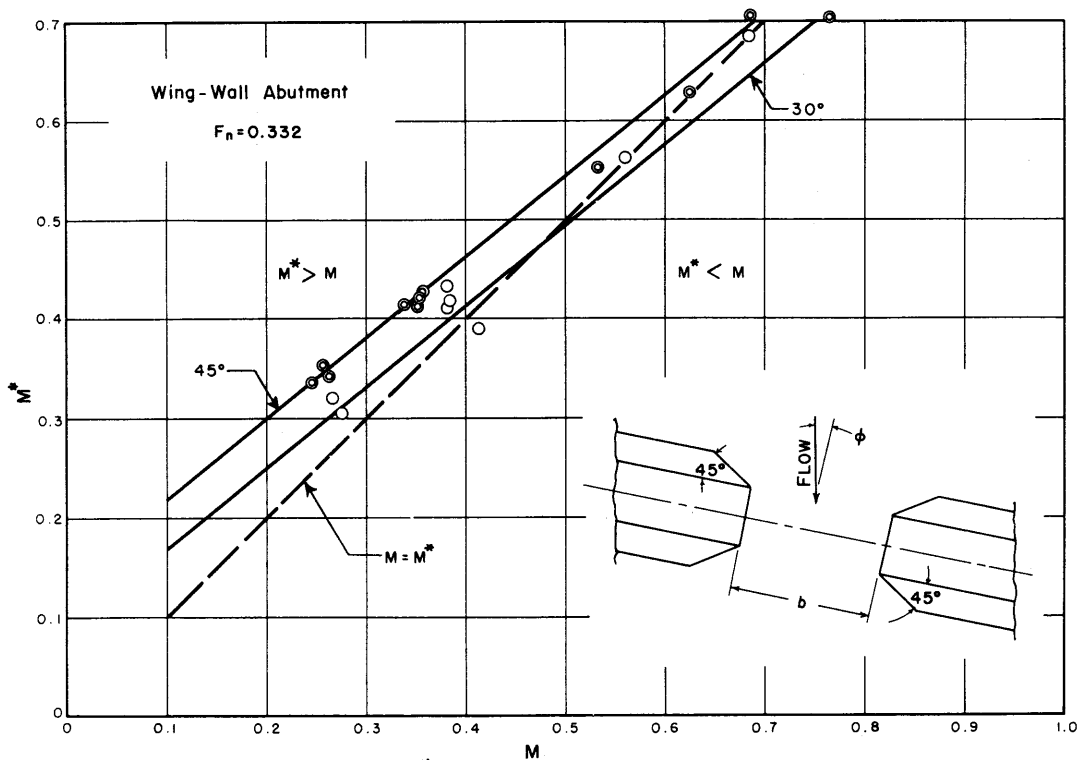


Fig. No. 5-61 Variation of M^* with M for skew crossing of wing-wall abutments with faces perpendicular to roadway

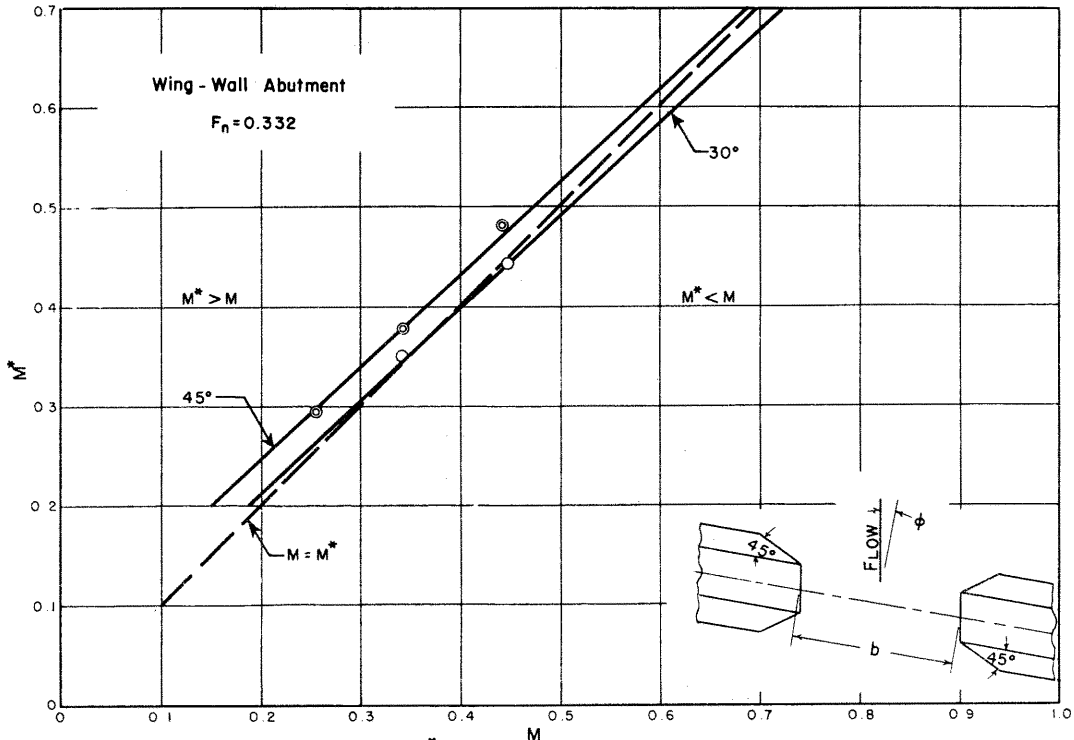


Fig. No. 5-62 Variation of M^* with M for skew crossing of wing-wall abutments with faces parallel to the main direction of flow

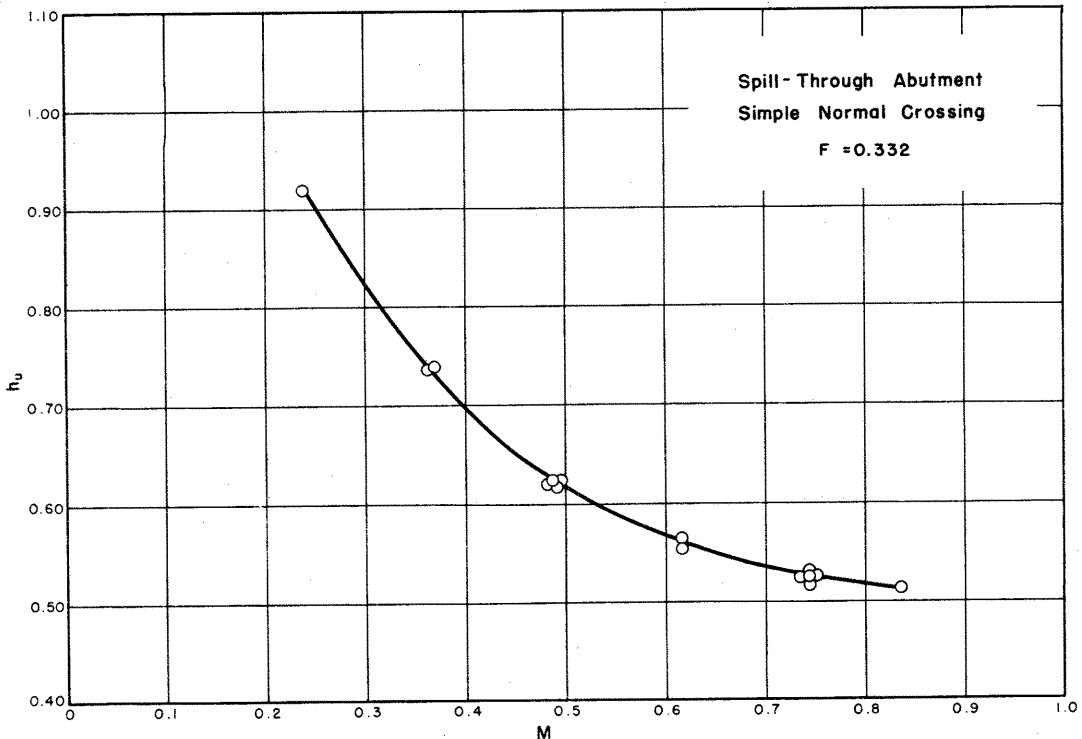


Fig. No. 5-63 Variation of h_u with M [base curve] for spill-through abutments at $F_n = 0.332$

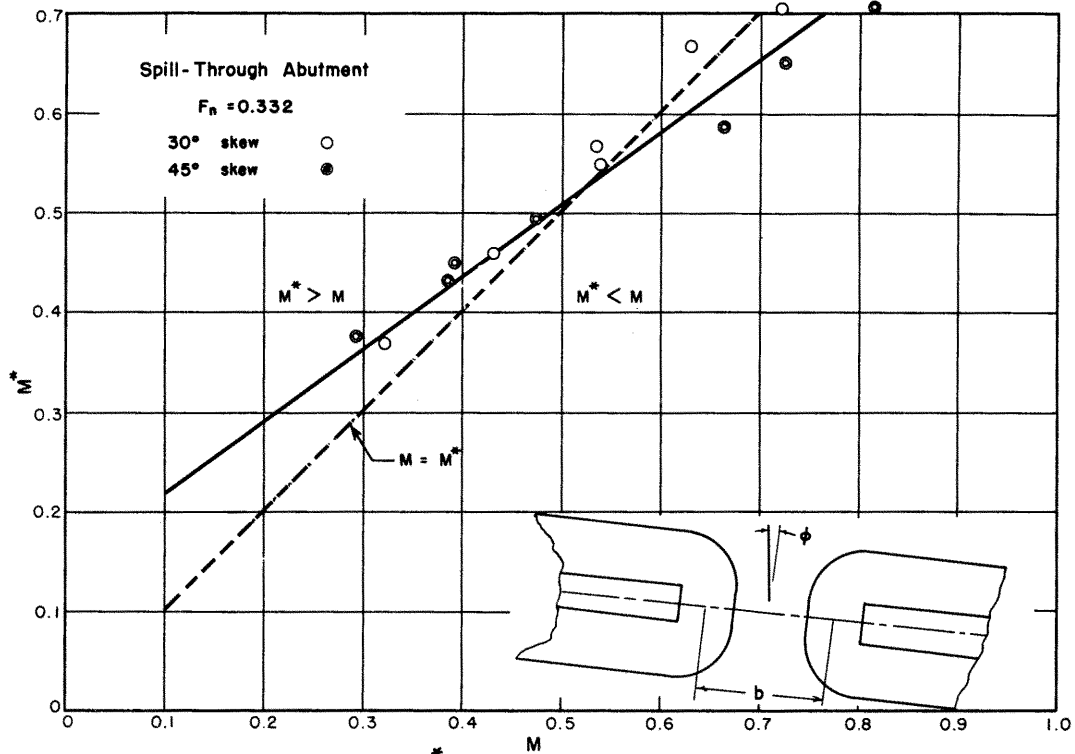


Fig. No. 5-64 Variation of M^* with M for skew crossing of spill-through abutment with faces perpendicular to roadway

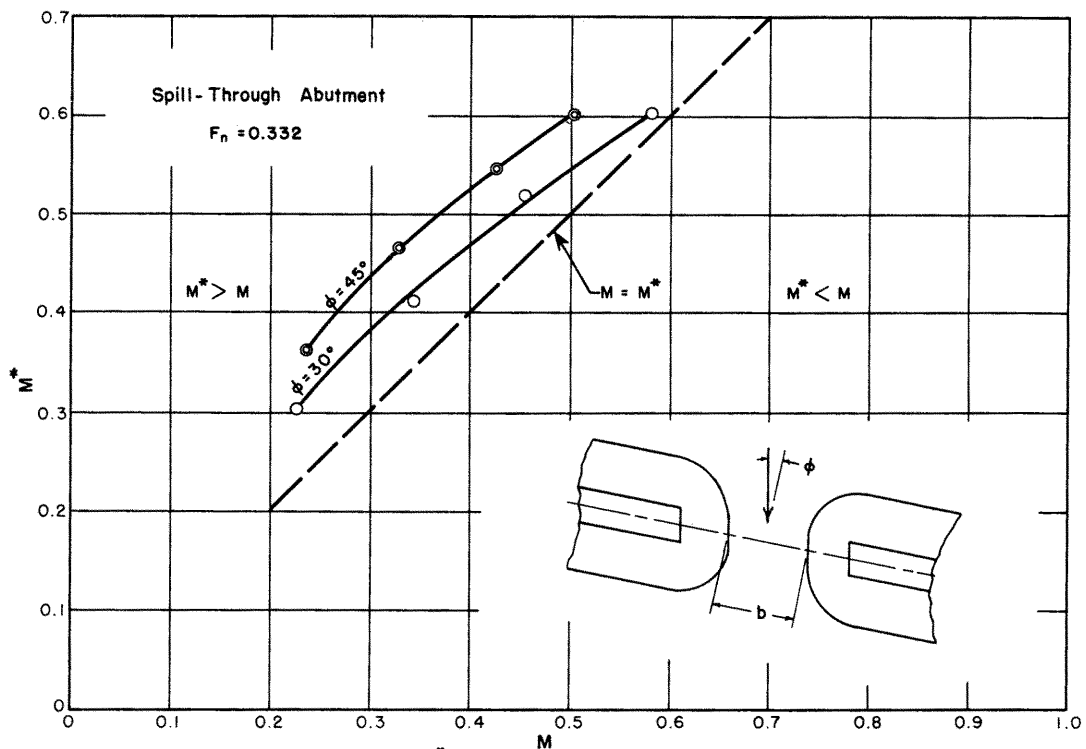


Fig. No. 5-65 Variation of M^* with M for skew crossing of spill-through abutment with faces parallel to the main direction of flow

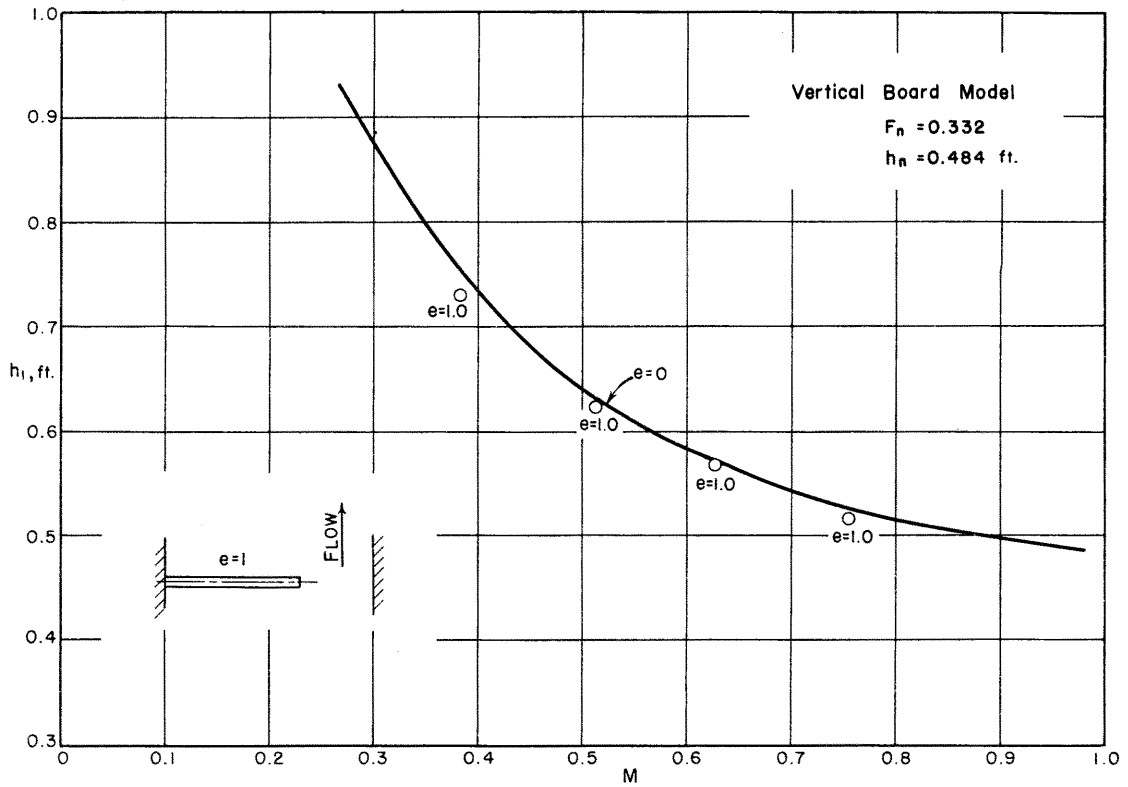


Fig. No. 5-66 Effect of eccentric crossing on h_1 for vertical-board model

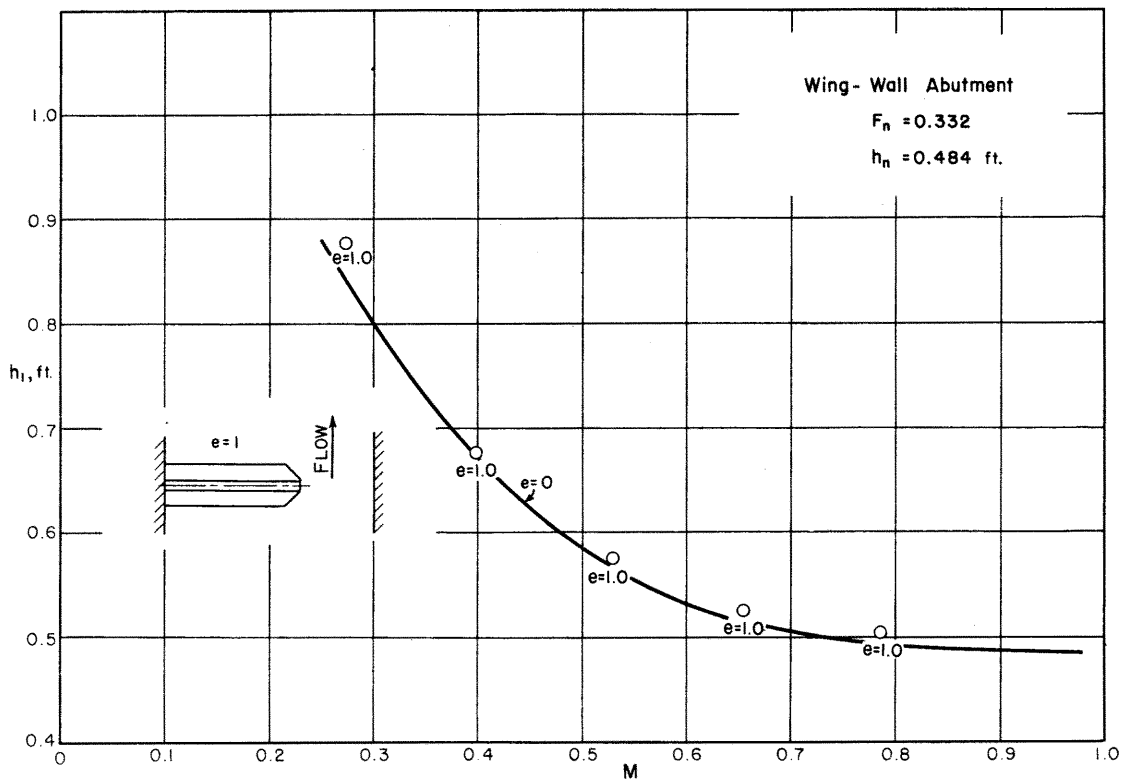


Fig. No. 5-67 Effect of eccentric crossing on h_1 for wing-wall abutments

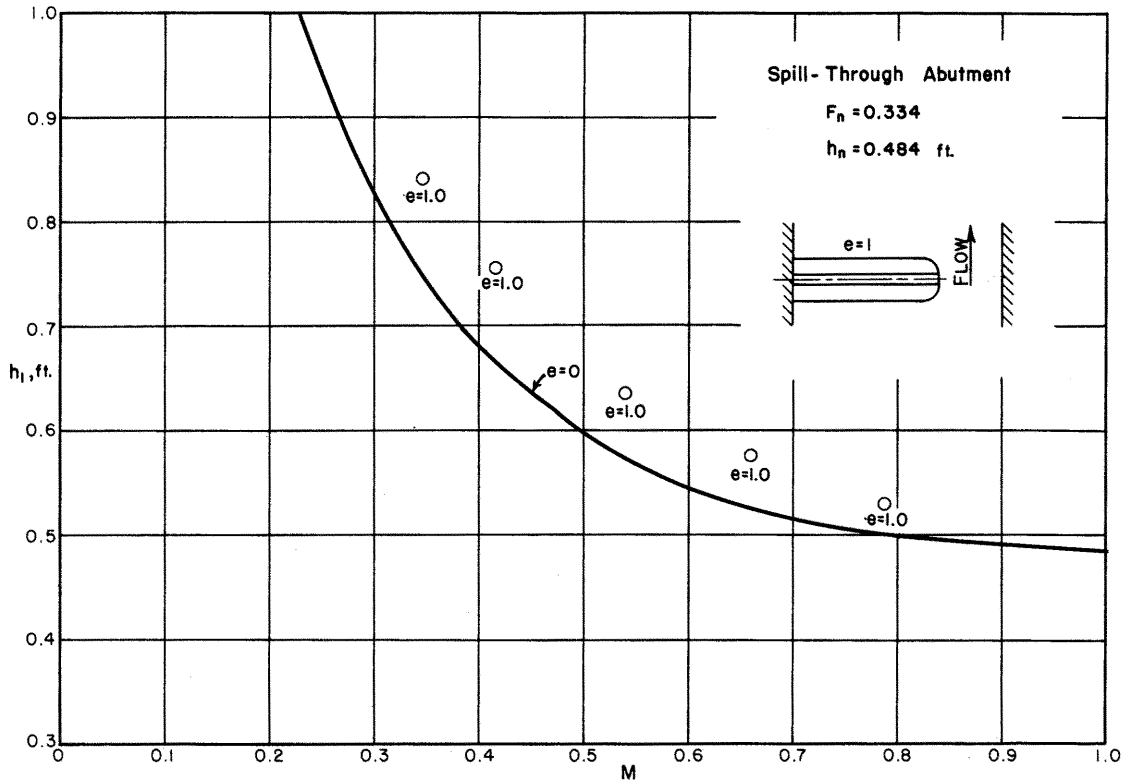


Fig. No. 5-68 Effect of eccentric crossing on h_1 for spill-through abutments

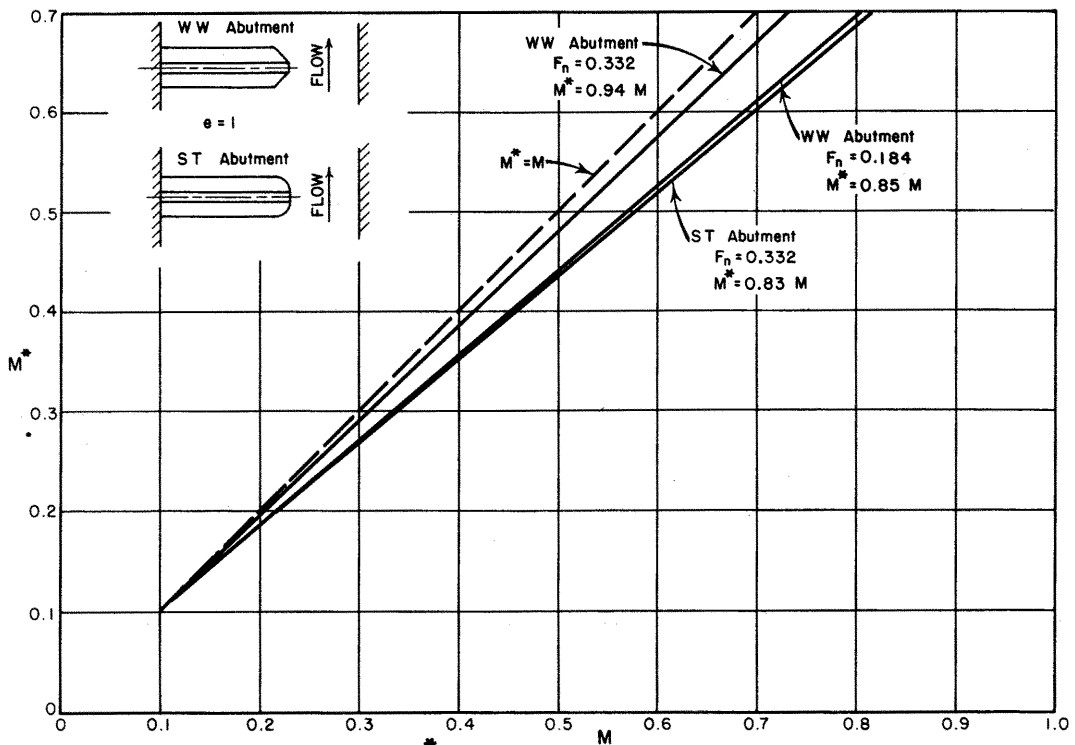


Fig. No. 5-69 Variation of M^* with M at $e=1$, for wing-wall and spill-through abutments

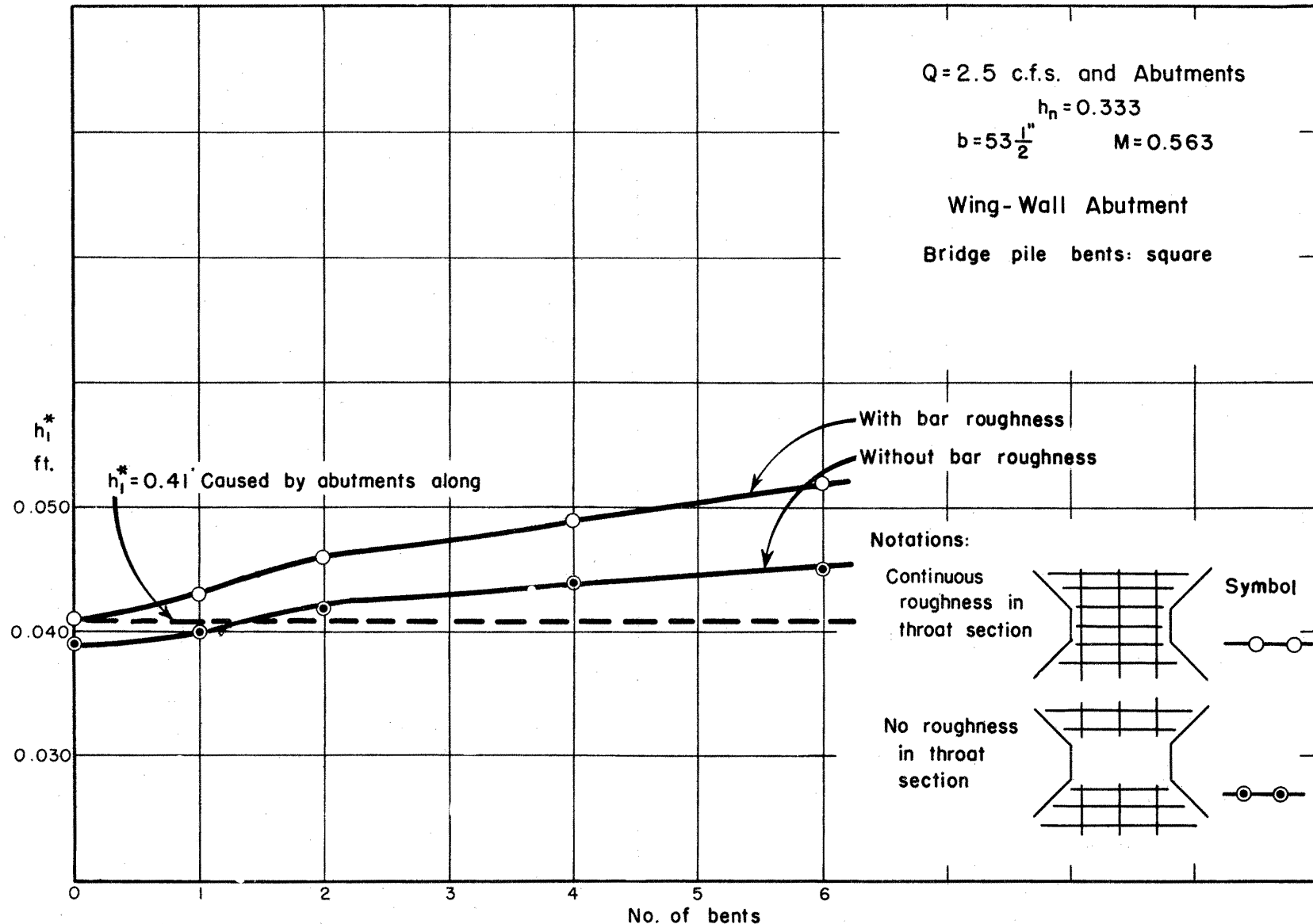


Fig. No. 5-70 Effect of bed roughness in the contraction on the maximum backwater

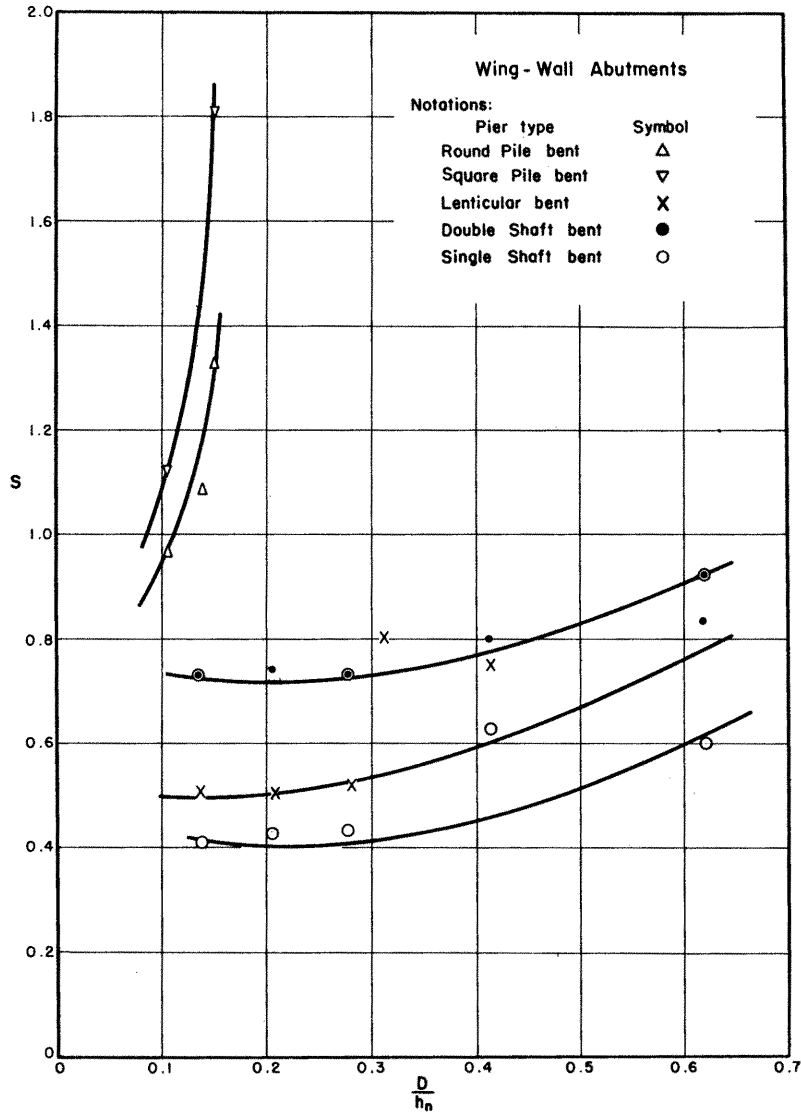


Fig. No. 5-71 Shape factor s for piers with wing-wall abutments

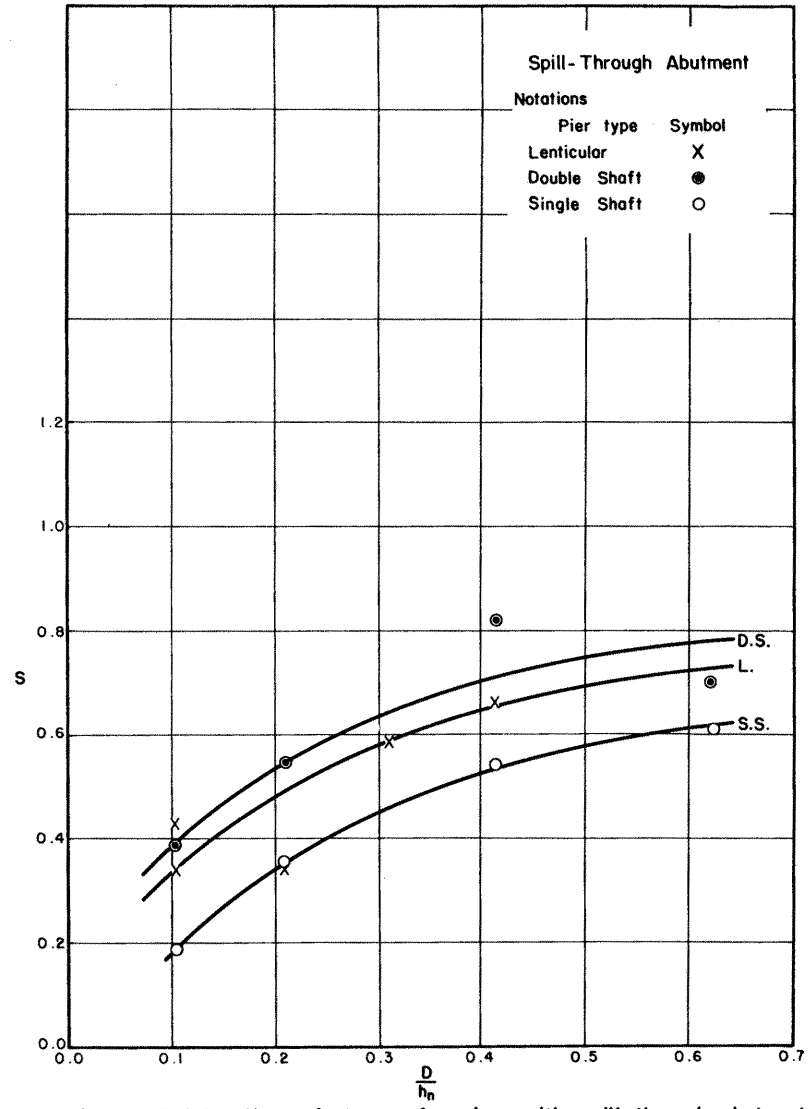


Fig. No. 5-72 Shape factor s for piers with spill-through abutment

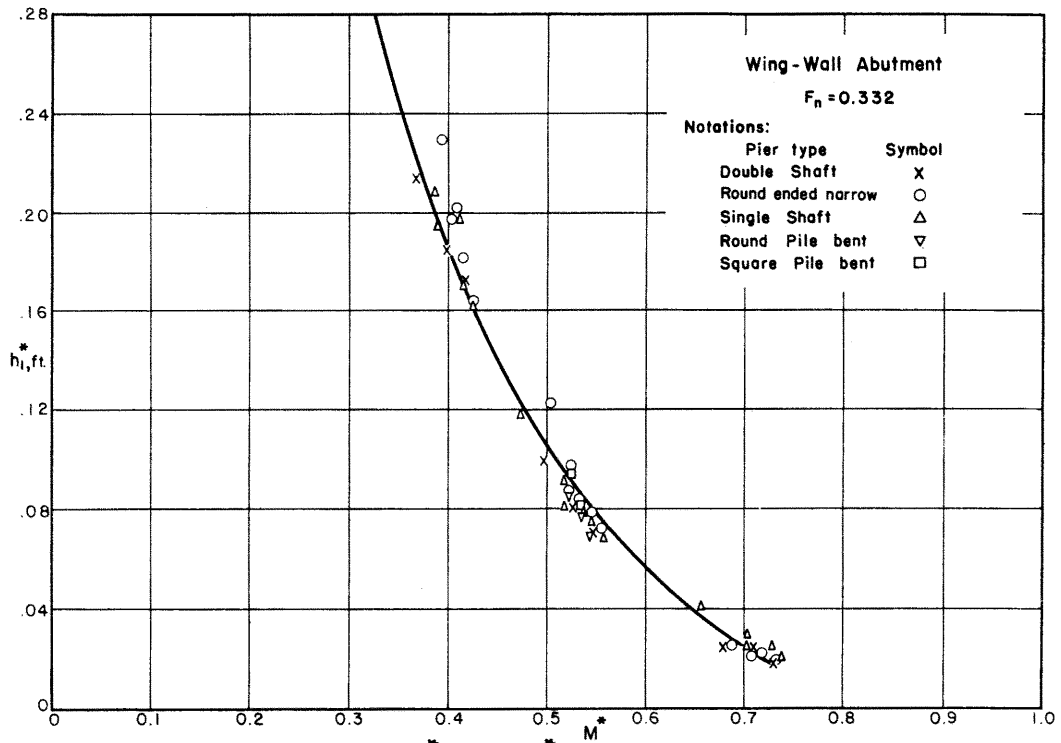


Fig. No. 5-73 Variation of h_1^* with M^* for wing-wall abutments with piers at $F_n = 0.332$

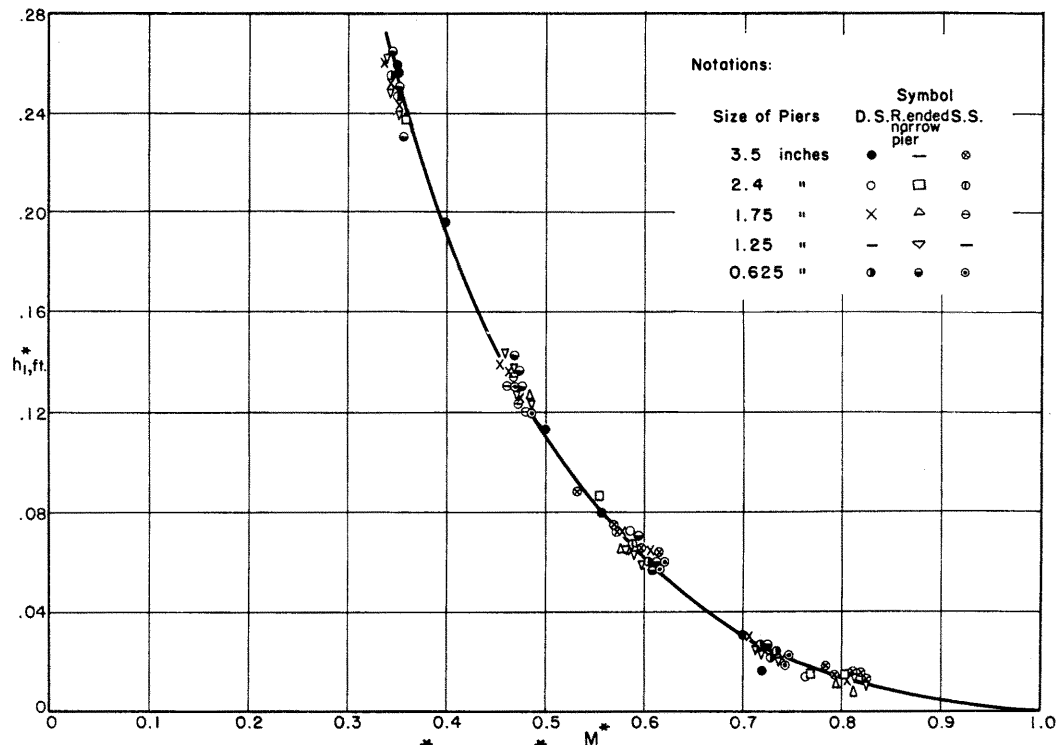


Fig. No. 5-74 Variation of h_1^* with M^* for spill-through abutments and piers at $F_n = 0.332$

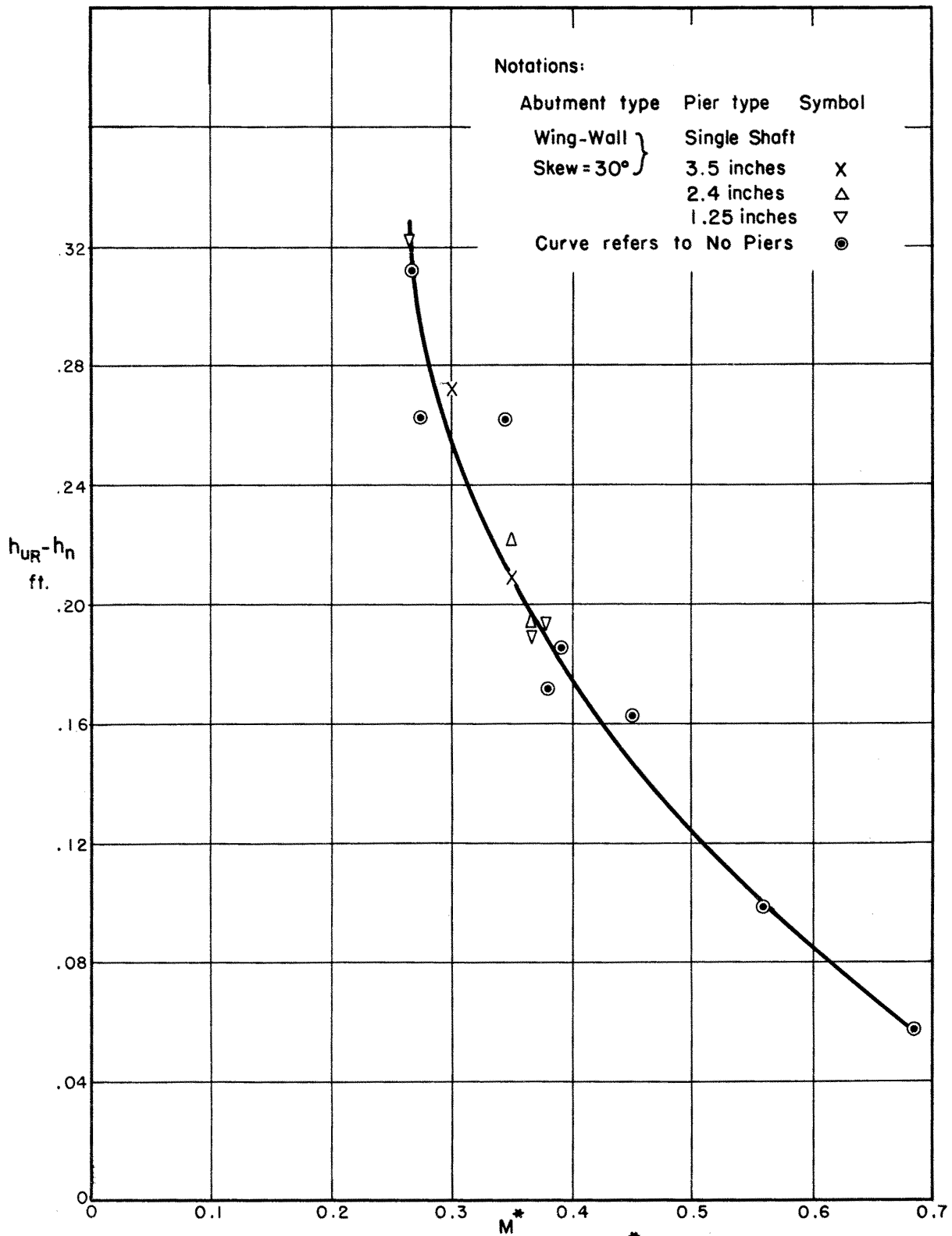


Fig. No. 5-75 Variation of $h_{UR} - h_n$ with M^* for skew crossing with piers and wing-wall abutments at $F_n = 0.332$, $\phi = 30^\circ$

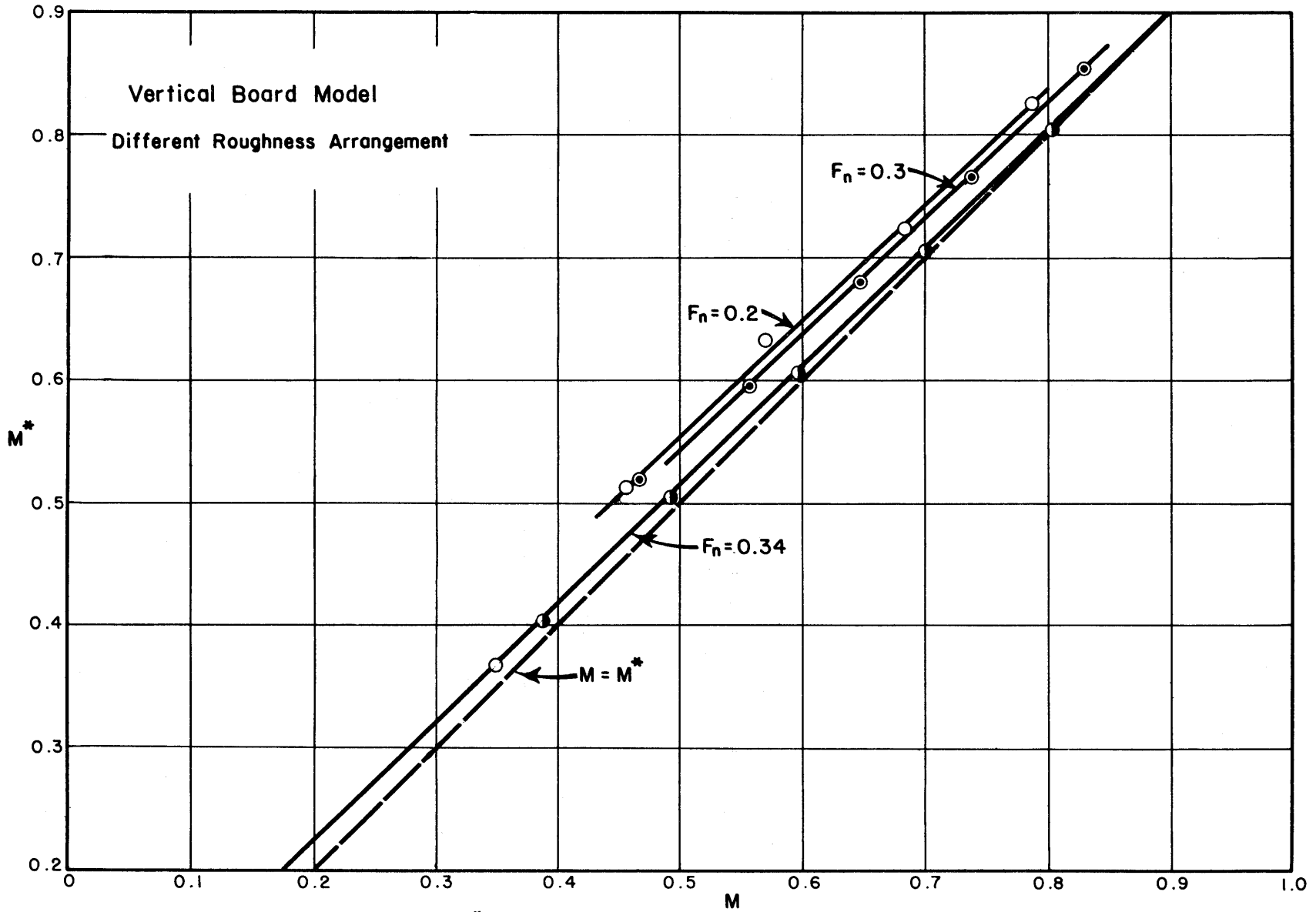


Fig. No. 5-76 Variation of M^* with M for flood-plain model with vertical board constriction

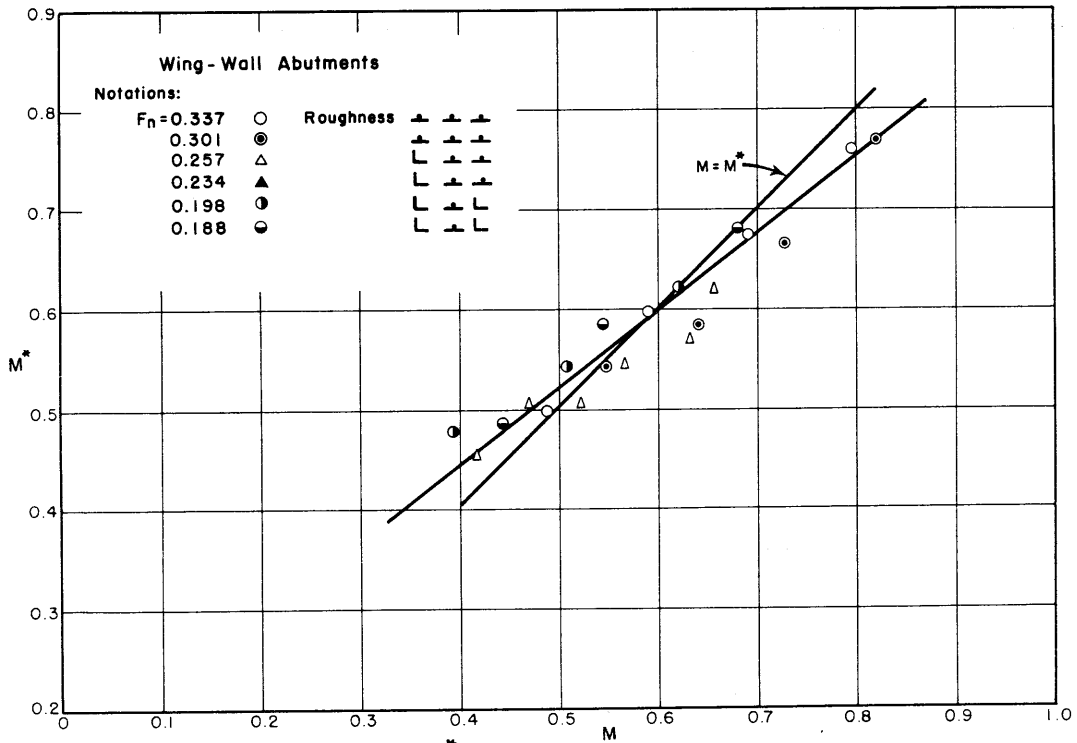


Fig. No. 5-77 Variation of M^* with M for flood-plain model with wing-wall abutments

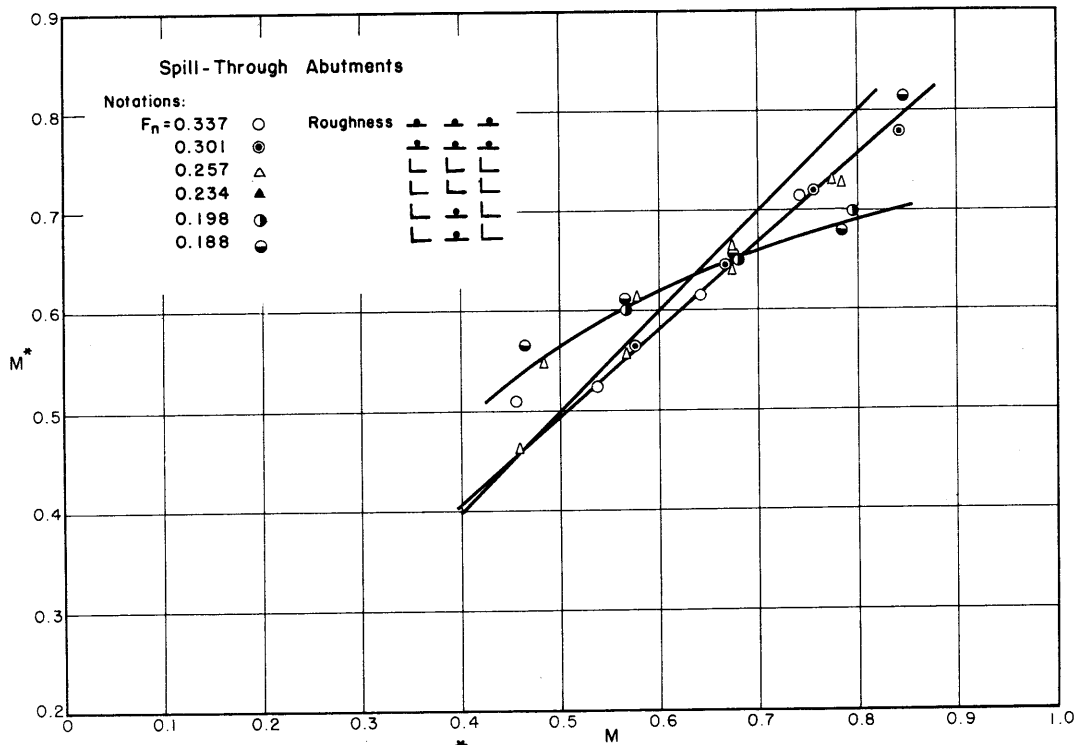


Fig. No. 5-78 Variation of M^* with M for flood-plain model with spill-through abutments

VI. ANALYSIS OF DATA FROM AN ENGINEERING APPROACH

This chapter is devoted entirely to treating experimental information in a manner acceptable to the bridge designer. In so doing a slight degree of accuracy may have been sacrificed for the sake of simplification. The reason for doing this will be self evident in the discussion which follows. Review of Chapter IV may be necessary in order to understand the laboratory crossing conditions upon which this method is based.

Dissimilarities in Model and Prototype

The model arrangement represented an idealized case in which the test channel was rectangular and of the same width throughout, the longitudinal slope was constant and the velocity distribution was more or less uniform and similar from section to section. This is the exception rather than the rule in nature. The variables were so numerous however, even for the idealized case, that individual consideration could not be given to each variable in the analysis. It is advisable to call attention to the principal differences in model and prototype and discuss the implications to understand the following practical approach.

Shape of channel cross section:- The model tests were performed mostly in rectangular channels of uniform width offering uniform resistance to flow throughout, while the typical prototype channels include flood plains, irregular cross-sections, which vary both upstream and downstream from the bridge, and boundary roughness which changes across the section as well as in the direction of flow, see Figs. 1-3 and 6-1. Although the

model analysis was based on a uniform cross sectional area, a reasonable amount of variation both upstream and downstream from the bridge was found permissible as will be shown later.

Continuity of bottom gradient:- The model tests were performed in a channel with constant bottom slope while this is seldom the case in the prototype. The prototype is subject to irregularities in the bottom slope in the vicinity of the bridge produced by deposition, boulders, scour holes, and the remains of old bridge piers and piling. Large irregularities do have an effect on the backwater. This latter phase is now under study at Colorado State University in which a flume 7.9 ft wide by 160 ft long with sand bed being utilized.

Width to depth ratio:- It is not practical or feasible to construct models of bridge waterways where very wide flood plains are involved because of the large width to depth ratio. Another way of saying this is that the depth of flow in the model would necessarily be so small compared to the width that frictional resistance of the channel and flood plains could not be reproduced to scale. The results when applied to the prototype would be questionable at best. To attempt a study of this kind with a distorted model would be even more questionable as the velocity and pressure distribution would be seriously distorted. As bridge backwater problems involve the transfer of potential to kinetic energy and vice versa, a distorted model is not a suitable tool.

The model testing was performed in a channel in which the minimum depth of flow was purposely limited to about 0.3 ft to avoid the possibility of errors due to scale effect. This limitation resulted in width to depth ratios up to 32 which is much

smaller than was desirable in attempting to compare model prototype conditions. The only satisfactory means of extending the present range materially would be to measure the backwater caused by full size structures during flood flows. This procedure will be pursued as time and conditions permit. For the time being however, information is lacking regarding the affect on the backwater of large values of the width to depth ratio.

Abutment shape:- It was not intended in this research to study fully the effect of abutment shape on backwater. As pointed out by Kindsvater and Carter, the abutment shape may have appreciable influence on the backwater. However, it is rather doubtful that such an effect obtained in a model can be accurately extrapolated to the prototype, unless the geometry of the abutment changes according to the same linear scale as that of the flow depth and width of channel.

Velocity distribution:- The approach velocity in the model was essentially uniform with small scale turbulence, while the approach velocity in the prototype is non-uniform with large scale turbulence. In the prototype the velocity distribution may be irregular because of the irregularities of the channel itself. Therefore, inclusion of a velocity head correction factor represents an attempt to correlate the prototype with the model in this respect.

Transverse water surface:- The transverse water surface across the approach channel of the model at section I, was found to be horizontal for the normal symmetrical contraction. In other words, the water surface elevation at section I was the same at the center of the channel as it was at the sides. As the only practical method of determining backwater in the prototype

is to measure the water surface elevation along the banks, it is desired to know the relation between center and bank elevations. Because of the difficulty and expense involved in obtaining it, very few data are available from field measurements, so it is necessary for the present to draw upon laboratory results, reason, and limited field experience for the answer.

Assuming the total energy across a river to be constant, the water surface at the center would be lower than at the banks because of the non-uniform velocity distribution. However, some observers [29] state that the water surface in a river cross-section, with extremely non-uniform velocity distribution, has been observed to be level or convex upward at the center where velocities are highest. Some further state that the latter could be an optical illusion produced by curvature of the earth's surface or the observer could have been misled by crests of standing waves existing in the center of the river. On the other hand, it is common knowledge among river boat pilots that floating debris is pushed toward the banks on a rising flood stage and moved back toward the center of the river on a falling stage. This would suggest that the water surface across a river is convex on the rising stage and possibly slightly concave on the falling stage. At some stage however, the water surface across the river must be essentially level. It seems reasonable to assume that this occurs near the flood crest, the condition with which the designer is most concerned. Furthermore, it can also be reasoned: that if velocity is directional while hydrostatic pressure is not, it is more logical to assume the water surface, rather than the energy to be horizontal across a river cross section at a stage approaching equilibrium.

The question remains controversial but in order to arrive at a working hypothesis on which to proceed with prototype computation, it is assumed that for a river channel where the general direction of flow is parallel to the banks, the water surface at any cross section is horizontal as peak flow is approached, see Fig. 6-2B. Thus the energy line is assumed to be convex upward. This may not be entirely true in the case of very wide rivers but the foregoing assumption offers a basis, at least for the present, by which model results and prototype measurements may be compared.

As the only practical means of measuring backwater in the prototype is near the banks, the method will be briefly illustrated. A drawing showing water surface measurements along the edge of the flood plain and along the roadway embankments at a typical normal but eccentric crossing is included as Fig. 6-3. Beginning at section I and following the right bank in a downstream direction, including the upstream side of the roadway embankment, it will be found that the measured elevations are essentially the same [with the exception of those in close proximity to the bridge abutment]. The differences observed are no greater than the inaccuracies involved in the measurements. The salient point is that the water surface measurements along the embankment are for practical purposes the same as those measured at section I. This is not true of the left bank as a fair velocity exists along that side.

Comparing the water surface profile along the right side of the river, Fig. 6-3, with the water surface profile along either side of the model channel, see Fig. 6-2A and C, it is apparent that these differ. The profile along the right bank of the river

from section I to the roadway embankment is essentially horizontal for the prototype while the model profile rises in a downstream direction approximately registering a full velocity head higher at the roadway embankment than at section I. The latter is produced by the uniform velocity distribution upstream. Studies of a number of field measurements -- such as those shown on Fig. 6-3, indicate that water surface measurements taken along the shore line and along the roadway embankments register little or no velocity head for streams with moderate or fairly wide flood plains.

As a matter of interest, attention is also called to the consistency of the water surface measurements along the right shore line downstream from the constriction, on Fig. 6-3. In the case of a symmetrical crossing, water surface measurements will be found essentially the same on both sides of the river.

Approach to Analysis

Bridge backwater analysis is far from simple or straight forward regardless of the method. As a dozen variables may be involved in a single bridge problem, it becomes evident that an ideal or extremely accurate solution will not be a simple one. Reasonable accuracy is acceptable in general highway bridge waterway design. Since a certain degree of simplification is imperative, the analysis which follows has been developed accordingly.

The Froude number and the normal depth of flow have been used extensively in the preceding model analysis. These two factors are difficult to define in channels of irregular cross section with non-uniform flow distribution such as encountered in natural streams. It is therefore necessary to alter the preceding method of analysis somewhat to make it adaptable to prototype design.

An expression for backwater has been formulated by applying the principle of conservation of energy between the point of maximum backwater upstream from the bridge, section I, and a point downstream from the bridge at which the normal stage has been re-established, section IV, see Fig. 1-1. The method, first suggested by C. F. Izzard [11], was developed on the basis that the channel in the vicinity of the bridge is essentially straight, the cross sectional area of the stream is reasonably uniform and the gradient of the bottom is constant between sections I and IV. Also the analysis applies only to steady tranquil flow.

Equating the energy between sections I and IV, Fig. 1-1

$$S_o L_{1-4} + h_1 + \alpha_1 \frac{V_1^2}{2g} = h_4 + \alpha_4 \frac{V_4^2}{2g} + E_{1-4} \quad [6-1]$$

where E_{1-4} is the total energy loss between sections I and IV.

As the testing procedure consisted of first establishing a normal water surface throughout the main channel -- parallel to the bottom -- the loss of head per foot of length, previous to installation of a bridge constriction, was the same as the bottom slope. Expressing the total loss as the normal boundary resistance $S_o L_{1-4}$, plus the remaining loss E_b , Eq 6-1 can be written:

$$h_1 - h_4 = \alpha_4 \frac{V_4^2}{2g} - \alpha_1 \frac{V_1^2}{2g} + E_b \quad [6-2]$$

Representing E_b as the product of a head loss coefficient K^* , and a known velocity head,

$$E_b = K^* \frac{V_4^2}{2g} \quad [6-3]$$

where V_{n2} is a hypothetical average velocity in the contracted section based on the flow area below normal water surface.

Replacing $h_1 - h_4$ with h_1^* , and E_p with $K^* V_{n2}^2 / 2g$, Eq 6-2 becomes

$$h_1^* = K^* \frac{V_{n2}^2}{2g} + \left[\alpha_4 \frac{V_4^2}{V_{n2}^2} - \alpha_1 \frac{V_1^2}{V_{n2}^2} \right] \frac{V_{n2}^2}{2g} \quad [6-4]$$

As the analysis is based on the assumption that the cross sectional areas at sections I and IV are essentially the same $\alpha_1 = \alpha_4$, the subscripts may be dropped. Also by referring to the equation of continuity $A_1 V_1 = A_4 V_4 = A_{n2} V_{n2}$, the velocities enclosed by parentheses in Eq 6-4 may be replaced with areas. The expression for the backwater is then

$$h_1^* = K^* \frac{V_{n2}^2}{2g} + \alpha \left[\frac{A_{n2}^2}{A_4^2} - \frac{A_{n2}^2}{A_1^2} \right] \frac{V_{n2}^2}{2g} \quad [6-5]$$

or if the backwater coefficient K^* is desired,

$$K^* = \frac{h_1^*}{V_{n2}^2 / 2g} - \alpha \left[\frac{A_{n2}^2}{A_4^2} - \frac{A_{n2}^2}{A_1^2} \right] \quad [6-6]$$

where the terms, applicable to prototype as well as model, are defined as follows:

h_1^* = backwater - ft

K^* = total backwater head loss coefficient

α = velocity head coefficient

A_{n2} = gross water area in constriction measured below normal stage - sq ft

V_{n2} = average velocity in constriction or Q/A_{n2} - fps

A_4 = water area at section IV [where normal stage has been re-established] - sq ft, and

A_1 = total water area at section I - sq ft.

If piers are present in the constriction, these are ignored in the determination of A_{n2} . The velocity V_{n2} does not represent an experimentally measured velocity but rather a reference velocity readily computed for both model and field structures.

For practical purposes, the backwater is simply the product of K^* , the backwater coefficient, which was determined experimentally, and the velocity head $V_{n2}^2/2g$. The expression

$$\alpha \left[\left(\frac{A_{n2}}{A_4} \right)^2 - \left(\frac{A_{n2}}{A_1} \right)^2 \right]$$

represents a correction term for the difference in kinetic energy between sections I and IV, expressed in areas rather than velocities. The term is significant primarily in cases where [1] α is large, [2] A_1 is substantially greater than A_4 , [3] the initial velocity in the natural stream is high, or [4] the contraction of the channel is severe.

Backwater Coefficient

The backwater coefficient K^* , in Eqs 6-5 and 6-6, which was determined experimentally, varies primarily with

1. Stream constriction as measured by the opening ratio M ,
2. Type and shape of bridge abutment - wing-wall, spill-through, etc.
3. Number, size, shape and orientation of piers in the constriction,
4. Eccentricity - or asymmetric position of bridge on the flood plain

5. Skew [bridge crosses river or flood plain at other than 90 degrees], and
6. Froude number.

There are other variables of a secondary nature which may have a cumulative or compensating effect in themselves depending on the problem at hand. From a practical standpoint, the unmentioned or secondary variables are unimportant. The Froude number as such does not appear in this analysis as it has no definite meaning when applied to irregular stream channels. It has not been entirely neglected, however, as the back-water coefficient can be also written

$$K^* = \frac{2h_1^*}{F_{n2}^2 h_n} .$$

Referring to section I, Fig. 1-3, the opening ratio M can be expressed as

$$M = \frac{Q_b}{Q_B} \quad [6-7]$$

where $Q_B = Q$
instead of

$$M = \frac{b}{B}$$

as previously defined; where Q_b is the discharge of the approaching flow having a channel width b ; and Q is the total discharge.

Because of changing roughness and the irregular shape of a natural stream channel, the discharge is not uniform across a river but varies in some such manner as indicated by the stream

tubes in Fig. 6-1. The channel opening ratio M , is most easily explained in terms of discharges but these quantities may not be known in the prototype.

In prototype computations, conveyance is used as a means of determining the distribution of flow in the natural river channel upstream from a bridge. The approach section is usually divided into subsections, differentiated according to channel roughness and marked changes in depth of flow. The conveyance of each subsection is computed individually from which the flow in each subsection is then determined.

Conveyance is a measure of the ability of a channel to transport flow. According to the Manning formula for open channel flow, the discharge in a subsection of a channel is

$$Q_{\sigma} = \frac{1.49}{n_{\sigma}} A_{\sigma} R_{\sigma}^{2/3} S^{1/3} \quad [6-8]$$

where Q_{σ} = discharge through a sub-section

A_{σ} = area of the sub-section

R_{σ} = hydraulic radius of the sub-section

n_{σ} = Manning n of the subsection.

By rearranging, the conveyance of the same sub-section is

$$\frac{Q_{\sigma}}{S_{\sigma}^{1/2}} = \frac{1.49}{n_{\sigma}} A_{\sigma} R_{\sigma}^{2/3} = \underline{K}_{\sigma} \quad [6-9]$$

in which \underline{K}_{σ} , the conveyance of sub-section σ can be expressed either in terms of flow factors or strictly geometric factors.

Since conveyance is proportional to discharge, assuming all subsections to have the same longitudinal slope, M also can be expressed in terms of conveyance as

$$M = \frac{K_b}{K_1} \quad [6-10]$$

where K_b and K_1 represent the conveyance at section I, corresponding to the projected opening width b and the total channel width B , respectively.

Establishing the opening ratio M is the most lengthy and difficult part of the bridge waterway analysis but this parameter is also the most important factor in the backwater determination. In practice, several state highway departments have contractual agreements with the U. S. Geological Survey by which the latter organization supplies a flood frequency curve, a stage discharge curve and conveyance curves for streams at proposed bridge sites.

Base curves - normal crossings:- The backwater coefficient K^* for normal crossing is denoted as K_b . Results of the first series of tests relating backwater coefficient K_b , to abutment geometry and the opening ratio M are included as Figs. 6-4A to 6-7A. The information is presented as several curves to show the experimental points. Fig. 6-4A relates K_b to M for a 45-degree wing-wall abutment with $1\frac{1}{2}$:1 embankment slopes. The points show some scatter but attention is called to the wide variety of conditions from which these data were gathered. These included two widths of test channel, four gradients of the channel and two degrees of bottom roughness. Points are also plotted for tests with a channel other than rectangular in cross section. Since several secondary variables appear in combination in the backwater coefficient K_b , the combined effect may be instrumental in the scatter. The essential experimental data from which the points were plotted is shown tabulated on Tables 1 and 2 of Appendix C. All reliable experimental data have been included in this Appendix for record purposes.

A factor which greatly aided in simplifying the analysis was the tilting flume. By setting the flume on a longitudinal slope and carefully adjusting the flow to the same depth throughout before beginning a test, both the slope of the flume S_o , and the boundary roughness n , are reflected in the normal depth of flow; thus neither S_o , nor n , appear as a separate factor in any of the design curves.

Curves relating K_b to M for all wing-wall abutments tested are shown on Fig. 6-5A. The experimental points are plotted for all but the 45 degree wing-wall abutment [Appendix C, Table 3]; the latter were shown on Fig. 6-4A. The embankment slope was $1:1\frac{1}{2}$ for each case. The curves show the 60 degree wing-wall abutments to be the most efficient of this group.

The proportions of the model were such that critical flow occurred in the constriction for some points with M values smaller than 0.5. Although some of these points are shown, they were disregarded in the drawing of curves.

Experimental results for the spill-through abutment with $1:1\frac{1}{2}$ embankment slopes are shown on Fig. 6-6A. As in the case of the 45 degree wing-wall abutment, the plotted points are representative of two channel widths, four channel slopes, two degrees of bottom roughness and include tests made on a flood-plain model [Appendix C, Tables 4 and 5]. The curve differs only slightly from those for the 45 and 60 degree wing-wall abutments.

The spill-through abutments were tested also for 1:2 and 1:1 embankment slopes to observe the effect on the back-water coefficient, K_b . The experimental points for the 1:2 and 1:1 embankment slopes are shown plotted on Fig. 6-7A

[Appendix C, Table 4]. It appears that the variations in embankment slopes tested are of minor importance in this practical analysis.

Roadway widths ranging from a single traffic lane to six lanes were tested by models for both wing-wall and spill-through abutments. It was found that variation of the width of bridge over this range produced only a negligible effect on the value of K_b , so this factor was treated as a secondary variable and not isolated in the analysis. The magnitude of this variable can be observed from the preceding model analysis in Chapter V and Figs. 5-30 and 5-31.

The charts on Fig. 6-5A and Fig. 6-7A are designated "base curves". These are for normal crossings without piers, eccentricity or skew. Backwater coefficients read from the base curve will be modified by the addition of incremental backwater coefficients when piers, eccentricity and skew are involved.

The procedure for computing backwater for a simple normal crossing without piers or other complications is to enter the appropriate curve on Fig. 6-5A or 6-7A with the computed value of M and obtain from the base curve the backwater coefficient K_b . In this particular case $K_b = K^*$. The backwater, h_1^* , is then determined by substituting appropriate values for the terms in Eq 6-5.

Piers:- The introduction of piers in a bridge constriction results in an increase in backwater and likewise an increase in the backwater coefficient over that shown by the base curves. This is illustrated on Fig. 6-8 where the backwater coefficient curves for circular pile bents, located between spill-through abutments, are compared with the base curve. The deviation

from the base curve increases as the value of J increases and is most pronounced for $M = 1.0$. The term J , for normal crossings, is the ratio of the area occupied by the piers A_p , to the gross area of the bridge constriction A_{n2} , both integrated between the normal water surface and the bed of the stream.

From an examination of Fig. 6-8, it may appear odd that the values of ΔK_p are greatest for $M = 1.0$. It is logical to reason that if the value of J is held constant, the backwater should rise as the severity of the constriction increases [value of M decreases]. This reasoning is correct. One might expect the value of ΔK_p to do likewise, but this is not true. If it is recalled that the incremental backwater coefficient $\Delta K_p = \frac{\Delta h_1^*}{V_{n2}^2/2g}$, it is apparent that ΔK_p varies as the reciprocal of the second power of the mean velocity in the constriction. As the value of M increases, the magnitude of the velocity head decreases at a much slower rate than Δh_1^* , accounting for larger values of ΔK_p for $M = 1.0$, Fig. 6-8.

The incremental backwater coefficient [or deviation from the base curve] for each pier type tested is shown plotted with respect to J for $M = 1.0$ on Fig. 6-9A. For values of M less than 1.0, the value of ΔK decreases as Fig. 6-8 indicates. Fortunately this rate of decrease in ΔK with M was essentially the same for all pier types and could be represented as a single curve, Fig. 6-9B. Thus to obtain the incremental backwater coefficient, enter Fig. 6-9A with the proper value of J and pier type and read ΔK from the ordinate for $M = 1.0$. Then enter Fig. 6-9B with the actual value of M and obtain the factor, θ . The incremental backwater coefficient for values of M less

than 1.0 is

$$\Delta K_p = \Delta K [\text{Fig. 6-9A}] \times \theta [\text{Fig. 6-9B}]$$

These curves are applicable to both wing-wall and spill-through abutments.

A more rigorous analysis of the effect of piers is hardly justified in that the coefficient of drag, which varies as the Reynold's number, will not scale up correctly to the prototype. In the conversion process the drag effect will be larger than that which will be experienced in the prototype for similar pier arrangements. In short, where similitude is dependent simultaneously on both the Froude and Reynold's laws, only one can be satisfied completely. In this case the Froude law has been chosen to interpret similitude for the following reason. Upon considering the prototype, there are equally unpredictable factors to be considered. Collection of trash and debris at piers during flood is the rule rather than the exception in field structures. Thus, if a pier is 2 ft in diameter, while collection of trash gives it an effective width of 3 ft, the model backwater computations would tend to compensate for this increase in pier diameter in the prototype.

The procedure for computing backwater for bridge contractions involving piers is to compute M as outlined previously, without regard for piers. With this value of M obtain K_b , from the appropriate base curve on Figs. 6-5A or 6-7A. The procedure so far is the same as would be followed were no piers involved. The value of J , is next computed for the piers in question. Then knowing M and J , and the pier type, the incremental backwater coefficient ΔK_p , due to piers, can be obtained

from Fig. 6-9. The over-all backwater coefficient for a normal crossing with piers will be

$$K^* = K_b + \Delta K_p \quad . \quad [6-11]$$

The backwater is then computed by substituting K^* in Eq 6-5. The term $V_{n2}^2/2g$ in Eq 6-5 is computed on the gross area under the bridge [ignoring piers] referred to the normal stage.

Although ΔK_p has been considered independent of pier diameter or width the value should be increased for bents with more than five piles. For example, a bent with 10 piles should be given a value of ΔK_p about 20 per cent higher than those shown for 5-pile bents [23].

Eccentricity:- A bridge is considered eccentric if the quantity of flow outside the projected length of the bridge is greater on one side than on the other. Eccentricity e , is defined here as unity minus the ratio of the lesser to the greater discharge or

$$e = [1 - \frac{Q_R}{Q_L}] \text{ where } Q_R < Q_L \quad [6-12]$$

or

$$e = [1 - \frac{Q_L}{Q_R}] \text{ where } Q_L < Q_R \quad .$$

Reference to the definition sketches on Figs. 1-8 and 6-12 will aid in clarifying the terminology.

For a given set of conditions, it was found that the backwater coefficient was larger than that for the base curve only for

severe eccentricity, e.g., when the flow outside the projected length of the bridge was approximately 80 per cent greater on one side than on the other. The incremental backwater coefficient curves for eccentric crossings ΔK_e , or differences from the base curve, are shown plotted with respect to M on Fig. 6-12A. The points shown represent both wing-wall and spill-through abutments for one value, $e = 1.0$. [Appendix C, Table 8] The scarcity of experimental results on eccentric crossings was due to the limited width of the test flume. It is planned to continue this work in a wider flume at a later date.

The over-all backwater coefficient for a normal bridge crossing with piers and eccentricity would be

$$K^* = K_b[\text{Fig. 6-5A or 6-7A}] + \Delta K_p[\text{Fig. 6-9}] + \Delta K_e[\text{Fig. 6-12}] \quad [6-13]$$

Skew crossings:- Testing on skew crossings was performed on two sizes of 45° wing-wall abutments and two sizes of spill-through abutments having embankment slopes of $1:1\frac{1}{2}$. The incremental backwater coefficient ΔK_s , or difference from the base curve, is shown plotted with respect to M and the angle of skew ϕ , for the wing-wall abutments on Fig. 6-13 [Appendix C, Table 9] and for the spill-through abutments on Fig. 6-14 [Appendix C, Table 10]. Note that these increments are negative when the abutment face is parallel with the flow [Figs. 6-13A and 6-14A] and have both positive and negative values, depending on M , when the abutment face is normal to the roadway coefficient falls below the base curve while the positive values fall above it. Negative values of the incremental backwater coefficient result from the definition of the opening ratio, which is different in the case of skew crossings.

The method of computation for skew crossings is altered in the following respect: The opening ratio M for skew crossings is computed as previously described except the bridge length is now projected against a section taken normal to the general direction of flood flow. Figs. 1-7 and 1-10 show a plan view of a typical skew crossing and the arrow indicates the general direction of flow as it existed before the embankments were in place. This is the flow direction used in the projection process. The length of the constricted opening is $b \cos \phi$ and the area A_{n2} is based on this length. The velocity head $V_{n2}^2 / 2g$, to be substituted in expression 6-5, is computed on the projected area A_{n2} .

It was observed during the testing that crossings with skew up to an angle of 15 degrees produced no particularly objectionable results, hydraulically, for any of the four abutment types. As the angle increased above this value however, the flow picture began to deteriorate; flow concentrations at abutments produced large eddies reducing the efficiency of the waterway and increasing the possibilities for scour.

When computing pier area A_p , for skew crossings, use the area obtained by projecting against the normal section as was done in computing M , see sketch on Fig. 6-9. Divide A_p , by the projected area A_{n2} in the same plane, to determine J . If piers are not set parallel to the flow, consult the sketch on Fig. 6-9 for method of computing A_p .

The total backwater coefficient for a skewed crossing with spill-through abutments and piers would be

$$K^* = K_b [\text{Fig. 6-7A}] + \Delta K_p [\text{Fig. 6-9}] + \Delta K_s [\text{Fig. 6-14A or 6-14B}] \quad [6-14]$$

The backwater h_1^* defined as the average of two stagnation depth h_{UL} and h_{UR} minus the head of approaching velocity is obtained by substituting K^* in expression 6-5. The location of h_1^* is rather indefinite in the case of skew crossings as the position of maximum backwater is dependent not only on the angle of skew but on the configuration of the stream channel. If the stream channel and flood plain are straight for a reasonable distance upstream from the bridge [as was the case in the model], the backwater will be essentially the same along both embankments. If the approach channel to the bridge entails a bend, the backwater will be higher at the embankment on the outside of the bend than at the embankment on the inside of the bend. In the case at hand h_1^* as computed would more nearly represent a mean of the two.

Location of Maximum Backwater

To determine the water surface elevations on the upstream and downstream sides of the approach roadway embankments, it will be necessary to locate the point of maximum backwater with respect to the bridge for the purpose of correcting for the natural fall in the stream. The location of the maximum backwater was discussed at length in Chapter V. Fig. 6-16 is recommended for engineering application. The horizontal distance L^* , normal to the center of the bridge, was measured from the water line on the upstream face of the embankment to the point of maximum backwater, denoted as point A, for each test [see sketch on Fig. 6-16]. For streams of moderate width, where the flood plain is inundated and the embankments constrict the flow, the elevation of the water surface throughout areas ABCD and AEFB will, for practical purposes, be the same as at point A where the backwater measurements were made. This characteristic was borne out from field

observations made by the U. S. Geological Survey on bridges up to 220 ft in length and inundated flood plains as wide as one-half mile. In the case of very wide rivers, the water surface measured at the banks may be higher than that observed in the center of the stream but this is still conjectural. The chart on Fig. 6-16 was prepared from the current model results plus three values obtained from a study by the U. S. Geological Survey on a model 98 ft wide, one observation by the Corps of Engineers on the Air Line Bridge over the Bonnet Carre' Floodway in Louisiana, and several field observations made by the U. S. Geological Survey on bridges up to 220 ft long.

To obtain the distance to maximum backwater L^* , for a normal crossing, enter Fig. 6-16 with the proper values of $b^2[1-J]/A_{n2}$ and $[bh_1^*/A_{n2} + 1]$; read off the corresponding value of L^*/b from the ordinate scale. The distance L^* is then the product of the chart value and b . If the backwater computation is based on the design discharge for normal stage at the bridge, the water surface elevation at section I [also throughout areas ABCD and AEFG] will be normal stage at bridge + $h_1^* + S_0L_{1-2}$. With the distance L^* and the cross section and height of the embankment known, L_{1-2} can be readily determined.

In the case of skew crossings, the water surface elevations along opposite banks of a stream are usually different than at point A; the difference depending on the angle of skew, the configuration of the approach channel and other factors. To obtain the approximate distance to maximum backwater L^* , for skew crossings [see Fig. 1-7B], the same procedure can apply as for normal crossings. For convenience, the projected length of the bridge and the projected area can be used for b and A_{n2} , respectively.

Difference in Level Across Embankments

Accurate measurement of backwater in the field is a rarity. The only satisfactory method entails preparing a reliable stage-discharge curve for the river immediately upstream from a site, before a bridge is constructed, and then obtaining a corresponding stage-discharge curve for flood flows after the bridge is completed. The difference in the two curves would represent the backwater produced by introduction of the bridge for any selected discharge. Of course, a long delay between establishment of the two stage-discharge curves, which may be unavoidable, could nullify the results.

Fortunately an indirect but reliable measurement can be made on the prototype during high water from which the backwater may be determined. The method consists of marking high water along banks and roadway embankments both upstream and downstream from the bridge and on both sides of the river while, at the same time, the discharge is measured by current-meter. Later, the elevation of these points can be determined with an engineer's level and the average differential across the embankments Δh_s computed. For prototype the Δh_s -value is the same as the Δh -value. In this chapter, Δh will be substituted for Δh_s hereafter.

A rather simple relation exists between the backwater and the differential level across embankments. The relationship between h_1^* and Δh was evolved through the medium of the model studies; thus by measuring Δh in the prototype, the backwater can be readily determined.

A rather simple relation exists between the backwater and the differential level across embankments. The relationship between h_1^* and Δh was evolved through the medium of

the model studies; thus by measuring Δh in the prototype, the backwater can be readily determined.

The differential level Δh , is also a factor in the computation of flow over roadway embankments. Provision for flow over roadway embankments shows much promise as a means of protecting bridges during superfloods. The roadway simulates a broad crested weir and its capacity is dependent on the depth of flow over the roadway and the degree of submergence from downstream.

Base curves - normal crossing:- Referring to Fig. 1-1,

$$\Delta h = h_3^* + h_1^* + S_0 L_{1-3} \quad [6-15]$$

where

h_3^* is the vertical distance between actual water surface and normal water surface at downstream side of embankments,

h_1^* is the maximum backwater produced by bridge, and

$S_0 L_{1-3}$ is the drop in channel bottom between sections I to III.

The ratio $h_1^*/[h_3^* + h_1^*] = \epsilon_b$ is plotted with respect to the opening ratio M for the 45 degree wing-wall abutment with $1:1\frac{1}{2}$ embankment slopes on Fig. 6-4B. The experimental points represent the same runs used to plot the K_b curve on Fig. 6-4A [Appendix C, Tables 1 and 2]. To aid in simplifying the test, the ratio $h_1^*/[h_3^* + h_1^*]$ will be designated as ϵ_b .

The curves on Fig. 6-5B show ϵ_b plotted with respect to M , for all wing-wall type abutments investigated, see Appendix C, Table 3. Note that the position of the ϵ_b curves vary with abutment shape as did the K_b curves.

Fig. 6-6B shows the experimental points for ϵ_b plotted with respect to M for the spill-through abutment with $1:1\frac{1}{2}$ embankment slopes [Appendix C, Tables 4 and 5]. A similar plot shows the experimental results for the three embankment slopes tested with the spill-through models on Fig. 6-7B [Appendix C, Table 4].

The plots on Figs. 6-5B and 6-7B are considered base curves, and the manner of adjusting for piers, eccentricity, and skew is handled in a like manner to that demonstrated previously for the backwater coefficient.

The procedure for obtaining h_3^* , for a simple normal crossing without piers, is to enter Figs. 6-5B or 6-7B with appropriate abutment shape and M , to obtain ϵ_b . With h_1^* , known from the backwater computation, $h_3^* = h_1^* / \epsilon_b - h_1^*$. To obtain Δh , the drop due to the channel gradient $S_0 L_{1-3}$ must be added or

$$\Delta h = \frac{h_1^*}{\epsilon_b} + S_0 L_{1-3} \quad .$$

Piers:- Any condition which alters the backwater coefficient K_b , from that given by the base curves, also affects the differential level across the embankments.

For the purpose of illustration, experimental values of $\epsilon_b + \Delta\epsilon_p$ plotted for round double shaft piers located between spill-through abutments on Fig. 6-10A. The incremental ratio $\Delta\epsilon_p$, represents the difference between the base curve values [Fig. 6-7B] and similar curves obtained with piers. Note how the lines deviate from the base curve as the value of J increases.

Also observe that the greatest deviation occurs for $M = 1.0$ while the deviation from the base curve is practically negligible at $M = 0.3$.

The deviation from the base curve $\Delta\epsilon_p$ or $\Delta[h_1^*/(h_3^* + h_1^*)]_p$, is plotted with respect to J and M for round double shaft piers located between spill-through abutments on Fig. 6-10B. Note that straight lines, intersecting at the origin have been used for constant values of M .

A dimensionless composite design curve [Fig. 6-11] was prepared by combining similar graphs for each of the several pier shapes. Again there was little or no difference between the results in which wing-wall [Appendix C, Table 6] and spill-through abutments [Appendix C, Table 7] were utilized.

The procedure for determining the drop across a roadway embankment when piers are present in a bridge constriction is to first obtain a value of ϵ_b from the appropriate base curve and add to this the incremental ratio $\Delta\epsilon_p$, for piers; e.g., for wing-wall abutments

$$\epsilon^* = \epsilon_b [\text{Fig. 6-5B}] + \Delta\epsilon_p [\text{Fig. 6-11}] \quad , \quad [6-16]$$

As $h_3^* = h_1^*/\epsilon^* - h_1^*$, where h_1^* is the computed backwater [including effect of piers], the drop across the roadway embankment

$$\Delta h = \frac{h_1^*}{\epsilon^*} + S_o L_{1-3} \quad . \quad [6-17]$$

Eccentricity:- In the case of severe eccentric crossings the differential level across embankments, as given here, applies

only to the side of the river having the greater flood plain discharge. The manner in which the experimental points plot, as deviations from the base curve, is shown on Fig. 6-12B. The incremental differential level ratio

$$\Delta \left[\frac{h_2^*}{h_3^* + h_1^*} \right]_e$$

which will be known as $\Delta\epsilon_e$, is plotted with respect to M . The points are for $e = 1.0$ and represent tests on both wing-wall and spill-through abutments [Appendix C, Table 8]. As is quite evident, additional information is likewise desirable on this phase of eccentric crossings.

For a normal but severe eccentric crossing with piers, the over-all differential level ratio

$$\epsilon^* = \epsilon_b + \Delta\epsilon_p + \Delta\epsilon_e \quad . \quad [6-18]$$

Skew Crossings:- The differential drop across roadway embankments for skew crossings is naturally different for opposite sides of the river. The amount depends on the configuration of the river, bends in the vicinity of the crossing and the degree of skew. The first two factors can be so variable that a generalized model study can shed but little light on the subject. The experimental information for the right embankment of the model, see sketch on Fig. 1-7B, was not reliable as the flow impinged against the right wall of the flume, downstream from the bridge, producing an unnatural condition, therefore, the test results for the differential level across the right embankment have been omitted.

The results for the left embankment have been included only as a matter of record. Caution should be exercised in the use of this information unless the prototype layout closely resembles that of the model tests [Fig. 1-7]. The incremental differential level ratio $\Delta \epsilon_s$, has been plotted with respect to M for both the wing-wall abutments [Appendix C, Table 9] and the spill-through abutments, for the left embankment only, [Appendix C, Table 10] on the single graph of Fig. 6-15. The opening ratio M , is based on the projected length of bridge explained previously for skew crossings.

Dual Bridges [Backwater]

With the advent of recent developments in divided highway construction, dual bridges of identical design placed parallel and only a short distance apart are becoming common. The backwater produced by dual bridges is naturally larger than that for a single bridge, yet less than the value which would result from two bridges computed separately. As the combinations of dual bridges encountered in the field would be legion, it was necessary to restrict the model tests to the simplest arrangement, namely: identical parallel bridges crossing the stream normal to the flow. The tests were limited to the 45 degree wing-wall and the spill-through type abutments both having embankment slopes of $1:1\frac{1}{2}$. The distance between bridges was limited by the range permissible in the model. The ratio h_d^*/h_1^* , is plotted in relation to the parameters bL_D/A_{n2} and M on Fig. 6-17, where h_d^* is the backwater for dual bridges measured upstream from the first bridge and L_D is the distance between the center lines of bridges. The resulting curves were established from test

results using wing-wall abutments, without and with piers. A record of the test data for identical dual bridges, without piers, is included in Appendix C, Table 11. The test data for wing-wall abutments and identical pier combinations for each bridge will be found in Appendix C, Table 12. The several points obtained for spill-through abutments [Appendix C, Table 11] showed lower values of h_d^*/h_1^* , but these were so few in number that no conclusions could be drawn. For design purposes the curves on Fig. 6-17 are recommended for both wing-wall and spill-through abutments.

The ratio h_d^*/h_1^* , which will be called the backwater multiplication factor and designated as η , increases as the bridges are moved apart apparently reaching a limit for bL_D/A_{n2} between 30 and 50, whereupon the value of η , then decreases as the distance is further lengthened between bridges. With the bridges in close proximity to one another the flow pattern is little different than for a single bridge. As the bridges are spaced farther apart, the downstream bridge interferes with the expanding jet from the first producing an additional loss of energy. This loss is progressive up to a value of bL_D/A_{n2} of 30 to 50 whereupon the effect of this interference diminishes.

To compute backwater for dual bridges meeting the above specifications, it is simply necessary to compute backwater h_1^* , for a single bridge [with or without piers] as previously outlined, then multiply this value by the backwater factor for dual bridges η which is obtained by entering Fig. 6-17 with the proper values of bL_D/A_{n2} and M .

Dual bridges [differential level across embankments];-

In the case of identical dual bridges, the designer may wish to know the water surface elevation on the downstream side of the roadway embankment of the second bridge, or the water surface elevation on the downstream side of the embankment of the first bridge. The water surface was measured at both locations and the results, which are for normal stream crossings, are included as Fig. 6-18 [Appendix C, Tables 11 and 12].

A similar procedure to that outlined in the preceding section on backwater for dual bridges was used to determine water surface levels across embankments. The procedure is to first compute $h_1^* + h_3^*$ between sections I and III for the upstream bridge alone, with or without piers, as outlined previously. Note from the sketch on Fig. 6-17 that section III is the same for dual bridges as for a single bridge, while the water surface immediately downstream from the embankment on the second bridge is referred to as section IIIB. The differential level between sections I and IIIB, which is $[h_d^* + h_3^*]_{3B}$, is obtained by multiplying the differential level $[h_1^* + h_3^*]$ for a single bridge by a factor obtained from Fig. 6-18A. The factor denoted as η_{3B} is obtained by entering Fig. 6-18A with the proper value of bL_D/A_{n2} . The factor η_{3B} is independent of M in this case.

$$[h_d^* + h_3^*]_{3B} = \eta_{3B}[h_1^* + h_3^*] \quad [6-19]$$

To determine the differential water surface level Δh_{1-3B} , between sections I and IIIB, the drop in the gradient of the channel must also be included or

$$\Delta h_{1-3B} = \eta_3 B [h_1^* + h_3^*] + S_0 L_{1-3B} \quad [6-20]$$

Should the differential level across the first bridge be desired, for a two-bridge combination, a similar procedure would be followed except the multiplication factor η_3 , is obtained from Fig. 6-18B. In this case

$$[h_d^* + h_3^*]_3 = \eta_3 [h_1^* + h_3^*] \quad \text{and} \quad [6-21]$$

$$\Delta h_{1-3} = \eta_3 [h_1^* + h_3^*] + S_0 L_{1-3} \quad [6-22]$$

As is evidenced by the scatter of experimental points on Fig. 6-18, considerable fluctuation of the water surface was experienced between bridges. In addition, there is no order to the manner in which the points plot so it is only possible to show the experimental results as a band. This was not the case downstream from the second bridge, as can be observed from Fig. 6-18A.

Abnormal Stage-Discharge Condition [Backwater]

Up to this point the discussion has concerned streams flowing at normal stage e.g., the natural flow of the stream has been influenced only by the slope of the bottom and the boundary resistance along channel bottom and flood plains. Often the stage at a bridge site is not normal but is influenced by flood conditions from the main river downstream. This condition produces a M1 backwater curve, beginning at the confluence of the tributary and main stream, and may extend a considerable distance upstream if the gradient of the tributary is flat.

Where bridges are placed close to the confluence of two streams, abnormal stage-discharge conditions can be of considerable importance in the design. It is often desirable to be able to compute the bridge backwater for abnormal stage-discharge conditions as it may be possible to use a shorter bridge near the mouth of a stream, for abnormal stage, than farther upstream where the stage is normal.

The model tests with abnormal stage were made with a channel slope of 0.0012 and a Manning roughness of 0.024. Due to the fact that normal depth was not maintained, but that the water surface assumed the profile of a backwater curve, the analysis as developed does not have general application. Strictly speaking, the results apply to the model for this one slope and roughness. On the other hand, if it is assumed that the model roughness scales up to prototype proportions as the one-sixth power of the scale ratio -- or approximately 1/40 -- it will be found that the resulting roughness will be commensurate with values encountered in many prototype problems.

The results do shed light on this phase of the backwater problem and may be used within reason. The computation of bridge backwater for abnormal stage-discharge conditions is considered a special case. To avoid confusion the backwater coefficient K_A^* , has been assigned a subscript to distinguish it from those preceding. As the solution for backwater is approximate, the term equating difference in kinetic energy between sections I and IV have been omitted.

Backwater coefficients for abnormal condition K_A [base curve] are plotted with respect to M on Fig. 6-19A for 45 degree wing-wall abutments [Appendix C, Table 13].

Backwater coefficients K_A , for normal crossings are plotted with respect to M for abnormal stage and spill-through abutments on Fig. 6-19B [Appendix C, Table 14]. It is interesting to note that the coefficients as computed do not plot greatly different from Fig. 6-4A and Fig. 6-6A, the base curves for simple normal crossings with the 45 degree wing-wall abutments and $1:1\frac{1}{2}$ spill-through abutments, respectively.

It should be noted however that the backwater coefficients for abnormal stage were computed differently than those previously for normal stage-discharge conditions. Referring to the sketch on Fig. 6-19, the backwater coefficients for abnormal stage, normal crossing without piers, is

$$K_A = \frac{h_1^*}{V_{A_2}^2 / 2g} \quad \text{where}$$

$$V_{A_2} = \frac{Q}{bh_A} \quad .$$

Since the points for abnormal stage fall on the previously established base curves, it is reasoned that a similar treatment of the incremental backwater coefficients is applicable to adjust for piers, eccentricity and skew. The incremental coefficients, which are of course approximate, will be those shown on Figs. 6-9, 6-12A, 6-13 and 6-14. Thus to obtain the over-all backwater coefficient for abnormal stage, spill-through abutments and piers

$$K_A^* = K_A [\text{Fig. 6-19B}] + \Delta K_p [\text{Fig. 6-9}] \quad [6-23]$$

The backwater then, measured above the abnormal stage at the bridge site, will be

$$h_1^* = K_A^* \frac{V_{A2}^2}{2g} \quad [6-24]$$

where

K_A^* = over-all backwater coefficient for abnormal stage,

and

$V_{A2} = \frac{Q}{A_{A2}}$ where $A_{A2} = bh_A$ or area of bridge constriction based on abnormal stage at section II.

The important step in the procedure with abnormal stage-discharge is to substitute the velocity for abnormal stage in Eq 6-24 rather than that for normal stage.

Abnormal stage-discharge condition [differential level across embankments]:- As in the case of the over-all backwater coefficient, the over-all differential level ratio ϵ_A , for abnormal stage-discharge conditions, has been assigned a subscript. The experimental points for the differential level ratio for simple normal crossings and wing-wall abutments are shown plotted on Fig. 6-20A [Appendix C, Table 13] and for spill-through abutments on Fig. 6-20B [Appendix C, Table 14]. The experimental points agree quite well with the base curve of simple normal crossings for wing-wall abutments but fall somewhat above the base curve for spill-through abutments.

The method for adjusting the differential level ratio for the effects of piers, eccentricity and skew remains unchanged, but it should be remembered that the result is approximate.

The over-all differential level ratio for spill-through abutments and abnormal stage-discharge conditions will be

$$\epsilon_A^* = \epsilon_A [\text{Fig. 6-20B}] + \Delta\epsilon_p [\text{Fig. 6-11}] + \Delta\epsilon_e [\text{Fig. 6-12B}] + \Delta\epsilon_s [\text{Fig. 6-15}] \quad [6-25]$$

Bridge Girder Partially Submerged [Backwater]

Problems occasionally arise in which it is desired to compute the backwater upstream from a bridge or the discharge under a bridge when flow is in contact with the girders. Once flow contacts the upstream girder of a bridge, orifice flow is established so that the discharge then varies as the square root of the effective head. The result is a sudden increase in backwater for essentially the same discharge. This is a backwater effect which the designer may seldom consider in new construction. A rather common source of bridge failure results from the superstructure being virtually shoved off the abutments and piers by a combination of buoyancy and dynamic force.

Two cases of flow were studied: [I], only the upstream girder was in the flow as indicated by the sketch accompanying Fig. 6-22. [II], the bridge constriction was flowing full and all girders were in the flow as shown on sketch accompanying Fig. 6-21. The procedure followed in the model tests for either case was to set a discharge and adjust the depth of flow such that it was constant throughout the flume. Normal depth, h_n , was measured and recorded. A pair of abutments was next placed in the flow and the backwater h_1^* , produced by these abutments, measured. Next a bridge, with girder depth exaggerated, was placed between the abutments and gradually lowered until the

upstream girder made contact with the water surface. Immediately the backwater increased; the deck was then firmly secured in place to prevent further movement. The new backwater denoted as h_s^* , was then measured, as well as the vertical distance between the bottom of the upstream girder and the floor of the channel, z . Other runs were made with the bridge deck further depressed, but in no case was flow over the bridge permitted. The above test procedure was then repeated for changes in abutment geometry using both wing-wall and spill-through abutments.

Several methods of procedure were attempted in the analysis of the data. It was found that for practical purposes the opening ratio M could be eliminated as a variable once orifice flow was established; the most logical and simple method of approach then being to treat this flow condition as a sluice gate problem [extreme case].

Using a common equation for sluice gate flow

$$Q = C_d b_N z \sqrt{2gh_1} \quad [6-26]$$

where Q = total discharge - cfs

b_N = net width of waterway [excluding piers] - ft

z = vertical distance - bottom of upstream girder to mean river bed under bridge - ft, and

h_1 = vertical distance - water surface at section I to mean river bed under bridge - ft.

For case [I], the coefficient of discharge C_d , is plotted with respect to the parameter z/h_1 on Fig. 6-22A [Appendix C, Table 15]. The points indicate that a single coefficient curve

will serve for both wing-wall and spill-through abutments. By substituting values in Eq 6-26, it is possible to solve for either the water surface upstream at section I or the discharge under the bridge, depending on the quantities known.

Case [II], where the entire area under the bridge is occupied by the flow, is handled in a different manner. To compute the water surface upstream from the bridge, in this case, the water surface on the downstream side and the discharge must be known. Or if the discharge under the bridge is desired the drop in water surface across the roadway embankments Δh , see sketch accompanying Fig. 6-21, must be known. The experimental points on Fig. 6-21, which are for both wing-wall and spill-through abutments, show the coefficient of discharge to be essentially 0.80 for the range of conditions tested [Appendix C, Table 16]. The equation recommended for the average two-lane bridge for Case [II] operation can be considered

$$Q = 0.80 b_N z \sqrt{2g\Delta h} \quad . \quad [6-27]$$

This type of operation compares favorably with that of a submerged short box culvert for which information is available. [9], [18].

Information in the two forms presented will be found helpful in computing discharge under a bridge for cases where flow is also spilling over the roadway embankments. As a reminder, if piers are present, the net width of waterway [width of piers deducted] should be substituted for b_N .

Bridge girders partially submerged [Differential level across embankments]:- The differential water surface level

across the roadway embankments is plotted only for Case [I] where the flow was in contact with the upstream girder. This was readily measured and the results are shown on Fig. 6-22B [Appendix C, Table 15]. Entering Fig. 6-22B with the discharge coefficient C_d - obtained from the preceding backwater or discharge computation - the ratio h_3/h_1 is read from the abscissa scale. With h_1 known, h_3 can be determined.

I. PROTOTYPE VERIFICATION

Even if the model experiments measured up to the height of perfection, the differences between model and prototype, as discussed previously, would lead to grave doubts as to whether the model results are applicable to prototype computation. This question could be satisfactorily answered in one manner only; obtain measurements from prototype structures during floods, then independently compute backwater and drop in water surface across embankments for the same floods utilizing the model results.

The United States Geological Survey, which has been very cooperative in the bridge waterway program, made available field measurements which that organization collected over a period of time at various bridges during floods. Utilizing only the basic data such as discharge, cross-section of approach channel, roughness factors and cross-section under bridge, the bridge backwater h_1^* , and the differential water surface across the embankments Δh , were computed for each bridge from the design curves established from the model studies.

A record of some of the pertinent data and a comparison of the measured and computed values of Δh , are shown on Table

6-1. The comparison involves several abutment types, and values of b varying from 20 to 220 ft. The first twelve are for crossings with freewater surface while the last three are for bridges with deck partially submerged. The value of M shows a wide variation and piers were present in several cases. Columns 9 and 11 show the backwater and differential level across the embankments, respectively, as computed from the model design charts. Column 10 lists the differential level across the embankments as measured in the field by the U. S. Geological Survey. The percentage difference between the measured values of Δh , and those computed are shown in Column 12. The percentage difference ranges from -8.5 to +13 per cent with ten out of the fifteen cases showing deviations of less than 7 per cent. The deviation is positive for six cases, negative for eight and shows no deviation for the one remaining. When it is considered that the possible error in prototype measurements taken during floods can likely be as much as ± 10 per cent, the agreement is quite encouraging. In addition to the comparison afforded, the prototype measurements were informative in pointing out differences that exist between model and prototype. By utilizing the two sources of information, it was possible to gain a better understanding of the bridge waterway problem in general than could have been obtained from either model or prototype alone.

Practical Applications

For practical application of the information contained in this report, the reader is referred to the Bridge Waterway Section of the U. S. Bureau of Public Roads Drainage Manual [9] which contains solutions of typical bridge waterway problems utilizing the design information presented in this chapter.

TABLE 6-1

COMPARISON OF MEASURED AND COMPUTED VALUES OF h
ON EXISTING FIELD STRUCTURES

Location of Bridge (1)	Date of Flood (2)	b ft (3)	Abut- ment Type (4)	Q cfs (5)	V_n^2 ft/sec (6)	M (7)	J (8)	h_1^* ft Computed (9)	Δh ft Measured (10)	Δh ft Computed (11)	% Diff. Δh (12)
West Branch Delaware River Hale Eddy, New York	3-22-48	220	90°VW	27,500	7.44	.904	.063	.28	0.83	0.76	- 8.5
"	12-31-48	220	90°VW	16,000	5.75	.958	.084	.08	0.24	0.23	- 4.2
Bond Brook Dunham Basin, N. Y.	12-31-48	20	45°WW	1,370	9.07	.996	0	1.07	1.99	1.90	- 4.5
Kaydencrosseros Creek Near W. Milton, N. Y.	4- 4-52	44	38°WW	774	4.00	.65	0	.23	0.44	0.43	- 2.3
"	6- 1-52	44	38°WW	1,320	5.13	.68	0	.22	0.50	0.48	- 4.0
"	4- 2-52	44	38°WW	1,450	5.43	.70	0	.30	0.69	0.66	- 4.4
"	4- 6-52	44	38°WW	2,620	7.75	.66	0	.63	1.15	1.23	+ 6.9
"	12-31-48	84	45°WW	4,340	6.83	.85	0.042	0.21	0.70	0.65	- 7.2
Schroon River River Bank, New York	4-18-52	83	30°WW	5,240	8.63	.603	0	1.03	1.60	1.81	+13.0
Wild Rice Creek Twin Valley, Minnesota	5- 9-50	58	45°WW	3,400	7.09	.82	0	0.18	0.55	0.61	+10.3
Short Creek	11-28-48	72	ST	12,000	10.20	.83	0.040	0.57	1.95	1.94	- 0.5
Crooked Creek Nye, Kansas	5-23-51	112.5	13°WW	9,640	9.0	.33	.084	1.80	2.24	2.53	+12.9
Oneida Creek Oneida, New York	3-28-50	68		7,230	Bridge	deck	submerged		1.48	1.53	+ 3.4
Town Creek Van Wert, Ohio	2-14-50	39		810	"	"	"		0.22	0.22	0
Blue River Kansas City, Mo	4-23-44	119.5		26,000	"	"	"		1.61	1.70	+ 5.6

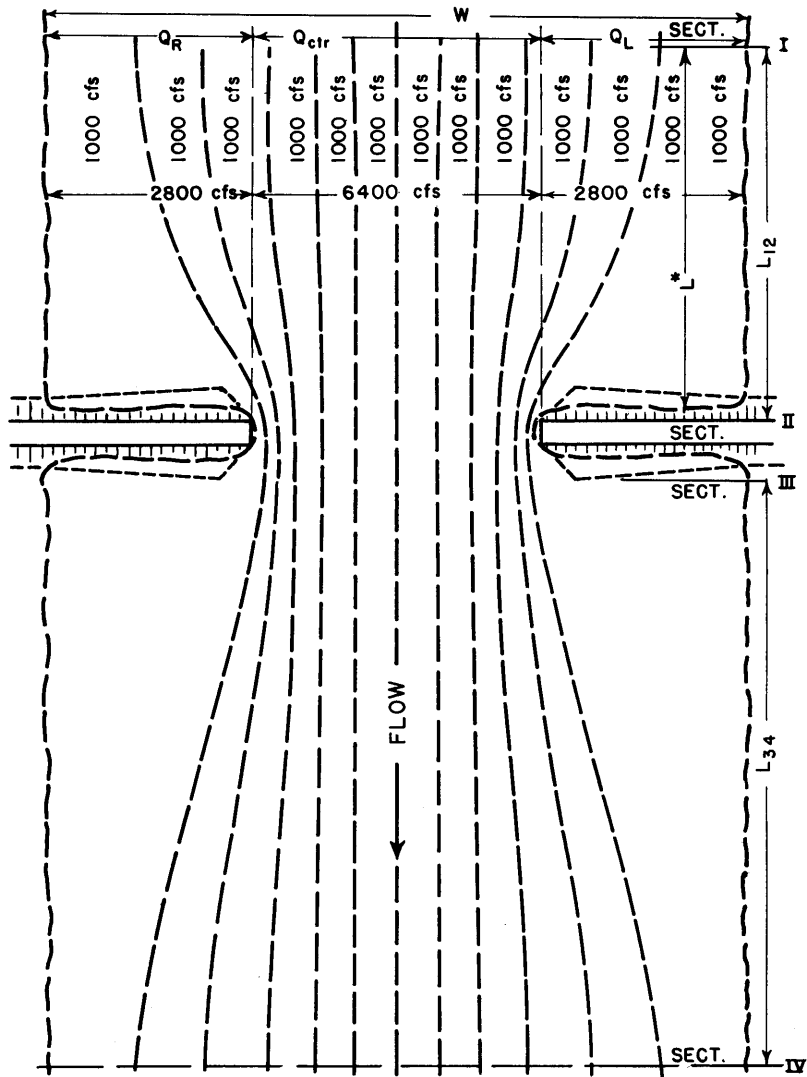


Fig. No. 6-1 Example of flow lines produced by channel contraction

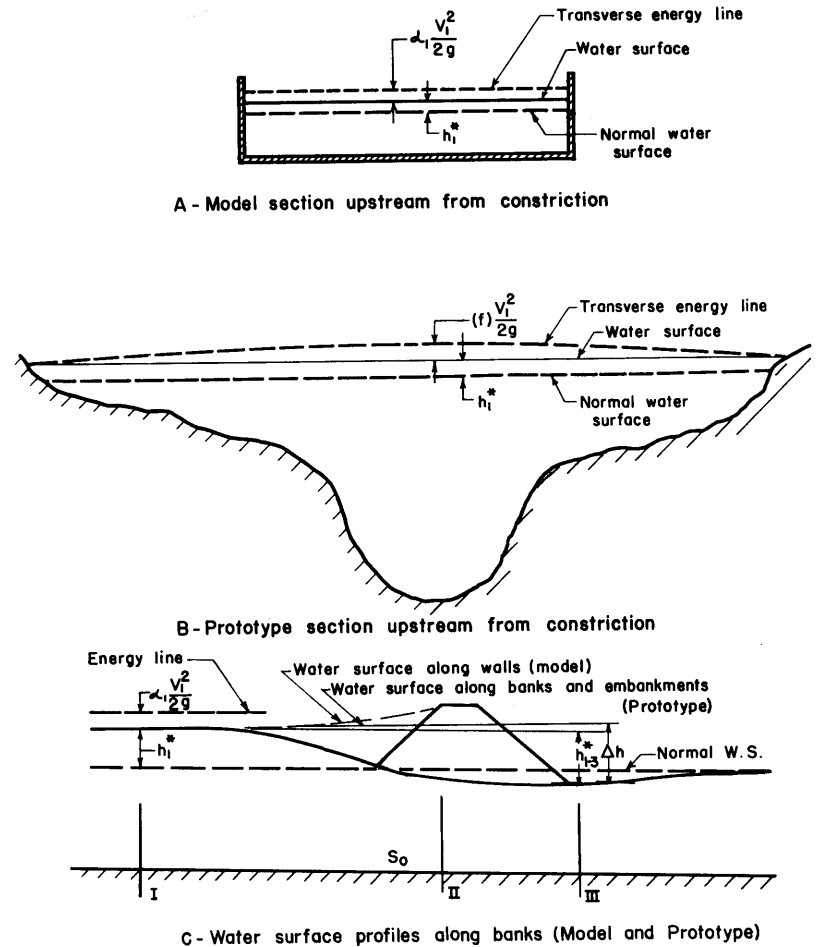


Fig. No. 6-2 Operational differences between model and prototype

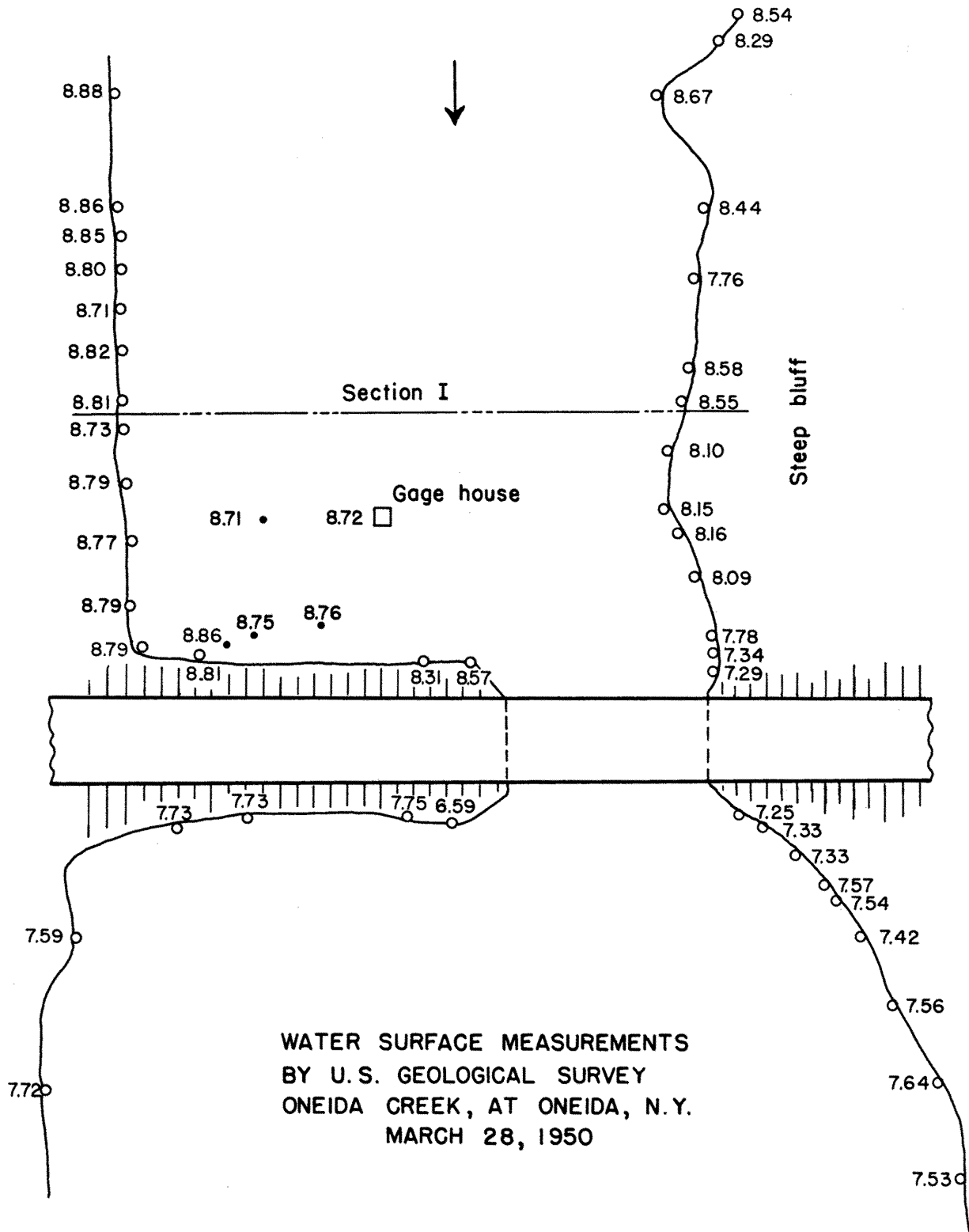


Fig. No. 6-3 Water surface measurements at shore line - Oneida Creek, N. Y.

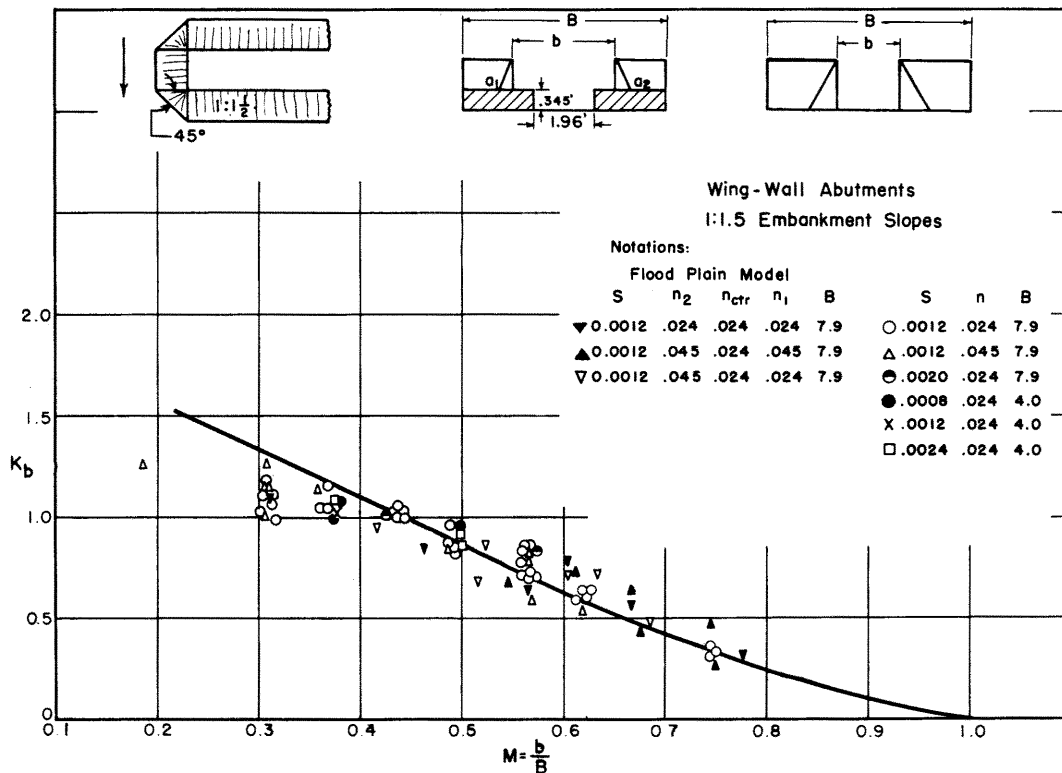


Fig. No. 6-4A Base curve of backwater coefficient K_b for 45 degrees wing-wall abutments

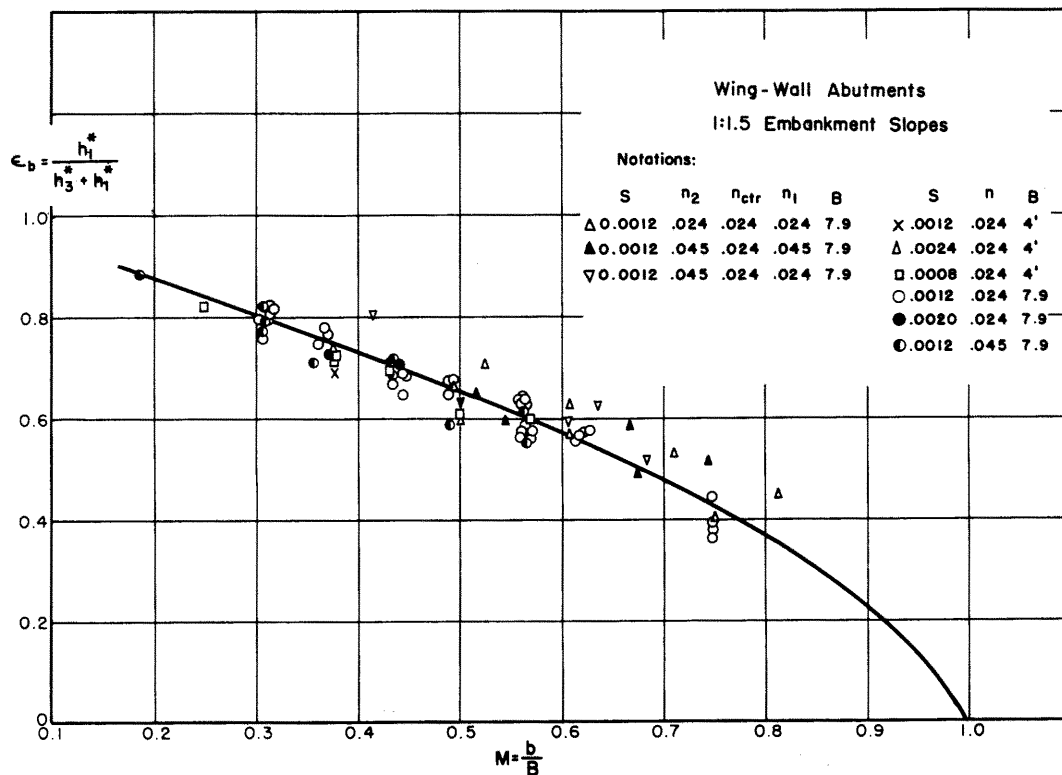


Fig. No. 6-4B Base curve of differential level ratio ϵ_b for 45 degrees wing-wall abutments

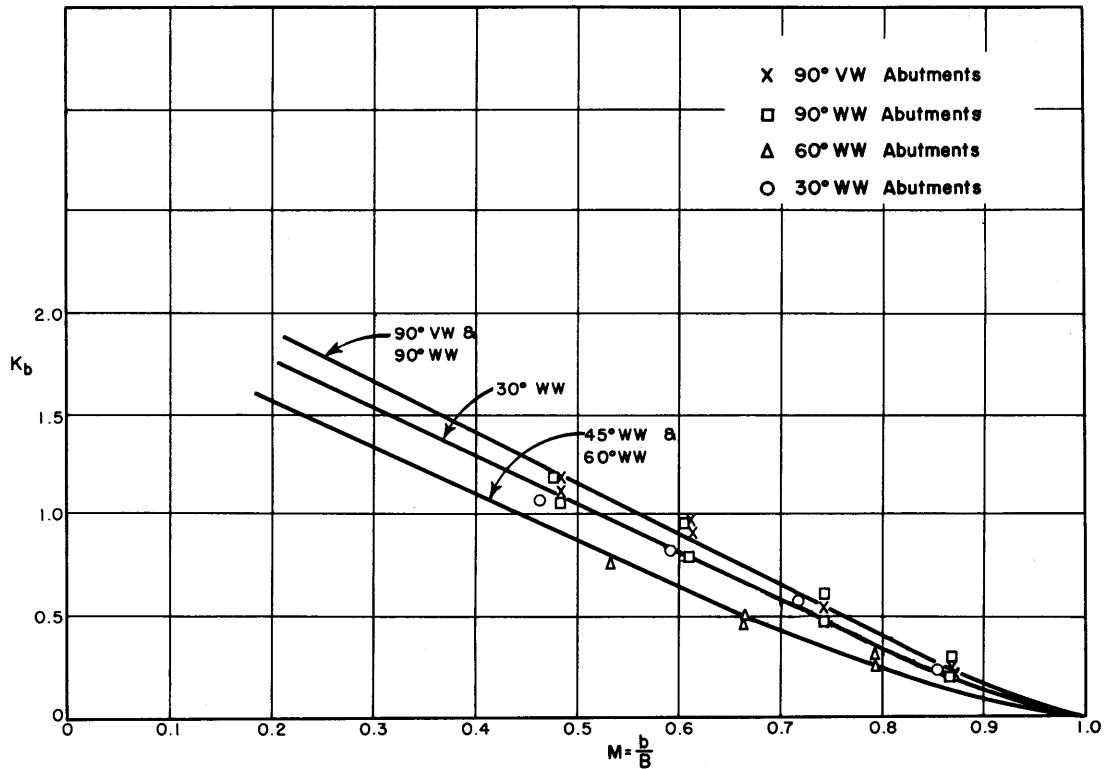


Fig. No. 6-5A Base curve of backwater coefficient K_b for all types of wing-wall abutments

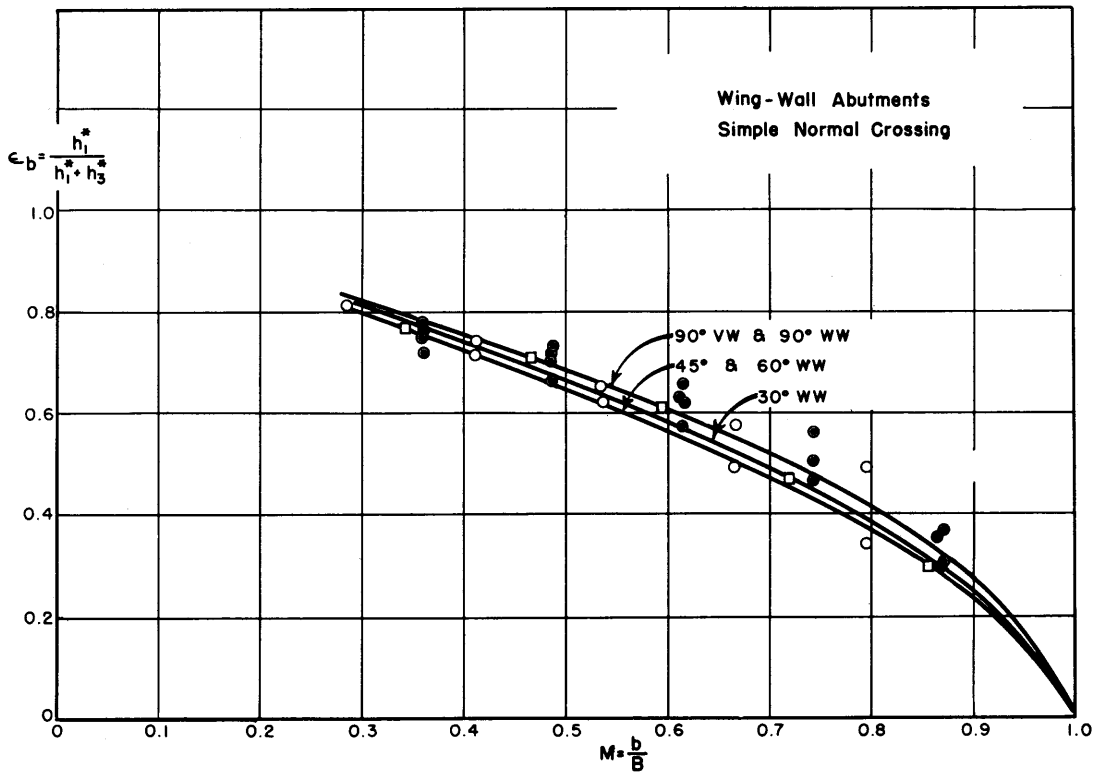


Fig. No. 6-5B Base curve of differential level ratio ϵ_b for all types of wing-wall abutments

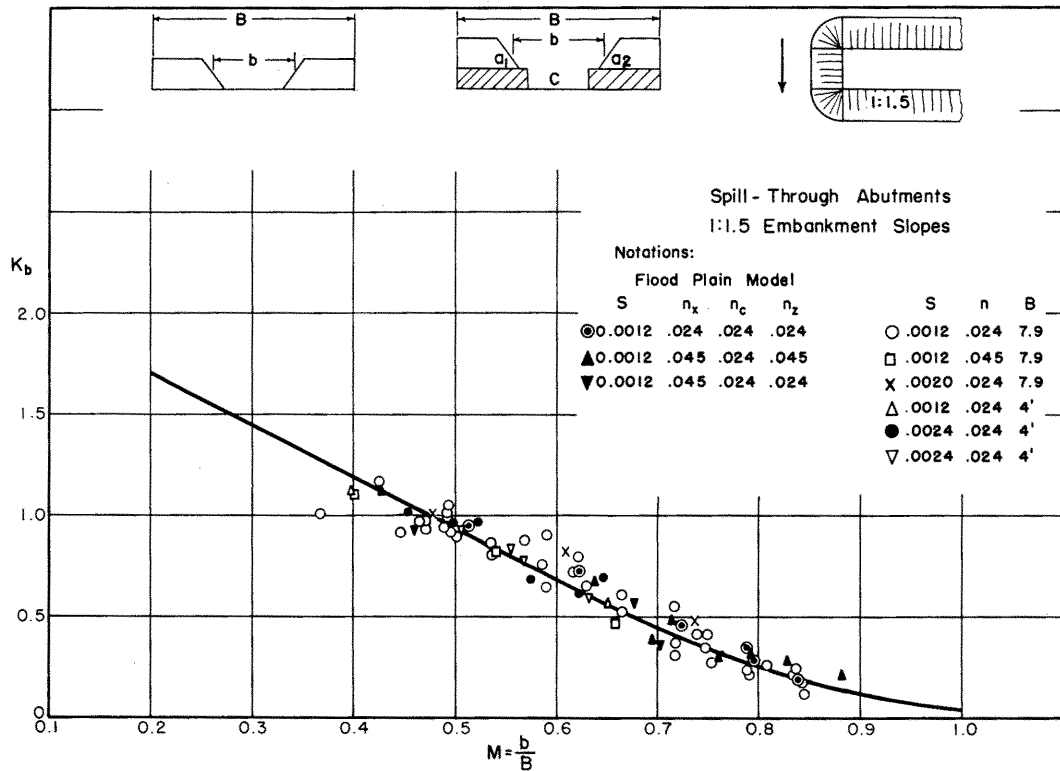


Fig. No. 6-6A Base curve of backwater coefficient K_b for 1:1.5 spill-through abutments

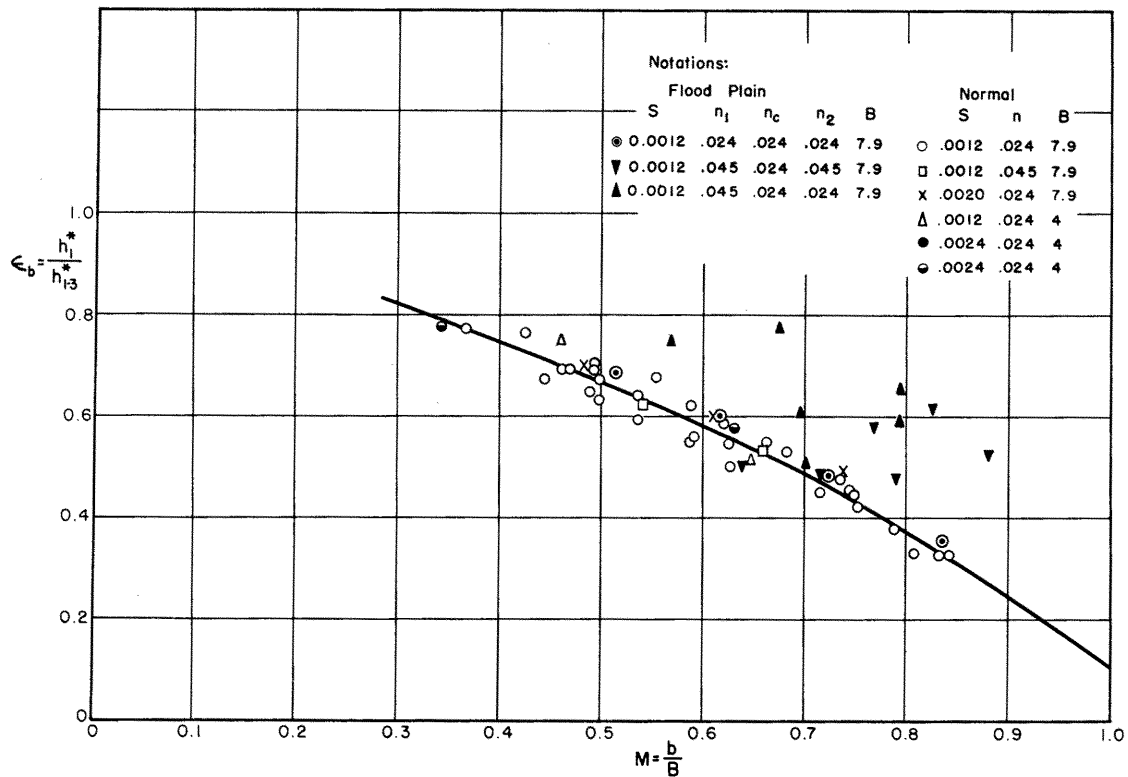


Fig. No. 6-6B Base curve of differential level ratio ϵ_b for 1:1.5 spill-through abutments

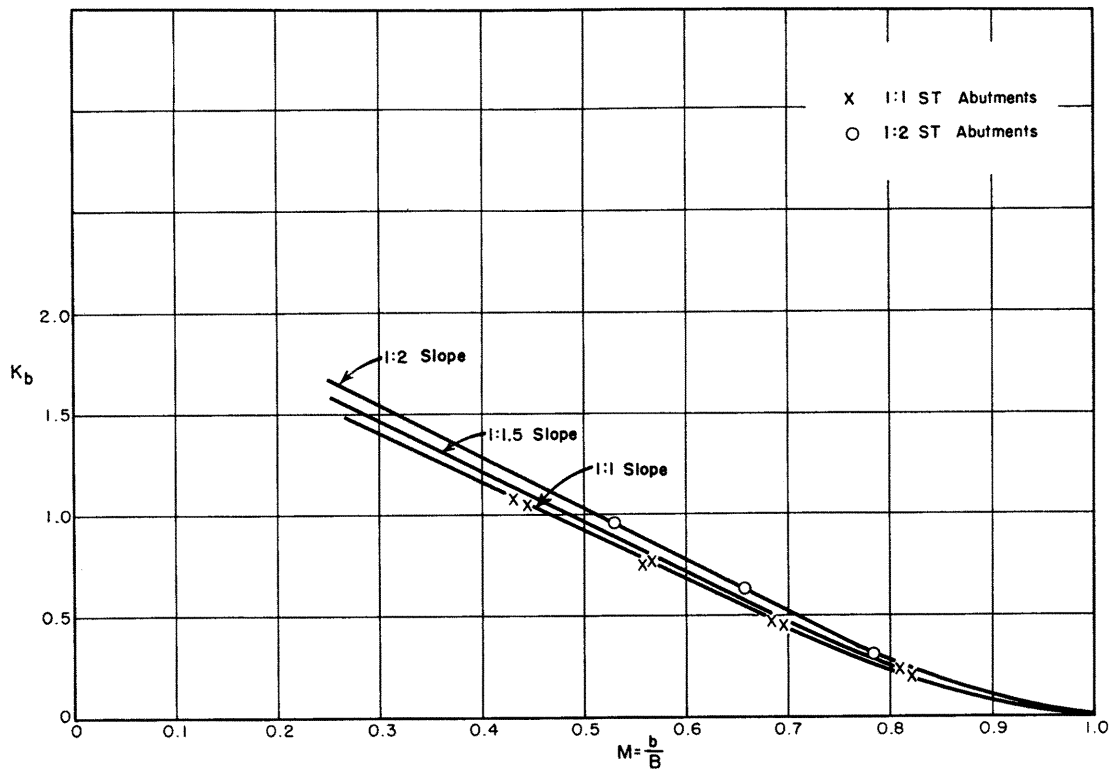


Fig. No. 6-7A Base curve of backwater coefficient K_b for all types of spill-through abutments

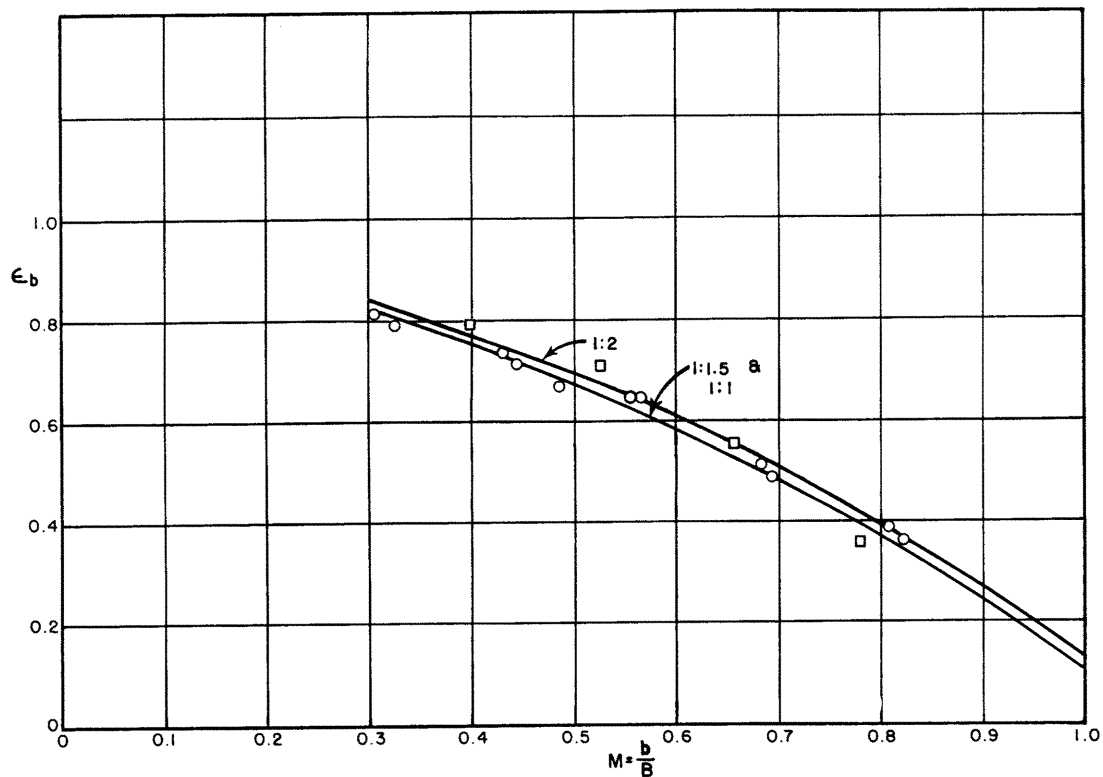


Fig. No. 6-7B Base curve of backwater coefficient ϵ_b for all types of spill-through abutments

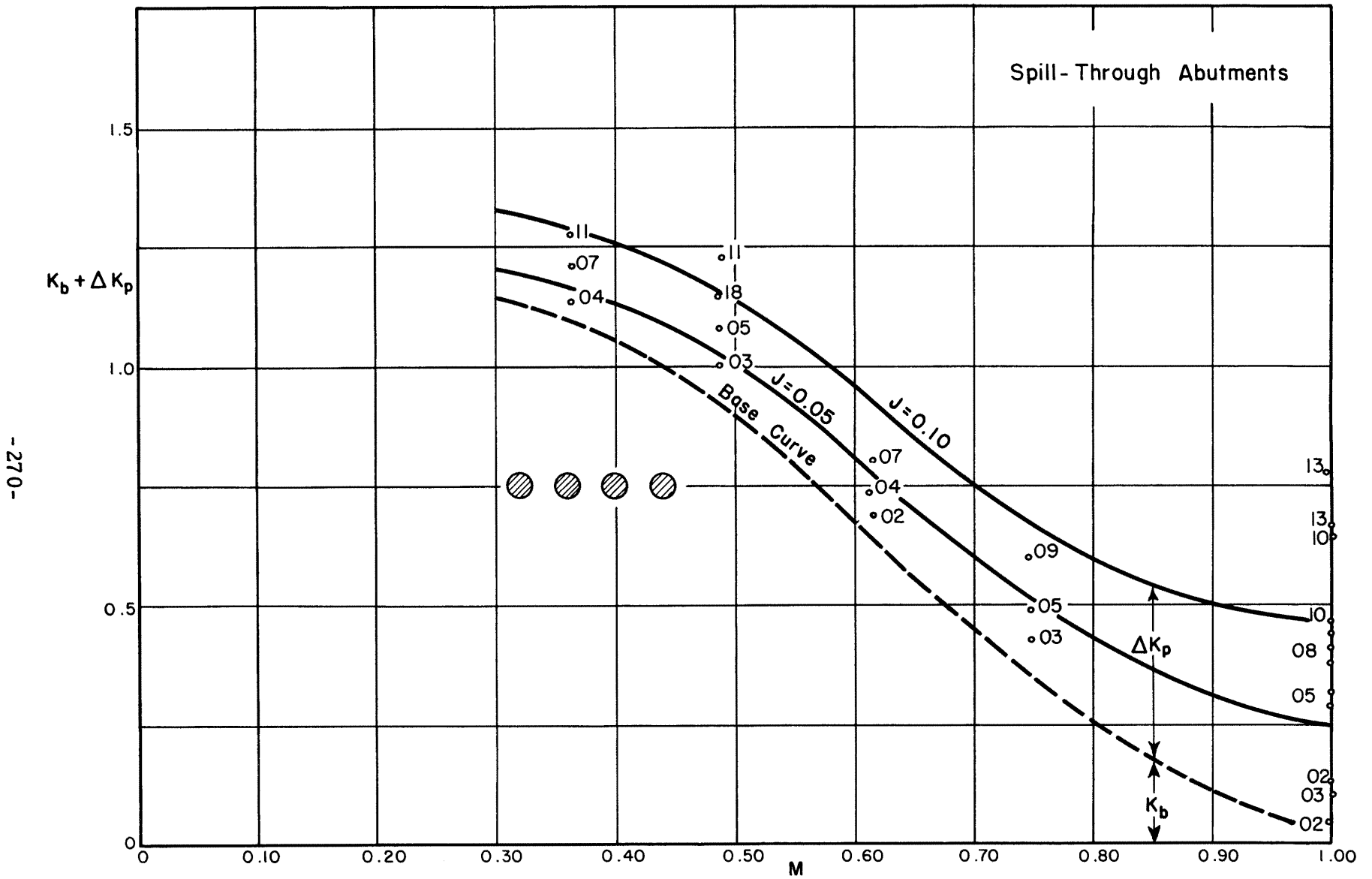


Fig. No. 6-8 Total backwater coefficient $K_b + \Delta K_p$ for bents with circular piles M and spill-through abutments

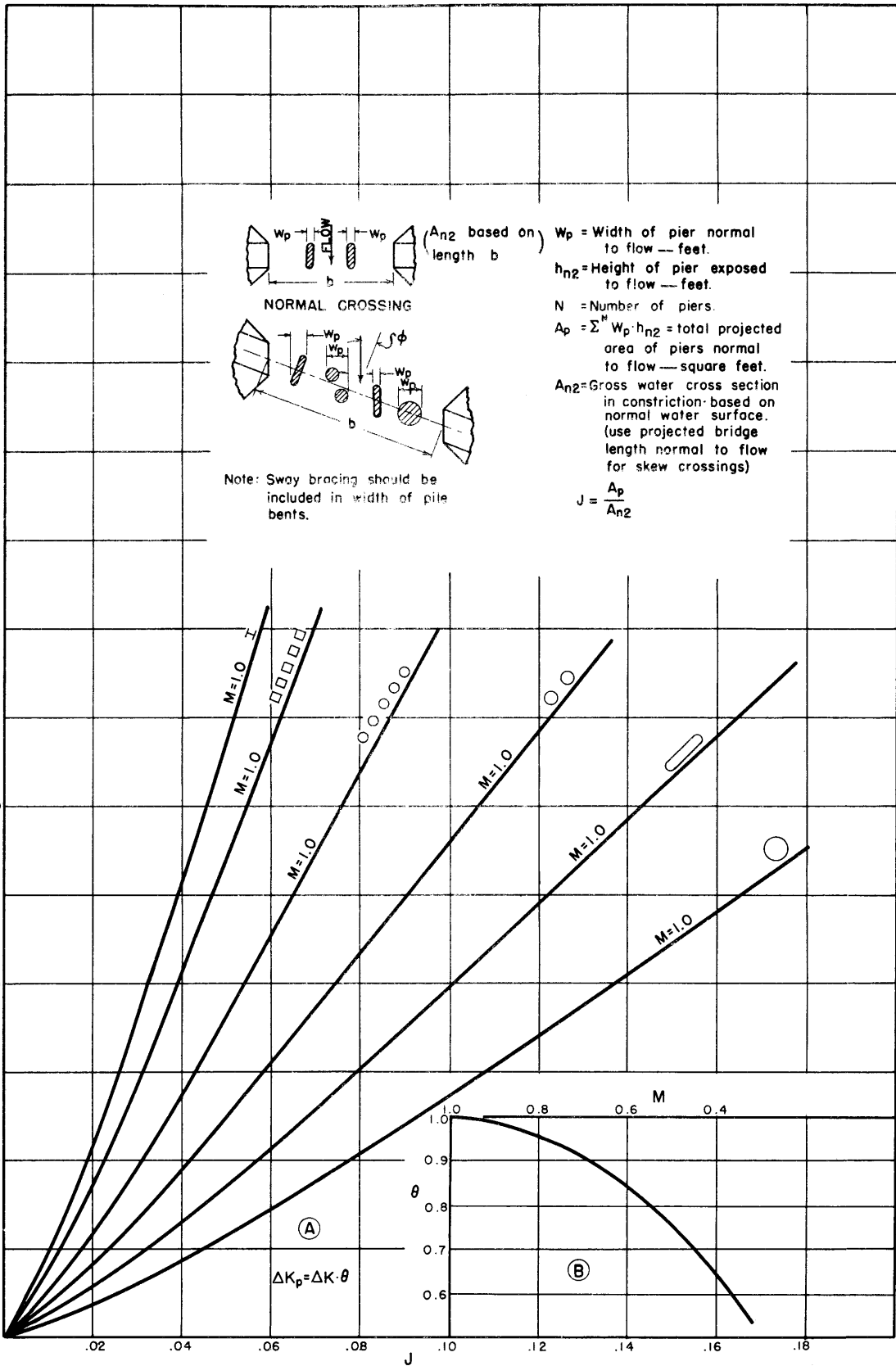


Fig. No. 6-9 Incremental backwater coefficient ΔK_p for piers, wing-wall, and spill-through abutments

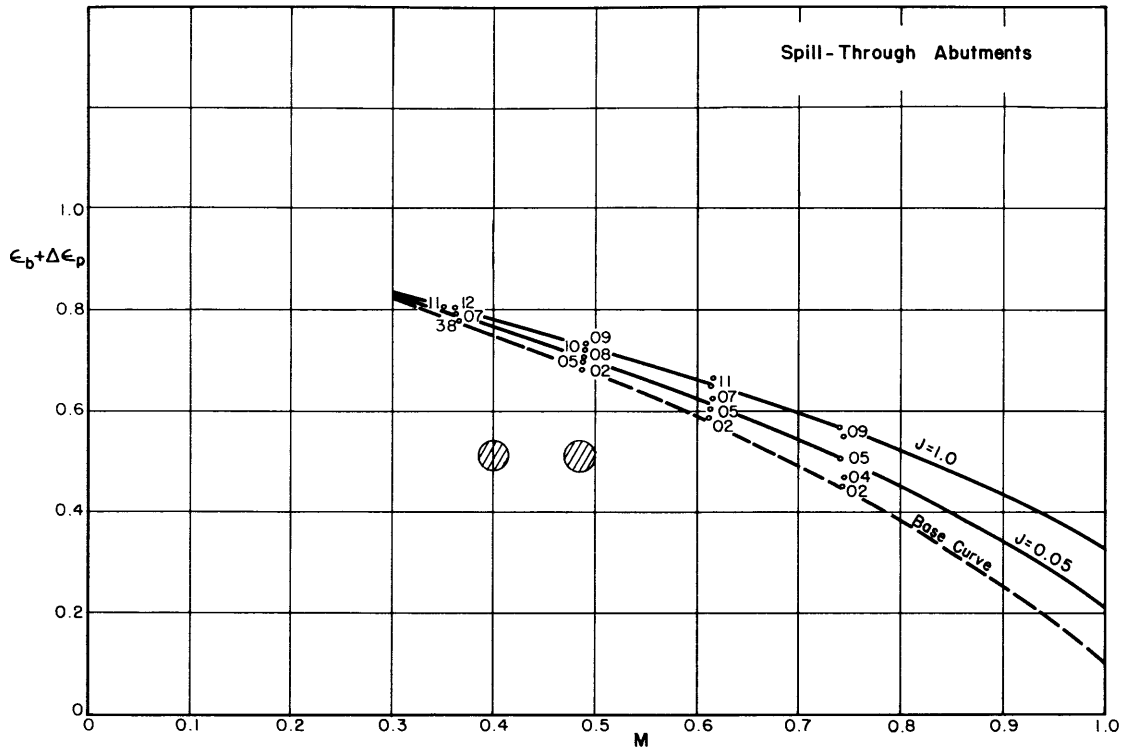


Fig. No. 6-10A Total differential level ratio $\epsilon_b + \Delta\epsilon_p$ for round double-shaft piers and spill-through abutments

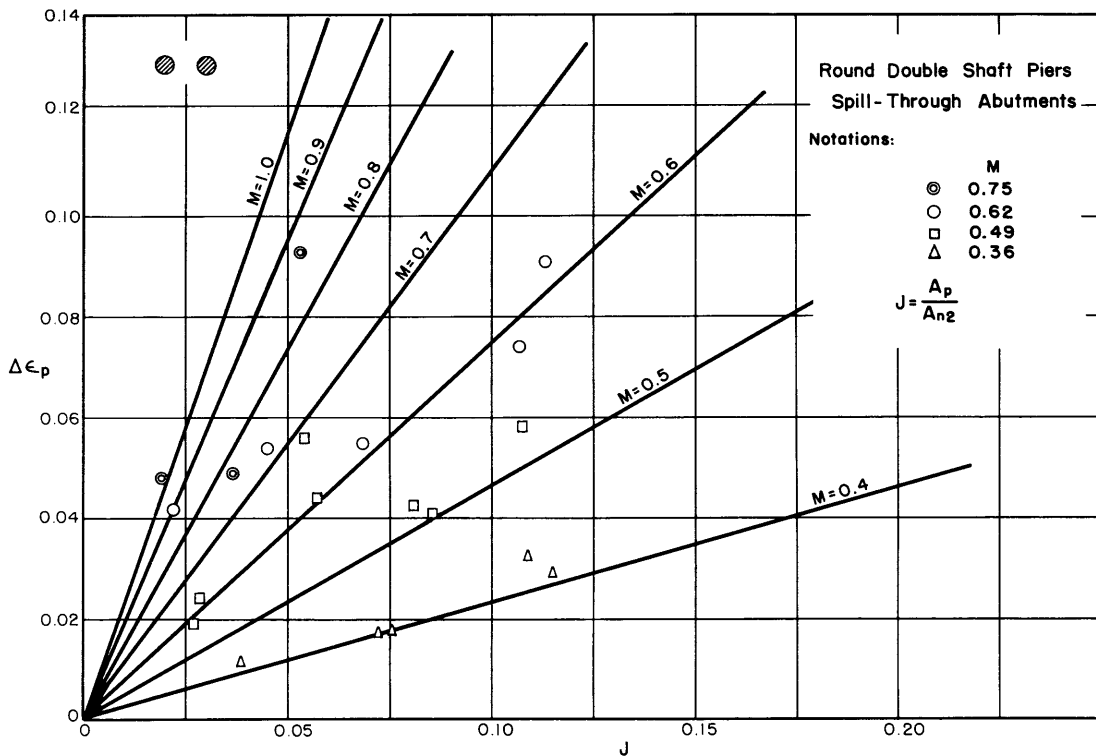


Fig. No. 6-10B Incremental differential level ratio $\Delta\epsilon_p$ for round double shaft piers and spill-through abutments

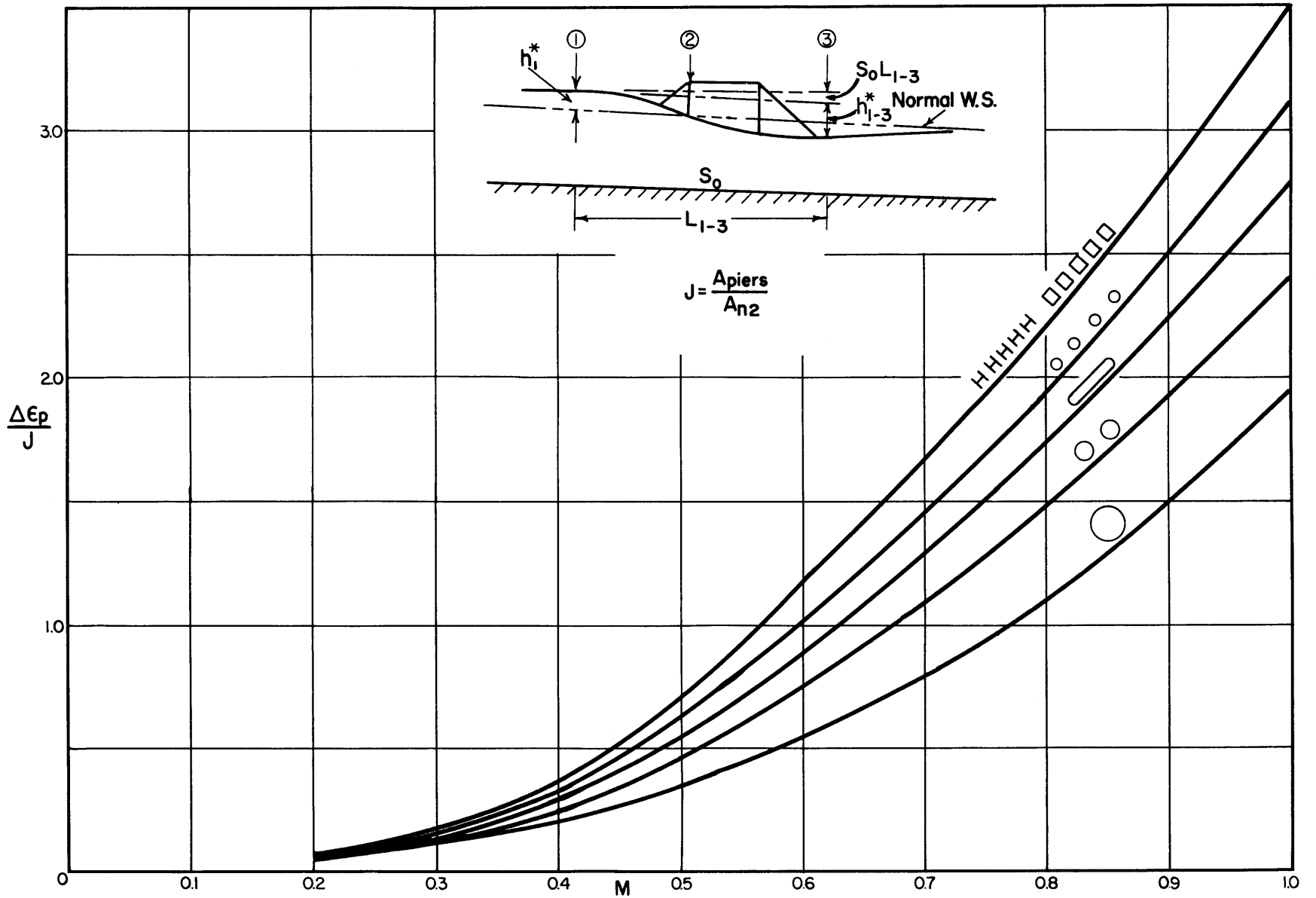
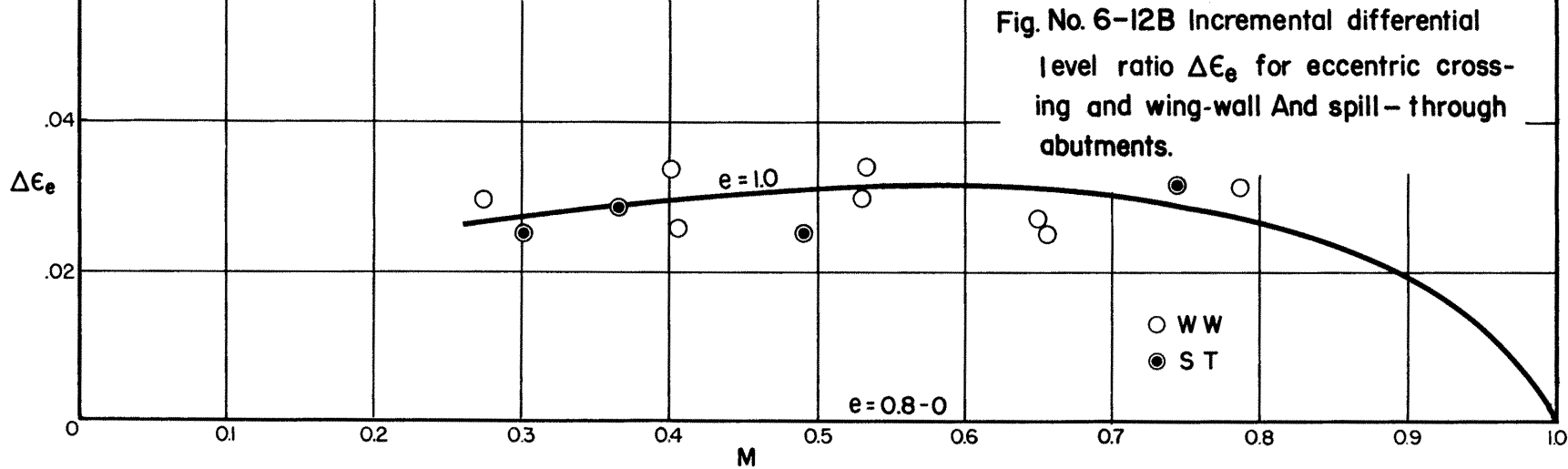
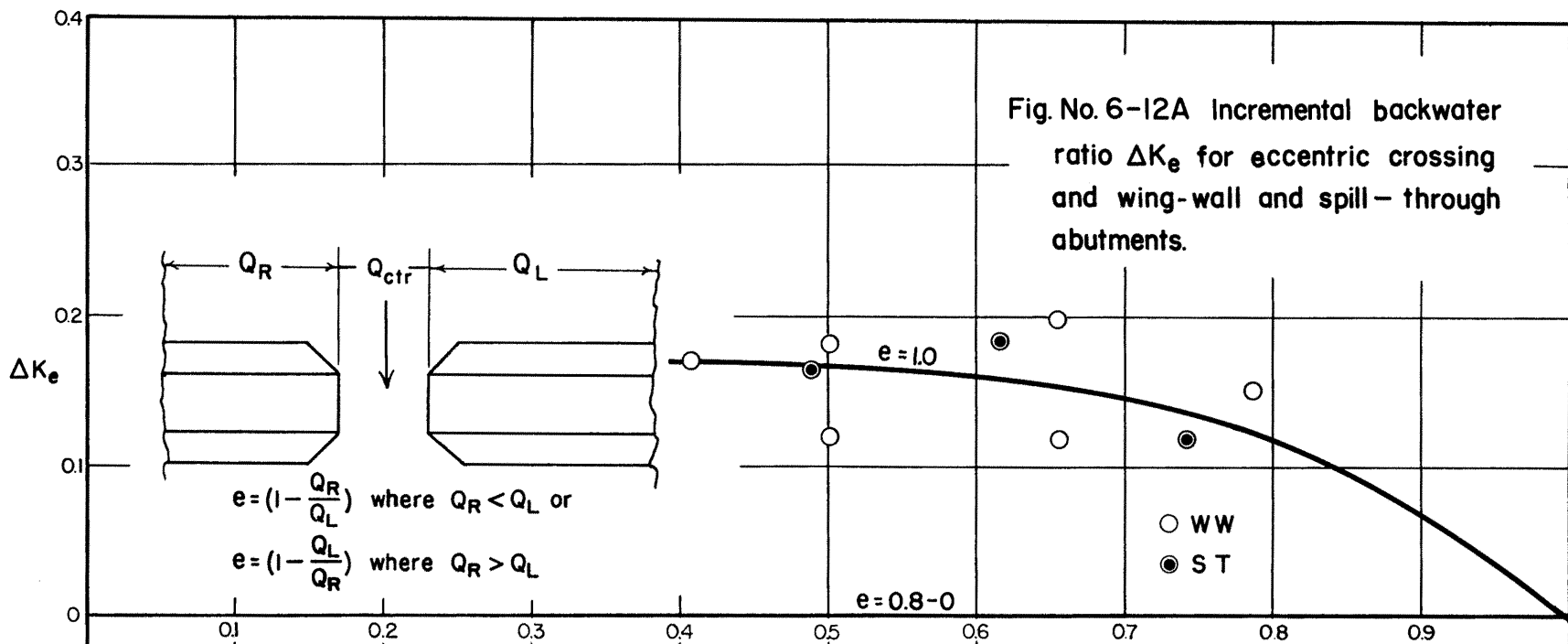


Fig. No. 6-11 Incremental differential level ratio $\Delta \epsilon_p$ for various Piers and Pile bents with wing-wall and spill-through abutments.



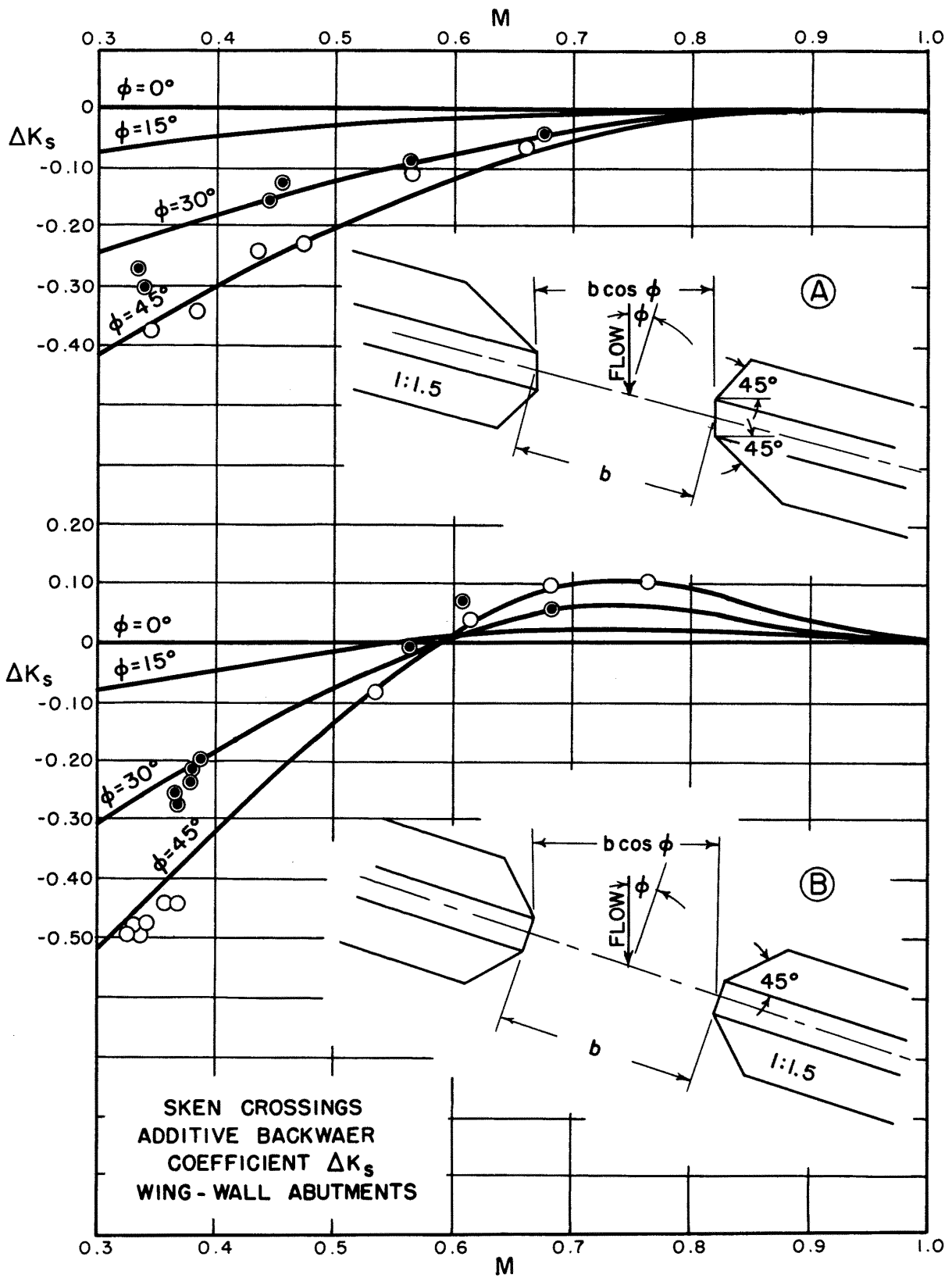


Fig. No. 6-13 Incremental backwater coefficient ΔK_s for skew crossing and wing-wall abutment

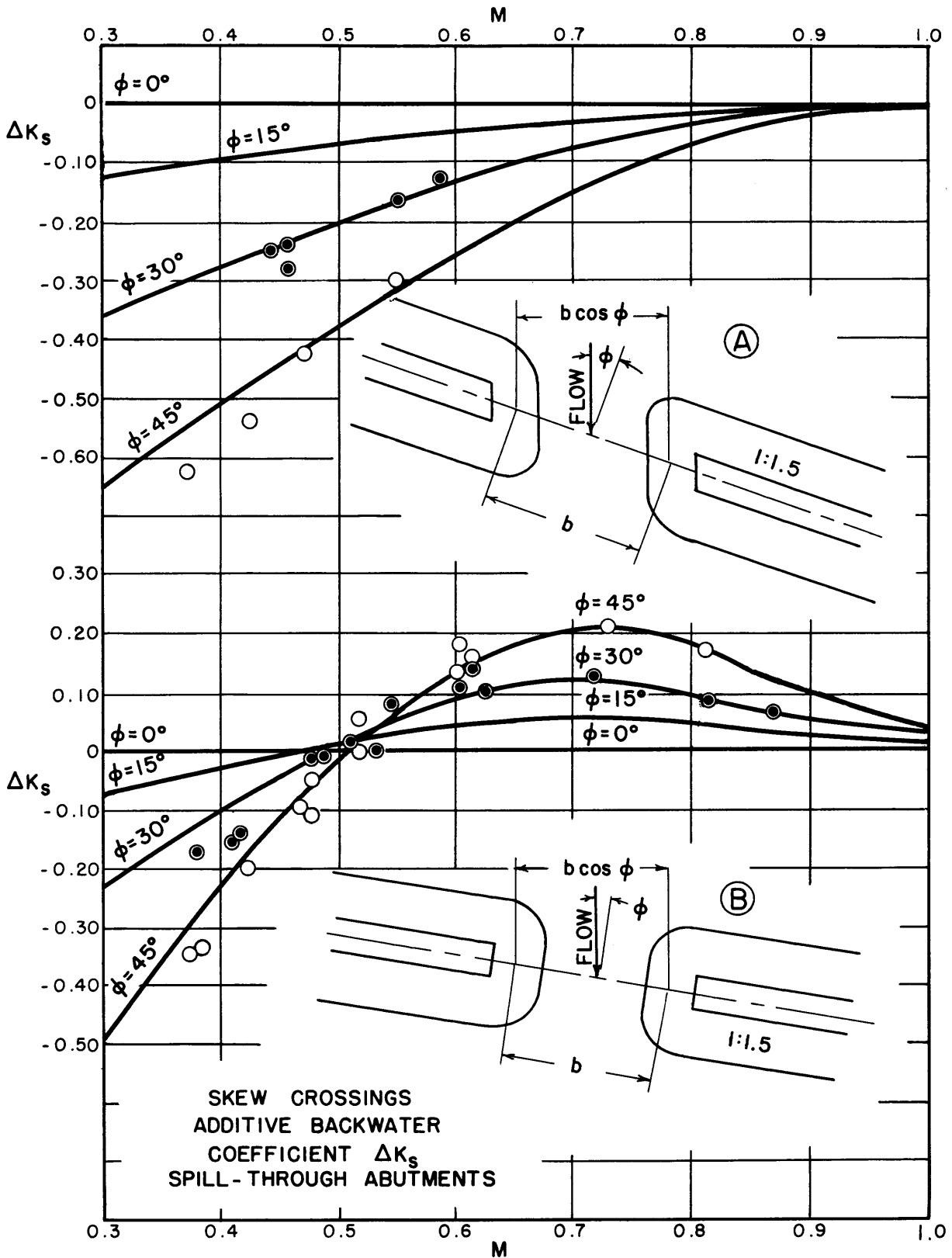


Fig. No. 6-14 Incremental backwater coefficient ΔK_s for skew crossing and spill-through abutment

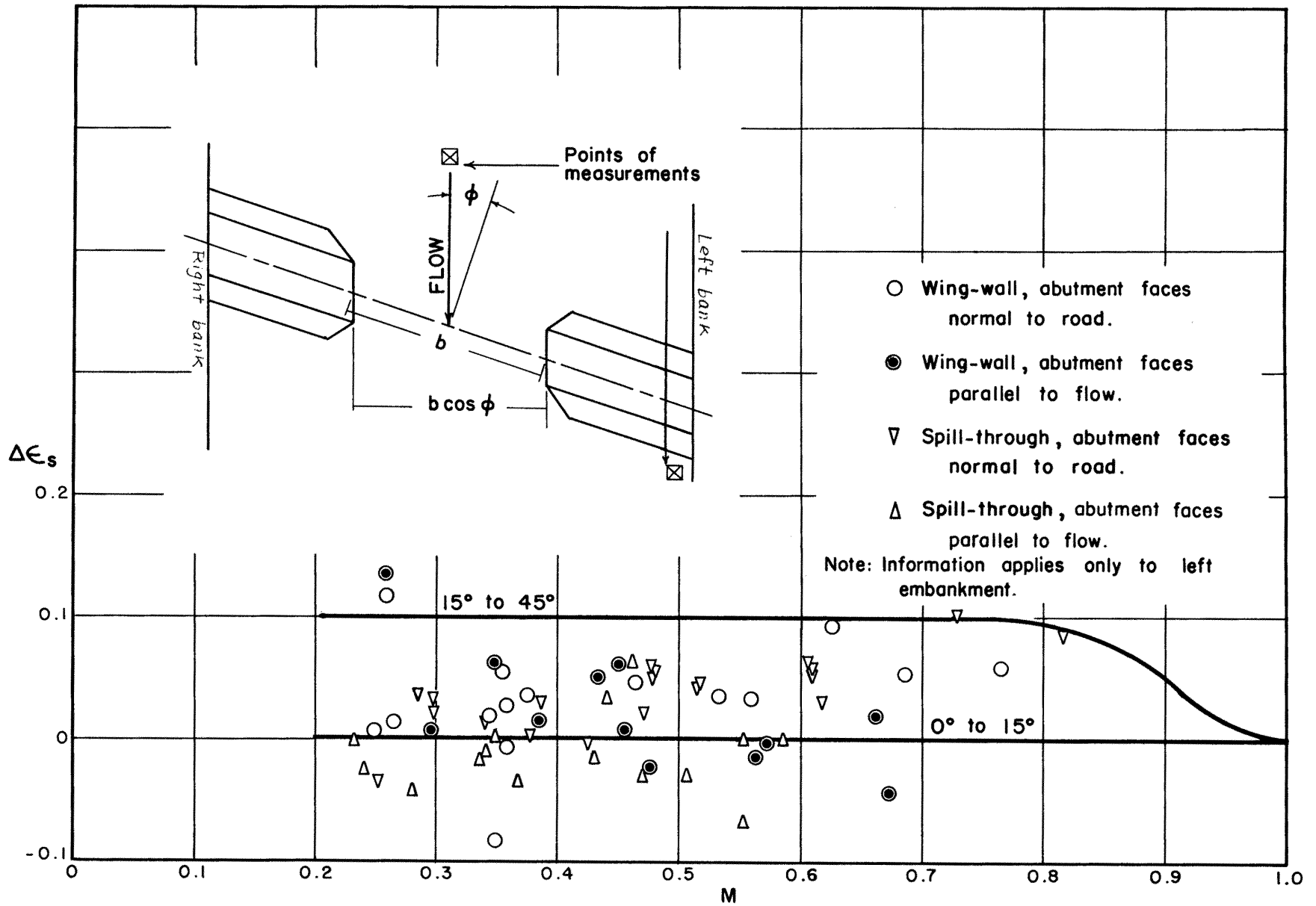


Fig. No. 6-15 Incremental differential level ratio $\Delta \epsilon_s$ for wing-wall and spill-through abutments

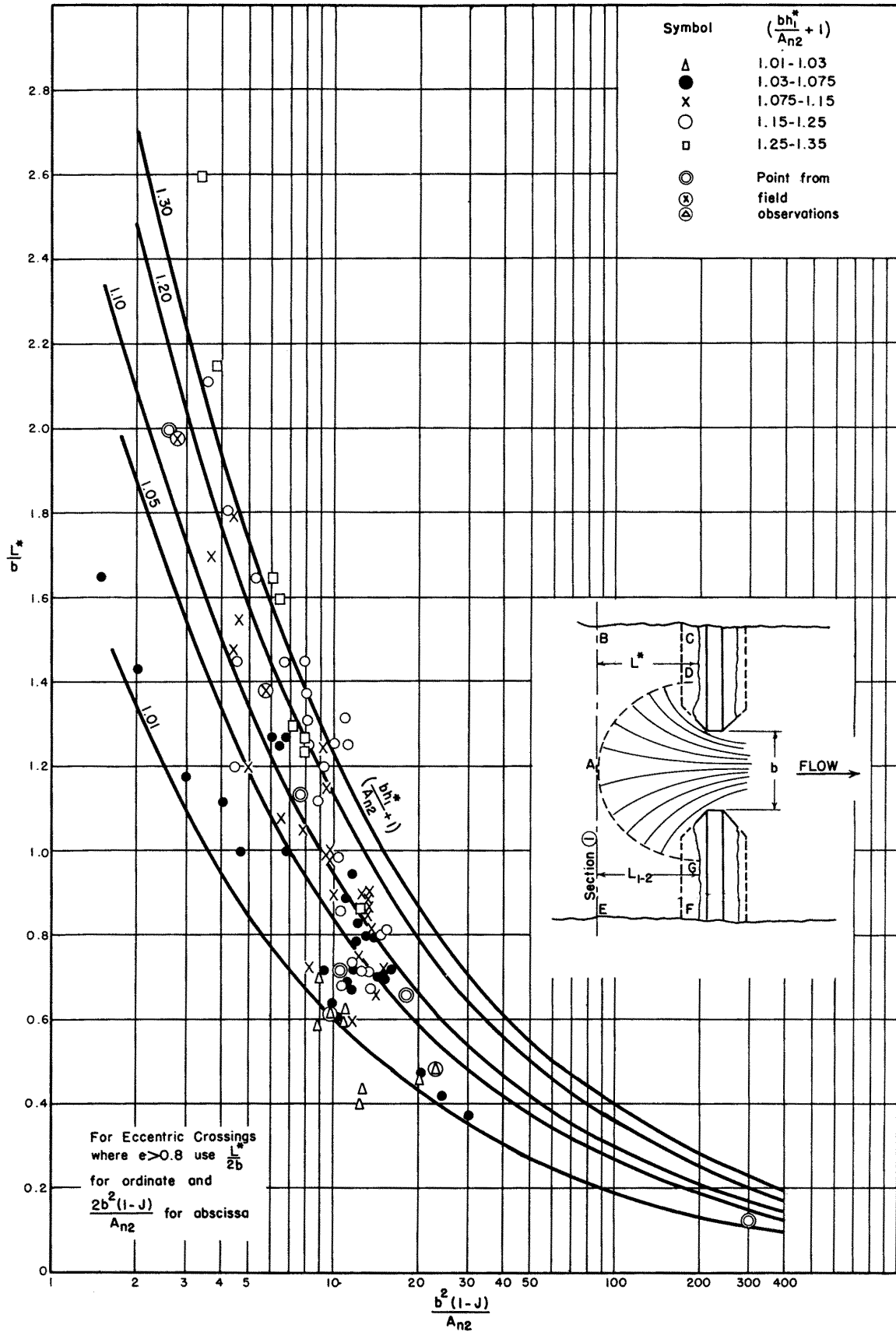


Fig. No. 6-16 Distance to point of maximum backwater with or without piers

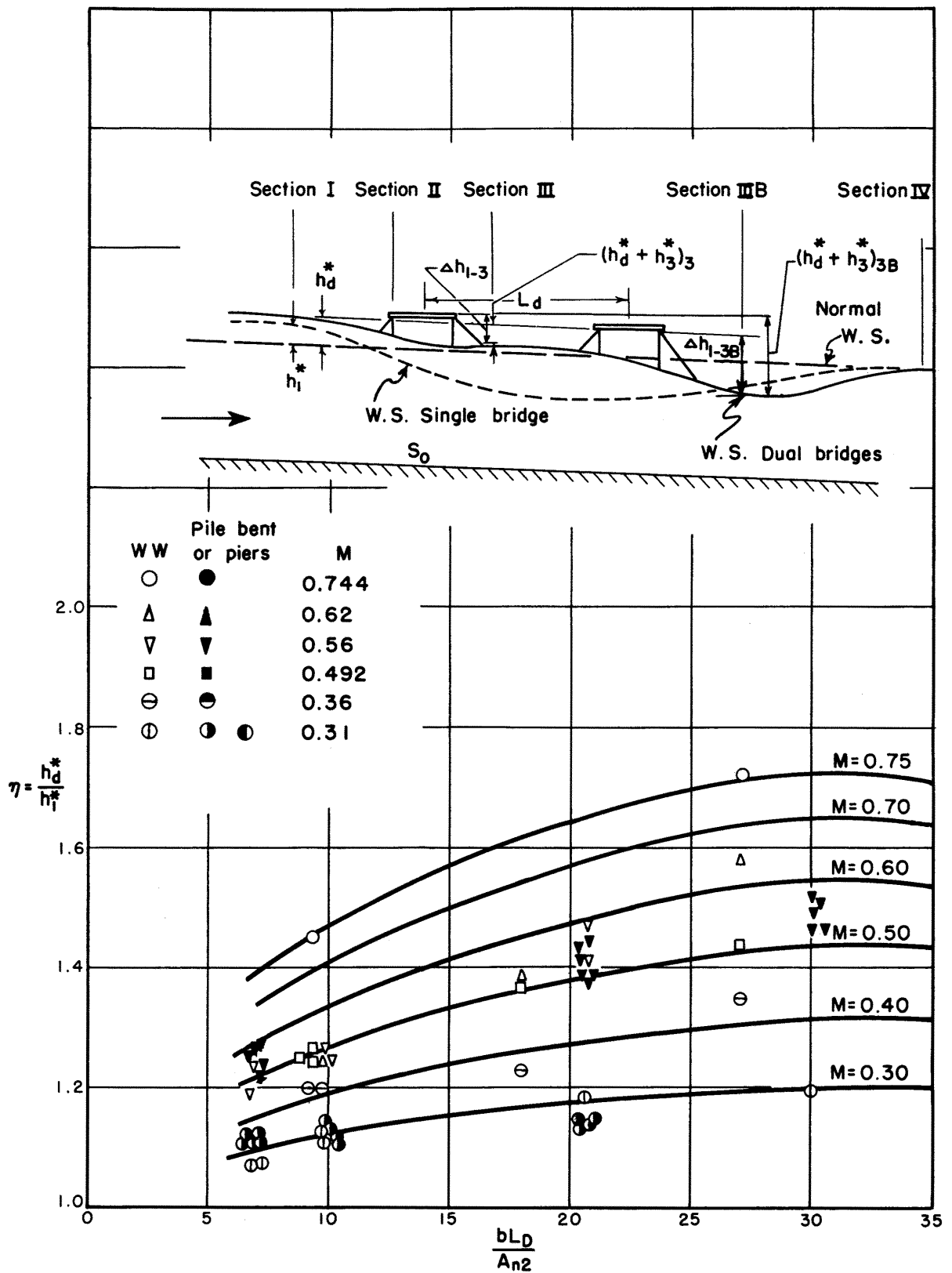


Fig. No. 6-17 Backwater multiplication factor η of dual bridges contraction for wing-wall and spill-through abutments

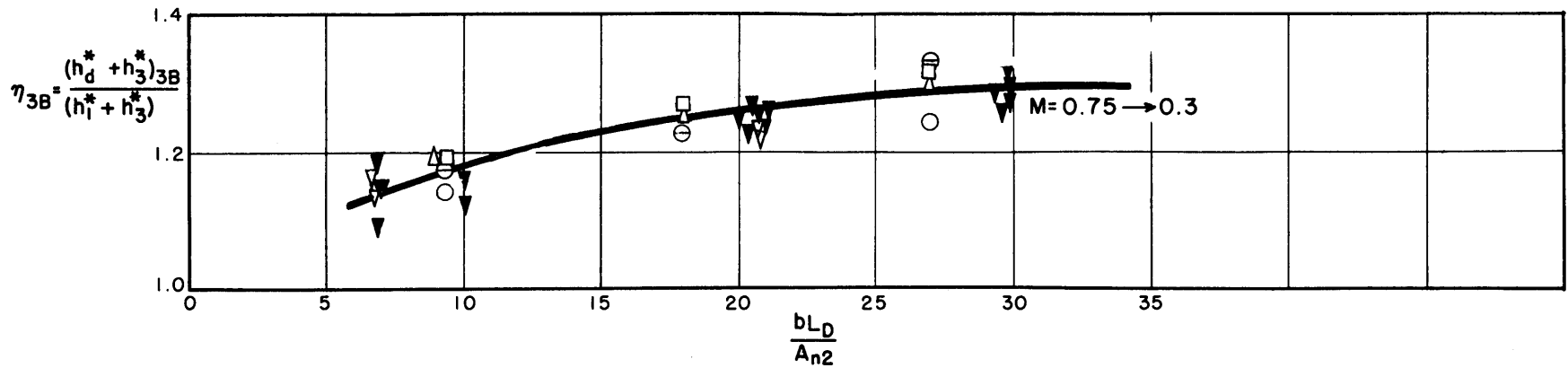


Fig. No. 6-18A Differential-level multiplication factor η_3 of dual bridges contraction for wing-wall and spill-through abutments

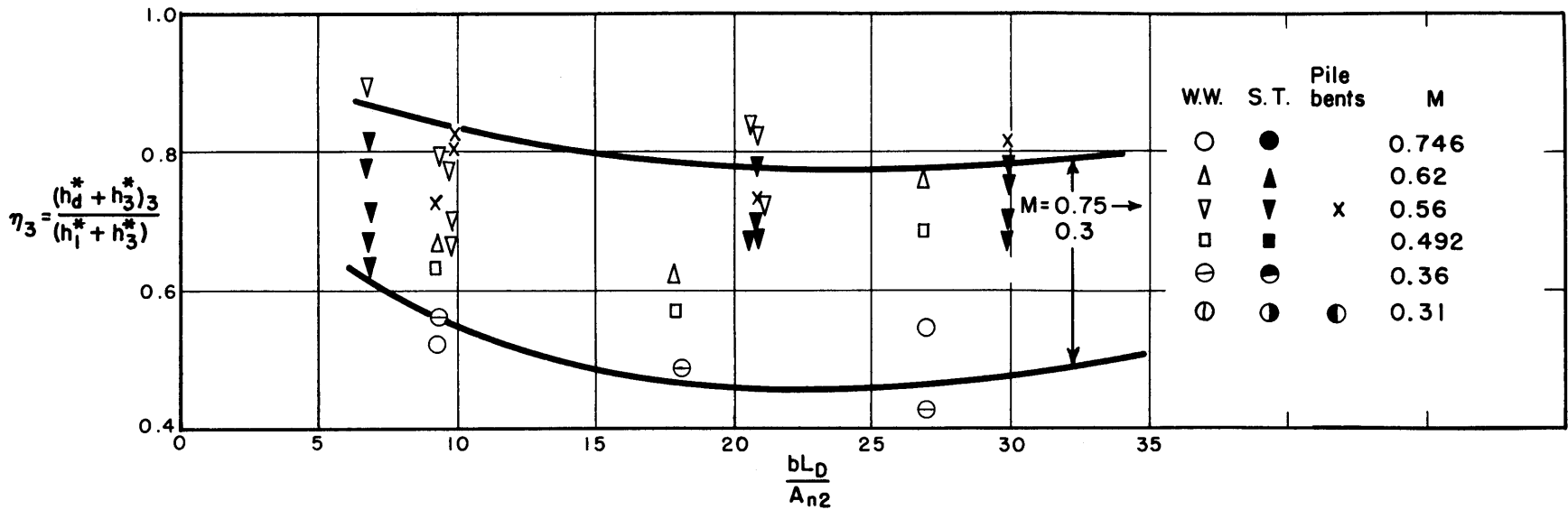


Fig. No. 6-18B Differential-level multiplication factor η_{3B} of dual bridges contraction for wing-wall and spill-through abutments

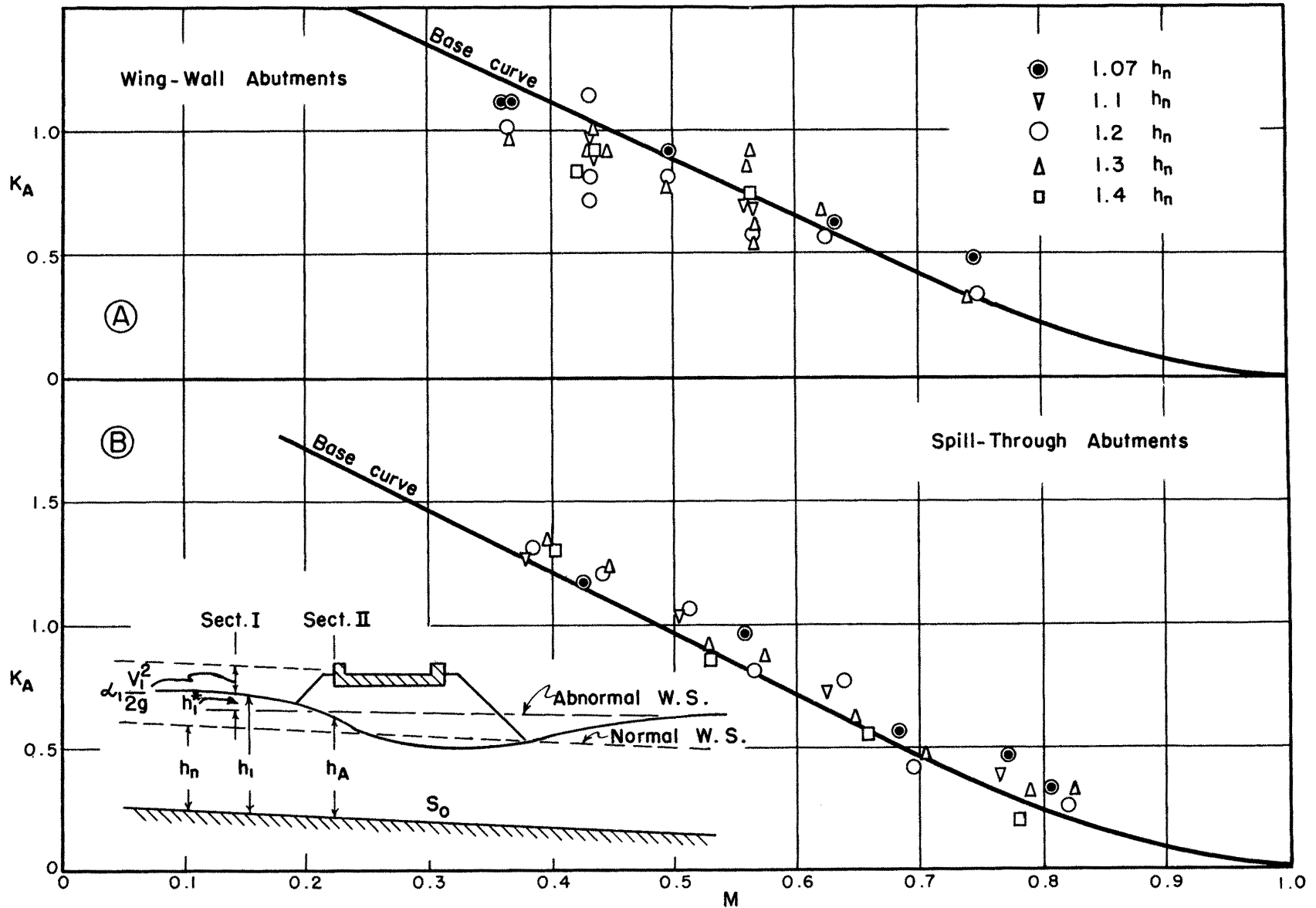


Fig. No. 6-19 Backwater coefficient K_A for abnormal stage-discharge condition

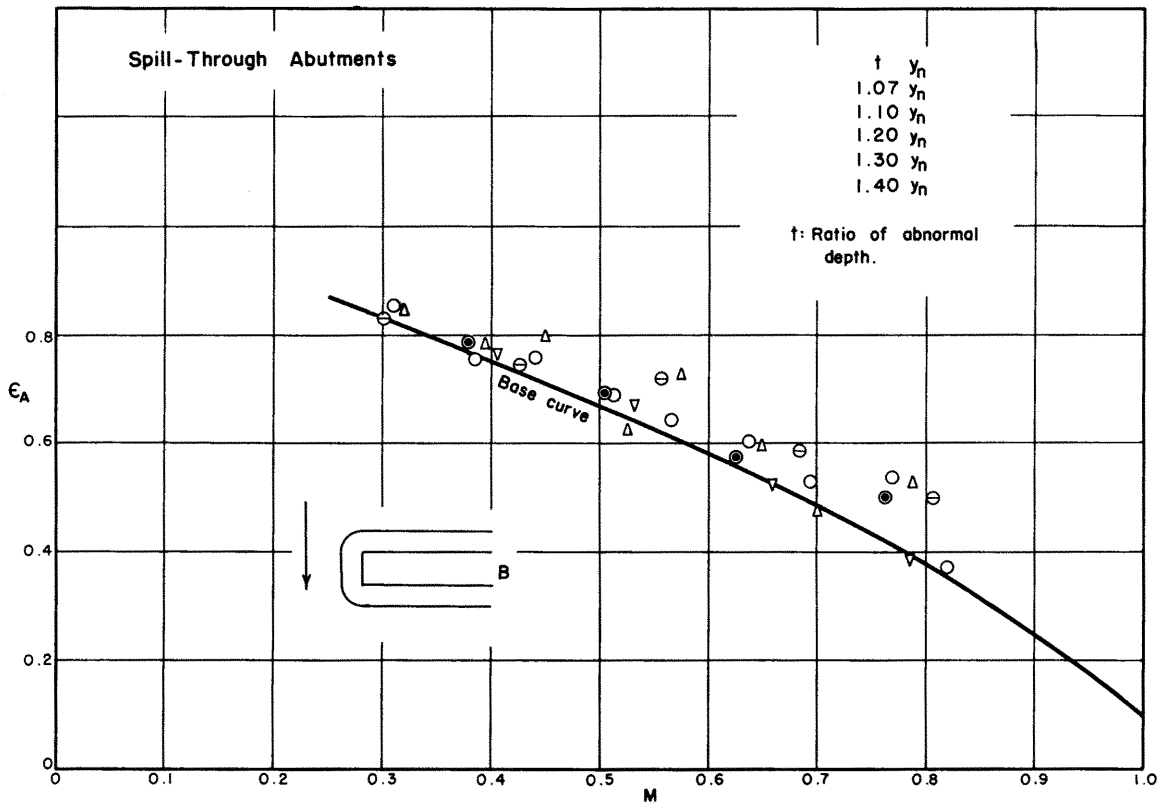
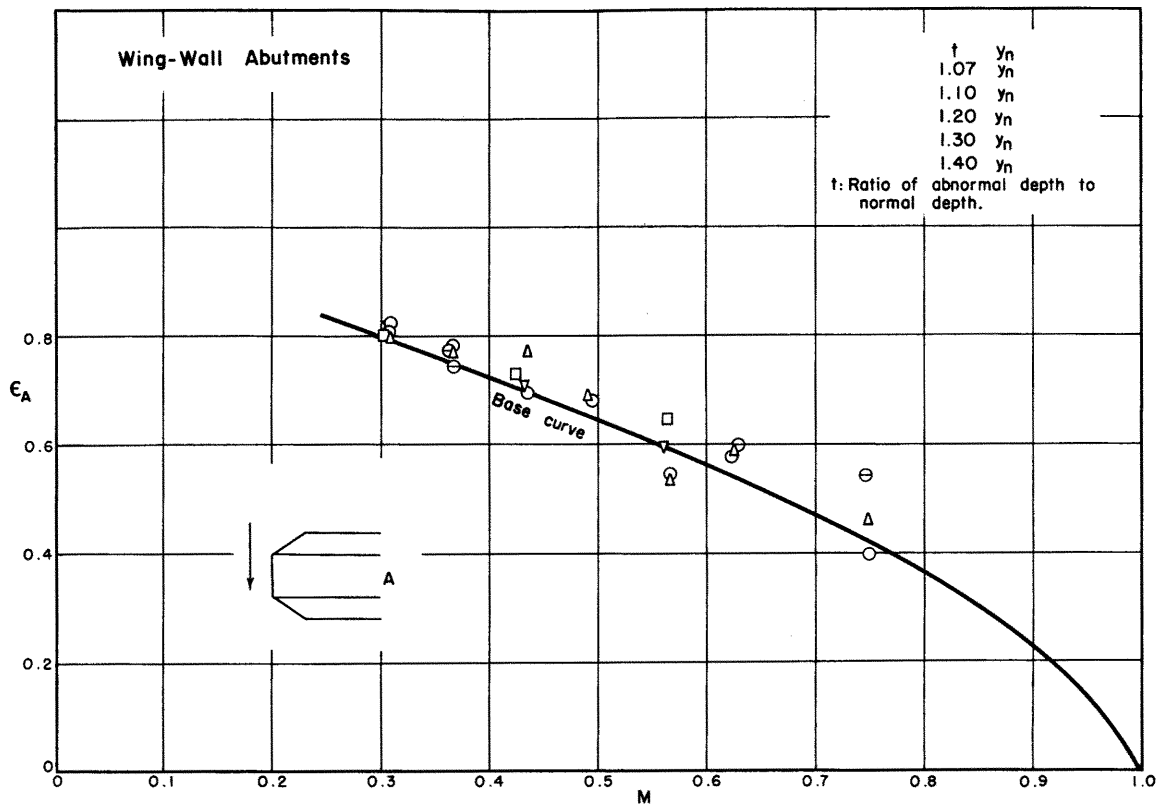


Fig. No. 6-20 Differential level ratio ϵ_A for abnormal stage conditions

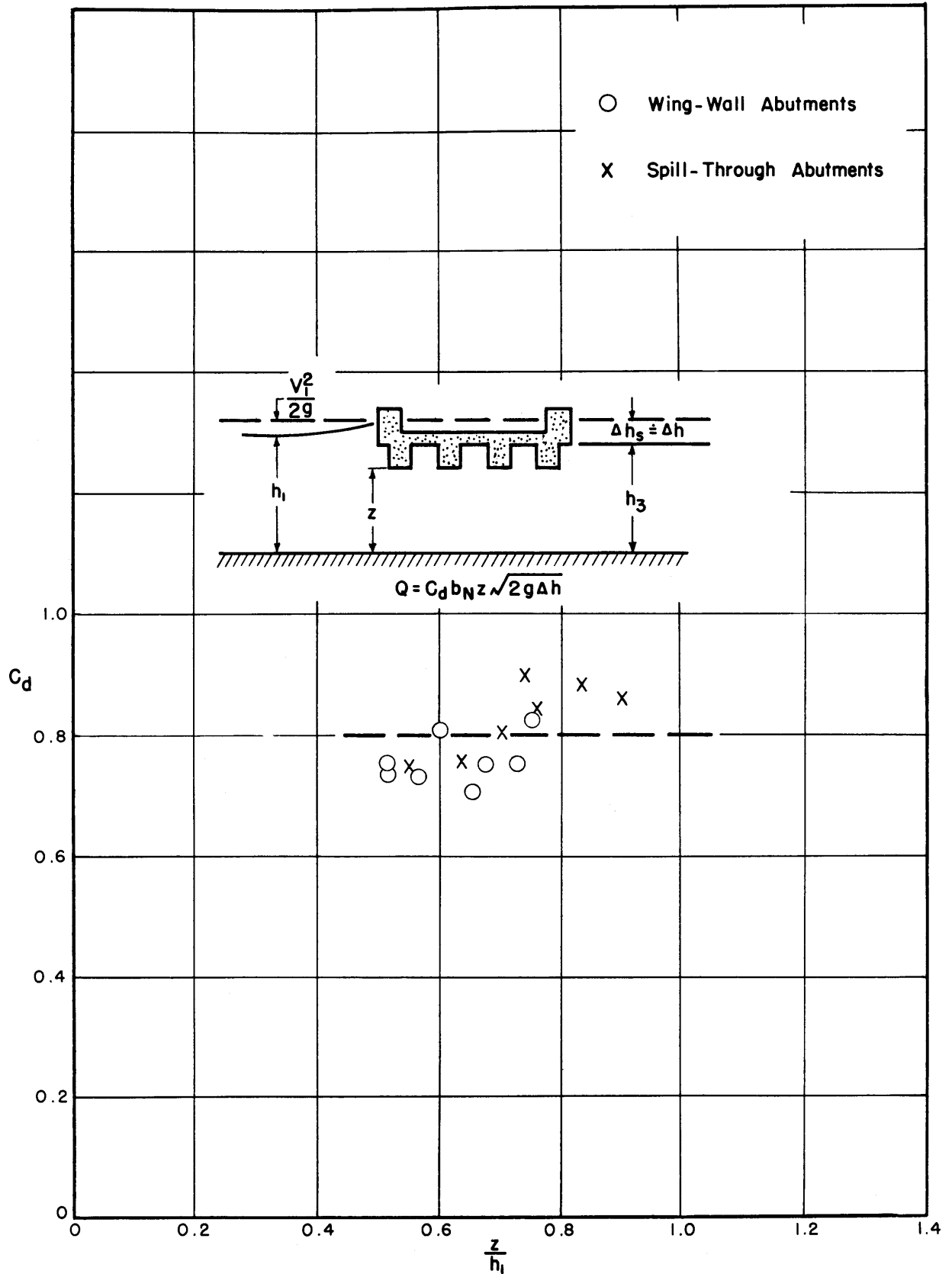


Fig. No. 6-21 Discharge coefficient for bridge girder submerged

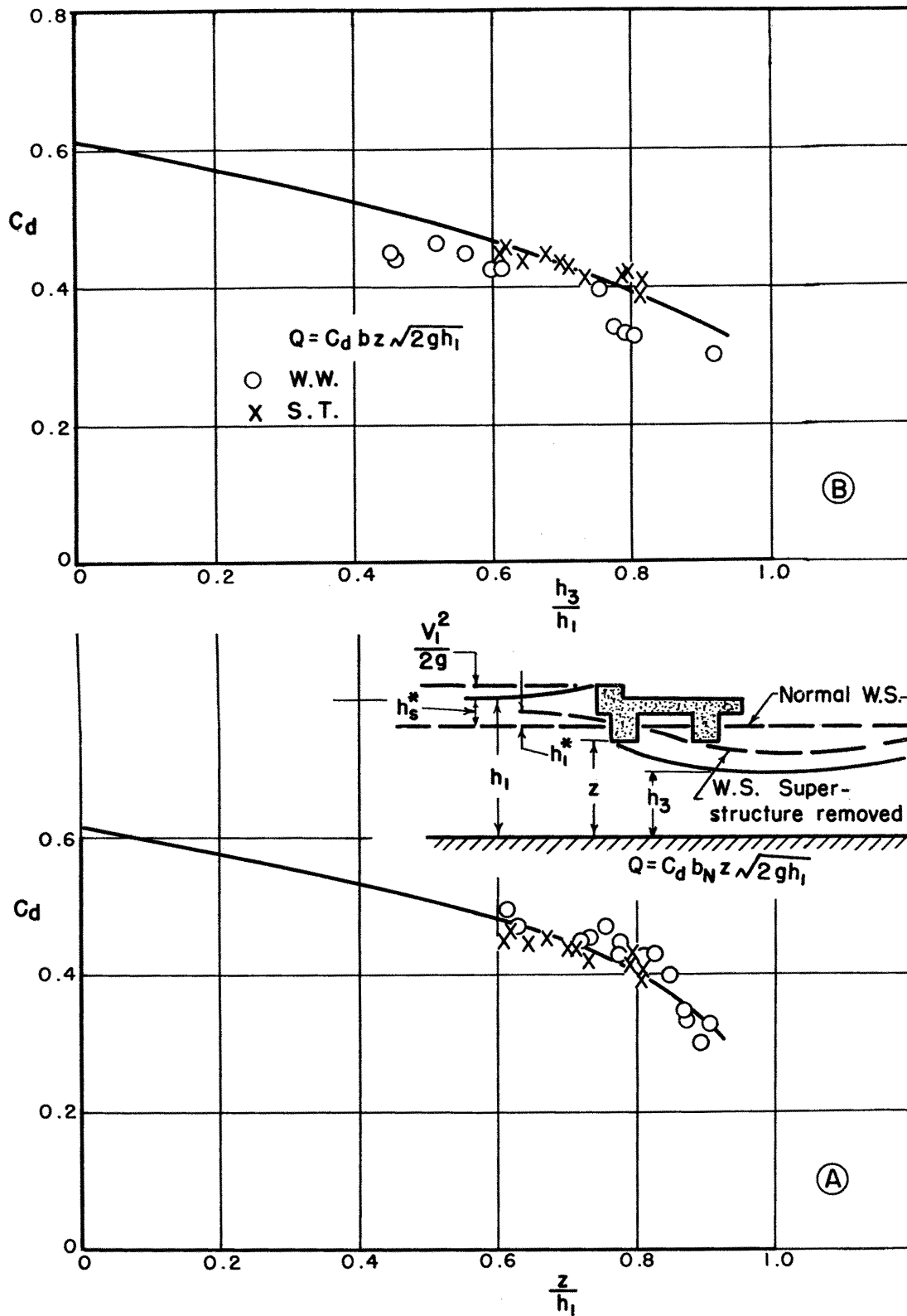


Fig. No. 6-22 Discharge coefficient for bridge girder partially submerged

VII. SUMMARY AND CONCLUSIONS

In this publication research on the maximum backwater caused by the open-channel contraction over a period of more than two years is reported. About 1400 runs have been made for this research. The main feature of the experiments was that the flow in a tilted flume was set uniform within the tested reach before the models were placed. Thus the normal depth and the Froude number of the un-contracted flow can be obtained for reference. The term opening ratio, denoting the ratio of the width of the opening to the channel width, has been used in the analysis instead of the term contraction ratio, denoting the degree of contraction.

The chapter on literature review discusses briefly the publications which are related directly to this research.

In Chapter III the mechanics of the open channel flow through a local contraction was discussed at length. The maximum backwater caused by the local constriction has been classified as [a] contraction backwater and [b] resistance backwater. When the flow is critical at the contracted section, the maximum backwater is called the contraction backwater, otherwise it is called the resistance backwater. For a given Froude number, the tranquil depth of the flow at the contraction decreases as the opening ratio decreases until the depth reaches the critical depth. The resistance backwater upstream from the contraction increases as the opening ratio decreases till the flow becomes critical at the contraction. The resistance backwater then becomes the contraction backwater. Further reduction of the opening ratio

will cause the increase of the contraction backwater. Based upon the principles of the specific energy diagram and the discharge diagram, and upon the condition that the flow is critical at the contraction, Eq 3-53 can be obtained

$$\left[\frac{h_1}{h_n}\right]^3 = \frac{F_n^2}{2} \frac{1}{\frac{3}{M} \sin\left[\frac{\theta}{3} - 30^\circ\right] - 1}, \quad [3-53]$$

Where $\text{Cos } \theta = M$. It is assumed that in both sections I and II the velocity distribution is uniform and the pressure distribution is uniform and the pressure distribution is hydrostatic. Eq 3-53 is both the lower limit of the contraction backwater and the upper limit of the resistance backwater.

If Eq 3-53 is modified:

- [a] it corrects for non-uniform distribution of velocity and non-hydrostatic distribution of pressure,
- [b] it correlates the ordinary resistance backwater to the upper limit of resistance backwater, and
- [c] its form can be made simpler.

An empirical coefficient $\bar{\phi}$ is needed. Introducing ϕ into Eq 3-53 yields:

$$\left[\frac{h_1}{h_n}\right]^3 = \frac{3}{2} F_n^2 \left[\frac{9\bar{\phi}}{4M^2} - 1 \right], \quad [3-60]$$

In order to analyze the flow pattern in the vicinity of the contraction, the theory of free streamline and the theory of the complex potential were employed.

Dimensional analysis was applied to this problem in order to plan an efficient testing program. For the case of a simple normal crossing, Eq 3-86 has been obtained.

$$\frac{h_1^*}{h_n} = f_s \left[\frac{V_n}{\sqrt{gh_n}}, \frac{V_n h_n}{v}, \frac{B}{h_n}, \frac{b}{B}, \text{model type} \right], \quad [3-80]$$

In Chapter V, the data have been analyzed thoroughly as a problem of fluid mechanics. In general the analysis is helpful to the basic understanding of the problem. In particular, the results of simple normal crossings can be applied to the prototype backwater problems. In Chapter VI, a method of estimating the maximum backwater from the viewpoint of a highway engineer has been presented. The analysis in Chapter V can be summarized as follows:

- I. The geometry of an open channel flow through a contracted opening has been compared to the outflow from a two-dimensional orifice plate. The method of free streamline analysis has been used to study the geometry of such an outflow from a two-dimensional orifice plate which is located perpendicularly to the approaching flow at the end of a straight channel. The measured water surface profiles taken upstream from the contraction have been compared satisfactorily with the theoretical profiles based upon free streamline theory, [see Fig. 5-1 and Fig. 5-2]. The coefficient of contraction of the jet from an open-channel contraction cannot be measured satisfactorily. Because the information of the coefficient of contraction is essential to the analysis of flow from an open-channel contraction, further laboratory work is needed to determine the coefficient of contraction. It is difficult to determine experimentally the location of the maximum backwater. An upper limit of the location of the maximum backwater has been found by use of the free streamline theory, see Fig. 5-7.

- II. The energy loss of an open channel flow through a contraction can be summarized as follows:
- [a] experiments show that the specific head at section I is approximately equal to that at section II.
 - [b] the energy loss can be classified mainly into three losses: energy loss owing to normal boundary resistance, energy loss owing to excess boundary resistance, and energy loss owing to lateral exchange of momentum.
 - [c] energy loss caused by excess boundary resistance between section III and section IV can be computed according to Eq 3-25.
 - [d] energy loss caused by lateral exchange of momentum between sections III and IV can be computed according to Eq 3-19.
 - [e] between sections I and IV, the distribution of energy loss can be seen from Figs. 5-14 to 5-17 for different abutments at different flow conditions.
- III. Analysis of the data of the maximum backwater can be summarized according to the crossing conditions:
- [a] Simple normal crossing. Based upon dimensional analysis and verified by experimental data, the maximum backwater can be expressed as a function of several important parameters:

$$\frac{h_1^*}{h_n} = \text{function} [M, F_n, \text{model type}] \quad . \quad [5-3]$$

The effects of channel slope, channel roughness, and discharge are included in Eq 5-3 as a result of using h_n and F_n . The effect of width-depth ratio B/h_n cannot

be determined owing to the limited width of the laboratory flume. Within the experimental range, the length of the contracted section does not affect the maximum backwater. That the maximum backwater is affected by abutment height is explained by the fact that the flow geometry of the abutments tested varies with the abutment height. Although the VB model does not have direct application in highway design practice, it does provide the most convenient means of investigating the relative influences of the basic variables on the maximum backwater.

From Chapter III, the equation for the maximum depth of resistance backwater can be written as

$$\left[\frac{h_1}{h_n}\right]^3 = \frac{3}{2} F_n^2 \left[\frac{9\phi}{4M^2} - 1 \right] \quad , \quad [3-60]$$

where ϕ is an empirical coefficient depending upon model type, Froude number and opening ratio. For the VB model

$$\phi = 1.33 \left[1 - \frac{2}{3} M^2 \left(2 - M - \frac{1}{3F_n^2} \right) \right] \quad [5-8]$$

The combination of Eqs 3-60 and 5-8 is equivalent to

$$\left[\frac{h_1}{h_n}\right]^3 - 1 = 4.83 F_n^2 \left[\frac{1}{M^2} - \frac{2}{3} (2.5 - M) \right] \quad [5-7]$$

Eq 5-7 indicates that if $\left[\frac{h_1}{h_n}\right]^3$ is plotted against F_n^2 with M as a third variable, data will form a set of straight lines whose slope is a function of M . All

the straight lines intersect the axis of $\left[\frac{h_1}{h_n}\right]^3 = 1$, see Fig. 5-35. For WW and ST abutments, data plotted as $\left[\frac{h_1}{h_n}\right]^3$ against F_n^2 do not follow straight lines for constant M-values, see Figs. 5-37 and 5-38. It can be concluded that for WW and ST abutments, $\left[\frac{h_1}{h_n}\right]^3 - 1$ does not vary linearly with F_n^2 , which means that the effect of abutment geometry on the maximum backwater changes with the Froude number F_n . Figs. 5-37 and 5-38 can be used in designing highway bridge crossings if the design values of F_n and M are within the range shown in these two figures.

A series of empirical curves have been found by plotting $\left[\frac{h_1}{h_n}\right]^3$ against $F_n^2 \left[\frac{1}{M^2} - 1\right]$, see Figs. 5-39 to 5-43. The advantage of using Figs. 5-39 to 5-43 instead of Figs. 5-37 to 5-38 is that the former has a wider application range of F_n and M than the latter.

[b] Abnormal stage-discharge condition. The abnormal stage-discharge conditions were obtained in the uncontracted channel with a slope by creating different M1-type backwater curves. The depth measured at section II before the installation of abutments has been chosen as the reference depth h_A . The test range of h_A varies from 100 to 140 per cent of h_n . The reference Froude number F_A has been defined as

$$F_A = \frac{Q}{h_A B \sqrt{gh_A}}, \quad [5-14]$$

and M remained to be b/B . Data of such abnormal stage-discharge conditions are shown in Figs. 5-45, 5-46 and 5-47.

Abnormal stage-discharge conditions in a contracted channel can also be created by using a horizontal channel. Limited experimental data of maximum backwater were obtained for this case, see Fig. 5-48.

All data of maximum backwater pertaining to abnormal stage-discharge conditions indicate that they deviate systematically from those pertaining to the simple normal crossing conditions. This abnormal stage-discharge condition is only a special case and cannot be accepted as a standard reference condition.

- [c] Dual bridges crossing. The analysis of the effect of dual-bridges crossing on the maximum backwater is handicapped by limited data. Data of dual-bridges crossing are plotted $[h_1/h_n]^3 - 1$ against $F_n^2[1/M^2 - 1]$ with the distance between the two crossings L_D as a third variable. [See Figs. 5-51 and 5-52] Fig. 5-53 indicates that the experimental range of L_D was not long enough for the maximum backwater to reach a maximum. Further research to determine the L_D value which will cause maximum effect of backwater is needed.
- [d] Bridge girder partially submerged. The experimental data of this crossing condition have been analyzed in two different ways, neither of which can be considered conclusive because of limited data. The first method is to plot the data according to dimensionless parameters which were obtained through dimensional analysis. The second method is to determine the effective opening ratio M^* for the same maximum backwater of bridge

girders partially submerged as caused by a simple normal crossing. The value $M-M^*$ has been plotted against Z/h_1 with M as third variable as shown in Fig. 5-56.

- [e] Skew crossings. Skew angle varied at 15 degrees, 30 degrees, and 45 degrees. Flow depth at one of the upstream stagnation points was chosen for analysis. Preliminary tests indicated that a skew angle at 15 degrees or less does not affect appreciably the flow depth at the two upstream stagnation points. The opening ratio is defined for skew crossings as

$$M = \frac{b \cos \phi}{B}$$

where ϕ is the skew angle.

The method of effective opening ratio M^* was applied to the analysis of this case. In most cases this method is satisfactory. In general the M^* values referred to the case of simple normal crossing is larger than the M -values of the skew crossing. This resulted from the fact that for the same opening ratio, according to the definition, the opening width of a skew crossing is greater than that of the simple normal crossing.

- [f] Eccentric crossing. It appeared that for the VB model, eccentric crossing does not affect the maximum backwater. For other types of abutments, curves of M versus M^* were plotted. Only eccentric crossings $e = 1$ were tested. More experimental data of eccentric crossings are needed.

[g] Piers. For the case that the backwater was caused by piers alone, it was found that the methods of Rehbock and d'Aubuisson, by use of coefficients given by Rehbock and Yarnell respectively, yield moderate agreement with the current data. A new set of pier coefficients is given in Table 5-2 of Chapter V. For the case that the backwater was caused by both piers and abutments, the method of effective opening ratio was used in analyzing the data in which a pier shape factor has been introduced so that

$$M^* = M - s \frac{ND}{B} \quad [5-20]$$

This method yields satisfactory results, and was extended satisfactorily to dual bridges crossing with piers and to skew crossings with piers.

[h] Flood plain model. Limited data have been obtained for this case. The normal depth and the Froude number for this case have been defined in such a way that methods used for previous cases can be applied to this case as well. The method of effective opening ratio was applied to this case with fair success. Considerable research is needed to study the effect of the flood plain on the maximum backwater.

The analysis in Chapter VI can be summarized as follows: A practical method of estimating the maximum backwater has been proposed in this chapter. In order to simplify the calculation, a slight degree of accuracy may have been sacrificed. This method which was first proposed by Izzard is based upon the

Bernoulli theorem applied to sections I and IV. The formula for estimating the maximum backwater is

$$h_1^* = K^* \frac{V_{n2}^2}{2g} + \alpha \left[\frac{A_{n2}^2}{A_4^2} - \frac{A_{n2}^2}{A_1^2} \right] \frac{V_{n2}^2}{2g} , \quad [6-5]$$

where K^* is an empirical backwater coefficient. The K^* -values have been determined by use of experimental data, so that:

- [a] For simple normal crossings the curves correlating K^* and M are called the base curves. See Fig. 6-4A to 6-7A. The backwater coefficient K^* is given a special symbol K_b for the base conditions.
- [b] For normal crossing with piers the increase of backwater coefficient above K_b is represented by ΔK_p such that

$$K^* = K_b + \Delta K_p \quad [6-11]$$

The ΔK_p -values are shown in Figs. 6-8 and 6-9.

- [c] For eccentric crossings the increase of backwater coefficient above base value K_b is represented by ΔK_e which is shown in Fig. 6-12A.
- [d] For skew crossings the increase of backwater coefficient ΔK_s is shown in Figs. 6-13 and 6-14.

In the prototype, the drop of the water surface across the roadway embankments Δh_s has been found equal to the total water surface drop along the center line of the channel Δh where $\Delta h = h_1^* + h_3^* + S_o L_{1-3}$.

The procedure is much the same as for determining the backwater coefficient K^* . In this case the symbol $\epsilon^* = \frac{h_1^*}{h_1^* + h_3^*}$ is used. Values of ϵ_b , or base curve, are shown on Figs. 6-4B to 6-7B. Figs. 6-10 and 6-11 show the incremental differential ratio $\Delta\epsilon_p$, or deviation from the base curve, for piers. Other figures are supplied to show this deviation for eccentricity $\Delta\epsilon_e$ and skew $\Delta\epsilon_s$.

For the case of dual bridges crossing, let h_d^* represent the maximum backwater of dual bridges crossing, and $\eta = h_d^*/h_1^*$. The curves of η as a function of M and bL_D/A_{n2} are shown in Fig. 6-17.

For the case of abnormal bridges crossing, the maximum backwater can be written as

$$h_1^* = K_A^* \frac{[Q/bh_A]^2}{2g}, \quad [6-24]$$

Where K_A^* is the total backwater coefficient, h_A is the abnormal depth of flow at section II before the contraction was installed. Similar to K^* , the value of K_A^* is a summation of K_A , ΔK_p , ΔK_s and ΔK_e ; where K_A is for simple abnormal crossings and ΔK_p , ΔK_s and ΔK_e are as defined previously.

VIII. RECOMMENDATIONS FOR FUTURE RESEARCH

The analysis reported in Chapters V and VI indicates that additional research is desirable on some phases of the fixed bed model study. Those phases needing additional attention are listed as follow:

1. Determination of the contraction coefficient of the jet measured at the vena contracta.
2. Further investigation of energy dissipation throughout the expanding jet by velocity measurements.
3. Determination of the energy gradient of the flow in the vicinity of the constriction by measurement of pressures and velocities throughout.
4. Determine more specifically the effect of eccentricity on the backwater. This phase has not been thoroughly explored.
5. Perform additional experiments on dual bridges to more clearly define the maximum value of h_d^* as the distance between bridges is further increased.
6. Continue study to determine how nonuniform distribution of flow affects the backwater. This would constitute extension of the studies performed using flood plain flow depths less than those in the main channel.
7. Determine effect of width to depth ratio [ratio of width of flood plain to depth of flow in main channel] on the backwater.

The objective throughout this research program has been threefold: [i] to understand the basic mechanics of open channel

flow through a constriction; [ii] to compute bridge backwater for the various conditions encountered in design; and [iii] to verify or compare the laboratory results with conditions experienced in the field.

Items 1 through 6 must of necessity be studied in the laboratory although certain checks for verification purposes can be made in the field for items 4, 5, and 6. Item 7 is limited to field observations.

In closing it may be stated that all phases of the foregoing backwater study amenable to prototype verification will be checked at every opportunity.

BIBLIOGRAPHY

1. Archer, W. H. Experimental determination of loss of head due to sudden enlargement in circular pipes. Trans. ASCE, Vol. LXXVI, 1913. p. 999.
2. Boussinesq, J. V. Essai sur la theorie des eaux courantes. Memoires presentes par divers savants a l'Academie des Sciences, Paris, 1877.
3. Escande, J. L. Notice sur les Travaux Scientifiques, Toulouse, 1953.
4. Garrett, Jerry. Relationship between the head loss at bridge piers and drag resistance of the piers. M.S. Thesis, University of Texas, Austin, Texas, 1956.
5. Gibson, A. H. Hydraulics and its applications. 4th ed., 1952.
6. Gibson, A. H. Conversion of kinetic to potential energy in the flow of water through passages having divergent boundaries. Engineering, Vol. 93, 1912. p. 205.
7. Gibson, A. H. On the flow of water through pipes and passages having converging or diverging boundaries. Proc. Royal Society of London, Series A, Vol. 83, 1910. p. 336.
8. Goldstein, S. Modern developments in fluid dynamics. Oxford Press, 1938.
9. Highway Drainage Manual, U. S. Bureau of Public Roads, Design Chart.
10. Ippen, A. T. Engineering hydraulics, edited by Hunter Rouse, Chapter VIII, John Wiley and Sons. p. 496.
11. Izzard, C. F. Discussion on "Tranquil flow through open-channel constrictions" by C. E. Kindsvater and R. W. Carter. Trans. ASCE, Vol. 120, 1955. p. 985-9.

12. Izzard, C. F. Discussion on "Backwater effects of open-channel constrictions" by H. J. Tracy and R. W. Carter. Trans. ASCE, Vol. 120, 1955, p. 1008-13.
13. Jaeger, C. The steady flow in open channels, the problem of Boussinesq. Journal of Institute of Civil Engineers, paper 5650, February, 1948.
14. Jaeger, C. Technisthe Hydraulik. Verlag Birkausen Basel, 1949.
15. Kalinske, A. A. Conversion of kinetic to potential energy in flow expansions. Trans. ASCE, Vol. III, 1946, p. 382.
16. Kindsvate, C. E. and R. W. Carter. Tranquil flow through open-channel constrictions. Trans. ASCE, Vol. 120, 1955. p. 955-80.
17. Kindsvater, C. E., Carter, R. W. and Tracy, H. J. Computation of peak discharge at constrictions. U. S. Geological Survey Circular 284, Washington, D. C., 1953.
18. King, Handbook of Hydraulics, 4th ed., 1954, Table 33. p. 3-43.
19. Lane, E. W. Experiments on the flow of water through contractions in an open channel. Trans. ASCE, Vol. 83, 1910-20. p. 1149-219.
20. Lencastre, Armando. Perdas de Carga Provocadas por Pilares. Laboraton'o Nacional de Engeharia Civil, Lisboa, 1954.
21. Mathes on roughness coefficients. Experimental Station Bul. No. 3, Vol. 1, NSWW Experiment Station, December, 1938.
22. McNown, John S. and Yih, C. S. Free streamline analyses of transition flow and jet deflection. State University of Iowa, Studies in Engineering, Bul. 35, 1953.

23. Nagler, F. A. Obstruction of bridge piers to the flow of water. Trans. ASCE, Vol. 82, 1918. p. 334-95.
24. Rehbock, Th. Verfahren zur bestimmung des bruckenstraues bei rein stromendem wasserdurchfluss. Tech. Univ. of Karlsruhe, November 26, 1921. A method for determining the backwater due to bridge piers in streaming flow. Translated by E. F. Wisely, Bureau of Reclamation.
25. Rehbock, Th., Bruckenstau and Walzenbildung. Untersuchungen aus dem FluBbau-Laboratorium der Technischen Hochschule zu Karlsruhe, July 15, 1921.
26. Rouse, Hunter. Elementary Mechanics of fluids. John Wiley and Sons, New York, 1946.
27. Rouse, Hunter. Fluid mechanics for hydraulic engineers. McGraw-Hill Book Co., Inc., 1938.
28. Schlichting, H. Boundary layer theory. McGraw-Hill, 1955.
29. Schnackenberg, E. C. Slope discharge formulae for alluvial streams and rivers. New Zealand Institute of Engineers, Proc., Vol. 37, 1951. p. 353, 411, 418, 419, 426, 427.
30. Streeter, V. L. Fluid dynamics. McGraw-Hill Book Co., Inc. 1948.
31. Thomas, A. R. Flow in expansions in open channels. Proc. Punjab Engr. Congress. Lahore, Paper No. 236, 1940. p. 179.
32. Tracy, H. J. and Carter, R. W. Backwater effects of open channel constrictions. Trans. ASCE, Vol. 120, 1955. p. 993-1006.
33. Van Driest, E. R. On dimensional analysis and the presentation of data in fluid flow problems. Journal of Applied Mechanics, Vol. 13, No. 1 P-A-34, March, 1946.
34. Von Mises, R. Berechnung von Ausfluss und Uberfallzahlen, Zeitschrift des Vereines Deutscher Ingenieure, 1917.

35. Woodward, S. M. and Posey, C. J. Hydraulics of steady flow in open channels. John Wiley and Sons, Inc., New York.
36. Yarnell, D. L. Bridge piers as channel obstructions. U. S. Dept. of Agriculture, Tech. Bul. No. 442, November, 1934. 25 p.
37. Yarnell, D. L. Pile trestles as channel obstructions. U. S. Dept. of Agriculture, Tech. Bul. No. 429.
38. Yarnell, D. L. and Nagler, F. A. Flow of flood waters over railroad and highway embankments. Public Roads, Vol. 11, No. 2, April 1930.

APPENDIX A

APPENDIX A

FREE STREAMLINE PROBLEM

The solution for flow out of a two-dimensional orifice plate which is at the end of a straight channel and is perpendicular to the channel boundary is one of the many free streamline problems.

It seems necessary to make a short introduction about the free streamline problems before such application to the particular problem is discussed. A more detailed discussion on free streamline by Birkhoff is recommended for further reference.

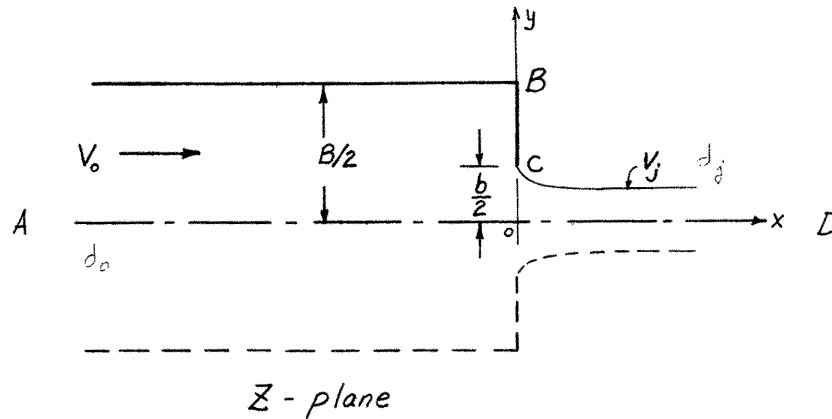
When a fluid is forced to turn a sudden corner, with radius of curvature zero, the acceleration of the fluid particle becomes infinite. This calls for an infinite force on the particle, which is obtained in ideal fluid flow by having the velocity to infinity. Since such a situation has no physical counterpart, the assumption may be made that the fluid particle separates from the boundary rather than making the sharp turn. This assumption leads to the so-called free streamline problems. The separation is assumed to occur at those points on the body where the body form makes a sudden turn, with the exception of stagnation points.

The fluid in contact with the body downstream from the separation points and separated from the main body of fluid in motion by the free streamline is known as the wake. The fluid in the wake is assumed to be at rest in steady flow problems. If the effects of gravity are neglected, the pressure intensity in the wake is, therefore, constant. According to the Bernoulli equation the velocity of the free streamline is constant. The velocity in the wake has been mentioned to be zero, therefore there exists a surface of discontinuity. In a non-viscous fluid, such a surface of discontinuity would give rise to no [viscous] shear forces, but is in unstable equilibrium. For real fluid flow it soon becomes wavy, and then breaks up into a turbulent "mixing zone". This turbulence is drawn into the wake and recirculated.

A streamline in contact with a boundary upstream from the separation point is referred to as a bounding streamline. When the bounding streamlines are straight, the shape of the free streamline in two-dimensional motion can be found by the methods of conformal mapping. The transformations are of a special character which takes advantage of the fact that the direction of the bounding streamlines is constant and the speed of the free streamlines is constant. It is convenient to start with the Z -plane showing the flow boundaries and the general form of the free streamlines. Then by suitable transformations the bounding streamlines and the free streamlines are mapped into straight-sided polygons from which the W -plane is obtained by use of the Schwarz-Christoffel theorem one or more times. Such applications of conformal transformation on free streamline problems are presented in standard references such as Streeter's *Fluid Dynamics*, Chapter VIII and in "Free Streamline Analyses" Bulletin 35 SUI Studies in Engineering.

The free streamline problem of an outflow from a two-dimensional orifice plate which is at the end of a straight channel and perpendicular to the channel boundary [Z -plane] has been presented by von Mises [34]. The following discussion of this problem has been done under the supervision of J. S. McNown.

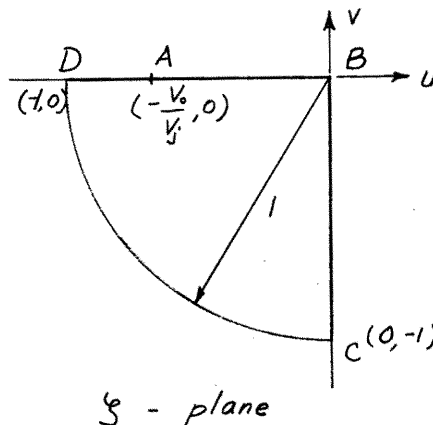
Because the flow is symmetrical with respect to the center line of the flow, only the upper half of the flow is considered in the transformation



By use of the transformation

$$\xi = \frac{1}{V_j} (-u + iv)$$

the ξ -plane can be obtained as shown. Straight solid boundaries in the Z -plane transform into radial lines in the ξ -plane. Free streamlines, along which the pressure and velocity are constant in the Z -plane, become circular arcs with centers at the origin in the ξ -plane. It is evident that the original boundary transforms into a circular sector.



Instead of transforming ξ -plane into a semi-infinite strip, and then transforming this semi-infinite strip into a half plane through Schwarz-Christoffel transformation, the transformation can be accomplished directly through the transformation:

$$t = \frac{1}{2} \left(\xi^2 + \frac{1}{\xi^2} \right)$$

The circular sector is mapped as the lower half of the t -plane; the boundary of the circular sector is mapped into the real axis. The infinite rectangle representing the potential and stream functions in the W -plane can be mapped into the lower half of the t -plane by means of the Schwarz-Christoffel theorem. However it is noted that in the t -plane, the flow pattern is simply that for a source with

a strength $V_0 \frac{B}{2}$ at A and a sink of equal strength at D for the flow occurring in the lower half of the plane. This latter requirement is satisfied if the strengths of the source and sink are doubled to provide an image pattern in the upper half (which actually represents the omitted half of the Z-plane). Application of the equations for a source and a sink on the real axis then results in the potential function (W-plane)

$$W = \frac{BV_0}{2\pi} [\ln(t - a) - \ln(t - 1)]$$

$$= \frac{BV_0}{2\pi} \ln(t - 1) - \ln(t - a)]$$

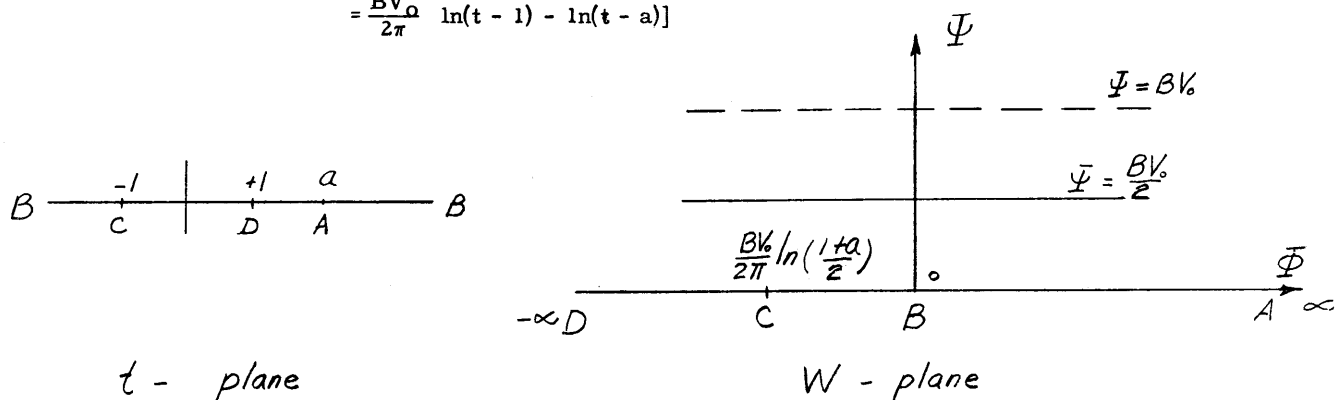


TABLE A

	Z	ζ	t	W
A	$-\alpha + i\left(\alpha \cot \frac{B}{2}\right)$	$-\frac{V_0}{V_j}$	$\frac{1}{2} \left(\frac{V_0^2 + V_j^2}{V_j^2} + \frac{V_j^2}{V_0^2} \right) = a$	∞
B	$i \frac{B}{2}$	0	∞	0
C	$i \frac{b}{2}$	-i1	$\frac{1}{2} \left(-V_j^2 + \frac{1}{-V_j^2} \right) = -1$	$-\frac{BV_0}{2\pi} \ln \frac{1+a}{2}$
D	$+\alpha + i\left(\alpha \cot \frac{C_0 b}{2}\right)$	-1	$\frac{1}{2} \left(V_j^2 + \frac{1}{V_j^2} \right) = 1$	$-\infty$

The coordinates of the various points are indicated in Table A.

By definition

$$d\phi = \frac{\partial \phi}{\partial x} dx + \frac{\partial \phi}{\partial y} dy$$

$$u = -\frac{\partial \phi}{\partial y}$$

$$v = -\frac{\partial \phi}{\partial x}$$

(A) Along BC, $x = \text{constant} = 0$, $dx = 0$, $V_x = 0$

$$d\phi = \frac{\partial \phi}{\partial y} dy = -v dy$$

or

$$dy = -\frac{d\phi}{u} = -\frac{d\phi/V_j}{v/V_j}$$

hence

$$y = \frac{B}{2} + \oint_{By} dy = \frac{B}{2} - \int \frac{d\phi/V_j}{v/V_j}$$

$$= \frac{B}{2} - \int \frac{d\phi}{v} \quad \text{where } V_j = 1$$

Since

$$W = \phi + i\Psi$$

$$= \frac{BV_0}{2\pi} [\ln(t-1) - \ln(t-a)]$$

Along BC, $\Psi = \text{constant}$, $d\Psi = 0$, $dW = d\phi$

$$d\phi = \frac{BV_0}{2\pi} \left[\frac{1}{t-1} - \frac{1}{t-a} \right] dt$$

Where

$$t = \frac{1}{2} \left(\zeta^2 + \frac{1}{\zeta^2} \right)$$

$$\zeta = \frac{1}{V_j} (-u + iv)$$

Along BC

$$\zeta = i \frac{v}{V_j} = iv \quad \text{where } V_j = 1$$

$$t = -\frac{1}{2} \left(v^2 + \frac{1}{v^2} \right)$$

$$dt = \left(\frac{1}{v^2} - v^2 \right) \frac{dv}{v}$$

Substituting t and dt into Eq

$$d\phi = \frac{BV_0}{2\pi} \left[-\frac{2v^2}{(v^2+1)^2} + \frac{2v^2}{v^4+2av^2+1} \right] \frac{(1-v^4)dv}{v^3}$$

Notice that from Table A,

$$a = \frac{1}{2} \left(V_0^2 + \frac{1}{V_0^2} \right)$$

It follows that

$$\frac{B}{2} - y = \frac{BV_0}{\pi} \int_0^v \left[-\frac{1-v^2}{v^2(1+v^2)} + \frac{1-v^4}{v^2(v^2+V_0^2)(v^2+\frac{1}{V_0^2})} \right] dv$$

$$= \frac{BV_0}{\pi} \left[-\int_0^v \frac{dv}{v^2} + 2 \int_0^v \frac{dv}{1+v^2} + \int_0^v \frac{dv}{v^2+V_0^2} - \int_0^v \frac{dv}{v^2+\frac{1}{V_0^2}} \right]$$

$$1 - \frac{y}{B/2} = \frac{2V_0}{\pi} \left[-2 \tan^{-1} v + \frac{1}{V_0} \tan^{-1} \frac{v}{V_0} + V_0 \tan^{-1} V_0 v \right]$$

At $y = \frac{b}{2}$, $v = 1$

$$1 - \frac{b}{B} = \frac{2V_0}{\pi} \left[-\frac{\pi}{2} + \frac{1}{V_0} \tan^{-1} \frac{1}{V_0} + V_0 \tan^{-1} V_0 \right]$$

With substitutions:

$$\tan^{-1} V_0 = \frac{\pi}{2} - \tan^{-1} \frac{1}{V_0}$$

$$C_c = \frac{bV_0}{B}$$

$$\tan^{-1} V_0 = \frac{1}{2} \text{Cot}^{-1} \left[\frac{1 - V_0^2}{2V_0} \right]$$

$$\frac{1}{C_c} = 1 + \frac{1}{\pi} \left[\frac{1}{V_0} - V_0 \right] \text{Cot}^{-1} \left[\frac{1}{2} \left(\frac{1}{V_0} - V_0 \right) \right]$$

which is the classic result.

(B) Along BA or AX, $y = \text{constant}$, $dy = 0$, $v = 0$,

so that $d\phi = \frac{\partial \phi}{\partial x} dx = -u dx$

$$dx = -\frac{d\phi}{u} = -\frac{d\phi/V_j}{u/V_j}$$

Along BA

$$x = -\frac{d\phi}{u} \quad \text{where } V_j = 1$$

$$d\phi = \frac{BV_0}{2\pi} \left[\frac{1}{t-1} - \frac{1}{t-a} \right] dt$$

Where

$$t = \frac{1}{2} \left(\zeta^2 + \frac{1}{\zeta^2} \right)$$

$$\zeta = -u$$

$$t = \frac{1}{2} \left(u^2 + \frac{1}{u^2} \right)$$

$$dt = \left(u^2 - \frac{1}{u^2} \right) \frac{du}{u}$$

$$d\phi = \frac{BV_0}{2\pi} \left[\frac{2u^2}{(u^2-1)^2} - \frac{2u^2}{u^4 - 2au^2 + 1} \right] dt$$

Substituting $a = \frac{1}{2} \left(V_0^2 + \frac{1}{V_0^2} \right)$

$$\begin{aligned}
d\phi &= \frac{BV_0}{\pi} \left[\frac{u^2+1}{u(u^2-1)} - \frac{(u^4-1)}{u(u^2-V_0^2)(u^2-\frac{1}{V_0^2})} \right] du \\
x &= \int_0^u \frac{d\phi}{u} \\
&= \frac{-BV_0}{\pi} \int_0^u \left(\frac{2}{u^2-1} - \frac{1}{u^2} + \frac{1}{u^2} - \frac{1}{u^2-V_0^2} - \frac{1}{u^2-\frac{1}{V_0^2}} \right) du \\
&= \frac{BV_0}{\pi} \left[\ln \frac{1+u}{1-u} - \frac{1}{2V_0} \ln \frac{V_0+u}{V_0-u} - \frac{V_0}{2} \ln \frac{1+uV_0}{1-uV_0} \right]_0^u
\end{aligned}$$

when $u = 0$, $x = 0$

Therefore
$$x = \frac{BV_0}{\pi} \left[\ln \frac{1+u}{1-u} - \frac{1}{2V_0} \ln \frac{V_0+u}{V_0-u} - \frac{V_0}{2} \ln \frac{1+uV_0}{1-uV_0} \right]_0^u$$

Note

$$V_0 = \frac{V_0}{V_j}, \quad u = \frac{u}{V_j} = \frac{u}{V_0} - \frac{V_0}{V_j} = \frac{v}{V_0} R$$

Where

$$R = \frac{V_0}{V_j} = \frac{C_c b}{B}$$

Therefore along BA

$$\frac{X}{B} = \frac{R}{\pi} \left[\ln \frac{1 + \frac{u}{V_0} R}{1 - \frac{u}{V_0} R} - \frac{1}{2R} \ln \frac{1 + \frac{u}{V_0}}{1 - \frac{u}{V_0}} + \frac{R}{2} \ln \frac{1 + \frac{u}{V_0} R^2}{1 - \frac{u}{V_0} R^2} \right]$$

pressure distribution along BA can be computed by use of the Bernoulli theorem

$$p_0 + \rho \frac{V_0^2}{2} = p + \rho \frac{u^2}{2}$$

$$\frac{p - p_0}{\frac{1}{2} \rho V_0^2} = 1 - \left(\frac{u}{V_0} \right)^2$$

Pressure and velocity distribution along BA have been computed as shown in the following table:

$\frac{u}{V_0}$	$\frac{b}{B} = 0.75, C_c = 0.717$ $R = 0.537$			$\frac{b}{B} = 0.50, C_c = 0.644$ $R = 0.322$			$\frac{b}{B} = 0.25, C_c = 0.619$ $R = 0.155$		
	$\frac{x}{B}$	$\frac{x}{b}$	$\frac{p-p_0}{\frac{1}{2}\rho V_0^2}$	$\frac{x}{B}$	$\frac{x}{b}$	$\frac{p-p_0}{\frac{1}{2}\rho V_0^2}$	$\frac{x}{B}$	$\frac{x}{b}$	$\frac{p-p_0}{\frac{1}{2}\rho V_0^2}$
0.995	0.775	1.031	0.011	0.890	1.780	0.011	0.939	3.756	0.011
0.99	0.666	0.890	0.021	0.779	1.558	0.021	0.823	3.292	0.021
0.98	0.557	0.744	0.041	0.668	1.336	0.041	0.716	2.864	0.041
0.96	0.449	0.599	0.080	0.556	1.112	0.080	0.603	2.412	0.080
0.94	0.388	0.517	0.119	0.491	0.982	0.119	0.536	2.144	0.119
0.92	0.345	0.460	0.154	0.450	0.900	0.154	0.480	1.920	0.154
0.90	0.315	0.420	0.190	0.408	0.816	0.190	0.452	1.808	0.190
0.87	0.274	0.366	0.244	0.368	0.736	0.244	0.410	1.640	0.244
0.84	0.244	0.326	0.295	0.335	0.670	0.295	0.375	1.500	0.295
0.80	0.213	0.284	0.360	0.297	0.594	0.360	0.337	1.348	0.360
0.75	0.182	0.243	0.438	0.259	0.518	0.438	0.298	1.192	0.438
0.60	0.122	0.163	0.640	0.183	0.366	0.640	0.211	0.844	0.640
0.30	0.051	0.068	0.910	0.080	0.160	0.910	0.094	0.376	0.910
0.10	0.016	0.021	0.990	0.025	0.050	0.990	0.030	0.120	0.990

Along the center line AX

$$x = -\frac{BV_0}{\pi} \left[\int_0^{V_0} \frac{du}{u(u^2-1)} + \int_{V_0}^u \left[\frac{u^2+1}{u(u^2-1)} - \frac{u^4-1}{u(u^2-V_0^2)(u^2-\frac{1}{V_0^2})} \right] du \right]$$

In general

$$x = -\frac{BV_0}{\pi} \int \left[\frac{u^2+1}{u(u^2-1)} - \frac{u^4-1}{u(u^2-V_0^2)(u^2-\frac{1}{V_0^2})} \right] du$$

Along BA

$$x = \frac{BV_0}{\pi} \left[\int \frac{2du}{1-u^2} - \int \frac{du}{V_0^2-u^2} - \int \frac{du}{\frac{1}{V_0^2}-u^2} \right], \quad 0 \leq u \leq V_0$$

Along AX

$$x = \frac{BV_0}{\pi} \left[\int \frac{2du}{1-u^2} + \int \frac{du}{u^2-V_0^2} - \int \frac{du}{\frac{1}{V_0^2}-u^2} \right], \quad V_j \geq u \geq V_0$$

$$= \frac{BV_0}{\pi} \left[\ln \frac{1+u}{1-u} + \frac{1}{2V_0} \ln \frac{u-V_0}{u+V_0} - \frac{V_0}{2} \ln \frac{1+uV_0}{1-uV_0} \right] + \text{constant}$$

Along BA, when $u = 0, x = 0$.

$$u = V_0, \quad x = -\infty \quad \text{upper limit}$$

Along AX , when $u = V_0$, $x = -\infty$ lower limit

Therefore

$$x = -\infty + 0 + \infty + \frac{BV_0}{\pi} \left[\ln \frac{1+u}{1-u} + \frac{1}{2V_0} \ln \frac{u-V_0}{u+V_0} - \frac{V_0}{2} \ln \frac{1+uV_0}{1-uV_0} \right]$$

or

$$\frac{x}{b} = \frac{C_c}{\pi} \left[\ln \frac{1 + \frac{u}{V_0} R}{1 - \frac{u}{V_0} R} + \frac{1}{2R} \ln \frac{\frac{u}{V_0} - 1}{\frac{u}{V_0} + 1} - \frac{R}{2} \ln \frac{1 + \frac{u}{V_0} R^2}{1 - \frac{u}{V_0} R^2} \right]$$

where

$$\frac{u}{V_0} > 1$$

The pressure distribution along the center line can be calculated by means of the Bernoulli theorem

$$p_0 + \frac{1}{2} \rho V_0^2 = p + \frac{1}{2} \rho u^2$$

$$p_0 - p = \frac{\rho}{2} (u^2 - V_0^2)$$

$$\frac{p_0 - p}{\frac{\rho}{2} V_0^2} = \left(\frac{u}{V_0} \right)^2 - 1$$

or

$$p_j + \frac{\rho V_j^2}{2} = p + \frac{\rho}{2} u^2$$

$$\frac{p - p_j}{\frac{1}{2} \rho V_j^2} = \frac{\rho}{2} (V_j^2 - u^2)$$

$$\frac{p - p_j}{\frac{1}{2} \rho V_j^2} = 1 - \left(\frac{u}{V_j} \right)^2$$

Pressure and velocity distribution along AX have been computed as shown in the following table.

$\frac{u}{V_0}$	$\frac{b}{B} = 0.75, C_c = 0.717$ R = 0.537				$\frac{b}{B} = 0.50, C_c = 0.644$ R = 0.322				$\frac{b}{B} = 0.25, C_c = 0.619$ R = 0.155			
	$\frac{u}{V_j}$	$\frac{x}{b}$	$\frac{p_0 - p}{\frac{1}{2}\rho V_0^2}$	$\frac{p - p_j}{\frac{1}{2}\rho V_j^2}$	$\frac{u}{V_j}$	$\frac{x}{b}$	$\frac{p_0 - p}{\frac{1}{2}\rho V_0^2}$	$\frac{p - p_j}{\frac{1}{2}\rho V_j^2}$	$\frac{u}{V_j}$	$\frac{x}{b}$	$\frac{p_0 - p}{\frac{1}{2}\rho V_0^2}$	$\frac{p - p_j}{\frac{1}{2}\rho V_j^2}$
1.005	0.539	-1.031	0.010	0.709	0.324	-1.775	0.010	0.895	0.156	-3.74	0.010	0.976
1.01	0.542	-0.890	0.020	0.706	0.326	-1.551	0.020	0.894	0.157	-3.28	0.020	0.975
1.05	0.564	-0.534	0.103	0.682	--	--	--	--	--	--	--	--
1.10	0.591	-0.376	0.210	0.650	0.364	-0.800	0.210	0.867	0.171	-1.85	0.210	0.971
1.20	0.645	-0.204	0.440	0.584	--	--	--	--	--	--	--	--
1.30	0.699	-0.086	0.690	0.511	--	--	--	--	--	--	--	--
1.40	0.752	+0.014	0.960	0.435	--	--	--	--	--	--	--	--
1.50	0.806	+0.111	1.250	0.350	0.484	-0.298	1.250	0.766	0.233	-0.93	1.250	0.946
1.60	0.860	+0.217	1.560	0.260	--	--	--	--	--	--	--	--
1.70	0.914	+0.356	1.890	0.165	--	--	--	--	--	--	--	--
1.80	0.968	+0.596	2.240	0.064	--	--	--	--	--	--	--	--
1.85	0.995	+0.995	2.423	0.010	--	--	--	--	--	--	--	--

$\frac{u}{V_0}$	$\frac{b}{B} = 0.75, C_c = 0.717$ R = 0.537				$\frac{b}{B} = 0.50, C_c = 0.644$ R = 0.322				$\frac{b}{B} = 0.25, C_c = 0.619$ R = 0.155			
	$\frac{u}{V_j}$	$\frac{x}{b}$	$\frac{p_0 - p}{\frac{1}{2}\rho V_0^2}$	$\frac{p - p_j}{\frac{1}{2}\rho V_j^2}$	$\frac{u}{V_j}$	$\frac{x}{b}$	$\frac{p_0 - p}{\frac{1}{2}\rho V_0^2}$	$\frac{p - p_j}{\frac{1}{2}\rho V_j^2}$	$\frac{u}{V_j}$	$\frac{x}{b}$	$\frac{p_0 - p}{\frac{1}{2}\rho V_0^2}$	$\frac{p - p_j}{\frac{1}{2}\rho V_j^2}$
2.0	--	--	--	--	0.644	-0.048	3.00	0.585	0.310	-0.575	3.00	0.900
2.5	--	--	--	--	0.805	+0.168	5.25	0.352	0.387	-0.382	5.25	0.850
3.0	--	--	--	--	0.966	+0.596	8.00	0.067	0.465	-0.36	8.00	0.784
3.5	--	--	--	--	--	--	--	--	0.542	-0.134	11.25	0.707
4.0	--	--	--	--	--	--	--	--	0.620	-0.04	15.00	0.615
4.2	--	--	--	--	--	--	--	--	0.650	-0.003	16.64	0.578
4.5	--	--	--	--	--	--	--	--	0.697	+0.051	19.25	0.514
5.0	--	--	--	--	--	--	--	--	0.776	+0.15	24.00	0.398
5.5	--	--	--	--	--	--	--	--	0.858	+0.27	29.25	0.265
6.0	--	--	--	--	--	--	--	--	0.935	+0.451	35.00	0.125

APPENDIX B

TABLE 1 : SIMPLE NORMAL CROSSING
45 degree wing-wall abutments

Run No	Model Type	Model height [ft]	Model length [ft]	Measured Data										Computed Data														
				b [ft]	B [ft]	Q [cfs]	h_n [ft]	Bottom Rdg.	Roughness	Slope	h_1 [ft]	R_{UR}	R_{UL}	R_{DR}	R_{DL}	L*	h_1^* [ft]	h_U [ft]	h_D [ft]	$\frac{h_1}{h_n}$	$(\frac{h_1}{h_n})^3$	F_n	F_n^2	M	$(\frac{1}{M^4}-1)F_n^3$	$\frac{B}{h_n}$		
219	WW	0.6	1.00	2.90	7.9	2.00	0.465	0.841	Baffle	.0012	0.513	1.363	1.357	1.286	1.287	3.3	0.048	0.519	0.446	1.100	1.341	0.140	.0196	0.367	0.126	16.99		
220	WW	0.6	1.00	1.88	7.9	2.00	0.465	0.841	Baffle	.0012	0.561	1.410	1.408	1.290	1.282	3.4	0.096	0.568	0.445	1.206	1.750	0.140	.0196	0.238	0.326	16.99		
279	WW	0.9	1.00	4.44	7.9	5.00	0.484	0.833		.0012	-	1.401	1.406	1.268	1.276	-	-	-	-	-	-	-	-	-	-	-	-	
280	WW	0.9	1.00	3.44	7.9	5.00	0.484	0.833		.0012	-	1.492	1.493	1.255	1.242	-	-	-	-	-	-	-	-	-	-	-	-	-
281	WW	0.9	1.00	2.45	7.9	5.00	0.484	0.833		.0012	-	1.643	1.649	1.227	1.248	-	-	-	-	-	-	-	-	-	-	-	-	-
455	WW	0.9	1.00	4.46	7.9	2.50	0.523	0.866	Baffle	.0012	0.539	1.410	1.410	1.378	1.377	3.8	0.016	0.544	0.512	1.030	1.095	0.147	.0216	0.565	0.046	15.10		
456	WW	0.9	1.00	3.42	7.9	2.50	0.523	0.866	Baffle	.0012	0.561	1.432	1.432	1.372	1.371	3.2	0.038	0.566	0.506	1.072	1.240	0.147	.0216	0.432	0.093	15.10		
457	WW	0.9	1.00	2.43	7.9	2.50	0.532	0.866	Baffle	.0012	0.609	1.479	1.479	1.371	1.370	3.1	0.086	0.613	0.505	1.164	1.579	0.147	.0216	0.307	0.208	15.10		
458	WW	0.9	1.00	1.46	7.9	2.50	0.523	0.866	Baffle	.0012	0.767	1.636	1.637	1.356	1.357	-	0.244	0.771	0.491	1.466	3.150	0.147	.0216	0.185	0.609	15.10		
782	WW	0.9	1.00	4.46	7.9	2.50	0.523	0.855	Baffle	.0012	0.541	1.403	1.399	1.364	1.363	-	0.018	0.546	0.509	1.036	1.110	0.147	.0216	0.560	0.047	15.10		
787	WW	0.9	1.00	2.36	7.9	2.50	0.523	0.855	Baffle	.0012	0.611	-	-	-	-	-	0.068	-	-	1.170	1.600	0.147	.0216	0.299	0.220	15.10		
586	WW	0.9	1.00	4.47	7.9	5.00	0.416	0.864	Bar	.002	0.522	1.409	1.411	1.206	1.200	4.0	0.106	0.536	0.339	1.254	1.976	0.416	.1731	0.565	0.367	19.00		
587	WW	0.9	1.00	3.42	7.9	5.00	0.416	0.864	Bar	.002	0.639	1.522	1.525	1.194	1.181	3.3	0.223	0.660	0.324	1.536	3.624	0.416	.1731	0.434	0.746	19.00		
588	WW	0.9	1.00	2.42	7.9	5.00	0.416	0.864	Bar	.002	0.799	1.678	1.683	1.187	1.200	3.3	0.383	0.817	0.330	1.920	7.085	0.416	.1731	0.306	1.676	19.00		
1161	RR	0.6	1.00	2.92	7.9	3.00	0.360	0.855	Bar	.0012	0.501	1.369	1.369	1.177	1.174	4.8	0.141	0.514	0.321	1.392	2.710	0.309	.0955	0.370	0.601	22.00		
1189	WW	0.6	1.00	3.89	7.9	3.00	0.360	0.855	Bar	.0012	0.425	1.299	1.293	1.187	1.182	5.1	0.065	0.441	0.330	1.180	1.650	0.309	.0955	0.492	0.300	22.00		
1216	WW	0.6	1.00	4.92	7.9	3.00	0.360	0.855	Bar	.0012	0.391	1.266	1.262	1.192	1.193	6.1	0.031	0.409	0.338	1.086	1.280	0.309	.0955	0.624	0.151	22.00		
1242	WW	0.6	1.00	5.90	7.9	3.00	0.360	0.855	Bar	.0012	0.371	1.246	1.243	1.198	1.197	5.5	0.011	0.390	0.343	1.031	1.100	0.309	.0955	0.746	0.755	22.00		
1344	WW	0.6	1.00	4.87	7.9	3.00	0.369	0.856	Bar	.0012	0.400	1.272	1.274	1.202	1.200	-	0.031	0.417	0.345	1.084	1.274	0.298	.089	0.616	0.145	21.40		
1348	WW	0.6	1.00	5.90	7.9	3.00	0.369	0.856	Bar	.0012	0.381	1.255	1.254	1.205	1.204	-	0.012	0.399	0.349	1.032	1.101	0.298	.089	0.746	0.071	21.40		
1354	WW	0.6	1.00	3.85	7.9	3.00	0.369	0.856	Bar	.0012	0.436	1.306	1.306	1.192	1.186	-	0.067	0.450	0.333	1.181	1.650	0.298	.089	0.487	0.284	21.40		
1355	WW	0.6	1.00	2.85	7.9	3.00	0.369	0.856	Bar	.0012	0.516	1.382	1.383	1.178	1.173	-	0.147	0.527	0.320	1.400	2.710	0.298	.089	0.361	0.594	21.40		
409	WW	0.6	1.00	5.90	7.9	2.50	0.333	0.866	Bar	.0012	0.347	1.225	1.222	1.188	1.186	3.1	0.014	0.358	0.321	1.041	1.138	0.289	.0835	0.746	0.067	23.70		
410	WW	0.6	1.00	4.85	7.9	2.50	0.333	0.866	Bar	.0012	0.357	1.235	1.232	1.181	1.179	4.3	0.024	0.368	0.314	1.072	1.240	0.289	.0835	0.614	0.139	23.70		
411	WW	0.6	1.00	3.87	7.9	2.50	0.333	0.866	Bar	.0012	0.393	1.268	1.264	1.171	1.169	3.6	0.060	0.400	0.304	1.180	1.644	0.289	.0835	0.490	0.264	23.70		
412	WW	0.6	1.00	2.90	7.9	2.50	0.333	0.866	Bar	.0012	0.462	1.334	1.332	1.159	1.161	3.2	0.129	0.467	0.294	1.387	2.670	0.289	.0835	0.367	0.536	23.70		
443	WW	0.6	1.00	1.85	7.9	2.50	0.333	0.866	Bar	.0012	0.622	1.491	1.490	1.142	1.143	2.7	0.289	0.625	0.277	1.870	6.520	0.289	.0835	0.234	1.444	23.70		
668	WW	0.9	1.00	4.46	7.9	2.50	0.333	0.857	Bar	.0012	0.374	1.241	1.241	1.166	1.166	-	0.041	0.384	0.309	1.123	1.417	0.289	.0835	0.564	0.178	23.70		
669	WW	0.9	1.00	3.44	7.9	2.50	0.333	0.857	Bar	.0012	0.414	1.281	1.279	1.156	1.155	-	0.081	0.423	0.299	1.241	1.910	0.289	.0835	0.435	0.357	23.70		
670	WW	0.9	1.00	2.44	7.9	2.50	0.333	0.857	Bar	.0012	0.514	1.379	1.379	1.145	1.141	-	0.181	0.522	0.286	1.540	3.650	0.289	.0835	0.309	0.790	23.70		
673	WW	0.6	1.00	4.85	7.9	2.50	0.333	0.857	Bar	.0012	0.359	-	-	-	-	-	0.016	0.366	-	1.078	1.253	0.289	.0835	0.613	0.138	23.70		
796	WW	0.9	1.00	4.46	7.9	2.50	0.333	0.854	Bar	.0012	0.372	1.240	1.237	1.159	1.159	-	0.039	0.385	0.305	1.117	1.395	0.289	.0835	0.556	0.182	23.70		
823	WW	0.9	1.00	2.42	7.9	2.50	0.333	0.855	Bar	.0012	0.509	1.370	1.368	1.142	1.142	-	0.176	0.514	0.287	1.528	3.560	0.289	.0835	0.306	0.801	23.70		
955	WW	0.9	1.00	4.46	7.9	2.50	0.333	0.855	Bar	.0012	0.374	1.245	1.242	1.164	1.164	-	0.041	0.389	0.309	1.121	1.410	0.289	.0835	0.564	0.178	23.70		
949	WW	0.9	1.00	4.46	7.9	2.50	0.333	0.855	Bar	.0012	0.372	1.241	1.240	1.162	1.164	-	0.039	0.386	0.308	1.117	1.399	0.289	.0835	0.564	0.178	23.70		
974	WW	0.9	1.00	4.42	7.9	2.50	0.333	0.855	Bar	.0012	0.373	1.242	1.241	1.167	1.170	-	0.040	-	-	-	-	-	-	-	-	-	-	
975	WW	0.9	1.00	4.42	7.9	2.50	0.484	0.855	Bar	.0012	0.552	1.432	1.430	1.290	1.286	-	0.068	-	-	-	-	-	-	-	-	-	-	
213	WW	0.9	1.00	4.46	7.9	4.95	0.718	0.833	Baffle	.0012	0.751	1.599	1.592	1.532	1.528	4.8	0.033	0.763	0.697	1.045	1.144	0.181	.0327	0.564	0.070	11.00		
214	WW	0.9	1.00	3.40	7.9	4.94	0.718	0.833	Baffle	.0012	0.792	1.635	1.633	1.519	1.520	4.3	0.074	0.801	0.687	1.101	1.345	0.181	.0327	0.430	0.144	11.00		
215	WW	0.9	1.00	2.42	7.9	4.91	0.718	0.833	Baffle	.0012	0.878	1.722	1.720	1.506	1.501	5.3	0.160	0.888	0.671	1.210	1.760	0.180	.0324	0.306	0.314	11.00		
467	WW	0.9	1.00	4.50	7.9	5.00	0.718	0.866	Baffle	.0012	0.745	1.622	1.622	1.557	1.557	3.2	0.027	0.756	0.691	1.037	1.117	0.184	.0339	0.569	0.071	11.00		
468	WW	0.9	1.00	3.44	7.9	5.00	0.718	0.866	Baffle	.0012	0.786	1.663	1.663	1.554	1.556	3.8	0.068	0.797	0.689	1.094	1.307	0.184	.0339	0.435	0.145	11.00		
469	WW	0.9	1.00	2.44	7.9	5.00	0.718	0.866	Baffle	.0012	0.888	1.763	1.763	1.540	1.540	3.6	0.170	0.897	0.674	1.236	1.892	0.184	.0339	0.309	0.321	11.00		
134	WW	0.9	3.00	3.38	7.9	5.00	0.484	0.835	Bar	.0012	0.693	1.554	1.551	1.289	1.287	-	0.209	0.718	0.453	1.432	2.95	0.332	.110	0.428	0.491	16.35		
135	WW	0.9	3.00	4.45	7.9	5.00	0.484	0.835	Bar	.0012	0.590	1.436	1.435	1.317	1.304	-	0.106	0.601	0.476	1.220	1.81	0.332	.110	0.564	0.236	16.35		
136	WW	0.9	1.00	4.46	7.9	5.00	0.484	0.835	Bar	.0012	0.586	1.441	1.429	1.310	1.298	-	0.102	0.600	0.469	1.211	1.78	0.332	.110	0.565	0.233	16.35		
137	WW	0.9	1.00	3.43	7.9	5.00	0.484	0.835	Bar	.0012	0.681	1.534	1.519	1.305	1.276	-	0.197	0.692	0.456	1.409	2.79	0.332	.110	0.434	0.475	16.35		
201	WW	0.9	1.00	3.42	7.9	4.87	0.484	0.834	Bar	.0012	0.631	1.481	1.479	1.245	1.257	4.6	0.147	0.646	0.417	1.303	2.216	0.324	.105	0.433	0.456	16.35		
202	WW	0.9	1.00	4.46	7.9	4.90	0.484																					

TABLE 1 SIMPLE NORMAL CROSSING [continued]
45 degree wing-wall abutments

Run No	Model Type	Model height [ft]	Model length [ft]	Measured Data										Computed Data											
				b [ft]	B [ft]	Q [cfs]	h_n [ft]	Bottom Rdg.	Roughness	Slope	h_1 [ft]	R_{UR}	R_{UL}	R_{DR}	R_{DL}	L^*	h_1^* [ft]	h_U [ft]	h_D [ft]	$\frac{h_1}{h_n}$	$\left(\frac{h_1}{h_n}\right)^3$	F_n	F_n^2	M	$\left[\frac{1}{M^2}-1\right]F_n^2$
2	WW	0.6	1.00	2.0	4	1.72	.384	.802	Bar	.0012	0.446	1.276	-	1.142	-	0.062	.474	.340	1.161	1.57	0.318	0.101	0.50	0.303	10.40
3	WW	0.6	1.00	1.0	4	1.71	.384	.802	Bar	.0012	0.653	-	-	-	-	0.269	-	-	-	-	-	-	-	-	10.40
6	WW	0.6	1.00	1.0	4	0.69	.215	.802	Bar	.0012	0.339	1.143	-	1.003	-	0.124	-	-	-	-	-	-	-	-	18.60
7	WW	0.6	1.00	2.0	4	0.66	.224	.849	Bar	.0012	0.250	1.102	-	1.053	-	0.026	.253	.204	1.114	1.39	0.274	0.075	0.50	0.225	17.85
10	WW	0.6	1.00	2.0	4	2.05	.457	.849	Bar	.0012	0.516	1.393	-	1.243	-	0.059	.544	.394	1.130	1.44	0.292	0.085	0.50	0.255	8.75
13	WW	0.6	1.00	1.5	4	1.98	.446	.849	Bar	.0012	0.592	1.440	-	1.230	-	0.146	.591	.381	1.327	2.34	0.294	0.086	0.375	0.525	8.96
14	WW	0.6	1.00	1.5	4	0.51	.170	.849	Bar	.0012	0.202	1.058	-	1.002	-	0.032	-	-	-	-	-	-	-	-	-
19	WW	0.6	1.00	2.0	4	1.06	.232	.849	Bar	.0036	0.327	1.189	-	1.048	-	0.095	.340	.199	1.409	2.80	0.417	0.174	0.50	0.522	17.22
20	WW	0.6	1.00	1.5	4	1.06	.232	.849	Bar	.0036	0.387	1.270	-	1.035	-	0.155	.421	.186	1.668	4.58	0.417	0.174	0.375	0.061	17.22
21	WW	0.6	1.00	2.0	4	2.25	.382	.849	Bar	.0024	0.532	1.392	-	1.144	-	0.150	.543	.295	1.393	2.71	0.419	0.176	0.50	0.528	10.48
28	WW	0.6	1.00	2.0	4	0.68	.202	.852	Bar	.0024	0.242	1.110	-	1.025	-	0.040	-	-	-	-	-	-	-	-	-
29	WW	0.6	1.00	1.5	4	0.66	.202	.841	Bar	.0024	0.296	1.146	-	1.020	-	0.094	-	-	-	-	-	-	-	-	-
30	WW	0.6	1.00	2.0	4	1.57	.318	.847	Bar	.0024	0.418	1.290	-	1.099	-	0.100	.443	.252	1.314	2.27	0.385	0.148	0.50	0.444	12.59
36	WW	0.6	1.00	2.0	4	0.51	.250	.859	Bar	.0008	0.266	1.120	-	1.088	-	0.016	-	-	-	-	-	-	-	-	-
37	WW	0.6	1.00	1.5	4	0.47	.256	.851	Bar	.0008	0.292	1.148	-	1.086	-	0.036	-	-	-	-	-	-	-	-	-
38	WW	0.6	1.00	1.0	4	0.48	.254	.854	Bar	.0008	0.346	1.191	-	1.078	-	0.092	-	-	-	-	-	-	-	-	-
39	WW	0.6	1.00	1.0	4	0.86	.351	.851	Bar	.0008	0.481	1.339	-	1.150	-	0.130	.488	.299	1.371	2.58	0.182	0.0331	0.25	0.497	11.40
40	WW	0.6	1.00	1.5	4	0.86	.345	.846	Bar	.0008	0.393	1.253	-	1.172	-	0.048	.407	.326	1.139	1.47	0.187	0.035	0.375	0.214	11.60
41	WW	0.6	1.00	2.0	4	0.87	.346	.847	Bar	.0008	0.370	1.212	-	1.167	-	0.024	.365	.320	1.069	1.22	0.188	0.0355	0.50	0.142	11.55
48	WW	0.6	1.00	2.0	4	1.54	.476	.854	Bar	.0008	0.504	1.378	-	1.295	-	0.028	.524	.441	1.059	1.19	0.206	0.0425	0.50	0.128	8.40
49	WW	0.6	1.00	1.5	4	1.53	.477	.853	Bar	.0008	0.551	1.410	-	1.280	-	0.074	.557	.427	1.155	1.54	0.207	0.0429	0.375	0.262	8.39
50	WW	0.6	1.00	2.0	4	0.40	.211	.858	Bar	.0004	0.218	1.078	-	1.070	-	0.007	-	-	-	-	-	-	-	-	-
51	WW	0.6	1.00	1.5	4	0.30	.213	.861	Bar	.0004	0.221	1.088	-	1.069	-	0.008	-	-	-	-	-	-	-	-	-
52	WW	0.6	1.00	1.0	4	0.30	.211	.857	Bar	.0004	0.241	1.108	-	1.065	-	0.030	-	-	-	-	-	-	-	-	-
59	WW	0.6	1.00	2.0	4	0.63	.332	.864	Bar	.0004	0.348	1.217	-	1.188	-	0.016	-	-	-	-	-	-	-	-	-
60	WW	0.6	1.00	1.5	4	0.61	.332	.859	Bar	.0004	0.367	1.237	-	1.183	-	0.035	-	-	-	-	-	-	-	-	-
61	WW	0.6	1.00	1.5	4	0.61	.344	.857	Bar	.0004	0.414	1.270	-	1.181	-	0.070	-	-	-	-	-	-	-	-	-
65	WW	0.6	1.00	2.0	4	2.40	.574	.863	Bar	.0004	0.629	-	-	1.404	-	0.055	-	-	-	-	-	-	-	-	-
66	WW	0.6	1.00	1.5	4	2.35	.558	.889	Bar	.0004	0.652	-	-	1.347	-	0.094	-	-	-	-	-	-	-	-	-
71	WW	0.6	1.00	2.9	7.9	2.36	.312	.841	Bar	.0012	0.452	1.303	1.296	1.128	1.118	0.140	-	-	-	-	-	-	-	-	-
72	WW	0.6	1.00	3.9	7.9	2.36	.312	.843	Bar	.0012	0.383	1.233	1.228	1.130	1.130	0.071	-	-	-	-	-	-	-	-	-
73	WW	0.6	1.00	4.9	7.9	2.36	.312	.843	Bar	.0012	0.355	1.211	1.210	1.143	1.137	0.043	-	-	-	-	-	-	-	-	-
74	WW	0.6	1.00	5.9	7.9	2.36	.312	.843	Bar	.0012	0.332	1.195	1.188	1.144	1.141	0.020	-	-	-	-	-	-	-	-	-
79	WW	0.6	3.00	2.9	7.9	2.36	.312	.841	Bar	.0012	0.463	1.318	1.306	1.123	1.128	0.151	-	-	-	-	-	-	-	-	-
80	WW	0.6	3.00	3.9	7.9	2.36	.312	.843	Bar	.0012	0.390	1.247	1.242	1.137	1.145	0.078	-	-	-	-	-	-	-	-	-
81	WW	0.6	3.00	4.9	7.9	2.36	.312	.842	Bar	.0012	0.354	1.205	1.217	1.137	1.136	0.042	-	-	-	-	-	-	-	-	-
82	WW	0.6	3.00	5.9	7.9	2.36	.312	.841	Bar	.0012	0.334	1.184	1.196	1.142	1.145	0.022	-	-	-	-	-	-	-	-	-
83	WW	0.6	2.00	4.9	7.9	2.36	.312	.841	Bar	.0012	0.353	1.205	1.210	1.134	1.137	0.041	-	-	-	-	-	-	-	-	-
84	WW	0.6	2.00	2.9	7.9	2.36	.312	.841	Bar	.0012	0.463	1.308	1.314	1.119	1.117	0.151	-	-	-	-	-	-	-	-	-
87	WW	0.6	3.00	5.9	7.9	5.30	.497	.842	Bar	.0012	0.516	1.384	1.392	1.318	1.317	0.019	.546	.476	1.038	1.118	0.338	.114	.746	.091	15.90
88	WW	0.6	3.00	4.9	7.9	5.30	.497	.844	Bar	.0012	0.544	1.427	1.411	1.304	1.307	0.047	.575	.462	1.091	1.300	0.338	.114	.620	.182	15.90
89	WW	0.6	1.00	4.9	7.9	5.30	.497	.844	Bar	.0012	0.546	1.403	1.408	1.291	1.288	0.049	.562	.446	1.100	1.341	0.338	.114	.620	.182	15.90
90	WW	0.6	1.00	5.9	7.9	5.30	.497	.844	Bar	.0012	0.512	1.372	1.388	1.307	1.308	0.015	.536	.464	1.030	1.093	0.338	.114	.746	.091	15.90
97	WW	0.9	1.00	4.5	7.9	5.30	.497	.844	Bar	.0012	0.562	1.427	1.433	1.291	1.291	0.065	.586	.447	1.130	1.443	0.338	.114	.569	.240	15.90
98	WW	0.9	1.00	3.5	7.9	5.30	.497	.844	Bar	.0012	0.654	1.510	1.519	1.250	1.258	0.157	.671	.410	1.315	2.274	0.338	.114	.443	.467	15.90
99	WW	0.9	3.00	4.5	7.9	5.30	.497	.844	Bar	.0012	0.567	1.426	1.436	1.285	1.302	0.070	.587	.450	1.140	1.482	0.338	.114	.569	.240	15.90
100	WW	0.9	3.00	3.5	7.9	5.30	.497	.844	Bar	.0012	0.647	-	1.527	-	1.272	0.150	.683	.428	1.301	2.202	0.338	.114	.443	.467	15.90
109	WW	0.9	2.00	2.5	7.9	5.30	.497	.844	Bar	.0012	0.787	-	1.655	-	-	0.290	.811	-	1.583	3.967	0.338	.114	.317	1.02	15.90
110	WW	0.9	1.00	4.5	7.9	9.00	.682	.844	Bar	.0012	0.767	1.640	1.653	1.434	1.456	0.085	.803	.601	1.124	1.420	0.355	.126	.569	.264	11.59
111	WW	0.9	3.00	4.5	7.9	9.00	.682	.844	Bar	.0012	0.761	1.629	1.640	1.428	1.445	0.079	.791	.593	1.115	1.386	0.356	.126	.569	.264	11.59
118	WW	0.9	1.00	0.5	7.9	2.22	.283	.744	Bar	.0012	0.948	-	-	-	-	0.665	-	-	-	-	-	-	-	-	-
119	WW	0.9	1.00	1.5	7.9	2.22	.283	.743	Bar	.0012	0.717	-	-	-	-	0.434	-	-	-	-	-	-	-	-	-
126	WW	0.6	3.00	1.87	7.9	2.45	.314	.835	Bar	.0012	0.531	1.440	1.427	1.096	1.107	0.277	-	-	-	-	-	-	-	-	-
127	WW	0.6	3.00	5.90	7.9	2.47	.314	.835	Bar	.0012	0.334	1.175	1.182	1.138	1.140	0.020	.344	.304	1.061	1.201	0.313	.098	.746	.0775	25.20
128	WW	0.6	1.00	5.90	7.9	2.47	.314	.835	Bar	.0012	0.334	1.185	1.180	1.141	1.136	0.020	.348	.304	1.063	1.201	0.313	.098	.746	.0775	25.20
129	WW	0.6	1.00	1.87	7.9	2.45	.314	.835	Bar	.0012	0.580	1.419	1.412	1.110	1.107	0.266	.581	.274	1.848	6.30	0.311	.097	.236	1.65	25.20
216	WW	0.6	1.00	5.92	7.9	2.00	.465	.833	Bar	.0012	0.474	1.322	1.311	1.300	1.295	0.009	-	-	-	-	-	-	-	-	-
217	WW	0.6	1.00	4.90	7.9	2.00	.465	.833	Bar	.0012	0.481	1.323	1.322	1.297											

TABLE 1: SIMPLE NORMAL CROSSING [continued]
45 degree wing-wall abutments

Run No	Model Type	Measured Data											Computed Data													
		Model height [ft]	Model length [ft]	b [ft]	B [ft]	Q [cfs]	h_n [ft]	Bottom Rdg.	Roughness	Slope	h_1 [ft]	R_{UR}	R_{UL}	R_{DR}	R_{DL}	L^*	h_1^* [ft]	h_U [ft]	h_D [ft]	$\frac{h_1}{h_n}$	$\left[\frac{h_1}{h_n}\right]^3$	F_n	F_n^2	M	$\left[\frac{1}{M^2}-1\right]F_n^2$	$\frac{B}{h_n}$
558	WW	0.9	0.5	2.46	7.9	5.00	0.484	0.866	Bar	.0012	0.797	1.670	1.673	1.282	1.268		0.313	0.806	0.409	1.650	4.50	0.332	.110	0.311	1.030	16.35
626	WW	0.6	1.00	5.92	7.9	5.00	0.484	0.853	Bar	.0012	0.502	1.378	1.381	1.309	1.310		0.018	0.806	0.409	1.650	4.50	0.332	.110	0.311	1.030	16.35
759	WW	0.9	1.00	3.44	7.9	5.00	0.484	0.862	Bar	.0012	0.646	1.528	1.526	1.282	1.270		0.162	0.665	0.414	1.339	2.40	0.332	.110	0.436	0.467	16.35
886	WW	0.9	1.00	4.46	7.9	5.00	0.484	0.855	Bar	.0012	0.550	1.436	1.424	1.304	1.295		0.066	0.575	0.445	1.139	1.48	0.332	.110	0.565	0.234	16.35
923	WW	0.9	1.00	4.42	7.9	5.00	0.484	0.855	Bar	.0012	0.546	1.435	1.427	1.293	1.297		0.062	0.576	0.440	1.130	1.44	0.332	.110	0.560	0.241	16.35
927	WW	0.9	1.00	2.42	7.9	5.00	0.484	0.855	Bar	.0012	0.789	1.666	1.665	1.256	1.228		0.305	0.811	0.387	1.630	4.331	0.332	.110	0.306	1.069	16.35

- R_{UR} - Point gage reading at upstream right stagnation point
- R_{UL} - Point gage reading at upstream left stagnation point
- R_{DR} - Point gage reading at downstream rightstagnation point
- R_{DL} - Point gage reading at downstream left stagnation point

TABLE 1: SIMPLE NORMAL CROSSING
1:1.5 spill-through abutment

Run No	Model Type	Model height [ft]	Model length [ft]	Measured Data										Computed Data												
				b [ft]	B [ft]	Q [cfs]	h_n [ft]	Bottom Rdg.	Roughness	Slope	h_1 [ft]	R_{UR}	R_{UL}	R_{DR}	R_{DL}	L^*	h_1^* [ft]	h_U [ft]	h_D [ft]	$\frac{h_1}{h_n}$	$\left(\frac{h_1}{h_n}\right)^3$	F_n	F_n^2	M	$[\frac{1}{M^2}-1]F_n^2$	$\frac{B}{h_n}$
16	ST	0.6	1.00	2.00	4.0	1.07	0.233	0.845	Bar	.0036	0.280	-	1.158	-	1.030	0.047	0.313	0.185	1.200	1.728	0.419	0.176	0.586	0.336	17.18	
18	ST	0.6	1.00	1.00	4.0	1.06	0.232	0.849	Bar	.0036	0.400	-	1.284	-	1.023	0.168	0.435	0.174	1.724	5.120	0.419	0.176	0.336	1.380	17.25	
120	ST	0.6	1.00	2.00	7.9	2.22	0.283	0.746	Bar	.0012	0.548	-	-	-	-	0.265	-	-	-	-	-	-	-	-	-	
121	ST	0.6	1.00	0.10	7.9	2.22	0.283	0.752	Bar	.0012	0.856	-	-	-	-	0.573	-	-	-	-	-	-	-	-	-	
122	ST	0.6	1.00	4.00	7.9	2.70	0.332	0.835	Bar	.0012	0.382	-	1.242	-	1.143	0.050	0.407	0.308	1.150	1.520	0.315	0.099	0.567	0.208	23.80	
123	ST	0.6	1.00	2.00	7.9	2.68	0.331	0.835	Bar	.0012	0.529	-	1.364	-	1.122	0.198	0.529	0.287	1.598	4.09	0.314	0.099	0.315	0.899	23.85	
124	ST	0.6	1.00	4.00	7.9	2.45	0.316	0.835	Bar	.0012	0.365	1.202	1.215	1.127	1.126	0.051	0.374	0.292	1.115	1.552	0.307	0.094	0.565	0.201	25.00	
125	ST	0.6	1.00	2.00	7.9	2.45	0.314	0.853	Bar	.0012	0.504	1.362	1.346	1.099	1.106	0.190	-	-	-	-	-	-	-	-	-	
31	ST	0.6	1.00	2.00	4.0	1.60	0.322	0.849	Bar	.0024	0.367	-	1.246	-	1.136	0.045	0.397	0.287	1.140	1.480	0.386	0.149	0.621	0.237	12.41	
32	ST	0.6	1.00	1.50	4.0	1.57	0.322	0.856	Bar	.0024	0.425	-	1.304	-	1.122	0.103	0.448	0.266	1.320	2.30	0.379	0.144	0.496	0.438	12.41	
53	ST	0.6	1.00	2.00	4.0	0.34	0.213	0.854	Bar	.0004	0.217	-	1.071	-	1.069	0.004	-	-	-	-	-	-	-	-	-	
54	ST	0.6	1.00	1.50	4.0	0.26	0.214	0.854	Bar	.0004	0.222	-	1.079	-	1.070	0.008	-	-	-	-	-	-	-	-	-	
55	ST	0.6	1.00	1.00	4.0	0.26	0.214	0.858	Bar	.0004	0.225	-	1.077	-	1.065	0.011	-	-	-	-	-	-	-	-	-	
56	ST	0.6	1.00	2.00	4.0	0.62	0.330	0.863	Bar	.0004	0.340	-	1.211	-	1.197	0.010	-	-	-	-	-	-	-	-	-	
57	ST	0.6	1.00	1.50	4.0	0.62	0.332	0.860	Bar	.0004	0.344	-	1.210	-	1.185	0.012	-	-	-	-	-	-	-	-	-	
58	ST	0.6	1.00	1.00	4.0	0.60	0.332	0.862	Bar	.0004	0.358	-	1.228	-	1.190	0.026	-	-	-	-	-	-	-	-	-	
62	ST	0.6	1.00	1.50	4.0	2.40	0.573	0.857	Bar	.0004	0.616	-	1.478	-	1.410	0.043	-	-	-	-	-	-	-	-	-	
63	ST	0.6	1.00	2.00	4.0	2.40	0.572	0.858	Bar	.0004	0.599	-	1.461	-	1.431	0.027	-	-	-	-	-	-	-	-	-	
64	ST	0.6	1.00	1.00	4.0	2.32	0.570	0.860	Bar	.0004	0.660	-	-	-	1.390	0.090	-	-	-	-	-	-	-	-	-	
67	ST	0.6	1.00	5.90	7.9	2.36	0.312	0.842	Bar	.0012	0.331	1.174	1.186	1.138	1.152	0.019	-	-	-	-	-	-	-	-	-	
68	ST	0.6	1.00	4.90	7.9	2.36	0.312	0.840	Bar	.0012	0.343	1.194	1.197	1.130	1.131	0.031	-	-	-	-	-	-	-	-	-	
69	ST	0.6	1.00	3.90	7.9	2.36	0.312	0.838	Bar	.0012	0.372	1.213	1.226	1.125	1.133	0.060	-	-	-	-	-	-	-	-	-	
70	ST	0.6	1.00	2.90	7.9	2.36	0.312	0.850	Bar	.0012	0.422	1.263	1.270	1.120	1.133	0.110	-	-	-	-	-	-	-	-	-	
75	ST	0.6	1.00	5.90	7.9	2.36	0.312	0.843	Bar	.0012	0.332	1.193	1.193	1.157	1.157	0.020	-	-	-	-	-	-	-	-	-	
76	ST	0.6	1.00	4.90	7.9	2.36	0.312	0.841	Bar	.0012	0.351	1.206	1.205	1.159	1.147	0.039	-	-	-	-	-	-	-	-	-	
77	ST	0.6	1.00	3.90	7.9	2.36	0.312	0.842	Bar	.0012	0.380	1.225	1.236	1.140	1.144	0.068	-	-	-	-	-	-	-	-	-	
78	ST	0.6	1.00	2.90	7.9	2.36	0.312	0.843	Bar	.0012	0.431	1.272	1.287	1.123	1.126	0.119	-	-	-	-	-	-	-	-	-	
85	ST	0.6	1.00	2.90	7.9	2.36	0.312	0.841	Bar	.0012	0.424	1.271	1.265	1.119	1.122	0.112	-	-	-	-	-	-	-	-	-	
86	ST	0.6	1.00	4.90	7.9	2.36	0.312	0.841	Bar	.0012	0.344	1.197	1.202	1.145	1.149	0.032	-	-	-	-	-	-	-	-	-	
444	ST	0.6	1.00	.82	7.9	2.50	0.333	0.866	Bar	.0012	0.712	1.582	1.581	1.139	1.149	2.9	0.379	0.716	0.278	2.140	9.80	0.289	.0835	0.167	2.91	23.70
445	ST	0.6	1.00	1.83	7.9	2.50	0.333	0.866	Bar	.0012	0.534	1.404	1.408	1.155	1.161	3.1	0.201	0.540	0.292	1.603	4.10	0.289	.0835	0.295	0.876	23.70
446	ST	0.6	1.00	2.86	7.9	2.50	0.333	0.866	Bar	.0012	0.431	1.303	1.301	1.171	1.167	3.3	0.098	0.436	0.306	1.294	2.17	0.289	.0835	0.425	0.377	23.70
447	ST	0.6	1.00	3.85	7.9	2.50	0.333	0.866	Bar	.0012	0.380	1.257	1.257	1.177	1.173	4.3	0.047	0.391	0.309	1.141	1.49	0.289	.0835	0.551	0.191	23.70
448	ST	0.6	1.00	4.88	7.9	2.50	0.333	0.866	Bar	.0012	0.355	1.231	1.230	1.180	1.180	4.3	0.022	0.365	0.314	1.066	1.210	0.289	.0835	0.681	0.097	23.70
449	ST	0.6	1.00	5.87	7.9	2.50	0.333	0.866	Bar	.0012	0.339	1.215	1.215	1.187	1.188	3.3	0.006	0.349	0.322	1.018	1.063	0.289	.0835	0.806	0.046	23.70
663	ST	0.9	1.00	5.17	7.9	2.50	0.333	0.857	Bar	.0012	0.342	1.212	1.212	1.174	1.174	4.8	0.009	-	-	-	-	-	-	-	-	-
664	ST	0.9	1.00	4.17	7.9	2.50	0.333	0.857	Bar	.0012	0.361	1.228	1.230	1.168	1.168	-	0.028	0.372	0.311	1.084	1.275	0.289	.0835	0.590	0.158	23.70
665	ST	0.9	1.00	3.17	7.9	2.50	0.333	0.857	Bar	.0012	0.402	1.269	1.269	1.160	1.160	5.4	0.069	0.412	0.303	1.207	1.76	0.289	.0835	0.465	0.302	23.70
666	ST	0.9	1.00	2.15	7.9	2.50	0.333	0.857	Bar	.0012	0.485	1.349	1.349	1.152	1.154	4.9	0.152	0.492	0.296	1.456	3.10	0.289	.0835	0.334	0.667	23.70
667	ST	0.9	1.00	1.125	7.9	2.50	0.333	0.857	Bar	.0012	0.630	1.491	1.491	1.145	1.135	4.8	0.297	0.634	0.283	1.891	6.78	0.289	.0835	0.206	1.88	23.70
866	ST	0.9	1.00	3.00	7.9	2.50	0.333	0.855	Bar	.0012	0.402	1.267	1.264	1.155	1.156	-	0.069	0.411	0.301	1.207	1.758	0.289	.0835	0.443	0.342	23.70
869	ST	0.9	1.00	5.17	7.9	2.50	0.333	0.855	Bar	.0012	0.349	1.215	1.214	1.176	1.173	-	0.016	0.360	0.320	1.048	1.151	0.289	.0835	0.717	0.080	23.70
42	ST	0.6	1.00	2.00	4.0	0.88	0.345	0.846	Bar	.0008	0.355	1.215	-	1.182	-	-	0.010	0.369	0.336	1.029	1.090	0.192	.0369	0.628	0.0569	11.60
43	ST	0.6	1.00	1.50	4.0	0.88	0.343	0.843	Bar	.0008	0.367	1.221	-	1.180	-	-	0.024	0.378	0.337	1.070	1.230	0.192	.0369	0.503	0.109	11.66
44	ST	0.6	1.00	1.00	4.0	0.88	0.344	0.854	Bar	.0008	0.394	1.250	-	1.172	-	-	0.050	0.396	0.318	1.145	1.500	0.192	.0369	0.379	0.219	11.61
1156R	ST	0.9	1.00	3.15	7.9	3.00	0.362	0.855	Bar	.0012	0.443	1.305	1.306	1.182	1.179	-	0.081	0.451	0.326	1.218	1.807	0.309	.096	0.467	0.343	12.80
1	ST	0.6	1.00	1.00	4.0	1.68	0.380	-	Bar	.0012	0.530	-	-	-	-	-	0.150	-	-	1.393	2.700	0.316	.100	0.392	0.55	10.51
4	ST	0.6	1.00	2.00	4.0	1.70	0.390	0.802	Bar	.0012	0.418	-	1.238	-	1.173	0.028	0.436	0.371	1.070	1.240	0.308	.095	0.646	0.133	10.24	
5	ST	0.6	1.00	2.00	4.0	0.65	0.220	0.802	Bar	.0012	0.232	-	1.040	-	1.011	0.012	-	-	-	-	-	-	-	-	-	-
8	ST	0.6	1.00	1.00	4.0	0.63	0.223	0.849	Bar	.0012	0.293	-	1.154	-	1.050	0.070	-	-	-	-	-	-	-	-	-	-
12	ST	0.6	1.00	1.50	4.0	2.00	0.450	0.849	Bar	.0012	0.504	-	1.368	-	1.253	0.054	-	-	-	-	-	-	-	-	-	-
15	ST	0.6	1.00	1.50	4.0	0.47	0.170	0.849	Bar	.0012	0.189	-	1.046	-	1.008	0.019	-	-	-	-	-	-	-	-	-	-
17	ST	0.6	1.00	1.50	4.0	1.06	0.230	0.849	Bar	.0036	0.330	-	1.194	-	1.030	0.100	-	-	-	-	-	-	-	-	-	-
22	ST	0.6	1.00	2.00	4.0	2.30	0.387	0.845	Bar	.0024	0.452	-	1.321	-	1.180	0.065	0.476	0.335	1.170	1.600	0.422	0.178	0.645	0.251	10.32	
23	ST	0.6	1.00	1.50	4.0	2.25	0.386	0																		

TABLE 1: SIMPLE NORMAL CROSSING [continued]
1:1.5 spill-through abutment

Run No	Model Type	Model height [ft]	Model length [ft]	Measured Data										Computed Data												
				b [ft]	B [ft]	Q [cfs]	h_n [ft]	Bottom Rdg.	Roughness	Slope	h_1 [ft]	R_{UR}	R_{UL}	R_{DR}	R_{DL}	L^*	h_1^* [ft]	h_u [ft]	h_D [ft]	$\frac{h_1}{h_n}$	$\left(\frac{h_1}{h_n}\right)^3$	F_n	F_n^2	M	$\frac{1}{M^2} F_n^2$	$\frac{B}{h_n}$
592	ST	0.9	1.00	5.19	7.9	5.00	0.416	0.864	Bar	.002	0.454	1.346	1.346	1.240	1.240	3.8	0.038	0.482	0.376	1.091	1.300	0.416	0.173	0.735	0.147	19.00
9	ST	0.6	1.00	1.00	4.0	2.00	0.444	0.849	Bar	.0012	0.583	-	1.444	-	1.247	0.139	0.595	0.398	1.312	2.260	0.298	0.089	0.416	0.425	9.00	
11	ST	0.6	1.00	2.00	4.0	2.02	0.450	0.849	Bar	.0012	0.467	-	1.340	-	1.270	0.017	0.491	0.421	1.038	1.114	0.295	0.0870	0.668	0.108	8.89	
25	ST	0.6	1.00	1.00	4.0	0.68	0.200	0.849	Bar	.0024	0.328	-	1.178	-	1.017	0.128	-	-	-	-	-	-	-	-	-	-
26	ST	0.6	1.00	1.50	4.0	0.68	0.205	0.849	Bar	.0024	0.262	-	1.137	-	1.027	0.057	-	-	-	-	-	-	-	-	-	-
27	ST	0.6	1.00	2.00	4.0	0.66	0.200	0.849	Bar	.0024	0.227	-	1.032	-	1.089	0.027	-	-	-	-	-	-	-	-	-	-
33	ST	0.6	1.00	2.00	4.0	0.45	0.250	0.854	Bar	.0008	0.260	-	1.126	-	1.088	0.010	-	-	-	-	-	-	-	-	-	-
34	ST	0.6	1.00	1.50	4.0	0.44	0.248	0.854	Bar	.0008	0.268	-	1.127	-	1.088	0.020	-	-	-	-	-	-	-	-	-	-
35	ST	0.6	1.00	1.00	4.0	0.50	0.250	0.854	Bar	.0008	0.298	-	1.154	-	1.086	0.048	-	-	-	-	-	-	-	-	-	-
45	ST	0.6	1.00	2.00	4.0	1.55	0.476	0.849	Bar	.0008	0.489	-	1.342	-	1.300	0.013	0.493	0.451	1.023	1.07	0.207	.043	0.678	.0504	8.40	
46	ST	0.6	1.00	1.50	4.0	1.54	0.476	0.849	Bar	.0008	0.505	-	1.361	-	1.301	0.029	0.512	0.452	1.06	1.19	0.206	.0425	0.554	.0964	8.40	
47	ST	0.6	1.00	1.00	4.0	1.54	0.476	0.849	Bar	.0008	0.541	-	1.379	-	1.284	0.065	0.530	0.435	1.138	1.473	0.206	.0425	0.428	0.189	8.40	
130	ST	0.9	1.00	3.16	7.9	5.00	0.484	0.835	Bar	.0012	0.610	1.458	1.452	1.298	1.259	0.126	0.620	0.444	1.262	2.010	0.332	0.110	0.492	0.334	16.35	
131	ST	0.9	1.00	5.16	7.9	5.00	0.484	0.833	Bar	.0012	0.512	1.363	1.363	1.297	1.284	0.028	0.530	0.458	1.060	1.190	0.332	0.110	0.744	0.890	16.35	
132	ST	0.9	1.00	5.16	7.9	5.00	0.484	0.834	Bar	.0012	0.500	1.345	1.359	1.294	1.297	0.016	0.518	0.462	1.035	1.11	0.332	0.110	0.744	0.890	16.35	
133	ST	0.9	1.00	3.16	7.9	5.00	0.484	0.844	Bar	.0012	0.604	1.462	1.463	1.257	1.268	0.120	0.619	0.419	1.247	1.940	0.332	0.110	0.491	0.346	16.35	
536	ST	0.9	1.00	4.19	7.9	5.00	0.484	0.866	Bar	.0012	0.545	1.424	1.427	1.309	1.306	0.061	0.560	0.442	1.126	1.428	0.332	0.110	0.622	0.174	16.35	
282	ST	0.9	1.00	5.15	7.9	5.00	0.484	0.834	Bar	.0012	-	1.355	1.357	1.290	1.290	-	-	-	-	-	-	-	-	-	-	-
283	ST	0.9	1.00	4.32	7.9	5.00	0.484	0.834	Bar	.0012	-	1.392	1.393	1.268	1.277	-	-	-	-	-	-	-	-	-	-	-
284	ST	0.9	1.00	3.19	7.9	5.00	0.484	0.834	Bar	.0012	-	1.452	1.453	1.257	1.269	-	-	-	-	-	-	-	-	-	-	-
552	ST	0.9	1.00	3.17	7.9	5.00	0.484	0.866	Bar	.0012	0.607	1.492	1.491	1.303	1.294	0.123	0.626	0.433	1.255	1.975	0.332	0.110	0.494	0.3431	16.35	
562	ST	0.9	1.00	5.19	7.9	5.00	0.484	0.866	Bar	.0012	0.507	1.390	1.392	1.320	1.323	0.023	0.525	0.456	1.048	1.150	0.332	0.110	0.750	0.086	16.35	
563	ST	0.9	1.00	2.19	7.9	5.00	0.484	0.866	Bar	.0012	0.724	1.604	1.605	1.292	1.285	0.240	0.739	0.423	1.497	3.350	0.332	0.110	0.370	0.692	16.35	
564	ST	0.9	1.00	1.17	7.9	5.00	0.484	0.866	Bar	.0012	0.910	1.786	1.785	1.247	1.270	0.425	0.920	0.393	1.885	6.690	0.332	0.110	0.240	1.810	16.35	
629	ST	0.6	1.00	5.87	7.9	5.00	0.484	0.853	Bar	.0012	0.495	1.363	1.366	1.313	1.315	0.011	0.512	0.461	1.023	1.070	0.332	0.110	0.835	0.048	16.35	
645	ST	0.6	1.00	5.87	7.9	5.00	0.484	0.855	Bar	.0012	0.492	-	-	-	-	0.008	-	-	1.019	1.059	0.332	0.110	0.835	0.048	16.35	
880	ST	0.9	1.00	5.08	7.9	5.00	0.484	0.854	Bar	.0012	0.508	1.380	1.378	1.315	1.314	0.024	0.525	0.461	1.05	1.158	0.332	0.110	0.735	0.094	16.35	
883	ST	0.9	1.00	3.17	7.9	5.00	0.484	0.856	Bar	.0012	0.604	1.484	1.469	1.293	1.279	0.120	0.621	0.430	1.250	1.950	0.332	0.110	0.493	0.343	16.35	
1086R	ST	0.9	1.00	3.15	7.9	5.00	0.484	0.855	Bar	.0012	0.599	1.475	1.473	1.280	1.275	5.5	0.115	0.619	0.423	1.240	1.910	0.332	0.110	0.490	0.348	16.35
1091R	ST	0.9	1.00	4.15	7.9	5.00	0.484	0.855	Bar	.0012	0.530	1.407	1.407	1.291	1.290	4.9	0.046	0.552	0.460	1.098	1.315	0.332	0.110	0.616	0.179	16.35
984	ST	0.9	1.00	5.17	7.9	5.00	0.484	0.855	Bar	.0012	0.504	1.381	1.378	1.318	1.313	0.020	0.525	0.461	1.041	1.128	0.332	0.110	0.746	0.088	16.35	
1007R	ST	0.9	1.00	4.15	7.9	5.00	0.484	0.855	Bar	.0012	0.541	1.418	1.415	1.302	1.298	4.9	0.057	0.562	0.445	1.119	1.400	0.332	0.110	0.616	0.178	16.35
1034	ST	0.9	1.00	3.13	7.9	5.00	0.484	0.855	Bar	.0012	0.603	1.475	1.476	1.277	1.272	5.7	0.119	0.621	0.420	1.247	1.939	0.332	0.110	0.488	0.352	16.35
1061	ST	0.9	1.00	2.15	7.9	5.00	0.484	0.855	Bar	.0012	0.719	1.593	1.592	1.279	1.259	4.7	0.235	0.738	0.414	1.486	3.280	0.332	0.110	0.364	0.717	16.35
112	ST	0.9	1.00	5.20	7.9	9.00	0.682	0.844	Bar	.0012	0.700	1.577	1.560	1.485	1.483	0.018	0.725	0.640	1.025	1.075	0.355	0.126	0.788	0.769	11.59	
113	ST	0.9	1.00	4.20	7.9	9.00	0.682	0.844	Bar	.0012	0.750	1.624	1.629	1.468	1.476	0.068	0.783	0.628	1.098	1.320	0.355	0.126	0.661	0.161	11.59	
114	ST	0.9	1.00	3.20	7.9	9.00	0.682	0.844	Bar	.0012	0.822	1.689	1.702	1.443	1.417	0.140	0.852	0.586	1.205	1.750	0.355	0.126	0.535	0.315	11.59	
115	ST	0.9	3.00	5.20	7.9	9.00	0.682	0.844	Bar	.0012	0.701	1.568	1.571	1.497	1.492	0.019	0.726	0.651	1.028	1.091	0.355	0.126	0.789	0.077	11.59	
116	ST	0.9	3.00	4.20	7.9	9.00	0.682	0.844	Bar	.0012	0.743	1.612	1.617	1.478	1.470	0.061	0.771	0.630	1.090	1.295	0.355	0.126	0.661	0.162	11.59	
117	ST	0.9	3.00	3.20	7.9	9.00	0.682	0.850	Bar	.0012	0.827	1.691	1.700	1.461	1.430	0.145	0.846	0.596	1.210	1.771	0.355	0.126	0.535	0.315	11.59	
91	ST	0.6	1.00	5.90	7.9	5.30	0.497	0.844	Bar	.0012	0.503	1.376	1.373	1.329	1.328	0.006	0.531	0.485	1.013	1.040	0.337	0.113	0.840	0.047	15.90	
92	ST	0.6	1.00	4.90	7.9	5.30	0.497	0.844	Bar	.0012	0.527	1.393	1.406	1.305	1.301	0.030	0.556	0.459	1.060	1.195	0.337	0.113	0.715	0.108	15.90	
93	ST	0.6	1.00	3.90	7.9	5.30	0.497	0.844	Bar	.0012	0.578	1.445	1.448	1.296	1.285	0.081	0.603	0.447	1.162	1.570	0.337	0.113	0.589	0.214	15.90	
94	ST	0.6	3.00	5.90	7.9	5.30	0.497	0.844	Bar	.0012	0.506	1.369	1.369	1.337	1.331	0.009	0.525	0.490	1.018	1.054	0.337	0.113	0.840	0.047	15.90	
95	ST	0.6	3.00	4.90	7.9	5.30	0.497	0.844	Bar	.0012	0.520	1.386	1.396	1.301	1.304	0.023	0.547	0.459	1.046	1.145	0.337	0.113	0.715	0.108	15.90	
96	ST	0.6	3.00	3.90	7.9	5.30	0.497	0.844	Bar	.0012	0.566	1.424	1.437	1.283	1.285	0.069	0.587	0.440	1.140	1.490	0.337	0.113	0.589	0.214	15.90	
101	ST	0.9	1.00	5.20	7.9	5.30	0.497	0.844	Bar	.0012	0.514	1.377	1.387	1.304	1.307	0.022	0.538	0.462	1.031	1.100	0.337	0.113	0.752	0.087	15.90	
102	ST	0.9	1.00	4.20	7.9	5.30	0.497	0.849	Bar	.0012	0.541	1.413	1.426	1.296	1.291	0.049	0.571	0.445	1.090	1.294	0.337	0.113	0.625	0.176	15.90	
103	ST	0.9	1.00	3.20	7.9	5.30	0.497	0.843	Bar	.0012	0.609	1.464	1.468	1.274	1.280	0.112	0.623	0.434	1.225	1.846	0.337	0.113	0.500	0.339	15.90	
104	ST	0.9	3.00	5.20	7.9	5.30	0.497	0.849	Bar	.0012	0.509	1.371	1.386	1.318	1.318	0.012	-	-	1.025	1.076	0.337	0.113	0.752	0.086	15.90	
105	ST	0.9	3.00	4.20	7.9	5.30	0.																			

TABLE 1: SIMPLE NORMAL CROSSING
vertical board model

Run No	Model Type	Model height [ft]	Model length [ft]	Measured Data										Computed Data													
				b [ft]	B [ft]	Q [cfs]	h_n [ft]	Bottom Rdg.	Roughness	Slope	h_1 [ft]	R_{UR}	R_{UL}	R_{DR}	R_{DL}	L*	h_1^* [ft]	h_U [ft]	h_D [ft]	$\frac{h_1}{h_n}$	$[\frac{h_1}{h_n}]^3$	F_n	F_n^2	M	$[\frac{1}{M^2}]F_n^2$	$\frac{B}{h_n}$	
357	VB	1.67	-	2.0	7.9	2.50	0.333	0.834	Bar	.0012	0.615	1.454	1.455	1.110	1.121	3.5	0.282	0.621	0.282	1.849	6.30	0.289	.0835	0.253	1.220	23.70	
358	VB	1.67	-	3.0	7.9	2.50	0.333	0.834	Bar	.0012	0.489	1.331	1.330	1.127	1.118	3.5	0.156	0.497	0.289	1.468	3.16	0.289	.0835	0.38	0.496	23.70	
359	VB	1.67	-	4.0	7.9	2.50	0.333	0.834	Bar	.0012	0.419	1.261	1.259	1.132	1.128	2.5	0.086	0.426	0.296	1.258	2.00	0.289	.0835	0.505	0.244	23.70	
360	VB	1.67	-	5.0	7.9	2.50	0.333	0.834	Bar	.0012	0.380	1.224	1.223	1.141	1.137	3.6	0.047	0.390	0.305	1.140	1.49	0.289	.0835	0.633	0.125	23.70	
361	VB	1.67	-	6.0	7.9	2.50	0.333	0.834	Bar	.0012	0.355	1.200	1.200	1.145	1.145	4.0	0.022	0.366	0.311	1.066	1.21	0.289	.0835	0.760	0.061	23.70	
267	VB	1.67	-	2.0	7.9	2.91	0.352	0.833	Bar	.0012	0.687	1.526	1.524	1.124	1.134	3.2	0.335	-	-	-	-	-	-	-	-	-	-
598	VB	1.67	-	6.0	7.9	5.00	0.416	0.864	Bar	.002	0.464	1.349	1.352	1.225	1.224	4.0	0.048	0.487	0.361	1.110	1.370	0.415	.172	0.760	0.126	19.00	
599	VB	1.67	-	5.0	7.9	5.00	0.416	0.864	Bar	.002	0.523	1.409	1.407	1.210	1.208	3.6	0.107	0.544	0.345	1.255	1.975	0.415	.172	0.633	0.258	19.00	
600	VB	1.67	-	4.0	7.9	5.00	0.416	0.864	Bar	.002	0.608	1.492	1.490	1.205	1.183	3.6	0.192	0.627	0.330	1.460	3.102	0.415	.172	0.505	0.503	19.00	
601	VB	1.67	-	3.0	7.9	5.00	0.416	0.864	Bar	.002	0.734	1.614	1.614	1.177	1.189	2.7	0.318	0.750	0.319	1.760	5.460	0.415	.172	0.380	1.025	19.00	
602	VB	1.67	-	2.0	7.9	5.00	0.416	0.864	Bar	.002	0.943	1.819	1.818	1.156	1.132	2.9	0.527	0.955	0.280	2.260	11.50	0.415	.172	0.253	2.510	19.00	
266	VB	1.67	-	2.0	7.9	3.95	0.418	0.833	Bar	.0012	0.835	1.673	1.673	1.167	1.182	3.5	0.417	-	-	-	-	-	-	-	-	-	-
754	VB	1.67	-	4.0	7.9	5.00	0.484	0.862	Bar	.0012	0.633	1.512	1.512	1.296	1.274	-	0.149	0.650	0.423	1.307	2.238	0.332	.110	0.505	0.321	16.35	
755	VB	1.67	-	3.0	7.9	5.00	0.484	0.862	Bar	.0012	0.750	1.631	1.624	1.272	1.254	3.5	0.266	0.766	0.404	1.550	3.724	0.332	.110	0.380	0.650	16.35	
756	VB	1.67	-	2.0	7.9	5.00	0.484	0.862	Bar	.0012	0.960	-	-	-	-	3.18	0.476	-	-	1.983	7.80	0.332	.110	0.253	1.608	16.35	
757	VB	1.67	-	5.0	7.9	5.00	0.484	0.862	Bar	.0012	0.567	1.448	1.447	1.290	1.302	2.62	0.083	0.586	0.434	1.171	1.610	0.332	.110	0.633	0.165	16.35	
758	VB	1.67	-	6.0	7.9	5.00	0.484	0.862	Bar	.0012	0.520	-	-	-	-	-	0.036	-	-	1.074	1.239	0.332	.110	0.760	.0805	16.35	
872	VB	1.67	-	3.00	7.9	5.00	0.484	0.855	Bar	.0012	0.758	1.624	1.619	1.280	1.258	2.90	0.274	0.767	0.414	1.566	3.840	0.332	.110	0.380	0.650	16.35	
873	VB	1.67	-	4.00	7.9	5.00	0.484	0.855	Bar	.0012	0.645	1.518	1.510	1.298	1.283	3.3	0.161	0.659	0.330	1.335	2.39	0.332	.110	0.505	0.321	16.35	
874R	VB	1.67	-	4.97	7.9	5.00	0.484	0.855	Bar	.0012	0.577	1.449	1.441	1.305	1.294	2.7	0.093	0.590	0.445	1.192	1.700	0.332	.110	0.630	0.167	16.35	
875	VB	1.67	-	5.96	7.9	5.00	0.484	0.855	Bar	.0012	0.534	1.415	1.402	1.319	1.315	2.1	0.050	-	-	-	-	-	-	-	-	-	-
301	VB	1.67	-	5.97	7.9	5.00	0.484	0.834	Bar	.0012	0.519	1.374	1.366	1.283	1.275	-	0.035	0.536	0.445	1.071	1.240	0.332	.110	0.756	0.083	16.35	
302	VB	1.67	-	5.00	7.9	5.00	0.484	0.834	Bar	.0012	0.567	1.419	1.410	1.274	1.260	4.3	0.083	0.581	0.433	1.171	1.606	0.332	.110	0.633	0.165	16.35	
303	VB	1.67	-	4.00	7.9	5.00	0.484	0.834	Bar	.0012	0.636	1.481	1.479	1.243	1.257	4.3	0.152	0.646	0.416	1.314	2.269	0.332	.110	0.505	0.322	16.35	
304	VB	1.67	-	3.00	7.9	5.00	0.484	0.834	Bar	.0012	0.758	1.602	1.595	1.248	1.223	4.4	0.274	0.765	0.402	1.566	3.840	0.332	.110	0.380	0.650	16.35	
305	VB	1.67	-	2.00	7.9	5.00	0.484	0.834	Bar	.0012	0.968	1.804	1.800	1.236	1.186	4.1	0.484	0.968	0.377	2.000	8.00	0.332	.110	0.253	1.598	16.35	
225	VB	1.67	-	6.00	7.9	5.00	0.484	0.834	Bar	.0012	0.520	1.369	1.371	1.282	1.279	4.7	0.036	0.536	0.447	1.074	1.239	0.332	.110	0.760	0.080	16.35	
226	VB	1.67	-	5.00	7.9	5.00	0.484	0.834	Bar	.0012	0.564	1.412	1.412	1.272	1.261	3.4	0.080	0.578	0.433	1.165	1.581	0.332	.110	0.633	0.165	16.35	
227	VB	1.67	-	4.00	7.9	5.00	0.484	0.834	Bar	.0012	0.637	1.487	1.481	1.260	1.246	4.2	0.153	0.650	0.419	1.316	2.279	0.332	.110	0.505	0.322	16.35	
228	VB	1.67	-	3.00	7.9	5.00	0.484	0.834	Bar	.0012	0.757	1.606	1.601	1.251	1.231	4.4	0.273	0.770	0.407	1.564	3.826	0.332	.110	0.380	0.650	16.35	
229	VB	1.67	-	2.00	7.9	5.00	0.484	0.834	Bar	.0012	0.962	1.802	1.800	1.201	1.239	3.2	0.478	0.967	0.386	1.988	7.857	0.332	.110	0.253	1.598	16.35	
234	VB	1.67	-	2.00	7.9	5.00	0.484	0.834	Bar	.0012	0.965	1.804	1.808	1.239	1.199	4.5	0.481	-	-	-	-	-	-	-	-	-	-
261	VB	1.67	-	2.00	7.9	5.00	0.484	0.834	Bar	.0012	0.965	1.807	1.807	1.218	1.231	3.3	0.481	0.973	0.391	1.994	7.928	0.332	.110	0.253	1.598	16.35	
603	VB	1.67	-	6.00	7.9	2.72	0.478	0.864	Baffle	.002	0.488	1.360	1.360	1.324	1.326	2.3	0.010	0.496	0.461	1.020	1.060	0.184	.0339	0.760	0.025	16.20	
604	VB	1.67	-	5.00	7.9	2.72	0.478	0.864	Baffle	.002	0.503	1.377	1.378	1.319	1.323	2.4	0.025	0.514	0.457	1.052	1.164	0.184	.0339	0.633	0.051	16.20	
605	VB	1.67	-	4.00	7.9	2.72	0.478	0.864	Baffle	.002	0.531	1.406	1.406	1.315	1.317	2.5	0.053	0.542	0.452	1.111	1.370	0.184	.0339	0.505	0.099	16.20	
606	VB	1.67	-	3.00	7.9	2.72	0.478	0.864	Baffle	.002	0.583	1.457	1.457	1.313	1.312	2.7	0.105	0.593	0.449	1.220	1.816	0.184	.0339	0.380	0.201	16.20	
607	VB	1.67	-	2.00	7.9	2.72	0.478	0.864	Baffle	.002	0.703	1.573	1.575	1.301	1.306	2.5	0.225	0.710	0.440	1.471	3.190	0.184	.0339	0.253	0.496	16.20	
450	VB	1.67	-	6.00	7.9	2.50	0.523	0.866	Baffle	.0012	0.532	1.401	1.401	1.376	1.376	2.4	0.009	0.535	0.510	1.018	1.052	0.148	.0219	0.760	0.16	15.10	
451	VB	1.67	-	5.00	7.9	2.50	0.523	0.866	Baffle	.0012	0.544	1.415	1.414	1.373	1.373	3.0	0.021	0.549	0.507	1.040	1.130	0.148	.0219	0.633	0.033	15.10	
452	VB	1.67	-	4.00	7.9	2.50	0.523	0.866	Baffle	.0012	0.566	1.437	1.436	1.371	1.372	2.9	0.043	0.571	0.506	1.082	1.172	0.148	.0219	0.505	0.064	15.10	
453	VB	1.67	-	3.00	7.9	2.50	0.523	0.866	Baffle	.0012	0.610	1.482	1.479	1.365	1.367	3.0	0.087	0.615	0.500	1.168	1.590	0.148	.0219	0.380	0.129	15.10	
454	VB	1.67	-	2.00	7.9	2.50	0.523	0.866	Baffle	.0012	0.708	1.580	1.581	1.362	1.362	2.7	0.185	0.715	0.496	1.354	2.490	0.148	.0219	0.253	0.320	15.10	
262	VB	1.67	-	2.00	7.9	5.75	0.523	0.834	Baffle	.0012	1.057	1.895	1.895	1.566	1.269	3.4	0.573	-	-	-	-	-	-	-	-	-	-
459	VB	1.67	-	6.00	7.9	5.00	0.718	0.866	Baffle	.0012	0.733	1.609	1.610	1.565	1.566	4.2	0.015	0.744	0.700	1.020	1.060	0.184	.0339	0.760	0.025	11.00	
460	VB	1.67	-	5.00	7.9	5.00	0.718	0.866	Baffle	.0012	0.756	1.634	1.633	1.556	1.557	2.5	0.038	0.768	0.691	1.053	1.168	0.184	.0339	0.633	0.051	11.00	
461	VB	1.67	-	4.00	7.9	5.00	0.718	0.866	Baffle	.0012	0.801	1.676	1.676	1.552	1.556	-	0.083	0.810	0.688	1.116	1.390	0.184	.0339	0.505	0.099	11.00	
462	VB	1.67	-	3.00	7.9	5.00	0.718	0.866	Baffle	.0012	0.882	1.754	1.760	1.545	1.547	3.6	0.164	0.891	0.680	1.228	1.852	0.184	.0339	0.380	0.201	11.00	
463	VB	1.67	-	2.00	7.9	5.00	0.718	0.866	Baffle	.0012	1.060	1.929	1.930	1.541	1.535	3.5	0.342	1.064	0.672	1.476							

TABLE 1: SIMPLE NORMAL CROSSING
vertical wall; 30 degree, 60 degree and 90 degree wing-wall models; 1:2 and 1:1 spill through abutments

Measured Data														Computed Data												
Run No	Model Type	Model height [ft]	Model length [ft]	b [ft]	B [ft]	Q [cfs]	h_n [ft]	Bottom Rdg.	Roughness	Slope	h_1 [ft]	R_{UR}	R_{UL}	R_{DR}	R_{DL}	L^*	h_1^* [ft]	h_U [ft]	h_D [ft]	$[\frac{h_1}{h_n}]$	$[\frac{h_1}{h_n}]^3$	F_n	F_n^2	M	$[\frac{1}{M^2}-1]F_n^2$	$\frac{B}{h_n}$
1288	VW	1.2	1.00	2.81	7.9	3.00	0.360	0.855	Bar	.0012	0.535	1.398	1.398	1.158	1.160		0.175	0.543	0.304	1.486	3.282	0.309	.095	0.356	0.653	21.98
1289	VW	1.2	1.00	3.82	7.9	3.00	0.360	0.855	Bar	.0012	0.452	1.317	1.319	1.177	1.179		0.092	0.463	0.323	1.256	1.979	0.309	.095	0.484	0.311	21.98
1290	VW	1.2	1.00	4.84	7.9	3.00	0.360	0.855	Bar	.0012	0.409	1.278	1.277	1.186	1.186		0.049	0.423	0.331	1.136	1.466	0.309	.095	0.612	0.152	21.98
1291	VW	1.2	1.00	5.87	7.9	3.00	0.360	0.855	Bar	.0012	0.387	1.254	1.252	1.195	1.193		0.027	0.398	0.339	1.075	1.242	0.309	.095	0.744	0.077	21.98
1292	VW	1.2	1.00	6.85	7.9	3.00	0.360	0.855	Bar	.0012	0.366	1.233	1.234	1.204	1.204		0.006	0.379	0.349	1.017	1.051	0.309	.095	0.866	0.029	21.98
1302	VW	1.42	1.00	2.83	7.9	5.00	0.484	0.856	Bar	.0012	0.745	1.611	1.608	1.235	1.256		0.261	0.754	0.390	1.549	3.65	0.332	.110	0.358	0.750	16.35
1303	VW	1.42	1.00	3.83	7.9	5.00	0.484	0.856	Bar	.0012	0.619	1.489	1.489	1.270	1.281		0.135	0.633	0.420	1.279	2.092	0.332	.110	0.484	0.357	16.35
1304	VW	1.42	1.00	4.85	7.9	5.00	0.484	0.856	Bar	.0012	0.554	1.427	1.425	1.286	1.292		0.070	0.570	0.433	1.145	1.500	0.332	.110	0.614	0.183	16.35
1305R	VW	1.42	1.00	5.85	7.9	5.00	0.484	0.856	Bar	.0012	0.513	1.382	1.383	1.309	1.308		0.029	0.527	0.453	1.060	1.191	0.332	.110	0.741	0.091	16.35
1306R	VW	1.42	1.00	6.87	7.9	5.00	0.484	0.856	Bar	.0012	0.492	1.362	1.360	1.324	1.321		0.008	0.505	0.467	1.017	1.051	0.332	.110	0.870	0.035	16.35
1274	WW30°	0.9	1.00	3.69	7.9	3.00	0.360	0.855	Bar	.0012	0.452	1.322	1.322	1.177	1.179		0.092	0.467	0.323	1.256	1.979	0.309	.095	0.467	0.342	21.98
1275	WW30°	0.9	1.00	2.69	7.9	3.00	0.360	0.855	Bar	.0012	0.542	1.407	1.408	1.164	1.156		0.182	0.553	0.305	1.506	3.413	0.309	.095	0.340	0.726	21.98
1276R	WW30°	0.9	1.00	4.69	7.9	3.00	0.360	0.855	Bar	.0012	0.405	1.276	1.279	1.187	1.188		0.045	0.423	0.333	1.125	1.424	0.309	.095	0.594	0.175	21.98
1277	WW30°	0.9	1.00	5.69	7.9	3.00	0.360	0.855	Bar	.0012	0.381	1.250	1.252	1.194	1.190		0.021	0.396	0.337	1.058	1.185	0.309	.095	0.720	0.088	21.98
1278	WW30°	0.9	1.00	6.77	7.9	3.00	0.360	0.855	Bar	.0012	0.366	1.234	1.234	1.202	1.200		0.006	0.379	0.346	1.016	1.051	0.309	.095	0.856	0.031	21.98
1293	WW60°	0.9	1.00	2.24	7.9	3.00	0.360	0.855	Bar	.0012	0.588	1.452	1.452	1.165	1.166		0.228	0.597	0.311	1.633	4.357	0.309	.095	0.284	1.08	21.98
1294	WW60°	0.9	1.00	3.25	7.9	3.00	0.360	0.855	Bar	.0012	0.468	1.334	1.336	1.176	1.182		0.108	0.480	0.324	1.300	2.197	0.309	.095	0.411	0.466	21.98
1295	WW60°	0.9	1.00	4.23	7.9	3.00	0.360	0.855	Bar	.0012	0.410	1.283	1.282	1.189	1.189		0.050	0.428	0.334	1.139	1.478	0.309	.095	0.534	0.239	21.98
1296	WW60°	0.9	1.00	5.27	7.9	3.00	0.360	0.855	Bar	.0012	0.381	1.254	1.256	1.201	1.199		0.021	0.400	0.345	1.058	1.185	0.309	.095	0.666	0.119	21.98
1297	WW60°	0.9	1.00	6.27	7.9	3.00	0.360	0.855	Bar	.0012	0.369	1.240	1.241	1.206	1.206		0.009	0.386	0.351	1.025	1.077	0.309	.095	0.794	0.056	21.98
1298	WW60°	0.9	1.00	3.24	7.9	5.00	0.484	0.856	Bar	.0012	0.642	1.513	1.512	1.274	1.284		0.158	0.657	0.423	1.33	2.35	0.332	.110	0.410	0.545	16.35
1299	WW60°	0.9	1.00	4.26	7.9	5.00	0.484	0.856	Bar	.0012	0.550	1.431	1.427	1.300	1.303		0.066	0.573	0.446	1.136	1.467	0.332	.110	0.540	0.266	16.35
1300	WW60°	0.9	1.00	5.25	7.9	5.00	0.484	0.856	Bar	.0012	0.513	1.393	1.395	1.311	1.311		0.029	0.538	0.455	1.060	1.191	0.332	.110	0.663	0.140	16.35
1301	WW60°	0.9	1.00	6.27	7.9	5.00	0.484	0.856	Bar	.0012	0.495	1.370	1.371	1.320	1.319		0.011	0.515	0.464	1.023	1.070	0.332	.110	0.792	0.065	16.35
1269	WW90°	0.9	1.00	2.83	7.9	3.00	0.360	0.855	Bar	.0012	0.544	1.409	1.409	1.164	1.168		0.184	0.554	0.311	1.511	3.451	0.309	.0955	0.358	0.650	21.98
1270	WW90°	0.9	1.00	3.84	7.9	3.00	0.360	0.855	Bar	.0012	0.453	1.323	1.321	1.182	1.182		0.093	0.467	0.327	1.258	1.992	0.309	.0955	0.486	0.310	21.98
1271	WW90°	0.9	1.00	4.87	7.9	3.00	0.360	0.855	Bar	.0012	0.407	1.276	1.278	1.191	1.191		0.047	0.422	0.336	1.131	1.445	0.309	.0955	0.616	0.155	21.98
1272	WW90°	0.9	1.00	5.88	7.9	3.00	0.360	0.855	Bar	.0012	0.381	1.252	1.252	1.199	1.199		0.021	0.397	0.344	1.058	1.185	0.309	.0955	0.742	0.078	21.98
1273	WW90°	0.9	1.00	6.87	7.9	3.00	0.360	0.855	Bar	.0012	0.367	1.240	1.240	1.204	1.203		0.007	0.385	0.349	1.019	1.059	0.309	.0955	0.870	0.031	21.98
1307	WW90°	0.9	1.00	2.84	7.9	5.00	0.484	0.856	Bar	.0012	0.749	1.619	1.619	1.252	1.270		0.265	0.763	0.405	1.548	3.706	0.332	.110	0.359	0.746	16.35
1308	WW90°	0.9	1.00	3.82	7.9	5.00	0.484	0.856	Bar	.0012	0.614	1.489	1.488	1.285	1.290		0.130	0.633	0.432	1.268	2.042	0.332	.110	0.483	0.363	16.35
1309	WW90°	0.9	1.00	4.83	7.9	5.00	0.484	0.856	Bar	.0012	0.546	1.422	1.428	1.306	1.305		0.062	0.569	0.450	1.128	1.436	0.332	.110	0.611	0.185	16.35
1310	WW90°	0.9	1.00	5.87	7.9	5.00	0.484	0.856	Bar	.0012	0.509	1.389	1.390	1.317	1.316		0.025	0.534	0.461	1.052	1.163	0.332	.110	0.741	0.090	16.35
1311	WW90°	0.9	1.00	6.85	7.9	5.00	0.484	0.856	Bar	.0012	0.491	1.370	1.372	1.326	1.323		0.007	0.515	0.469	1.014	1.044	0.332	.110	0.866	0.036	16.35
1284	ST 1:2	0.6	1.00	2.44	7.9	3.00	0.360	0.855	Bar	.0012	0.489	1.357	1.355	1.184	1.178		0.129	0.501	0.326	1.358	2.506	0.309	.0955	0.40	0.501	21.98
1285	ST 1:2	0.6	1.00	3.44	7.9	3.00	0.360	0.855	Bar	.0012	0.425	1.297	1.298	1.189	1.188		0.065	0.443	0.334	1.181	1.645	0.309	.0955	0.525	0.321	21.98
1286	ST 1:2	0.6	1.00	4.48	7.9	3.00	0.360	0.855	Bar	.0012	0.388	1.262	1.263	1.190	1.195		0.028	0.408	0.338	1.078	1.252	0.309	.0955	0.657	0.126	21.98
1287	ST 1:2	0.6	1.00	5.45	7.9	3.00	0.360	0.855	Bar	.0012	0.369	1.240	1.238	1.200	1.199		0.009	0.384	0.345	1.025	1.077	0.309	.0955	0.781	0.058	21.98
1279	ST 1:1	0.9	1.00	2.04	7.9	3.00	0.360	0.855	Bar	.0012	0.568	1.431	1.432	1.172	1.162		0.208	0.577	0.312	1.578	3.928	0.309	.0955	0.304	0.936	21.98
1280	ST 1:1	0.9	1.00	3.04	7.9	3.00	0.360	0.855	Bar	.0012	0.465	1.334	1.335	1.179	1.175		0.105	0.480	0.322	1.292	2.155	0.309	.0955	0.43	0.396	21.98
1281	ST 1:1	0.9	1.00	4.04	7.9	3.00	0.360	0.855	Bar	.0012	0.405	1.278	1.275	1.191	1.190		0.045	0.422	0.336	1.125	1.424	0.309	.0955	0.556	0.213	21.98
1282	ST 1:1	0.9	1.00	5.04	7.9	3.00	0.360	0.855	Bar	.0012	0.379	1.250	1.249	1.198	1.197		0.019	0.395	0.343	1.053	1.167	0.309	.0955	0.682	0.110	21.98
1283	ST 1:1	0.9	1.00	6.04	7.9	3.00	0.360	0.855	Bar	.0012	0.367	1.239	1.233	1.205	1.204		0.007	0.381	0.350	1.019	1.059	0.309	.0955	0.811	0.050	21.98
1312	ST 1:1	0.9	1.00	2.06	7.9	5.00	0.484	0.856	Bar	.0012	0.770	1.637	1.635	1.255	1.272		0.286	0.780	0.408	1.591	4.027	0.332	.110	0.322	0.945	16.35
1313	ST 1:1	0.9	1.00	3.02	7.9	5.00	0.484	0.856	Bar	.0012	0.633	1.505	1.504	1.275	1.288		0.149	0.649	0.426	1.308	2.237	0.332	.110	0.443	0.452	16.35
1314	ST 1:1	0.9	1.00	3.98	7.9	5.00	0.484	0.856	Bar	.0012	0.552	1.430	1.428	1.300	1.306		0.068	0.573	0.447	1.141	1.490	0.332	.110	0.564	0.237	16.35
1315	ST 1:1	0.9	1.00	5.00	7.9	5.00	0.484	0.856	Bar	.0012	0.511	1.388	1.391	1.314	1.310		0.027	0.534	0.456	1.056	1.177	0.332	.110	0.693	0.119	16.

TABLE 2 : ABNORMAL STAGE DISCHARGE CONDITION
45 degree wing-wall abutment

Measured Data														Computed Data											
Run No	Model Type	Model height [ft]	Model length [ft]	b [ft]	B [ft]	Q [cfs]	h_1 [ft]	Bottom Rdg.	Roughness	Slope	% Ponding	h_A [ft]	h_1 [ft]	R_{UR}	R_{UL}	R_{DR}	R_{DL}	h^*_{1A} [ft]	h_U [ft]	h_D [ft]	$\frac{h_1}{h_A}$	$[\frac{h_1}{h_A}]^3$	F_A	F_A^2	M
147A	WW	0.9	1.00	4.46	7.9	4.92	0.484	0.835	Bar	.0012	10	0.532	0.594	1.442	1.439	1.362	1.345	0.062	0.606	0.519	1.115	1.502	0.283	0.080	0.565
148A	WW	0.9	1.00	3.42	7.9	4.92	0.484	0.835	Bar	.0012	10	0.532	0.657	1.509	1.507	1.346	1.345	0.125	0.673	0.511	1.231	1.870	0.288	0.080	0.434
149A	WW	0.9	1.00	2.40	7.9	4.92	0.484	0.835	Bar	.0012	10	0.532	0.800	1.650	1.650	1.292	1.315	0.268	0.815	0.468	1.50	3.39	0.288	0.080	0.304
150A	WW	0.9	1.00	2.40	7.9	4.91	0.484	0.835	Bar	.0012	20	0.581	0.803	1.648	1.646	1.368	1.366	0.222	0.812	0.532	1.381	2.631	0.246	0.060	0.304
151A	WW	0.9	1.00	3.40	7.9	4.90	0.484	0.835	Bar	.0012	20	0.581	0.681	1.536	1.529	1.384	1.402	0.100	0.698	0.558	1.171	1.610	0.246	0.060	0.430
152A	WW	0.9	1.00	4.44	7.9	4.90	0.484	0.835	Bar	.0012	20	0.581	0.621	1.479	1.477	1.395	1.391	0.040	0.643	0.558	1.069	1.22	0.246	0.060	0.561
349	WW	0.9	1.00	2.44	7.9	5.00	0.484	0.834	Bar	.0012	10	0.532	0.809	1.652	1.652	1.313	1.292	0.176	0.818	0.491	1.519	3.500	0.287	0.0822	0.308
350	WW	0.9	1.00	3.42	7.9	5.00	0.484	0.834	Bar	.0012	10	0.532	0.653	1.496	1.497	1.319	1.313	0.121	0.663	0.482	1.229	1.856	0.287	0.0822	0.432
351	WW	0.9	1.00	4.46	7.9	5.00	0.484	0.834	Bar	.0012	10	0.532	0.584	1.433	1.431	1.334	1.326	0.052	0.598	0.496	1.095	1.313	0.287	0.0822	0.564
205	WW	0.9	1.00	2.45	7.9	5.00	0.484	0.834	Bar	.0012	20	0.581	0.796	1.639	1.633	1.380	1.361	0.215	0.802	0.537	1.370	2.56	0.252	0.634	0.310
206	WW	0.9	1.00	3.42	7.9	5.00	0.484	0.834	Bar	.0012	20	0.581	0.701	1.552	1.559	1.412	1.404	0.023	0.722	0.574	1.207	1.755	0.252	0.634	0.433
207	WW	0.9	1.00	4.47	7.9	5.00	0.484	0.834	Bar	.0012	20	0.581	0.637	1.488	1.480	1.407	1.394	0.056	0.650	0.567	1.096	1.310	0.252	0.634	0.565
346	WW	0.9	1.00	4.48	7.9	5.00	0.484	0.834	Bar	.0012	20	0.581	0.616	1.465	1.464	1.392	1.385	0.035	0.631	0.555	1.060	1.195	0.252	0.634	0.567
347	WW	0.9	1.00	3.44	7.9	5.00	0.484	0.834	Bar	.0012	20	0.581	0.674	1.524	1.522	1.372	1.380	0.094	0.689	0.542	1.160	1.561	0.252	0.634	0.435
348	WW	0.9	1.00	2.44	7.9	5.00	0.484	0.834	Bar	.0012	20	0.581	0.817	1.661	1.659	1.352	1.368	0.236	0.826	0.526	1.405	2.780	0.252	0.634	0.309
138	WW	0.9	1.00	3.42	7.9	4.95	0.484	0.835	Bar	.0012	30	0.629	0.723	1.579	1.575	1.453	1.461	0.094	0.742	0.622	1.15	1.52	0.222	0.0494	0.432
139	WW	0.9	1.00	4.46	7.9	4.95	0.484	0.835	Bar	.0012	30	0.629	0.692	1.534	1.527	1.464	1.466	0.063	0.696	0.630	1.100	1.331	0.222	0.0494	0.564
140	WW	0.9	1.00	4.46	7.9	4.98	0.484	0.835	Bar	.0012	30	0.629	0.688	1.538	1.540	1.459	1.477	0.059	0.704	0.633	1.092	1.310	0.223	0.0495	0.564
141	WW	0.9	1.00	3.42	7.9	4.96	0.484	0.835	Bar	.0012	30	0.629	0.731	1.569	1.567	1.460	1.469	0.102	0.733	0.630	1.161	1.570	0.224	0.0494	0.433
208	WW	0.9	1.00	2.42	7.9	4.98	0.484	0.834	Bar	.0012	30	0.629	0.813	1.653	1.653	1.390	1.405	0.184	0.819	0.564	1.291	2.155	0.223	0.0495	0.306
209	WW	0.9	1.00	3.44	7.9	4.96	0.484	0.834	Bar	.0012	30	0.629	0.695	1.541	1.540	1.417	1.421	0.066	0.707	0.585	1.105	1.350	0.222	0.0494	0.435
210	WW	0.9	1.00	4.46	7.9	4.94	0.484	0.834	Bar	.0012	30	0.629	0.656	1.507	1.503	1.436	1.427	0.027	0.671	0.598	1.045	1.145	0.221	0.0490	0.564
336A	WW	0.9	1.00	4.46	7.9	5.00	0.484	0.834	Bar	.0012	30	0.629	0.660	1.504	1.503	1.439	1.432	0.031	0.670	0.602	1.15	1.155	0.2235	0.0499	0.565
337	WW	0.9	1.00	3.42	7.9	5.00	0.484	0.834	Bar	.0012	30	0.629	0.709	1.554	1.552	1.436	1.440	0.080	0.719	0.604	1.128	1.44	0.2235	0.0499	0.433
356	WW	0.9	1.00	2.42	7.9	5.00	0.484	0.834	Bar	.0012	30	0.629	0.821	1.662	1.661	1.422	1.406	0.192	0.828	0.580	1.306	2.24	0.2235	0.0499	0.306
329	WW	0.9	1.00	4.44	7.9	5.00	0.484	0.834	Bar	.0012	40	0.678	0.712	1.559	1.559	1.496	1.490	0.034	0.725	0.659	1.050	1.160	0.200	0.040	0.562
330	WW	0.9	1.00	3.36	7.9	5.00	0.484	0.834	Bar	.0012	40	0.678	0.743	1.592	1.588	1.484	1.492	0.065	0.756	0.654	1.095	1.313	0.200	0.040	0.425
335	WW	0.9	1.00	2.42	7.9	5.00	0.484	0.834	Bar	.0012	40	0.678	0.838	1.680	1.678	1.464	1.484	0.160	0.845	0.640	1.235	1.890	0.200	0.040	0.306
362	WW	0.6	1.00	5.90	7.9	2.50	0.333	0.834	Bar	.0012	6.9	0.356	0.368	1.213	1.211	1.182	1.182	0.012	0.378	0.348	1.035	1.1087	0.2617	0.0685	0.747
363	WW	0.6	1.00	4.89	7.9	2.50	0.333	0.834	Bar	.0012	6.9	0.356	0.376	1.223	1.219	1.177	1.175	0.020	0.387	0.342	1.057	1.180	0.2617	0.0685	0.618
364	WW	0.6	1.00	3.89	7.9	2.50	0.333	0.834	Bar	.0012	6.9	0.356	0.405	1.251	1.248	1.169	1.164	0.049	0.416	0.333	1.139	1.47	0.2617	0.0685	0.492
365	WW	0.6	1.00	2.90	7.9	2.50	0.333	0.866	Bar	.0012	6.9	0.356	0.464	1.337	1.333	1.189	1.186	0.108	0.469	0.322	1.300	2.197	0.2617	0.0685	0.366
366	WW	0.6	1.00	1.89	7.9	2.50	0.333	0.866	Bar	.0012	6.9	0.356	0.602	1.473	1.475	1.186	1.162	0.246	0.608	0.308	1.695	4.87	0.2617	0.0685	0.239
367	WW	0.9	1.00	2.86	7.9	2.50	0.333	0.866	Bar	.0012	6.9	0.356	0.466	1.338	1.338	1.194	1.185	0.110	0.472	0.324	1.310	2.250	0.2617	0.0685	0.362
378	WW	0.6	1.00	5.92	7.9	2.50	0.333	0.866	Bar	.0012	20	0.400	0.406	1.278	1.276	1.257	1.257	0.006	0.411	0.391	1.015	1.046	0.2205	0.0486	0.750
379	WW	0.6	1.00	4.92	7.9	2.50	0.333	0.866	Bar	.0012	20	0.400	0.415	1.285	1.290	1.256	1.254	0.015	0.422	0.389	1.039	1.122	0.2205	0.0486	0.622
380	WW	0.6	1.00	3.92	7.9	2.50	0.333	0.866	Bar	.0012	20	0.400	0.433	1.310	1.306	1.252	1.249	0.033	0.442	0.385	1.083	1.270	0.2205	0.0486	0.496
381	WW	0.6	1.00	2.90	7.9	2.50	0.333	0.866	Bar	.0012	20	0.400	0.476	1.350	1.350	1.250	1.240	0.076	0.484	0.379	1.190	1.689	0.2205	0.0486	0.367
382	WW	0.6	1.00	1.90	7.9	2.50	0.333	0.866	Bar	.0012	20	0.400	0.614	1.487	1.487	1.228	1.240	0.214	0.621	0.368	1.535	3.600	0.2205	0.0486	0.240
383	WW	0.6	1.00	5.90	7.9	2.50	0.333	0.866	Bar	.0012	30	0.433	0.436	1.311	1.311	1.292	1.290	0.003	0.445	0.425	1.007	1.025	0.196	0.0384	0.746
384	WW	0.6	1.00	4.92	7.9	2.50	0.333	0.866	Bar	.0012	30	0.433	0.445	1.320	1.319	1.287	1.287	0.012	0.454	0.421	1.030	1.093	0.196	0.0384	0.622
385	WW	0.6	1.00	3.90	7.9	2.50	0.333	0.866	Bar	.0012	30	0.433	0.459	1.333	1.333	1.285	1.283	0.026	0.467	0.418	1.060	1.190	0.196	0.0384	0.494
386	WW	0.6	1.00	2.90	7.9	2.50	0.333	0.866	Bar	.0012	30	0.433	0.492	1.367	1.367	1.276	1.280	0.059	0.501	0.412	1.137	1.468	0.196	0.0384	0.367

TABLE 2 : ABNORMAL STAGE DISCHARGE CONDITION
1:1.5 spill-through abutment

Measured Data														Computed Data											
Run No	Model Type	Model height [ft]	Model length [ft]	b [ft]	B [ft]	Q [cfs]	h_n [ft]	Bottom Rdg.	Roughness	Slope	% Ponding	h_A [ft]	h_1 [ft]	R_{UR}	R_{UL}	R_{DR}	R_{DL}	h^*_{1A} [ft]	h_U [ft]	h_D [ft]	$\frac{h_1}{h_A}$	$\left[\frac{h_1}{h_A}\right]^3$	F_A	F_A^2	M
146A	ST	0.9	1.00	4.17	7.9	4.97	0.484	0.835	Bar	.0012	10	0.532	0.587	1.443	1.431	1.363	1.361	0.055	0.602	0.527	1.103	1.342	0.286	0.0818	0.630
352	ST	0.9	1.00	5.17	7.9	5.00	0.484	0.834	Bar	.0012	10	0.532	0.548	1.401	1.395	1.349	1.351	0.016	0.564	0.516	1.03	1.093	0.288	0.083	0.756
353	ST	0.9	1.00	4.13	7.9	5.00	0.484	0.834	Bar	.0012	10	0.532	0.577	1.427	1.425	1.333	1.333	0.045	0.592	0.499	1.084	1.273	0.288	0.083	0.624
354	ST	0.9	1.00	3.17	7.9	5.00	0.484	0.834	Bar	.0012	10	0.532	0.628	1.478	1.477	1.330	1.316	0.096	0.644	0.489	1.178	1.641	0.288	0.083	0.502
355	ST	0.9	1.00	2.19	7.9	5.00	0.484	0.834	Bar	.0012	10	0.532	0.737	1.580	1.580	1.300	1.320	0.205	0.746	0.476	1.384	2.6521	0.288	0.083	0.378
342	ST	0.9	1.00	2.17	7.9	5.00	0.484	0.834	Bar	.0012	20	0.581	0.751	1.593	1.588	1.358	1.367	0.170	0.757	0.529	1.293	2.162	0.252	0.633	0.385
343	ST	0.9	1.00	3.17	7.9	5.00	0.484	0.834	Bar	.0012	20	0.581	0.660	1.508	1.504	1.376	1.386	0.079	0.672	0.547	1.136	1.467	0.252	0.0633	0.511
344	ST	0.9	1.00	4.17	7.9	5.00	0.484	0.834	Bar	.0012	20	0.581	0.615	1.460	1.462	1.393	1.395	0.034	0.627	0.560	1.059	1.19	0.252	0.0633	0.637
345	ST	0.9	1.00	5.21	7.9	5.00	0.484	0.834	Bar	.0012	20	0.581	0.596	1.439	1.437	1.403	1.404	0.015	0.604	0.570	1.026	1.080	0.252	0.0633	0.770
142	ST	0.9	1.00	3.33	7.9	4.90	0.484	0.835	Bar	.0012	30	0.629	0.685	1.534	1.523	1.418	1.440	0.056	0.694	0.594	1.090	1.300	0.219	0.048	0.541
143	ST	0.9	1.00	5.17	7.9	4.95	0.484	0.835	Bar	.0012	30	0.629	0.639	1.478	1.477	1.450	1.444	0.010	0.643	0.612	1.017	1.050	0.221	0.049	0.774
144	ST	0.9	3.00	5.17	7.9	4.99	0.484	0.835	Bar	.0012	30	0.629	0.634	1.481	1.480	1.459	1.448	0.005	0.646	0.619	1.006	1.018	0.219	0.048	0.774
145	ST	0.9	3.00	4.17	7.9	4.93	0.484	0.835	Bar	.0012	30	0.629	0.643	1.498	1.493	1.453	1.453	0.014	0.661	0.618	1.022	1.067	0.220	0.0485	0.649
338	ST	0.9	1.00	5.29	7.9	5.00	0.484	0.834	Bar	.0012	30	0.629	0.637	1.484	1.479	1.455	1.456	0.008	0.648	0.622	1.014	1.043	0.224	0.050	0.789
339	ST	0.9	1.00	4.15	7.9	5.00	0.484	0.834	Bar	.0012	30	0.629	0.655	1.501	1.496	1.448	1.443	0.026	0.665	0.612	1.041	1.1281	0.2245	0.050	0.645
340	ST	0.9	1.00	3.21	7.9	5.00	0.484	0.834	Bar	.0012	30	0.629	0.685	1.531	1.532	1.436	1.422	0.056	0.698	0.595	1.089	1.290	0.2245	0.050	0.526
341	ST	0.9	1.00	2.17	7.9	5.00	0.484	0.834	Bar	.0012	30	0.629	0.769	1.616	1.614	1.417	1.434	0.140	0.781	0.592	1.222	1.825	0.224	0.050	0.394
331	ST	0.9	1.00	5.17	7.9	5.00	0.484	0.834	Bar	.0012	40	0.678	0.683	1.523	1.521	1.503	1.504	0.005	0.688	0.670	1.008	1.024	0.1994	0.398	0.784
332	ST	0.9	1.00	4.19	7.9	5.00	0.484	0.834	Bar	.0012	40	0.678	0.696	1.539	1.537	1.495	1.496	0.018	0.704	0.662	1.027	1.084	0.1994	0.398	0.660
333	ST	0.9	1.00	3.17	7.9	5.00	0.484	0.834	Bar	.0012	40	0.678	0.722	1.567	1.564	1.484	1.496	0.044	0.732	0.656	1.066	1.205	0.1994	0.398	0.529
334	ST	0.9	1.00	2.17	7.9	5.00	0.484	0.834	Bar	.0012	40	0.678	0.791	1.635	1.635	1.472	1.485	0.113	0.801	0.645	1.166	1.584	0.1994	0.398	0.404
368	ST	0.6	1.00	1.85	7.9	2.5	0.333	0.866	Bar	.0012	6.9	0.356	0.535	1.407	1.406	1.189	1.181	0.179	0.541	0.319	1.503	3.394	0.262	0.0685	0.302
369	ST	0.6	1.00	2.85	7.9	2.5	0.333	0.866	Bar	.0012	6.9	0.356	0.439	1.311	1.312	1.195	1.194	0.083	0.446	0.329	1.231	1.860	0.262	0.0685	0.428
370	ST	0.6	1.00	3.85	7.9	2.5	0.333	0.866	Bar	.0012	6.9	0.356	0.397	1.274	1.272	1.206	1.206	0.041	0.407	0.340	1.115	1.390	0.262	0.0688	0.555
371	ST	0.6	1.00	4.85	7.9	2.5	0.333	0.866	Bar	.0012	6.9	0.356	0.372	1.253	1.252	1.211	1.210	0.016	0.387	0.345	1.045	1.141	0.262	0.0688	0.681
372	ST	0.6	1.00	5.85	7.9	2.5	0.333	0.866	Bar	.0012	6.9	0.356	0.364	1.237	1.232	1.215	1.215	0.008	0.369	0.349	1.021	1.060	0.262	0.0688	0.809
373	ST	0.6	1.00	5.87	7.9	2.5	0.333	0.866	Bar	.0012	20	0.400	0.403	1.275	1.276	1.260	1.261	0.003	0.410	0.395	1.008	1.026	0.220	0.0484	0.820
374	ST	0.6	1.00	4.87	7.9	2.5	0.333	0.866	Bar	.0012	20	0.400	0.409	1.288	1.284	1.259	1.257	0.009	0.420	0.392	1.023	1.070	0.220	0.0484	0.692
375	ST	0.6	1.00	3.87	7.9	2.5	0.333	0.866	Bar	.0012	20	0.400	0.425	1.300	1.299	1.252	1.251	0.025	0.433	0.386	1.063	1.200	0.220	0.0484	0.566
376	ST	0.6	1.00	2.87	7.9	2.5	0.333	0.866	Bar	.0012	20	0.400	0.463	1.339	1.336	1.249	1.243	0.063	0.472	0.380	1.158	1.550	0.220	0.0484	0.440
377	ST	0.6	1.00	1.85	7.9	2.5	0.333	0.866	Bar	.0012	20	0.400	0.540	1.411	1.411	1.244	1.240	0.140	0.545	0.376	1.350	2.460	0.220	0.0484	0.323
387	ST	0.6	1.00	5.90	7.9	2.5	0.333	0.866	Bar	.0012	30	0.433	0.435	1.306	1.302	1.295	1.295	0.002	0.438	0.429	1.005	1.01	0.196	0.0384	0.829
388	ST	0.6	1.00	4.88	7.9	2.5	0.333	0.866	Bar	.0012	30	0.433	0.439	1.312	1.310	1.288	1.289	0.006	0.445	0.423	1.013	1.048	0.196	0.0384	0.700
389	ST	0.6	1.00	3.88	7.9	2.5	0.333	0.866	Bar	.0012	30	0.433	0.452	1.327	1.325	1.289	1.289	0.019	0.460	0.423	1.044	1.145	0.196	0.0384	0.573
390	ST	0.6	1.00	2.88	7.9	2.5	0.333	0.866	Bar	.0012	30	0.433	0.484	1.356	1.357	1.287	1.279	0.051	0.491	0.417	1.118	1.395	0.196	0.0384	0.446
391	ST	0.6	1.00	1.87	7.9	2.5	0.333	0.866	Bar	.0012	30	0.433	0.548	1.417	1.420	1.270	1.282	0.115	0.553	0.410	1.267	2.04	0.196	0.0384	0.319

TABLE 2 : ABNORMAL STAGE DISCHARGE CONDITION
vertical board model

Run No	Model Type	Model height [ft]	Model length [ft]	b [ft]	B [ft]	Q [cfs]	h _n [ft]	Bottom Rdg.	Roughness	Slope	% Ponding	h _A [ft]	h ₁ [ft]	R _{UR}	R _{UL}	R _{DR}	R _{DL}	Computed Data								
																		h* _{1A} [ft]	h _U [ft]	h _D [ft]	$\frac{h_1}{h_A}$	$[\frac{h_1}{h_A}]^3$	F _A	F _A ²	M	
306	VB	1.67	-	2.00	7.9	5.00	0.484	0.834	Bar	.0012	10	0.532	0.972	1.818	1.812	1.309	1.270	0.440	0.981	0.456	1.825	6.078	0.2875	0.0827	0.253	
307	VB	1.67	-	3.00	7.9	5.00	0.484	0.834	Bar	.0012	10	0.532	0.778	1.620	1.617	1.314	1.289	0.246	0.785	0.468	1.463	3.131	0.2857	0.0827	0.380	
308	VB	1.67	-	4.00	7.9	5.00	0.484	0.834	Bar	.0012	10	0.532	0.665	1.509	1.507	1.322	1.307	0.133	0.674	0.481	1.250	1.953	0.2875	0.0827	0.506	
309A	VB	1.67	-	5.00	7.9	5.00	0.484	0.834	Bar	.0012	10	0.532	0.598	-	-	-	-	0.066	-	-	1.122	1.420	0.2875	0.0827	0.633	
310	VB	1.67	-	6.00	7.9	5.00	0.484	0.834	Bar	.0012	10	0.532	0.560	1.413	1.406	1.339	1.332									
311	VB	1.67	-	6.00	7.9	5.00	0.484	0.834	Bar	.0012	20	0.581	0.600	1.449	1.442	1.391	1.383									
312	VB	1.67	-	5.00	7.9	5.01	0.484	0.834	Bar	.0012	20	0.581	0.642	1.494	1.479	1.396	1.375									
313	VB	1.67	-	4.00	7.9	5.00	0.484	0.834	Bar	.0012	20	0.581	0.696	1.545	1.531	1.389	1.360									
314	VB	1.67	-	6.00	7.9	5.00	0.484	0.834	Bar	.0012	20	0.581	0.603	1.450	1.442	1.393	1.385	0.022	0.612	0.555	1.038	1.118	0.2516	0.0633	0.760	
315	VB	1.67	-	5.00	7.9	5.00	0.484	0.834	Bar	.0012	20	0.581	0.638	1.486	1.485	1.377	1.375	0.057	0.652	0.542	1.098	1.324	0.2516	0.0633	0.633	
316	VB	1.67	-	4.00	7.9	5.00	0.484	0.834	Bar	.0012	20	0.581	0.692	1.540	1.539	1.365	1.378	0.111	0.706	0.538	1.191	1.698	0.2516	0.0633	0.506	
317	VB	1.67	-	3.00	7.9	5.00	0.484	0.834	Bar	.0012	20	0.581	0.796	1.639	1.632	1.349	1.370	0.215	0.802	0.526	1.371	2.577	0.2516	0.0633	0.380	
318	VB	1.67	-	2.00	7.9	5.00	0.484	0.834	Bar	.0012	20	0.581	0.992	1.830	1.834	1.366	1.325	0.411	0.998	0.512	1.709	4.992	0.2516	0.0633	0.253	
319	VB	1.67	-	2.00	7.9	5.00	0.484	0.834	Bar	.0012	30	0.629	1.008	1.846	1.846	1.423	1.386	0.379	1.012	0.571	1.604	4.127	0.2234	0.0499	0.253	
320	VB	1.67	-	3.00	7.9	5.00	0.484	0.834	Bar	.0012	30	0.629	0.817	1.660	1.653	1.424	1.407	0.188	0.823	0.582	1.299	2.192	0.2234	0.0499	0.380	
321	VB	1.67	-	4.00	7.9	5.00	0.484	0.834	Bar	.0012	30	0.629	0.723	1.568	1.566	1.432	1.416	0.094	0.733	0.590	1.150	1.521	0.2234	0.0499	0.506	
322	VB	1.67	-	5.00	7.9	5.00	0.484	0.834	Bar	.0012	30	0.629	0.677	1.520	1.518	1.439	1.429	0.048	0.685	0.600	1.076	1.246	0.2234	0.0499	0.633	
323	VB	1.67	-	6.00	7.9	5.00	0.484	0.834	Bar	.0012	30	0.629	0.643	1.498	1.482	1.439	1.433	0.014	0.652	0.602	1.022	1.067	0.2234	0.0499	0.760	
324	VB	1.67	-	6.00	7.9	5.00	0.484	0.834	Bar	.0012	40	0.678	0.683	1.529	1.522	1.483	1.475	0.005	0.692	0.645	1.007	1.021	0.1994	0.0398	0.760	
325	VB	1.67	-	5.00	7.9	5.00	0.484	0.834	Bar	.0012	40	0.678	0.714	1.558	1.557	1.490	1.478	0.036	0.724	0.650	1.053	1.168	0.1994	0.0398	0.633	
326	VB	1.67	-	4.00	7.9	5.00	0.484	0.834	Bar	.0012	40	0.678	0.760	1.603	1.602	1.474	1.485	0.082	0.769	0.646	1.119	1.401	0.1994	0.0398	0.506	
327	VB	1.67	-	3.00	7.9	5.00	0.484	0.834	Bar	.0012	40	0.678	0.842	1.685	1.678	1.478	1.456	0.164	0.848	0.633	1.243	1.921	0.1994	0.0398	0.380	
328	VB	1.67	-	2.00	7.9	5.00	0.484	0.834	Bar	.0012	40	0.678	1.029	1.869	1.866	1.468	1.435	0.351	1.033	0.618	1.517	3.491	0.1994	0.0398	0.253	
743	VB	1.66	-	6.00	7.9	5.00	-	0.859	Baffle	0.00	-	0.796	0.804	1.670	1.669	1.639	1.640	0.811	0.781	1.009	1.03	0.157	0.0247	0.760		
744	VB	1.66	-	5.00	7.9	5.00	-	0.859	Baffle	0.00	-	0.805	0.824	1.687	1.688	1.634	1.640	0.829	0.778	1.021	1.065	0.155	0.024	0.633		
745	VB	1.66	-	4.00	7.9	5.00	-	0.859	Baffle	0.00	-	0.827	0.855	1.719	1.715	1.641	1.626	0.858	0.775	1.031	1.10	0.148	0.022	0.505		
746	VB	1.66	-	3.00	7.9	5.00	-	0.859	Baffle	0.00	-	0.863	0.918	1.782	1.781	1.618	1.632	0.923	0.766	1.063	1.200	0.139	0.0194	0.380		
747	VB	1.66	-	6.00	7.9	2.50	-	0.859	Bar	0.00	-	0.420	0.428	1.291	1.288	1.266	1.259	0.431	0.404	1.019	1.055	0.200	0.040	0.760		
748	VB	1.66	-	4.00	7.9	2.50	-	0.859	Bar	0.00	-	0.450	0.475	1.339	1.337	1.260	1.250	0.479	0.396	1.055	1.175	0.186	0.0348	0.505		
749	VB	1.66	-	3.00	7.9	2.50	-	0.859	Bar	0.00	-	0.486	0.527	1.393	1.387	1.249	1.251	0.531	0.391	1.084	1.28	0.167	0.0279	0.380		
750	VB	1.66	-	6.00	7.9	5.00	-	0.859	Bar	0.00	-	0.501	0.524	1.396	1.392	1.310	1.301	0.535	0.447	1.041	1.140	0.315	0.099	0.760		
751	VB	1.66	-	5.00	7.9	5.00	-	0.859	Bar	0.00	-	0.524	0.565	1.443	1.441	1.300	1.287	0.583	0.435	1.080	1.255	0.295	0.087	0.633		
752	VB	1.66	-	4.00	7.9	5.00	-	0.859	Bar	0.00	-	0.574	0.637	1.506	1.498	1.289	1.266	0.643	0.419	1.110	1.365	0.259	0.067	0.505		
753	VB	1.66	-	3.00	7.9	5.00	-	0.859	Bar	0.00	-	0.669	0.743	1.610	1.604	1.275	1.249	0.748	0.403	1.110	1.365	0.204	0.0416	0.380		

TABLE 3: DUAL BRIDGES CROSSING
45 degree wing-wall abutment and 1:1.5 spill-through abutment

Run No	Model Type	Model height [ft]	Model length [ft]	b [ft]	B [ft]	Q [cfs]	h _n	Bottom Rdg.	Roughness	Slope	L _D [ft]	h ₁ [ft]	Measured Data		Computed Data																		
													Upstream abutment		Downstream abutment		Upstream abutment		Downstream abutment		h ₁ ** [ft]	h _U [ft]	h _D [ft]	h _U [ft]	h _D [ft]	h ₁ ** / h _n	L _D / b	L _D / h _n	(h ₁ / h _n) ³	F _n	F _n ²	M	[1/M ² -1]F _n ²
													R _{Uav.}	R _{DAv.}	R _{Uav.}	R _{DAv.}	R _{Uav.}	R _{DAv.}	R _{Uav.}	R _{DAv.}													
809	2WW	0.9	1.00	4.46	7.9	2.50	0.333	0.855	Bar	.0012	3.33	0.384	1.250	1.185	1.185	1.161	0.051	0.395	0.330	0.330	0.308	0.153	0.753	10.00	1.532	0.289	.0835	0.566	0.177				
833	2WW	0.9	1.00	2.42	7.9	2.50	0.333	0.855	Bar	.0012	3.33	0.528	1.390	1.270	1.270	1.143	0.195	0.535	0.415	0.415	0.288	1.585	1.378	10.00	3.982	0.289	.0835	0.306	0.810				
840	2WW	0.9	1.00	2.42	7.9	2.50	0.333	0.855	Bar	.0012	10.00	0.550	1.410	1.308	1.321	1.150	0.055	0.400	0.327	0.344	0.310	0.165	2.26	30.00	1.581	0.289	.0835	0.559	1.184				
816R	2WW	0.9	1.00	4.42	7.9	2.50	0.333	0.855	Bar	.0012	10.00	0.388	1.255	1.182	1.199	1.165	0.217																
960	2WW	0.9	1.00	2.42	7.9	2.50	0.333	0.855	Bar	.0012	10.00	0.544	1.410	1.309	1.325	1.150	0.211	0.555	0.454	0.470	0.295	0.633	4.13	30.00	4.358	0.289	.0835	0.305	0.808				
967	2WW	0.9	1.00	2.42	7.9	2.50	0.333	0.855	Bar	.0012	10.00	0.529	1.396	1.292	1.311	1.151	0.196																
1329	2WW	0.6	1.00	2.85	7.9	3.00	0.370	0.855	Bar	.0012	3.33	0.540	1.405	1.284	1.293	1.179	0.170	0.550	0.429	0.438	0.324	0.468	1.170	9.00	3.102	0.297	.0882	0.360	0.592				
1330	2WW	0.6	1.00	3.87	7.9	3.00	0.370	0.855	Bar	.0012	3.33	0.451	1.320	1.235	1.240	1.192	0.081	0.465	0.380	0.385	0.337	0.219	0.860	9.00	1.811	0.297	.0882	0.490	0.279				
1331	2WW	0.6	1.00	4.87	7.9	3.00	0.370	0.855	Bar	.0012	3.33	0.409	1.280	1.220	1.218	1.200	0.039	0.425	0.363	0.365	0.345	0.105	0.683	9.00	1.349	0.297	.0882	0.617	0.144				
1332	2WW	0.6	1.00	5.90	7.9	3.00	0.370	0.855	Bar	.0012	3.33	0.386	1.260	1.216	1.220	1.208	0.016	0.405	0.361	0.365	0.353	0.043	0.564	9.00	1.140	0.297	.0882	0.747	0.0696				
1333	2WW	0.6	1.00	2.85	7.9	3.00	0.370	0.855	Bar	.0012	6.66	0.544	1.410	1.302	1.324	1.178	0.174	0.555	0.447	0.469	0.323	0.471	2.340	18.00	3.177	0.297	.0882	0.360	0.592				
1334	2WW	0.6	1.00	3.85	7.9	3.00	0.370	0.855	Bar	.0012	6.66	0.459	1.328	1.249	1.262	1.192	0.089	0.473	0.394	0.407	0.337	0.240	1.730	18.08	1.900	0.297	.0882	0.486	0.283				
1335	2WW	0.6	1.00	4.87	7.9	3.00	0.370	0.855	Bar	.0012	6.66	0.413	1.283	1.223	1.235	1.200	0.043	0.428	0.368	0.380	0.345	0.116	1.368	18.08	1.389	0.297	.0882	0.616	0.144				
1336	2WW	0.6	1.00	5.87	7.9	3.00	0.370	0.855	Bar	.0012	6.66	0.390	1.260	1.218	1.232	1.207	0.020	0.405	0.363	0.377	0.352	0.054	1.134	18.08	1.171	0.297	.0882	0.743	0.072				
1337	2WW	0.6	1.00	2.85	7.9	3.00	0.370	0.855	Bar	.0012	10.00	0.560	1.425	1.327	1.359	1.173	0.190	0.570	0.472	0.504	0.318	0.514	3.510	27.03	3.470	0.297	.0882	0.360	0.592				
1338	2WW	0.6	1.00	3.85	7.9	3.00	0.370	0.855	Bar	.0012	10.00	0.464	1.330	1.243	1.263	1.192	0.094	0.475	0.388	0.408	0.337	0.254	2.595	27.03	1.973	0.297	.0882	0.487	0.284				
1339	2WW	0.6	1.00	4.87	7.9	3.00	0.370	0.855	Bar	.0012	10.00	0.419	1.288	1.224	1.243	1.198	0.049	0.433	0.369	0.388	0.343	0.133	2.051	27.03	1.450	0.297	.0882	0.616	0.144				
1340	2WW	0.6	1.00	5.87	7.9	3.00	0.370	0.855	Bar	.0012	10.00	0.389	1.259	1.218	1.240	1.208	0.019	0.404	0.363	0.385	0.353	0.051	1.701	27.03	1.160	0.297	.0882	0.743	0.072				
895R	2WW	0.9	1.00	4.42	7.9	5.00	0.484	0.855	Bar	.0012	3.33	0.566	1.443	1.325	1.326	1.293	0.082	0.588	0.470	0.471	0.438	0.169	0.753	6.88	1.600	0.332	.110	0.559	0.242				
902	2WW	0.9	1.00	2.42	7.9	5.00	0.484	0.855	Bar	.0012	3.33	0.817	1.688	1.499	1.510	1.249	0.333	0.833	0.644	0.655	0.394	0.688	1.378	6.88	4.810	0.332	.110	0.306	1.069				
909	2WW	0.9	1.00	2.42	7.9	5.00	0.484	0.855	Bar	.0012	10.00	0.845	1.714	1.556	1.590	1.266	0.361	0.859	0.701	0.735	0.411	0.745	4.13	20.6	5.314	0.332	.110	0.306	1.069				
916RR	2WW	0.9	1.00	4.42	7.9	5.00	0.484	0.855	Bar	.0012	10.00	0.579	1.453	1.344	1.374	1.303	0.095	0.598	0.489	0.519	0.448	0.196	2.26	20.6	1.711	0.332	.110	0.560	0.241				
1325	2ST	0.9	1.00	2.14	7.9	5.00	0.484	0.856	Bar	.0012	3.75	0.730	1.598	1.381	1.377	1.270	0.246	0.742	0.525	0.521	0.414	0.508	1.752	7.750	3.431	0.332	.110	0.364	0.722				
1326	2ST	0.9	1.00	3.17	7.9	5.00	0.484	0.856	Bar	.0012	3.75	0.621	1.493	1.344	1.351	1.291	0.137	0.637	0.488	0.495	0.435	0.283	1.182	7.750	2.110	0.332	.110	0.492	0.345				
1327	2ST	0.9	1.00	4.13	7.9	5.00	0.484	0.856	Bar	.0012	3.75	0.542	1.422	1.316	1.315	1.312	0.058	0.566	0.460	0.459	0.456	0.120	0.909	7.750	1.404	0.332	.110	0.616	0.179				
1328	2ST	0.9	1.00	5.17	7.9	5.00	0.484	0.856	Bar	.0012	3.75	0.509	1.384	1.328	1.330	1.318	0.025	0.528	0.472	0.474	0.462	0.0516	0.725	7.750	1.163	0.332	.110	0.745	0.089				
1321	2ST	0.9	1.00	2.13	7.9	5.00	0.484	0.856	Bar	.0012	6.66	0.750	1.619	1.472	1.498	1.274	0.266	0.763	0.616	0.642	0.418	0.549	3.126	13.76	3.74	0.332	.110	0.361	0.736				
1322R	2ST	0.9	1.00	3.15	7.9	5.00	0.484	0.856	Bar	.0012	6.66	0.626	1.502	1.364	1.401	1.296	0.142	0.646	0.508	0.545	0.440	0.293	2.121	13.76	2.163	0.332	.110	0.490	0.348				
1323	2ST	0.9	1.00	4.15	7.9	5.00	0.484	0.856	Bar	.0012	6.66	0.553	1.430	1.331	1.345	1.313	0.069	0.574	0.475	0.489	0.457	0.143	1.612	13.76	1.491	0.332	.110	0.615	0.182				
1324	2ST	0.9	1.00	5.15	7.9	5.00	0.484	0.856	Bar	.0012	6.66	0.516	1.390	1.329	1.352	1.323	0.032	0.534	0.473	0.496	0.467	0.0661	1.293	13.76	1.212	0.332	.110	0.744	0.089				
1317	2ST	0.9	1.00	2.15	7.9	5.00	0.484	0.856	Bar	.0012	10.00	0.749	1.819	1.459	1.491	1.280	0.265	0.963	0.603	0.635	0.424	0.547	3.48	20.66	3.706	0.332	.110	0.366	0.710				
1318	2ST	0.9	1.00	3.17	7.9	5.00	0.484	0.856	Bar	.0012	10.00	0.624	1.497	1.368	1.399	1.296	0.140	0.641	0.512	0.543	0.440	0.289	3.154	20.66	2.143	0.332	.110	0.492	0.346				
1319	2ST	0.9	1.00	4.27	7.9	5.00	0.484	0.856	Bar	.0012	10.00	0.552	1.427	1.336	1.364	1.312	0.068	0.571	0.480	0.508	0.456	0.143	2.398	20.66	1.483	0.332	.110	0.617	0.179				
1320	2ST	0.9	1.00	5.17	7.9	5.00	0.484	0.856	Bar	.0012	10.00	0.514	1.390	1.332	1.365	1.323	0.030	0.534	0.476	0.509	0.467	0.0619	1.930	20.66	1.197	0.332	.110	0.744	0.089				

TABLE 4 PARTIALLY SUBMERGED BRIDGE GIRDER
45 degree wing-wall abutment and 1:1.5 spill-through abutment

Measured Data													Computed Data											
Run No	Model Type	Model height [ft]	Model length [ft]	b [ft]	B [ft]	Q [cfs]	h_n [ft]	Bottom Rdg.	Roughness	Slope	z [ft]	h_1 [ft]	R_{UR}	R_{UL}	R_{DR}	R_{DL}	h_1^* [ft]	h_U [ft]	h_D [ft]	M	$\frac{z}{h_1}$	F_n	M^*	
807	WW	0.9	1.00	4.46	7.9	2.50	0.333	0.855	Bar	.0012	0.316	0.392	1.262	1.254	1.163	1.161	0.059	0.403	0.307	0.565	0.806	0.289	0.492	
830	WW	0.9	1.00	2.42	7.9	2.50	0.333	0.855	Bar	.0012	0.348	0.575	-	-	-	-	0.242	-	-	0.306	0.605	0.289	0.290	
831	WW	0.9	1.00	2.42	7.9	2.50	0.333	0.855	Bar	.0012	0.392	0.515	-	-	-	-	0.182	-	-	0.306	0.761	0.289	0.298	
760	WW	0.9	1.00	3.44	7.9	5.00	0.484	0.863	Bar	.0012	0.530	-	1.548	-	-	-	-	-	-	-	-	-	-	-
788	WW	0.9	1.00	2.44	7.9	2.50	0.523	0.855	Baffle	.0012	0.519	0.613	1.478	1.473	1.360	1.357	0.090	0.621	0.504	0.309	0.846	0.147	0.496	
789	WW	0.9	1.00	2.44	7.9	2.50	0.523	0.855	Baffle	.0012	0.508	0.623	1.485	1.485	1.363	1.358	0.100	0.630	0.506	0.309	0.815	0.147	0.481	
1353	WW	0.6	1.00	3.85	7.9	3.00	0.369	0.855	Bar	.0012	0.372	0.441	1.312	1.309	1.192	1.185	0.072	0.456	0.334	0.487	0.845	0.298	0.479	
1356	WW	0.6	1.00	2.85	7.9	3.00	0.369	0.855	Bar	.0012	0.426	0.526	1.392	1.391	1.175	1.168	0.157	0.537	0.317	0.360	0.810	0.298	0.352	
1357	WW	0.6	1.00	2.85	7.9	3.00	0.369	0.855	Bar	.0012	0.371	0.590	1.457	1.454	1.164	1.167	0.220	0.601	0.311	0.360	0.629	0.298	0.313	
1358	WW	0.6	1.00	2.85	7.9	3.00	0.369	0.855	Bar	.0012	0.397	0.555	1.419	1.421	1.169	1.165	0.186	0.565	0.312	0.360	0.715	0.298	0.330	
1359	WW	0.6	1.00	2.85	7.9	3.00	0.369	0.855	Bar	.0012	0.431	0.521	1.385	1.386	1.187	1.170	0.152	0.531	0.324	0.360	0.829	0.298	0.356	
893	WW	0.9	1.00	4.46	7.9	5.00	0.484	0.855	Bar	.0012	0.482	0.559	1.442	1.432	1.294	1.288	0.075	0.582	0.436	0.565	0.863	0.332	0.551	
894	WW	0.9	1.00	4.46	7.9	5.00	0.484	0.855	Bar	.0012	0.470	0.563	1.446	1.439	1.296	1.291	0.079	0.588	0.439	0.565	0.834	0.332	0.545	
937	WW	0.9	1.00	2.42	7.9	5.00	0.484	0.855	Bar	.0012	0.645	0.830	1.705	1.696	1.232	1.257	0.346	0.845	0.390	0.306	0.776	0.332	0.294	
938	WW	0.9	1.00	2.42	7.9	5.00	0.484	0.855	Bar	.0012	0.620	0.848	1.723	1.719	1.233	1.255	0.364	0.866	0.389	0.306	0.730	0.332	0.290	
867	ST	0.9	1.00	3.00	7.9	2.50	0.333	0.855	Bar	.0012	0.302	0.447	1.291	1.284	1.161	1.154	0.114	0.433	0.303	0.443	0.675	0.289	0.388	
884	ST	0.9	1.00	3.17	7.9	5.00	0.484	0.855	Bar	.0012	0.435	0.702	1.573	1.562	1.281	1.261	0.218	0.713	0.416	0.493	0.619	0.332	0.371	
885	ST	0.9	1.00	3.17	7.9	5.00	0.484	0.855	Bar	.0012	0.488	0.613	1.486	1.485	1.285	1.276	0.129	0.631	0.426	0.493	0.796	0.332	0.480	
1360	ST	0.9	1.00	3.15	7.9	5.00	0.484	0.855	Bar	.0012	0.492	0.621	1.494	1.494	1.296	1.273	0.137	0.639	0.430	0.491	0.794	0.332	0.466	
1361	ST	0.9	1.00	3.15	7.9	5.00	0.484	0.855	Bar	.0012	0.464	0.664	1.533	1.537	1.287	1.266	0.180	0.680	0.422	0.491	0.699	0.332	0.414	
1362	ST	0.9	1.00	3.15	7.9	5.00	0.484	0.855	Bar	.0012	0.438	0.712	1.578	1.582	1.274	1.260	0.228	0.725	0.412	0.491	0.616	0.332	0.511	
1363	ST	0.9	1.00	2.12	7.9	5.00	0.484	0.855	Bar	.0012	0.596	0.732	1.602	1.602	1.259	1.276	0.248	0.747	0.413	0.361	0.817	0.332	0.359	
1364	ST	0.9	1.00	2.12	7.9	5.00	0.484	0.855	Bar	.0012	0.534	0.831	1.699	1.698	1.273	1.243	0.347	0.844	0.403	0.361	0.644	0.332	0.308	
1365	ST	0.9	1.00	2.12	7.9	5.00	0.484	0.855	Bar	.0012	0.556	0.793	1.660	1.658	1.282	1.251	0.309	0.804	0.412	0.361	0.702	0.332	0.324	
1366	ST	0.9	1.00	4.19	7.9	5.00	0.484	0.855	Bar	.0012	0.446	0.548	1.426	1.424	1.295	1.300	0.064	0.570	0.443	0.623	0.816	0.332	0.604	

TABLE 4 : PARTIALLY SUBMERGED BRIDGE GIRDER [All Girders Submerged]
45 degree wing-wall abutment and 1:1.5 spill-through abutment

Run No	Model Type	Model height [ft]	Model length [ft]	Measured Data										Computed Data									
				b [ft]	B [ft]	Q [cfs]	h_n [ft]	Bottom Rdg.	Roughness	Slope	z [ft]	h_n [ft]	R_{UR}	R_{UL}	R_{DR}	R_{DL}	h_n [ft]	h_U [ft]	h_D [ft]	M	$\frac{z}{h_1}$	F_n	M*
808	WW	0.9	1.00	4.46	7.9	2.50	0.333	0.855	Bar	.0012	0.266	0.437	1.302	1.295	1.159	1.159	0.104	0.444	0.304	0.565	0.608	0.289	0.397
784	WW	0.9	1.00	4.42	7.9	2.50	0.523	0.854	Baffle	.0012	0.479	0.557	1.414	1.415	1.369	1.368	0.034	0.561	0.515	0.559	0.859	0.147	0.620
785	WW	0.9	1.00	4.42	7.9	2.50	0.523	0.854	Baffle	.0012	0.450	0.567	1.423	1.420	1.365	1.364	0.044	0.568	0.511	0.559	0.793	0.147	0.590
786	WW	0.9	1.00	4.42	7.9	2.50	0.523	0.855	Baffle	.0012	0.415	0.583	1.443	1.441	1.368	1.367	0.060	0.587	0.513	0.559	0.712	0.147	0.553
1341	WW	0.6	1.00	4.87	7.9	3.00	0.369	0.856	Bar	.0012	0.327	0.414	1.285	1.283	1.202	1.201	0.045	0.428	0.346	0.616	0.790	0.298	0.557
1342	WW	0.6	1.00	4.87	7.9	3.00	0.369	0.856	Bar	.0012	0.299	0.442	1.313	1.314	1.201	1.199	0.073	0.458	0.344	0.616	0.676	0.298	0.473
1343	WW	0.6	1.00	4.87	7.9	3.00	0.369	0.856	Bar	.0012	0.254	0.490	1.360	1.358	1.200	1.198	0.121	0.503	0.343	0.616	0.518	0.298	0.390
1345	WW	0.6	1.00	5.90	7.9	3.00	0.369	0.856	Bar	.0012	0.343	0.383	1.255	1.259	1.208	1.208	0.014	0.401	0.352	0.746	0.895	0.298	0.733
1346	WW	0.6	1.00	5.90	7.9	3.00	0.369	0.856	Bar	.0012	0.301	0.400	1.272	1.274	1.208	1.207	0.031	0.417	0.352	0.746	0.752	0.298	0.616
1347	WW	0.6	1.00	5.90	7.9	3.00	0.369	0.856	Bar	.0012	0.258	0.431	1.299	1.303	1.211	1.209	0.062	0.445	0.354	0.746	0.600	0.298	0.505
1349	WW	0.6	1.00	4.87	7.9	3.00	0.369	0.856	Bar	.0012	0.316	0.434	1.302	1.304	1.200	1.199	0.065	0.447	0.344	0.616	0.728	0.298	0.494
1350	WW	0.6	1.00	4.87	7.9	3.00	0.369	0.856	Bar	.0012	0.271	0.479	1.347	1.346	1.200	1.196	0.110	0.491	0.342	0.616	0.565	0.298	0.405
1351	WW	0.6	1.00	3.85	7.9	3.00	0.369	0.856	Bar	.0012	0.328	0.471	1.339	1.339	1.190	1.187	0.102	0.483	0.333	0.487	0.696	0.298	0.418
1352	WW	0.6	1.00	3.85	7.9	3.00	0.369	0.856	Bar	.0012	0.279	0.538	1.404	1.402	1.186	1.182	0.169	0.547	0.328	0.487	0.522	0.298	0.344
868R	ST	0.9	1.00	3.00	7.9	2.50	0.333	0.855	Bar	.0012	0.266	0.485	1.351	1.348	1.156	1.147	0.152	0.495	0.297	0.443	0.548	0.289	0.338
870	ST	0.9	1.00	5.00	7.9	2.50	0.333	0.855	Bar	.0012	0.264	0.403	1.270	1.264	1.181	1.176	0.070	0.412	0.324	0.696	0.655	0.289	0.470
871	ST	0.9	1.00	5.00	7.9	2.50	0.333	0.855	Bar	.0012	0.285	0.377	1.246	1.242	1.178	1.174	0.044	0.389	0.321	0.696	0.753	0.289	0.535
881	ST	0.9	1.00	5.08	7.9	5.00	0.484	0.856	Bar	.0012	0.399	0.538	1.422	1.410	1.231	1.321	0.055	0.560	0.465	0.735	0.741	0.332	0.625
882	ST	0.9	1.00	5.08	7.9	5.00	0.484	0.856	Bar	.0012	0.393	0.555	1.433	1.428	1.310	1.309	0.071	0.575	0.454	0.735	0.708	0.332	0.582
1367	ST	0.9	1.00	4.19	7.9	5.00	0.484	0.856	Bar	.0012	0.418	0.571	1.448	1.448	1.300	1.294	0.087	0.592	0.441	0.623	0.732	0.332	0.545
1368	ST	0.9	1.00	4.19	7.9	5.00	0.484	0.856	Bar	.0012	0.391	0.617	1.484	1.485	1.295	1.289	0.133	0.629	0.436	0.623	0.633	0.332	0.469
1369	ST	0.9	1.00	5.17	7.9	5.00	0.484	0.856	Bar	.0012	0.458	0.509	1.383	1.386	1.316	1.315	0.025	0.529	0.460	0.747	0.899	0.332	0.724
1370	ST	0.9	1.00	5.17	7.9	5.00	0.484	0.856	Bar	.0012	0.433	0.517	1.391	1.393	1.317	1.312	0.033	0.536	0.459	0.747	0.837	0.332	0.693
1371	ST	0.9	1.00	5.17	7.9	5.00	0.484	0.856	Bar	.0012	0.407	0.536	1.409	1.410	1.312	1.311	0.052	0.554	0.456	0.747	0.760	0.332	0.629

TABLE 5: SKEW CROSSING
45 degree wing-wall abutment

Measured Data												Computed Data														
Run No	Model Type	Model height [ft]	Model length [ft]	b [ft]	B [ft]	Q [cfs]	h_n [ft]	Bottom Rdg.	Roughness	Slope	degree of Skew	R_{UR}	R_{UL}	R_{DR}	R_{DL}	h_{UR} [ft]	h_{UL} [ft]	h_{DR} [ft]	h_{DL} [ft]	$\left(\frac{h_{UR}}{h_n}\right)$	$\left(\frac{h_{UR}}{h_n}\right)^3$	M	F_n	F_n^2	$\left(\frac{1}{M^2}-1\right)F_n^2$	M*
396	WW	0.6	1.00	7.37	7.9	2.50	0.333	0.866	Bar	.0012	45°	1.230	1.223	1.194	1.184	0.364	0.357	0.328	0.318	1.092	1.301	0.659	0.289	0.0835	0.1094	0.680
397	WW	0.6	1.00	6.33	7.9	2.50	0.333	0.866	Bar	.0012	45°	1.247	1.247	1.196	1.177	0.381	0.381	0.330	0.311	1.141	1.490	0.566	0.289	0.0835	0.177	0.578
398	WW	0.6	1.00	5.29	7.9	2.50	0.333	0.866	Bar	.0012	45°	1.264	1.265	1.195	1.172	0.398	0.399	0.329	0.306	1.195	1.710	0.473	0.289	0.0835	0.290	0.507
399	WW	0.6	1.00	4.27	7.9	2.50	0.333	0.866	Bar	.0012	45°	1.301	1.310	1.199	1.171	0.435	0.444	0.333	0.305	1.308	2.240	0.382	0.289	0.0835	0.489	0.411
400	WW	0.6	1.00	3.27	7.9	2.50	0.333	0.866	Bar	.0012	45°	1.378	1.376	1.185	1.166	0.512	0.510	0.319	0.300	1.539	3.630	0.292	0.289	0.0835	0.895	0.310
401	WW	0.6	1.00	6.12	7.9	2.50	0.333	0.866	Bar	.0012	30°	1.233	1.229	1.187	1.180	0.367	0.363	0.321	0.314	1.102	1.340	0.670	0.289	0.0835	0.102	0.651
402	WW	0.6	1.00	5.12	7.9	2.50	0.333	0.866	Bar	.0012	30°	1.253	1.250	1.187	1.175	0.387	0.384	0.321	0.309	1.162	1.540	0.560	0.289	0.0835	0.182	0.546
403	WW	0.6	1.00	4.14	7.9	2.50	0.333	0.866	Bar	.0012	30°	1.288	1.286	1.183	1.171	0.422	0.420	0.317	0.305	1.269	2.05	0.454	0.289	0.0835	0.314	0.440
404	WW	0.6	1.00	3.16	7.9	2.50	0.333	0.866	Bar	.0012	30°	1.349	1.353	1.162	1.175	0.483	0.487	0.296	0.309	1.450	3.05	0.346	0.289	0.0835	0.612	0.341
485	WW	0.9	1.00	4.94	7.9	5.00	0.484	0.866	Bar	.0012	45°	1.485	1.493	1.350	1.308	0.619	0.627	0.484	0.442	1.278	2.08	0.441	0.332	0.110	0.454	0.481
486	WW	0.9	1.00	3.85	7.9	5.00	0.484	0.866	Bar	.0012	45°	1.571	1.576	1.345	1.307	0.705	0.710	0.479	0.441	1.456	3.09	0.344	0.332	0.110	0.820	0.378
487	WW	0.9	1.00	2.85	7.9	5.00	0.484	0.866	Bar	.0012	45°	1.717	1.730	1.275	1.288	0.851	0.864	0.409	0.422	1.758	0.542	0.255	0.332	0.110	1.580	0.295
496	WW	0.9	1.00	4.10	7.9	5.00	0.484	0.866	Bar	.0012	30°	1.509	1.513	1.316	1.309	0.643	0.647	0.450	0.443	1.328	2.34	0.449	0.332	0.110	0.435	0.445
497	WW	0.9	1.00	3.12	7.9	5.00	0.484	0.866	Bar	.0012	30°	1.604	1.613	1.271	1.298	0.738	0.747	0.405	0.432	1.524	3.54	0.344	0.332	0.110	0.820	0.350
294	WW	0.6	1.00	6.25	7.9	2.54	0.333	0.833	Bar	.0012	45°	1.219	1.222	1.164	1.146	0.386	0.389	0.331	0.314	1.145	1.50	0.559	0.289	0.0835	0.183	0.572
295	WW	0.6	1.00	5.18	7.9	2.53	0.333	0.833	Bar	.0012	45°	1.234	1.239	1.170	1.147	0.401	0.406	0.337	0.314	1.204	1.74	0.463	0.289	0.0835	0.306	0.516
296	WW	0.6	1.00	4.16	7.9	2.55	0.333	0.833	Bar	.0012	45°	1.258	1.264	1.174	1.148	0.425	0.431	0.341	0.315	1.278	2.09	0.372	0.289	0.0835	0.520	0.443
297	WW	0.6	1.00	5.56	7.9	2.55	0.333	0.833	Bar	.0012	30°	1.220	1.225	1.158	1.153	0.387	0.392	0.325	0.320	1.160	1.56	0.609	0.289	0.0835	0.141	0.569
298	WW	0.6	1.00	4.56	7.9	2.50	0.333	0.833	Bar	.0012	30°	1.242	1.248	1.161	1.150	0.409	0.415	0.328	0.317	1.228	1.85	0.500	0.289	0.0835	0.250	0.486
299	WW	0.6	1.00	3.56	7.9	2.50	0.333	0.833	Bar	.0012	30°	1.272	1.280	1.167	1.145	0.439	0.447	0.334	0.312	1.318	2.29	0.391	0.289	0.0835	0.454	0.415
285	WW	0.9	1.00	3.48	7.9	5.00	0.484	0.834	Bar	.0012	30°	1.483	1.490	1.314	1.271	0.649	0.656	0.480	0.437	1.340	2.41	0.381	0.332	0.110	0.649	0.435
286	WW	0.9	1.00	2.45	7.9	5.00	0.484	0.834	Bar	.0012	30°	1.622	1.629	1.323	1.262	0.788	0.795	0.489	0.428	1.630	4.33	0.269	0.332	0.110	1.420	0.320
287	WW	0.9	1.00	2.97	7.9	5.00	0.484	0.834	Bar	.0012	15°	1.547	1.548	1.266	1.262	-	-	-	-	-	-	-	-	-	-	-
288	WW	0.9	1.00	1.98	7.9	5.00	0.484	0.834	Bar	.0012	15°	-	-	-	-	-	-	-	-	-	-	-	-	-	-	-
300	WW	0.9	1.00	3.56	7.9	5.00	0.482	0.833	Bar	.0012	30°	1.501	1.501	1.307	1.264	0.668	0.668	0.474	0.431	1.386	2.65	0.390	0.332	0.110	0.620	0.414
576	WW	0.9	1.00	3.54	7.9	5.00	0.484	0.864	Bar	.0012	30°	1.527	1.536	1.337	1.295	0.663	0.672	0.473	0.431	1.369	2.56	0.388	0.332	0.110	0.621	0.42
582	WW	0.9	1.00	2.54	7.9	5.00	0.484	0.864	Bar	.0012	30°	1.659	1.666	1.347	1.291	0.795	0.802	0.483	0.427	1.642	4.42	0.279	0.332	0.110	1.300	0.319
1382	WW	0.9	1.00	3.48	7.9	5.00	0.486	0.855	Bar	.0012	30°	1.527	1.535	1.333	1.288	0.672	0.680	0.478	0.433	1.382	2.64	0.382	0.328	0.108	0.631	0.411
1383	WW	0.9	1.00	5.10	7.9	5.00	0.486	0.855	Bar	.0012	30°	1.435	1.440	1.328	1.300	0.580	0.585	0.473	0.445	1.191	1.699	0.560	0.328	0.108	0.236	0.562
1384	WW	0.9	1.00	6.25	7.9	5.00	0.486	0.855	Bar	.0012	30°	1.398	1.393	1.323	1.307	0.543	0.538	0.468	0.452	1.117	1.391	0.685	0.328	0.108	0.124	0.686
211	WW	0.9	1.00	3.96	7.9	4.99	0.484	0.834	Bar	.0012	45°	1.494	1.489	1.340	1.275	0.660	0.655	0.506	0.441	1.365	2.540	0.355	0.331	0.110	0.765	0.422
212	WW	0.9	1.00	2.94	7.9	4.98	0.484	0.834	Bar	.0012	45°	1.584	1.591	1.362	1.272	0.750	0.757	0.528	0.438	1.551	3.72	0.263	0.331	0.110	1.48	0.342
289	WW	0.9	1.00	3.92	7.9	5.00	0.484	0.834	Bar	.0012	45°	1.503	1.504	1.360	1.278	0.669	0.670	0.526	0.444	1.384	2.645	0.351	0.332	0.110	0.785	0.411
290	WW	0.9	1.00	2.87	7.9	5.00	0.484	0.834	Bar	.0012	45°	1.567	1.578	1.385	1.272	0.733	0.744	0.551	0.438	1.516	3.48	0.257	0.332	0.110	1.56	0.354
565	WW	0.9	1.00	3.80	7.9	5.00	0.484	0.864	Bar	.0012	45°	1.531	1.536	1.382	1.303	0.667	0.672	0.518	0.439	1.378	2.62	0.340	0.332	0.110	0.841	0.415
572	WW	0.9	1.00	2.75	7.9	5.00	0.484	0.864	Bar	.0012	45°	1.623	1.632	1.418	1.301	0.759	0.768	0.554	0.437	1.568	3.85	0.246	0.332	0.110	1.71	0.338
1377	WW	0.9	1.00	3.99	7.9	5.00	0.485	0.856	Bar	.0012	45°	1.513	1.514	1.364	1.288	0.657	0.658	0.508	0.432	1.353	2.48	0.357	0.330	0.109	0.755	0.428
1378	WW	0.9	1.00	5.94	7.9	5.00	0.485	0.856	Bar	.0012	45°	1.439	1.439	1.355	1.302	0.583	0.583	0.499	0.446	1.201	1.73	0.532	0.330	0.109	0.280	0.554
1379	WW	0.9	1.00	7.00	7.9	5.00	0.485	0.856	Bar	.0012	45°	1.412	1.412	1.347	1.311	0.556	0.556	0.491	0.455	1.150	1.516	0.627	0.330	0.109	0.168	0.630
1380	WW	0.9	1.00	7.67	7.9	5.00	0.485	0.856	Bar	.0012	45°	1.393	1.389	1.337	1.309	0.537	0.533	0.481	0.453	1.106	1.352	0.687	0.330	0.109	0.122	0.711
1381	WW	0.9	1.00	8.54	7.9	5.00	0.485	0.856	Bar	.0012	45°	1.382	1.378	1.336	1.314	0.526	0.522	0.480	0.458	1.084	1.272	0.765	0.330	0.109	0.078	-

TABLE 5: SKEW CROSSING
1:1.5 spill-through abutment

Run No.	Model Type	Model height [ft]	Model length [ft]	Measured Data										Computed Data												
				b [ft]	B [ft]	Q [cfs]	h_n [ft]	Bottom Rdg.	Roughness	Slope	degree of Skew	R_{UR}	R_{UL}	R_{DR}	R_{DL}	h_{UR}	h_{UL}	h_{DR}	h_{DL}	$\frac{h_{UR}}{h_n}$	$\frac{h_{UL}}{h_n}$	M	F_n	F_n^2	$\frac{1}{M^2-1}F_n^2$	M^*
405	ST	0.6	1.00	4.54	7.9	2.50	0.333	0.866	Bar	.0012	30°	1.248	1.242	1.190	1.178	0.382	0.376	0.324	0.312	1.147	1.509	0.552	0.289	0.0835	0.189	0.570
406	ST	0.6	1.00	3.50	7.9	2.50	0.333	0.866	Bar	.0012	30°	1.274	1.275	1.190	1.177	0.408	0.409	0.324	0.311	1.225	1.840	0.439	0.289	0.0835	0.350	0.485
407	ST	0.6	1.00	2.58	7.9	2.50	0.333	0.866	Bar	.0012	30°	1.339	1.340	1.191	1.166	0.473	0.474	0.325	0.300	1.420	2.87	0.338	0.289	0.0835	0.649	0.365
408	ST	0.6	1.00	1.58	7.9	2.50	0.333	0.866	Bar	.0012	30°	1.435	1.434	1.177	1.162	0.569	0.568	0.311	0.296	1.708	4.98	0.228	0.289	0.0835	1.520	0.261
492	ST	0.9	1.00	4.58	7.9	5.00	0.484	0.866	Bar	.0012	30°	1.429	1.430	1.333	1.317	0.563	0.564	0.467	0.451	1.163	1.570	0.582	0.332	0.110	0.214	0.602
493	ST	0.9	1.00	3.44	7.9	5.00	0.484	0.866	Bar	.0012	30°	1.470	1.473	1.341	1.312	0.604	0.607	0.475	0.446	1.247	1.940	0.456	0.332	0.110	0.417	0.520
494	ST	0.9	1.00	2.42	7.9	5.00	0.484	0.866	Bar	.0012	30°	1.550	1.553	1.335	1.301	0.684	0.687	0.469	0.435	1.413	2.83	0.345	0.332	0.110	0.815	0.412
495	ST	0.9	1.00	1.35	7.9	5.00	0.484	0.866	Bar	.0012	30°	1.691	1.704	1.322	1.295	0.825	0.838	0.456	0.429	1.704	0.494	0.228	0.332	0.110	2.00	0.302
488	ST	0.9	1.00	1.92	7.9	5.00	0.484	0.866	Bar	.0012	45°	1.608	1.617	1.394	1.302	0.742	0.751	0.528	0.436	1.535	3.62	0.236	0.332	0.110	1.86	0.362
489	ST	0.9	1.00	2.98	7.9	5.00	0.484	0.866	Bar	.0012	45°	1.504	1.515	1.371	1.308	0.638	0.649	0.505	0.442	1.318	2.29	0.332	0.332	0.110	0.892	0.468
490	ST	0.9	1.00	4.04	7.9	5.00	0.484	0.866	Bar	.0012	45°	1.456	1.467	1.352	1.314	0.590	0.601	0.486	0.448	1.219	1.81	0.427	0.332	0.110	0.49	0.545
491	ST	0.9	1.00	4.92	7.9	5.00	0.484	0.866	Bar	.0012	45°	1.430	1.439	1.342	1.312	0.564	0.573	0.476	0.446	1.165	1.58	0.504	0.332	0.110	0.32	0.600
392	ST	0.6	1.00	5.66	7.9	2.50	0.333	0.866	Bar	.0012	45°	1.240	1.236	1.195	1.177	0.374	0.370	0.329	0.311	1.123	1.42	0.551	0.289	0.0835	0.191	0.601
393	ST	0.6	1.00	4.75	7.9	2.50	0.333	0.866	Bar	.0012	45°	1.255	1.249	1.202	1.177	0.389	0.383	0.336	0.311	1.168	1.59	0.469	0.289	0.0835	0.296	0.543
394	ST	0.6	1.00	3.58	7.9	2.50	0.333	0.866	Bar	.0012	45°	1.280	1.278	1.206	1.173	0.414	0.412	0.340	0.307	1.243	1.92	0.365	0.289	0.0835	0.544	0.469
395	ST	0.6	1.00	2.63	7.9	2.50	0.333	0.866	Bar	.0012	45°	1.325	1.327	1.217	1.167	0.459	0.461	0.351	0.301	1.378	2.62	0.280	0.289	0.0835	1.020	0.385
676	ST	0.9	1.00	4.18	7.9	2.50	0.333	0.857	Bar	.0012	30°	1.253	1.254	1.178	1.166	0.396	0.397	0.321	0.309	1.189	1.68	0.513	0.289	0.0835	0.234	0.521
677	ST	0.9	1.00	3.25	7.9	2.50	0.333	0.857	Bar	.0012	30°	1.280	1.283	1.182	1.161	0.423	0.426	0.325	0.304	1.270	2.05	0.411	0.289	0.0835	0.410	0.450
678	ST	0.9	1.00	2.29	7.9	2.50	0.333	0.857	Bar	.0012	30°	1.335	1.339	1.198	1.156	0.478	0.482	0.341	0.299	1.435	2.96	0.306	0.289	0.0835	0.810	0.359
674	ST	0.6	1.00	5.02	7.9	2.50	0.333	0.857	Bar	.0012	30°	1.239	1.242	1.177	1.165	0.382	0.385	0.320	0.308	1.147	1.51	0.605	0.289	0.0835	0.145	0.569
675	ST	0.6	1.00	4.02	7.9	2.50	0.333	0.857	Bar	.0012	30°	1.263	1.270	1.179	1.165	0.406	0.413	0.322	0.308	1.220	1.81	0.495	0.289	0.0835	0.256	0.491
661	ST	0.6	1.00	2.98	7.9	2.50	0.333	0.857	Bar	.0012	30°	1.302	1.310	1.180	1.158	0.445	0.453	0.323	0.301	1.336	2.39	0.382	0.289	0.0835	0.489	0.406
662	ST	0.6	1.00	2.16	7.9	2.50	0.333	0.857	Bar	.0012	30°	1.358	1.364	1.196	1.160	0.501	0.507	0.339	0.303	1.504	3.40	0.292	0.289	0.0835	0.895	0.330
659	ST	0.6	1.00	5.02	7.9	2.50	0.333	0.857	Bar	.0012	30°	1.241	1.240	1.178	1.167											
660	ST	0.6	1.00	4.02	7.9	2.50	0.333	0.857	Bar	.0012	30°	1.262	1.268	1.178	1.165											
654	ST	0.6	1.00	6.29	7.9	2.50	0.333	0.857	Bar	.0012	45°	1.241	1.242	1.188	1.167	0.384	0.385	0.331	0.310	1.153	1.534	0.606	0.289	0.0835	0.144	0.560
655	ST	0.6	1.00	5.23	7.9	2.50	0.333	0.857	Bar	.0012	45°	1.258	1.263	1.193	1.165	0.401	0.406	0.336	0.308	1.204	1.745	0.512	0.289	0.0835	0.236	0.505
656	ST	0.6	1.00	4.23	7.9	2.50	0.333	0.857	Bar	.0012	45°	1.279	1.283	1.199	1.159	0.422	0.426	0.342	0.302	1.267	2.03	0.424	0.289	0.0835	0.383	0.450
657	ST	0.6	1.00	3.25	7.9	2.50	0.333	0.857	Bar	.0012	45°	1.311	1.316	1.207	1.162	0.454	0.459	0.350	0.305	1.363	2.53	0.335	0.289	0.0835	0.661	0.391
658	ST	0.6	1.00	2.27	7.9	2.50	0.333	0.857	Bar	.0012	45°	1.367	1.376	1.221	1.155	0.510	0.519	0.364	0.298	1.531	3.59	0.248	0.289	0.0835	1.27	0.320
671	ST	0.9	1.00	6.27	7.9	2.50	0.333	0.857	Bar	.0012	45°	1.240	1.242	1.187	1.169	0.383	0.385	0.330	0.312	1.150	1.521	0.605	0.289	0.0835	0.145	0.565
672	ST	0.9	1.00	5.25	7.9	2.50	0.333	0.857	Bar	.0012	45°	1.253	1.254	1.191	1.167	0.396	0.397	0.334	0.310	1.189	1.68	0.514	0.289	0.0835	0.233	0.521
679	ST	0.9	1.00	4.75	7.9	2.50	0.333	0.857	Bar	.0012	45°	1.260	1.266	1.196	1.164	0.403	0.409	0.339	0.307	1.210	1.77	0.470	0.289	0.0835	0.294	0.500
680	ST	0.9	1.00	3.69	7.9	2.50	0.333	0.857	Bar	.0012	45°	1.287	1.290	1.206	1.160	0.430	0.433	0.349	0.303	1.291	2.15	0.374	0.289	0.0835	0.512	0.433
681	ST	0.9	1.00	2.65	7.9	2.50	0.333	0.857	Bar	.0012	45°	1.322	1.330	1.214	1.156	0.465	0.473	0.357	0.299	1.396	2.72	0.282	0.289	0.0835	0.976	0.375
682	ST	0.9	1.00	1.60	7.9	2.50	0.333	0.857	Bar	.0012	45°	1.403	1.411	1.242	1.158	0.546	0.554	0.385	0.301	1.639	4.40	0.188	0.289	0.0835	2.30	0.283
646	ST	0.9	1.00	4.19	7.9	5.00	0.484	0.855	Bar	.0012	30°	1.443	1.447	1.324	1.293	0.588	0.592	0.469	0.438	1.214	1.79	0.540	0.332	0.110	0.266	0.549
647	ST	0.9	1.00	3.21	7.9	5.00	0.484	0.855	Bar	.0012	30°	1.499	1.508	1.336	1.293	0.644	0.653	0.481	0.438	1.330	2.35	0.431	0.332	0.110	0.481	0.460
648	ST	0.9	1.00	2.21	7.9	5.00	0.484	0.855	Bar	.0012	30°	1.589	1.594	1.350	1.284	0.734	0.739	0.495	0.429	1.516	3.48	0.322	0.332	0.110	0.950	0.370
1385	ST	0.9	1.00	5.83	7.9	5.00	0.486	0.855	Bar	.0012	30°	1.398	1.394	1.321	1.307	0.543	0.539	0.466	0.452	1.122	1.415	0.721	0.332	0.110	0.101	0.710
1386	ST	0.9	1.00	4.15	7.9	5.00	0.486	0.855	Bar	.0012	30°	1.448	1.449	1.333	1.303	0.593	0.594	0.478	0.448	1.22	1.806	0.535	0.332	0.110	0.275	0.568
1387	ST	0.6	1.00	7.19	7.9	5.00	0.486	0.855	Bar	.0012	30°	1.411	1.413	1.324	1.308	0.556	0.558	0.469	0.453	1.114	1.50	0.859	0.332	0.110	0.037	0.666
1388	ST	0.6	1.00	6.70	7.9	5.00	0.486	0.855	Bar	.0012	30°	1.387	1.374	1.319	1.316	0.532	0.519	0.464	0.460	1.092	1.305	0.815	0.332	0.110	0.055	0.775
649	ST	0.6	1.00	4.94	7.9	5.00	0.484	0.855	Bar	.0012	30°	1.420	1.428	1.311	1.301											
650	ST	0.9	1.00	4.62	7.9	5.00	0.484	0.855	Bar	.0012	45°	1.472	1.479	1.358	1.295	0.617	0.624	0.503	0.440	1.274	2.07	0.478	0.332	0.110	0.373	0.498
651	ST	0.9	1.00	3.67	7.9	5.00	0.484	0.855	Bar	.0012	45°	1.507	1.516	1.369	1.295	0.652	0.661	0.514	0.440	1.347	2.44	0.394	0.332	0.110	0.600	0.450
652	ST	0.9	1.00	2.54	7.9	5.00	0.484	0.855	Bar	.0012	45°	1.579	1.591	1.401	1.291	0.724	0.736	0.546	0.436	1.495	3.34	0.292	0.332	0.110	1.18	0.378
291	ST	0.9	1.00	4.58	7.9	5.00	0.484	0.834	Bar	.0012	45°	1.454	1.456	1.345	1.											

TABLE 5: SKEW CROSSING
vertical board model

Run No	Model Type	Model height [ft]	Model length [ft]	Measured Data										Computed Data												
				b [ft]	B [ft]	Q [cfs]	h_n [ft]	Bottom Rdg.	Roughness	Slope	degree of Skew	R_{UR}	R_{UL}	R_{DR}	R_{DL}	h_{UR} [ft]	h_{UL} [ft]	h_{DR} [ft]	h_{DL} [ft]	$\left(\frac{h_{US}}{h_n}\right)$	$\left(\frac{h_{US}}{h_n}\right)^3$	M	F_n	F_n^2	$\left(\frac{1}{M^2}-1\right)F_n^2$	M^*
256	VB	1.67	-	2.21	7.9	4.99	0.484	0.834	Bar	.0012	15°	1.741	1.759	1.233	1.254	0.737	0.744	0.417	0.428	1.522	3.525	0.394	0.332	0.110	0.600	0.405
257	VB	1.67	-	3.22	7.9	4.98	0.484	0.834	Bar	.0012	15°	1.571	1.578	1.251	1.262	0.635	0.640	0.426	0.436	1.311	2.253	0.515	0.332	0.110	0.306	0.526
258	VB	1.67	-	4.21	7.9	4.99	0.484	0.834	Bar	.0012	15°	1.469	1.474	1.260	1.270	0.577	0.580	0.435	0.446	1.192	1.694	0.638	0.332	0.110	0.161	0.642
259	VB	1.67	-	5.22	7.9	5.00	0.484	0.834	Bar	.0012	15°	1.411	1.414	1.269	1.280	0.536	0.534	0.444	0.456	1.110	1.360	0.760	0.332	0.110	0.0803	0.776
260	VB	1.67	-	6.21	7.9	4.98	0.484	0.834	Bar	.0012	15°	1.370	1.368	1.278	1.290	0.508	0.512	0.462	0.457	1.049	1.154	0.826	0.332	0.110	0.0506	-
235	VB	1.67	-	9.23	7.9	4.98	0.484	0.834	Bar	.0012	45°	1.342	1.346	1.296	1.291	0.525	0.527	0.462	0.450	1.084	1.274	0.735	0.332	0.110	0.094	-
236	VB	1.67	-	8.21	7.9	5.00	0.484	0.834	Bar	.0012	45°	1.359	1.361	1.296	1.283	0.544	0.547	0.465	0.447	1.123	1.416	0.647	0.332	0.110	0.153	0.746
237	VB	1.67	-	7.23	7.9	4.98	0.484	0.834	Bar	.0012	45°	1.378	1.381	1.299	1.281	0.576	0.579	0.470	0.443	1.190	1.685	0.557	0.332	0.110	0.244	0.645
238	VB	1.67	-	6.22	7.9	4.98	0.484	0.834	Bar	.0012	45°	1.410	1.413	1.304	1.277	0.615	0.618	0.483	0.438	1.270	2.05	0.468	0.332	0.110	0.392	0.560
239	VB	1.67	-	5.23	7.9	4.97	0.484	0.834	Bar	.0012	45°	1.449	1.425	1.317	1.272	0.665	0.664	0.494	0.434	1.371	2.577	0.393	0.332	0.110	0.605	0.485
240	VB	1.67	-	4.39	7.9	4.97	0.484	0.834	Bar	.0012	45°	1.499	1.498	1.328	1.268	0.750	0.750	0.507	0.433	1.550	3.720	0.304	0.332	0.110	1.08	0.394
241	VB	1.67	-	3.37	7.9	4.99	0.484	0.834	Bar	.0012	45°	1.584	1.584	1.341	1.267											
242	VB	1.67	-	2.37	7.9	4.99	0.484	0.834	Bar	.0012	45°	1.736	1.734	1.352	1.255	0.352	0.349	0.320	0.319	1.057	1.181	0.829	0.289	0.0835	0.0384	-
413	VB	1.67	-	9.25	7.9	2.50	0.333	0.866	Bar	.0012	45°	1.218	1.215	1.186	1.185	0.361	0.359	0.322	0.315	1.084	1.274	0.739	0.289	0.0835	0.0694	-
414	VB	1.67	-	8.25	7.9	2.50	0.333	0.866	Bar	.0012	45°	1.227	1.225	1.188	1.181	0.374	0.371	0.322	0.315	1.123	1.416	0.649	0.289	0.0835	0.115	0.705
415	VB	1.67	-	7.25	7.9	2.50	0.333	0.866	Bar	.0012	45°	1.240	1.237	1.188	1.181	0.387	0.387	0.327	0.308	1.162	1.569	0.560	0.289	0.0835	0.182	0.698
416	VB	1.67	-	6.25	7.9	2.50	0.333	0.866	Bar	.0012	45°	1.253	1.253	1.193	1.174	0.410	0.408	0.330	0.306	1.231	1.869	0.470	0.289	0.0835	0.295	0.552
417	VB	1.67	-	5.25	7.9	2.50	0.333	0.866	Bar	.0012	45°	1.276	1.274	1.196	1.172	0.486	0.493	0.345	0.304	1.459	3.100	0.303	0.289	0.0835	0.825	0.400
418	VB	1.67	-	3.38	7.9	2.50	0.333	0.866	Bar	.0012	45°	1.352	1.359	1.211	1.170	0.580	0.588	0.361	0.301	1.741	5.280	0.211	0.289	0.0835	1.800	0.291
419	VB	1.67	-	2.36	7.9	2.50	0.333	0.866	Bar	.0012	45°	1.446	1.454	1.227	1.167	0.522	0.523	0.451	0.456	1.078	1.251	0.781	0.331	0.110	0.071	-
251	VB	1.67	-	7.12	7.9	4.98	0.484	0.834	Bar	.0012	30°	1.356	1.357	1.285	1.290	0.549	0.549	0.449	0.446	1.132	1.460	0.675	0.330	0.109	0.133	0.730
252	VB	1.67	-	6.16	7.9	4.97	0.484	0.834	Bar	.0012	30°	1.383	1.383	1.283	1.280	0.587	0.590	0.451	0.442	1.212	1.779	0.567	0.330	0.109	0.232	0.618
253	VB	1.67	-	5.17	7.9	4.97	0.484	0.834	Bar	.0012	30°	1.421	1.424	1.285	1.276	0.650	0.656	0.451	0.431	1.342	2.418	0.456	0.330	0.109	0.419	0.504
254	VB	1.67	-	4.16	7.9	4.97	0.484	0.834	Bar	.0012	30°	1.484	1.490	1.285	1.265	0.746	0.755	0.454	0.428	1.541	3.660	0.346	0.330	0.109	0.800	0.395
255	VB	1.67	-	3.16	7.9	4.96	0.484	0.834	Bar	.0012	30°	1.580	1.589	1.288	1.262	0.361	0.357	0.316	0.315	1.084	1.265	0.784	0.289	0.0835	0.0532	0.785
421	VB	1.67	-	7.15	7.9	2.50	0.333	0.866	Bar	.0012	30°	1.227	1.223	1.182	1.181	0.376	0.376	0.317	0.312	1.129	1.44	0.674	0.289	0.0835	0.100	0.694
422	VB	1.67	-	6.15	7.9	2.50	0.333	0.866	Bar	.0012	30°	1.242	1.242	1.183	1.178	0.398	0.398	0.317	0.309	1.195	1.703	0.567	0.289	0.0835	0.176	0.595
423	VB	1.67	-	5.17	7.9	2.50	0.333	0.866	Bar	.0012	30°	1.264	1.264	1.183	1.175	0.432	0.434	0.319	0.303	1.297	2.18	0.458	0.289	0.0835	0.315	0.494
424	VB	1.67	-	4.18	7.9	2.50	0.333	0.866	Bar	.0012	30°	1.298	1.300	1.185	1.169	0.492	0.495	0.318	0.299	1.477	3.22	0.350	0.289	0.0835	0.598	0.390
425	VB	1.67	-	3.19	7.9	2.50	0.333	0.866	Bar	.0012	30°	1.358	1.361	1.184	1.165	0.587	0.590	0.321	0.295	1.762	5.47	0.254	0.289	0.0835	1.21	0.284
426	VB	1.67	-	2.31	7.9	2.50	0.333	0.866	Bar	.0012	30°	1.453	1.456	1.187	1.161											
420	VB	1.67	-	1.34	7.9	2.50	0.333	0.866	Bar	.0012	45°	1.646	1.654	1.244	1.165											
427	VB	1.67	-	1.31	7.9	2.50	0.333	0.866	Bar	.0012	30°	1.670	1.674	1.190	1.165											
1327	VB	1.67	-	5.23	7.9	3.00	0.369	0.853	Bar	.0012	45°	1.317	1.320	1.231	1.193											

TABLE 6 : ECCENTRIC CROSSING
45 degree wing-wall abutment and 1:1.5 spill-through abutment and vertical board model

Measured Data														Computed Data										
Run No.	Model Type	Model height [ft]	Model length [ft]	b [ft]	B [ft]	Q [cfs]	[ft]	Bottom Rdg.	Roughness	Slope	h ₁ [ft]	R _{UR}	R _{UL}	R _{DR}	R _{DL}	e	h ₁ *	h _{UR} [ft]	h _{UL} [ft]	h _{DR} [ft]	h _{DL} [ft]	M	M*	F _n
470A	WW	0.9	1.00	6.21	7.9	5.00	0.718	0.866	Baffle	.0012	0.725	-	1.602	-	1.568	1.00	0.007	-	0.736	-	0.702	0.785	0.783	0.184
471	WW	0.9	1.00	5.19	7.9	5.00	0.718	0.866	Baffle	.0012	0.743	-	1.623	-	1.562	1.00	0.025	-	0.757	-	0.696	0.655	0.590	0.184
472	WW	0.9	1.00	4.19	7.9	5.00	0.718	0.866	Baffle	.0012	0.769	-	1.654	-	1.558	1.00	0.051	-	0.788	-	0.692	0.53	0.492	0.184
473	WW	0.9	1.00	3.17	7.9	5.00	0.718	0.864	Baffle	.0012	0.830	-	1.710	-	1.552	1.00	0.112	-	0.846	-	0.688	0.400	0.375	0.184
474	WW	0.9	1.00	2.65	7.9	5.00	0.718	0.864	Baffle	.0012	0.881	-	1.766	-	1.552	1.00	0.163	-	0.902	-	0.688	0.336	0.310	0.184
475	WW	0.9	1.00	6.21	7.9	5.00	0.484	0.866	Bar	.0012	0.505	-	1.396	-	1.321	1.00	0.021	-	0.530	-	0.455	0.786	0.710	0.332
476	WW	0.9	1.00	5.19	7.9	5.00	0.484	0.866	Bar	.0012	0.528	-	1.419	-	1.312	1.00	0.044	-	0.553	-	0.446	0.655	0.619	0.332
477	WW	0.9	1.00	4.19	7.9	5.00	0.484	0.866	Bar	.0012	0.577	-	1.471	-	1.302	1.00	0.093	-	0.605	-	0.436	0.530	0.513	0.332
478	WW	0.9	1.00	3.17	7.9	5.00	0.484	0.866	Bar	.0012	0.679	-	1.565	-	1.286	1.00	0.195	-	0.699	-	0.420	0.400	0.390	0.332
479	WW	0.9	1.00	2.17	7.9	5.00	0.484	0.866	Bar	.0012	0.877	-	1.757	-	1.278	1.00	0.393	-	0.891	-	0.412	0.274	0.259	0.332
480	ST	0.9	1.00	2.00	7.9	5.00	0.484	0.866	Bar	.0012	0.831	-	1.707	-	1.279	1.00	0.347	-	0.841	-	0.413	0.345	0.295	0.332
481	ST	0.9	1.00	2.50	7.9	5.00	0.484	0.866	Bar	.0012	0.736	-	1.623	-	1.284	1.00	0.252	-	0.757	-	0.418	0.413	0.357	0.332
482	ST	0.9	1.00	3.50	7.9	5.00	0.484	0.866	Bar	.0012	0.617	-	1.502	-	1.291	1.00	0.133	-	0.636	-	0.425	0.540	0.469	0.332
483	ST	0.9	1.00	4.50	7.9	5.00	0.484	0.866	Bar	.0012	0.550	-	1.442	-	1.311	1.00	0.066	-	0.576	-	0.445	0.660	0.588	0.332
484	ST	0.9	1.00	5.50	7.9	5.00	0.484	0.866	Bar	.0012	0.511	-	1.396	-	1.318	1.00	0.027	-	0.530	-	0.452	0.789	0.720	0.332
230	VB	1.67	-	2.07	7.9	4.97	0.484	0.834	Bar	.0012	-	1.764	1.767	1.151	1.249	0.804	-	0.930	0.933	0.317	0.415	0.262	-	0.332
231	VB	1.67	-	3.07	7.9	4.97	0.484	0.834	Bar	.0012	-	1.580	1.586	1.201	1.259	0.752	-	0.746	0.752	0.367	0.425	0.388	-	0.332
232	VB	1.67	-	4.0	7.9	4.99	0.484	0.834	Bar	.0012	-	1.476	1.479	1.240	1.264	0.676	-	0.642	0.645	0.406	0.430	0.506	-	0.332
233	VB	1.67	-	5.5	7.9	5.00	0.484	0.834	Bar	.0012	-	1.391	1.392	1.267	1.280	0.335	-	0.557	0.558	0.433	0.446	0.695	-	0.332
428	VB	1.67	-	2.06	7.9	2.5	0.333	0.866	Bar	.0012	-	1.470	1.475	1.095	1.160	0.801	-	0.604	0.609	0.229	0.294	0.260	-	0.289
429A	VB	1.67	-	2.06	7.9	2.5	0.333	0.866	Bar	.0012	-	1.476	1.478	1.133	1.157	0.665	-	0.610	0.612	0.267	0.291	0.260	-	0.289
430	VB	1.67	-	2.06	7.9	2.5	0.333	0.866	Bar	.0012	-	1.475	1.481	1.140	1.160	0.495	-	0.609	0.615	0.274	0.294	0.260	-	0.289
431	VB	1.67	-	2.06	7.9	2.5	0.333	0.866	Bar	.0012	-	1.481	1.484	1.146	1.159	0.276	-	0.615	0.618	0.280	0.293	0.260	-	0.289
432	VB	1.67	-	3.06	7.9	2.5	0.333	0.866	Bar	.0012	-	1.348	1.351	1.150	1.159	0.754	-	0.482	0.485	0.284	0.293	0.387	-	0.289
433A	VB	1.67	-	3.06	7.9	2.5	0.333	0.866	Bar	.0012	-	1.353	1.356	1.152	1.161	0.574	-	0.487	0.490	0.286	0.295	0.387	-	0.289
434B	VB	1.67	-	3.06	7.9	2.5	0.333	0.866	Bar	.0012	-	1.354	1.351	1.161	1.150	0.256	-	0.488	0.485	0.295	0.284	0.387	-	0.289
435	VB	1.67	-	4.07	7.9	2.5	0.333	0.866	Bar	.0012	-	1.290	1.287	1.162	1.166	0.395	-	0.424	0.421	0.296	0.300	0.515	-	0.289
436	VB	1.67	-	4.07	7.9	2.5	0.333	0.866	Bar	.0012	-	1.290	1.288	1.162	1.168	0.666	-	0.424	0.422	0.296	0.302	0.515	-	0.289
464	VB	1.67	-	2.04	7.9	2.5	0.718	0.866	Baffle	.0012	1.062	-	1.944	-	1.544	1.00	0.344	-	1.078	-	0.678	0.258	-	0.184
465	VB	1.67	-	2.04	7.9	2.5	0.523	0.866	Baffle	.0012	0.706	-	1.582	-	1.366	1.00	0.183	-	0.716	-	0.500	0.258	-	0.148
862	VB	1.67	-	3.04	7.9	2.5	0.333	0.855	Bar	.0012	0.477	-	-	-	-	1.00	0.144	-	-	-	-	0.385	-	0.289
863	VB	1.67	-	4.06	7.9	2.5	0.333	0.855	Bar	.0012	0.409	-	-	-	-	1.00	0.076	-	-	-	-	0.515	-	0.289
864	VB	1.67	-	4.97	7.9	2.5	0.333	0.855	Bar	.0012	0.392	-	1.253	-	1.160	1.00	0.059	-	0.368	-	0.305	0.630	-	0.289
865	VB	1.67	-	5.94	7.9	2.5	0.333	0.855	Bar	.0012	0.356	-	1.228	-	1.165	1.00	0.023	-	0.373	-	0.310	0.750	-	0.289
876R	VB	1.67	-	5.96	7.9	5.00	0.484	0.855	Bar	.0012	0.518	-	1.396	-	1.303	1.00	0.034	-	0.541	-	0.448	0.755	-	0.332
877	VB	1.67	-	4.96	7.9	5.00	0.484	0.855	Bar	.0012	0.569	-	1.442	-	1.292	1.00	0.085	-	0.587	-	0.437	0.629	-	0.332
878R	VB	1.67	-	4.04	7.9	5.00	0.484	0.855	Bar	.0012	0.623	-	1.497	-	1.271	1.00	0.139	-	0.642	-	0.416	0.511	-	0.332
879	VB	1.67	-	3.02	7.9	5.00	0.484	0.855	Bar	.0012	0.730	-	1.603	-	1.261	1.00	0.246	-	0.748	-	0.406	0.382	-	0.332

TABLE 6 : ECCENTRIC AND SKEW CROSSING
vertical board model.

Run No.	Model Type	Measured Data										Computed Data										
		Model height [ft]	Model length [ft]	b [ft]	B [ft]	Q [cfs]	h_n [ft]	Bottom Rdg	Roughness	Slope	Degree of Skew	h_1 [ft]	R_{UR}	R_{UL}	R_{DR}	R_{DL}	e	h_1^*	h_{UR} [ft]	h_{UL} [ft]	h_{DR} [ft]	h_{DL} [ft]
243	VB	1.67	-	2.37	7.9	4.99	0.484	0.834	Bar	.0012	45°	-	1.772	1.779	1.547	1.237	0.794	-	0.938	0.945	0.713	0.403
244	VB	1.67	-	2.88	7.9	4.99	0.484	0.834	Bar	.0012	45°	-	1.690	1.689	1.495	1.256	0.779	-	0.856	0.855	0.661	0.422
245	VB	1.67	-	3.38	7.9	4.99	0.484	0.834	Bar	.0012	45°	-	1.609	1.623	1.462	1.263	0.761	-	0.775	0.789	0.628	0.429
246	VB	1.67	-	4.39	7.9	4.98	0.484	0.834	Bar	.0012	45°	-	1.512	1.528	1.398	1.265	0.715	-	0.678	0.694	0.564	0.431
247	VB	1.67	-	5.31	7.9	4.99	0.484	0.834	Bar	.0012	45°	-	1.455	1.465	1.365	1.271	0.656	-	0.621	0.631	0.531	0.437
248	VB	1.67	-	5.82	7.9	4.99	0.484	0.834	Bar	.0012	45°	-	1.432	1.441	1.348	1.274	0.613	-	0.598	0.607	0.514	0.440
249	VB	1.67	-	6.75	7.9	4.98	0.484	0.834	Bar	.0012	45°	-	1.397	1.406	1.322	1.280	0.485	-	0.563	0.572	0.488	0.446
250	VB	1.67	-	7.75	7.9	4.99	0.484	0.834	Bar	.0012	45°	-	1.368	1.374	1.302	1.285	0.245	-	0.534	0.540	0.468	0.451
269	VB	1.67	-	5.66	7.9	5.00	0.484	0.834	Bar	.0012	30°	-	1.403	1.403	1.289	1.273	0.210	-	0.569	0.569	0.455	0.439
270	VB	1.67	-	5.18	7.9	4.99	0.484	0.834	Bar	.0012	30°	-	1.421	1.429	1.294	1.270	0.384	-	0.587	0.595	0.460	0.436
271	VB	1.67	-	4.64	7.9	4.99	0.484	0.834	Bar	.0012	30°	-	1.453	1.463	1.304	1.264	0.492	-	0.619	0.629	0.470	0.430
272	VB	1.67	-	3.73	7.9	5.00	0.484	0.834	Bar	.0012	30°	-	1.526	1.535	1.326	1.258	0.612	-	0.692	0.701	0.492	0.424
273	VB	1.67	-	3.26	7.9	5.00	0.484	0.834	Bar	.0012	30°	-	1.589	1.599	1.345	1.265	0.654	-	0.755	0.765	0.511	0.431
274	VB	1.67	-	2.30	7.9	5.00	0.484	0.834	Bar	.0012	30°	-	1.750	1.758	1.368	1.254	0.718	-	0.916	0.924	0.534	0.420
275	VB	1.67	-	4.72	7.9	5.00	0.484	0.834	Bar	.0012	15°	-	1.437	1.438	1.267	1.270	0.245	-	0.603	0.604	0.433	0.426
276	VB	1.67	-	3.72	7.9	5.00	0.484	0.834	Bar	.0012	15°	-	1.519	1.523	1.264	1.262	0.500	-	0.685	0.689	0.420	0.428
277	VB	1.67	-	2.80	7.9	5.00	0.484	0.834	Bar	.0012	15°	-	1.635	1.638	1.263	1.256	0.618	-	0.801	0.804	0.429	0.422
278	VB	1.67	-	2.30	7.9	5.00	0.484	0.834	Bar	.0012	15°	-	1.727	1.730	1.253	1.259	0.661	-	0.893	0.896	0.419	0.425

TABLE 7 : PIERS WITH ABUTMENTS
45 degree wing-wall abutment

Measured Data														Computed Data													
Run No.	Model Type	Model height [ft]	Model length [ft]	b [ft]	B [ft]	Q [cfs]	h ₁ [ft]	Bottom Rdg.	Roughness	Slope	Type of Piers	Number of Piers	Diameter of Piers [in]	h ₁ [ft]	R _{UR}	R _{UL}	R _{DR}	R _{DL}	L*	h ₁ * [ft]	h _U	h _D	h _L / h _n	ND / B	M	S	M*
1180	WW	0.6	1.00	2.90	7.9	3.00	0.362	0.855	Bar	.0012	ss	6	0.625	0.519	1.386	1.387	1.179	1.172	4.7	0.161	0.532	0.321	1.440	.0396	0.329	0.41	0.351
1181	WW	0.6	1.00	2.90	7.9	3.00	0.362	0.855	Bar	.0012	ss	4	0.625	0.515	1.381	1.381	1.181	1.172	4.7	0.157	0.526	0.321	1.422	.0264	0.342	0.41	0.356
1182	WW	0.6	1.00	2.90	7.9	3.00	0.362	0.855	Bar	.0012	ss	2	0.625	0.509	1.376	1.375	1.179	1.172	5.5	0.151	0.521	0.321	1.406	.0132	0.355	0.41	0.361
1186	WW	0.6	1.00	2.90	7.9	3.00	0.362	0.855	Bar	.0012	ss	1	1.25	0.509	1.376	1.378	1.171	1.174	4.7	0.151	0.522	0.318	1.406	.0132	0.355	0.42	0.361
1187	WW	0.6	1.00	2.90	7.9	3.00	0.362	0.855	Bar	.0012	ss	2	1.25	0.515	1.385	1.383	1.177	1.172	4.2	0.157	0.529	0.319	1.422	.0264	0.342	0.42	0.356
1188	WW	0.6	1.00	2.90	7.9	3.00	0.362	0.855	Bar	.0012	ss	3	1.25	0.522	1.390	1.389	1.175	1.169	4.5	0.164	0.535	0.317	1.442	.0396	0.329	0.42	0.351
1204	WW	0.6	1.00	3.89	7.9	3.00	0.362	0.855	Bar	.0012	ss	8	0.625	0.436	1.309	1.306	1.185	1.183	5.1	0.078	0.453	0.329	1.205	.0527	0.440	0.41	0.470
1205	WW	0.6	1.00	3.89	7.9	3.00	0.362	0.855	Bar	.0012	ss	6	0.625	0.433	1.303	1.302	1.183	1.179	5.7	0.075	0.447	0.326	1.198	.0396	0.453	0.41	0.476
1206	WW	0.6	1.00	3.90	7.9	3.00	0.362	0.855	Bar	.0012	ss	4	0.625	0.432	1.301	1.301	1.184	1.183	.070								
1210	WW	0.6	1.00	3.89	7.9	3.00	0.362	0.855	Bar	.0012	ss	4	1.25	0.433	1.302	1.301	1.183	1.180	5.0	0.075	0.447	0.326	1.198	.0527	0.440	0.42	0.470
1211	WW	0.6	1.00	3.89	7.9	3.00	0.362	0.855	Bar	.0012	ss	3	1.25	0.431	1.301	1.299	1.184	1.180	5.0	0.073	0.445	0.327	1.192	.0396	0.453	0.42	0.475
1212	WW	0.6	1.00	3.89	7.9	3.00	0.362	0.855	Bar	.0012	ss	2	1.25	0.430	1.303	1.302	1.184	1.182	5.1	0.072	0.447	0.328	1.191	.0264	0.466	0.42	0.481
1217	WW	0.6	1.00	4.92	7.9	3.00	0.362	0.855	Bar	.0012	ss	10	0.625	0.396	1.269	1.271	1.192	1.192	5.0	0.038	0.415	0.337	1.095	.0659	0.557	0.41	0.597
1218	WW	0.6	1.00	4.92	7.9	3.00	0.362	0.855	Bar	.0012	ss	8	0.625	0.395	1.267	1.268	1.191	1.191	5.2	0.037	0.413	0.336	1.090	.0527	0.570	0.41	0.613
1219	WW	0.6	1.00	4.92	7.9	3.00	0.362	0.855	Bar	.0012	ss	4	0.625	0.393	1.266	1.265	1.192	1.191	5.0	0.035	0.410	0.336	1.086	.0264	0.596	0.41	0.602
1226	WW	0.6	1.00	4.92	7.9	3.00	0.362	0.855	Bar	.0012	ss	5	1.25	0.398	1.267	1.267	1.194	1.193	5.0	0.040	0.413	0.338	1.100	.0659	0.557	0.42	0.596
1227	WW	0.6	1.00	4.92	7.9	3.00	0.362	0.855	Bar	.0012	ss	4	1.25	0.396	1.268	1.267	1.197	1.193	4.8	0.038	0.413	0.340	1.095	.0527	0.570	0.42	0.602
1228	WW	0.6	1.00	4.92	7.9	3.00	0.362	0.855	Bar	.0012	ss	2	1.25	0.393	1.264	1.263	1.194	1.192	5.0	0.035	0.409	0.338	1.083	.0264	0.596	0.42	0.613
1249R	WW	0.6	1.00	5.90	7.9	3.00	0.362	0.855	Bar	.0012	ss	12	0.625	0.376	1.248	1.247	1.200	1.201	-	0.018	0.393	0.345	1.040	.0791	0.667	0.41	0.714
1250R	WW	0.6	1.00	5.90	7.9	3.00	0.362	0.855	Bar	.0012	ss	8	0.625	0.374	1.246	1.246	1.200	1.198	4.5	0.016	0.391	0.344	1.032	.0527	0.691	0.41	0.725
1251	WW	0.6	1.00	5.90	7.9	3.00	0.362	0.855	Bar	.0012	ss	4	0.625	0.372	1.247	1.243	1.199	1.199	5.3	0.014	0.390	0.344	1.029	.0264	0.718	0.41	0.736
1256	WW	0.6	1.00	5.90	7.9	3.00	0.362	0.855	Bar	.0012	ss	6	1.25	0.377	1.249	1.247	1.200	1.199	4.8	0.019	0.393	0.345	1.041	.0791	0.667	0.42	0.714
1257	WW	0.6	1.00	5.90	7.9	3.00	0.362	0.855	Bar	.0012	ss	4	1.25	0.374	1.247	1.246	1.200	1.200	5.1	0.016	0.391	0.345	1.032	.0527	0.691	0.42	0.725
1258	WW	0.6	1.00	5.90	7.9	3.00	0.362	0.855	Bar	.0012	ss	2	1.25	0.373	1.245	1.245	1.200	1.200	5.0	0.015	0.390	0.345	1.030	.0264	0.718	0.42	0.736
1177	WW	0.6	1.00	2.91	7.9	3.00	0.360	0.855	Bar	.0012	ds	6	0.625	0.526	1.392	1.391	1.178	1.173	4.9	0.166	0.537	0.321	1.46	.039	0.329	0.72	0.340
1178	WW	0.6	1.00	2.91	7.9	3.00	0.360	0.855	Bar	.0012	ds	4	0.625	0.518	1.383	1.381	1.178	1.172	4.8	0.158	0.527	0.320	1.44	.026	0.342	0.72	0.350
1179	WW	0.6	1.00	2.91	7.9	3.00	0.360	0.855	Bar	.0012	ds	2	0.625	0.510	1.376	1.375	1.178	1.173	4.9	0.150	0.521	0.321	1.42	.013	0.355	0.72	0.359
1183	WW	0.6	1.00	2.91	7.9	3.00	0.360	0.855	Bar	.0012	ds	3	1.25	0.529	1.397	1.396	1.183	1.171	4.5	0.169	0.542	0.322	1.47	.039	0.329	0.73	0.339
1184	WW	0.6	1.00	2.91	7.9	3.00	0.360	0.855	Bar	.0012	ds	2	1.25	0.519	1.385	1.387	1.177	1.170	5.1	0.159	0.531	0.319	1.44	.026	0.342	0.73	0.349
1185	WW	0.6	1.00	2.91	7.9	3.00	0.360	0.855	Bar	.0012	ds	1	1.25	0.511	1.380	1.381	1.176	1.172	4.7	0.151	0.526	0.319	1.42	.013	0.355	0.73	0.358
1207	WW	0.6	1.00	3.89	7.9	3.00	0.360	0.855	Bar	.0012	ds	8	0.625	0.443	1.314	1.310	1.184	1.181	5.4	0.083	0.457	0.328	1.23	.0526	0.440	0.72	0.454
1208	WW	0.6	1.00	3.89	7.9	3.00	0.360	0.855	Bar	.0012	ds	6	0.625	0.440	1.309	1.309	1.184	1.184	5.7	0.080	0.454	0.329	1.22	.0394	0.453	0.72	0.464
1209	WW	0.6	1.00	3.89	7.9	3.00	0.360	0.855	Bar	.0012	ds	4	0.625	0.436	1.308	1.305	1.183	1.185	5.0	0.076	0.452	0.329	1.21	.0263	0.466	0.72	0.474
1213	WW	0.6	1.00	3.89	7.9	3.00	0.360	0.855	Bar	.0012	ds	4	1.25	0.441	1.311	1.309	1.183	1.180	5.2	0.081	0.455	0.327	1.23	.0526	0.440	0.73	0.453
1214	WW	0.6	1.00	3.89	7.9	3.00	0.360	0.855	Bar	.0012	ds	3	1.25	0.437	1.307	1.304	1.183	1.183	5.1	0.077	0.452	0.328	1.21	.0394	0.453	0.73	0.463
1215	WW	0.6	1.00	3.89	7.9	3.00	0.360	0.855	Bar	.0012	ds	2	1.25	0.432	1.304	1.304	1.183	1.185	5.1	0.072	0.449	0.329	1.20	.0263	0.466	0.73	0.473
1220	WW	0.6	1.00	4.92	7.9	3.00	0.360	0.855	Bar	.0012	ds	10	0.625	0.402	1.273	1.274	1.191	1.192	5.4	0.042	0.418	0.337	1.12	.0660	0.557	0.72	0.576
1221	WW	0.6	1.00	4.92	7.9	3.00	0.360	0.855	Bar	.0012	ds	8	0.625	0.399	1.271	1.270	1.193	1.192	4.8	0.039	0.416	0.338	1.11	.0526	0.570	0.72	0.586
1222	WW	0.6	1.00	4.92	7.9	3.00	0.360	0.855	Bar	.0012	ds	4	0.625	0.394	1.267	1.266	1.194	1.191	5.0	0.034	0.412	0.338	1.09	.0263	0.598	0.72	0.605
1223	WW	0.6	1.00	4.92	7.9	3.00	0.360	0.855	Bar	.0012	ds	5	1.25	0.403	1.276	1.277	1.194	1.194	5.3	0.043	0.422	0.339	1.12	.0660	0.557	0.73	0.576
1224	WW	0.6	1.00	4.92	7.9	3.00	0.360	0.855	Bar	.0012	ds	4	1.25	0.400	1.274	1.273	1.194	1.192	5.0	0.040	0.419	0.338	1.11	.0526	0.570	0.73	0.586
1225	WW	0.6	1.00	4.92	7.9	3.00	0.360	0.855	Bar	.0012	ds	2	1.25	0.396	1.266	1.266	1.195	1.193	-	0.036	0.411	0.339	1.10	.0263	0.598	0.73	0.605
1252	WW	0.6	1.00	5.9	7.9	3.00	0.360	0.855	Bar	.0012	ds	12	0.625	0.381	1.251	1.252	1.199	1.199	4.5	0.021	0.397	0.344	1.06	.0791	0.667	0.72	0.690
1253R	WW	0.6	1.00	5.9	7.9	3.00	0.360	0.855	Bar	.0012	ds	8	0.625	0.377	1.249	1.249	1.201	1.200	5.0	0.017	0.394	0.345	1.05	.0526	0.693	0.72	0.709
1254	WW	0.6	1.00	5.9	7.9	3.00	0.360	0.855	Bar	.0012	ds	6	0.625	0.374	1.247	1.247	1.199	1.198	4.7	0.014							
1255	WW	0.6	1.00	5.9	7.9	3.00	0.360	0.855	Bar	.0012	ds	4	0.625	0.374	1.246	1.245	1.200	1.199	5.0	0.014	0.391	0.345	1.04	.0263	0.720	0.72	0.728
1259	WW	0.6	1.00	5.9	7.9	3.00	0.360	0.855	Bar	.0012	ds	2	1.25	0.375	1.246	1.244	1.200	1.198	4.5	0.015	0.390	0.344	1.04	.0263	0.720	0.73	0.728
1260	WW	0.6	1.00	5.9	7.9	3.00																					

TABLE 7 : PIERS WITH ABUTMENTS [continued]
45 degree wing-wall abutment

Measured Data														Computed Data													
Run No.	Model Type	Model height [ft]	Model length [ft]	b [ft]	B [ft]	Q [cfs]	h _n [ft]	Bottom Rdg.	Roughness	Slope	Type of Piers	Number of Piers	Diameter of Piers [in]	h ₁ [ft]	R _{UR}	R _{UL}	R _{DR}	R _{DL}	L*	h ₁ * [ft]	h _U	h _D	h _L / h _n	ND / B	M	S	M*
1233	WW	0.6	1.00	4.92	7.9	3.00	0.360	0.855	Bar	.0012	rn	8	0.625	0.394	1.265	1.266	1.192	1.192	4.8	0.034	0.411	0.337	1.094	.0526	0.570	0.49	0.598
1234	WW	0.6	1.00	4.92	7.9	3.00	0.360	0.855	Bar	.0012	rn	4	0.625	0.391	1.261	1.260	1.195	1.191	5.4	0.031	0.406	0.338	1.086	.0263	0.597	0.49	0.611
1243	WW	0.6	1.00	5.90	7.9	3.00	0.360	0.855	Bar	.0012	rn	12	0.625	0.377	1.250	1.247	1.199	1.198	4.5	0.017	0.394	0.344	1.047	.0788	0.669	0.49	0.708
1244	WW	0.6	1.00	5.90	7.9	3.00	0.360	0.855	Bar	.0012	rn	8	0.625	0.373	1.246	1.243	1.201	1.201	4.8	0.013	0.390	0.346	1.036	.0526	0.595	0.49	0.722
1245	WW	0.6	1.00	5.90	7.9	3.00	0.360	0.855	Bar	.0012	rn	6	0.625	0.373	1.244	1.242	1.201	1.199	4.5	0.013	0.388	0.345	1.038	.0396	0.707	0.49	0.729
1246	WW	0.6	1.00	5.90	7.9	3.00	0.360	0.855	Bar	.0012	rn	6	1.25	0.376	1.248	1.246	1.202	1.200	5.0	0.016	0.392	0.346	1.044	.0788	0.669	0.52	0.709
1247	WW	0.6	1.00	5.90	7.9	3.00	0.360	0.855	Bar	.0012	rn	4	1.25	0.374	1.244	1.246	1.202	1.200	4.5	0.014	0.391	0.346	1.040	.0526	0.695	0.52	0.722
1248	WW	0.6	1.00	5.90	7.9	3.00	0.360	0.855	Bar	.0012	rn	2	1.25	0.373	1.244	1.245	1.203	1.199	4.7	0.013	0.390	0.346	1.038	.0263	0.722	0.52	0.735
1169	WW	0.6	1.00	2.91	7.9	3.00	0.360	0.855	Bar	.0012	Sq	6	0.625	0.550	1.416	1.416	1.175	1.166	4.2	0.190	0.561	0.316	1.530	.0396	0.328	1.46	0.310
1170	WW	0.6	1.00	2.91	7.9	3.00	0.360	0.855	Bar	.0012	Sq	4	0.625	0.531	1.399	1.401	1.176	1.170	5.0	0.171	0.545	0.318	1.476	.0263	0.342	1.46	0.330
1171	WW	0.6	1.00	2.91	7.9	3.00	0.360	0.855	Bar	.0012	Sq	2	0.625	0.513	1.383	1.381	1.177	1.167	5.3	0.153	0.527	0.317	1.425	.0131	0.355	1.46	0.349
1201	WW	0.6	1.00	3.89	7.9	3.00	0.360	0.855	Bar	.0012	Sq	8	0.625	0.462	1.331	1.334	1.183	1.182	4.4	0.102	0.478	0.328	1.284	.0526	0.441	1.46	0.416
1202	WW	0.6	1.00	3.89	7.9	3.00	0.360	0.855	Bar	.0012	Sq	6	0.625	0.451	1.321	1.321	1.183	1.180	5.0	0.091	0.466	0.327	1.254	.0394	0.453	1.46	0.435
1203	WW	0.6	1.00	3.89	7.9	3.00	0.360	0.855	Bar	.0012	Sq	4	0.625	0.441	1.310	1.310	1.185	1.183	5.1	0.081	0.455	0.329	1.228	.0263	0.442	1.46	0.455
1237	WW	0.6	1.00	4.92	7.9	3.00	0.360	0.855	Bar	.0012	Sq	10	0.625	0.415	1.285	1.285	1.191	1.191	5.1	0.055	0.430	0.336	1.152	.0526	0.558	1.46	0.528
1238	WW	0.6	1.00	4.92	7.9	3.00	0.360	0.855	Bar	.0012	Sq	8	0.625	0.408	1.278	1.278	1.191	1.190	4.5	0.048	0.423	0.336	1.132	.0656	0.570	1.46	0.547
1239R	WW	0.6	1.00	4.92	7.9	3.00	0.360	0.855	Bar	.0012	Sq	4	0.625	0.396	1.266	1.266	1.190	1.191	4.5	0.036	0.411	0.336	1.110	.0263	0.598	1.46	0.586
1265	WW	0.6	1.00	5.90	7.9	3.00	0.360	0.855	Bar	.0012	Sq	12	0.625	0.392	1.265	1.260	1.200	1.201	5.3	0.032	0.408	0.346	1.090	.0788	0.669	1.46	0.643
1266	WW	0.6	1.00	5.90	7.9	3.00	0.360	0.855	Bar	.0012	Sq	8	0.625	0.384	1.256	1.255	1.201	1.201	5.0	0.024	0.401	0.346	1.069	.0526	0.695	1.46	0.671
1267	WW	0.6	1.00	5.90	7.9	3.00	0.360	0.855	Bar	.0012	Sq	4	0.625	0.378	1.251	1.247	1.201	1.200	5.1	0.018	0.394	0.346	1.050	.0263	0.722	1.46	0.710
1172	WW	0.6	1.00	2.91	7.9	3.00	0.360	0.855	Bar	.0012	r	6	0.625	0.540	1.406	1.405	1.175	1.173	4.9	0.180	0.551	0.319	1.50	.0396	0.329	1.28	0.317
1173R	WW	0.6	1.00	2.91	7.9	3.00	0.360	0.855	Bar	.0012	r	4	0.625	0.528	1.396	1.394	1.181	1.172	4.7	0.168	0.540	0.322	1.46	.0263	0.342	1.28	0.335
1174	WW	0.6	1.00	2.91	7.9	3.00	0.360	0.855	Bar	.0012	r	2	0.625	0.512	1.379	1.379	1.177	1.170	4.5	0.152	0.524	0.319	1.42	.0131	0.355	1.28	0.352
1198	WW	0.6	1.00	3.89	7.9	3.00	0.360	0.855	Bar	.0012	r	8	0.625	0.454	1.325	1.323	1.184	1.181	4.5	0.094	0.469	0.329	1.26	.0526	0.439	1.28	0.426
1199	WW	0.6	1.00	3.89	7.9	3.00	0.360	0.855	Bar	.0012	r	6	0.625	0.444	1.313	1.314	1.184	1.182	5.9	0.084	0.459	0.328	1.23	.0396	0.453	1.28	0.443
1200	WW	0.6	1.00	3.89	7.9	3.00	0.360	0.855	Bar	.0012	r	4	0.625	0.436	1.304	1.304	1.183	1.183	4.5	0.076	0.449	0.328	1.21	.0263	0.466	1.28	0.460
1240	WW	0.6	1.00	4.92	7.9	3.00	0.360	0.855	Bar	.0012	r	10	0.625	0.409	1.282	1.279	1.192	1.190	4.5	0.049	0.426	0.336	1.13	.0656	0.557	1.28	0.540
1241	WW	0.6	1.00	4.92	7.9	3.00	0.360	0.855	Bar	.0012	r	8	0.625	0.403	1.276	1.283	1.191	1.190	4.5	0.043	0.425	0.336	1.12	.0526	0.570	1.28	0.545
1242	WW	0.6	1.00	4.92	7.9	3.00	0.360	0.855	Bar	.0012	r	4	0.625	0.395	1.266	1.265	1.193	1.191	4.9	0.035	0.411	0.337	1.10	.0263	0.598	1.28	0.590
1262	WW	0.6	1.00	5.9	7.9	3.00	0.360	0.855	Bar	.0012	r	12	0.625	0.388	1.261	1.258	1.202	1.199	5.3	0.028	0.405	0.346	1.08	.0788	0.668	1.28	0.646
1263	WW	0.6	1.00	5.9	7.9	3.00	0.360	0.855	Bar	.0012	r	8	0.625	0.383	1.255	1.252	1.201	1.200	4.9	0.023	0.399	0.346	1.06	.0526	0.694	1.28	0.679
1264	WW	0.6	1.00	5.9	7.9	3.00	0.360	0.855	Bar	.0012	r	4	0.625	0.377	1.250	1.247	1.201	1.201	5.0	0.017	0.394	0.346	1.05	.0263	0.721	1.28	0.713
1175	WW	0.6	1.00	2.91	7.9	3.00	0.360	0.855	Bar	.0012	H	3	0.625	0.529	1.396	1.393	1.176	1.170	4.7	0.169	0.540	0.318	1.47	.0198	0.349		
1176	WW	0.6	1.00	2.91	7.9	3.00	0.360	0.855	Bar	.0012	H	2	0.625	0.519	1.385	1.383	1.179	1.174	4.5	0.159	0.529	0.322	1.44	.0131	0.355		
1196	WW	0.6	1.00	3.89	7.9	3.00	0.360	0.855	Bar	.0012	H	3	0.625	0.438	1.307	1.306	1.185	1.183	5.6	0.078	0.452	0.329	1.22	.0198	0.473		
1197	WW	0.6	1.00	3.89	7.9	3.00	0.360	0.855	Bar	.0012	H	2	0.625	0.432	1.298	1.302	1.185	1.185	5.5	0.072	0.445	0.330	1.20	.0131	0.479		
1235	WW	0.6	1.00	4.92	7.9	3.00	0.360	0.855	Bar	.0012	H	4	0.625	0.399	1.269	1.268	1.195	1.192	4.8	0.039	0.414	0.339	1.11	.0263	0.597		
1236	WW	0.6	1.00	4.92	7.9	3.00	0.360	0.855	Bar	.0012	H	2	0.625	0.392	1.263	1.262	1.191	1.190	4.7	0.032	0.408	0.336	1.09	.0131	0.610		
1268	WW	0.6	1.00	5.90	7.9	3.00	0.360	0.855	Bar	.0012	H	4	0.625	0.379	1.250	1.249	1.202	1.200	5.2	0.019	0.395	0.346	1.05	.0263	0.721		
627	WW	0.6	1.00	5.91	7.9	5.00	0.484	0.853	Bar	.0012	ds	2	3.5	0.509	1.387	1.382	1.316	1.317	-	0.025	0.532	0.464	1.052	.0739	0.675	0.92	0.681
628	WW	0.6	1.00	5.91	7.9	5.00	0.484	0.853	Bar	.0012	ds	2	1.125	0.503	1.375	1.378	1.311	1.310	-	0.019	0.524	0.458	1.039	.0253	0.724	0.72	0.726
499	WW	0.9	1.00	4.48	7.9	5.00	0.484	0.866	Bar	.0012	rn	2	1.125	0.556	1.441	1.443	1.301	1.308	-	0.072	0.576	0.439	1.149	.0253	0.540	0.50	0.552
500	WW	0.9	1.00	4.46	7.9	5.00	0.484	0.866	Bar	.0012	rn	4	1.125	0.564	1.449	1.441	1.300	1.293	-	0.080	0.579	0.431	1.165	.0506	0.514	0.50	0.540
501	WW	0.9	1.00	4.46	7.9	5.00	0.484	0.866	Bar	.0012	rn	4	1.75	0.582	1.467	1.462	1.299	1.304	-	0.098	0.599	0.435	1.202	.0739	0.491	0.54	0.525
502	WW	0.9	1.00	4.46	7.9	5.00	0.484	0.866	Bar	.0012	rn	2	1.75	0.563	1.447	1.445	1.304	1.304	-	0.079	0.580	0.438	1.163	.0369	0.528	0.54	0.545
503	WW	0.9	1.00	4.46	7.9	5.00	0.484	0.866	Bar	.0012	rn	2	2.40	0.568	1.454	1.450	1.305	1.301	-	0.084	0.586	0.437	1.174	.0506	0.514	0.60	0.534
504	WW	0.9	1.00	4.46	7.9	5.00	0.484	0.866	Bar	.0012	rn	4	2.40	0.607	1.483	1.481	1.298	1.293	-	0.123	0.616	0.430	1.254	.1012	0.464	0.60	0.504
523	WW	0.9	1.00	3.44	7.9	5.00	0.484																				

TABLE 7 : PIERS WITH ABUTMENTS [continued]
45 degree wing-wall abutment

Measured Data													Computed Data														
Run No.	Model Type	Model height [ft]	Model length [ft]	b [ft]	B [ft]	Q [cfs]	h_1 [ft]	Bottom Rdg.	Roughness	Slope	Type of Piers	Number of Piers	Diameter of Piers [in]	h_1 [ft]	R_{UR}	R_{UL}	R_{DR}	R_{DL}	L^*	h_1^* [ft]	h_U	h_D	$\frac{h_1}{h_n}$	$\frac{ND}{B}$	M	S	M*
520	WW	0.9	1.00	3.44	7.9	5.00	0.484	0.866	Bar	.0012	ss	2	2.4	0.662	1.543	1.543	1.283	1.277	-	0.178	0.677	0.414	1.368	.051	0.384	0.48	0.410
521	WW	0.9	1.00	3.44	7.9	5.00	0.484	0.866	Bar	.0012	ss	4	2.4	0.692	1.570	1.570	1.285	1.276	-	0.208	0.704	0.414	1.430	.101	0.334	0.48	0.386
522	WW	0.9	1.00	3.44	7.9	5.00	0.484	0.866	Bar	.0012	ss	2	3.5	0.679	1.559	1.556	1.280	1.272	-	0.195	0.692	0.410	1.403	.074	0.361	0.62	0.386
529	WW	0.9	1.00	2.44	7.9	5.00	0.484	0.866	Bar	.0012	ss	2	2.4	0.848	1.713	1.727	1.276	1.248	-	0.364							
530	WW	0.9	1.00	2.44	7.9	5.00	0.484	0.866	Bar	.0012	ss	2	1.125	0.820	1.691	1.694	1.266	1.253	-	0.336	0.827	0.394	1.694	.024	0.285	0.41	0.299
535	WW	0.9	1.00	2.44	7.9	5.00	0.484	0.866	Bar	.0012	ss	2	2.4	0.843	1.716	1.716	1.247	1.273	-	0.359	0.850	0.394	1.742	.051	0.258	0.48	0.288
511	WW	0.9	1.00	4.46	7.9	5.00	0.484	0.866	Bar	.0012	ds	2	1.125	0.555	1.444	1.438	1.300	1.317	-	0.071	0.574	0.442	1.147	.024	0.541	0.72	0.548
512	WW	0.9	1.00	4.46	7.9	5.00	0.484	0.866	Bar	.0012	ds	2	2.4	0.564	1.443	1.443	1.300	1.302	-	0.080	0.577	0.435	1.165	.051	0.514	0.78	0.525
513	WW	0.9	1.00	4.46	7.9	5.00	0.484	0.866	Bar	.0012	ds	2	3.5	0.583	1.467	1.461	1.302	1.304	-	0.099	0.598	0.437	1.205	.074	0.491	0.92	0.497
515	WW	0.9	1.00	3.46	7.9	5.00	0.484	0.866	Bar	.0012	ds	2	3.5	0.698	1.604	1.602	1.297	1.283	-	0.214	0.737	0.424	1.442	.074	0.364	0.92	0.373
516	WW	0.9	1.00	3.46	7.9	5.00	0.484	0.866	Bar	.0012	ds	2	2.4	0.669	1.548	1.546	1.289	1.287	-	0.185	0.681	0.422	1.382	.051	0.387	0.78	0.398
517	WW	0.9	1.00	3.44	7.9	5.00	0.484	0.866	Bar	.0012	ds	2	1.125	0.657	1.539	1.537	1.285	1.276	-	0.173	0.672	0.415	1.357	.024	0.411	0.72	0.418
531	WW	0.9	1.00	2.44	7.9	5.00	0.484	0.866	Bar	.0012	ds	2	1.125	0.827	1.703	1.701	1.253	1.281	-	0.343	0.836	0.401	1.709	.024	0.285	0.73	0.292
532	WW	0.9	1.00	2.44	7.9	5.00	0.484	0.866	Bar	.0012	ds	2	2.4	0.867	1.742	1.742	1.261	1.283	-	0.383	0.876	0.406	1.791	.051	0.258	0.78	0.269
625	WW	0.6	1.00	5.91	7.9	5.00	0.484	0.853	Bar	.0012	ds	2	2.4	0.508	1.382	1.375	1.314	1.312	-	0.024	0.523	0.460	1.049	.051	0.698	0.78	0.709
612	WW	0.6	1.00	5.92	7.9	5.00	0.484	0.866	Bar	.0012	ss	2	3.5	0.511	1.393	1.396	1.318	1.325	-	0.026	0.529	0.456	1.056	.074	0.675	0.62	0.703
613	WW	0.6	1.00	5.92	7.9	5.00	0.484	0.866	Bar	.0012	ss	4	3.5	0.524	1.408	1.412	1.323	1.325	-	0.040	0.544	0.458	1.073	.148	0.601	0.62	0.657
614	WW	0.6	1.00	5.92	7.9	5.00	0.484	0.866	Bar	.0012	ss	4	2.4	0.514	1.398	1.399	1.322	1.323	-	0.030	0.533	0.457	1.062	.100	0.649	0.476	0.701
615	WW	0.6	1.00	5.92	7.9	5.00	0.484	0.866	Bar	.0012	ss	2	2.4	0.508	1.392	1.391	1.318	1.326	-	0.024	0.526	0.456	1.050	.050	0.699	0.476	0.725
616	WW	0.6	1.00	5.92	7.9	5.00	0.484	0.866	Bar	.0012	ss	2	1.25	0.504	1.388	1.391	1.321	1.324	-	0.020	0.524	0.457	1.041	.026	0.723	0.41	0.736
617	WW	0.6	1.00	5.92	7.9	5.00	0.484	0.866	Bar	.0012	ss	4	1.25	0.508	1.390	1.393	1.319	1.321	-	0.024	0.526	0.454	1.050	.053	0.696	0.41	0.727
890	WW	0.9	1.00	4.46	7.9	5.00	0.484	0.855	Bar	.0012	Sq	6	0.625	0.579	1.461	1.448	1.296	1.290	-	0.095	0.600	0.438	1.196	.040	0.525	1.1	0.521
891R	WW	0.9	1.00	4.46	7.9	5.00	0.484	0.855	Bar	.0012	Sq	4	0.625	0.571	1.452	1.449	1.296	1.300	-	0.087	0.596	0.443	1.179	.026	0.539	1.1	0.536
892R	WW	0.9	1.00	4.46	7.9	5.00	0.484	0.855	Bar	.0012	Sq	2	0.625	0.569	1.451	1.447	1.295	1.296	-	0.085	0.594	0.441	1.176	.013	0.552	1.1	0.530
934	WW	0.9	1.00	2.42	7.9	5.00	0.484	0.855	Bar	.0012	Sq	1	0.625	0.814	1.686	1.686	1.250	1.269	-	0.330	0.831	0.405	1.682	.007	0.299	1.1	0.298
935	WW	0.9	1.00	2.42	7.9	5.00	0.484	0.855	Bar	.0012	Sq	2	0.625	0.824	1.691	1.689	1.241	1.265	-	0.340	0.835	0.398	1.702	.013	0.293	1.1	0.291
936	WW	0.9	1.00	2.42	7.9	5.00	0.484	0.855	Bar	.0012	Sq	3	0.625	0.841	1.707	1.706	1.241	1.267	-	0.357	0.852	0.399	1.738	.020	0.286	1.1	0.284
887RR	WW	0.9	1.00	4.46	7.9	5.00	0.484	0.855	Bar	.0012	r	2	0.625	0.565	1.443	1.436	1.299	1.293	-	0.081	0.585	0.441	1.167	.013	0.552	0.96	0.552
888R	WW	0.9	1.00	4.46	7.9	5.00	0.484	0.855	Bar	.0012	r	4	0.625	0.570	1.449	1.449	1.302	1.300	-	0.086	0.594	0.446	1.177	.026	0.539	0.96	0.540
889RR	WW	0.9	1.00	4.46	7.9	5.00	0.484	0.855	Bar	.0012	r	6	0.625	0.575	1.453	1.453	1.300	1.304	-	0.091	0.598	0.447	1.188	.040	0.525	0.96	0.527
931	WW	0.9	1.00	2.42	7.9	5.00	0.484	0.855	Bar	.0012	r	3	0.625	0.832	1.700	1.703	1.242	1.262	-	0.348	0.847	0.397	1.719	.020	0.286	0.96	0.268
932	WW	0.9	1.00	2.42	7.9	5.00	0.484	0.855	Bar	.0012	r	2	0.625	0.821	1.700	1.688	1.256	1.268	-	0.337	0.839	0.407	1.696	.013	0.293	0.96	0.293
933	WW	0.9	1.00	2.42	7.9	5.00	0.484	0.855	Bar	.0012	r	1	0.625	0.808	1.682	1.677	1.252	1.264	-	0.324	0.825	0.403	1.669	.007	0.299	0.96	0.300
924	WW	0.9	1.00	4.42	7.9	5.00	0.484	0.855	Bar	.0012	H	1	0.625	0.553	1.436	1.430	1.291	1.301	-	0.069	0.578	0.445	1.143	.007	0.551		
925	WW	0.9	1.00	4.42	7.9	5.00	0.484	0.855	Bar	.0012	H	2	0.625	0.556	1.440	1.433	1.293	1.295	-	0.072	0.582	0.439	1.149	.013	0.546		
926	WW	0.9	1.00	4.42	7.9	5.00	0.484	0.855	Bar	.0012	H	3	0.625	0.555	1.440	1.434	1.290	1.294	-	0.071	0.582	0.437	1.147	.020	0.539		
928	WW	0.9	1.00	2.42	7.9	5.00	0.484	0.855	Bar	.0012	H	1	0.625	0.801	1.625	1.673	1.257	1.236	-	0.317	0.796	0.392	1.657	.007	0.299		
929	WW	0.9	1.00	2.42	7.9	5.00	0.484	0.855	Bar	.0012	H	2	0.625	0.822	1.692	1.685	1.262	1.242	-	0.338	0.834	0.397	1.698	.013	0.293		
930	WW	0.9	1.00	2.42	7.9	5.00	0.484	0.856	Bar	.0012	H	3	0.625	0.830	1.703	1.701	1.255	1.240	-	0.346	0.846	0.392	1.715	.020	0.286		
801	WW	0.9	1.00	4.46	7.9	2.50	0.333	0.854	Bar	.0012	Sq	6	0.625	0.386	1.255	1.249	1.162	1.161	-	0.053	0.398	0.308	1.156	.040	0.525	1.80	0.493
802	WW	0.9	1.00	4.46	7.9	2.50	0.333	0.854	Bar	.0012	Sq	4	0.625	0.378	1.246	1.241	1.163	1.162	-	0.045	0.390	0.309	1.135	.026	0.539	1.80	0.518
803	WW	0.9	1.00	4.46	7.9	2.50	0.333	0.855	Bar	.0012	Sq	2	0.625	0.373	1.243	1.238	1.161	1.162	-	0.040							
804R	WW	0.9	1.00	4.46	7.9	2.50	0.333	0.855	Bar	.0012	Sq	1	0.625	0.374	1.240	1.242	1.166	1.167	-	0.041	0.386	0.312	1.123	.007	0.558	1.80	0.552
824	WW	0.9	1.00	2.42	7.9	2.50	0.333	0.855	Bar	.0012	Sq	1	0.625	0.514	1.382	1.375	1.138	1.133	-	0.181	0.524	0.281	1.543	.007	0.299	1.80	0.293
825	WW	0.9	1.00	2.42	7.9	2.50	0.333	0.855	Bar	.0012	Sq	2	0.625	0.528	1.392	1.387	1.137	1.135	-	0.195	0.535	0.281	1.585	.013	0.293	1.80	0.283
826	WW	0.9	1.00	2.42	7.9	2.50	0.333	0.855	Bar	.0012	Sq	4	0.625	0.542	1.407	1.402	1.141	1.133	-	0.209	0.550	0.282	1.628	.026	0.280	1.80	0.259
950	WW	0.9	1.00	4.46	7.9	2.50	0.333	0.855	Bar	.0012	Sq	1	0.625	0.373	1.242	1.239	1.160	1.159	-	0.040	0.386	0.305	1.120	.007	0.558	1.80	0.552
951	WW	0.9	1.00	4.46	7.9	2.50	0.333	0.855	Bar	.0012	Sq	2	0.625	0.375	1.245	1.243	1.163	1.162	-	0.042	0.389	0.308	1.126	.013	0.552	1.80	0.541
952	WW	0.9	1.00	4.46	7.9	2.50	0.333	0.855																			

TABLE 7 : PIERS WITH ABUTMENTS [continued]
45 degree wing-wall abutment

Measured Data																	Computed Data											
Run No.	Model Type	Model height [ft]	Model length [ft]	b [ft]	B [ft]	Q [cfs]	h_n [ft]	Bottom Rdg.	Roughness	Slope	Type of Piers	Number of Piers	Diameter of Piers [in]	h_1 [ft]	R_{UR}	R_{UL}	R_{DR}	R_{DL}	L*	h_1^* [ft]	h_U	h_D	$\frac{h_L}{h_n}$	$\frac{ND}{B}$	M	S	M*	
829	WW	0.9	1.00	2.42	7.9	2.50	0.333	0.855	Bar	.0012	r	1	0.625	0.514	1.400	1.375	1.145	1.133	-	0.181	0.533	0.284	1.543	.007	0.299	1.30	0.297	
805	WW	0.9	1.00	4.42	7.9	2.50	0.333	0.855	Bar	.0012	H	1	0.625	0.370	1.238	1.237	1.160	1.159	-	0.037	0.382	0.305	1.111	.007	0.553			
806	WW	0.9	1.00	4.42	7.9	2.50	0.333	0.855	Bar	.0012	H	3	0.625	0.373	1.243	1.238	1.162	1.161	-	0.040	0.386	0.307	1.120	.021	0.553			
777	WW	0.9	1.00	4.42	7.9	2.50	0.523	0.856	Baffle	.0012	r	2	0.625	0.544	1.403	1.399	1.368	1.364	-	0.021								
778	WW	0.9	1.00	4.42	7.9	2.50	0.523	0.856	Baffle	.0012	r	4	0.625	0.544	1.407	1.403	1.364	1.367	-	0.021								
779	WW	0.9	1.00	4.42	7.9	2.50	0.523	0.855	Baffle	.0012	r	6	0.625	0.545	1.408	1.405	1.369	1.366	-	0.022								
793	WW	0.9	1.00	2.44	7.9	2.50	0.523	0.854	Baffle	.0012	r	4	0.625	0.633	1.491	1.488	1.359	1.355	-	0.110								
794	WW	0.9	1.00	2.44	7.9	2.50	0.523	0.855	Baffle	.0012	r	2	0.625	0.627	1.487	1.486	1.358	1.356	-	0.104								
795	WW	0.9	1.00	2.44	7.9	2.50	0.523	0.854	Baffle	.0012	r	1	0.625	0.619	-	-	-	-	-	-	0.096							

Type of Piers

- ss - Single shaft pier
- ds - Double shaft pier
- rn - Round-ended narrow pier
- r - Round rod pile bents
- H - H-beam pile bents

TABLE 7 : PIERS WITH ABUTMENTS
1:1.5 spill-through abutment

Measured Data														Computed Data													
Run No	Model Type	Model height [ft]	Model length [ft]	b [ft]	B [ft]	Q [cfs]	h ₁ [ft]	Bottom Rdg.	Roughness	Slope	Type of Piers	Number of Piers	Diameter of Piers [in]	h ₁ [ft]	R _{UR}	R _{UL}	R _{DR}	R _{DL}	L*	h ₁ * [ft]	h _U	h _D	h ₁ h _n	ND B	M	S	M*
1083R	ST	0.90	1.00	2.44	7.9	5.00	0.484	0.855	Bar	.0012	rn	2	0.625	0.730	1.600	1.603	1.261	1.275	4.5	0.246	0.747	0.413	1.510	.013	0.388	0.34	0.396
1084R	ST	0.90	1.00	2.44	7.9	5.00	0.484	0.855	Bar	.0012	rn	4	0.625	0.742	1.612	1.614	1.271	1.257	4.5	0.258	0.758	0.409	1.537	.026	0.375	0.34	0.390
1085R	ST	0.90	1.00	2.44	7.9	5.00	0.484	0.855	Bar	.0012	rn	6	0.625	0.756	1.627	1.629	1.274	1.258	4.1	0.272	0.773	0.411	1.565	.039	0.361	0.34	0.387
1087R	ST	0.90	1.00	3.15	7.9	5.00	0.484	0.855	Bar	.0012	rn	2	0.625	0.601	1.477	1.476	1.280	1.272	5.5	0.117	0.622	0.421	1.243	.013	0.477	0.34	0.485
1088R	ST	0.90	1.00	3.15	7.9	5.00	0.484	0.855	Bar	.0012	rn	4	0.625	0.613	1.492	1.487	1.292	1.279	-	0.129	0.635	0.431	1.270	.026	0.464	0.34	0.479
1089R	ST	0.90	1.00	3.15	7.9	5.00	0.484	0.855	Bar	.0012	rn	6	0.625	0.622	1.498	1.495	1.295	1.283	4.3	0.138	0.642	0.434	1.288	.039	0.450	0.34	0.476
1090R	ST	0.90	1.00	3.15	7.9	5.00	0.484	0.855	Bar	.0012	rn	8	0.625	0.626	1.503	1.500	1.278	1.269	5.1	0.142	0.647	0.419	1.296	.053	0.437	0.34	0.472
1092R	ST	0.90	1.00	4.14	7.9	5.00	0.484	0.855	Bar	.0012	rn	2	0.625	0.541	1.423	1.422	1.297	1.294	5.3	0.057	0.568	0.441	1.120	.013	0.602	0.34	0.610
1093R	ST	0.90	1.00	4.14	7.9	5.00	0.484	0.855	Bar	.0012	rn	4	0.625	0.544	1.422	1.424	1.298	1.295	5.5	0.060	0.568	0.442	1.123	.026	0.589	0.34	0.604
1094R	ST	0.90	1.00	4.14	7.9	5.00	0.484	0.855	Bar	.0012	rn	6	0.625	0.546	1.423	1.426	1.300	1.297	5.3	0.062	0.570	0.444	1.130	.039	0.575	0.34	0.601
1095	ST	0.90	1.00	4.14	7.9	5.00	0.484	0.855	Bar	.0012	rn	10	0.625	0.553	1.430	1.432	1.300	1.304	5.1	0.069	0.576	0.447	1.132	.066	0.549	0.34	0.593
1104	ST	0.90	1.00	5.15	7.9	5.00	0.484	0.855	Bar	.0012	rn	10	0.625	0.511	1.385	1.391	1.314	1.317	6.0	0.027	0.533	0.461	1.057	.066	0.679	0.34	0.723
1105	ST	0.90	1.00	5.15	7.9	5.00	0.484	0.855	Bar	.0012	rn	8	0.625	0.508	1.377	1.386	1.314	1.315	4.9	0.024	0.527	0.460	1.050	.053	0.692	0.34	0.727
1106	ST	0.90	1.00	5.15	7.9	5.00	0.484	0.855	Bar	.0012	rn	6	0.625	0.507	1.378	1.383	1.316	1.315	5.9	0.023	0.526	0.461	1.049	.039	0.705	0.34	0.731
1080R	ST	0.90	1.00	2.15	7.9	5.00	0.484	0.855	Bar	.0012	rn	1	1.25	0.728	1.600	1.606	1.260	1.282	5.3	0.244	0.748	0.416	1.506	.013	0.350	0.49	0.357
1081R	ST	0.90	1.00	2.15	7.9	5.00	0.484	0.855	Bar	.0012	rn	2	1.25	0.741	1.609	1.612	1.279	1.260	4.9	0.257	0.756	0.415	1.531	.026	0.337	0.49	0.350
1082R	ST	0.90	1.00	2.15	7.9	5.00	0.484	0.855	Bar	.0012	rn	3	1.25	0.752	1.621	1.624	1.264	1.278	4.5	0.268	0.768	0.416	1.569	.039	0.323	0.49	0.343
1096R	ST	0.90	1.00	4.14	7.9	5.00	0.484	0.855	Bar	.0012	rn	2	1.25	0.544	1.421	1.422	1.294	1.295	-	0.060	0.567	0.440	1.121	.026	0.589	0.49	0.602
1097R	ST	0.90	1.00	4.14	7.9	5.00	0.484	0.855	Bar	.0012	rn	3	1.25	0.545	1.422	1.421	1.292	1.293	4.1	0.061	0.567	0.438	1.129	.039	0.577	0.49	0.598
1098R	ST	0.90	1.00	4.14	7.9	5.00	0.484	0.855	Bar	.0012	rn	4	1.25	0.548	1.424	1.424	1.296	1.295	5.1	0.064	0.569	0.441	1.132	.053	0.564	0.49	0.591
1099R	ST	0.90	1.00	4.14	7.9	5.00	0.484	0.855	Bar	.0012	rn	5	1.25	0.549	1.426	1.426	1.300	1.301	4.7	0.065	0.571	0.446	1.138	.066	0.551	0.49	0.585
1100R	ST	0.90	1.00	3.15	7.9	5.00	0.484	0.855	Bar	.0012	rn	4	1.25	0.627	1.503	1.503	1.291	1.274	5.1	0.143	0.648	0.428	1.298	.053	0.437	0.49	0.464
1101R	ST	0.90	1.00	3.15	7.9	5.00	0.484	0.855	Bar	.0012	rn	3	1.25	0.617	1.491	1.492	1.272	1.285	4.7	0.133	0.637	0.424	1.278	.039	0.450	0.49	0.471
1102R	ST	0.90	1.00	3.15	7.9	5.00	0.484	0.855	Bar	.0012	rn	2	1.25	0.611	1.489	1.488	1.286	1.272	5.5	0.127	0.634	0.424	1.265	.026	0.464	0.49	0.477
1103R	ST	0.90	1.00	3.15	7.9	5.00	0.606	1.481	1.483	1.279	1.281	4.9	1.25	0.606	1.481	1.483	1.279	1.281	4.9	0.122	0.627	0.425	1.255	.013	0.477	0.49	0.483
1107	ST	0.90	1.00	5.15	7.9	5.00	0.484	0.855	Bar	.0012	rn	5	1.25	0.509	1.381	1.387	1.313	1.315	-	0.025	0.529	0.459	1.052	.066	0.680	0.49	0.714
1108	ST	0.90	1.00	5.15	7.9	5.00	0.508	1.377	1.386	1.314	1.315	5.1	1.25	0.508	1.377	1.386	1.314	1.315	5.1	0.024	0.527	0.460	1.050	.053	0.693	0.49	0.720
1109	ST	0.90	1.00	5.15	7.9	5.00	0.484	0.855	Bar	.0012	rn	2	1.25	0.506	1.376	1.382	1.312	1.314	6.2	0.022	0.524	0.458	1.049	.026	0.720	0.49	0.733
550	ST	0.90	1.00	4.17	7.9	5.00	0.546	1.432	1.428	1.306	1.302	-	1.25	0.546	1.432	1.428	1.306	1.302	-	0.062	0.564	0.438	1.130	.053	0.567	0.49	0.594
551	ST	0.90	1.00	4.17	7.9	5.00	0.484	0.866	Bar	.0012	rn	2	1.25	0.542	1.430	1.427	1.311	1.311	-	0.058	0.563	0.445	1.120	.026	0.594	0.49	0.607
640	ST	0.60	1.00	5.87	7.9	5.00	0.495	1.364	1.360	1.317	1.316	-	1.25	0.495	1.364	1.360	1.317	1.316	-	0.011	0.507	0.462	1.022	.026	0.810	0.49	0.823
641	ST	0.60	1.00	5.87	7.9	5.00	0.484	0.855	Bar	.0012	rn	4	1.25	0.498	1.368	1.361	1.319	1.317	-	0.014	0.510	0.463	1.030	.053	0.783	0.49	0.810
642	ST	0.60	1.00	5.87	7.9	5.00	0.493	1.362	1.358	1.316	1.317	-	1.75	0.493	1.362	1.358	1.316	1.317	-	0.009	0.505	0.462	1.020	.037	0.799	0.59	0.814
643	ST	0.60	1.00	5.87	7.9	5.00	0.484	0.855	Bar	.0012	rn	4	1.75	0.496	1.364	1.361	1.320	1.320	-	0.012	0.508	0.465	1.028	.074	0.762	0.59	0.792
548	ST	0.90	1.00	4.17	7.9	5.00	0.546	1.436	1.431	1.306	1.309	-	1.75	0.546	1.436	1.431	1.306	1.309	-	0.062	0.568	0.442	1.130	.037	0.583	0.59	0.598
549	ST	0.90	1.00	4.17	7.9	5.00	0.484	0.866	Bar	.0012	rn	4	1.75	0.559	1.443	1.439	1.304	1.304	-	0.075	0.575	0.438	1.156	.074	0.546	0.59	0.576
546	ST	0.90	1.00	4.17	7.9	5.00	0.551	1.435	1.431	1.301	1.306	-	2.4	0.551	1.435	1.431	1.301	1.306	-	0.067	0.567	0.438	1.140	.037	0.583	0.66	0.586
547	ST	0.90	1.00	4.18	7.9	5.00	0.484	0.866	Bar	.0012	rn	4	2.4	0.571	1.454	1.452	1.299	1.300	-	0.087	0.587	0.434	1.181	.101	0.519	0.66	0.554
639	ST	0.60	1.00	5.87	7.9	5.00	0.499	1.366	1.363	1.316	1.314	-	2.4	0.499	1.366	1.363	1.316	1.314	-	0.015	0.512	0.462	1.031	.051	0.784	0.66	0.802
644	ST	0.60	1.00	5.87	7.9	5.00	0.484	0.855	Bar	.0012	rn	4	2.4	0.499	1.367	1.365	1.318	1.316	-	0.015	0.511	0.462	1.031	.101	0.734	0.66	0.769
993	ST	0.90	1.00	5.17	7.9	5.00	0.504	1.378	1.374	1.316	1.312	-	2.4	0.504	1.378	1.374	1.316	1.312	-	0.020	0.521	0.459	1.040	.013	0.733	0.19	0.743
994	ST	0.90	1.00	5.17	7.9	5.00	0.484	0.855	Bar	.0012	ss	4	0.625	0.505	1.380	1.379	1.316	1.315	4.9	0.021	0.525	0.461	1.043	.026	0.720	0.19	0.741
995	ST	0.90	1.00	5.17	7.9	5.00	0.484	0.855	Bar	.0012	ss	6	0.625	0.506	1.383	1.381	1.315	1.315	5.5	0.022	0.527	0.460	1.049	.039	0.706	0.19	0.738
996	ST	0.90	1.00	5.17	7.9	5.00	0.484	0.855	Bar	.0012	ss	10	0.625	0.508	1.386	1.382	1.318	1.314	6.1	0.024	0.529	0.461	1.050	.066	0.680	0.19	0.733
1816	ST	0.90	1.00	4.14	7.9	5.00	0.484	0.855	Bar	.0012	ss	10	0.625	0.548	1.426	1.425	1.303	1.301	4.5	0.064	0.571	0.447	1.132	.066	0.552	0.19	0.605
1017R	ST	0.90	1.00	4.14	7.9	5.00	0.484	0.855	Bar	.0012	ss	6	0.625	0.543	1.421	1.419	1.305	1.303	4.7	0.059	0.565	0.449	1.122	.039	0.578	0.19	0.610
1018	ST	0.90	1.00	4.14	7.9	5.00	0.542	1.419	1.418	1.302	1.300	4.9	0.625	0.542	1.419	1.418	1.302										

TABLE 7: PIERS WITH ABUTMENTS [continued]
1:1.5 spill-through abutment

Measured Data													Computed Data															
Run No.	Model Type	Model height [ft]	Model length [ft]	b [ft]	B [ft]	Q [cfs]	h_n [ft]	Bottom Rdg	Roughness	Slope	Type of Piers	Number of Piers	Diameter of Piers [in]	h_i [ft]	R_{UR}	R_{UL}	R_{DR}	R_{DL}	L^*	h_i^* [ft]	h_U	h_D	h_n	$\frac{ND}{B}$	M	S	M*	
1056	ST	0.90	1.00	3.13	7.9	5.00	0.484	0.855	Bar	.0012	ss	4	1.25	0.613	1.484	1.482	1.288	1.280	5.5	0.129	0.628	0.429	1.268	.053	0.436	0.36	0.470	
1074	ST	0.90	1.00	2.15	7.9	5.00	0.484	0.855	Bar	.0012	ss	1	1.25	0.724	1.593	1.593	1.279	1.255	4.7	0.240	0.738	0.412	1.499	.013	0.351	0.36	0.359	
1075	ST	0.90	1.00	2.15	7.9	5.00	0.484	0.855	Bar	.0012	ss	2	1.25	0.729	1.599	1.599	1.279	1.253	4.7	0.245	0.744	0.413	1.508	.026	0.338	0.36	0.355	
1076	ST	0.90	1.00	2.15	7.9	5.00	0.484	0.855	Bar	.0012	ss	3	1.25	0.735	1.602	1.601	1.280	1.254	5.1	0.251	0.747	0.412	1.520	.039	0.325	0.36	0.350	
537	ST	0.90	1.00	4.19	7.9	5.00	0.484	0.866	Bar	.0012	ss	2	3.5	0.556	1.442	1.439	1.312	1.312	-	0.072	0.575	0.446	1.150	.074	0.547	0.61	0.576	
538	ST	0.90	1.00	4.19	7.9	5.00	0.484	0.866	Bar	.0012	ss	4	3.5	0.572	1.449	1.452	1.311	1.311	-	0.088	0.585	0.445	1.183	.148	0.473	0.61	0.571	
633	ST	0.60	1.00	5.88	7.9	5.00	0.484	0.853	Bar	.0012	ss	2	3.5	0.499	1.368	1.361	1.315	1.318	-	0.015	0.512	0.464	1.031	.074	0.761	0.61	0.790	
638	ST	0.60	1.00	5.88	7.9	5.00	0.484	0.853	Bar	.0012	ss	4	3.5	0.508	1.377	1.370	1.319	1.319	-	0.024	0.521	0.466	1.050	.148	0.687	0.61	0.745	
539	ST	0.90	1.00	4.19	7.9	5.00	0.484	0.866	Bar	.0012	ss	2	2.4	0.551	1.436	1.434	1.314	1.304	-	0.067	0.569	0.443	1.140	.051	0.570	0.52	0.594	
540	ST	0.90	1.00	4.19	7.9	5.00	0.484	0.866	Bar	.0012	ss	4	2.4	0.558	1.442	1.437	1.316	1.314	-	0.074	0.574	0.449	1.151	.101	0.520	0.52	0.569	
634	ST	0.60	1.00	5.88	7.9	5.00	0.484	0.853	Bar	.0012	ss	2	2.4	0.499	1.368	1.363	1.317	1.318	-	0.015	0.513	0.465	1.031	.051	0.784	0.52	0.809	
637	ST	0.60	1.00	5.88	7.9	5.00	0.484	0.853	Bar	.0012	ss	4	2.4	0.503	1.371	1.365	1.319	1.319	-	0.019	0.515	0.466	1.040	.101	0.734	0.52	0.783	
541	ST	0.90	1.00	4.19	7.9	5.00	0.484	0.866	Bar	.0012	ss	4	1.25	0.547	1.436	1.430	1.315	1.308	-	0.063	0.567	0.446	1.131	.053	0.568	0.36	0.602	
542	ST	0.90	1.00	4.19	7.9	5.00	0.484	0.866	Bar	.0012	ss	2	1.25	0.548	1.434	1.430	1.313	1.309	-	0.064	0.566	0.445	1.132	.026	0.595	0.36	0.612	
635	ST	0.60	1.00	5.88	7.9	5.00	0.484	0.853	Bar	.0012	ss	2	1.25	0.497	1.366	1.359	1.318	1.319	-	0.013	0.510	0.466	1.029	.026	0.809	0.36	0.826	
636	ST	0.60	1.00	5.88	7.9	5.00	0.484	0.853	Bar	.0012	ss	4	1.25	0.499	1.367	1.364	1.319	1.319	-	0.015	0.513	0.466	1.031	.053	0.782	0.36	0.816	
997	ST	0.90	1.00	5.17	7.9	5.00	0.484	0.855	Bar	.0012	ds	10	0.625	0.511	1.386	1.383	1.320	1.319	5.5	0.027	0.530	0.465	1.059	.066	0.680	0.39	0.720	
998	ST	0.90	1.00	5.17	7.9	5.00	0.484	0.855	Bar	.0012	ds	6	0.625	0.507	1.384	1.382	1.318	1.319	5.3	0.023	0.528	0.464	1.049	.039	0.707	0.39	0.731	
1020	ST	0.90	1.00	4.15	7.9	5.00	0.484	0.855	Bar	.0012	ds	2	0.625	0.545	1.422	1.420	1.305	1.303	-	0.061								
1021	ST	0.90	1.00	4.14	7.9	5.00	0.484	0.855	Bar	.0012	ds	10	0.625	0.551	1.425	1.425	1.304	1.300	5.7	0.067	0.570	0.447	1.140	.066	0.550	0.39	0.590	
1022	ST	0.90	1.00	4.14	7.9	5.00	0.484	0.855	Bar	.0012	ds	6	0.625	0.546	1.422	1.422	1.304	1.302	5.5	0.062	0.567	0.448	1.130	.039	0.577	0.39	0.601	
1023	ST	0.90	1.00	4.14	7.9	5.00	0.484	0.855	Bar	.0012	ds	4	0.625	0.544	1.421	1.419	1.302	1.301	5.5	0.060	0.565	0.447	1.122	.026	0.590	0.39	0.606	
1049	ST	0.90	1.00	3.13	7.9	5.00	0.484	0.855	Bar	.0012	ds	8	0.625	0.618	1.493	1.489	1.298	1.280	5.5	0.134	0.636	0.434	1.280	.053	0.435	0.39	0.467	
1050RR	ST	0.90	1.00	3.13	7.9	5.00	0.484	0.855	Bar	.0012	ds	6	0.625	0.615	1.488	1.487	1.290	1.281	5.9	0.131	0.633	0.430	1.272	.039	0.449	0.39	0.473	
1051R	ST	0.90	1.00	3.13	7.9	5.00	0.484	0.855	Bar	.0012	ds	4	0.625	0.611	1.483	1.482	1.299	1.283	6.1	0.127	0.628	0.436	1.266	.026	0.462	0.39	0.478	
1052	ST	0.90	1.00	3.13	7.9	5.00	0.484	0.855	Bar	.0012	ds	2	0.625	0.608	1.481	1.479	1.286	1.279	5.3	0.124	0.625	0.428	1.259	.013	0.475	0.39	0.483	
1071	ST	0.90	1.00	2.15	7.9	5.00	0.484	0.855	Bar	.0012	ds	2	0.625	0.724	1.597	1.594	1.292	1.256	5.3	0.240	0.741	0.419	1.497	.013	0.351	0.39	0.359	
1072	ST	0.90	1.00	2.15	7.9	5.00	0.484	0.855	Bar	.0012	ds	4	0.625	0.731	1.602	1.600	1.281	1.256	4.7	0.247	0.746	0.414	1.512	.026	0.338	0.39	0.354	
1073	ST	0.90	1.00	2.15	7.9	5.00	0.484	0.855	Bar	.0012	ds	6	0.625	0.739	1.609	1.611	1.281	1.262	4.7	0.255	0.755	0.417	1.529	.039	0.325	0.39	0.349	
1003	ST	0.90	1.00	5.17	7.9	5.00	0.484	0.855	Bar	.0012	ds	5	1.25	0.514	1.385	1.386	1.316	1.318	6.1	0.030	0.531	0.462	1.060	.066	0.680	0.55	0.710	
1004R	ST	0.90	1.00	5.17	7.9	5.00	0.484	0.855	Bar	.0012	ds	3	1.25	0.508	1.384	1.383	1.318	1.317	5.9	0.024	0.529	0.463	1.050	.039	0.707	0.55	0.725	
1005	ST	0.90	1.00	5.17	7.9	5.00	0.484	0.855	Bar	.0012	ds	2	1.25	0.507	1.380	1.379	1.315	1.314	5.7	0.023	0.525	0.460	1.049	.026	0.720	0.55	0.732	
1006	ST	0.90	1.00	5.17	7.9	5.00	0.484	0.855	Bar	.0012	ds	1	1.25	0.506	1.382	1.376	1.315	1.315	5.7	0.022	0.524	0.460	1.047	.013	0.733	0.55	0.739	
1028	ST	0.90	1.00	4.14	7.9	5.00	0.484	0.855	Bar	.0012	ds	5	1.25	0.556	1.434	1.433	1.304	1.300	5.5	0.072	0.579	0.447	1.151	.066	0.550	0.55	0.580	
1029	ST	0.90	1.00	4.14	7.9	5.00	0.484	0.855	Bar	.0012	ds	3	1.25	0.549	1.427	1.426	1.300	1.299	5.5	0.065	0.572	0.445	1.133	.039	0.577	0.55	0.595	
1030	ST	0.90	1.00	4.14	7.9	5.00	0.484	0.855	Bar	.0012	ds	2	1.25	0.547	1.422	1.421	1.302	1.300	5.3	0.063	0.567	0.446	1.130	.026	0.590	0.55	0.602	
1031	ST	0.90	1.00	4.14	7.9	5.00	0.484	0.855	Bar	.0012	ds	1	1.25	0.544	1.421	1.420	1.303	1.298	4.9	0.060	0.566	0.446	1.123	.013	0.603	0.55	0.609	
1057	ST	0.90	1.00	3.13	7.9	5.00	0.484	0.855	Bar	.0012	ds	4	1.25	0.622	1.500	1.498	1.290	1.282	5.3	0.138	0.644	0.431	1.286	.053	0.435	0.55	0.459	
1058	ST	0.90	1.00	3.13	7.9	5.00	0.484	0.855	Bar	.0012	ds	3	1.25	0.620	1.493	1.490	1.295	1.283	5.5	0.136	0.637	0.434	1.281	.039	0.449	0.55	0.466	
1059	ST	0.90	1.00	3.13	7.9	5.00	0.484	0.855	Bar	.0012	ds	2	1.25	0.614	1.489	1.489	1.295	1.289	5.5	0.130	0.634	0.437	1.269	.026	0.462	0.55	0.474	
1060	ST	0.90	1.00	3.13	7.9	5.00	0.484	0.855	Bar	.0012	ds	1	1.25	0.609	1.487	1.481	1.294	1.284	5.3	0.125	0.629	0.434	1.260	.013	0.475	0.55	0.481	
1077	ST	0.90	1.00	2.15	7.9	5.00	0.484	0.855	Bar	.0012	ds	3	1.25	0.745	1.611	1.615	1.281	1.257	5.5	0.261	0.758	0.414	1.540	.039	0.325	0.55	0.343	
1078	ST	0.90	1.00	2.15	7.9	5.00	0.484	0.855	Bar	.0012	ds	2	1.25	0.735	1.602	1.601	1.278	1.256	5.1	0.251	0.747	0.412	1.520	.026	0.338	0.55	0.350	
1079	ST	0.90	1.00	2.15	7.9	5.00	0.484	0.855	Bar	.0012	ds	1	1.25	0.727	1.597	1.597	1.277	1.257	5.1	0.243	0.742	0.412	1.502	.013	0.351	0.55	0.358	
543	ST	0.90	1.00	4.18	7.9	5.00	0.484	0.866	Bar	.0012	ds	2	1.25	0.548	1.431	1.420	1.316	1.307	-	0.064	0.560	0.446	1.132	.026	0.594	0.55	0.606	
632	ST	0.60	1.00	5.87	7.9	5.00	0.484	0.853	Bar	.0012	ds	2	1.25	0.497	1.367	1.363	1.317	1.317	-	0.013	0.512	0.464	1.029	.026	0.809	0.55	0.821	
631	ST	0.60	1.00	5.87	7.9	5.00	0.484	0.853	Bar	.0012	ds	2	2.4	0.499	1.364	1.359	1.315	1.315	-	0.015	0.509	0.462	1.031	.051	0.784	0.71	0.799	
544	ST	0.90	1.00	4.18	7.9	5.																						

TABLE 7 : PIERS WITH ABUTMENTS
1:1.5 spill-through abutment and vertical board model

Run No.	Model Type	Model height [ft]	Model length [ft]	b [ft]	B [ft]	Q [cfs]	Measured Data					Computed Data															
							h_1 [ft]	Bottom Rdg.	Roughness	Slope	Type of Piers	Number of Piers	Diameter of Piers [in]	h_1 [ft]	R_{UR}	R_{UL}	R_{DR}	R_{DL}	L^*	h_1^* [ft]	h_U	h_D	$\frac{h_L}{h_n}$	$\frac{ND}{B}$	M	S	M*
989	ST	0.90	1.00	5.17	7.9	5.00	0.484	0.855	Bar	.0012	Sq	2	0.625	0.505	1.379	1.380	1.317	1.316	5.3	0.021	0.525	0.462	1.043	.013	0.732	1.016	0.732
990	ST	0.90	1.00	5.17	7.9	5.00	0.484	0.855	Bar	.0012	Sq	4	0.625	0.508	1.381	1.381	1.318	1.316	6.3	0.024	0.526	0.462	1.050	.026	0.719	1.016	0.719
991	ST	0.90	1.00	5.17	7.9	5.00	0.484	0.855	Bar	.0012	Sq	6	0.625	0.513	1.388	1.387	1.319	1.318	5.3	0.029	0.533	0.464	1.060	.039	0.706	1.016	0.705
992	ST	0.90	1.00	5.17	7.9	5.00	0.484	0.855	Bar	.0012	Sq	10	0.625	0.521	1.395	1.394	1.318	1.319	5.9	0.037	0.540	0.464	1.079	.066	0.679	1.016	0.678
1012	ST	0.90	1.00	4.14	7.9	5.00	0.484	0.855	Bar	.0012	Sq	2	0.625	0.547	1.421	1.425	1.302	1.301	5.5	0.063	0.568	0.447	1.130	.013	0.603	1.016	0.603
1013	ST	0.90	1.00	4.14	7.9	5.00	0.484	0.855	Bar	.0012	Sq	4	0.625	0.552	1.429	1.426	1.309	1.305	5.3	0.068	0.573	0.452	1.140	.026	0.590	1.016	0.590
1014	ST	0.90	1.00	4.14	7.9	5.00	0.484	0.855	Bar	.0012	Sq	6	0.625	0.558	1.435	1.433	1.302	1.298	4.9	0.074	0.579	0.445	1.153	.039	0.577	1.016	0.576
1015	ST	0.90	1.00	4.14	7.9	5.00	0.484	0.855	Bar	.0012	Sq	10	0.625	0.575	1.450	1.451	1.305	1.302	5.5	0.091	0.596	0.449	1.190	.066	0.550	1.016	0.549
1039	ST	0.90	1.00	3.13	7.9	5.00	0.484	0.855	Bar	.0012	Sq	2	0.625	0.613	1.485	1.487	1.281	1.278	5.1	0.129	0.631	0.425	1.269	.013	0.475	1.016	0.475
1040	ST	0.90	1.00	3.13	7.9	5.00	0.484	0.855	Bar	.0012	Sq	4	0.625	0.623	1.495	1.498	1.284	1.277	4.7	0.139	0.642	0.426	1.289	.026	0.462	1.016	0.462
1041	ST	0.90	1.00	3.13	7.9	5.00	0.484	0.855	Bar	.0012	Sq	6	0.625	0.635	1.508	1.508	1.287	1.279	4.7	0.151	0.653	0.428	1.311	.039	0.449	1.016	0.448
1042	ST	0.90	1.00	3.13	7.9	5.00	0.484	0.855	Bar	.0012	Sq	8	0.625	0.647	1.517	1.519	1.288	1.279	5.5	0.163	0.663	0.429	1.339	.053	0.435	1.016	0.434
1065	ST	0.90	1.00	2.14	7.9	5.00	0.484	0.855	Bar	.0012	Sq	2	0.625	0.734	1.601	1.602	1.274	1.249	4.7	0.250	0.747	0.407	1.518	.013	0.350	1.016	0.350
1066	ST	0.90	1.00	2.14	7.9	5.00	0.484	0.855	Bar	.0012	Sq	4	0.625	0.752	1.621	1.622	1.275	1.249	5.5	0.268	0.767	0.407	1.557	.026	0.337	1.016	0.337
1067	ST	0.90	1.00	2.14	7.9	5.00	0.484	0.855	Bar	.0012	Sq	6	0.625	0.771	1.636	1.637	1.274	1.250	4.7	0.287	0.782	0.407	1.594	.039	0.324	1.016	0.323
1032	ST	0.90	1.00	4.14	7.9	5.00	0.484	0.855	Bar	.0012	H	2	0.625	0.546	1.419	1.421	1.304	1.298	5.3	0.062	0.565	0.446	1.130	.013	0.603		
1033	ST	0.90	1.00	4.14	7.9	5.00	0.484	0.855	Bar	.0012	H	4	0.625	0.552	1.425	1.426	1.301	1.300	5.5	0.068	0.571	0.446	1.141	.026	0.590		
1043	ST	0.90	1.00	3.13	7.9	5.00	0.484	0.855	Bar	.0012	H	2	0.625	0.613	1.486	1.485	1.294	1.276	5.5	0.129	0.631	0.430	1.268	.013	0.475		
1044	ST	0.90	1.00	3.13	7.9	5.00	0.484	0.855	Bar	.0012	H	4	0.625	0.623	1.497	1.496	1.298	1.284	4.7	0.139	0.642	0.436	1.289	.026	0.462		
1157	ST	0.90	1.00	3.15	7.9	3.00	0.360	0.855	Bar	.0012	rn	6	0.625	0.459	1.327	1.326	1.185	1.185	5.3	0.099							
1158	ST	0.90	1.00	3.15	7.9	3.00	0.360	0.855	Bar	.0012	rn	4	0.625	0.451	1.320	1.317	1.188	1.186	5.5	0.091							
1159	ST	0.90	1.00	3.15	7.9	3.00	0.360	0.855	Bar	.0012	rn	2	0.625	0.445	1.312	1.313	1.187	1.185	5.5	0.085							
1160	ST	0.90	1.00	3.15	7.9	3.00	0.360	0.855	Bar	.0012	rn	1	0.625	0.442	1.310	1.308	1.187	1.186	5.3	0.082							
438	VB	1.67	-	5.00	7.9	2.50	0.333	0.866	Bar	.0012	ss	4	1.25	0.382	1.258	1.257	1.173	1.171	-	0.049							
439	VB	1.67	-	5.00	7.9	2.50	0.333	0.866	Bar	.0012	ss	2	2.4	0.384	1.256	1.255	1.167	1.168	-	0.051							
440	VB	1.67	-	5.00	7.9	2.50	0.333	0.866	Bar	.0012	ss	4	2.4	0.390	1.267	1.266	1.174	1.172	-	0.057							
441	VB	1.67	-	5.00	7.9	2.50	0.333	0.866	Bar	.0012	ss	2	3.5	0.388	1.262	1.260	1.172	1.170	-	0.055							
442	VB	1.67	-	5.00	7.9	2.50	0.333	0.866	Bar	.0012	ss	4	3.5	0.401	1.276	1.274	1.173	1.171	-	0.068							

TABLE 7: PIERS WITH ABUTMENTS [DUAL BRIDGES]
45 degree wing-wall abutments

Run No.	Model Type	Model height [ft]	Model length [ft]	b [ft]	B [ft]	Q [cfs]	h _n [ft]	Bottom Rdg.	Roughness	Slope	Type of Piers	Number of Piers	Diameter of Piers [in]	h _i [ft]	Measured Data		Computed Data		Upstream abutment		Downstream abutment		L _D [ft]	h _i *	Upstream abutment		Downstream abutment		h _i / h _n	ND/B	M	S	M*
															R _U	R _D	R _U	R _D	h _U	h _D	h _U	h _D											
899	2WW	0.90	1.00	4.46	7.9	5.00	0.484	0.855	Bar	.0012	Sq	6	0.625	0.600	1.475	1.361	1.364	1.292	3.3	0.116	0.620	0.506	0.509	0.437	1.239	.040	0.524	1.1	0.520				
900	2WW	0.90	1.00	4.46	7.9	5.00	0.484	0.855	Bar	.0012	Sq	4	0.625	0.587	1.469	1.344	1.349	1.296	3.3	0.103	0.614	0.489	0.494	0.441	1.212	.026	0.538	1.1	0.535				
901	2WW	0.90	1.00	4.46	7.9	5.00	0.484	0.855	Bar	.0012	Sq	2	0.625	0.575	1.453	1.344	1.348	1.297	3.3	0.091	0.598	0.489	0.493	0.442	1.188	.013	0.551	1.1	0.550				
906R	2WW	0.90	1.00	2.42	7.9	5.00	0.484	0.855	Bar	.0012	Sq	3	0.625	0.902	1.769	1.593	1.607	1.255	3.3	0.418	0.914	0.738	0.752	0.400	1.863	.020	0.286	1.1	0.284				
907R	2WW	0.90	1.00	2.42	7.9	5.00	0.484	0.855	Bar	.0012	Sq	2	0.625	0.868	1.738	1.566	1.574	1.238	3.3	0.384	0.883	0.711	0.719	0.383	1.793	.013	0.293	1.1	0.292				
908	2WW	0.90	1.00	2.42	7.9	5.00	0.484	0.855	Bar	.0012	Sq	1	0.625	0.835	1.699	1.517	1.525	1.246	3.3	0.351	0.844	0.662	0.670	0.391	1.725	.007	0.299	1.1	0.298				
913	2WW	0.90	1.00	2.42	7.9	5.00	0.484	0.855	Bar	.0012	Sq	3	0.625	0.892	1.761	1.577	1.606	1.253	10.00	0.408	0.906	0.722	0.751	0.398	1.842	.020	0.286	1.1	0.284				
914	2WW	0.90	1.00	2.42	7.9	5.00	0.484	0.855	Bar	.0012	Sq	2	0.625	0.875	1.743	1.577	1.605	1.258	10.00	0.391	0.888	0.702	0.750	0.403	1.807	.013	0.293	1.1	0.292				
915	2WW	0.90	1.00	2.42	7.9	5.00	0.484	0.855	Bar	.0012	Sq	1	0.625	0.856	1.731	1.573	1.615	1.261	10.00	0.372	0.876	0.718	0.760	0.406	1.768	.007	0.299	1.1	0.298				
920	2WW	0.90	1.00	4.42	7.9	5.00	0.484	0.855	Bar	.0012	Sq	6	0.625	0.618	1.491	1.379	1.408	1.299	10.00	0.134	0.636	0.524	0.553	0.444	1.276	.040	0.519	1.1	0.526				
921	2WW	0.90	1.00	4.42	7.9	5.00	0.484	0.855	Bar	.0012	Sq	4	0.625	0.599	1.475	1.363	1.389	1.298	10.00	0.115	0.620	0.508	0.534	0.443	1.237	.026	0.533	1.1	0.531				
922	2WW	0.90	1.00	4.42	7.9	5.00	0.484	0.855	Bar	.0012	Sq	2	0.625	0.580	1.459	1.349	1.378	1.292	10.00	0.096	0.604	0.494	0.523	0.437	1.198	.013	0.546	1.1	0.546				
896	2WW	0.90	1.00	4.46	7.9	5.00	0.484	0.855	Bar	.0012	r	2	0.625	0.574	1.451	1.338	1.339	1.307	3.3	0.090	0.596	0.483	0.484	0.452	1.185	.013	0.551	0.96	0.552				
897	2WW	0.90	1.00	4.46	7.9	5.00	0.484	0.855	Bar	.0012	r	4	0.625	0.583	1.460	1.353	1.355	1.298	3.3	0.099	0.605	0.498	0.500	0.443	1.204	.026	0.538	0.96	0.539				
898	2WW	0.90	1.00	4.46	7.9	5.00	0.484	0.855	Bar	.0012	r	6	0.625	0.592	1.470	1.359	1.362	1.293	3.3	0.108	0.615	0.504	0.507	0.438	1.221	.040	0.524	0.96	0.526				
903	2WW	0.90	1.00	2.42	7.9	5.00	0.484	0.855	Bar	.0012	r	1	0.625	0.851	1.711	1.528	1.544	1.241	3.3	0.367	0.856	0.673	0.689	0.386	1.578	.007	0.299	0.96	0.299				
904	2WW	0.90	1.00	2.42	7.9	5.00	0.484	0.855	Bar	.0012	r	2	0.625	0.854	1.723	1.543	1.558	1.261	3.3	0.370	0.868	0.688	0.703	0.406	1.764	.013	0.293	0.96	0.294				
905	2WW	0.90	1.00	2.42	7.9	5.00	0.484	0.855	Bar	.0012	r	3	0.625	0.871	1.756	1.586	1.592	1.256	3.3	0.387	0.901	0.731	0.737	0.401	1.800	.020	0.286	0.96	0.287				
910	2WW	0.90	1.00	2.42	7.9	5.00	0.484	0.855	Bar	.0012	r	1	0.625	0.854	1.722	1.555	1.616	1.245	10.00	0.370	0.867	0.700	0.761	0.390	1.764	.007	0.299	0.96	0.300				
911	2WW	0.90	1.00	2.42	7.9	5.00	0.484	0.855	Bar	.0012	r	2	0.625	0.870	1.735	1.556	1.596	1.254	10.00	0.386	0.880	0.701	0.741	0.411	1.800	.013	0.293	0.96	0.294				
917R	2WW	0.90	1.00	4.42	7.9	5.00	0.484	0.855	Bar	.0012	r	2	0.625	0.584	1.454	1.351	1.378	1.299	10.00	0.100	0.599	0.496	0.523	0.444	1.207	.013	0.547	0.96	0.547				
918R	2WW	0.90	1.00	4.42	7.9	5.00	0.484	0.855	Bar	.0012	r	4	0.625	0.599	1.471	1.371	1.399	1.303	10.00	0.115	0.616	0.516	0.544	0.448	1.225	.026	0.534	0.96	0.534				
919	2WW	0.90	1.00	4.42	7.9	5.00	0.484	0.855	Bar	.0012	r	6	0.625	0.605	1.486	1.371	1.398	1.299	10.00	0.121	0.631	0.516	0.543	0.444	1.250	.040	0.520	0.96	0.522				
813	2WW	0.90	1.00	4.42	7.9	2.50	0.333	0.855	Bar	.0012	Sq	6	0.625	0.393	1.260	1.190	1.191	1.163	3.3	0.060	0.405	0.335	0.336	0.308	1.179	.040	0.520	1.8	0.488				
814	2WW	0.90	1.00	4.42	7.9	2.50	0.333	0.855	Bar	.0012	Sq	4	0.625	0.368	1.256	1.183	1.184	1.163	3.3	0.055	0.401	0.328	0.329	0.308	1.104	.026	0.534	1.8	0.513				
815R	2WW	0.90	1.00	4.42	7.9	2.50	0.333	0.855	Bar	.0012	Sq	2	0.625	0.387	1.254	1.178	1.177	1.163	3.3	0.054	0.399	0.323	0.322	0.308	1.161	.013	0.547	1.8	0.537				
817	2WW	0.90	1.00	4.42	7.9	2.50	0.333	0.855	Bar	.0012	Sq	2	0.625	0.395	1.261	1.400	1.205	1.175	10.00	0.062	0.406	0.345	0.350	0.320	1.185	.013	0.547	1.8	0.537				
818	2WW	0.90	1.00	4.42	7.9	2.50	0.333	0.855	Bar	.0012	Sq	4	0.625	0.400	1.265	1.202	1.208	1.174	10.00	0.067	0.410	0.347	0.353	0.319	1.200	.026	0.534	1.8	0.513				
819	2WW	0.90	1.00	4.42	7.9	2.50	0.333	0.855	Bar	.0012	Sq	6	0.625	0.409	1.267	1.208	1.226	1.178	10.00	0.076	0.412	0.353	0.371	0.323	1.227	.040	0.520	1.8	0.488				
834	2WW	0.90	1.00	2.42	7.9	2.50	0.333	0.855	Bar	.0012	Sq	1	0.625	0.541	1.404	1.232	1.286	1.145	3.3	0.208	0.549	0.377	0.431	0.290	1.623	.007	0.299	1.8	0.293				
835	2WW	0.90	1.00	2.42	7.9	2.50	0.333	0.855	Bar	.0012	Sq	2	0.625	0.561	1.422	1.298	1.297	1.145	3.3	0.228	0.567	0.443	0.442	0.290	1.683	.013	0.293	1.8	0.283				
836	2WW	0.90	1.00	2.42	7.9	2.50	0.333	0.855	Bar	.0012	Sq	4	0.625	0.579	1.440	1.314	1.314	1.139	3.3	0.246	0.585	0.459	0.459	0.284	1.737	.026	0.280	1.8	0.259				
845	2WW	0.90	1.00	2.42	7.9	2.50	0.333	0.855	Bar	.0012	Sq	4	0.625	0.592	1.450	1.339	1.355	1.155	10.00	0.259	0.595	0.484	0.500	0.300	1.776	.026	0.280	1.8	0.259				
846	2WW	0.90	1.00	2.42	7.9	2.50	0.333	0.855	Bar	.0012	Sq	2	0.625	0.567	1.424	1.317	1.339	1.154	10.00	0.234	0.569	0.462	0.484	0.299	1.701	.013	0.293	1.8	0.283				
847	2WW	0.90	1.00	2.42	7.9	2.50	0.333	0.855	Bar	.0012	Sq	1	0.625	0.553	1.412	1.313	1.333	1.153	10.00	0.220	0.557	0.458	0.478	0.298	1.655	.007	0.299	1.8	0.293				
810	2WW	0.90	1.00	4.46	7.9	2.50	0.333	0.855	Bar	.0012	r	2	0.625	0.382	1.251	1.185	1.185	1.167	3.3	0.049	0.396	0.330	0.330	0.312	1.146	.013	0.552	1.3	0.548				
811R	2WW	0.90	1.00	4.46	7.9	2.50	0.333	0.855	Bar	.0012	r	4	0.625	0.387	1.255	1.179	1.178	1.166	3.3	0.054	0.400	0.324	0.323	0.311	1.161	.026	0.539	1.3	0.531				
812	2WW	0.90	1.00	4.46	7.9	2.50	0.333	0.855	Bar	.0012	r	6	0.625	0.391	1.256	1.191	1.193	1.166	3.3	0.058	0.401	0.336	0.338	0.311	1.173	.040	0.525	1.3	0.513				
820	2WW	0.90	1.00	4.46	7.9	2.50	0.333	0.855	Bar	.0012	r	6	0.625	0.404	1.269	1.205	1.225	1.177	10.00	0.071	0.414	0.350	0.370	0.322	1.212	.040	0.525	1.3	0.513				
821R	2WW	0.90	1.00	4.46	7.9	2.50	0.333	0.855	Bar	.0012	r	4	0.625	0.400	1.265	1.198	1.216	1.167	10.00	0.067	0.410	0.343	0.361	0.312	1.200	.026	0.539	1.3	0.531				
822R	2WW	0.90	1.00	4.46	7.9	2.50	0.333	0.855	Bar	.0012	r	2	0.625	0.395	1.259	1.188	1.207	1.168	10.00	0.062	0.404	0.333	0.352	0.313	1.185	.013	0.552	1.3	0.548				
837	2WW	0.90	1.00	2.42	7.9	2.50	0.333	0.855	Bar	.0012	r	4	0.625	0.569	1.427	1.305	1.305	1.143	3.3	0.236	0.572	0.450	0.450	0.288	1.707	.026	0.280	1.3	0.272				
838R	2WW	0.90	1.00	2.42	7.9	2.50	0.333	0.855	Bar	.0012	r	2	0.625	0.548	1.409	1.293	1.																

TABLE 7 : PIERS WITHOUT ABUTMENTS

Run No.	Measured Data										Computed Data					
	b [ft]	B [ft]	Q [cfs]	h_n [ft]	Bottom Rdg.	Roughness	Slope	Type of Piers	Number of Piers	Diameter of Piers [in]	h_1 [ft]	h_1^* [ft]	$\frac{h_1}{h_n}$	$\frac{ND}{B}$	δ_o	C_{DA}
1133	7.1	7.9	3.00	0.360	0.855	Bar	.0012	rn	16	0.625	0.364	0.004	1.011	0.105	4.15	1.060
1134	7.3	7.9	3.00	0.360	0.855	Bar	.0012	rn	12	0.625	0.362	0.002	1.006	0.079	2.85	1.055
1135	7.5	7.9	3.00	0.360	0.855	Bar	.0012	rn	8	0.625	0.361	0.001	1.003	0.053	2.19	1.039
1136	7.1	7.9	3.00	0.360	0.855	Bar	.0012	rn	8	1.25	0.362	0.002	1.006	0.105	2.01	1.083
1137	7.3	7.9	3.00	0.360	0.855	Bar	.0012	rn	6	1.25	0.361	0.001	1.003	0.079	1.38	1.067
594	7.1	7.9	5.00	0.416	0.864	Bar	.0012	rn	4	2.4	0.423	0.007	1.017	0.101	3.42	1.076
595	7.5	7.9	5.00	0.416	0.864	Bar	.0012	rn	2	2.4	0.419	0.003	1.007	0.051	3.20	1.035
1118	7.7	7.9	5.00	0.484	0.855	Bar	.0012	rn	4	0.625	0.485	0.001				
1119R	7.5	7.9	5.00	0.484	0.855	Bar	.0012	rn	8	0.625	0.487	0.003				
1120	7.3	7.9	5.00	0.484	0.855	Bar	.0012	rn	12	0.625	0.488	0.004	1.008	0.079	3.68	1.044
1121	7.1	7.9	5.00	0.484	0.855	Bar	.0012	rn	16	0.625	0.490	0.006	1.012	0.105	4.00	1.065
1122	7.1	7.9	5.00	0.484	0.855	Bar	.0012	rn	8	1.25	0.490	0.006	1.012	0.105	4.00	1.065
1123	7.3	7.9	5.00	0.484	0.855	Bar	.0012	rn	6	1.25	0.488	0.004	1.008	0.079	3.55	1.044
1124	7.5	7.9	5.00	0.484	0.855	Bar	.0012	rn	4	1.25	0.487	0.003	1.006	0.053	4.28	1.030
1125	7.7	7.9	5.00	0.484	0.855	Bar	.0012	rn	2	1.25	0.485	0.001	1.002	0.026	3.00	1.015
1145	7.1	7.9	3.00	0.360	0.855	Bar	.0012	ss	16	0.625	0.363	0.003	1.008	0.105	3.20	1.073
1147	7.3	7.9	3.00	0.360	0.855	Bar	.0012	ss	12	0.625	0.361	0.001	1.003	0.079	1.45	1.066
1151	7.1	7.9	3.00	0.360	0.855	Bar	.0012	ss	8	1.25	0.362	0.002	1.006	0.105	2.10	1.093
1152	7.3	7.9	3.00	0.360	0.855	Bar	.0012	ss	6	1.25	0.361	0.001	1.003	0.079	1.45	1.066
1154	7.5	7.9	3.00	0.360	0.855	Bar	.0012	ss	4	1.25	0.361	0.001	1.003	0.053	2.40	1.038
596	6.7	7.9	5.00	0.416	0.864	Bar	.002	ss	4	3.6	0.429	0.013	1.031	0.152	4.21	1.108
597	7.3	7.9	5.00	0.416	0.864	Bar	.002	ss	2	3.6	0.423	0.007	1.017	0.076	4.34	1.042
608	7.3	7.9	5.00	0.484	0.866	Bar	.0012	ss	2	3.6	0.486	0.002	1.004	0.076	2.00	1.067
609	6.7	7.9	5.00	0.484	0.866	Bar	.0012	ss	4	3.6	0.492	0.008	1.017	0.152	3.75	1.112
610	7.5	7.9	5.00	0.484	0.866	Bar	.0012	ss	2	2.4	0.487	0.003	1.006	0.051	4.81	1.030
611	7.1	7.9	5.00	0.484	0.866	Bar	.0012	ss	4	2.4	0.490	0.006	1.012	0.101	4.45	1.018
1110	7.8	7.9	5.00	0.484	0.855	Bar	.0012	ss	2	1.25	0.485	0.001				
1111	7.5	7.9	5.00	0.484	0.855	Bar	.0012	ss	4	1.25	0.487	0.003	1.006	0.053	4.82	1.005
1112	7.3	7.9	5.00	0.484	0.855	Bar	.0012	ss	6	1.25	0.490	0.006	1.012	0.079	5.95	0.990
1113	7.1	7.9	5.00	0.484	0.855	Bar	.0012	ss	8	1.25	0.492	0.008	1.017	0.105	5.69	0.988
1126	7.5	7.9	5.00	0.484	0.855	Bar	.0012	ss	8	0.625	0.486	0.002	1.004	0.053	3.20	1.020
1127	7.3	7.9	5.00	0.484	0.855	Bar	.0012	ss	12	0.625	0.487	0.003	1.006	0.079	2.93	0.990
1128	7.1	7.9	5.00	0.484	0.855	Bar	.0012	ss	16	0.625	0.487	0.003	1.006	0.105	2.06	1.018
1146	7.1	7.9	3.00	0.360	0.855	Bar	.0012	ds	16	0.625	0.366	0.006	1.017	0.105	6.60	0.968
1148	7.3	7.9	3.00	0.360	0.855	Bar	.0012	ds	12	0.625	0.363	0.003	1.008	0.079	4.56	1.008
1149	7.5	7.9	3.00	0.360	0.855	Bar	.0012	ds	8	0.625	0.361	0.001	1.003	0.053	2.29	1.028
1150	7.1	7.9	3.00	0.360	0.855	Bar	.0012	ds	8	1.25	0.364	0.004	1.011	0.105	4.34	1.012
1153	7.3	7.9	3.00	0.360	0.855	Bar	.0012	ds	6	1.25	0.362	0.002	1.006	0.079	3.02	1.028
1155	7.5	7.9	3.00	0.360	0.855	Bar	.0012	ds	4	1.25	0.362	0.002	1.006	0.053	4.64	1.000
623	7.3	7.9	5.00	0.484	0.853	Bar	.0012	ds	2	3.5	0.490	0.006	1.012	0.074	6.28	0.990
624	7.5	7.9	5.00	0.484	0.853	Bar	.0012	ds	2	2.4	0.488	0.004	1.008	0.051	6.30	0.990
1114	7.1	7.9	5.00	0.484	0.855	Bar	.0012	ds	8	1.25	0.495	0.011	1.023	0.105	7.68	0.954
1115	7.3	7.9	5.00	0.484	0.855	Bar	.0012	ds	6	1.25						
1116	7.5	7.9	5.00	0.484	0.855	Bar	.0012	ds	4	1.25	0.489	0.005	1.010	0.053	7.48	0.975
1129	7.1	7.9	5.00	0.484	0.855	Bar	.0012	ds	16	0.625	0.491	0.007	1.014	0.105	4.84	1.005
1130	7.3	7.9	5.00	0.484	0.855	Bar	.0012	ds	12	0.625	0.490	0.006	1.012	0.079	5.83	0.990
1131	7.5	7.9	5.00	0.484	0.855	Bar	.0012	ds	8	0.625	0.488	0.004	1.008	0.053	5.98	0.990
1132	7.7	7.9	5.00	0.484	0.855	Bar	.0012	ds	4	0.625	0.485	0.001	1.002	0.026	3.39	1.009
771	7.4	7.9	2.50	0.535	0.855	Baffle	.0012	r	10	0.625	0.538	0.003	1.006	0.066	18.80	0.862
772	7.2	7.9	2.50	0.536	0.855	Baffle	.0012	r	14	0.625	0.539	0.003	1.007	0.092	13.15	0.884
773	7.0	7.9	2.50	0.536	0.854	Baffle	.0012	r	18	0.625	0.540	0.004	1.008	0.119	12.80	0.855
848	7.7	7.9	2.50	0.333	0.855	Bar	.0012	r	4	0.625	0.337	0.004	1.011	0.026	24.20	0.913
849	7.5	7.9	2.50	0.333	0.855	Bar	.0012	r	8	0.625	0.338	0.005	1.015	0.053	14.35	0.915
850	7.3	7.9	2.50	0.333	0.855	Bar	.0012	r	12	0.625	0.339	0.006	1.018	0.079	11.10	0.920
851	7.1	7.9	2.50	0.333	0.855	Bar	.0012	r	16	0.625	0.343	0.010	1.030	0.105	13.50	0.865
852	6.9	7.9	2.50	0.333	0.855	Bar	.0012	r	20	0.625	0.345	0.012	1.036	0.132	12.30	0.855
1138	7.1	7.9	3.00	0.360	0.855	Bar	.0012	r	16	0.625	0.368	0.008	1.022	0.105	8.55	0.930
1139	7.3	7.9	3.00	0.360	0.855	Bar	.0012	r	12	0.625	0.365	0.005	1.014	0.079	7.35	0.962
1140	7.5	7.9	3.00	0.360	0.855	Bar	.0012	r	8	0.625	0.362	0.002	1.006	0.053	4.54	1.000

TABLE 7 : PIERS WITHOUT ABUTMENTS [continued]

Run No.	Measured Data										Computed Data					
	b [ft]	B [ft]	Q [cfs]	h _n [ft]	Bottom Rdg.	Roughness	Slope	Type of Piers	Number of Piers	Diameter of Piers [in]	h ₁ [ft]	h ₁ * [ft]	h ₁ /h _n	ND/B	φ	C _{DA}
939	7.7	7.9	5.00	0.484	0.855	Bar	.0012	r	4	0.625	0.485	0.001	1.002	0.026	3.40	1.010
940	7.5	7.9	5.00	0.484	0.855	Bar	.0012	r	8	0.625	0.488	0.004	1.010	0.053	5.82	0.995
941	7.3	7.9	5.00	0.484	0.855	Bar	.0012	r	12	0.625	0.497	0.013	1.027	0.079	12.40	0.905
942	7.1	7.9	5.00	0.484	0.855	Bar	.0012	r	16	0.625	0.498	0.014	1.029	0.105	9.60	0.917
943	6.9	7.9	5.00	0.484	0.855	Bar	.0012	r	20	0.625	0.503	0.019	1.039	0.132	10.00	0.894
980	7.7	7.9	5.00	0.484	0.855	Bar	.0012	r	4	0.625	0.488	0.004				
981	7.3	7.9	5.00	0.484	0.855	Bar	.0012	r	12	0.625	0.497	0.003				
774	7.0	7.9	2.50	0.536	0.854	Baffle	.0012	Sq	18	0.625	0.541	0.005	1.009	0.119	16.10	0.815
775	7.2	7.9	2.50	0.536	0.854	Baffle	.0012	Sq	14	0.625	0.539	0.003	1.006	0.092	13.15	0.887
776	7.4	7.9	2.50	0.536	0.854	Baffle	.0012	Sq	10	0.625	0.538	0.002	1.004	0.066	12.62	0.915
853	6.9	7.9	2.50	0.333	0.855	Bar	.0012	Sq	20	0.625	0.346	0.013	1.039	0.132	13.30	0.839
854	7.1	7.9	2.50	0.333	0.855	Bar	.0012	Sq	16	0.625	0.343	0.010	1.030	0.105	13.51	0.868
855	7.3	7.9	2.50	0.333	0.855	Bar	.0012	Sq	12	0.625	0.340	0.007	1.021	0.079	13.08	0.900
856	7.5	7.9	2.50	0.333	0.855	Bar	.0012	Sq	8	0.625	0.338	0.005	1.015	0.053	14.20	0.910
857	7.7	7.9	2.50	0.333	0.855	Bar	.0012	Sq	4	0.625	0.336	0.003	1.009	0.026	18.10	0.940
1141	7.1	7.9	3.00	0.360	0.855	Bar	.0012	Sq	16	0.625	0.368	0.008	1.022	0.105	8.70	0.935
1142	7.3	7.9	3.00	0.360	0.855	Bar	.0012	Sq	12	0.625	0.366	0.006	1.017	0.079	9.10	0.945
1143	7.5	7.9	3.00	0.360	0.855	Bar	.0012	Sq	8	0.625	0.364	0.004	1.011	0.053	9.34	0.959
1144	7.7	7.9	3.00	0.360	0.855	Bar	.0012	Sq	4	0.625	0.362	0.002	1.006	0.026	9.78	0.977
944	7.7	7.9	5.00	0.484	0.855	Bar	.0012	Sq	4	0.625	0.485	0.001	1.002	0.026	3.18	1.010
945	7.5	7.9	5.00	0.484	0.855	Bar	.0012	Sq	8	0.625	0.486	0.002	1.004	0.053	2.96	1.023
946	7.3	7.9	5.00	0.484	0.855	Bar	.0012	Sq	12	0.625	0.492	0.008	1.017	0.079	7.76	0.962
947	7.1	7.9	5.00	0.484	0.855	Bar	.0012	Sq	16	0.625	0.495	0.011	1.023	0.105	7.43	0.950
948	6.9	7.9	5.00	0.484	0.855	Bar	.0012	Sq	20	0.625	0.499	0.015	1.031	0.132	8.05	0.932

- 340 -

TABLE 7 : PIERS WITH ABUTMENTS [SKEW]
30 degree and 45 degree wing-wall abutments

Run No.	Model Type	Model height [ft]	Model length [ft]	Measured Data										Computed Data												
				b [ft]	B [ft]	Q [cfs]	h _n [ft]	Bottom Rdg.	Roughness	Slope	Type of Piers	Number of Piers	Diameter of Piers [ft]	h ₁ [ft]	R _{UR}	R _{UL}	R _{DR}	R _{DL}	h ₁ *	h _U	h _D	h ₁ /h _n	ND/B	M	S	M*
577	30°WW	0.9	1.00	3.54	7.9	5.00	0.484	0.864	Bar	.0012	ss	2	3.5	0.692	1.542	1.556	1.353	1.296	0.208	0.685	0.461	1.430	.074	0.324	0.62	0.348
581 _B	30°WW	0.9	1.00	3.46	7.9	5.00	0.484	0.864	Bar	.0012	ss	4	3.5	0.756	1.611	1.621	1.358	1.301	0.272	0.752	0.466	1.562	.148	0.251	0.62	0.300
578	30°WW	0.9	1.00	3.54	7.9	5.00	0.484	0.864	Bar	.0012	ss	2	2.4	0.679	1.535	1.543	1.349	1.295	0.195	0.675	0.458	1.403	.050	0.345	0.46	0.368
579	30°WW	0.9	1.00	3.54	7.9	5.00	0.484	0.864	Bar	.0012	ss	4	2.4	0.705	1.558	1.569	1.357	1.298	0.221	0.700	0.463	1.457	.101	0.300	0.46	0.348
583	30°WW	0.9	1.00	2.54	7.9	5.00	0.484	0.864	Bar	.0012	ss	2	2.4	0.831	1.689	1.695	1.351	1.291	0.347	0.828	0.457	1.717	.050	0.236	0.46	0.259
580	30°WW	0.9	1.00	3.54	7.9	5.00	0.484	0.864	Bar	.0012	ss	4	1.25	0.674	1.530	1.538	1.350	1.297	0.190	0.670	0.459	1.393	.053	0.342	0.40	0.370
581	30°WW	0.9	1.00	3.54	7.9	5.00	0.484	0.864	Bar	.0012	ss	2	1.25	0.677	1.525	1.541	1.340	1.297	0.193	0.669	0.454	1.399	.027	0.365	0.40	0.379
584	30°WW	0.9	1.00	2.54	7.9	5.00	0.484	0.864	Bar	.0012	ss	2	1.25	0.806	1.666	1.670	1.349	1.293	0.322	0.804	0.457	1.665	.027	0.256	0.40	0.269
585	30°WW	0.9	1.00	2.54	7.9	5.00	0.484	0.864	Bar	.0012	ss	4	1.25	0.829	1.681	1.693	1.352	1.292	0.345	0.823	0.458	1.713	.053	0.233	0.40	0.260
566	45°WW	0.9	1.00	3.81	7.9	5.00	0.484	0.864	Bar	.0012	ss	2	3.5	0.690	1.547	1.554	1.390	1.293	0.206	0.686	0.478	1.426	.074	0.289	0.62	0.309
567	45°WW	0.9	1.00	3.81	7.9	5.00	0.484	0.864	Bar	.0012	ss	4	3.5	0.723	1.576	1.587	1.419	1.300	0.239	0.718	0.496	1.494	.148	0.237	0.62	0.276
573	45°WW	0.9	1.00	2.75	7.9	5.00	0.484	0.864	Bar	.0012	ss	2	3.5	0.822	1.678	1.686	1.434	1.299	0.338	0.818	0.503	1.700	.074	0.194	0.62	0.213
568	45°WW	0.9	1.00	3.81	7.9	5.00	0.484	0.864	Bar	.0012	ss	2	2.4	0.687	1.546	1.551	1.393	1.299	0.203	0.685	0.482	1.419	.050	0.306	0.46	0.325
569	45°WW	0.9	1.00	3.81	7.9	5.00	0.484	0.864	Bar	.0012	ss	4	2.4	0.699	1.552	1.563	1.400	1.297	0.215	0.693	0.487	1.444	.101	0.270	0.46	0.309
574	45°WW	0.9	1.00	2.75	7.9	5.00	0.484	0.864	Bar	.0012	ss	2	2.4	0.787	1.648	1.651	1.424	1.299	0.303	0.786	0.499	1.626	.050	0.211	0.46	0.230
570	45°WW	0.9	1.00	3.81	7.9	5.00	0.484	0.864	Bar	.0012	ss	2	1.25	0.678	1.528	1.542	1.378	1.300	0.194	0.671	0.475	1.401	.027	0.322	0.403	0.334
571	45°WW	0.9	1.00	3.81	7.9	5.00	0.484	0.864	Bar	.0012	ss	4	1.25	0.680	1.540	1.544	1.383	1.300	0.196	0.678	0.478	1.405	.053	0.304	0.403	0.327
575	45°WW	0.9	1.00	2.75	7.9	5.00	0.484	0.864	Bar	.0012	ss	2	1.25	0.774	1.630	1.638	1.419	1.301	0.290	0.770	0.497	1.599	.027	0.227	0.403	0.238

TABLE 8 : FLOOD PLAIN MODEL
45 degree wing-wall abutment; 1:1.5 spill-through abutment and vertical board model

Run No.	Model Type	Model height [ft]	Model length [ft]	Measured Data										Computed Data										
				b [ft]	B [ft]	Q [cfs]	h _m [ft]	Bottom Rdg.	Slope	Roughness arrangement			R _{UR}	R _{UL}	R _{DR}	R _{DL}	h ₁ * [ft]	h _U [ft]	h _D [ft]	h _m - γ [ft]	M	F _n	M*	
										n _S	n _C	n _N												h ₁ [ft]
683	WW	0.6	1.00	5.92	7.9	5.00	0.721	0.859	.0012	Bar	Bar	Bar	0.738	1.619	1.619	1.559	1.559	0.017	0.760	0.700	0.376	0.796	0.338	0.759
684	WW	0.6	1.00	4.90	7.9	5.00	0.721	0.859	.0012	Bar	Bar	Bar	0.756	1.639	1.639	1.550	1.546	0.035	0.780	0.689	0.376	0.692	0.338	0.674
685	WW	0.6	1.00	3.92	7.9	5.00	0.721	0.859	.0012	Bar	Bar	Bar	0.782	1.669	1.667	1.532	1.534	0.061	0.809	0.674	0.376	0.590	0.338	0.598
686	WW	0.6	1.00	2.92	7.9	5.00	0.721	0.859	.0012	Bar	Bar	Bar	0.835	1.712	1.715	1.524	1.520	0.114	0.855	0.663	0.376	0.489	0.338	0.499
715	WW	0.9	1.00	4.46	7.9	5.00	0.929	0.860	.0012	Baffle	Bar	Baffle	0.949	1.822	1.821	1.770	1.770	0.020	0.962	0.910	0.584	0.620	0.198	0.622
716	WW	0.9	1.00	3.42	7.9	5.00	0.929	0.860	.0012	Baffle	Bar	Baffle	0.969	1.840	1.840	1.760	1.761	0.040	0.980	0.901	0.584	0.506	0.198	0.544
717	WW	0.9	1.00	2.40	7.9	5.00	0.929	0.860	.0012	Baffle	Bar	Baffle	0.996	1.865	1.866	1.745	1.742	0.067	1.006	0.884	0.584	0.392	0.198	0.478
740	WW	0.9	1.00	2.46	7.9	5.00	0.817	0.859	.0012	Baffle	Bar	Bar	0.922	1.787	1.802	1.639	1.632	0.105	0.936	0.777	0.472	0.416	0.257	0.452
741	WW	0.9	1.00	3.44	7.9	5.00	0.817	0.859	.0012	Baffle	Bar	Bar	0.889	1.756	1.773	1.650	1.642	0.072	0.906	0.787	0.472	0.523	0.257	0.506
742	WW	0.9	1.00	4.44	7.9	5.00	0.817	0.859	.0012	Baffle	Bar	Bar	0.864	1.729	1.749	1.664	1.653	0.047	0.880	0.800	0.472	0.632	0.257	0.567
702	WW	0.6	1.00	5.90	7.9	2.50	0.560	0.859	.0012	Bar	Bar	Bar	0.571	1.438	1.438	1.409	1.409	0.011	0.579	0.550	0.215	0.820	0.301	0.770
703	WW	0.6	1.00	4.90	7.9	2.50	0.560	0.859	.0012	Bar	Bar	Bar	0.582	1.449	1.450	1.402	1.400	0.022	0.591	0.542	0.215	0.728	0.301	0.665
704	WW	0.6	1.00	3.90	7.9	2.50	0.560	0.859	.0012	Bar	Bar	Bar	0.595	1.465	1.463	1.396	1.396	0.035	0.605	0.537	0.215	0.640	0.301	0.582
705	WW	0.6	1.00	2.90	7.9	2.50	0.560	0.859	.0012	Bar	Bar	Bar	0.609	1.479	1.478	1.390	1.389	0.049	0.620	0.531	0.215	0.549	0.301	0.544
726	WW	0.9	1.00	4.54	7.9	2.50	0.687	0.859	.0012	Baffle	Bar	Baffle	0.692	1.555	1.555	1.536	1.536	0.005	0.696	0.677	0.342	0.660	0.188	0.715
727	WW	0.9	1.00	3.40	7.9	2.50	0.687	0.859	.0012	Baffle	Bar	Baffle	0.702	1.566	1.565	1.531	1.529	0.015	0.707	0.671	0.342	0.545	0.188	0.585
728	WW	0.9	1.00	2.40	7.9	2.50	0.687	0.859	.0012	Baffle	Bar	Baffle	0.723	1.586	1.586	1.537	1.536	0.036	0.727	0.678	0.342	0.441	0.188	0.485
729	WW	0.9	1.00	4.42	7.9	2.50	0.622	0.860	.0012	Baffle	Bar	Bar	0.638	1.500	1.512	1.472	1.463	0.016	0.646	0.608	0.277	0.660	0.234	0.620
730	WW	0.9	1.00	3.40	7.9	2.50	0.622	0.860	.0012	Baffle	Bar	Bar	0.653	1.514	1.526	1.466	1.457	0.031	0.660	0.602	0.277	0.566	0.234	0.546
731	WW	0.9	1.00	2.38	7.9	2.50	0.622	0.860	.0012	Baffle	Bar	Bar	0.664	1.526	1.539	1.461	1.456	0.042	0.673	0.599	0.277	0.466	0.234	0.506
687	ST	0.6	1.00	5.83	7.9	5.00	0.721	0.859	.0012	Bar	Bar	Bar	0.731	1.616	1.612	1.561	1.562	0.010	0.755	0.703	0.376	0.846	0.338	0.815
688	ST	0.6	1.00	4.83	7.9	5.00	0.721	0.859	.0012	Bar	Bar	Bar	0.749	1.635	1.629	1.551	1.549	0.028	0.773	0.691	0.376	0.742	0.338	0.716
689	ST	0.6	1.00	3.83	7.9	5.00	0.721	0.859	.0012	Bar	Bar	Bar	0.784	1.661	1.663	1.537	1.539	0.063	0.803	0.679	0.376	0.640	0.338	0.615
690	ST	0.6	1.00	2.83	7.9	5.00	0.721	0.859	.0012	Bar	Bar	Bar	0.830	1.712	1.713	1.530	1.529	0.109	0.853	0.671	0.376	0.534	0.338	0.525
718	ST	0.9	1.00	3.10	7.9	5.00	0.929	0.860	.0012	Baffle	Bar	Baffle	0.952	1.824	1.825	1.764	1.766	0.023	0.964	0.905	0.584	0.567	0.198	0.602
719	ST	0.9	1.00	2.06	7.9	5.00	0.929	0.860	.0012	Baffle	Bar	Baffle	0.980	1.846	1.849	1.740	1.740	0.051	0.988	0.880	0.584	0.453	0.198	0.510
720	ST	0.9	1.00	4.11	7.9	5.00	0.929	0.860	.0012	Baffle	Bar	Baffle	0.944	1.816	1.816	1.780	1.776	0.015	0.956	0.918	0.584	0.678	0.198	0.652
721	ST	0.9	1.00	5.18	7.9	5.00	0.929	0.860	.0012	Baffle	Bar	Baffle	0.938	1.800	1.804	1.785	1.785	0.009	0.942	0.925	0.584	0.797	0.198	0.700
736	ST	0.9	1.00	5.15	7.9	5.00	0.817	0.859	.0012	Baffle	Bar	Bar	0.832	1.693	1.712	1.672	1.664	0.015	0.844	0.809	0.472	0.782	0.257	0.729
737	ST	0.9	1.00	4.13	7.9	5.00	0.817	0.859	.0012	Baffle	Bar	Bar	0.847	1.714	1.735	1.670	1.665	0.030	0.866	0.809	0.472	0.673	0.257	0.640
738	ST	0.9	1.00	3.13	7.9	5.00	0.817	0.859	.0012	Baffle	Bar	Bar	0.874	1.741	1.760	1.657	1.656	0.057	0.892	0.798	0.472	0.565	0.257	0.556
739	ST	0.9	1.00	2.13	7.9	5.00	0.817	0.859	.0012	Baffle	Bar	Bar	0.919	1.787	1.797	1.648	1.634	0.102	0.933	0.782	0.472	0.458	0.257	0.464
706	ST	0.6	1.00	2.85	7.9	2.50	0.560	0.859	.0012	Bar	Bar	Bar	0.607	1.475	1.476	1.391	1.391	0.047	0.617	0.532	0.215	0.575	0.301	0.564
707	ST	0.6	1.00	3.85	7.9	2.50	0.560	0.859	.0012	Bar	Bar	Bar	0.587	1.455	1.456	1.403	1.400	0.027	0.597	0.543	0.215	0.666	0.301	0.646
708	ST	0.6	1.00	4.83	7.9	2.50	0.560	0.859	.0012	Bar	Bar	Bar	0.576	1.443	1.444	1.407	1.407	0.016	0.585	0.548	0.215	0.755	0.301	0.708
709	ST	0.6	1.00	5.83	7.9	2.50	0.560	0.859	.0012	Bar	Bar	Bar	0.570	1.438	1.438	1.415	1.413	0.010	0.579	0.555	0.215	0.844	0.301	0.760
722	ST	0.9	1.00	5.17	7.9	2.50	0.687	0.859	.0012	Baffle	Bar	Baffle	0.692	1.522	1.552	1.543	1.543	0.005	0.678	0.684	0.342	0.774	0.188	0.680
723	ST	0.9	1.00	4.15	7.9	2.50	0.687	0.859	.0012	Baffle	Bar	Baffle	0.695	1.554	1.555	1.540	1.542	0.008	0.696	0.682	0.342	0.672	0.188	0.653
724	ST	0.9	1.00	3.13	7.9	2.50	0.687	0.859	.0012	Baffle	Bar	Baffle	0.700	1.562	1.563	1.537	1.538	0.013	0.704	0.679	0.342	0.568	0.188	0.610
725	ST	0.9	1.00	2.08	7.9	2.50	0.687	0.859	.0012	Baffle	Bar	Baffle	0.706	1.566	1.567	1.530	1.530	0.019	0.708	0.671	0.342	0.462	0.188	0.568
732	ST	0.9	1.00	5.13	7.9	2.50	0.622	0.860	.0012	Baffle	Bar	Bar	0.627	1.487	1.500	1.477	1.473	0.005	0.634	0.615	0.277	0.773	0.234	0.730
733	ST	0.9	1.00	4.08	7.9	2.50	0.622	0.860	.0012	Baffle	Bar	Bar	0.633	1.493	1.508	1.474	1.465	0.011	0.641	0.610	0.277	0.673	0.234	0.665
734	ST	0.9	1.00	3.08	7.9	2.50	0.622	0.860	.0012	Baffle	Bar	Bar	0.641	1.502	1.513	1.466	1.462	0.019	0.648	0.604	0.277	0.577	0.234	0.617
735	ST	0.9	1.00	2.13	7.9	2.50	0.622	0.860	.0012	Baffle	Bar	Bar	0.656	1.517	1.529	1.457	1.457	0.034	0.663	0.597	0.277	0.484	0.234	0.549
691	VB	-	-	2.00	7.9	5.00	0.721	0.859	.0012	Bar	Bar	Bar	0.987	1.861	1.860	1.498	1.476	0.266	1.002	0.628	0.376	0.389	0.338	0.406
692	VB	-	-	3.00	7.9	5.00	0.721	0.859	.0012	Bar	Bar	Bar	0.891	1.768	1.765	1.489	1.511	0.170	0.908	0.641	0.376	0.493	0.338	0.505
693	VB	-	-	4.00	7.9	5.00	0.721	0.859	.0012	Bar	Bar	Bar	0.825	1.702	1.700	1.517	1.522	0.104	0.842	0.661	0.376	0.598	0.338	0.608
694	VB	-	-	5.00	7.9	5.00	0.721	0.859	.0012	Bar	Bar	Bar	0.780	1.663	1.658	1.532	1.534	0.059	0.802	0.674	0.376	0.700	0.338	0.708
695	VB	-	-	6.00	7.9	5.00	0.721	0.859	.0012	Bar	Bar	Bar	0.751	1.630	1.627	1.545	1.546	0.030	0.770	0.687	0.376	0.804	0.338	0.805
696	VB	-	-	5.00	7.9	5.00	0.721	0.859	.0012	Bar	Bar	Bar	0.777	-	-	-	-	0.056	-	-	0.376	0.700	0.338	0.714
710	VB	-	-	6.00	7.9	5.00	0.929	0.860	.0012	Baffle	Bar	Baffle	0.940	1.805	1.808	1.772	1.770	0.011	0.947	0.911	0.584	0.789	0.198	0.828
711	VB	-	-	5.00	7.9	5.00	0.929	0.860	.0012	Baffle	Bar	Baffle	0.956	1.824	1.824	1.762	1.762	0.027	0.964	0.902	0.584	0.681	0.198	0.723
712	VB	-	-	4.00	7																			

APPENDIX C

TABLE 1: SIMPLE NORMAL CROSSING
45 degree wing-wall abutment

Run No.	Abutment Type	L [ft]	l [ft]	B [ft]	b [ft]	S _o	n	Q [cfs]	h ₁ * [ft]	h _n [ft]	M	K _b	h ₁ * + h ₃ *	$\frac{h_1^*}{h_1^* + h_3^*}$	L*
13	WW	1.00	0.60	4.00	1.50	0.0012	0.024	1.98	0.146	0.446	0.375	1.013	0.211	0.692	4.0
28	WW	1.00	0.60	4.00	2.00	0.0024	0.024	0.68	0.043	0.202	0.50	0.886	0.069	0.623	1.5
29	WW	1.00	0.60	4.00	1.50	0.0024	0.024	0.66	0.086	0.202	0.375	1.089	0.117	0.735	1.5
30	WW	1.00	0.60	4.00	2.00	0.0024	0.024	1.57	0.098	0.318	0.50	0.929	0.166	0.590	2.3
40	WW	1.00	0.60	4.00	1.50	0.0008	0.024	0.86	0.048	0.345	0.375	1.092	0.066	0.727	2.0
41	WW	1.00	0.60	4.00	2.00	0.0008	0.024	0.87	0.025	0.346	0.50	0.950			3.7
49	WW	1.00	0.60	4.00	1.50	0.0008	0.024	1.53	0.074	0.477	0.375	1.000			3.9
87	WW	3.00	0.60	7.90	5.90	0.0012	0.022	5.30	0.019	0.497	0.746	0.324	0.043	0.442	
88	WW	3.00	0.60	7.90	4.90	0.0012	0.022	5.30	0.047	0.497	0.62	0.575	0.083	0.566	
89	WW	1.00	0.60	7.90	4.90	0.0012	0.022	5.30	0.049	0.497	0.62	0.589			
97	WW	1.00	0.60	7.90	4.50	0.0012	0.022	5.30	0.068	0.497	0.57	0.709	0.118	0.551	
409	WW	1.00	0.60	7.90	5.90	0.0012	0.023	2.50	0.014	0.333	0.746	0.523			2.7
410	WW	1.00	0.60	7.90	4.85	0.0012	0.023	2.50	0.024	0.333	0.614	0.596	0.043	0.558	3.9
411	WW	1.00	0.60	7.90	3.87	0.0012	0.023	2.50	0.060	0.333	0.49	0.967	0.089	0.674	3.3
412	WW	1.00	0.60	7.90	2.90	0.0012	0.023	2.50	0.129	0.333	0.367	1.173	0.168	0.768	3.0
626	WW	1.00	0.60	7.90	5.91	0.0012	0.024	5.00	0.018	0.484	0.748	0.355	0.046	0.391	
1161R	WW	1.00	0.60	7.90	2.91	0.0012	0.024	3.00	0.141	0.360	0.368	1.046			4.9
1161RR	WW	1.00	0.60	7.90	2.91	0.0012	0.024	3.00	0.141	0.360	0.368	1.046	0.181	0.779	4.7
1189R	WW	1.00	0.60	7.90	3.89	0.0012	0.022	3.00	0.065	0.360	0.492	0.842	0.096	0.677	4.8
1189RR	WW	1.00	0.60	7.90	3.89	0.0012	0.022	3.00	0.064	0.360	0.492	0.828			4.8
1261	WW	1.00	0.60	7.90	4.92	0.0012	0.024	3.00	0.031	0.360	0.624	0.634	0.054	0.574	5.8
1242	WW	1.00	0.60	7.90	5.90	0.0012	0.024	3.00	0.011	0.360	0.748	0.313	0.029	0.379	5.2
1344	WW	1.00	0.60	7.90	4.87	0.0012	0.024	3.00	0.031	0.360	0.618	0.643	0.055	0.564	
1348	WW	1.00	0.60	7.90	5.90	0.0012	0.024	3.00	0.012	0.360	0.748	0.345	0.033	0.364	
1354	WW	1.00	0.60	7.90	3.85	0.0012	0.024	3.00	0.067	0.360	0.488	0.845	0.103	0.650	
1355	WW	1.00	0.60	7.90	2.85	0.0012	0.024	3.00	0.147	0.360	0.361	1.043	0.197	0.746	
98	WW	1.00	0.90	7.90	3.50	0.0012	0.022	5.30	0.158	0.497	0.443	1.005	0.245	0.645	
99	WW	3.00	0.90	7.90	4.50	0.0012	0.022	5.30	0.070	0.497	0.57	0.732	0.118	0.593	
100	WW	3.00	0.90	7.90	3.50	0.0012	0.022	5.30	0.154	0.497	0.443	0.992	0.223	0.693	
109	WW	2.00	0.90	7.90	2.50	0.0012	0.022	5.30	0.297	0.497	0.316	0.988	0.365	0.814	
201	WW	1.00	0.90	7.90	3.42	0.0012	0.022	4.87	0.147	0.484	0.433	1.022	0.220	0.668	4.2
202	WW	1.00	0.90	7.90	4.46	0.0012	0.022	4.90	0.058	0.484	0.565	0.669	0.101	0.584	5.2
498	WW	1.00	0.90	7.90	4.48	0.0012	0.022	5.00	0.065	0.484	0.567	0.715	0.114	0.570	
514	WW	1.00	0.90	7.90	3.46	0.0012	0.022	5.00	0.154	0.484	0.438	1.033	0.220	0.700	
553	WW	0.50	0.90	7.90	4.46	0.0012	0.022	5.00	0.077	0.484	0.565	0.850	0.127	0.606	
554	WW	2.00	0.90	7.90	4.46	0.0012	0.022	5.00	0.066	0.484	0.565	0.717	0.110	0.627	
557	WW	2.00	0.90	7.90	2.46	0.0012	0.022	5.00	0.318	0.484	0.311	1.100	0.394	0.807	
558	WW	0.50	0.90	7.90	2.46	0.0012	0.022	5.00	0.313	0.484	0.311	1.082	0.388	0.807	
668	WW	1.00	0.90	7.90	4.46	0.0012	0.022	2.50	0.041	0.333	0.565	0.864	0.065	0.600	
669	WW	1.00	0.90	7.90	3.44	0.0012	0.022	2.50	0.081	0.333	0.435	1.026	0.116	0.698	
670	WW	1.00	0.90	7.90	2.44	0.0012	0.022	2.50	0.181	0.333	0.309	1.177	0.228	0.794	
759	WW	1.00	0.90	7.90	3.44	0.0012	0.022	5.00	0.162	0.484	0.436	1.075	0.233	0.695	
796	WW	1.00	0.90	7.90	4.42	0.0012	0.022	2.50	0.039	0.333	0.56	0.799	0.068	0.574	
796R	WW	1.00	0.90	7.90	4.42	0.0012	0.022	2.50	0.038	0.333	0.56	0.777	0.60	0.633	
823	WW	1.00	0.90	7.90	2.416	0.0012	0.022	2.50	0.176	0.333	0.305	1.119	0.222	0.793	

TABLE 1: SIMPLE NORMAL CROSSING [continued]

Run No.	Abutment Type	L [ft]	l [ft]	B [ft]	b [ft]	S _o	n	Q [cfs]	h ₁ * [ft]	h _n [ft]	M	K _b	h ₁ * + h ₃ * [ft]	$\frac{h_1^*}{h_1^* + h_3^*}$	L*
886RR	WW	1.00	0.90	7.90	4.42	0.0012	0.022	5.00	0.066	0.484	0.56	0.712	0.106	0.623	
927	WW	1.00	0.90	7.90	2.416	0.0012	0.022	5.00	0.305	0.484	0.305	1.015	0.402	0.759	
949	WW	1.00	0.90	7.90	4.46	0.0012	0.022	2.50	0.039	0.333	0.565	0.818	0.064	0.609	
955	WW	1.00	0.90	7.90	4.46	0.0012	0.022	5.00	0.041	0.333	0.565	0.864	0.065	0.631	
217	WW	1.00	0.60	7.90	4.90	0.0012	0.052	2.00	0.008	0.435	0.62	0.545			3.1
218	WW	1.00	0.60	7.90	3.85	0.0012	0.052	2.02	0.020	0.435	0.487	0.850	0.034	0.588	3.1
219	WW	1.00	0.60	7.90	2.84	0.0012	0.052	2.00	0.048	0.435	0.359	1.139	0.068	0.706	3.1
213	WW	1.00	0.90	7.90	4.47	0.0012	0.042	4.95	0.035	0.678	0.566	0.826	0.056	0.589	4.5
214	WW	1.00	0.90	7.90	3.42	0.0012	0.042	4.94	0.073	0.678	0.433	1.013	0.104	0.702	4.1
215	WW	1.00	0.90	7.90	2.42	0.0012	0.042	4.91	0.166	0.678	0.306	1.158	0.207	0.773	5.2
455	WW	1.00	0.90	7.90	4.46	0.0012	0.046	2.50	0.016	0.493	0.565	0.781	0.29	0.552	3.2
456	WW	1.00	0.90	7.90	3.42	0.0012	0.046	2.50	0.035	0.493	0.433	1.018	0.057	0.684	2.6
457	WW	1.00	0.90	7.90	2.43	0.0012	0.046	2.50	0.087	0.493	0.308	1.258	0.106	0.821	2.6
458	WW	1.00	0.90	7.90	1.46	0.0012	0.046	2.50	0.244	0.493	0.185	1.287	0.277	0.881	2.7
467	WW	1.00	0.90	7.90	4.50	0.0012	0.039	5.00	0.027	0.678	0.57	0.584			2.9
468	WW	1.00	0.90	7.90	3.43	0.0012	0.039	5.00	0.075	0.678	0.434	1.006	0.98	0.704	3.6
469	WW	1.00	0.90	7.90	2.44	0.0012	0.039	5.00	0.170	0.678	0.309	1.166	0.214	0.794	3.5
586	WW	1.00	0.90	7.90	4.47	0.0020	0.024	5.00	0.106	0.416	0.565	0.832	0.183	0.579	3.4
587	WW	1.00	0.90	7.90	3.42	0.0020	0.024	5.00	0.223	0.416	0.433	1.053	0.316	0.706	2.9

- 344 -

TABLE 2: FLOOD PLAIN MODEL
45 degree wing-wall abutment

Run No.	Abutment Type	L [ft]	l [ft]	B [ft]	b [ft]	S _o	n			Q [cfs]			h _n [ft]	h ₁ * [ft]	K _b	M	h ₁ * + h ₃ * [ft]	$\frac{h_1^*}{h_1^* + h_3^*}$
							Left 2.97'	Center 1.96'	Right 2.97'	Left 2.97'	Center 1.96'	Right 2.97'						
683	WW	1.00	0.60	7.90	5.92	0.0012	0.024	0.024	0.024	1.470	1.810	1.620	0.721	0.017	0.324	0.775	0.038	0.447
684	WW	1.00	0.60	7.90	4.89	0.0012	0.024	0.024	0.024	1.470	1.810	1.620	0.721	0.035	0.509	0.667	0.067	0.524
685	WW	1.00	0.60	7.90	3.92	0.0012	0.024	0.024	0.024	1.470	1.810	1.620	0.721	0.061	0.650	0.566	0.108	0.565
686	WW	1.00	0.60	7.90	2.92	0.0012	0.024	0.024	0.024	1.470	1.810	1.620	0.721	0.114	0.843	0.462	0.172	0.663
715	WW	1.00	0.90	7.90	4.45	0.0012	0.042	0.024	0.042	1.10	2.80	1.10	0.929	0.020	0.491	0.744	0.039	0.516
716	WW	1.00	0.90	7.90	3.41	0.0012	0.042	0.024	0.042	1.10	2.80	1.10	0.929	0.040	0.653	0.667	0.069	0.580
717	WW	1.00	0.90	7.90	2.39	0.0012	0.042	0.024	0.042	1.14	2.72	1.14	0.929	0.066	0.673	0.547	0.112	0.590
726	WW	1.00	0.90	7.90	4.54	0.0012	0.042	0.024	0.042	0.457	1.456	0.507	0.687	0.006	0.266	0.75	0.015	0.400
727	WW	1.00	0.90	7.90	3.39	0.0012	0.042	0.024	0.042	0.457	1.456	0.507	0.687	0.015	0.443	0.675	0.031	0.484
728	WW	1.00	0.90	7.90	2.39	0.0012	0.042	0.024	0.042	0.457	1.456	0.507	0.687	0.036	0.739	0.61		
729	WW	1.00	0.90	7.90	4.31	0.0012	0.042	0.024	0.024	0.825	1.210	0.445	0.622	0.016	0.494	0.684	0.031	0.516
730	WW	1.00	0.90	7.90	3.40	0.0012	0.042	0.024	0.024	0.825	1.210	0.445	0.622	0.031	0.738	0.607	0.052	0.597
731	WW	1.00	0.90	7.90	2.38	0.0012	0.042	0.024	0.024	0.825	1.210	0.445	0.622	0.042	0.692	0.519	0.065	0.646
740	WW	1.00	0.90	7.90	2.44	0.0012	0.042	0.024	0.024	1.310	1.840	1.850	0.817	0.116	0.906	0.418	0.145	0.800
741	WW	1.00	0.90	7.90	3.44	0.0012	0.042	0.024	0.024	1.310	1.840	1.850	0.817	0.072	0.876	0.525	0.102	0.705
742	WW	1.00	0.90	7.90	4.44	0.0012	0.042	0.024	0.024	1.310	1.840	1.850	0.817	0.041	0.713	0.631	0.065	0.630

TABLE 3 : SIMPLE NORMAL CROSSING
 90 degree vertical-wall; 90 degree, 60 degree and 30 degree wing-wall abutments

Run No.	Abutment Type	L [ft]	l [ft]	B [ft]	b [ft]	S _o	n	Q [cfs]	h ₁ * [ft]	h ₂ [ft]	M	K _b	h ₁ * + h ₃ * [ft]	$\frac{h_1^*}{h_1^* + h_3^*}$
1288	90°VW	1.00	0.90	7.90	2.81	0.0012	0.024	3.00	0.175	0.360	0.356	1.217	0.231	0.758
1289	90°VW	1.00	0.90	7.90	3.83	0.0012	0.024	3.00	0.092	0.360	0.484	1.174	0.129	0.713
1290	90°VW	1.00	0.90	7.90	4.84	0.0012	0.024	3.00	0.049	0.360	0.613	0.980	0.078	0.628
1292	90°VW	1.00	0.90	7.90	6.85	0.0012	0.024	3.00	0.006	0.360	0.867	0.237	0.017	0.353
1302	90°VW	1.00	0.90	7.90	2.84	0.0012	0.024	5.00	0.261	0.484	0.359	1.198	0.356	0.733
1303	90°VW	1.00	0.90	7.90	3.83	0.0012	0.024	5.00	0.135	0.484	0.485	1.104	0.200	0.675
1304	90°VW	1.00	0.90	7.90	4.85	0.0012	0.024	5.00	0.070	0.484	0.614	0.910	0.121	0.579
1305R	90°VW	1.00	0.90	7.90	5.85	0.0012	0.024	5.00	0.029	0.484	0.741	0.543	0.061	0.475
1306R	90°VW	1.00	0.90	7.90	6.87	0.0012	0.024	5.00	0.008	0.484	0.870	0.203	0.026	0.308
1269	90°WW	1.00	0.90	7.90	2.83	0.0012	0.024	3.00	0.184	0.360	0.358	1.291	0.233	0.790
1270	90°WW	1.00	0.90	7.90	3.84	0.0012	0.024	3.00	0.093	0.360	0.486	1.187	0.126	0.738
1271	90°WW	1.00	0.90	7.90	4.87	0.0012	0.024	3.00	0.047	0.360	0.616	0.962	0.071	0.662
1272	90°WW	1.00	0.90	7.90	5.88	0.0012	0.024	3.00	0.021	0.360	0.744	0.617	0.037	0.568
1273	90°WW	1.00	0.90	7.90	6.87	0.0012	0.024	3.00	0.007	0.360	0.870	0.275	0.019	0.368
1307	90°WW	1.00	0.90	7.90	2.84	0.0012	0.024	5.00	0.265	0.484	0.359	1.217	0.344	0.770
1308	90°WW	1.00	0.90	7.90	3.82	0.0012	0.024	5.00	0.130	0.484	0.484	1.051	0.183	0.710
1309	90°WW	1.00	0.90	7.90	4.83	0.0012	0.024	5.00	0.062	0.484	0.611	0.794	0.097	0.639
1310	90°WW	1.00	0.90	7.90	5.87	0.0012	0.024	5.00	0.025	0.484	0.743	0.469	0.049	0.510
1311	90°WW	1.00	0.90	7.90	6.85	0.0012	0.024	5.00	0.007	0.484	0.867	0.179	0.023	0.304
1293	60°WW	1.00	0.90	7.90	2.24	0.0012	0.024	3.00	0.228	0.360	0.284	1.010	0.278	0.820
1294	60°WW	1.00	0.90	7.90	3.25	0.0012	0.024	3.00	0.108	0.360	0.411	0.990	0.144	0.750
1295	60°WW	1.00	0.90	7.90	4.23	0.0012	0.024	3.00	0.050	0.360	0.535	0.767	0.076	0.658
1296	60°WW	1.00	0.90	7.90	5.27	0.0012	0.024	3.00	0.021	0.360	0.667	0.490	0.036	0.583
1297	60°WW	1.00	0.90	7.90	6.27	0.0012	0.024	3.00	0.009	0.360	0.704	0.302	0.018	0.500
1298	60°WW	1.00	0.90	7.90	3.24	0.0012	0.024	5.00	0.158	0.484	0.410	0.927	0.219	0.721
1299	60°WW	1.00	0.90	7.90	4.26	0.0012	0.024	5.00	0.066	0.484	0.539	0.660	0.105	0.629
1300	60°WW	1.00	0.90	7.90	5.25	0.0012	0.024	5.00	0.029	0.484	0.665	0.435	0.058	0.500
1301	60°WW	1.00	0.90	7.90	6.27	0.0012	0.024	5.00	0.011	0.484	0.794	0.234	0.032	0.344
1274	30°WW	1.00	0.90	7.90	3.68	0.0012	0.024	3.00	0.092	0.360	0.466	1.071	0.129	0.713
1275	30°WW	1.00	0.90	7.90	2.69	0.0012	0.024	3.00	0.182	0.360	0.341	1.156	0.237	0.768
1276R	30°WW	1.00	0.90	7.90	4.69	0.0012	0.024	3.00	0.045	0.360	0.594	0.844	0.037	0.616
1277	30°WW	1.00	0.90	7.90	5.69	0.0012	0.024	3.00	0.021	0.360	0.720	0.580	0.044	0.477
1278	30°WW	1.00	0.90	7.90	6.77	0.0012	0.024	3.00	0.006	0.360	0.857	0.227	0.020	0.300

TABLE 4 : SIMPLE NORMAL CROSSING
spill-through abutment

Run No.	Abutment Type	L [ft]	l [ft]	B [ft]	b _m [ft]	b [ft]	S _o	n	Q [cfs]	h ₁ * [ft]	h _n [ft]	M	K _D	h ₁ * + h ₃ * [ft]	$\frac{h_1^*}{h_1^* + h_3^*}$	L*
1	1:1.5ST	1.00	0.60	4.00	1.00	1.570	0.0012	0.024	1.68	0.150	0.380	0.392	1.147			2.4
4	1:1.5ST	1.00	0.60	4.00	2.00	2.585	0.0012	0.024	1.70	0.029	0.390	0.646	0.583	0.054	0.537	3.3
22	1:1.5ST	1.00	0.60	4.00	2.00	2.58	0.0024	0.024	2.30	0.68	0.387	0.645	0.718	0.120	0.542	3.8
23	1:1.5ST	1.00	0.60	4.00	1.50	2.079	0.0024	0.024	2.25	0.135	0.386	0.520	0.985	0.194	0.696	2.7
26	1:1.5ST	1.00	0.60	4.00	1.50	1.808	0.0024	0.024	0.68	0.057	0.205	0.452	1.027	0.084	0.679	2.4
27	1:1.5ST	1.00	0.60	4.00	2.00	2.300	0.0024	0.024	0.66	0.025	0.200	0.575	0.700	0.042	0.642	1.4
31	1:1.5ST	1.00	0.60	4.00	2.00	2.483	0.0024	0.024	1.60	0.045	0.322	0.621	0.630	0.080	0.562	2.6
32	1:1.5ST	1.00	0.60	4.00	1.50	1.983	0.0024	0.024	1.57	0.103	0.322	0.496	0.988	0.159	0.648	3.2
42	1:1.5ST	1.00	0.60	4.00	2.00	2.518	0.008	0.024	0.88	0.010	0.345	0.630	0.603	0.019	0.579	3.8
43	1:1.5ST	1.00	0.60	4.00	1.50	2.014	0.008	0.024	0.88	0.024	0.343	0.504	0.946			4.0
46	1:1.5ST	1.00	0.60	4.00	1.50	2.214	0.008	0.024	1.54	0.029	0.476	0.554	0.845			2.2
47	1:1.5ST	1.00	0.60	4.00	1.00	1.714	0.008	0.024	1.54	0.064	0.476	0.428	1.125			2.7
91	1:1.5ST	1.00	0.60	7.90	5.90	6.646	0.0012	0.024	5.30	0.006	0.497	0.841	0.118	0.018	0.333	
92	1:1.5ST	1.00	0.60	7.90	4.90	5.646	0.0012	0.024	5.30	0.031	0.497	0.615	0.507	0.069	0.449	
122	1:1.5ST	1.00	0.60	7.90	4.00	4.498	0.0012	0.024	2.70	0.050	0.332	0.569	0.892			3.0
130	1:1.5ST	1.00	0.60	7.90	3.16	3.886	0.0012	0.024	4.95	0.126	0.484	0.492	1.073			3.5
133	1:1.5ST	1.00	0.60	7.90	3.16	3.886	0.0012	0.024	4.95	0.120	0.484	0.492	1.027			2.5
446	1:1.5ST	1.00	0.60	7.90	2.86	3.360	0.0012	0.024	2.50	0.098	0.333	0.425	1.178	0.128	0.766	3.0
449	1:1.5ST	1.00	0.60	7.90	5.87	6.370	0.0012	0.024	2.50	0.006	0.333	0.806	0.259	0.018	0.333	2.9
629	1:1.5ST	1.00	0.60	7.90	5.87	6.596	0.0012	0.024	5.00	0.011	0.484	0.835	0.250	0.034	0.324	
645	1:1.5ST	1.00	0.60	7.90	5.87	6.596	0.0012	0.024	5.00	0.010	0.484	0.835	0.224			
94	1:1.5ST	3.00	0.60	7.90	5.90	6.646	0.0012	0.024	5.30	0.009	0.497	0.841	0.193			
95	1:1.5ST	3.00	0.60	7.90	4.90	5.646	0.0012	0.024	5.30	0.023	0.497	0.715	0.380			
96	1:1.5ST	3.00	0.60	7.90	3.90	4.646	0.0012	0.024	5.30	0.069	0.497	0.588	0.768			
104	1:1.5ST	3.00	0.90	7.90	5.20	5.946	0.0012	0.024	5.30	0.017	0.497	0.753	0.293	0.040	0.425	
105	1:1.5ST	3.00	0.90	7.90	4.20	4.946	0.0012	0.024	5.30	0.045	0.497	0.626	0.566	0.082	0.549	
106	1:1.5ST	3.00	0.90	7.90	3.20	3.946	0.0012	0.024	5.30	0.113	0.497	0.499	0.919	0.167	0.677	
115	1:1.5ST	3.00	0.90	7.90	5.20	6.223	0.0012	0.024	9.00	0.019	0.682	0.788	0.236	0.050	0.380	
116	1:1.5ST	3.00	0.90	7.90	4.20	5.223	0.0012	0.024	9.00	0.061	0.682	0.661	0.543	0.113	0.540	
117	1:1.5ST	3.00	0.90	7.90	3.20	4.223	0.0012	0.024	9.00	0.145	0.682	0.535	0.859	0.225	0.644	
101	1:1.5ST	1.00	0.90	7.90	5.20	5.946	0.0012	0.024	5.30	0.017	0.497	0.752	0.294			
102	1:1.5ST	1.00	0.90	7.90	4.20	4.946	0.0012	0.024	5.30	0.048	0.497	0.626	0.608	0.095	0.505	
103	1:1.5ST	1.00	0.90	7.90	3.20	3.946	0.0012	0.024	5.30	0.112	0.497	0.499	0.910	0.176	0.636	
112	1:1.5ST	1.00	0.90	7.90	5.20	6.223	0.0012	0.024	9.00	0.018	0.682	0.787	0.222			
113	1:1.5ST	1.00	0.90	7.90	4.20	5.223	0.0012	0.024	9.00	0.068	0.682	0.661	0.614	0.122	0.557	
114	1:1.5ST	1.00	0.90	7.90	3.20	4.223	0.0012	0.024	9.00	0.140	0.682	0.535	0.826	0.236	0.593	
536	1:1.5ST	1.00	0.90	7.90	4.18	4.906	0.0012	0.024	5.00	0.061	0.484	0.62	0.802	0.104	0.587	4.0
552	1:1.5ST	1.00	0.90	7.90	3.17	3.896	0.0012	0.024	5.00	0.123	0.484	0.492	1.041	0.175	0.703	
562	1:1.5ST	1.00	0.90	7.90	5.19	5.916	0.0012	0.024	5.00	0.022	0.484	0.748	0.418	0.049	0.449	
664	1:1.5ST	1.00	0.90	7.90	4.16	4.660	0.0012	0.024	2.50	0.028	0.333	0.59	0.653	0.050	0.560	
665	1:1.5ST	1.00	0.90	7.90	3.16	3.660	0.0012	0.024	2.50	0.069	0.333	0.463	0.986	0.099	0.697	4.7
866	1:1.5ST	1.00	0.90	7.90	3.00	3.500	0.0012	0.024	2.50	0.069	0.333	0.444	0.917	0.102	0.676	
880	1:1.5ST	1.00	0.90	7.90	5.08	5.806	0.0012	0.024	5.00	0.023	0.484	0.736	0.419	0.048	0.479	
883	1:1.5ST	1.00	0.90	7.90	3.16	3.886	0.0012	0.024	5.00	0.121	0.484	0.492	1.013	0.174	0.695	
984	1:1.5ST	1.00	0.90	7.90	5.167	5.893	0.0012	0.024	5.00	0.020	0.484	0.745	0.360	0.044	0.455	
1007R	1:1.5ST	1.00	0.90	7.90	4.14	4.866	0.0012	0.024	5.00	0.057	0.484	0.616	0.735	0.096	0.594	4.3
1034	1:1.5ST	1.00	0.90	7.90	3.125	3.851	0.0012	0.024	5.00	0.119	0.484	0.488	0.977	0.184	0.647	5.3
1061	1:1.5ST	1.00	0.90	7.90	2.146	2.872	0.0012	0.024	5.00	0.235	0.484	0.364	1.099	0.305	0.770	4.4
1156	1:1.5ST	1.00	0.90	7.90	3.15	3.690	0.0012	0.024	3.00	0.081	0.360	0.467	0.959	0.116	0.698	4.4

TABLE 4 : SIMPLE NORMAL CROSSING
spill-through abutments

Run No.	Abutment Type	L [ft]	l [ft]	B [ft]	b _m [ft]	b [ft]	S _o	n	Q [cfs]	h ₁ * [ft]	h _n [ft]	M	K _b	h ₁ **+h ₃ * [ft]	$\frac{h_1^*}{h_1^{**}+h_3^*}$	L*
1156R	1:1.5ST	1.00	0.90	7.90	3.15	3.690	0.0012	0.024	3.00	0.080	0.360	0.467	0.947			
222	1:1.5ST	1.00	0.90	7.90	4.12	5.137	0.0012	0.045	5.00	0.016	0.678	0.658	0.484	0.030	0.533	5.8
223	1:1.5ST	1.00	0.90	7.90	3.18	4.197	0.0012	0.045	4.95	0.041	0.678	0.539	0.846	0.066	0.621	5.3
224	1:1.5ST	1.00	0.90	7.90	2.07	3.087	0.0012	0.045	4.95	0.099	0.678	0.398	1.100			4.8
590	1:1.5ST	1.00	0.90	7.90	3.16	3.784	0.0020	0.024	5.00	0.177	0.416	0.479	1.013	0.253	0.700	3.3
592	1:1.5ST	1.00	0.90	7.90	5.19	5.814	0.0020	0.024	5.00	0.038	0.416	0.736	0.488	0.078	0.487	3.1
1279	1:1 ST	1.00	0.90	7.90	2.04	2.400	0.0012	0.024	3.00	0.208	0.360	0.304	1.057	0.256	0.812	
1280	1:1 ST	1.00	0.90	7.90	3.04	3.400	0.0012	0.024	3.00	0.105	0.360	0.43	1.055	0.143	0.734	
1281	1:1 ST	1.00	0.90	7.90	4.04	4.400	0.0012	0.024	3.00	0.045	0.360	0.557	0.739	0.070	0.643	
1282	1:1 ST	1.00	0.90	7.90	5.04	5.400	0.0012	0.024	3.00	0.019	0.360	0.684	0.467	0.037	0.514	
1283	1:1 ST	1.00	0.90	7.90	6.04	6.400	0.0012	0.024	5.00	0.007	0.484	0.810	0.245	0.018	0.389	
1312	1:1 ST	1.00	0.90	7.90	2.06	2.544	0.0012	0.024	5.00	0.286	0.484	0.322	1.054	0.363	0.788	
1313	1:1 ST	1.00	0.90	7.90	3.02	3.504	0.0012	0.024	5.00	0.149	0.484	0.444	1.022	0.208	0.716	
1314	1:1 ST	1.00	0.90	7.90	3.98	4.464	0.0012	0.024	5.00	0.068	0.484	0.565	0.746	0.105	0.648	
1315	1:1 ST	1.00	0.90	7.90	5.00	5.484	0.0012	0.024	5.00	0.027	0.484	0.694	0.441	0.055	0.491	
1316	1:1 ST	1.00	0.90	7.90	6.00	6.484	0.0012	0.024	5.00	0.008	0.484	0.821	0.182	0.022	0.364	
1284	2:1 ST	1.00	0.90	7.90	2.43	3.150	0.0012	0.024	3.00	0.129	0.360	0.399	1.110	0.163	0.791	
1285	2:1 ST	1.00	0.90	7.90	3.44	4.160	0.0012	0.024	3.00	0.065	0.360	0.527	0.969	0.092	0.707	
1286	2:1 ST	1.00	0.90	7.90	4.48	5.200	0.0012	0.024	3.00	0.028	0.360	0.658	0.640	0.051	0.549	
1287	2:1 ST	1.00	0.90	7.90	5.45	6.170	0.0012	0.024	3.00	0.009	0.360	0.781	0.292	0.025	0.360	

- 347 -

TABLE 5 : FLOOD PLAIN MODEL
1:1.5 spill-through abutment

Run No.	Abutment Type	L [ft]	l [ft]	B [ft]	b _m [ft]	b [ft]	S _o	n			Q [cfs]			h _n [ft]	h ₁ * [ft]	K _b	M	h ₁ **+h ₃ * [ft]	$\frac{h_1^*}{h_1^{**}+h_3^*}$	
								Left 2.97'	Center 1.96'	Right 2.97'	Left 2.97'	Center 1.96'	Right 2.97'							
687	1:1.5ST	1.00	0.60	7.90	5.83	6.394	0.0012	0.024	0.024	0.024	0.024	1.470	1.810	1.620	0.721	0.010	0.216	0.835	0.028	0.357
688	1:1.5ST	1.00	0.60	7.90	4.83	5.394	0.0012	0.024	0.024	0.024	0.024	1.470	1.810	1.620	0.721	0.028	0.468	0.720	0.058	0.483
689	1:1.5ST	1.00	0.60	7.90	3.83	4.394	0.0012	0.024	0.024	0.024	0.024	1.470	1.810	1.620	0.721	0.060	0.744	0.615	0.105	0.600
690	1:1.5ST	1.00	0.60	7.90	2.83	3.394	0.0012	0.024	0.024	0.024	0.024	1.470	1.810	1.620	0.721	0.109	0.970	0.511	0.159	0.686
718	1:1.5ST	1.00	0.90	7.90	3.10	3.976	0.0012	0.042	0.024	0.042	1.10	2.80	1.10	0.929	0.023	0.498	0.712	0.049	0.490	
719	1:1.5ST	1.00	0.90	7.90	2.06	2.936	0.0012	0.042	0.024	0.042	1.11	2.78	1.11	0.929	0.051	0.680	0.634	0.100	0.510	
720	1:1.5ST	1.00	0.90	7.90	4.11	4.986	0.0012	0.042	0.024	0.042	1.09	2.82	1.09	0.929	0.012	0.344	0.788	0.025	0.480	
721	1:1.5ST	1.00	0.90	7.90	5.18	6.056	0.0012	0.042	0.024	0.042	0.99	3.02	0.99	0.929	0.006	0.219	0.878	0.113	0.531	
722	1:1.5ST	1.00	0.90	7.90	5.17	5.683	0.0012	0.042	0.024	0.042	0.457	1.456	0.507	0.687	0.005	0.287	0.824	0.008	0.626	
723	1:1.5ST	1.00	0.90	7.90	4.14	4.653	0.0012	0.042	0.024	0.042	0.457	1.456	0.507	0.687	0.007	0.304	0.757	0.012	0.583	
724	1:1.5ST	1.00	0.90	7.90	3.12	3.633	0.0012	0.042	0.024	0.042	0.457	1.456	0.507	0.687	0.012	0.390	0.691	0.020	0.600	
732	1:1.5ST	1.00	0.90	7.90	5.12	5.536	0.0012	0.042	0.024	0.024	0.825	1.210	0.445	0.622	0.007	0.307	0.790	0.012	0.584	
733	1:1.5ST	1.00	0.90	7.90	4.08	4.496	0.0012	0.042	0.024	0.024	0.825	1.210	0.445	0.622	0.012	0.384	0.700	0.024	0.500	
736	1:1.5ST	1.00	0.90	7.90	5.15	5.858	0.0012	0.042	0.024	0.024	1.310	1.840	1.850	0.817	0.015	0.396	0.782	0.023	0.652	
737	1:1.5ST	1.00	0.90	7.90	4.12	4.828	0.0012	0.042	0.024	0.024	1.310	1.840	1.850	0.817	0.030	0.585	0.672	0.039	0.770	
738	1:1.5ST	1.00	0.90	7.90	3.12	3.828	0.0012	0.042	0.024	0.024	1.310	1.840	1.850	0.817	0.057	0.795	0.556	0.077	0.740	
739	1:1.5ST	1.00	0.90	7.90	2.12	2.828	0.0012	0.042	0.024	0.024	1.310	1.840	1.850	0.817	0.102	0.955	0.460	0.137	0.745	

TABLE 6 : PIERS
45 degree wing-wall abutment

B = 7.90 ft., L = 1.00 ft.

Run No.	l [ft]	Type of Pier	N Number of Piers	D Width of Piers	J	b [ft]	S _o	n	Q [cfs]	h ₁ * [ft]	h _n [ft]	M	K _b	ΔK _p	h ₁ * + h ₃ * [ft]	$\frac{h_1^*}{h_1^* + h_3^*}$	$\frac{h_1^*}{h_1^* + h_3^*}$	L*
520	0.90	sing. shft.	2	0.200	0.117	3.44	0.0012	0.024	5.00	0.178	0.484	0.435	1.183	1.054				
616	0.90	sing. shft.	2	0.094	0.031	5.92	0.0012	0.024	5.00	0.020	0.484	0.749	0.382	0.343				
1111	0.90	sing. shft.	4	0.104	0.053	7.90	0.0012	0.024	5.00	0.003	0.484	1.000	0.099	0.099				
1126	0.90	sing. shft.	8	0.052	0.053	7.90	0.0012	0.024	5.00	0.002	0.484	1.000	0.066	0.066				
1127	0.90	sing. shft.	12	0.052	0.079	7.90	0.0012	0.024	5.00	0.003	0.484	1.000	0.099	0.099				
1128	0.90	sing. shft.	16	0.052	0.105	7.90	0.0012	0.024	5.00	0.005	0.484	1.000	0.165	0.165				
1154	0.90	sing. shft.	4	0.104	0.053	7.90	0.0012	0.024	3.00	0.001	0.360	1.000	0.053	0.053				
1161R	0.90	none				2.91	0.0012	0.024	3.00	0.141	0.360	0.368	1.045	1.080	0.181	0.779	0.770	
1180	0.90	sing. shft.	6	0.052	0.107	2.91	0.0012	0.024	3.00	0.159	0.360	0.368	1.183	0.103	0.199	0.799	0.029	4.6
1181	0.90	sing. shft.	4	0.052	0.072	2.91	0.0012	0.024	3.00	0.155	0.360	0.368	1.152	0.072	0.194	0.799	0.029	4.6
1182	0.90	sing. shft.	2	0.052	0.035	2.91	0.0012	0.024	3.00	0.149	0.360	0.368	1.106	0.026	0.189	0.788	0.018	5.4
1186	0.90	sing. shft.	1	0.104	0.035	2.91	0.0012	0.024	3.00	0.149	0.360	0.368	1.106	0.026	0.192	0.776	0.006	4.6
1187	0.90	sing. shft.	2	0.104	0.072	2.91	0.0012	0.024	3.00	0.155	0.360	0.368	1.152	0.072	0.196	0.791	0.021	4.1
1189R	0.90	sing. shft.				3.89	0.0012	0.024	3.00	0.065	0.360	0.492	0.847	0.870	0.096	0.677	0.670	
1204	0.90	sing. shft.	8	0.052	0.107	3.89	0.0012	0.024	3.00	0.076	0.360	0.492	0.993	0.123	0.107	0.710	0.040	
1205	0.90	sing. shft.	6	0.052	0.080	3.89	0.0012	0.024	3.00	0.073	0.360	0.492	0.953	0.083	0.107	0.682	0.012	
1210	0.90	sing. shft.	4	0.104	0.107	3.89	0.0012	0.024	3.00	0.073	0.360	0.492	0.953	0.840	0.107	0.682	0.012	4.8
1211	0.90	sing. shft.	3	0.104	0.080	3.89	0.0012	0.024	3.00	0.071	0.360	0.492	0.927	0.087	0.104	0.683	0.013	4.8
1212	0.90	sing. shft.	2	0.104	0.054	3.89	0.0012	0.024	3.00	0.070	0.360	0.492	0.914	0.074	0.102	0.686	0.016	4.8
1216	0.90	none				4.92	0.0012	0.024	3.00	0.031	0.360	0.623	0.629	0.629	0.054	0.574	0.574	
1226	0.90	sing. shft.	5	0.104	0.106	4.92	0.0012	0.024	3.00	0.038	0.360	0.623	0.773	0.144	0.060	0.633	0.059	4.7
1227	0.90	sing. shft.	4	0.104	0.085	4.92	0.0012	0.024	3.00	0.036	0.360	0.623	0.732	0.103	0.056	0.643	0.069	4.5
1228	0.90	sing. shft.	2	0.104	0.042	4.92	0.0012	0.024	3.00	0.033	0.360	0.623	0.670	0.041	0.055	0.600	0.026	4.7
1242	0.90	none				5.90	0.0012	0.024	3.00	0.011	0.360	0.747	0.323	0.323	0.029	0.379	0.400	
1249R	0.90	sing. shft.	12	0.052	0.105	5.90	0.0012	0.024	3.00	0.016	0.360	0.747	0.469	0.146	0.031	0.516	0.116	
1250R	0.90	sing. shft.	8	0.052	0.071	5.90	0.0012	0.024	3.00	0.014	0.360	0.747	0.411	0.088	0.030	0.467	0.67	4.2
1251	0.90	sing. shft.	4	0.052	0.035	5.90	0.0012	0.024	3.00	0.012	0.360	0.747	0.352	0.029	0.028	0.428	0.028	5.0
1257	0.90	sing. shft.	4	0.104	0.071	5.90	0.0012	0.024	3.00	0.014	0.360	0.747	0.411	0.088	0.029	0.483	0.083	4.8
512	0.90	dbl. shft.	1	0.200	0.045	4.46	0.0012	0.024	5.00	0.081	0.484	0.565	0.880	0.800	0.130	0.615	0.574	
623	0.90	dbl. shft.	2	0.290	0.073	7.90	0.0012	0.024	5.00	0.006	0.484	1.000	0.198	0.198				
624	0.90	dbl. shft.	2	0.200	0.051	7.90	0.0012	0.024	5.00	0.004	0.484	1.000	0.132	0.132				
1114	0.90	dbl. shft.	8	0.104	0.105	7.90	0.0012	0.024	5.00	0.011	0.484	1.000	0.363	0.363				
1115	0.90	dbl. shft.	6	0.104	0.079	7.90	0.0012	0.024	5.00	0.008	0.484	1.000	0.264	0.264				
1116	0.90	dbl. shft.	4	0.104	0.053	7.90	0.0012	0.024	5.00	0.005	0.484	1.000	0.165	0.165				
1129	0.90	dbl. shft.	16	0.052	0.105	7.90	0.0012	0.024	5.00	0.007	0.484	1.000	0.231	0.231				
1129R	0.90	dbl. shft.	16	0.052	0.105	7.90	0.0012	0.024	5.00	0.007	0.484	1.000	0.231	0.231				
1130	0.90	dbl. shft.	12	0.052	0.079	7.90	0.0012	0.024	5.00	0.006	0.484	1.000	0.198	0.198				
1131	0.90	dbl. shft.	8	0.052	0.053	7.90	0.0012	0.024	5.00	0.004	0.484	1.000	0.132	0.132				
1132	0.90	dbl. shft.	4	0.052	0.026	7.90	0.0012	0.024	5.00	0.001	0.484	1.000	0.033	0.033				
1146	0.90	dbl. shft.	16	0.052	0.105	7.90	0.0012	0.024	3.00	0.006	0.360	1.000	0.321	0.321				
1148	0.90	dbl. shft.	12	0.052	0.079	7.90	0.0012	0.024	3.00	0.003	0.360	1.000	0.160	0.160				
1155	0.90	dbl. shft.	4	0.104	0.053	7.90	0.0012	0.024	3.00	0.002	0.360	1.000	0.106	0.106				

TABLE 6 : PIERS
45 degree wing-wall abutment

B = 7.90 ft., L = 1.00 ft.

Run No.	l [ft]	Type of Pier	N Number of Piers	D Width of Piers	J	b [ft]	S _o	n	Q [cfs]	h ₁ * [ft]	h _n [ft]	M	K _b	ΔK _p	h ₁ *+h ₃ * [ft]	$\frac{h_1^*}{h_1^*+h_3^*}$	$\Delta \frac{h_1^*}{h_1^*+h_3^*}$	L*
1161R	0.90	none				2.91	0.0012	0.024	3.00	0.141	0.360	0.368	1.045	1.045	0.181	0.779	0.770	
1177	0.90	dbl. shft.	6	0.052	0.107	2.91	0.0012	0.024	3.00	0.166	0.360	0.368	1.236	0.191	0.206	0.806	0.036	4.8
1178	0.90	dbl. shft.	4	0.052	0.072	2.91	0.0012	0.024	3.00	0.158	0.360	0.368	1.175	0.130	0.198	0.798	0.028	4.7
1179	0.90	dbl. shft.	2	0.052	0.035	2.91	0.0012	0.024	3.00	0.150	0.360	0.368	1.114	0.069	0.190	0.789	0.019	4.8
1183	0.90	dbl. shft.	3	0.104	0.107	2.91	0.0012	0.024	3.00	0.169	0.360	0.368	1.259	0.214	0.207	0.816	0.046	4.4
1184	0.90	dbl. shft.	2	0.104	0.072	2.91	0.0012	0.024	3.00	0.159	0.360	0.368	1.183	0.138	0.201	0.791	0.021	5.0
1185	0.90	dbl. shft.	1	0.104	0.035	2.91	0.0012	0.024	3.00	0.151	0.360	0.368	1.122	0.077	0.192	0.786	0.016	4.6
1189R	0.90	none				3.89	0.0012	0.024	3.00	0.065	0.360	0.492	0.847	0.870	0.096	0.677	0.670	
1207	0.90	dbl. shft.	8	0.052	0.107	3.89	0.0012	0.024	3.00	0.083	0.360	0.492	1.087	0.217	0.116	0.716	0.046	5.2
1208	0.90	dbl. shft.	6	0.052	0.080	3.89	0.0012	0.024	3.00	0.080	0.360	0.492	1.047	0.177	0.111	0.721	0.051	5.5
1209	0.90	dbl. shft.	4	0.052	0.054	3.89	0.0012	0.024	3.00	0.076	0.360	0.492	0.993	0.123	0.107	0.710	0.040	4.8
1213	0.90	dbl. shft.	4	0.104	0.107	3.89	0.0012	0.024	3.00	0.081	0.360	0.492	1.061	0.191	0.115	0.704	0.034	4.8
1214	0.90	dbl. shft.	3	0.104	0.080	3.89	0.0012	0.024	3.00	0.077	0.360	0.492	1.007	0.137	0.109	0.706	0.036	4.8
1215	0.90	dbl. shft.	2	0.104	0.054	3.89	0.0012	0.024	3.00	0.072	0.360	0.492	0.940	0.070	0.103	0.699	0.029	4.8
1216	0.90	none				4.92	0.0012	0.024	3.00	0.031	0.360	0.623	0.629	0.629	0.054	0.574	0.574	
1220	0.90	dbl. shft.	10	0.052	0.106	4.92	0.0012	0.024	3.00	0.042	0.360	0.623	0.856	0.227	0.066	0.636	0.062	5.1
1221	0.90	dbl. shft.	8	0.052	0.085	4.92	0.0012	0.024	3.00	0.039	0.360	0.623	0.795	0.166	0.062	0.629	0.055	4.5
1222	0.90	dbl. shft.	4	0.052	0.042	4.92	0.0012	0.024	3.00	0.034	0.360	0.623	0.692	0.063	0.057	0.596	0.022	4.7
1223	0.90	dbl. shft.	5	0.104	0.106	4.92	0.0012	0.024	3.00	0.043	0.360	0.623	0.877	0.248	0.064	0.672	0.098	5.0
1225	0.90	dbl. shft.	2	0.104	0.042	4.92	0.0012	0.024	3.00	0.036	0.360	0.623	0.732	0.103	0.057	0.632	0.058	
1242	0.90	none				5.90	0.0012	0.024	3.00	0.011	0.360	0.747	0.323	0.323	0.029	0.379	0.400	
1252	0.90	dbl. shft.	12	0.052	0.105	5.90	0.0012	0.024	3.00	0.021	0.360	0.747	0.609	0.286	0.037	0.568	0.168	4.3
1253R	0.90	dbl. shft.	8	0.052	0.071	5.90	0.0012	0.024	3.00	0.017	0.360	0.747	0.498	0.175	0.032	0.531	0.131	4.7
1255	0.90	dbl. shft.	4	0.052	0.035	5.90	0.0012	0.024	3.00	0.014	0.360	0.747	0.411	0.088	0.030	0.467	0.067	4.7
1259	0.90	dbl. shft.	2	0.104	0.035	5.90	0.0012	0.024	3.00	0.015	0.360	0.747	0.440	0.117	0.031	0.484	0.084	
1260	0.90	dbl. shft.	4	0.104	0.071	5.90	0.0012	0.024	3.00	0.018	0.360	0.747	0.529	0.206	0.033	0.545	0.145	
498	0.90	none				4.48	0.0012	0.024	5.00	0.065	0.484	0.567	0.712	0.712	0.114	0.570	0.570	
499	0.90	Lenticular	2	0.10	0.044	4.48	0.0012	0.024	5.00	0.072	0.484	0.567	0.790	0.078	0.118	0.610	0.040	
500	0.90	Lenticular	4	0.10	0.089	4.46	0.0012	0.024	5.00	0.080	0.484	0.565	0.879	0.167	0.133	0.602	0.032	
502	0.90	Lenticular	2	0.145	0.065	4.46	0.0012	0.024	5.00	0.079	0.484	0.565	0.868	0.156	0.125	0.632	0.062	
503	0.90	Lenticular	2	0.200	0.090	4.46	0.0012	0.024	5.00	0.084	0.484	0.565	0.924	0.212	0.131	0.641	0.071	
514	0.90	none				3.46	0.0012	0.024	5.00	0.154	0.484	0.438	1.034	1.034	0.220	0.700	0.700	
525	0.90	Lenticular	2	0.145	0.084	3.44	0.0012	0.024	5.00	0.184	0.484	0.435	1.239	0.205	0.263	0.707	0.007	
526	0.90	Lenticular	2	0.100	0.058	3.44	0.0012	0.024	5.00	0.164	0.484	0.435	1.088	0.054	0.233	0.704	0.004	
528	0.90	none				2.44	0.0012	0.024	5.00	0.323	0.484	0.309	1.101	1.101	0.412	0.784	0.784	
533	0.90	Lenticular	2	0.100	0.081	2.44	0.0012	0.024	5.00	0.350	0.484	0.309	1.196	0.095	0.442	0.792	0.008	
534	0.90	Lenticular	2	0.145	0.119	2.44	0.0012	0.024	5.00	0.372	0.484	0.309	1.274	0.173	0.458	0.812	0.028	
618	0.90	Lenticular	2	0.208	0.071	5.92	0.0012	0.024	5.00	0.023	0.484	0.749	0.439	0.343	0.051	0.451	0.420	
1120	0.90	Lenticular	12	0.052	0.079	7.9	0.0012	0.024	5.00	0.004	0.484	1.000	0.132	0.132				
1121	0.90	Lenticular	16	0.052	0.105	7.9	0.0012	0.024	5.00	0.006	0.484	1.000	0.198	0.198				
1122	0.90	Lenticular	8	1.04	0.105	7.9	0.0012	0.024	5.00	0.006	0.484	1.000	0.198	0.198				
1123	0.90	Lenticular	6	1.04	0.079	7.9	0.0012	0.024	5.00	0.004	0.484	1.000	0.132	0.132				
1124	0.90	Lenticular	4	1.04	0.053	7.9	0.0012	0.024	5.00	0.003	0.484	1.000	0.099	0.099				

TABLE 6 : PIERS
45 degree wing-wall abutment

B = 7.90 ft., L = 1.00 ft.

Run No.	l [ft]	Type of Pier	N Number of Piers	D Width of Piers	J	b [ft]	S _o	n	Q [cfs]	h ₁ * [ft]	h ₂ [ft]	M	K _b	ΔK _p	h ₁ *+h ₃ * [ft]	$\frac{h_1^*}{h_1^*+h_3^*}$	$\Delta \frac{h_1^*}{h_1^*+h_3^*}$	L*
1125	0.90	Rd. Narrow	2	1.04	0.026	7.90	0.0012	0.024	5.00	0.001	0.484	0.565	0.033	0.033				
1161RR	0.90	none				2.91	0.0012	0.024	3.00	0.141	0.360	0.368	1.045	1.045	0.181	0.779	0.770	
1163	0.90	Rd. Narrow	4	0.052	0.072	2.91	0.0012	0.024	3.00	0.161	0.360	0.368	1.198	0.153	0.202	0.797	0.027	5.0
1164	0.90	Rd. Narrow	2	0.052	0.036	2.91	0.0012	0.024	3.00	0.147	0.360	0.368	1.091	0.046	0.187	0.786	0.016	4.8
1165	0.90	Rd. Narrow	1	0.052	0.018	2.91	0.0012	0.024	3.00	0.144	0.360	0.368	1.068	0.023	0.183	0.787	0.017	4.2
1189R	0.90	none				3.89	0.0012	0.024	3.00	0.065	0.360	0.492	0.847	0.870	0.096	0.677	0.670	
1190	0.90	Rd. Narrow	4	0.104	0.107	3.89	0.0012	0.024	3.00	0.086	0.360	0.492	1.127	0.257	0.120	0.716	0.046	4.8
1191	0.90	Rd. Narrow	3	0.104	0.080	3.89	0.0012	0.024	3.00	0.078	0.360	0.492	1.021	0.151	0.110	0.709	0.039	4.7
1192	0.90	Rd. Narrow	2	0.104	0.054	3.89	0.0012	0.024	3.00	0.073	0.360	0.492	0.953	0.083	0.106	0.689	0.019	4.8
1193	0.90	Rd. Narrow	8	0.052	0.107	3.89	0.0012	0.024	3.00	0.087	0.360	0.492	1.140	0.270	0.119	0.731	0.061	5.2
1194	0.90	Rd. Narrow	6	0.052	0.080	3.89	0.0012	0.024	3.00	0.079	0.360	0.492	1.034	0.164	0.111	0.712	0.042	5.7
1195	0.90	Rd. Narrow	4	0.052	0.054	3.89	0.0012	0.024	3.00	0.072	0.360	0.492	0.940	0.070	0.103	0.699	0.029	
1242	0.60	none				5.90	0.0012	0.024	3.00	0.011	0.360	0.744	0.323	0.323	0.029	0.379	0.400	
1243	0.60	Rd. Narrow	12	0.052	0.105	5.90	0.0012	0.024	3.00	0.017	0.360	0.744	0.498	0.175	0.034	0.500	0.100	4.2
1245	0.60	Rd. Narrow	6	0.052	0.053	5.90	0.0012	0.024	3.00	0.013	0.360	0.744	0.381	0.058	0.028	0.464	0.064	4.2
1247	0.60	Rd. Narrow	4	0.104	0.071	5.90	0.0012	0.024	3.00	0.014	0.360	0.744	0.411	0.088	0.028	0.500	0.100	4.2
1248	0.60	Rd. Narrow	2	0.104	0.035	5.90	0.0012	0.024	3.00	0.013	0.360	0.744	0.381	0.058	0.027	0.481	0.081	4.4
594	0.60	Rd. Narrow	4	0.198	0.100	7.90	0.0020	0.024	5.00	0.007	0.416	1.000	0.160	0.160				
595	0.60	Rd. Narrow	2	0.198	0.050	7.90	0.0020	0.024	5.00	0.003	0.416	1.000	0.069	0.069				
777	0.60	Rd. pile bts.	2	0.052	0.024	4.416	0.0012	0.042	2.50	0.021	0.483	0.552	0.975	0.836	0.032	0.656	0.094	
778	0.60	Rd. pile bts.	4	0.052	0.048	4.416	0.0012	0.042	2.50	0.021	0.483	0.552	0.975	0.139	0.033	0.636	0.074	
796R	0.60	none				4.42	0.0012	0.024	2.50	0.039	0.333	0.552	0.784	0.790	0.060	0.633	0.574	
797	0.60	Rd. pile bts.	1	0.052	0.012	4.42	0.0012	0.024	2.50	0.039	0.333	0.552	0.806	0.016	0.066	0.591	0.018	
798	0.60	Rd. pile bts.	2	0.052	0.024	4.42	0.0012	0.024	2.50	0.042	0.333	0.552	0.868	0.078	0.063	0.667	0.093	
823	0.60	none				2.416	0.0012	0.024	2.50	0.176	0.333	0.302	1.118	1.100	0.222	0.793	0.790	
827	0.60	Rd. pile bts.	4	0.052	0.086	2.416	0.0012	0.024	2.50	0.204	0.333	0.302	1.304	0.204	0.246	0.829		
828	0.60	Rd. pile bts.	2	0.052	0.044	2.416	0.0012	0.024	2.50	0.192	0.333	0.302	1.226	0.126	0.242	0.793		
828R	0.60	Rd. pile bts.	2	0.052	0.044	2.400	0.0012	0.024	2.50	0.189	0.333	0.302	1.189	0.089	0.232	0.815		
829	0.60	Rd. pile bts.	1	0.052	0.021	2.416	0.0012	0.024	2.50	0.181	0.333	0.302	1.152	0.052	0.230	0.787		
849	0.60	Rd. pile bts.	8	0.052	0.052	7.98	0.0012	0.024	2.50	0.005	0.333	1.000	0.327	0.327	0.005	1.000	1.00	
850	0.60	Rd. pile bts.	12	0.052	0.079	7.98	0.0012	0.024	2.50	0.006	0.333	1.000	0.393	0.393	0.004	1.500	1.500	
851	0.60	Rd. pile bts.	16	0.052	0.104	7.98	0.0012	0.024	2.50	0.010	0.333	1.000	0.654	0.654	0.007	1.429	1.429	
852	0.60	Rd. pile bts.	20	0.052	0.130	7.98	0.0012	0.024	2.50	0.012	0.333	1.000	0.788	0.788	0.009	1.333	1.333	
886RR	0.60	none				4.42	0.0012	0.024	5.00	0.066	0.484	0.552	0.706	0.706	0.106	0.623	0.623	
887RR	0.60	Rd. pile bts.	2	0.052	0.023	4.42	0.0012	0.024	5.00	0.071	0.484	0.552	0.767	0.061	0.112	0.634	0.011	
888R	0.60	Rd. pile bts.	4	0.052	0.047	4.42	0.0012	0.024	5.00	0.080	0.484	0.552	0.859	0.153	0.116	0.690	0.067	
888RR	0.60	Rd. pile bts.	4	0.052	0.047	4.42	0.0012	0.024	5.00	0.077	0.484	0.552	0.827	0.121	0.127	0.606	-0.017	
889RR	0.60	Rd. pile bts.	6	0.052	0.071	4.42	0.0012	0.024	5.00	0.087	0.484	0.552	0.937	0.231	0.135	0.644	0.021	
927	0.60	none				2.416	0.0012	0.024	5.00	0.305	0.484	0.302	1.015	1.035	0.402	0.759	0.780	
931	0.60	Rd. pile bts.	3	0.052	0.064	2.416	0.0012	0.024	5.00	0.348	0.484	0.302	1.163	0.128	0.435	0.800	0.020	
932	0.60	Rd. pile bts.	2	0.052	0.043	2.416	0.0012	0.024	5.00	0.338	0.484	0.302	1.128	0.103	0.412	0.820	0.040	
933	0.60	Rd. pile bts.	1	0.052	0.021	2.416	0.0012	0.024	5.00	0.324	0.484	0.302	1.080	0.055	0.405	0.800	0.020	
939	0.60	Rd. pile bts.	4	0.052	0.026	7.90	0.0012	0.024	5.00	0.001	0.484	1.000	0.033	0.033				

TABLE 6 : PIERS
45 degree wing-wall abutment

B = 7.90 ft., L = 1.00 ft.

Run No.	l [ft]	Type of Pier	N Number of Piers	D Width of Piers	J	b [ft]	S _o	n	Q [cfs]	h ₁ * [ft]	h ₂ [ft]	M	K _b	ΔK _p	h ₁ * + h ₃ * [ft]	$\frac{h_1^*}{h_1^* + h_3^*}$	$\Delta \frac{h_1^*}{h_1^* + h_3^*}$	L*
940	0.60	Rd. pile bts.	8	0.052	0.053	7.90	0.0012	0.024	5.00	0.004	0.484	1.000	0.132	0.132				
941	0.60	Rd. pile bts.	12	0.052	0.079	7.90	0.0012	0.024	5.00	0.013	0.484	1.000	0.430	0.430				
942	0.60	Rd. pile bts.	16	0.052	0.105	7.90	0.0012	0.024	5.00	0.014	0.484	1.000	0.464	0.464				
943	0.60	Rd. pile bts.	20	0.052	0.132	7.90	0.0012	0.024	5.00	0.020	0.484	1.000	0.663	0.663				
979	0.60	Rd. pile bts.	8	0.052	0.053	7.90	0.0012	0.024	5.00	0.009	0.484	1.000	0.297	0.297				
980	0.60	Rd. pile bts.	4	0.052	0.026	7.90	0.0012	0.024	5.00	0.004	0.484	1.000	0.132	0.132	0.004	1.00	1.00	
981	0.60	Rd. pile bts.	12	0.052	0.079	7.90	0.0012	0.024	5.00	0.013	0.484	1.000	0.430	0.430	0.013	1.00	1.00	
1138	0.60	Rd. pile bts.	16	0.052	0.105	7.90	0.0012	0.024	3.00	0.008	0.360	1.000	0.427	0.427				
1139	0.60	Rd. pile bts.	12	0.052	0.079	7.90	0.0012	0.024	3.00	0.005	0.360	1.000	0.266	0.266				
1140	0.60	Rd. pile bts.	8	0.052	0.053	7.90	0.0012	0.024	3.00	0.002	0.360	1.000	0.106	0.106				
1161R	0.60	none				2.91	0.0012	0.024	3.00	0.141	0.360	0.368	1.045	1.045	0.181	0.779	0.770	
1172	0.60	Rd. pile bts.	6	0.052	0.107	2.91	0.0012	0.024	3.00	0.180	0.360	0.368	1.343	0.298	0.221	0.814	0.044	4.8
1172R	0.60	Rd. pile bts.	6	0.052	0.107	2.91	0.0012	0.024	3.00	0.181	0.360	0.368	1.350	0.305	0.221	0.819	0.049	4.4
1173R	0.60	Rd. pile bts.	4	0.052	0.072	2.91	0.0012	0.024	3.00	0.167	0.360	0.368	1.244	0.199	0.206	0.811	0.041	4.6
1174	0.60	Rd. pile bts.	2	0.052	0.035	2.91	0.0012	0.024	3.00	0.152	0.360	0.368	1.129	0.084	0.194	0.784	0.014	4.4
1189R	0.60	none				3.89	0.0012	0.024	3.00	0.065	0.360	0.492	0.847	0.870	0.096	0.677	0.670	
1198	0.60	Rd. pile bts.	8	0.052	0.107	3.89	0.0012	0.024	3.00	0.094	0.360	0.492	1.234	0.364	0.127	0.740	0.070	4.3
1199	0.60	Rd. pile bts.	6	0.052	0.080	3.89	0.0012	0.024	3.00	0.084	0.360	0.492	1.100	0.230	0.116	0.724	0.054	5.7
1200	0.60	Rd. pile bts.	4	0.052	0.054	3.89	0.0012	0.024	3.00	0.076	0.360	0.492	0.993	0.123	0.108	0.704	0.034	4.3
1216	0.60	none				4.92	0.0012	0.024	3.00	0.031	0.360	0.623	0.629	0.629	0.054	0.574	0.574	
1240	0.60	Rd. pile bts.	10	0.052	0.106	4.92	0.0012	0.024	3.00	0.048	0.360	0.623	0.980	0.351	0.072	0.667	0.093	4.3
1241	0.60	Rd. pile bts.	8	0.052	0.085	4.92	0.0012	0.024	3.00	0.043	0.360	0.623	0.877	0.248	0.068	0.632	0.058	4.3
774	0.60	Sq. pile bts.	18	0.052	0.118	7.90	0.0012	0.042	2.50	0.005	0.496	1.000	0.813	0.813	0.004	1.250	1.250	
775	0.60	Sq. pile bts.	14	0.052	0.092	7.90	0.0012	0.042	2.50	0.003	0.496	1.000	0.488	0.488	0.001	3.000	3.000	
776	0.60	Sq. pile bts.	10	0.052	0.066	7.90	0.0012	0.042	2.50	0.002	0.496	1.000	0.325	0.325	0.000	0.000	0.000	
801	0.60	Sq. pile bts.	6	0.052	0.071	4.42	0.0012	0.024	2.50	0.052	0.333	0.552	1.078	0.790	0.078	0.667	0.574	
802	0.60	Sq. pile bts.	4	0.052	0.047	4.42	0.0012	0.024	2.50	0.044	0.333	0.552	0.911	0.121	0.070	0.629	0.055	
804R	0.60	Sq. pile bts.	1	0.052	0.016	4.42	0.0012	0.024	2.50	0.041	0.333	0.552	0.847	0.057	0.062	0.661	0.087	
823	0.60	none				2.416	0.0012	0.024	2.50	0.176	0.333	0.302	1.118	1.100	0.222	0.793	0.790	
824	0.60	Sq. pile bts.	1	0.052	0.021	2.416	0.0012	0.024	2.50	0.181	0.333	0.302	1.152	0.052	0.234	0.774	-0.016	
824R	0.60	Sq. pile bts.	1	0.052	0.021	2.416	0.0012	0.024	2.50	0.182	0.333	0.302	1.158	0.058	0.230	0.791	0.001	
824RR	0.60	Sq. pile bts.	1	0.052	0.021	2.416	0.0012	0.024	2.50	0.185	0.333	0.302	1.178	0.078	0.232	0.797	0.007	
825	0.60	Sq. pile bts.	2	0.052	0.044	2.416	0.0012	0.024	2.50	0.195	0.333	0.302	1.245	0.145	0.247	0.789	-0.001	
826	0.60	Sq. pile bts.	4	0.052	0.086	2.416	0.0012	0.024	2.50	0.209	0.333	0.302	1.333	0.233	0.260	0.804	0.014	
853	0.60	Sq. pile bts.	20	0.052	0.130	7.90	0.0012	0.024	2.50	0.013	0.333	1.000	0.854	0.854				
854	0.60	Sq. pile bts.	16	0.052	0.104	7.90	0.0012	0.024	2.50	0.010	0.333	1.000	0.654	0.654				
855	0.60	Sq. pile bts.	12	0.052	0.079	7.90	0.0012	0.024	2.50	0.007	0.333	1.000	0.458	0.458				
856	0.60	Sq. pile bts.	8	0.052	0.052	7.90	0.0012	0.024	2.50	0.005	0.333	1.000	0.327	0.327				
857	0.60	Sq. pile bts.	4	0.052	0.026	7.90	0.0012	0.024	2.50	0.003	0.333	1.000	0.196	0.196				
886RR	0.60	none				4.42	0.0012	0.024	5.00	0.066	0.484	0.552	0.706	0.706	0.106	0.623	0.623	
890	0.60	Sq. pile bts.	6	0.052	0.070	4.42	0.0012	0.024	5.00	0.095	0.484	0.552	1.036	0.330	0.141	0.674	0.051	
890RR	0.60	Sq. pile bts.	6	0.052	0.071	4.42	0.0012	0.024	5.00	0.093	0.484	0.552	1.002	0.296	0.142	0.655	0.032	

TABLE 6 : PIERS
45 degree wing-wall abutment

B = 7.90ft., L = 1.00 ft.

Run No.	l	Type of Pier	N Number of Piers	D Width of Piers	J	b [ft]	S _o	n	Q [cfs]	h ₁ * [ft]	h _n [ft]	M	K _b	K _p	h ₁ *+h ₃ * [ft]	$\frac{h_1^*}{h_1^*+h_3^*}$	$\frac{h_1^*}{h_1^*+h_3^*}$	L*
891R	0.60	Sq. pile bts.	4	0.052	0.047	4.42	0.0012	0.024	5.00	0.085	0.484	0.552	0.914	0.208	0.122	0.697	0.074	
891RR	0.60	Sq. pile bts.	4	0.052	0.047	4.42	0.0012	0.024	5.00	0.081	0.484	0.552	0.870	0.164	0.130	0.623	0	
892R	0.60	Sq. pile bts.	2	0.052	0.023	4.42	0.0012	0.024	5.00	0.070	0.484	0.552	0.751	0.045	0.112	0.625	0.002	
892RR	0.60	Sq. pile bts.	2	0.052	0.023	4.42	0.0012	0.024	5.00	0.072	0.484	0.552	0.772	0.066	0.120	0.600	0.023	
927	0.60	none				2.416	0.0012	0.024	5.00	0.305	0.484	0.302	1.015	1.035	0.402	0.759	0.780	
935	0.60	Sq. pile bts.	2	0.052	0.043	2.416	0.0012	0.024	5.00	0.340	0.484	0.302	1.135	0.110	0.425	0.800	0.020	
936	0.60	Sq. pile bts.	3	0.052	0.064	2.416	0.0012	0.024	5.00	0.357	0.484	0.302	1.194	0.169	0.442	0.808	0.028	
1141	0.60	Sq. pile bts.	16	0.052	0.105	7.90	0.0012	0.024	3.00	0.008	0.360	1.000	0.427	0.427				
1142	0.60	Sq. pile bts.	12	0.052	0.079	7.90	0.0012	0.024	3.00	0.006	0.360	1.000	0.321	0.321				
1143	0.60	Sq. pile bts.	8	0.052	0.053	7.90	0.0012	0.024	3.00	0.004	0.360	1.000	0.224	0.224				
1144	0.60	Sq. pile bts.	4	0.052	0.026	7.90	0.0012	0.024	3.00	0.002	0.360	1.000	0.106	0.106				
1161R	0.60	none				2.91	0.0012	0.024	3.00	0.141	0.360	0.368	1.045	1.045	0.181	0.779	0.770	
1169	0.60	Sq. pile bts.	6	0.052	0.107	2.91	0.0012	0.024	3.00	0.190	0.360	0.368	1.419	0.374	0.235	0.809	0.039	4.1
1170	0.60	Sq. pile bts.	4	0.052	0.072	2.91	0.0012	0.024	3.00	0.171	0.360	0.368	1.273	0.228	0.213	0.803	0.033	4.9
1171	0.60	Sq. pile bts.	2	0.052	0.035	2.91	0.0012	0.024	3.00	0.153	0.360	0.368	1.137	0.092	0.196	0.781	0.011	5.2
1189R	0.60	none				3.89	0.0012	0.024	3.00	0.065	0.360	0.492	0.847	0.870	0.096	0.677	0.670	
1201	0.60	Sq. pile bts.	8	0.052	0.107	3.89	0.0012	0.024	3.00	0.102	0.360	0.492	1.342	0.472	0.135	0.756	0.086	4.2
1202	0.60	Sq. pile bts.	6	0.052	0.080	3.89	0.0012	0.024	3.00	0.091	0.360	0.492	1.194	0.324	0.125	0.728	0.058	4.8
1203	0.60	Sq. pile bts.	4	0.052	0.054	3.89	0.0012	0.024	3.00	0.081	0.360	0.492	1.061	0.191	0.112	0.723	0.053	4.9
1216	0.60	none				4.92	0.0012	0.024	3.00	0.031	0.360	0.623	0.629	0.629	0.054	0.574	0.574	
1237	0.60	Sq. pile bts.	10	0.052	0.106	4.92	0.0012	0.024	3.00	0.055	0.360	0.623	1.126	0.497	0.079	0.696	0.122	4.8
1238	0.60	Sq. pile bts.	8	0.052	0.085	4.92	0.0012	0.024	3.00	0.048	0.360	0.623	0.980	0.351	0.073	0.658	0.084	4.3
1239R	0.60	Sq. pile bts.	4	0.052	0.042	4.92	0.0012	0.024	3.00	0.038	0.360	0.623	0.773	0.144	0.063	0.603	0.029	4.3
1242	0.60	none				5.90	0.0012	0.024	3.00	0.011	0.360	0.747	0.323	0.323	0.029	0.379	0.400	
1265	0.60	Sq. pile bts.	12	0.052	0.105	5.90	0.0012	0.024	3.00	0.032	0.360	0.747	0.945	0.622	0.047	0.681	0.281	
1266	0.60	Sq. pile bts.	8	0.052	0.071	5.90	0.0012	0.024	3.00	0.024	0.360	0.747	0.706	0.383	0.038	0.632	0.232	
1267	0.60	Sq. pile bts.	4	0.052	0.035	5.90	0.0012	0.024	3.00	0.018	0.360	0.747	0.529	0.206	0.033	0.545	0.145	
923	0.60	none				4.42	0.0012	0.024	5.00	0.062	0.484	0.552	0.663	0.663	0.106	0.585	0.585	
924	0.60	H pile bts.	1	0.050	0.011	4.42	0.0012	0.024	5.00	0.069	0.484	0.552	0.740	0.077	0.112	0.616	0.031	
925	0.60	H pile bts.	2	0.050	0.022	4.42	0.0012	0.024	5.00	0.072	0.484	0.552	0.772	0.109	0.117	0.615	0.030	
926	0.60	H pile bts.	3	0.050	0.034	4.42	0.0012	0.024	5.00	0.071	0.484	0.552	0.767	0.104	0.119	0.597	0.012	
1161R	0.60	none				2.91	0.0012	0.024	3.00	0.141	0.360	0.368	1.045	1.045	0.181	0.779	0.770	
1175	0.60	H pile bts.	3	0.052	0.053	2.91	0.0012	0.024	3.00	0.169	0.360	0.368	1.259	0.214	0.211	0.801	0.031	5.0
1176	0.60	H pile bts.	2	0.052	0.035	2.91	0.0012	0.024	3.00	0.159	0.360	0.368	1.183	0.138	0.198	0.803	0.033	
1189R	0.60	none				3.89	0.0012	0.024	3.00	0.065	0.360	0.492	0.847	0.870	0.096	0.677	0.670	
1196	0.60	H pile bts.	3	0.052	0.040	3.89	0.0012	0.024	3.00	0.078	0.360	0.492	1.021	0.151	0.109	0.716	0.046	
1197	0.60	H pile bts.	2	0.052	0.026	3.89	0.0012	0.024	3.00	0.076	0.360	0.492	0.940	0.070	0.102	0.706	0.036	
1216	0.60	none				4.92	0.0012	0.024	3.00	0.031	0.360	0.623	0.629	0.629	0.054	0.574	0.574	
1235	0.60	H pile bts.	4	0.052	0.042	4.92	0.0012	0.024	3.00	0.039	0.360	0.623	0.795	0.166	0.061	0.639	0.065	
1242	0.60	none				5.90	0.0012	0.024	3.00	0.011	0.360	0.747	0.323	0.323	0.029	0.379	0.400	
1268	0.60	H pile bts.	4	0.052	0.035	5.90	0.0012	0.024	3.00	0.019	0.360	0.747	0.558	0.324	0.033	0.576	0.176	

TABLE 7 : PIERS
1:1.5 spill-through abutment

B = 7.90 ft. , L = 1.00 ft. , $S_o = 0.0012$, n = 0.024

Run No.	l [ft]	Type of pier	N Number of piers	D Width of pier	J	b_m [ft]	b [ft]	Q [cfs]	h_1^* [ft]	h_n [ft]	M	K_b	ΔK_p	$h_1^* + h_3^*$ [ft]	$\frac{h_1^*}{h_1^* + h_3^*}$	$\frac{h_1^*}{h_1^* + h_3^*}$	L*
984	0.90	none				5.167	5.893	5.00	0.020	0.484	0.746	0.373	0.353	0.044	0.455	0.430	
993	0.90	sing. shft.	2	0.052	0.018	5.167	5.893	5.00	0.020	0.484	0.746	0.373	0.020	0.045	0.444	0.014	
994	0.90	sing. shft.	4	0.052	0.035	5.167	5.893	5.00	0.021	0.484	0.746	0.396	0.043	0.044	0.477	0.047	4.3
995	0.90	sing. shft.	6	0.052	0.053	5.167	5.893	5.00	0.022	0.484	0.746	0.411	0.058	0.046	0.478	0.048	4.9
996	0.90	sing. shft.	10	0.052	0.088	5.167	5.893	5.00	0.024	0.484	0.746	0.449	0.096	0.047	0.511	0.081	5.5
999	0.90	sing. shft.	1	0.110	0.019	5.167	5.893	5.00	0.022	0.484	0.746	0.411	0.390	0.042	0.524	0.094	4.5
1000	0.90	sing. shft.	2	0.110	0.037	5.167	5.893	5.00	0.023	0.484	0.746	0.429	0.039	0.044	0.523	0.093	4.8
1002	0.90	sing. shft.	5	0.110	0.094	5.167	5.893	5.00	0.026	0.484	0.746	0.486	0.096	0.050	0.520	0.090	5.1
1007R	0.90	none				4.14	4.866	5.00	0.057	0.484	0.617	0.739	0.720	0.096	0.594	0.570	
1018	0.90	sing. shft.	4	0.052	0.042	4.14	4.866	5.00	0.058	0.484	0.617	0.752	0.032	0.096	0.604	0.034	4.4
1019	0.90	sing. shft.	2	0.052	0.021	4.14	4.866	5.00	0.057	0.484	0.617	0.739	0.019	0.095	0.600	0.030	5.0
1024R	0.90	sing. shft.	5	0.110	0.113	4.14	4.866	5.00	0.065	0.484	0.617	0.845	0.745	0.100	0.650	0.080	
1025	0.90	sing. shft.	3	0.110	0.068	4.14	4.866	5.00	0.062	0.484	0.617	0.805	0.060	0.100	0.620	0.050	5.2
1026	0.90	sing. shft.	2	0.110	0.045	4.14	4.866	5.00	0.061	0.484	0.617	0.791	0.046	0.100	0.610	0.040	5.2
1027	0.90	sing. shft.	1	0.110	0.022	4.14	4.866	5.00	0.059	0.484	0.617	0.765	0.020	0.098	0.602	0.032	5.0
1034	0.90	none				3.125	3.851	5.00	0.119	0.484	0.488	0.978	0.978	0.184	0.647	0.670	
1045	0.90	sing. shft.	2	0.052	0.027	3.125	3.851	5.00	0.122	0.484	0.488	1.003	0.028	0.179	0.682	0.012	5.1
1046	0.90	sing. shft.	4	0.052	0.054	3.125	3.851	5.00	0.123	0.484	0.488	1.012	0.034	0.176	0.699	0.029	5.1
1047	0.90	sing. shft.	6	0.052	0.081	3.125	3.851	5.00	0.125	0.484	0.488	1.029	0.051	0.179	0.698	0.028	5.5
1048	0.90	sing. shft.	8	0.052	0.108	3.125	3.851	5.00	0.127	0.484	0.488	1.046	0.068	0.184	0.690	0.020	
1053R	0.90	sing. shft.	1	0.110	0.028	3.125	3.851	5.00	0.121	0.484	0.488	0.995	0.017	0.174	0.695	0.025	4.9
1054R	0.90	sing. shft.	2	0.110	0.057	3.125	3.851	5.00	0.124	0.484	0.488	1.021	0.043	0.178	0.697	0.027	5.1
1055	0.90	sing. shft.	3	0.110	0.086	3.125	3.851	5.00	0.126	0.484	0.488	1.038	0.060	0.174	0.724	0.054	5.1
1056	0.90	sing. shft.	4	0.110	0.114	3.125	3.851	5.00	0.129	0.484	0.488	1.063	0.085	0.184	0.701	0.031	5.1
1061	0.90	none				2.146	2.872	5.00	0.235	0.484	0.363	1.097	1.077	0.305	0.770	0.760	5.1
1068	0.90	sing. shft.	2	0.052	0.036	2.146	2.872	5.00	0.237	0.484	0.363	1.107	0.030	0.307	0.772	0.012	5.0
1069	0.90	sing. shft.	4	0.052	0.072	2.146	2.872	5.00	0.239	0.484	0.363	1.116	0.039	0.309	0.773	0.013	5.0
1070	0.90	sing. shft.	6	0.052	0.109	2.146	2.872	5.00	0.243	0.484	0.363	1.136	0.059	0.312	0.779	0.019	4.6
1074	0.90	sing. shft.	1	0.110	0.038	2.146	2.872	5.00	0.240	0.484	0.363	1.121	0.024	0.312	0.769	0.009	4.4
1075	0.90	sing. shft.	2	0.110	0.076	2.146	2.872	5.00	0.245	0.484	0.363	1.145	0.048	0.318	0.770	0.010	4.4
1076	0.90	sing. shft.	3	0.110	0.115	2.146	2.872	5.00	0.251	0.484	0.363	1.174	0.077	0.323	0.777	0.017	4.9
984	0.90	none				5.167	5.893	5.00	0.020	0.484	0.746	0.373		0.044	0.455		
997	0.90	dbl. shft.	10	0.052	0.088	5.167	5.893	5.00	0.027	0.484	0.746	0.503	0.170	0.046	0.587	0.157	4.9
998	0.90	dbl. shft.	6	0.052	0.053	5.167	5.893	5.00	0.023	0.484	0.746	0.429	0.096	0.044	0.523	0.093	4.7
1003	0.90	dbl. shft.	5	0.110	0.094	5.167	5.893	5.00	0.030	0.484	0.746	0.561	0.188	0.052	0.577	0.147	5.5
1003R	0.90	dbl. shft.	5	0.110	0.094	5.167	5.893	5.00	0.031	0.484	0.746	0.580	0.207				
1005	0.90	dbl. shft.	2	0.110	0.037	5.167	5.893	5.00	0.023	0.484	0.746	0.429	0.056	0.048	0.479	0.049	5.1
1006	0.90	dbl. shft.	1	0.110	0.019	5.167	5.893	5.00	0.022	0.484	0.746	0.411	0.038	0.046	0.478	0.048	5.1
1007R	0.90	none				4.14	4.866	5.00	0.057	0.484	0.617	0.739	0.720	0.096	0.594	0.570	
1021	0.90	dbl. shft.	10	0.052	0.107	4.14	4.866	5.00	0.067	0.484	0.617	0.871	0.151	0.104	0.644	0.074	5.2
1028	0.90	dbl. shft.	5	0.110	0.113	4.14	4.866	5.00	0.072	0.484	0.617	0.937	0.745	0.109	0.661	0.091	5.0
1029	0.90	dbl. shft.	3	0.110	0.068	4.14	4.866	5.00	0.065	0.484	0.617	0.845	0.100	0.104	0.625	0.055	5.0
1030	0.90	dbl. shft.	2	0.110	0.045	4.14	4.866	5.00	0.063	0.484	0.617	0.818	0.073	0.101	0.624	0.054	4.8

TABLE 7 : PIERS
1:1.5 spill-through abutment

B = 7.90 ft. , L = 1.00 ft. , $S_o = 0.0012$, n = 0.024

Run No.	l [ft]	Type of pier	N Number of piers	D Width of pier	J	b_m [ft]	b [ft]	Q [cfs]	h_1^* [ft]	h_m [ft]	M	K_b	ΔK_p	$h_1^* + h_3^*$ [ft]	$\frac{h_1^*}{h_1^* + h_3^*}$	$\frac{h_1^*}{h_1^* + h_3^*}$	L*
1031	0.90	dbl. shft.	1	0.110	0.022	4.14	4.866	5.00	0.060	0.484	0.617	0.778	0.033	0.098	0.612	0.042	4.4
1034	0.90	none				3.125	3.851	5.00	0.119	0.484	0.488	0.978	0.978	0.184	0.647	0.670	
1049	0.90	dbl. shft.	8	0.052	0.108	3.125	3.851	5.00	0.134	0.484	0.488	1.105	0.127	0.184	0.728	0.058	5.1
1049R	0.90	dbl. shft.	8	0.052	0.108	3.125	3.851	5.00	0.135	0.484	0.488	1.113	0.135				
1050RR	0.90	dbl. shft.	6	0.052	0.081	3.125	3.851	5.00	0.131	0.484	0.488	1.080	0.102	0.184	0.712	0.042	5.6
1051R	0.90	dbl. shft.	4	0.052	0.054	3.125	3.851	5.00	0.127	0.484	0.488	1.046	0.068	0.175	0.726	0.056	5.7
1052	0.90	dbl. shft.	2	0.052	0.027	3.125	3.851	5.00	0.124	0.484	0.488	1.021	0.043	0.180	0.689	0.019	4.9
1058	0.90	dbl. shft.	3	0.110	0.086	3.125	3.851	5.00	0.136	0.484	0.488	1.122	0.144	0.186	0.731	0.690	5.1
1059	0.90	dbl. shft.	2	0.110	0.057	3.125	3.851	5.00	0.130	0.484	0.488	1.071	1.082	0.177	0.734	0.044	5.1
1060	0.90	dbl. shft.	1	0.110	0.028	3.125	3.851	5.00	0.125	0.484	0.488	1.029	0.051	0.175	0.714	0.024	4.9
1071	0.90	dbl. shft.	2	0.052	0.036	2.146	2.872	5.00	0.240	0.484	0.363	1.121	0.039	0.315	0.762	0.760	5.0
1072	0.90	dbl. shft.	4	0.052	0.072	2.146	2.872	5.00	0.247	0.484	0.363	1.155	0.073	0.318	0.777	0.017	4.4
1073	0.90	dbl. shft.	6	0.052	0.109	2.146	2.872	5.00	0.255	0.484	0.363	1.194	0.112	0.322	0.792	0.032	4.5
1077	0.90	dbl. shft.	3	0.110	0.115	2.146	2.872	5.00	0.261	0.484	0.363	1.222	1.097	0.331	0.789	0.029	5.3
1078	0.90	dbl. shft.	2	0.110	0.076	2.146	2.872	5.00	0.251	0.484	0.363	1.174	0.077	0.323	0.777	0.017	4.9
1079	0.90	dbl. shft.	1	0.110	0.038	2.146	2.872	5.00	0.243	0.484	0.363	1.136	0.039	0.315	0.771	0.011	4.8
1061	0.90	none				2.146	2.872	5.00	0.235	0.484	0.363	1.097	1.127	0.305	0.770	0.770	
1081R	0.90	Rd. Narrow	2	0.104	0.072	2.146	2.892	5.00	0.257	0.484	0.366	1.222	0.095	0.326	0.788	0.018	4.7
1082R	0.90	Rd. Narrow	3	0.104	0.108	2.146	2.892	5.00	0.268	0.484	0.366	1.276	0.149	0.336	0.798	0.028	4.3
1083R	0.90	Rd. Narrow	2	0.052	0.036	2.146	2.892	5.00	0.246	0.484	0.366	1.167	0.060	0.317	0.776	0.006	4.2
1084R	0.90	Rd. Narrow	4	0.052	0.072	2.146	2.892	5.00	0.258	0.484	0.366	1.226	0.099	0.333	0.775	0.005	4.3
1085R	0.90	Rd. Narrow	6	0.052	0.108	2.146	2.892	5.00	0.272	0.484	0.366	1.295	0.168	0.345	0.788	0.018	3.9
1086R	0.90	none				3.145	3.891	5.00	0.119	0.484	0.492	1.006	1.006	0.184	0.647	0.647	
1087R	0.90	Rd. Narrow	2	0.052	0.026	3.145	3.891	5.00	0.124	0.484	0.492	1.050	0.044	0.187	0.663	0.016	5.1
1091R	0.90	none				4.14	4.886	5.00	0.055	0.484	0.618	0.723	0.700	0.084	0.665	0.545	
1092R	0.90	Rd. Narrow	2	0.052	0.021	4.14	4.886	5.00	0.057	0.484	0.618	0.750	0.050	0.100	0.570	0.025	4.8
1093R	0.90	Rd. Narrow	4	0.052	0.042	4.14	4.886	5.00	0.060	0.484	0.618	0.790	0.090	0.102	0.588	0.043	5.0
1094R	0.90	Rd. Narrow	6	0.052	0.064	4.14	4.886	5.00	0.062	0.484	0.618	0.816	0.116	0.102	0.608	0.063	4.8
1095R	0.90	Rd. Narrow	10	0.052	0.106	4.14	4.886	5.00	0.069	0.484	0.618	0.911	0.211	0.106	0.056	0.106	4.6
1096RR	0.90	Rd. Narrow	2	0.104	0.042	4.14	4.886	5.00	0.058	0.484	0.618	0.763	0.063	0.102	0.569	0.520	
1097R	0.90	Rd. Narrow	3	0.104	0.064	4.14	4.886	5.00	0.061	0.484	0.618	0.803	0.103	0.108	0.565	0.045	3.6
1098R	0.90	Rd. Narrow	4	0.104	0.085	4.14	4.886	5.00	0.064	0.484	0.618	0.844	0.144	0.108	0.593	0.073	4.6
1099RR	0.90	Rd. Narrow	5	0.104	0.106	4.14	4.886	5.00	0.066	0.484	0.618	0.870	0.170	0.104	0.635	0.115	4.2
1100R	0.90	Rd. Narrow	4	0.104	0.107	3.145	3.891	5.00	0.143	0.484	0.492	1.202	0.966	0.200	0.715	0.647	4.7
1101R	0.90	Rd. Narrow	3	0.104	0.080	3.145	3.891	5.00	0.133	0.484	0.492	1.116	0.150	0.194	0.686	0.039	4.3
1102R	0.90	Rd. Narrow	2	0.104	0.054	3.145	3.891	5.00	0.127	0.484	0.492	1.064	0.098	0.187	0.679	0.032	5.1
1103R	0.90	Rd. Narrow	1	0.104	0.029	3.145	3.891	5.00	0.122	0.484	0.492	1.021	0.055	0.184	0.663	0.016	4.5
984	0.90	none				5.167	5.893	5.00	0.020	0.484	0.746	0.373	0.313	0.044	0.455	0.440	
986	0.90	Rd. pile bts.	4	0.052	0.035	5.167	5.893	5.00	0.023	0.484	0.746	0.429	0.116	0.051	0.451	0.021	5.7
987R	0.90	Rd. pile bts.	6	0.052	0.053	5.167	5.893	5.00	0.026	0.484	0.746	0.486	0.173	0.046	0.565	0.125	3.9
988	0.90	Rd. pile bts.	10	0.052	0.088	5.167	5.893	5.00	0.032	0.484	0.746	0.660	0.287	0.050	0.640	0.200	4.1
1007R	0.90	none				4.14	4.866	5.00	0.057	0.484	0.617	0.739	0.710	0.096	0.594	0.570	
1008	0.90	Rd. pile bts.	2	0.052	0.021	4.14	4.866	5.00	0.060	0.484	0.617	0.778	0.068	0.097	0.619	0.049	5.0

TABLE 7 : PIERS
1:1.5 spill-through abutment

B = 7.90 ft. , L = 1.00 ft. , $S_o = 0.0012$, n = 0.024

Run No.	l [ft]	Type of pier	N Number of piers	D Width of pier	J	b_m [ft]	b [ft]	Q [cfs]	h_1^* [ft]	h_2 [ft]	M	K_b	ΔK_p	$h_1^* + h_3^*$ [ft]	$\frac{h_1^*}{h_1^* + h_3^*}$	$\frac{h_1^*}{h_1^* + h_3^*}$	L*
1009	0.90	Rd. pile bts.	4	0.052	0.042	4.14	4.866	5.00	0.064	0.484	0.617	0.831	0.121	0.098	0.653	0.083	5.4
1010	0.90	Rd. pile bts.	6	0.052	0.064	4.14	4.866	5.00	0.069	0.484	0.617	0.898	0.188	0.099	0.697	0.127	4.8
1034	0.90	none				3.125	3.851	5.00	0.119	0.484	0.488	0.978	0.978	0.184	0.647	0.670	
1035	0.90	Rd. pile bts.	2	0.052	0.027	3.125	3.851	5.00	0.126	0.484	0.488	1.038	0.060	0.184	0.685	0.015	5.1
1036	0.90	Rd. pile bts.	4	0.052	0.054	3.125	3.851	5.00	0.134	0.484	0.488	1.109	0.131	0.192	0.698	0.028	4.9
1037	0.90	Rd. pile bts.	6	0.052	0.081	3.125	3.851	5.00	0.142	0.484	0.488	1.173	0.195	0.202	0.703	0.033	4.5
1038	0.90	Rd. pile bts.	8	0.052	0.108	3.125	3.851	5.00	0.153	0.484	0.488	1.266	0.288	0.208	0.736	0.066	4.9
1061	0.90	none				2.146	2.872	5.00	0.235	0.484	0.363	1.097	1.077	0.305	0.770	0.760	
1062R	0.90	Rd. pile bts.	2	0.052	0.036	2.146	2.872	5.00	0.245	0.484	0.363	1.145	0.068	0.321	0.763	0.008	5.1
1063	0.90	Rd. pile bts.	4	0.052	0.073	2.146	2.872	5.00	0.258	0.484	0.363	1.208	0.131	0.337	0.766	0.011	5.3
1064	0.90	Rd. pile bts.	6	0.052	0.109	2.146	2.872	5.00	0.272	0.484	0.363	1.275	0.198	0.350	0.777	0.022	5.3
984	0.90	none				5.167	5.893	5.00	0.020	0.484	0.746	0.373	0.313	0.044	0.455	0.440	
989	0.90	Sq. pile bts.	2	0.052	0.018	5.167	5.893	5.00	0.021	0.484	0.746	0.392	0.079	0.044	0.477	0.037	4.7
991	0.90	Sq. pile bts.	6	0.052	0.053	5.167	5.893	5.00	0.029	0.484	0.746	0.543	0.230	0.050	0.580	0.140	4.7
992	0.90	Sq. pile bts.	10	0.052	0.088	5.167	5.893	5.00	0.037	0.484	0.746	0.694	0.381	0.058	0.638	0.198	5.3
1007R	0.90	none				4.14	4.866	5.00	0.057	0.484	0.617	0.739	0.739	0.096	0.594	0.570	
1012	0.90	Sq. pile bts.	2	0.052	0.021	4.14	4.866	5.00	0.063	0.484	0.617	0.818	0.079	0.100	0.630	0.060	5.0
1013	0.90	Sq. pile bts.	4	0.052	0.042	4.14	4.866	5.00	0.068	0.484	0.617	0.884	0.145	0.100	0.680	0.110	4.8
1013R	0.90	Sq. pile bts.	4	0.052	0.042	4.14	4.866	5.00	0.069	0.484	0.617	0.898	0.159				
1014	0.90	Sq. pile bts.	6	0.052	0.064	4.14	4.866	5.00	0.074	0.484	0.617	0.963	0.224	0.113	0.655	0.085	4.4
1034	0.90	none				3.125	3.851	5.00	0.119	0.484	0.488	0.978	0.978	0.184	0.647	0.670	
1039	0.90	Sq. pile bts.	2	0.052	0.027	3.125	3.851	5.00	0.129	0.484	0.488	1.063	0.085	0.188	0.686	0.016	4.7
1040	0.90	Sq. pile bts.	4	0.052	0.054	3.125	3.851	5.00	0.139	0.484	0.488	1.148	0.170	0.198	0.702	0.032	4.3
1041	0.90	Sq. pile bts.	6	0.052	0.081	3.125	3.851	5.00	0.151	0.484	0.488	1.249	0.271	0.207	0.729	0.059	4.3
1042	0.90	Sq. pile bts.	8	0.052	0.108	3.125	3.851	5.00	0.163	0.484	0.488	1.351	0.373	0.218	0.748	0.078	5.1
1062R	0.90	none				2.146	2.872	5.00	0.235	0.484	0.363	1.097	1.085	0.305	0.770	0.760	
1065	0.90	Sq. pile bts.	2	0.052		2.146	2.872	5.00	0.250	0.484	0.363	1.170	0.085	0.328	0.762	0.002	4.5
1066	0.90	Sq. pile bts.	4	0.052		2.146	2.872	5.00	0.268	0.484	0.363	1.256	0.171	0.345	0.777	0.017	5.3
1067	0.90	Sq. pile bts.	6	0.052		2.146	2.872	5.00	0.287	0.484	0.363	1.348	0.263	0.364	0.788	0.028	4.5
1007R	0.90	none				4.14	4.866	5.00	0.057	0.484	0.617	0.739	0.745	0.096	0.594	0.570	
1032	0.90	H pile bents	2	0.050	0.020	4.14	4.866	5.00	0.062	0.484	0.617	0.805	0.060	0.100	0.620	0.050	4.8
1033	0.90	H pile bents	4	0.050	0.041	4.14	4.866	5.00	0.068	0.484	0.617	0.884	0.139	0.106	0.642	0.072	5.0
1034	0.90	none				3.125	3.851	5.00	0.119	0.484	0.488	0.978	0.978	0.184	0.647	0.670	
1043	0.90	H pile bents	2	0.050	0.026	3.125	3.851	5.00	0.129	0.484	0.488	1.063	0.085	0.183	0.705	0.035	5.1
1044	0.90	H pile bents	4	0.050	0.052	3.125	3.851	5.00	0.139	0.484	0.488	1.148	0.170	0.187	0.743	0.073	4.3

TABLE 8 : ECCENTRIC CROSSING

Run No.	Abutment Type	L [ft]	l [ft]	B [ft]	b_m [ft]	b [ft]	S_o	n	Q [cfs]	h_1^* [ft]	h_n	M	K_b	e	$h_1^* + h_3^*$ [ft]	$\frac{h_1^*}{h_1^* + h_3^*}$	ΔK_b	$\Delta \frac{h_1^*}{h_1^* + h_3^*}$
475	45°WW	1.00	0.90	7.90		6.20	0.0012	0.024	5.00	0.021	0.484	0.785	0.437	1.00	0.050	0.420	0.187	0.040
476	45°WW	1.00	0.90	7.90		5.19	0.0012	0.024	5.00	0.044	0.484	0.657	0.646	1.00	0.082	0.537	0.156	0.027
477	45°WW	1.00	0.90	7.90		4.19	0.0012	0.024	5.00	0.093	0.484	0.530	0.903	1.00	0.142	0.655	0.133	0.037
478	45°WW	1.00	0.90	7.90		3.17	0.0012	0.024	5.00	0.195	0.484	0.401	1.101	1.00	0.260	0.750	0.081	0.035
470R	45°WW	1.00	0.90	7.90		6.20	0.0012	0.042	5.00	0.009	0.678	0.785	0.394				0.144	
471	45°WW	1.00	0.90	7.90		5.19	0.0012	0.042	5.00	0.025	0.678	0.657	0.766	1.00	0.047	0.532	0.276	0.022
472	45°WW	1.00	0.90	7.90		4.19	0.0012	0.042	5.00	0.051	0.678	0.530	1.011	1.00	0.077	0.662	0.241	0.044
473	45°WW	1.00	0.90	7.90		3.17	0.0012	0.042	5.00	0.110	0.678	0.401	1.268	1.00	0.142	0.764	0.268	0.049
474	45°WW	1.00	0.90	7.90		2.66	0.0012	0.042	5.00	0.163	0.678	0.337	1.208	1.00	0.195	0.836	0.183	0.071
479	45°WW	1.00	0.90	7.90		2.17	0.0012	0.042	5.00	0.393	0.678	0.275	1.063	1.00	0.465	0.846		0.036
480	1:1.5ST	1.00	0.90	7.90	2.00	2.363	0.0012	0.024	5.00	0.347	0.484	0.300	1.109	1.00	0.418	0.830		0.010
481	1:1.5ST	1.00	0.90	7.90	2.50	2.863	0.0012	0.024	5.00	0.253	0.484	0.363	1.174	1.00	0.319	0.793	0.074	0.018
482	1:1.5ST	1.00	0.90	7.90	3.50	3.863	0.0012	0.024	5.00	0.135	0.484	0.490	1.134	1.00	0.194	0.696	0.199	0.021
483	1:1.5ST	1.00	0.90	7.90	4.50	4.863	0.0012	0.024	5.00	0.067	0.484	0.615	0.858	1.00	0.106	0.632	0.218	0.059
484	1:1.5ST	1.00	0.90	7.90	5.50	5.863	0.0012	0.024	5.00	0.027	0.484	0.742	0.505	1.00	0.059	0.458	0.155	0.018

TABLE 9 : SKEW CROSSING
45 degree wing-wall abutment

Run No.	Abutment Type	Angle of Skew	L [ft]	l [ft]	B [ft]	b [ft]	bCosφ [ft]	S _o	n	Q [cfs]	h _n [ft]	h ₁ * + $\frac{u^2}{2g}$	K _b	M	Approx. h ₁ * [ft]	h ₁ * + h ₃ * [ft]	$\frac{h_1^*}{h_1^* + h_3^*}$	ΔK _s	$\Delta \frac{h_1^*}{h_1^* + h_3^*}$
211	45°WW	45°	1.00	0.90	7.90	3.96	2.800	0.0012	0.024	4.99	0.484	0.180	0.695	0.355	0.166	0.209	0.793	-0.375	0.028
212	45°WW	45°	1.00	0.90	7.90	2.94	2.079	0.0012	0.024	4.98	0.484	0.270	0.642	0.263	0.260	0.306	0.849	-0.458	0.014
289	45°WW	45°	1.00	0.90	7.90	3.92	2.771	0.0012	0.024	5.00	0.484	0.184	0.729	0.351	0.170	0.210	0.810	-0.341	0.055
290	45°WW	45°	1.00	0.90	7.90	2.87	2.029	0.0012	0.024	5.00	0.484	0.268	0.599	0.257	0.157	0.217	0.723	-0.501	0.117
294	45°WW	45°	1.00	0.60	7.90	6.25	4.419	0.0012	0.024	2.54	0.337	0.050	0.799	0.559	0.040	0.063	0.634	+0.059	0.033
295	45°WW	45°	1.00	0.60	7.90	5.18	3.662	0.0012	0.024	2.53	0.337	0.066	0.800	0.464	0.056	0.077	0.727	-0.130	0.047
296	45°WW	45°	1.00	0.60	7.90	4.16	2.941	0.0012	0.024	2.55	0.337	0.090	0.736	0.372	0.081	0.103	0.787	-0.324	0.037
565	45°WW	45°	1.00	0.90	7.90	3.81	2.694	0.0012	0.024	5.00	0.484	0.186	0.700	0.341	0.172	0.217	0.793	-0.370	0.018
572	45°WW	45°	1.00	0.90	7.90	2.75	1.944	0.0012	0.024	5.00	0.484	0.280	0.578	0.246	0.269	0.316	0.852	-0.522	0.006
1377	45°WW	45°	1.00	0.90	7.90	3.99	2.821	0.0012	0.024	5.00	0.484	0.178	0.729	0.357	0.164	0.217	0.756	-0.341	-0.009
1378	45°WW	45°	1.00	0.90	7.90	5.94	4.200	0.0012	0.024	5.00	0.484	0.095	0.728	0.532	0.076	0.115	0.662	-0.052	0.037
1379	45°WW	45°	1.00	0.90	7.90	7.00	4.949	0.0012	0.024	5.00	0.484	0.073	0.682	0.626	0.053	0.083	0.638	+0.112	0.095
1380	45°WW	45°	1.00	0.90	7.90	7.67	5.423	0.0012	0.024	5.00	0.484	0.058	0.565	0.686	0.037	0.069	0.536	+0.125	0.053
1381	45°WW	45°	1.00	0.90	7.90	8.54	6.038	0.0012	0.024	5.00	0.484	0.045	0.416	0.764	0.023	0.050	0.460	+0.116	0.060
235	45°WW	30°	1.00	0.90	7.90	3.48	3.014	0.0012	0.024	5.00	0.484	0.180	0.843	0.382	0.166	0.213	0.780	-0.202	0.038
286	45°WW	30°	1.00	0.90	7.90	2.45	2.122	0.0012	0.024	4.99	0.484	0.317	0.792	0.269	0.307	0.363	0.845	-0.308	0.013
297	45°WW	30°	1.00	0.60	7.90	5.56	4.815	0.0012	0.024	2.55	0.337	0.042	0.733	0.609	0.032	0.048	0.666	+0.113	0.107
299	45°WW	30°	1.00	0.60	7.90	3.56	3.083	0.0012	0.024	2.50	0.337	0.098	0.937	0.391	0.040	0.115	0.782	-0.093	0.045
300	45°WW	30°	1.00	0.90	7.90	3.56	3.083	0.0012	0.024	5.00	0.482	0.186	0.905	0.390	0.177	0.228	0.775	-0.125	0.038
576	45°WW	30°	1.00	0.90	7.90	3.54	3.066	0.0012	0.024	5.00	0.484	0.184	0.894	0.388	0.176	0.357	0.493	-0.146	-0.246
582	45°WW	30°	1.00	0.90	7.90	2.54	2.200	0.0012	0.024	5.00	0.484	0.314	0.840	0.278	0.304	0.361	0.843	-0.260	0.021
1382	45°WW	30°	1.00	0.90	7.90	3.48	3.017	0.0012	0.024	5.00	0.484	0.190	0.898	0.382	0.176	0.229	0.768	-0.132	0.025
1383	45°WW	30°	1.00	0.90	7.90	5.104	4.425	0.0012	0.024	5.00	0.484	0.090	0.757	0.560	0.071	0.112	0.634	+0.027	0.033
1384	45°WW	30°	1.00	0.90	7.90	6.25	5.419	0.0012	0.024	5.00	0.484	0.052	0.511	0.686	0.030	0.064	0.469	+0.066	-0.015
287	45°WW	15°	1.00	0.90	7.90	7.97	2.869	0.0012	0.024	5.00	0.484	0.230	1.012	0.363	0.218	0.274	0.796	-0.058	0.041
396	45°WW	45°	1.00	0.60	7.90	7.37	5.211	0.0012	0.024	2.50	0.333	0.029	0.472	0.660	0.017	0.032	0.532	-0.028	0.022
397	45°WW	45°	1.00	0.60	7.90	6.34	4.482	0.0012	0.024	2.50	0.333	0.042	0.633	0.567	0.031	0.053	0.585	-0.092	-0.009
398	45°WW	45°	1.00	0.60	7.90	5.29	3.740	0.0012	0.024	2.50	0.333	0.060	0.728	0.473	0.050	0.077	0.649	-0.179	-0.021
399	45°WW	45°	1.00	0.60	7.90	4.27	3.019	0.0012	0.024	2.50	0.333	0.095	0.843	0.382	0.087	0.115	0.756	-0.202	0.016
400	45°WW	45°	1.00	0.60	7.90	3.27	2.312	0.0012	0.024	2.50	0.333	0.155	0.859	0.293	0.148	0.181	0.817	-0.246	0.007
485	45°WW	45°	1.00	0.90	7.90	4.93	3.486	0.0012	0.024	5.00	0.484	0.140	0.835	0.441	0.124	0.166	0.746	-0.130	0.051
486	45°WW	45°	1.00	0.90	7.90	3.84	2.715	0.0012	0.024	5.00	0.484	0.226	0.886	0.344	0.214	0.257	0.833	-0.189	0.063
487	45°WW	45°	1.00	0.90	7.90	2.85	2.015	0.0012	0.024	5.00	0.484	0.376	0.857	0.255	0.371	0.433	0.857	-0.243	0.133
401	45°WW	30°	1.00	0.60	7.90	6.12	5.300	0.0012	0.024	2.50	0.333	0.028	0.453	0.671	0.016	0.035	0.457	-0.017	-0.043
402	45°WW	30°	1.00	0.60	7.90	5.12	4.434	0.0012	0.024	2.50	0.333	0.045	0.685	0.561	0.034	0.058	0.586	-0.040	-0.014
403	45°WW	30°	1.00	0.60	7.90	4.14	3.585	0.0012	0.024	2.50	0.333	0.075	0.897	0.454	0.065	0.093	0.698	-0.098	0.010
404	45°WW	30°	1.00	0.60	7.90	3.15	2.728	0.0012	0.024	2.50	0.333	0.125	0.940	0.345	0.118	0.142	0.831	-0.135	0.061
496	45°WW	30°	1.00	0.90	7.90	4.10	3.551	0.0012	0.024	5.00	0.484	0.140	0.867	0.449	0.124	0.165	0.752	-0.083	0.062
497	45°WW	30°	1.00	0.90	7.90	3.17	2.745	0.0012	0.024	5.00	0.484	0.225	0.902	0.347	0.113	0.165	0.685	-0.173	-0.085

TABLE 10 : SKEW CROSSING
1:1.5 spill- through abutment

B = 7.90 ft. , L = 1.00 ft. , $S_o = 0.0012$, n = 0.024

Run No.	Abutment Type	Angle of Skew	l [ft]	b_m [ft]	b [ft]	bCos ϕ [ft]	Q [cfs]	h_n [ft]	h_1^* [ft]	K_b	M	Approx. h_1^* [ft]	$h_1^* + h_3^*$ [ft]	$\frac{h_1^*}{h_1^* + h_3^*}$	ΔK_s	$\Delta \frac{h_1^*}{h_1^* + h_3^*}$
291	1:1.5 ST	45°	0.90	4.58	5.306	3.751	5.00	0.484	0.137	0.890	0.475	0.121	0.162	0.747	-0.070	0.060
292	1:1.5 ST	45°	0.90	3.56	4.286	3.030	5.00	0.484	0.183	0.870	0.384	0.169	0.215	0.786	-0.225	0.031
293	1:1.5 ST	45°	0.90	2.58	3.306	2.337	4.99	0.484	0.249	0.734	0.296	0.237	0.282	0.840	-0.411	0.020
650	1:1.5 ST	45°	0.90	4.62	5.346	3.780	5.00	0.484	0.137	0.952	0.478	0.121	0.165	0.734	-0.006	0.051
651	1:1.5 ST	45°	0.90	3.66	4.386	3.101	5.00	0.484	0.178	0.881	0.293	0.164	0.208	0.788	-0.264	0.034
652	1:1.5 ST	45°	0.90	2.54	3.266	2.309	5.00	0.484	0.246	0.719	0.292	0.234	0.282	0.830	-0.426	0.008
653	1:1.5 ST	45°	0.60	6.16	6.886	4.868	5.00	0.484	0.085	0.835	0.616	0.066	0.110	0.600	+0.185	0.032
654	1:1.5 ST	45°	0.60	6.29	6.790	4.801	2.50	0.333	0.050	0.946	0.608	0.039	0.062	0.628	+0.276	0.053
655	1:1.5 ST	45°	0.60	5.23	5.730	4.051	2.50	0.333	0.067	1.001	0.513	0.057	0.082	0.696	+0.116	0.043
656	1:1.5 ST	45°	0.60	4.23	4.730	3.344	2.50	0.333	0.088	0.949	0.423	0.079	0.110	0.718	-0.099	-0.009
657	1:1.5 ST	45°	0.60	3.25	3.750	2.651	2.50	0.333	0.124	0.887	0.336	0.117	0.145	0.806	-0.243	0.016
658	1:1.5 ST	45°	0.60	2.27	2.770	1.958	2.50	0.333	0.160	0.640	0.248	0.154	0.189	0.815	-0.505	-0.035
671	1:1.5 ST	45°	0.90	6.26	6.760	4.779	2.50	0.333	0.048	0.897	0.605	0.037	0.058	0.639	+0.227	0.062
672	1:1.5 ST	45°	0.90	5.25	5.750	4.065	2.50	0.333	0.064	0.943	0.515	0.054	0.077	0.702	+0.058	0.047
679	1:1.5 ST	45°	0.90	4.75	5.250	3.712	2.50	0.333	0.073	0.920	0.470	0.064	0.090	0.711	-0.030	0.021
680	1:1.5 ST	45°	0.90	3.69	4.190	2.962	2.50	0.333	0.103	0.889	0.375	0.095	0.125	0.760	-0.211	0.000
681	1:1.5 ST	45°	0.90	2.64	3.140	2.220	2.50	0.333	0.136	0.685	0.281	0.129	0.163	0.791	-0.460	0.039
1389	1:1.5 ST	45°	0.60	8.38	9.106	6.438	5.00	0.484	0.043	0.411	0.815	0.021	0.047	0.447	+0.166	0.087
1390	1:1.5 ST	45°	0.90	7.38	8.106	5.731	5.00	0.484	0.062	0.714	0.725	0.041	0.073	0.562	+0.294	0.102
1391	1:1.5 ST	45°	0.90	4.60	5.326	3.765	5.00	0.484	0.138	0.952	0.476	0.122	0.165	0.740	-0.003	0.056
646	1:1.5 ST	30°	0.90	4.21	4.936	4.275	5.00	0.484	0.110	0.916	0.541	0.092	0.138	0.666	+0.086	0.036
647	1:1.5 ST	30°	0.90	3.21	3.936	3.409	5.00	0.484	0.169	0.996	0.414	0.154	0.200	0.770	-0.064	0.035
648	1:1.5 ST	30°	0.90	2.21	2.936	2.543	5.00	0.484	0.255	0.892	0.322	0.243	0.298	0.815	-0.248	0.015
649	1:1.5 ST	30°	0.60	4.94	5.666	4.907	5.00	0.484	0.081	0.788	0.621	0.061	0.099	0.617	+0.148	0.055
659	1:1.5 ST	30°	0.60	5.02	5.520	4.780	2.50	0.333	0.048	0.897	0.605	0.037	0.060	0.617	+0.217	0.039
660	1:1.5 ST	30°	0.60	4.02	4.520	3.914	2.50	0.333	0.070	0.883	0.495	0.060	0.085	0.707	+0.058	0.037
661	1:1.5 ST	30°	0.60	2.98	3.480	3.014	2.50	0.333	0.110	1.000	0.382	0.102	0.134	0.762	-0.095	0.004
662	1:1.5 ST	30°	0.60	2.16	2.660	2.304	2.50	0.333	0.165	0.915	0.292	0.159	0.189	0.842	-0.230	0.019
674	1:1.5 ST	30°	0.60	5.02	5.520	4.780	2.50	0.333	0.045	0.818	0.605	0.033	0.058	0.574	+0.145	-0.001
675	1:1.5 ST	30°	0.60	4.02	4.520	3.914	2.50	0.333	0.070	0.983	0.495	0.060	0.085	0.706	+0.058	0.036
676	1:1.5 ST	30°	0.90	4.18	4.680	4.053	2.50	0.333	0.064	0.945	0.513	0.054	0.078	0.692	+0.060	0.037
677	1:1.5 ST	30°	0.90	3.25	3.750	3.248	2.50	0.333	0.093	0.951	0.411	0.084	0.113	0.744	-0.109	0.010
678	1:1.5 ST	30°	0.90	2.29	2.790	2.416	2.50	0.333	0.149	0.899	0.306	0.142	0.176	0.806	-0.246	-0.004
1385	1:1.5 ST	30°	0.90	5.83	6.556	5.684	5.00	0.484	0.055	0.561	0.719	0.034	0.066	0.516	+0.131	0.048
1286	1:1.5 ST	30°	0.90	4.15	4.876	4.227	5.00	0.484	0.108	0.875	0.535	0.090	0.126	0.715	+0.035	0.077
1387	1:1.5 ST	30°	0.60	7.19	7.916	6.863	5.00	0.484	0.035	0.245	0.869	0.012	0.043	0.279	+0.075	-0.003
1388	1:1.5 ST	30°	0.60	6.70	7.426	6.438	5.00	0.484	0.040	0.336	0.815	0.017	0.040	0.425	+0.091	0.065
392	1:1.5 ST	45°	0.60	5.66	6.160	4.355	2.50	0.333	0.039	0.544	0.551	0.028	0.050	0.560	-0.256	-0.068
393	1:1.5 ST	45°	0.60	4.75	5.250	3.712	2.50	0.333	0.053	0.607	0.470	0.043	0.065	0.662	-0.363	-0.028
394	1:1.5 ST	45°	0.60	3.58	4.080	2.885	2.50	0.333	0.080	0.629	0.365	0.071	0.097	0.733	-0.481	-0.037
395	1:1.5 ST	45°	0.60	2.59	3.090	2.185	2.50	0.333	0.127	0.617	0.277	0.120	0.152	0.790	-0.528	-0.045
438	1:1.5 ST	45°	0.90	1.94	2.666	1.885	5.00	0.484	0.263	0.506	0.239	0.252	0.300	0.840	-0.639	-0.027
489	1:1.5 ST	45°	0.90	2.98	3.706	2.620	5.00	0.484	0.160	0.554	0.332	0.145	0.187	0.775	-0.589	-0.019

TABLE 10 : SKEW CROSSING
1:1.5 spill-through abutment

B = 7.90 ft. , L = 1.00 ft. , S_o = 0.0012 , n = 0.024

Run No.	Abutment Type	Angle of Skew	l [ft]	b _m [ft]	b [ft]	bCosφ [ft]	Q [cfs]	h _n [ft]	h ₁ * [ft]	K _b	M	Approx. h ₁ * [ft]	h ₁ *+h ₃ * [ft]	$\frac{h_1^*}{h_1^*+h_3^*}$	ΔK _s	$\Delta \frac{h_1^*}{h_1^*+h_3^*}$
490	1:1.5 ST	45°	0.90	4.04	4.766	3.370	5.00	0.484	0.112	0.585	0.427	0.094	0.132	0.712	-.455	-.013
491	1:1.5 ST	45°	0.90	4.92	5.646	3.992	5.00	0.484	0.085	0.562	0.505	0.066	0.104	0.635	-.398	-.030
405	1:1.5 ST	30°	0.60	4.52	5.020	4.347	2.50	0.333	0.046	0.697	0.550	0.035	0.056	0.625	-.103	-.002
406	1:1.5 ST	30°	0.60	3.50	4.000	3.464	2.50	0.333	0.076	0.848	0.438	0.067	0.089	0.753	-.182	0.035
407	1:1.5 ST	30°	0.60	2.58	3.080	2.667	2.50	0.333	0.115	0.821	0.338	0.117	0.150	0.780	-.319	-.013
408	1:1.5 ST	30°	0.60	1.58	2.080	1.801	2.50	0.333	0.235	0.818	0.228	0.230	0.267	0.862	-.327	-.010
492	1:1.5 ST	30°	0.90	4.58	5.306	4.595	5.00	0.484	0.077	0.648	0.582	0.057	0.095	0.600	-.092	0.00
493	1:1.5 ST	30°	0.90	3.44	4.166	3.608	5.00	0.484	0.122	0.752	0.457	0.105	0.138	0.761	-.238	0.060
494	1:1.5 ST	30°	0.90	2.42	3.146	2.724	5.00	0.484	0.202	0.783	0.345	0.189	0.238	0.794	-.347	0.006
495	1:1.5 ST	30°	0.90	1.35	2.076	1.798	5.00	0.484	0.370	0.669	0.228	0.361	0.416	0.867	-.476	-.005

TABLE 11 : DUAL BRIDGES
pile bents

B = 7.90 ft. , L = 1.00 ft. , $S_o = 0.0012$, n = 0.024

Run No.	Abutment Type	l [ft]	b_m [ft]	b [ft]	Q [cfs]	h_n [ft]	h_1^* [ft]	h_d^* [ft]	$\frac{h_d^*}{h_1^*}$	M	L_D [ft]	$\frac{L_D}{h_n}$	$h_1^* + h_3^*$ [ft]	$h_d^* + h_{3A}^*$ [ft]	$h_d^* + h_{3B}^*$ [ft]	$\frac{h_d^* + h_{3A}^*}{h_1^* + h_3^*}$	$\frac{h_d^* + h_{3B}^*}{h_1^* + h_3^*}$	K_b	K_d	$\frac{K_d}{K_b}$
833	45°WW	0.90		2.416	2.50	0.333	0.176	0.195	1.108	0.306	3.3	9.90	0.222	0.113	0.240	0.510	1.080	1.090	1.119	1.245
895R	45°WW	0.90		4.42	5.00	0.484	0.066	0.082	1.240	0.560	3.3	6.82	0.106	0.095	0.128	0.895	1.208	0.690	0.881	1.275
902	45°WW	0.90		2.416	5.00	0.484	0.305	0.333	1.090	0.306	3.3	6.82	0.402	0.174	0.424	0.432	1.055	1.090	1.112	1.020
909	45°WW	0.90		2.416	5.00	0.484	0.305	0.361	1.182	0.306	10.00	20.70	0.402	0.144	0.434	0.358	1.078	1.090	1.208	1.110
916R	45°WW	0.90		4.42	5.00	0.484	0.066	0.091	1.420	0.560	10.00	20.70	0.106	0.088	0.131	0.830	1.235	0.690	0.981	1.420
916RR	45°WW	0.90		4.42	5.00	0.484	0.066	0.095	1.480	0.560	10.00	20.70	0.106	0.089	0.130	0.840	1.225	0.690	1.025	1.485
960	45°WW	0.90		2.416	2.50	0.333	0.176	0.211	1.200	0.306	10.00	30.10	0.222	0.090	0.248	0.405	1.116	1.090	1.348	1.235
1329	45°WW	0.60		2.90	3.00	0.360	0.141	0.169	1.200	0.367	3.33	9.25	0.181	0.102	0.213	0.563	1.177	1.050	1.200	1.142
1330	45°WW	0.60		3.88	3.00	0.360	0.065	0.081	1.245	0.491	3.33	9.25	0.096	0.061	0.114	0.635	1.188	0.850	1.045	1.230
1331	45°WW	0.60		4.90	3.00	0.360	0.031	0.039	1.255	0.619	3.33	9.25	0.054	0.036	0.064	0.667	1.185	0.550	0.797	1.450
1332	45°WW	0.60		5.90	3.00	0.360	0.011	0.016	1.455	0.746	3.33	9.25	0.029	0.015	0.033	0.517	1.138	0.290	0.469	1.610
1333	45°WW	0.60		2.90	3.00	0.360	0.141	0.174	1.235	0.366	6.67	18.00	0.088	0.088	0.222	0.486	1.225	1.050	1.237	1.180
1334	45°WW	0.60		3.87	3.00	0.360	0.065	0.089	1.370	0.490	6.67	18.00	0.096	0.055	0.122	0.573	1.270	0.860	1.151	1.340
1335	45°WW	0.60		4.90	3.00	0.360	0.031	0.043	1.385	0.619	6.67	18.00	0.054	0.034	0.068	0.630	1.260	0.550	0.881	1.600
1337	45°WW	0.60		2.90	3.00	0.360	0.141	0.190	1.350	0.366	10.00	27.00	0.181	0.078	0.242	0.431	1.337	1.050	1.355	1.290
1338	45°WW	0.60		3.87	3.00	0.360	0.065	0.094	1.445	0.490	10.00	27.00	0.096	0.066	0.128	0.687	1.335	0.860	1.200	1.400
1339	45°WW	0.60		4.90	3.00	0.360	0.031	0.049	1.580	0.619	10.00	27.00	0.054	0.041	0.076	0.759	1.410	0.550	1.005	1.830
1340	45°WW	0.60		5.88	3.00	0.360	0.011	0.019	1.725	0.744	10.00	27.00	0.029	0.016	0.036	0.552	1.240	0.290	0.559	1.925
1317	1:1.5ST	0.90	2.14	2.866	5.00	0.484	0.240	0.265	1.105	0.363	10.00	20.70	0.299	0.146	0.325	0.488	1.088	1.100	1.235	1.123
1318	1:1.5ST	0.90	3.16	3.866	5.00	0.484	0.123	0.140	1.140	0.492	10.00	20.70	0.175	0.112	0.184	0.640	1.052	0.940	1.177	0.250
1319	1:1.5ST	0.90	4.16	4.886	5.00	0.484	0.061	0.068	1.110	0.619	10.00	20.70	0.104	0.072	0.096	0.692	0.925	0.640	0.898	1.400
1320	1:1.5ST	0.90	5.16	5.886	5.00	0.484	0.022	0.030	1.365	0.745	10.00	20.70	0.049	0.039	0.048	0.796	0.980	0.350	0.563	1.605
1321	1:1.5ST	0.90	2.12	2.846	5.00	0.484	0.240	0.266	1.110	0.360	6.67	13.80	0.299	0.134	0.333	0.448	1.113	1.100	1.222	1.110
1322R	1:1.5ST	0.90	3.14	3.866	5.00	0.484	0.123	0.142	1.155	0.490	6.67	13.80	0.175	0.118	0.186	0.674	1.064	0.940	1.183	1.260
1323	1:1.5ST	0.90	4.13	4.856	5.00	0.484	0.057	0.069	1.210	0.615	6.67	13.80	0.096	0.078	0.097	0.812	1.010	0.640	0.897	1.400
1324	1:1.5ST	0.90	5.15	5.876	5.00	0.484	0.022	0.032	1.455	0.744	6.67	13.80	0.049	0.044	0.049	0.898	1.000	0.350	0.600	1.715
1325	1:1.5ST	0.90	2.15	2.876	5.00	0.484	0.240	0.246	1.025	0.364	3.75	7.75	0.299	0.205	0.317	0.686	1.060	1.100	1.156	1.050
1326R	1:1.5ST	0.90	3.16	3.886	5.00	0.484	0.123	0.129	1.050	0.492	3.75	7.75	0.104	0.131	0.181	1.260	1.740	0.940	1.082	1.155
1328	1:1.5ST	0.90	5.16	5.886	5.00	0.484	0.022	0.025	1.135	0.745	3.75	7.75	0.049	0.037	0.048	0.755	0.980	0.350	0.469	1.335

TABLE 12 : DUAL BRIDGES CONTRACTION
with pile bents

B = 7.90 , L = 1.00 , S_o = 0.0012 , n = 0.0024

Run No.	Abutment Type	l [ft]	b [ft]	Q [cfs]	h _n [ft]	h ₁ * [ft]	h _d * [ft]	$\frac{h_d^*}{h_1^*}$	M	L _D	$\frac{L_D}{h_n}$	Type of bent	Width of piles [ft]	Number of bents	J = $\frac{A_p}{A_n^3}$	h ₁ ** + h ₃ * [ft]	h _d ** + h _{3A} * [ft]	h _d ** + h _{3B} * [ft]	$\frac{h_d^{**} + h_{3A}^*}{h_1^{**} + h_3^*}$	$\frac{h_d^{**} + h_{3B}^*}{h_1^{**} + h_3^*}$
811	45°WW	0.90	4.42	2.50	0.333	0.044	0.056	1.273	0.559	3.3	9.91	Circular	0.052	4	0.0472	0.069	0.055	0.077	0.797	1.116
811R	45°WW	0.90	4.42	2.50	0.333	0.044	0.054	1.227	0.559	3.3	9.91	lar	0.052	4	0.0472	0.069	0.055	0.077	0.797	1.116
812	45°WW	0.90	4.42	2.50	0.333	0.049	0.058	1.184	0.559	3.3	9.91	5	0.052	6	0.0706	0.077	0.056	0.083	0.727	1.078
812R	45°WW	0.90	4.42	2.50	0.333	0.049	0.054	1.102	0.559	3.3	9.91	piles	0.052	6	0.0706	0.077	0.051	0.076	0.662	0.987
820	45°WW	0.90	4.42	2.50	0.333	0.049	0.071	1.449	0.559	10.00	30.00		0.052	6	0.0706	0.077	0.054	0.083	0.701	1.078
821	45°WW	0.90	4.42	2.50	0.333	0.044	0.066	1.500	0.559	10.00	30.00		0.052	4	0.0472	0.069	0.054	0.080	0.782	1.160
821R	45°WW	0.90	4.42	2.50	0.333	0.044	0.067	1.523	0.559	10.00	30.00		0.052	4	0.0472	0.069	0.057	0.088	0.826	1.275
822	45°WW	0.90	4.42	2.50	0.333	0.042	0.059	1.405	0.559	10.00	30.00		0.052	2	0.0236	0.063	0.048	0.072	0.762	1.143
822R	45°WW	0.90	4.42	2.50	0.333	0.042	0.062	1.476	0.559	10.00	30.00		0.052	2	0.0236	0.063	0.062	0.082	0.984	1.301
837	45°WW	0.90	2.416	2.50	0.333	0.204	0.236	1.157	0.306	3.3	9.91		0.052	4	0.0862	0.246	0.119	0.281	0.484	1.142
838R	45°WW	0.90	2.416	2.50	0.333	0.192	0.216	1.125	0.306	3.3	9.91		0.052	2	0.0432	0.242	0.111	0.264	0.459	1.091
839	45°WW	0.90	2.416	2.50	0.333	0.181	0.206	1.138	0.306	3.3	9.91		0.052	1	0.0215	0.230	0.119	0.254	0.517	1.104
839R	45°WW	0.90	2.416	2.50	0.333	0.181	0.203	1.122	0.306	3.3	9.91		0.052	1	0.0215	0.230	0.105	0.251	0.456	1.091
896	45°WW	0.90	4.42	5.00	0.484	0.071	0.090	1.268	0.559	3.3	6.82		0.052	2	0.0236	0.112	0.091	0.122	0.812	1.089
897	45°WW	0.90	4.42	5.00	0.484	0.078	0.099	1.269	0.559	3.3	6.82		0.052	4	0.0472	0.122	0.086	0.140	0.711	1.157
898	45°WW	0.90	4.42	5.00	0.484	0.087	0.107	1.230	0.559	3.3	6.82		0.052	6	0.0707	0.135	0.087	0.154	0.644	1.141
903R	45°WW	0.90	2.416	5.00	0.484	0.324	0.360	1.111	0.306	3.3	6.82		0.052	1	0.0216	0.405	0.171	0.459	0.422	1.133
904	45°WW	0.90	2.416	5.00	0.484	0.338	0.370	1.095	0.306	3.3	6.82		0.052	2	0.0432	0.415	0.166	0.448	0.400	1.081
905	45°WW	0.90	2.416	5.00	0.484	0.348	0.387	1.112	0.306	3.3	6.82		0.052	3	0.0646	0.435	0.166	0.457	0.382	1.051
905R	45°WW	0.90	2.416	5.00	0.484	0.348	0.400	1.149	0.306	3.3	6.82		0.052	3	0.0646	0.435	0.154	0.483	0.354	1.110
910	45°WW	0.90	2.416	5.00	0.484	0.324	0.370	1.142	0.306	10.00	20.70		0.052	1	0.0216	0.405	0.154	0.464	0.380	1.146
911	45°WW	0.90	2.416	5.00	0.484	0.338	0.386	1.142	0.306	10.00	20.70		0.052	2	0.0432	0.415	0.170	0.472	0.410	1.137
917R	45°WW	0.90	4.42	5.00	0.484	0.071	0.110	1.408	0.559	10.00	20.70		0.052	2	0.0236	0.112	0.088	0.140	0.786	1.250
918	45°WW	0.90	4.44	5.00	0.484	0.078	0.109	1.397	0.562	10.00	20.70		0.052	4	0.0467	0.120	0.087	0.150	0.731	1.260
918R	45°WW	0.90	4.44	5.00	0.484	0.078	0.114	1.462	0.559	10.00	20.70		0.052	4	0.0472	0.120	0.083	0.150	0.697	1.260
919	45°WW	0.90	4.44	5.00	0.484	0.088	0.121	1.375	0.559	10.00	20.70		0.052	6	0.071	0.131	0.089	0.161	0.679	1.229
813	45°WW	0.90	4.42	2.50	0.333	0.052	0.060	1.154	0.559	3.3	9.91	Square	0.052	6	0.0706	0.078	0.064	0.085	0.820	1.090
814	45°WW	0.90	4.42	2.50	0.333	0.044	0.055	1.250	0.559	3.3	9.91	5	0.052	4	0.0472	0.069	0.057	0.061	0.826	0.884
818	45°WW	0.90	4.42	2.50	0.333	0.044	0.067	1.523	0.559	10.00	30.00	piles	0.052	4	0.0472	0.069	0.054	0.081	0.783	1.174
819	45°WW	0.90	4.42	2.50	0.333	0.052	0.076	1.462	0.559	10.00	30.00		0.052	6	0.0706	0.078	0.056	0.087	0.718	1.115
834	45°WW	0.90	2.416	2.50	0.333	0.183	0.208	1.137	0.306	3.3	9.91		0.052	1	0.0215	0.231	0.116	0.251	0.502	1.086
835	45°WW	0.90	2.416	2.50	0.333	0.195	0.228	1.170	0.306	3.3	9.91		0.052	2	0.0432	0.247	0.117	0.271	0.474	1.097
836	45°WW	0.90	2.416	2.50	0.333	0.209	0.246	1.177	0.306	3.3	9.91		0.052	4	0.0862	0.260	0.121	0.295	0.465	1.135
899	45°WW	0.90	4.42	5.00	0.484	0.093	0.116	1.247	0.559	3.3	6.82		0.052	6	0.0707	0.141	0.095	0.167	0.674	1.184
900	45°WW	0.90	4.42	5.00	0.484	0.083	0.103	1.241	0.559	3.3	6.82		0.052	4	0.0472	0.126	0.098	0.147	0.778	1.167
906R	45°WW	0.90	2.416	5.00	0.484	0.357	0.418	1.171	0.306	3.3	6.82		0.052	3	0.0646	0.442	0.165	0.502	0.373	1.136
907R	45°WW	0.90	2.416	5.00	0.484	0.340	0.384	1.129	0.306	3.3	6.82		0.052	2	0.0432	0.425	0.157	0.485	0.369	1.141
908	45°WW	0.90	2.416	5.00	0.484	0.330	0.351	1.064	0.306	3.3	6.82		0.052	1	0.0216	0.410	0.173	0.444	0.422	1.083
908R	45°WW	0.90	2.416	5.00	0.484	0.330	0.350	1.061	0.306	3.3	6.82		0.052	1	0.0216	0.410	0.169	0.463	0.412	1.129
914	45°WW	0.90	2.416	5.00	0.484	0.340	0.391	1.150	0.306	10.00	20.70		0.052	2	0.0432	0.425	0.174	0.473	0.409	1.113
915	45°WW	0.90	2.416	5.00	0.484	0.330	0.372	1.127	0.306	10.00	20.70		0.052	1	0.0216	0.410	0.138	0.450	0.337	1.097
920	45°WW	0.90	4.46	5.00	0.484	0.094	0.134	1.426	0.564	10.00	20.70		0.052	6	0.0708	0.141	0.094	0.175	0.667	1.241
921	45°WW	0.90	4.46	5.00	0.484	0.083	0.115	1.386	0.564	10.00	20.70		0.052	4	0.0467	0.126	0.092	0.156	0.730	1.238

TABLE 13 : ABNORMAL STAGE-DISCHARGE CONDITION
45 degree wing-wall abutment

Run No.	Abutment Type	L [ft]	l [ft]	B [ft]	b [ft]	S _o	n	Q [cfs]	t ^h _n	h ₁ * [ft]	h _n [ft]	M	K _A *	K _b	h ₁ * + h ₃ * [ft]	$\frac{h_1^*}{h_1^* + h_3^*}$
362	45°WW	1.00	0.60	7.90	5.91	0.0012	0.024	2.50	1.07y _n	0.012	0.333	0.748	0.485	0.431	0.022	0.545
363	45°WW	1.00	0.60	7.90	4.98	0.0012	0.024	2.50	1.07y _n	0.021	0.333	0.63	0.634	0.530	0.035	0.600
364	45°WW	1.00	0.60	7.90	3.90	0.0012	0.024	2.50	1.07y _n	0.049	0.333	0.494	0.916	0.787	0.072	0.680
365	45°WW	1.00	0.60	7.90	2.90	0.0012	0.024	2.50	1.07y _n	0.107	0.333	0.367	1.118	0.959	0.143	0.748
367	45°WW	1.00	0.60	7.90	2.85	0.0012	0.024	2.50	1.07y _n	0.110	0.333	0.361	1.115	0.978	0.142	0.774
147A	45°WW	1.00	0.90	7.90	4.45	0.0012	0.024	4.95	1.10y _n	0.050	0.484	0.563	0.683	0.571		
148A	45°WW	1.00	0.90	7.90	3.41	0.0012	0.024	4.95	1.10y _n	0.111	0.484	0.432	0.899	0.825		
149A	45°WW	1.00	0.90	7.90	2.40	0.0012	0.024	4.95	1.10y _n	0.256	0.484	0.304	1.050	0.869		
349	45°WW	1.00	0.90	7.90	2.44	0.0012	0.024	5.00	1.10y _n	0.277	0.484	0.309	1.153	0.917	0.341	0.812
350	45°WW	1.00	0.90	7.90	3.42	0.0012	0.024	5.00	1.10y _n	0.121	0.484	0.433	0.975	0.803	0.171	0.708
351	45°WW	1.00	0.90	7.90	4.46	0.0012	0.024	5.00	1.10y _n	0.052	0.484	0.565	0.695	0.579	0.088	0.591
150A	45°WW	1.00	0.90	7.90	2.40	0.0012	0.024	4.95	1.20y _n	0.209	0.484	0.304	1.003	0.713		
151A	45°WW	1.00	0.90	7.90	3.40	0.0012	0.024	4.95	1.20y _n	0.086	0.484	0.430	0.815	0.585		
151B	45°WW	1.00	0.90	7.90	3.40	0.0012	0.024	4.95	1.20y _n	0.076	0.484	0.430	0.715	0.514		
205	45°WW	1.00	0.90	7.90	2.45	0.0012	0.024	5.00	1.20y _n	0.215	0.484	0.310	1.076	0.770	0.260	0.827
206	45°WW	1.00	0.90	7.90	3.42	0.0012	0.024	5.00	1.20y _n	0.119	0.484	0.433	1.160	0.724		
207	45°WW	1.00	0.90	7.90	4.47	0.0012	0.024	4.99	1.20y _n	0.055	0.484	0.566	0.891	0.468		
346	45°WW	1.00	0.90	7.90	4.48	0.0012	0.024	5.00	1.20y _n	0.034	0.484	0.567	0.574	0.391	0.062	0.548
347	45°WW	1.00	0.90	7.90	3.44	0.0012	0.024	5.00	1.20y _n	0.092	0.484	0.435	0.913	0.632	0.132	0.697
348	45°WW	1.00	0.90	7.90	2.44	0.0012	0.024	5.00	1.20y _n	0.235	0.484	0.309	1.174	0.815	0.291	0.808
378	45°WW	1.00	0.60	7.90	5.92	0.0012	0.024	2.50	1.20y _n	0.006	0.333	0.749	0.321	0.262	0.015	0.399
379	45°WW	1.00	0.60	7.90	4.92	0.0012	0.024	2.50	1.20y _n	0.015	0.333	0.623	0.572	0.399	0.026	0.577
380	45°WW	1.00	0.60	7.90	3.92	0.0012	0.024	2.50	1.20y _n	0.033	0.333	0.496	0.805	0.549	0.048	0.687
381	45°WW	1.00	0.60	7.90	2.90	0.0012	0.024	2.50	1.20y _n	0.076	0.333	0.367	1.018	0.698	0.097	0.784
138	45°WW	1.00	0.90	7.90	3.41	0.0012	0.024	4.95	1.30y _n	0.079	0.484	0.432	0.909	0.540		
139	45°WW	1.00	0.90	7.90	4.45	0.0012	0.024	4.95	1.30y _n	0.048	0.484	0.563	0.928	0.556		
140	45°WW	1.00	0.90	7.90	4.45	0.0012	0.024	4.95	1.30y _n	0.045	0.484	0.563	0.867	0.519		
141	45°WW	1.00	0.90	7.90	3.41	0.0012	0.024	4.95	1.30y _n	0.087	0.484	0.432	1.006	0.597		
208	45°WW	1.00	0.90	7.90	2.42	0.0012	0.024	4.98	1.30y _n	0.183	0.484	0.306	1.063	0.578		
210	45°WW	1.00	0.90	7.90	4.46	0.0012	0.024	4.94	1.30y _n	0.027	0.484	0.565	0.536	0.317		
336	45°WW	1.00	0.90	7.90	4.46	0.0012	0.024	5.00	1.30y _n	0.031	0.484	0.565	0.600	0.351	0.059	0.525
337	45°WW	1.00	0.90	7.90	3.42	0.0012	0.024	5.00	1.30y _n	0.080	0.484	0.433	0.908	0.537	0.105	0.762
356	45°WW	1.00	0.90	7.90	2.44	0.0012	0.024	5.00	1.30y _n	0.192	0.484	0.309	1.123	0.654	0.241	0.797
383	45°WW	1.00	0.60	7.90	5.90	0.0012	0.024	2.50	1.30y _n	0.005	0.333	0.747	0.309	0.192	0.011	0.454
384	45°WW	1.00	0.60	7.90	4.92	0.0012	0.024	2.50	1.30y _n	0.014	0.333	0.623	0.660	0.382	0.024	0.583
385	45°WW	1.00	0.60	7.90	3.90	0.0012	0.024	2.50	1.30y _n	0.028	0.333	0.494	0.785	0.459	0.041	0.684
386	45°WW	1.00	0.60	7.90	2.90	0.0012	0.024	2.50	1.30y _n	0.061	0.333	0.367	0.963	0.559	0.080	0.763
329	45°WW	1.00	0.90	7.90	4.44	0.0012	0.024	5.00	1.40y _n	0.034	0.484	0.562	0.754	0.385	0.053	0.642
330	45°WW	1.00	0.90	7.90	3.35	0.0012	0.024	5.00	1.40y _n	0.065	0.484	0.424	0.833	0.425	0.089	0.730
335	45°WW	1.00	0.90	7.90	2.42	0.0012	0.024	5.00	1.40y _n	0.160	0.484	0.306	1.082	0.551	0.198	0.808

TABLE 14 : ABNORMAL STAGE-DISCHARGE CONDITION
1:1.5 spill-through abutment

Run No.	Abutment Type	L [ft]	l [ft]	B [ft]	b _m [ft]	b [ft]	S _o	n	Q [cfs]	t ^h _n	h ₁ * [ft]	h _n [ft]	M	K _A *	K _b	h ₁ * + h ₃ * [ft]	$\frac{h_1^*}{h_1^* + h_3^*}$
368	1:1.5ST	1.00	0.60	7.90	1.85	2.384	0.0012	0.024	2.50	1.07y _n	0.179	0.333	0.302	1.272	1.088	0.216	0.829
369	1:1.5ST	1.00	0.60	7.90	2.85	3.384	0.0012	0.024	2.50	1.07y _n	0.083	0.333	0.428	1.174	1.024	0.111	0.747
370	1:1.5ST	1.00	0.60	7.90	3.85	4.384	0.0012	0.024	2.50	1.07y _n	0.041	0.333	0.555	0.967	0.844	0.057	0.720
371	1:1.5ST	1.00	0.60	7.90	4.85	5.384	0.0012	0.024	2.50	1.07y _n	0.016	0.333	0.682	0.573	0.469	0.027	0.592
372	1:1.5ST	1.00	0.60	7.90	5.85	6.384	0.0012	0.024	2.50	1.07y _n	0.007	0.333	0.808	0.347	0.298	0.014	0.500
352	1:1.5ST	1.00	0.90	7.90	5.21	6.008	0.0012	0.024	5.00	1.10y _n	0.016	0.484	0.761	0.396	0.311	0.032	0.500
353	1:1.5ST	1.00	0.90	7.90	4.12	4.918	0.0012	0.024	5.00	1.10y _n	0.045	0.484	0.623	0.736	0.590	0.078	0.577
354	1:1.5ST	1.00	0.90	7.90	3.17	3.968	0.0012	0.024	5.00	1.10y _n	0.096	0.484	0.502	1.035	0.807	0.139	0.691
355	1:1.5ST	1.00	0.90	7.90	2.19	2.988	0.0012	0.024	5.00	1.10y _n	0.205	0.484	0.378	1.260	0.990	0.261	0.785
342	1:1.5ST	1.00	0.90	7.90	2.17	3.042	0.0012	0.024	5.00	1.20y _n	0.169	0.484	0.385	1.312	0.826	0.223	0.758
343	1:1.5ST	1.00	0.90	7.90	3.17	4.042	0.0012	0.024	5.00	1.20y _n	0.078	0.484	0.512	1.067	0.684	0.113	0.690
344	1:1.5ST	1.00	0.90	7.90	4.17	5.042	0.0012	0.024	5.00	1.20y _n	0.034	0.484	0.638	0.726	0.473	0.056	0.607
345	1:1.5ST	1.00	0.90	7.90	5.21	6.082	0.0012	0.024	5.00	1.20y _n	0.014	0.484	0.770	0.472	0.310	0.026	0.538
373	1:1.5ST	1.00	0.60	7.90	5.88	6.480	0.0012	0.024	2.50	1.20y _n	0.003	0.333	0.820	0.257	0.141	0.008	0.375
374	1:1.5ST	1.00	0.60	7.90	4.88	5.480	0.0012	0.024	2.50	1.20y _n	0.009	0.333	0.694	0.418	0.280	0.017	0.529
375	1:1.5ST	1.00	0.60	7.90	3.88	4.480	0.0012	0.024	2.50	1.20y _n	0.025	0.333	0.567	0.812	0.527	0.039	0.641
376	1:1.5ST	1.00	0.60	7.90	2.88	3.480	0.0012	0.024	2.50	1.20y _n	0.063	0.333	0.441	1.206	0.783	0.083	0.759
377	1:1.5ST	1.00	0.60	7.90	1.85	2.450	0.0012	0.024	2.50	1.20y _n	0.140	0.333	0.310	1.340	0.862	0.164	0.854
338	1:1.5ST	1.00	0.90	7.90	5.29	6.234	0.0012	0.024	5.00	1.30y _n	0.009	0.484	0.789	0.337	0.180	0.017	0.529
339	1:1.5ST	1.00	0.90	7.90	4.17	5.114	0.0012	0.024	5.00	1.30y _n	0.026	0.484	0.647	0.634	0.365	0.044	0.591
340	1:1.5ST	1.00	0.90	7.90	3.20	4.144	0.0012	0.024	5.00	1.30y _n	0.056	0.484	0.525	0.935	0.498	0.090	0.622
341	1:1.5ST	1.00	0.90	7.90	2.17	3.114	0.0012	0.024	5.00	1.30y _n	0.140	0.484	0.394	1.340	0.686	0.178	0.787
387	1:1.5ST	1.00	0.60	7.90	5.90	6.550	0.0012	0.024	2.50	1.30y _n	0.004	0.333	0.829	0.313	0.184		
388	1:1.5ST	1.00	0.60	7.90	4.88	5.530	0.0012	0.024	2.50	1.30y _n	0.008	0.333	0.700	0.451	0.259	0.017	0.471
389	1:1.5ST	1.00	0.60	7.90	3.88	4.530	0.0012	0.024	2.50	1.30y _n	0.022	0.333	0.573	0.872	0.471	0.030	0.733
390	1:1.5ST	1.00	0.60	7.90	2.88	3.530	0.0012	0.024	2.50	1.30y _n	0.053	0.333	0.447	1.229	0.671	0.067	0.792
391	1:1.5ST	1.00	0.60	7.90	1.86	2.510	0.0012	0.024	2.50	1.30y _n	0.117	0.333	0.318	1.387	0.729	0.139	0.842
331	1:1.5ST	1.00	0.90	7.90	5.17	6.187	0.0012	0.024	5.00	1.40y _n	0.005	0.484	0.783	0.205	0.091	0.013	0.385
332	1:1.5ST	1.00	0.90	7.90	4.19	5.207	0.0012	0.024	5.00	1.40y _n	0.018	0.484	0.659	0.566	0.254	0.034	0.529
333	1:1.5ST	1.00	0.90	7.90	3.17	4.187	0.0012	0.024	5.00	1.40y _n	0.043	0.484	0.530	0.865	0.384	0.064	0.672
334	1:1.5ST	1.00	0.90	7.90	2.17	3.187	0.0012	0.024	5.00	1.40y _n	0.112	0.484	0.403	1.308	0.547	0.147	0.769

TABLE 15 : PARTIALLY SUBMERGED BRIDGE DECK
upstream girder submerged

Run No.	Abutment Type	L [ft]	l [ft]	B [ft]	b_m [ft]	b [ft]	S_o	n	Q [cfs]	h_n [ft]	h_s^* [ft]	h_1 [ft]	Z [ft]	M	C_d	$\frac{Z}{h_1}$	$\frac{h_3}{h_1}$ [ft]	$\frac{h_3}{h_1}$
788	WW	1.00	0.90	7.90		2.44	0.0012	0.042	2.50	0.483	0.090	0.573	0.519	0.309	0.324	0.906	0.463	0.807
789	WW	1.00	0.90	7.90		2.44	0.0012	0.042	2.50	0.483	0.100	0.583	0.508	0.309	0.329	0.871	0.465	0.798
830	WW	1.00		7.90		2.416	0.0012	0.024	2.50	0.333	0.242	0.575	0.348	0.306	0.488	0.605		
831	WW	1.00		7.90		2.416	0.0012	0.024	2.50	0.333	0.182	0.515	0.389	0.309	0.463	0.755		
760	WW	1.00	0.90	7.90		3.44	0.0012	0.024	5.00	0.484	0.186	0.670	0.522	0.435	0.422	0.779		
893	WW	1.00	0.90	7.90		4.42	0.0012	0.024	5.00	0.484	0.075	0.559	0.482	0.559	0.338	0.862	0.435	0.778
937	WW	1.00	0.90	7.90		2.416	0.0012	0.024	5.00	0.484	0.346	0.830	0.644	0.306	0.438	0.776	0.389	0.468
938	WW	1.00	0.90	7.90		2.416	0.0012	0.024	5.00	0.484	0.364	0.848	0.619	0.306	0.448	0.730	0.389	0.459
1345	WW	1.00	0.60	7.90		5.90	0.0012	0.024	3.00	0.369	0.014	0.383	0.343	0.747	0.298	0.896	0.352	0.920
1353	WW	1.00	0.60	7.90		3.85	0.0012	0.024	3.00	0.369	0.071	0.440	0.372	0.487	0.394	0.845	0.332	0.755
1356	WW	1.00	0.60	7.90		2.85	0.0012	0.024	3.00	0.369	0.155	0.524	0.426	0.361	0.425	0.813	0.315	0.600
1357	WW	1.00	0.60	7.90		2.85	0.0012	0.024	3.00	0.369	0.220	0.589	0.371	0.361	0.462	0.630	0.309	0.525
1358	WW	1.00	0.60	7.90		2.85	0.0012	0.024	3.00	0.369	0.185	0.554	0.397	0.361	0.447	0.717	0.311	0.562
1359	WW	1.00	0.60	7.90		2.85	0.0012	0.024	3.00	0.369	0.151	0.520	0.431	0.361	0.423	0.829	0.322	0.618
867	ST	1.00		7.90	3.00	3.453	0.0012	0.024	2.50	0.333	0.114	0.447	0.302	0.443	0.447	0.676	0.302	0.676
884	ST	1.00	0.90	7.90	3.16	3.813	0.0012	0.024	5.00	0.484	0.218	0.702	0.435	0.492	0.450	0.620	0.416	0.620
885	ST	1.00	0.90	7.90	3.16	3.894	0.0012	0.024	5.00	0.484	0.129	0.613	0.488	0.492	0.417	0.796	0.426	0.796
1360	ST	1.00	0.90	7.90	3.14	3.878	0.0012	0.024	5.00	0.484	0.135	0.619	0.492	0.490	0.415	0.795	0.428	0.795
1361	ST	1.00	0.90	7.90	3.14	3.836	0.0012	0.024	5.00	0.484	0.179	0.663	0.464	0.490	0.431	0.700	0.420	0.700
1362	ST	1.00	0.90	7.90	2.1	3.797	0.0012	0.024	5.00	0.484	0.227	0.711	0.438	0.490	0.443	0.616	0.411	0.616
1363	ST	1.00	0.90	7.90	2.12	3.014	0.0012	0.024	5.00	0.484	0.245	0.729	0.596	0.300	0.406	0.818	0.411	0.818
1364	ST	1.00	0.90	7.90	2.12	2.921	0.0012	0.024	5.00	0.484	0.345	0.829	0.534	0.300	0.439	0.644	0.402	0.644
1365	ST	1.00	0.90	7.90	2.12	2.954	0.0012	0.024	5.00	0.484	0.307	0.791	0.556	0.300	0.426	0.703	0.410	0.703
1366	ST	1.00	0.90	7.90	4.18	4.849	0.0012	0.024	5.00	0.484	0.062	0.546	0.446	0.621	0.389	0.817	0.441	0.817
1367	ST	1.00	0.90	7.90	4.18	4.807	0.0012	0.024	5.00	0.484	0.087	0.571	0.418	0.621	0.410	0.732	0.441	0.732

TABLE 16 : PARTIALLY SUBMERGED BRIDGE DECK
all girders submerged

Run No.	Abutment Type	L [ft]	l [ft]	B [ft]	b_m [ft]	b [ft]	S_o	n	Q [cfs]	h_n [ft]	h_s^* [ft]	h_1 [ft]	Z [ft]	M	C_d	$\frac{Z}{h_1}$	Δh [ft]
808	WW	1.00		7.90		4.42	0.0012	0.024	2.50	0.333	0.104	0.407	0.266	0.579	0.709	0.654	0.139
1342	WW	1.00	0.60	7.90		4.87	0.0012	0.024	3.00	0.369	0.073	0.442	0.299	0.617	0.759	0.676	0.114
1343	WW	1.00	0.60	7.90		4.87	0.0012	0.024	3.00	0.369	0.121	0.490	0.254	0.617	0.755	0.518	0.160
1349	WW	1.00	0.60	7.90		4.87	0.0012	0.024	3.00	0.369	0.065	0.434	0.316	0.617	0.756	0.728	0.103
1350	WW	1.00	0.60	7.90		4.87	0.0012	0.024	3.00	0.369	0.110	0.479	0.271	0.617	0.731	0.566	0.149
1346	WW	1.00	0.60	7.90		5.90	0.0012	0.024	3.00	0.369	0.031	0.400	0.301	0.747	0.824	0.752	0.065
1347	WW	1.00	0.60	7.90		5.90	0.0012	0.024	3.00	0.369	0.061	0.430	0.258	0.747	0.813	0.600	0.091
1352	WW	1.00	0.60	7.90		3.85	0.0012	0.024	3.00	0.369	0.169	0.538	0.279	0.487	0.742	0.518	0.219
868R	ST	1.00		7.90	3.00	3.399	0.0012	0.024	2.50	0.333	0.152	0.485	0.266	0.443	0.751	0.548	0.199
881	ST	1.00	0.90	7.90	5.06	5.599	0.0012	0.024	5.00	0.484	0.055	0.539	0.399	0.735	0.905	0.740	0.095
882	ST	1.00	0.90	7.90	5.08	5.669	0.0012	0.024	5.00	0.484	0.072	0.556	0.393	0.735	0.807	0.707	0.120
1368	ST	1.00	0.90	7.90	4.18	4.767	0.0012	0.024	5.00	0.484	0.133	0.617	0.391	0.621	0.760	0.634	0.193
1369	ST	1.00	0.90	7.90	5.17	5.857	0.0012	0.024	5.00	0.484	0.025	0.509	0.458	0.746	0.867	0.900	0.069
1370	ST	1.00	0.90	7.90	5.17	5.819	0.0012	0.024	5.00	0.484	0.033	0.517	0.433	0.746	0.882	0.838	0.078
1371	ST	1.00	0.90	7.90	5.17	5.781	0.0012	0.024	5.00	0.484	0.051	0.535	0.407	0.746	0.845	0.761	0.098